UNIVERSITY OF CAMBRIDGE

Development of stapled peptide targeted covalent inhibitors and synthesis of novel ADC payloads for applications in cancer therapy

Jiraborrirak Charoenpattarapreeda

Trinity College

University of Cambridge

November 2020

Supervised by Professor David R Spring

This dissertation is submitted for the degree of Doctor of Philosophy.

Declaration

This thesis is the result of my own work and includes nothing which is the outcome of work done in collaboration except as declared in the Preface and specified in the text. It is not substantially the same as any that I have submitted, or, is being concurrently submitted for a degree or diploma or other qualification at the University of Cambridge or any other University or similar institution except as declared in the Preface and specified in the text. I further state that no substantial part of my thesis has already been submitted, or, is being concurrently submitted for any such degree, diploma or other qualification at the University of Cambridge or any other University or similar institution except as declared in the Preface and specified in the text. It does not exceed the prescribed word limit for the relevant Degree Committee

Jiraborrirak Charoenpattarapreeda

Trinity College, University of Cambridge

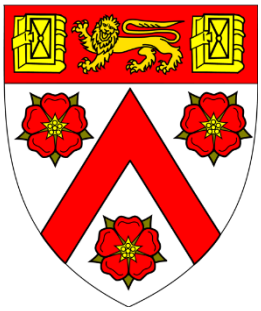

Abstract

Development of stapled peptide targeted covalent inhibitors and synthesis of novel ADC payloads for applications in cancer therapy

Jiraborrirak Charoenpattarapreeda

Cancer is one of the leading causes of deaths worldwide with 1 in 2 people estimated to develop the disease during their lifetimes. While great progress has been made in curing cancers, new therapeutics are still necessary to tackle this collection of diseases and minimise side-effects. This thesis presents two approaches towards the development of novel bioactive molecules with application in cancer therapeutics.

1) Development of stapled peptide–targeted covalent inhibitors (SPTCIs) of p53–MDM2 protein–protein interaction (PPI).

Herein, the development and synthesis of three novel electrophilic staples and four stapled peptides are described. The stapled peptides bear moieties to covalently target a surface-exposed lysine residue on MDM2, an important anti-apoptotic protein overexpressed in many cancer cells. Led by computational modelling and kinetic studies on stability and reactivity of the electrophiles, an SPTCI with an apparent K_d of 7.1 nM was discovered. The stapled peptide was built using two-component Cu-catalysed azide-alkyne cycloaddition (CuAAC) and an activated ester electrophile for targeted covalent inhibition. The peptide showed selective and complete covalent binding to MDM2. Crucially, this proof-of-concept study sets the basis for the development of SPTCIs for a wider range of PPIs.

2) Novel total synthesis of hemiasterlin and its use as a payload in antibody–drug conjugates (ADCs).

This thesis details the novel synthesis of hemiasterlin, an anti-mitotic marine natural product with low- to sub-nM potencies against several cancer cell lines. Rapid construction of hemiasterlin was achieved, through a four-component Ugi reaction, in total 14 steps (longest linear sequence of 10 steps) in 11% overall yield. The convergent synthetic route also enabled the synthesis of taltobulin (HTI-286), a similarly potent synthetic analogue. Through the synthesis of complex linker-drug molecules, two ADCs were made to investigate the potential of the two molecules as payloads. Remarkably, the conjugates were found to have mid-pM cytotoxicity against antigen-expressing breast cancer cell lines and no appreciable activity against antigen-negative cancer cells.

Acknowledgements

First and foremost, I would like to express my gratitude to Prof David Spring for giving me the opportunity to be working in his research group and allowing me to work on this fascinating research in the past four years. Thank you for all the advice, support, and the belief in me that I can get to the finish line. I would like to thank Trinity College for funding and being my home in the past eight years. More thanks go to the Development and Promotion of Science and Technology Talents Project (DPST), Royal Thai Government for funding. I would also like to thank all the collaborators: Dr Yaw Sing Tan, Dr Elaine Fowler, Dr Rohan Eapen, Teodors Pantelejevs. Without all of them, the projects would not be successful.

Massive thanks to my two mentors during my PhD, Dr Jessica Iegre and Dr Stephen Walsh. To Jessy, I thank you for being patient with me since the first year, pushing me forward, and not giving up on me. To Steve, thanks for introducing me to the ADC world, always being kind and supportive. I have learned a lot from you two and would not get to the end of my PhD without your guidance. You two have my eternal gratitude.

I would like to thank Dr Jessica Iegre, Dr Stephen Walsh, Dr Javi Perez-Areales, Dr Kim Mortensen, Dr Bee Ha Gan, Beth Cooper, and Tom King for sacrificing their time to proofread this thesis. I owe all of you a cake or a pint if you prefer.

Thanks to all past and present Spring Group members for always making me feel welcome in the Group. Special mention to Dr Hannah Sore for always looking out for me and giving me advice. Thanks also to Kim and Tom, my bay-buddies, for keeping me company and the tolerance to my strange music taste.

Thanks also to the technicians: Kevin, Gary, Nick, Nic, and Naomi for all the assistance and help with technical questions. More thanks to the NMR team: Duncan, Andrew, and Peter, for their assistance with NMR experiments.

Immense gratitude goes to my family, who always believe in me and let me pursue my own path in my life. It has been a long journey since I left home; without you, Mum and Dad, I would not be able to get here.

Big thanks to Keng, Neptune, Aim, and Tangtang—my real friends for keeping me sane and support me all the way during my PhD. I will sorely miss our weekend dinners and mahjong sessions.

Last but not least, thanks to Toei for always being with me and encouraging me through all the ups and downs. Your love and your smiles kept me going, and this thesis will not be possible without you.

Abbreviations

[α]	specific rotation
°C	degree(s) Celsius
2C-PS	two-component peptide stapling
9-BBN	9-borabicyclo[3.3.1]nonane
Å	ångström
Ac	acetyl
AcBut	4-(4'-acetylphenoxy)butanoic acid
ADC	antibody–drug conjugate
ADCC	antibody-dependent cell-mediated cytotoxicity
Ahx	6-aminohexanoic acid
AIBN	azobisisobutyronitrile
Alloc	allyloxycarbonyl
AML	acute myeloid leukaemia
ASAP	atmospheric solids analysis probe
ATP	adenosine triphosphate
ATR	attenuated total reflectance
BAD	Bcl-2-associated death promoter
BC	before Christ
Bcl-2	B-cell lymphoma 2
Bcl-X_L	B-cell lymphoma-extra large
BEP	2-bromo-*N*-ethylpyridinium tetrafluoroborate
BH3	Bcl-2 homology domain 3
BINOL	1,1'-bi-2-naphthol
Bn	benzyl
Boc	*tert*-butyloxycarbonyl
brsm	based on recovered starting material
BTFFH	Fluoro-*N*,*N*,*N'*,*N'*-bis(tetramethylene)formamidinium hexafluorophosphate
Bts	benzothiazol-2-sulfonyl
calcd	calculated
Cba	3-cyclobutyl-L-alanine
Cbz	carboxybenzyl
CD	circular dichroism

CD33	sialic acid–binding Ig-like lectin 3
CDI	1,1'-carbonyldiimidazole
CDK2	cyclin-dependent kinase 2
CDR	complementary binding region
Cit	citrulline
CLL	chronic lymphocytic leukaemia
cm^{-1}	wavenumber
CML	chronic myeloid leukaemia
CPA	chiral phosphoric acid
CSA	camphorsulfonic acid
CuAAC	copper(I)-catalysed azide–alkyne cycloaddition
CV	column volume(s)
Cy	cyclohexyl
Da	Dalton
DABSO	1,4-diazabicyclo[2.2.2]octane–bis(sulfur dioxide)
Dap	dolaproine
DAR	drug-to-antibody ratio
dba	dibenzylideneacetone
DBDMH	1,3-dibromo-5,5-dimethylhydantoin
DBU	1,8-diazabicyclo[5.4.0]undec-7-ene
DCC	*N*,*N*'-dicyclohexylcarbodiimide
dec	decomposed
DEPC	diethyl phosphorocyanidate
DIBAL-H	diisobutylaluminium hydride
DIC	diisopropylcarbodiimide
Dil	dolaisoleuine
DIPEA	*N*,*N*-diisopropylethylamine
DM1	emtansine
DM4	ravtansine
DMAP	*N*,*N*-dimethyl-4-aminopyridine
DMF	*N*,*N*-dimethylformamide
DMH	3-mercapto-3-methylbutyryl hydrazide
DMSO	dimethylsulfoxide
DNA	deoxyribonucleic acid
dPEG	discrete poly(ethylene glycol)

DPPA	diphenylphosphoryl azide
dr	diastereomeric ratio
DTC	dithiocarbamate
DTT	dithiothreitol
DUBA	duocarmycin-hydroxybenzamide-azaindole
DVP	divinylpyrimidine
EDC	*N*-(3-(dimethylamino)propyl)-*N*'-ethylcarbodiimide hydrochloride
EDTA	ethylenediaminetetraacetic acid
EGFR	epidermal growth factor receptor
eIF	eukaryotic translation initiation factor
ELISA	enzyme-linked immunosorbent assay
equiv.	equivalent(s)
ES	electrospray
ESI	electrospray ionisation
Fab	fragment, antigen-binding
FBS	foetal-bovine serum
Fc	fragment, crystallisable
FcγR	Fc-γ receptor
FDA	Food and Drug Administration
Fmoc	Fluorenylmethyloxycarbonyl
FP	fluorescence polarisation
FSBA	5'-*p*-fluorosulfonylbenzoyladenosine
GSH	glutathione
GTP	guanosine triphosphate
h	hour(s)
HATU	1-[bis(dimethylamino)methylene]-1*H*-1,2,3-triazolo[4,5-*b*]pyridinium 3-oxide hexafluorophosphate
HBTU	2-(1*H*-benzotriazol-1-yl)-1,1,3,3-tetramethyluronium hexafluorophosphate
HC	heavy chain
HER2	human epidermal growth factor 2
HOAt	1-hydroxy-7-azabenzotriazole
HOBt	1-hydroxybenzotriazole
HPLC	high-performance liquid chromatography
HRMS	high-resolution mass spectrometry
HSP	heat shock protein

IAP	inhibitors of apoptosis protein
IBX	2-iodoxybenzoic acid
IC_{50}	half-maximal inhibitory concentration
Ig	immunoglobulin
IGN	indolinobenzodiazepine dimer
IMCR	isonitrile-based multi-component reaction
IR	infrared
K	Kelvin
K_a	acid dissociation constant
K_d	dissociation constant
$K_{d,app}$	apparent dissociation constant
KHMDS	potassium hexamethyldisilazide
K_i	inhibition constant
LC	light chain
LCMS	liquid chromatography–mass spectrometry
lit.	literature
LL	low-loading
LLS	longest linear sequence
Lyz	lysozyme
M	molar
m/z	mass-to-charge ratio
mAb	monoclonal antibody
Mal	maleimide
$\tilde{\nu}_{max}$	absorption maximum in wavenumber
mc	maleimidocaproyl
Mcl-1	myeloid cell leukaemia 1
MD	molecular dynamics
MDM2	murine double minute 2
MDMX	murine double minute X
MED	minimum effective dose
MeVal	*N*-methylvaline
min	minute(s)
MMAE	monomethyl auristatin E
MMAF	monomethyl auristatin F
MOM	methoxymethyl

MQ	Milli-Q®
Ms	mesyl
MS	mass spectrometry; molecular sieves
MTD	maximum tolerated dose
MWCO	molecular weight cut-off
NBS	*N*-bromosuccinimide
NFSI	*N*-fluorobenzenesulfonimide
NHS	*N*-hydroxysuccinimide
NIS	*N*-iodosuccinimide
NK	natural killer
NMM	*N*-methylmorpholine
NMO	*N*-methylmorpholine *N*-oxide
NMR	nuclear magnetic resonance
Ns	nosyl
NSCLC	non-small-cell lung carcinoma
Orn	ornithine
Orn(N_3)	azido-ornithine
o-Tol	*ortho*-tolyl
PABC	*p*-aminobenzyloxycarbonyl
PBD	pyrrolobenzodiazepine
PBS	phosphate-buffered saline
PD	pharmacodynamics
PDB	protein database
PDI	peptide dual inhibitor
PEG	poly(ethylene glycol)
PI3K	phosphatidylinositol 3-kinases
Ph	phenyl
PK	pharmacokinetics
PMI	p53–MDM2/MDMX inhibitor
PNGase F	peptide:*N*-glycosidase F
PNP	*p*-nitrophenyl
PPI	protein–protein interaction
PPTS	pyridinium *p*-toluenesulfonate
propargylGly	L-propargylglycine
py	pyridine

PyBOP	benzotriazol-1-yl-oxytripyrrolidinophosphonium hexafluorophosphate
PyBroP	bromotripyrrolidinophosphonium hexafluorophosphate
quant.	quantitative
ReBiL	recombinase enhanced bimolecular luciferase complementation
ref.	reference
R_f	retardation factor
RING	really interesting new gene
RNA	ribonucleic acid
RP-HPLC	reverse-phase high-performance liquid chromatography
rt	room temperature
s	second(s)
SAH	stabilised α-helix
SDS-PAGE	sodium dodecylsulfate–polyacrylamide gel electrophoresis
SEC	size-exclusion chromatography
Selectfluor™	1-chloromethyl-4-fluoro-1,4-diazoniabicyclo[2.2.2]octane bis(tetrafluoroborate)
SMCC	succinimidyl 4-(*N*-maleimidomethyl)cyclohexane-1-carboxylate
S_N2	bimolecular nucleophilic substitution
S_NAr	nucleophilic aromatic substitution
S_NV	nucleophilic vinylic substitution
SPAAC	strain-promoted azide–alkyne cycloaddition
SPINOL	1,1'-spirobiindane-7,7'-diol
SPPS	solid-phase peptide synthesis
SPTCI	stapled peptide targeted covalent inhibitor
STP	sulfotetrafluorophenyl
subsp.	subspecies
SWD	Sondheimer-Wong diyne
T	temperature
$t_{1/2}$	half-life
TAMRA	5(6)-carboxytetramethylrhodamine
TBAF	tetrabutylammonium fluoride
TBS	*tert*-butyldimethylsilyl
TBS	Tris-buffered saline
TCCA	trichloroisocyanuric acid
TCEP	tris(2-carboxyethyl)phosphine hydrochloride

TCI	targeted covalent inhibitor
TEB	1,3,5-triethynylbenzene
TEMPO	(2,2,6,6-tetramethylpiperidin-1-yl)oxyl
Tf	triflyl
TFA	trifluoroacetic acid
TFAA	trifluoroacetic anhydride
THF	tetrahydrofuran
THPTA	tris(3-hydroxypropyltriazolymethyl)amine
TIPS	triisopropylsilyl
Tle	*tert*-leucine
TMS	trimethylsilyl
TOF	time of flight
TPAP	tetrapropylammonium perruthenate
TPS-N_3	2,4,6-triisopropylbenzenesulfonyl azide
TPX2	targeting protein for Xklp2
t_R	retention time
Tras	trastuzumab
Ugi-4CR	Ugi four-component reaction
UV	ultraviolet
V	volt
v/v	volume by volume
WT	wild-type
δ_X	chemical shift of element X
λ_{max}	absorption maximum in wavelength
µw	microwave

Standard one- and three-letter codes are used for amino acids and nucleotide bases. Standard abbreviations are used for alkyl groups with one to four carbon atoms.

Table of Contents

Section II: Results and Discussion

Section I:

Introduction

Chapter 1 — Introduction to Cancer

The term cancer is used to describe a large collection of diseases whose primary characteristic is an abnormal cell growth which can spread to other parts of the body. In 2018, it was estimated that 18.1 million people around the globe were diagnosed with cancer, and 9.6 million people died because of the disease.[1] With the expectation that the case number would rise even further in the future, cancer poses an ever-increasing threat to the health of humanity.

A prominent feature of cancer is rapidly and uncontrollably dividing cells, which are caused by mutations in their proto-oncogenes and tumour-suppressor genes.[2,3] The mutations can originate from several sources including amongst others: physical (e.g. ultraviolet radiation), chemical (e.g. polycyclic aromatic hydrocarbons and aromatic amines in tobacco), biological (e.g. human papillomavirus, also known as HPV), inherited mutation in certain genes, and random errors in DNA replication.[4,5] More than 600 types of cancer have been categorised by the International Classification of Diseases (revision 11, ICD-11).[1,6] While most of these cancers require different diagnosis and treatment approaches, many can now be completely cured.[7]

The earliest form of cancer treatment was the use of surgery, which was documented by the Greek physician Hippocrates of Kos (460 – ca. 360 BC).[8–10] Radiotherapy became an option after the discovery of X-ray by Wilhelm Conrad Röntgen in 1895.[11,12] Up until the 1960s, surgery and radiation therapy dominated the field of treatment of solid tumours. However, it was found that the cure rates plateaued at 33% due to unnoticed micrometastases.[13] It was then observed that combination chemotherapy was able to cure various advanced cancers.

Chemotherapy was first coined by Paul Ehrlich in the early 1900s. Traditional chemotherapeutic agents target vital mechanisms for cellular division or survival and have been widely used for eliminating cancerous cells since the 1940s.[13,14] Early examples include the DNA alkylating agent chlormethine for Hodgkin lymphoma patients,[15,16] anti-folate methotrexate (amethopterin) for childhood leukaemia,[17] anti-metabolites 5-fluorouracil (5-FU) for solid tumours[18] and 6-mercaptopurine for acute leukaemia,[19,20] and anti-mitotic Vinca alkaloids[21] such as vincristine and vinblastine (Figure 1). The Vinca alkaloids act as a suppressor of microtubule dynamics, blocking mitosis and causing cell apoptosis.[22,23] Later, Pt-based drugs like cisplatin, carboplatin, and oxaliplatin,[24] the microtubule stabiliser paclitaxel (Taxol®),[25] nitrogen mustard cyclophosphamide,[26] topoisomerase I inhibitor irinotecan[27] entered clinical use (Figure 1). While these compounds affect rapidly proliferating cells (i.e. cancerous cells) more than healthy cells, their low selectivity means they have a narrow therapeutic window, and the collateral death of healthy tissues and subsequent side effects of varying severities cannot be avoided.[28]

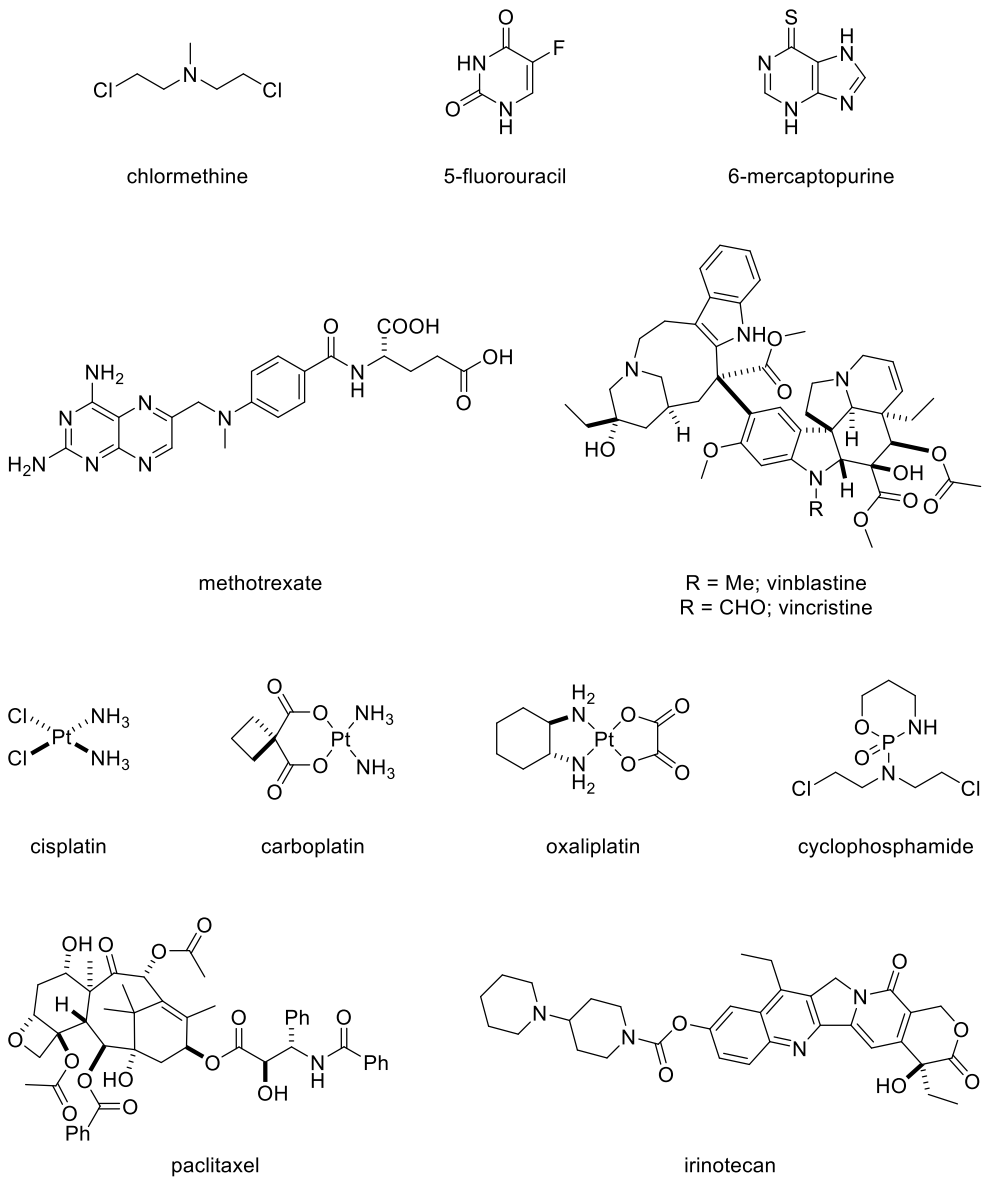

Figure 1 Examples of chemotherapeutic agents: DNA-alkylating agent chlormethine and cyclophosphamide, anti-metabolites 5-fluorouracil and 6-mercaptopurine, anti-folate methotrexate, anti-microtubule agents vinblastine and vincristine, Pt-based DNA cross-linking agents, cisplatin, carboplatin and oxaliplatin, microtubule stabiliser paclitaxel, and topoisomerase I inhibitor irinotecan.

To mitigate the side-effects arising from the low selectivity against tumour cells, more targeted approaches were taken. One major area in this field is the development of kinase inhibitors as dysregulation of kinases are implicated in many cancers.[29–31] The first small molecule to use this targeted approach was imatinib (Figure 2), for treating chronic myeloid leukaemia (CML).[32] Imatinib targets the kinase activity of the oncogenic fusion protein Bcr-Abl, the formation of which is involved in the pathogenesis of CML.[14,33,34] Other drugs targeting other kinases soon followed, such as gefitinib for the treatment of EGFR mutation–positive metastatic NSCLC,[35] dasatinib for the treatment of imatinib-resistant CML,[36,37] lapatinib for HER2-positive advanced breast cancer patients,[38] and trametinib for $BRAF^{V600E}$-positive advanced melanoma (Figure 2).[39] Despite these advances, adverse effects arising from damaging healthy cells are still common.[30,31,40]

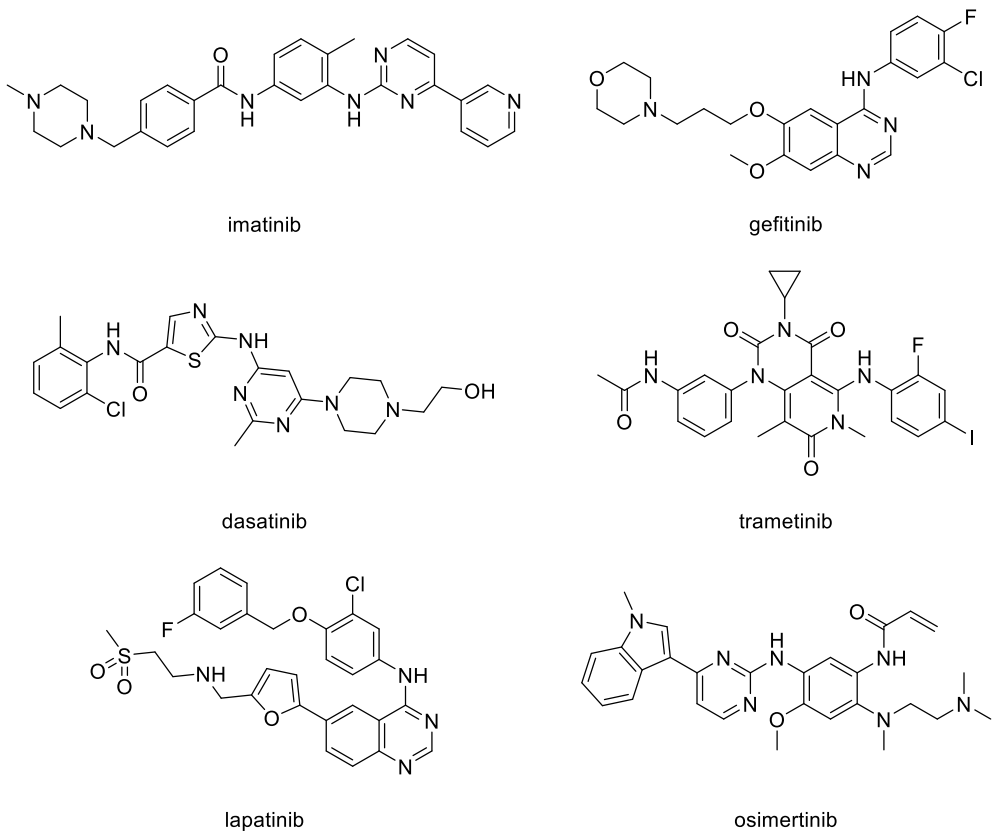

Figure 2 Examples of kinase inhibitors for cancer treatments: imatinib, gefitinib, dasatinib, trametinib, lapatinib, and osimertinib.

One common problem encountered in cancer treatment is the decrease in treatment efficacy due to the emergence of drug resistance.[40,41] Consequently, several strategies have been developed to overcome the resistance, e.g. combination therapy employing a cocktail of chemotherapeutic agents with distinct mechanisms of action,[42] targeted degradation using proteolysis targeting chimaeras (PROTACs),[43–46] designing compounds with multiple binding modes,[47] and irreversible covalent inhibitors.[48] Irreversible covalent inhibitors, in particular, were exemplified by osimertinib (Figure 2), a drug used for treating patients with $EGFR^{T790M}$-mutated NSCLC by binding covalently to Cys797 of the mutated EGFR.[49,50]

Apart from the use of small molecules for treating cancer, the use of biologics has gained more interests in the past few decades. Among the fastest-growing and most developable biologics are monoclonal antibodies (mAbs), which were first approved by the United States Food and Drug Administration (US FDA) in 1986. Currently, more than 80 mAbs have been approved by the US FDA for a multitude of diseases, and approximately half of them are used in oncological indications.[51,52] A subset of antibody-based therapeutics, called antibody–drug conjugates (ADCs), has also gained rapid traction in cancer treatment. Nine ADCs have already been approved for various cancers, and over 80 ADCs are being evaluated in clinical trials.[53]

Another approach to oncotherapy, which is currently being researched, is the inhibition of protein–protein interactions (PPIs). Numerous aberrant PPIs have been identified to have a

link with oncogenesis or poor disease prognosis.[54,55] As PPIs have large contact surfaces, it is challenging for small molecule inhibitors to be successfully developed. Conformationally constrained peptides, also known as stapled peptides, are one of the most promising ways to inhibit PPIs, as these peptides possess a native binding motif, with enhanced pharmacokinetics compared to native peptides.[56,57] Stapled peptides have been used successfully for probing several PPIs implicated in cancer, such as p53–MDM2/MDMX, Bcl-2 family, and Aurora-A/TPX2, with one such stapled peptide advancing through late-stage clinical trials.[58,59]

The rest of the introduction section will outline in detail three modalities, namely, stapled peptides and covalent inhibitors in Chapter 2, and ADCs in Chapter 3 as other types of therapeutics fall outside the scope of the work being described.

Chapter 2 — Targeting the p53–MDM2 Protein–Protein Interaction with Stapled Peptides and Covalent Inhibitors

2.1. Protein–protein interactions

Proteins are essential not only for cell structure and functions, being involved in enzymatic catalysis, and cell signalling, but also they can act as antibodies and transporters. To exert their functions, most proteins must interact with each other. Therefore, anomalous interactions and protein dysregulation can disrupt cellular processes, resulting in several human diseases.[60] In recent years, attaining the ability to selectively modulate protein–protein interactions (PPIs) has unlocked new opportunities for potentially powerful therapeutics.[61,62] Historically, PPIs were deemed 'undruggable'[63], and less than 0.01% of the estimated 650,000 PPIs have been targeted by inhibitors.[64] This was due to challenges in identifying small molecules via a classic drug discovery paradigm. PPI surfaces are large (1,000–6,000 $Å^2$)[62], generally flat, and lack pockets and grooves to accommodate small molecules (Figure 3a).[65] Therefore, it is not surprising that there are no known small-molecule ligands as a starting point for drug design, making it challenging for high binding affinity to be achieved. Despite these hurdles, there has been a rapid progression towards PPI inhibition within the last two decades with small molecules, biologics, and peptidomimetics.[65–70] These PPI inhibitors that are approved by the FDA are exemplified by the followings (Figure 1b):

- tirofiban, a small molecule antiplatelet drug inhibiting the interaction between fibrinogen and platelet integrin receptor GP IIb/IIIa;[71,72]
- trastuzumab (Herceptin®), monoclonal antibody biologic for treatment of breast cancer by binding to human epidermal growth factor receptor 2 (HER2);[73,74]
- eptifibatide, a cyclic peptide peptidomimetic antiplatelet drug acting similarly to tirofiban.[75]

For the scope of this dissertation, only the p53–MDM2 PPI and two approaches for its disruption, namely stapled peptides and covalent inhibitors, will be discussed in detail.

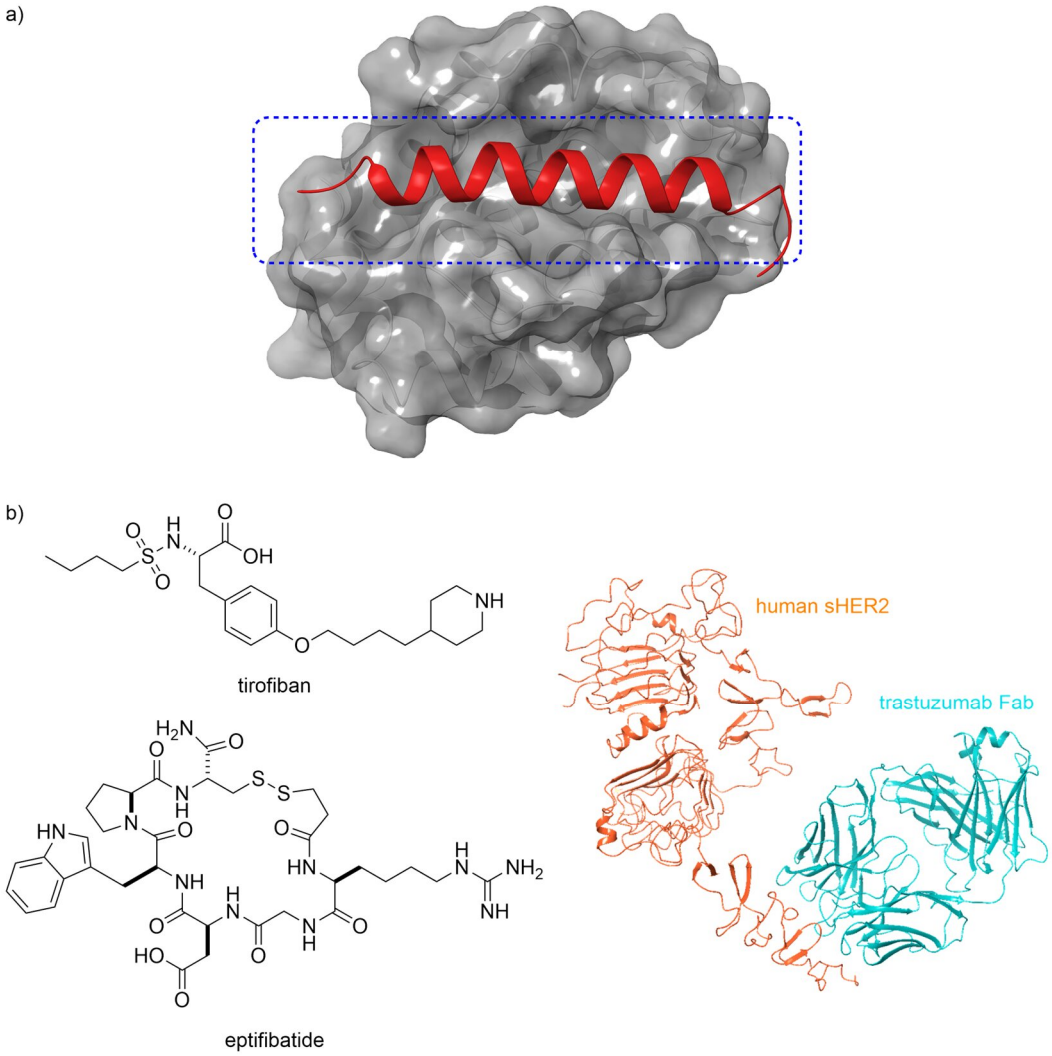

Figure 3 Protein-protein interactions and examples of FDA-approved inhibitors. a) PPI of Bcl-X_L (grey) and BAD (red). Dotted blue box highlights the large PPI interface. (PDB ID: 2BZW)[76] b) Examples of FDA-approved PPI inhibitors: the small molecule tirofiban, the peptidomimetic eptifibatide and the biologic trastuzumab. In the case of trastuzumab, the crystal structure of its Fab region (cyan) is shown interacting with human soluble HER2 (orange). (PDB ID: 1N8Z)[73]

2.1.1. p53–MDM2 protein–protein interaction

The tumour suppressor protein p53, sometimes dubbed "the guardian of the genome", is a pro-apoptotic protein present at a low concentration in normal cells.[77] Various stress signals such as oncogene activation or DNA damage can raise the level of p53 and cause its translocation and aggregation in the nucleus to trigger repairing pathways, cell cycle arrest, or ultimately apoptosis.[78] It has been estimated that approximately 50% of human cancers contain mutated p53.[79]

MDM2, an E3 ubiquitin ligase, is a negative regulator of p53, where MDM2 ubiquitinates p53, thus limiting its transcriptional activity.[80,81] The structure of MDM2 consists of four main regions: an *N*-terminal p53-binding domain,[82] a central acidic domain,[83–85] a Zn-finger

domain,[86] and a *C*-terminal RING finger domain (Figure 4).[87] The RING finger domain is mainly responsible for ubiquitination of p53, which eventually leads to its proteasomal degradation. The central acidic domain also contributes to this process.[83–85,87] In the interest of this report, only the *N*-terminal domain will be described in detail.

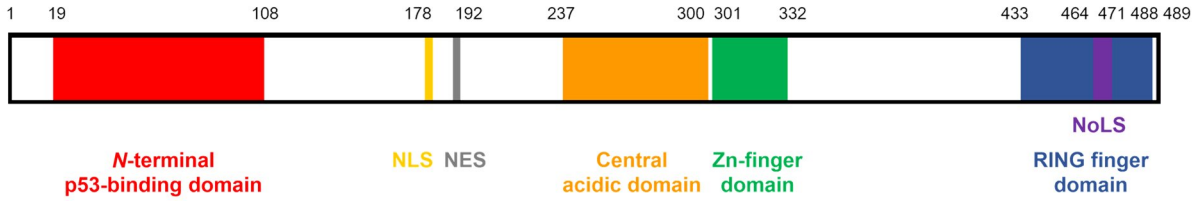

Figure 4 Schematic representation of the structure of full-length MDM2. Known motifs are shown. NLS = nuclear localisation signal; NES = nuclear export signal; NoLS = nucleolar localisation signal. The numbers above the drawing indicate the amino acid positions.[88]

The *N*-terminal domain contains four α-helices and two β-sheets arranged in a pseudosymmetrical fashion.[82] The trans-activation domain of p53 binds to the hydrophobic cleft, which consists of the α2 helix on one side and both β-sheets on the other side. The primary contacts from p53 are made by its amphipathic α-helix. The hydrophobic face of this α-helix buries into the MDM2 hydrophobic cleft. Phe19, Trp23, and Leu26, often referred to as 'hot spots', are the three key residues that most strongly interact with MDM2 and sit deep into the cleft (Figure 5).

As the trans-activation domain of p53 binds to MDM2, its transcriptional machinery is shielded from functioning.[82] In abnormal cells where MDM2 is overexpressed, the p53 becomes deactivated, causing uncontrolled cell proliferation and tumour development.[89,90] Inhibition of p53–MDM2 interaction is, therefore, vital to the restoration of p53 cellular function and suppression of tumour growth.[91–93]

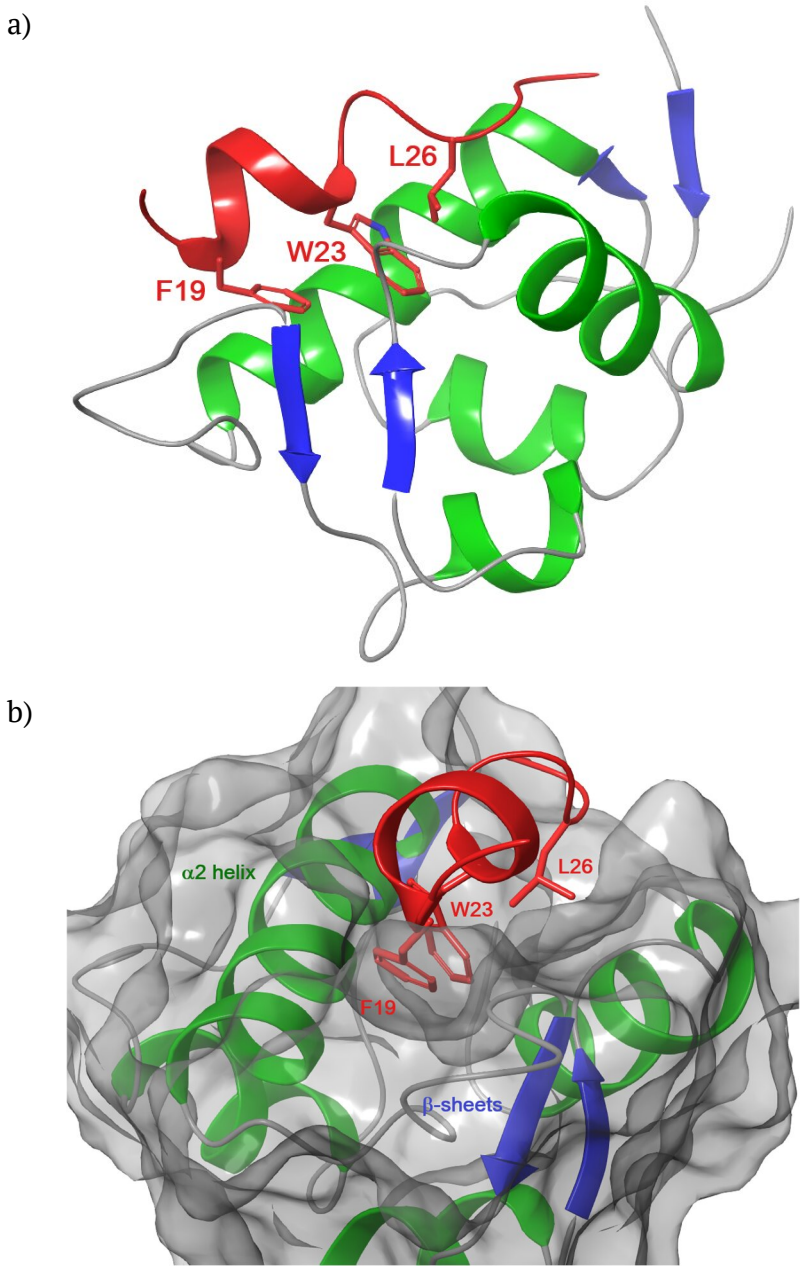

Figure 5 Structure of complex of the trans-activation domain of p53 (red) and the *N*-terminal domain of MDM2 (PDB ID: 1YCR).[82] The α-helices of MDM2 are shown in green, and the β-sheets are shown in blue. a) The overview of the p53–MDM2. b) Details of the hydrophobic cleft showing the three key residues of p53 that drive the hydrophobic contact: Phe19, Trp23, and Leu26.

At least 14 inhibitors of the p53–MDM2 (or closely related MDMX) PPI have progressed to clinical trials.[94–96] Among these, RG7388 (Figure 6),[97] a small molecule inhibitor developed by Hoffmann-La Roche, advanced to phase III clinical trial for the treatment of acute myeloid leukaemia, and ALRN-6924,[98] a hydrocarbon stapled peptide (see section 2.2) with an undisclosed structure developed by Aileron Therapeutics, reached phase II clinical trial for the treatment of peripheral T-cell lymphoma.[57,99–105] Both molecules bind to the *N*-terminal hot-spot region of MDM2, which the trans-activation domain of p53 typically occupies, and hence prevent the binding of native p53. Currently, no drugs targeting the p53–MDM2 PPI have been released into the market. As MDM2 overexpression is one of the leading causes of

development and progression for a variety of cancer types, there is an unmet need for the swift development of new inhibitors to maximise the chances of clinical success.[77]

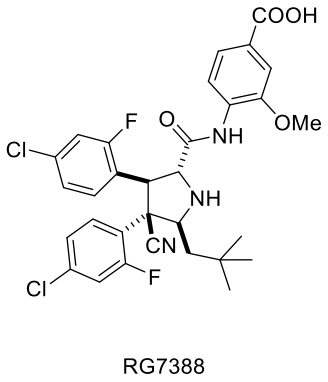

RG7388

Figure 6 Structure of RG7388, a small molecule inhibitor of MDM2.

2.2. Stapled peptides

Because PPIs generally have relatively large surfaces and lack obvious binding pockets,[62,65] peptides are a suitable strategy for their inhibition due to the high similarity to native proteins and greater coverage of contact surface area compared to small molecules.[106] However, peptides may suffer from poor proteolytic stability and bioavailability.[56,57,102,107] Aiming to overcome these intrinsic limitations, stapled peptides—i.e. peptides constrained into their binding conformation by chemically cross-linking two amino acid side chains—has emerged as a very promising approach.[56,57,107] While generally the term 'stapling' is applied to α-helical peptides, it can also be used more widely to refer to other types of secondary structures.[57] In this section, only the α-helix definition will be discussed.

A single turn of an α-helix contains 3.6 residues, and therefore, stapling involves cross-linking between residues at the *i* and *i* + 4, *i* + 7, or *i* + 11 positions corresponding to the same face of an α-helix after 1, 2, and 3 turns, respectively (Figure 7). These residues can either be mutated to non-native amino acids prior to cross-linking or directly joined together (i.e. 'stapled') using appropriate techniques. By optimising the length of the side chain and position of the staple, a more rigid structure with a greater degree of helicity can be achieved. This process generally results in improved binding affinity, proteolytic stability, and cell permeability.[56,102,107]

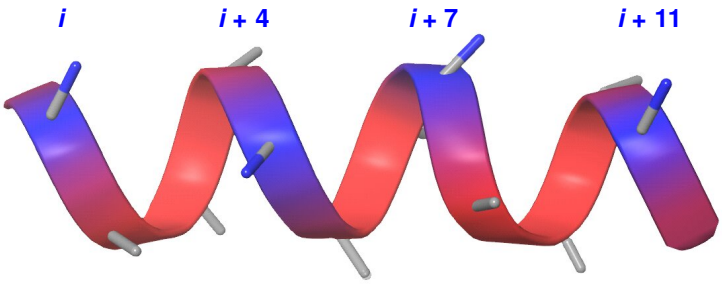

Figure 7 Shown in blue are amino acid residues at positions *i*, *i* + 4, *i* + 7, and *i* + 11, which are on the same face and suitable for stapling.

Several techniques exist for peptide stapling where a variety of macrocyclisation chemistries were employed, resulting in different bioactivities.[56,57,108] These are covered in detail in the following section.

2.2.1. Techniques in peptide stapling

Stapling techniques are broadly categorised into three classes: one-component, two-component, and multi-component stapling. One-component stapling refers to covalent bond formation between two usually non-native amino acid side chains of the same linear sequence. In contrast, two-component and multi-component staplings involve another molecule(s) bridging the two amino acid side-chains of the same sequence together (Scheme 1). For this dissertation, only two-component techniques will be covered. For one- and multi-component techniques, more information can be found in these excellent reviews.[56,108,109]

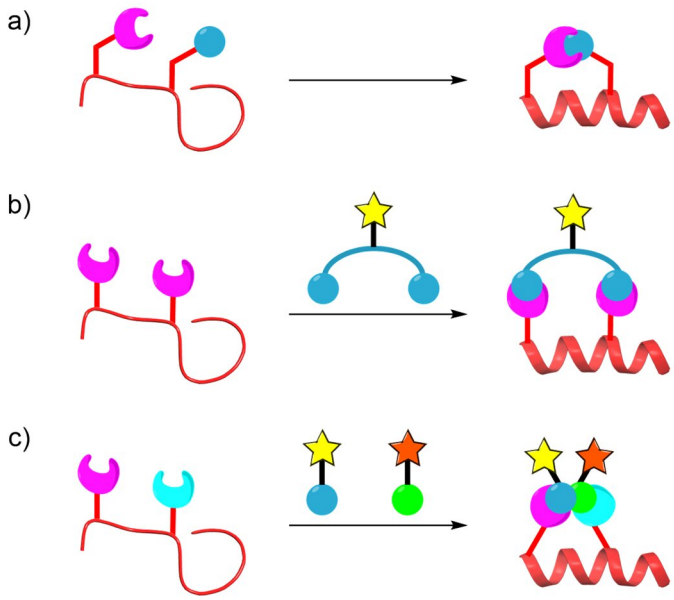

Scheme 1 Schematic representation of a) one-component, b) two-component, and c) multi-component peptide stapling (shown here with three components). Stars refer to optional functionalisation possible on external components.

2.2.1.1. Two-component peptide stapling techniques

Two-component peptide stapling (2C-PS) involves a bifunctional linker that reacts with two complementary, usually non-native amino acids in the peptide of interest. Compared to the one-component stapling, two-component methodologies offer a simpler way of diversifying both peptide sequences and staple linkages, which can be both elaborated independently. Thus, chemically or biologically different stapled peptides can be accessed more efficiently.[102] Moreover, the use of external linkers allows for further functionalisation on the staples.[57,102] The functionalisation can be used to modulate the pharmacological properties of the stapled peptides, such as an addition of cell-permeable motif or PEGylation to improve their solubility, binding to plasma proteins, and protease stability.[102,110,111] In addition, fluorophores or affinity tags can be added to the staples to aid biological assays.[57,102,112,113] Attachment of these moieties on the staple position, rather than at the traditional *N*-, *C*-terminus or side chains, has advantages such as combinatorial diversification of the peptides, lower risk of decreased binding affinity by altering the peptide conformation, and avoidance of steric clashes between the target protein and the added functionality.[57]

Nevertheless, this highly attractive methodology involves certain complications to be considered. Most of the two-component reactions are performed in solution phase due to potential issues of site-isolation on resin, which necessitates an extra purification step.[56] Another issue is the potential of side reactions, such as a formation of double coupled linear peptides and an oligomerisation due to a more complicated reaction pathway. Regardless of these disadvantages, several effective two-component stapling techniques have been developed and optimised with success in biological contexts. For this report, the focus will be on the technique using functionalised double-click linkers.

One of the most prominent strategies of functionalisable 2C-PS is the use of bioorthogonal copper-catalysed azide–alkyne cycloaddition (CuAAC) or "copper-click" reaction. By incorporating two unnatural azido amino acids into a peptide sequence, functionalisable bis-alkyne linkers can be used for stapling. The first example of the CuAAC reaction in a 2C-PS was reported by Bong and co-workers.[114] Azidoalanine was used to replace the *i* and *i* + 4 residues in a peptide derived from the GCN4 leucine zipper. Unfunctionalised 1,5-hexadiyne was employed as the optimal bis-alkyne linker. Based on this work, the Spring group developed a protocol for *i*, *i* + 7 stapling to generate functionalised stapled peptides targeting the p53–MDM2 interaction (Scheme 2a).[102,115] Using p53-based diazidopeptide stapled with 1,3-diethynylbenzene, a nanomolar inhibitor was obtained, but cell permeability could not be observed. By introducing three Arg residues onto the linker, enhanced cell permeability and p53 reactivation in cells were observed, showcasing the importance of peptide functionalisation. Further development of this methodology by Pedersen and co-workers saw the use of 1,3,5-triethylnylbenzene (TEB) as a linker that allows extra functionalisation through a second CuAAC reaction post-stapling (Scheme 2b).[111]

Another bioorthogonal click reaction that has recently gained popularity is the strain-promoted azide–alkyne cycloaddition (SPAAC) reaction.[116–118] The use of a strained alkyne avoids the need for a copper catalyst, which is cytotoxic. The Spring Group devised a protocol based on the SPAAC reaction using Sondheimer-Wong diyne (SWD, R = H)[119] and a phage display PDI-based peptide to generate *i*, *i* + 7 stapled peptides targeting the p53–MDM2 interaction (Scheme 2c).[103] The generated stapled peptide was shown to bind MDM2 strongly, with a K_d of 7.5 nM. *In situ* stapling could also be performed but with moderate loss in cellular activity compared to the use of pure stapled peptides. Further investigation by the Spring group added fluorine or methoxy substituents to the SWD linker (Scheme 2c).[120] While the *m*-fluoro derivative resulted in a slightly diminished binding affinity (K_d = 17.3 nM), an *in situ* stapling of this analogue provided an improved cellular activity compared to the use of unsubstituted SWD linker.

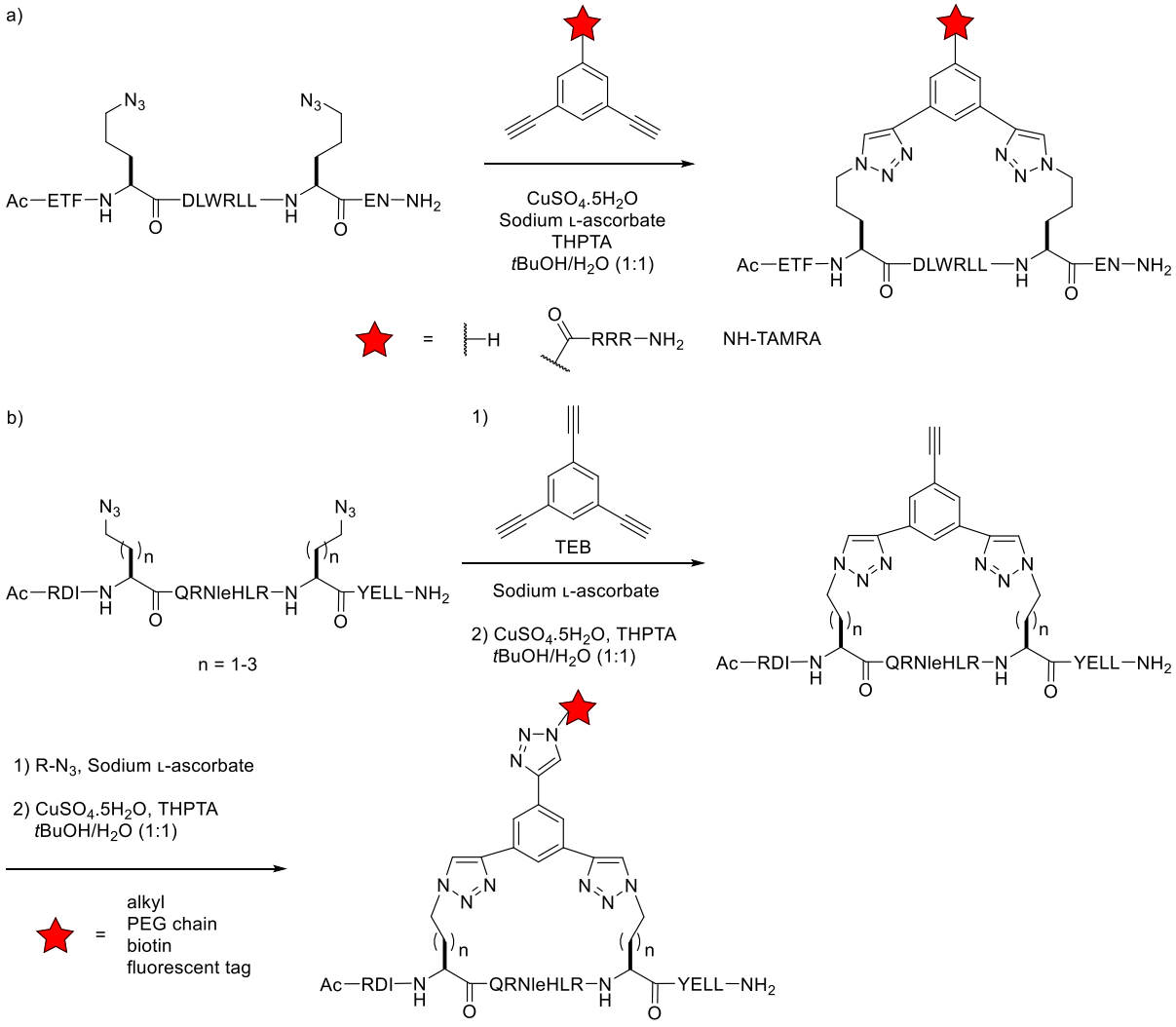

Scheme 2 Azide-alkyne cycloadditions in two-component peptide stapling a) CuAAC reaction for *i*, *i* + 7 peptide stapling.[102,115] THPTA = tris(3-hydroxypropyltriazolymethyl)amine; TAMRA = 5-(and-6)-carboxytetramethylrhodamine. b) CuAAC reaction using TEB as the staple allows functionalisation with another azide after the stapling.[111] TEB = 1,3,5-triethynylbenzene.

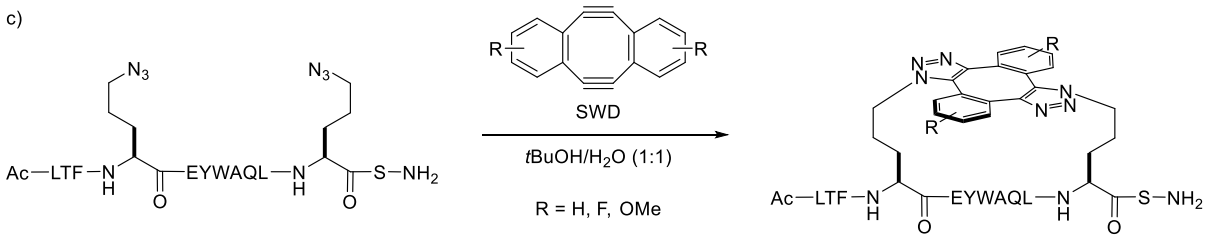

Scheme 2 (continued) c) SPAAC reaction for *i*, *i* + 7 peptide stapling to generate MDM2 inhibitors.[103,120]

Whilst azido amino acids are the most used unnatural amino acids for functionalisable 2C-PS, cysteines are the most exploited proteinogenic amino acids for these applications owing to their unique nucleophilicity and low abundance in the proteome, as evidenced by the plethora of methodologies developed.[57] The use of natural amino acids entails an advantage of high availability, which simplifies and reduces the cost of peptide synthesis. However, issues of chemoselectivity and orthogonality may arise. S_N2 reaction and conjugate addition are the most frequently reported reactions for Cys-based 2C-PS, with S_NAr and nucleophilic vinylic substitution (S_NV) also being employed (Figure 8).

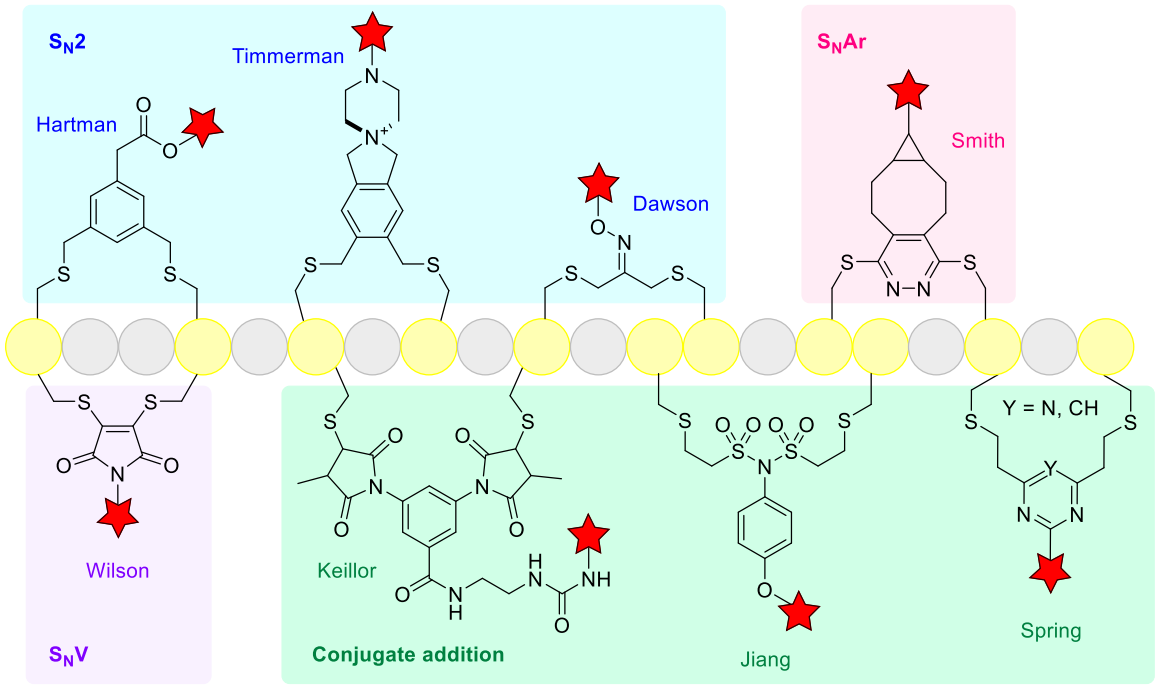

Figure 8 Various functionalised 2C-PS through cysteine residues. The linkages are categorised according to their chemistries: S_N2 in cyan background, S_NAr in pink background, S_NV in lavender background, and conjugate addition in green background. Each linker is annotated with its inventor. Stars indicate functionalisation with various moieties such as fluorophores, cell-permeable motifs, or affinity tags. Yellow circles represent cysteine residues, but distances between any two cysteines do not indicate actual numbers of residues across the stapling.

Hartman *et al*. first introduced the use of derivatives of 1,3-bis(bromomethyl)benzene for peptide macrocyclisation and functionalisation through an S_N2 reaction with cysteine side-chains (Figure 8).[121] Timmerman *et al*. then disclosed the incorporation of quaternary ammonium to aryl halide linkers for functionalisation and improved water solubility.[122] They termed the linkage between cysteine thiols and aryl halides "CLIPS (chemical ligation of

peptide onto scaffolds)", which is being used to generate bi-, tri-, and tetracyclic peptides by pharmaceutical companies.[123,124] Another example of the use of S_N2 reaction for peptide stapling was demonstrated by Dawson *et al*., who employed 1,3-dichloroacetone, with functionalisation achieved through post-stapling oxime formation.[125]

Pentelute *et al*. pioneered the adoption of perfluoroaromatic compounds for S_NAr cross-linking of cysteines or lysines, but functionalisation on the staple was not possible.[126,127] Subsequently, Brown and Smith utilised 3,6-dichloro-1,2,4,5-tetrazine as the linker, which allows post-stapling modification through inverse-electron-demand Diels–Alder reaction with bicyclo[6.1.0]non-4-yne for incorporation of fluorescent dyes (Figure 8).[128]

Dibromomaleimides were employed by Wilson *et al*. for reversible cysteine or homo-cysteine peptide stapling via nucleophilic vinylic substitution (S_NV; Figure 8).[110] Peptides can be unstapled through a reaction with glutathione, and functionalisation can be done on the imide nitrogen.

Several examples of thiol–ene conjugate addition for peptide stapling and macrocyclisation have been reported (Figure 8). First, Keillor *et al*. reported the use of functionalised dimaleimide compounds to incorporate a fluorescent tag.[129] Further example by Jiang *et al*. showed the use of functionalised divinylsulfonamides as linkers.[130] Recently, the Spring Group reported similar reactions using divinylheteroarenes (pyrimidine or 1,3,5-triazine) staples with the possibility of dual functionalisation through the pyrimidine version.[113,131]

With wide-ranging stapling methodologies, each one displaying unique features, the choice of a stapling technique to be used depends on the nature of the targeted PPI and the biological aspects being explored.[108] Thanks to the functionalities that can be easily introduced with two-component stapling, stapled peptides have become not only potential therapeutics but also chemical tools for probing and understanding biological processes.[57–59,132]

2.2.2. Stapled peptide inhibitors of p53–MDM2 PPI

Several stapled peptides have been developed using various methodologies to target p53–MDM2 PPI (Table 1). While a majority of the stapled peptides utilised a classic one-component hydrocarbon stapling effected by an olefin metathesis,[99–101,133,134] CuAAC and SPAAC 2C-PS developed by the Spring group also generated a number of potent MDM2 binders.[102,103,120,135,136]

In general, an appropriate peptide stapling leads not only to increased binding affinity against MDM2, but also to improvement in their α-helicity, protease stability, and cell permeability. In the case of peptide "11B", the inclusion of triarginine (RRR) tag on the staple imparted cell permeability onto the stapled peptide—otherwise, cell permeability was not observed.[135] Sub-nanomolar binding affinity was also attainable in three stapled peptides shown in Table 1. Thus, it is evident that stapled peptides are a valid modality for targeting the p53–MDM2 PPI.

Table 1 Selected stapled peptides active against p53–MDM2 PPI.

Name	Linear sequence	Staple type	K_d (nM)	Active in cells?	Remarks	Reference
One-component stapling						
SAH-p53-8	Ac-QSQQTFX_RNLWRLLX_SQN-NH_2	HC	55	Yes	Increased helicity* from 11 to 85%	99
ATSP-7041	Ac-LTFX_REYWAQCbaX_SSAA-NH_2	HC	0.91	Yes	Increased helicity* from 11 to 70%, suppressed tumour growth in mice	100
sMTide-02A	Ac-TSFX_REYW$_{Cl}$ALLX_S-NH_2	HC	6.76	Yes		101
M06	Ac-TSFX_REYWYLLX_S-NH_2	HC	107.5	Yes		133
mSF-SAH	Ac-QSQQTFX_RNZWRLLX_SQN-NH_2	HC	1300[§]	No	Covalent inhibitor	134
peptide "3a"	Ac-LTFαHYWARLβS-NH_2	UV cycloaddition	15[†]	Yes		137
PhR	Ac-LTFCHYW($S_5$2-Ph)QLTS-NH_2	UV thiol-ene	500	Yes	Suppressed tumour growth in mice	104
Two-component stapling						
peptide "11B"	Ac-ETFX_3DLWKLLX_3EN-NH_2	CuAAC	8.9	Yes	Functionalised with RRR	135
peptide "A1"	TAMRA-Ahx-ETFX_3DLWRLLX_3EN-NH_2	CuAAC	18	No	Photoaffinity probe	112
peptide "E1"	Ac-LTFX_3EYWAQLX_3S-NH_2	SPAAC	7.5	Yes	Increased protease stability*	103
peptide "22"	Ac-LTFX_3EYWAQLX_3S-NH_2	SPAAC	17.3	Yes		120
peptide "7 "open""	Ac-LTFX_4EYWAQLX_4S-NH_2	CuAAC	0.4[‡]	N/A	Photoisomerisable diarylethene linker, "closed" form (K_i = 7.2 nM)	136
^{DTC}PMI	Ac-TSFKQYWCLLSR-NH_2	DTC	0.87	Yes	Increased helicity* from 10 to 62%	105

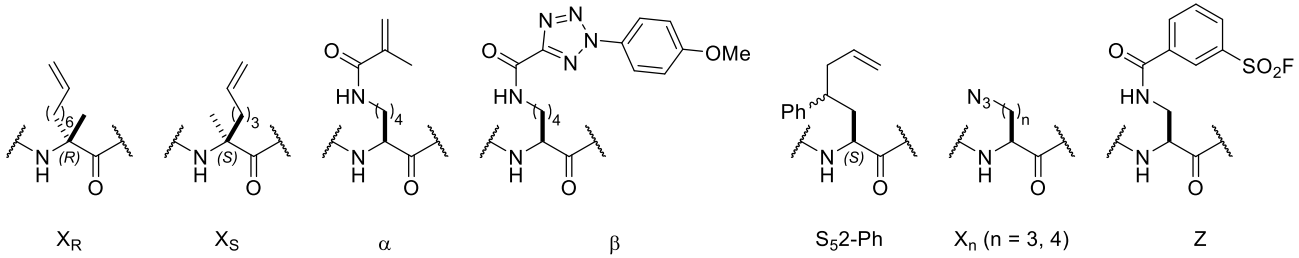

X_R X_S α β $S_5$2-Ph X_n (n = 3, 4) Z

When peptides were not named, they are referred to by the numbering in their respective references. Amino acids in red indicate stapling positions. Cba = 3-cyclobutyl-L-alanine, W_{Cl} = 6-chloro-l-tryptophan, TAMRA = 5(6)-carboxytetramethylrhodamine, Ahx = 6-aminohexanoic acid. HC = hydrocarbon stapling via olefin metathesis, UV = ultraviolet-mediated, DTC = dithiocarbamate. All peptides have increased bioactivity compared to their wild-type versions. *compared to their wild-type peptides. [§]IC_{50} from recombinase enhanced bimolecular luciferase complementation (ReBiL) assay in cell lysate. [†]IC_{50} value from ELISA. [‡]K_i.

2.3. Covalent inhibitors

In addition to peptides, covalent inhibitors can be used in targeting shallow, 'undruggable' pockets such as those at PPI surfaces. Covalent inhibitors are molecules that contain reactive functionalities leading to a covalent bond formation with the targeted protein. Despite the historical success of aspirin and amoxicillin, covalent inhibitors have been generally excluded from high-throughput screenings, citing concerns in potential toxicity.[138] Recent developments in the field, namely 'targeted covalent inhibitors' (TCI), have sparked renewed interest in this class of compounds.[139–146] Using this approach, a compound is rationally designed to form a specific and controlled covalent binding to a site on the target of interest.

2.3.1. General mechanisms

A general mechanism for TCIs involves two steps (Scheme 3).[147] First, the inhibitor binds to the target protein reversibly to form a non-covalent complex [**PI**], governed by the equilibrium constant $K_i = k_{on}/k_{off}$. Then, a covalent bond is formed to give the protein–inhibitor covalent complex **P–I**, the rate of which is governed by the first-order rate constant k_{inact}.

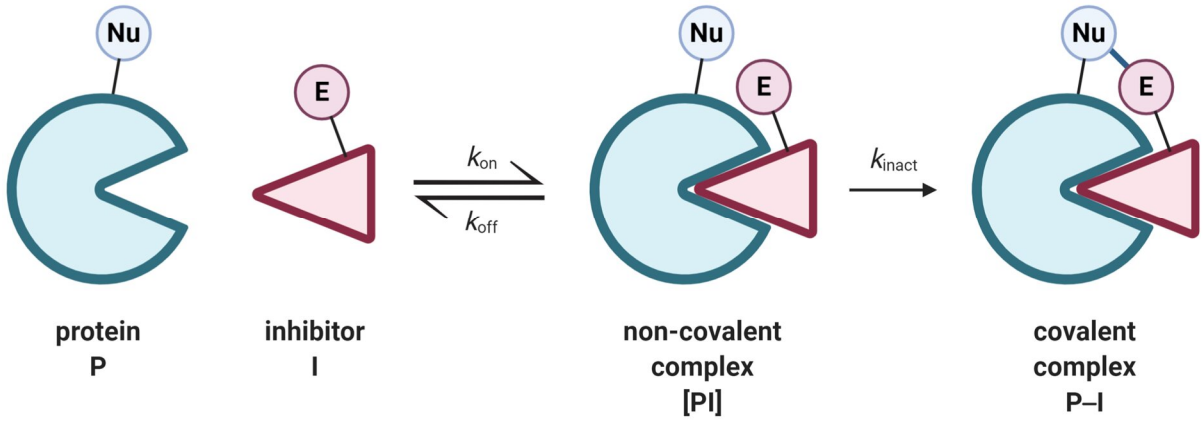

Scheme 3 General mechanism of action for targeted covalent inhibitor **I** against a generic protein target **P**. Created with BioRender.com

For a TCI to achieve selective binding, two criteria must be satisfied. Firstly, the non-covalent binding affinity $(K_i)^*$ must be sufficiently high to attain a good non-covalent binding to the desired target. Secondly, the electrophile should be stable enough to avoid off-target reactivity, while reactive enough so that the covalent bond formation occurs within the lifetime of the [**PI**] complex. This reactivity will arise from the careful placement of the electrophile spatially close to the nucleophilic site on the target.[139]

---

* $K_i = \frac{k_{on}}{k_{off}} = \frac{[\boldsymbol{P}][\boldsymbol{I}]}{[[\boldsymbol{PI}]]}$

2.3.2. Advantages of covalent inhibitors

Some of the advantages of covalent inhibitors over non-covalent inhibitors are listed below:

1) Overcoming competing endogenous substrate binding more easily

   It has been estimated that approximately 80% of approved drugs compete with endogenous ligands in binding with the same protein binding site.[148] A non-equilibrium binding mode can potentially mitigate any competing endogenous substrates, e.g. ATP substrate in the case of kinase inhibition.[149]

2) Extended duration of action due to "permanent" binding of the inhibitor

   With covalent binding, an irreversible inhibitor can exert an effect on its target protein for a prolonged period, even if the drug has been cleared from the system—i.e. its pharmacodynamics and pharmacokinetics can be decoupled. A good example is omeprazole (Scheme 4), a proton pump inhibitor targeting H^+/K^+-ATPase, which has a half-life of 1-2 hours. Due to its covalent binding, omeprazole can be administered daily and be efficacious up to 28 hours.[150] This increased duration of action could result in less frequent drug administration and propel the development of efficient drugs that can be cleared from the system quickly to reduce a patient's drug burden.[147]

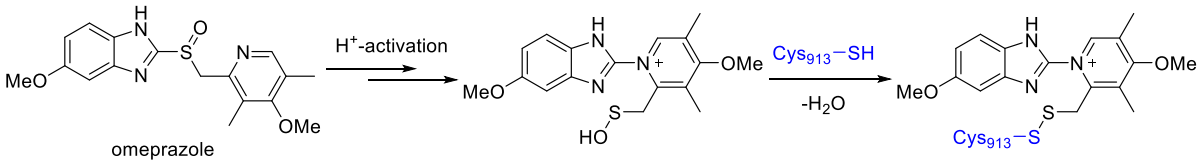

Scheme 4 Structure of omeprazole, a small-molecule proton pump inhibitor, and its mechanism of action. Omeprazole is activated in an acidic environment to a sulfenic acid intermediate before an attack by Cys913 of H^+/K^+-ATPase, its target, forms a covalent disulfide bond.[150,151]

3) Ability to combat drug resistance caused by a mutation

   It has been reported that irreversible covalent inhibitors could overcome some drug-resistant mutations acquired after treatment in cancer and infectious diseases.[139] For example, 50% of patients with NSCLC developed resistance against non-covalent EGFR inhibitors due to mutations in the ATP binding site (T790M or L858R).[152–154] The use of irreversible inhibitors such as osimertinib (Tagrisso) and WZ4002 was shown to be effective against these mutated cells and may reduce side-effects associated with the inhibition of wild-type EGFR in healthy cells (Scheme 5).[152,155–157] Osimertinib is now approved for the treatment of advanced NSCLC.

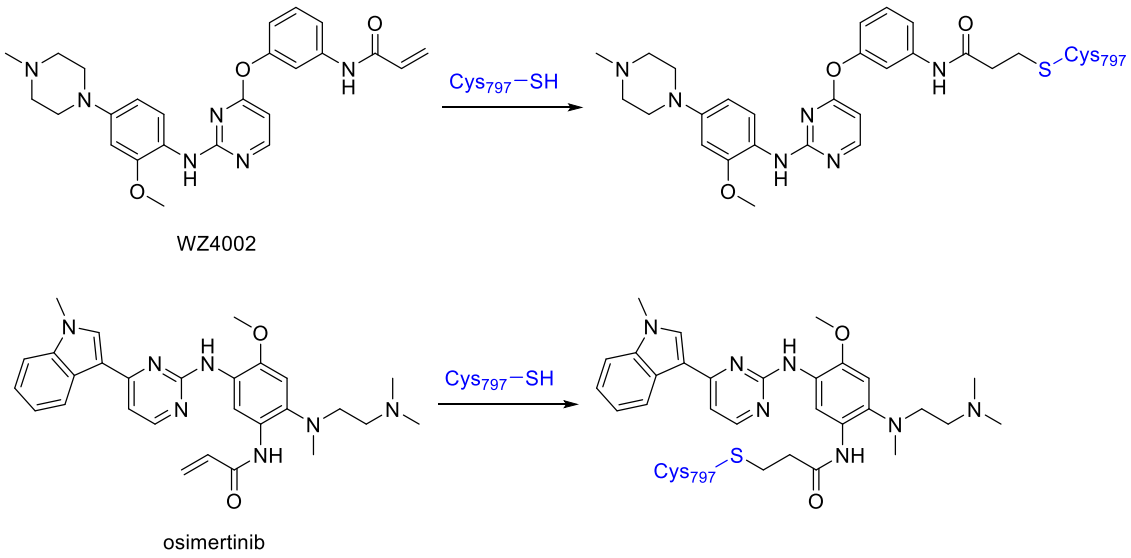

Scheme 5 Structures of WZ4002 and osimertinib, EGFR^{T790M} covalent inhibitors, and their bound structures with Cys797.

4) Ability to target shallow, 'undruggable' targets

Covalent inhibitors have been shown to be efficacious for tackling more challenging and 'undruggable' targets. For example, while Cathepsin K (Cat K) had previously been identified as an 'undruggable' target due to its small and solvent-exposed binding site,[158] odanacatib could be used as its covalent inhibitor (Scheme 6).[159] The nitrile group reacts reversibly with a cysteine residue in the Cat K active site generating a thioimidate linkage.[138] Odanacatib could advance to phase III clinical trials for the treatment of osteoporosis,[160] though its development was stopped due to an associated increase in the risk of stroke.[161] Another example is AMG 510, an inhibitor of KRAS^{G12C} mutant, present in approximately 13% of lung adenocarcinoma (Scheme 6).[162] AMG 510 features an acrylamide and specifically targets the Cys12 residue of KRAS^{G12C}. The inhibitor is now in clinical trial phase 1/2 for the treatment of advanced solid tumours and NSCLC with the mutated KRAS (NCT03600883).

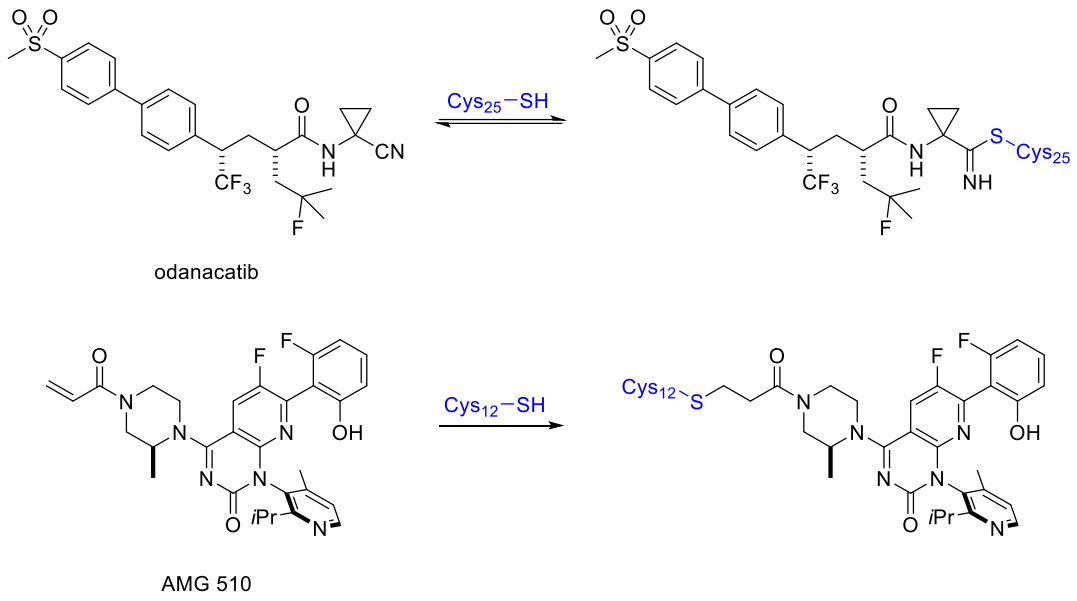

Scheme 6 Structures and mechanisms of action of odanacatib, a covalent inhibitor of Cat K, and AMG 510, a $KRAS^{G12C}$ covalent inhibitor.

2.3.3. Lysine-targeting covalent inhibitors

Most covalent inhibitors have been designed to target a cysteine residue near the substrate binding site.[163,164] The advantages of targeting cysteines include high selectivity due to its low abundance in the proteome and its unique reactivity as a thiol, a soft and reactive nucleophile, which can react even with a modest electrophile.[165,166] But its low abundance is also its limitation, as not all binding sites have a cysteine in their proximity. Therefore, other nucleophilic residues, such as lysine, serine, threonine, tyrosine, glutamate, and aspartate, have also been targeted.[142,143,172,144,147,166–171] Whilst TCIs exist for all these nucleophilic amino acids, this section will focus only on lysine-targeting inhibitors, considering the scope of this dissertation.

Although the ε-NH_2 group of lysine could potentially be an excellent nucleophile, unless perturbed, its pK_a value (10.3) renders it challenging to target at physiological pH.[173] The perturbation depends on the microenvironment around the lysine, which is affected by the nearby residues and the binding ligand. Lysine residues in catalytic sites are more likely to have pK_a values perturbed to act as a nucleophile, while those located outside are less likely to do so. Despite the challenges, examples of inhibitors that target different types of lysine residues have been published.[172] Electrophiles that have been reported include aldehydes, aryl sulfonyl fluorides, fluorosulfates, vinyl sulfones, and acrylate esters, and notable examples are outlined in the following section.

2.3.4. Examples of covalent inhibitors targeting lysine residues

2.3.4.1. Natural products

One of the early sources of lysine-targeting covalent inhibitors is natural products. An example is wortmannin, a steroidal antibiotic produced by *Penicillium wortmanni*. Wortmannin was found to irreversibly inhibit a family of phosphatidylinositol 3-kinases (PI3K), a promising target in oncology.[147,174,175] Depending on the isoform, Lys802 or Lys833 attacks the enoate in a furan ring of wortmannin resulting in the ring-opening and the bound enamine product (Scheme 7).[176,177] PX-866, a wortmannin analogue, was developed to address the poor selectivity and biological instability of wortmannin by replacing the furan ring with an open-chain enamine (Scheme 7).[178] PX-866 has advanced into phase II clinical trials for the treatment of glioblastoma, castration-resistant prostate cancer, and NSCLC.[179–181]

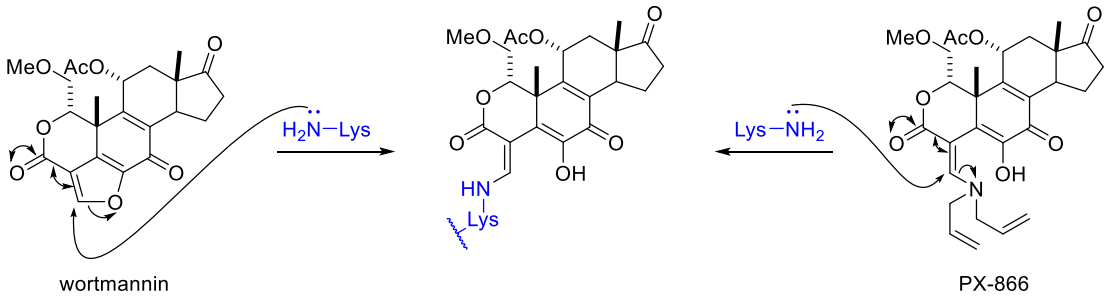

Scheme 7 Wortmannin and its analogue PX-866. Both target Lys802 or Lys833 of PI3K to form an enamine covalent complex.

2.3.4.2. Targeting catalytic lysine residues

Catalytic lysine residues are the simplest to target as they tend to have sufficiently perturbed pK_a such that the amino group becomes nucleophilic at physiological pH.[172] Recently, Dalton *et al*. developed a selective, irreversible inhibitor **1** targeting PI3Kδ at its conserved catalytic Lys779 (Scheme 8).[182] The design of **1** was based on the clinical candidate GSK2292767, a potent and selective PI3Kδ inhibitor.[183] The Lys779 in PI3Kδ attacks the activated ester in **1** to form the covalently bound amide complex. The inhibitor was found to be selective to the δ isoform over α, β, and γ isoforms of PI3K and had a duration of action for over 48 hours in cellular washout studies.[182]

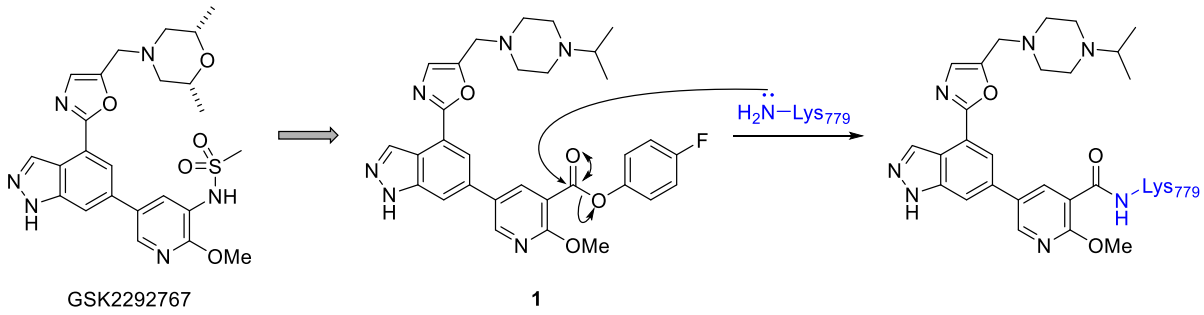

Scheme 8 A selective irreversible PI3Kδ inhibitor **1** equipped with an activated ester. Its design was based on GSK2292767, a reversible inhibitor.

Gushwa *et al*. developed the covalent inhibitor **2** targeting the Src-family tyrosine kinases, a potential drug target for cancer treatment.[184] The design combined the affinity-labelling agent 5'-*p*-fluorosulfonylbenzoyladenosine (FSBA) and the Src-family inhibitor PP1 whose *p*-tolyl group can interact with a hydrophobic pocket found in all Src-family kinases (Scheme 9).[185] The catalytic Lys295 covalently binds **2** through the attack on the sulfonyl fluoride group. The alkynyl group was appended to the solvent-exposed 2' position for monitoring the covalent cross-linking via CuAAC.[186]

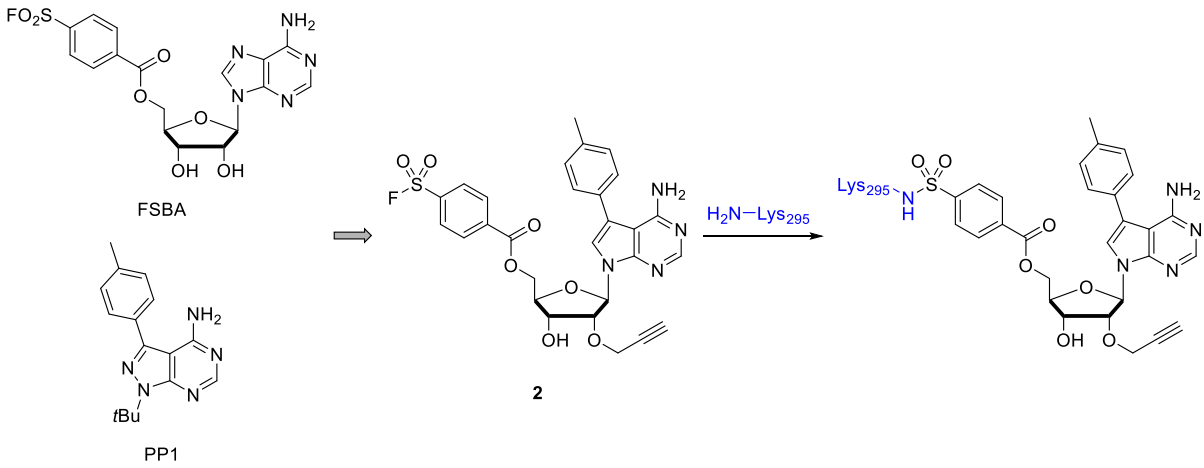

Scheme 9 Irreversible Src-family kinase inhibitor **2**, designed by combining affinity-labelling agent FSBA and the reversible inhibitor PP1. The catalytic Lys295 binds to **2** by attacking the sulfonyl fluoride.

2.3.4.3. Targeting non-catalytic lysine residues

Targeting non-catalytic lysine residues, while more challenging because the pK_a may not be perturbed adequately,[187] can be achieved, and a few examples have been reported in the literature. NU6300, an irreversible inhibitor for cyclin-dependent kinase 2 (CDK2), is one such example (Scheme 10).[188] CDK2 is involved in cell cycles and is an important target in oncology.[189] Anscombe *et al*. developed NU6300 based on the structure of NU6102,[190] a potent reversible inhibitor of CDK2 lacking in cellular activity.[188] It was noticed that the sulfonamide in NU6102 is close to Lys89, so the electrophilic vinyl sulfone analogue NU6300 was made.

NU6300 binds CDK2 via Michael addition (Scheme 10). The covalent analogue was shown to have a better cellular activity compared to its reversible version.

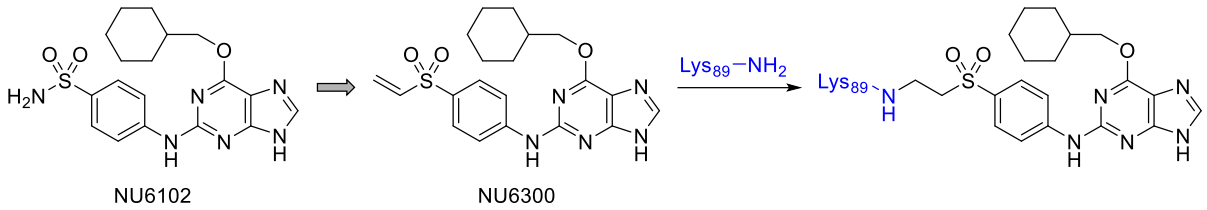

Scheme 10 The vinyl sulfone NU6300, an irreversible CDK2 inhibitor based on NU6102, was developed by Anscombe *et al.*[188] Lys89 forms a covalent bond with NU6300 via Michael addition.

The 70 kilodalton heat shock proteins (HSP70s) are a family of molecular chaperones, which regulate protein folding and refolding and are essential to protein homeostasis.[191] The inducible isoform HSP72 has been established as an oncological target and linked to drug resistance.[192] Pettinger *et al.* disclosed the development of the adenosine-derived HSP72 inhibitor **4** in a series of publications (Scheme 11).[193,194] The design was based on the previous high-affinity reversible inhibitor **3**, with the inclusion of an aryl sulfonyl fluoride moiety at position 5' and a change in the purine substituent. The inhibitor was confirmed to react with the non-catalytic Lys56 and showed efficient covalent binding.

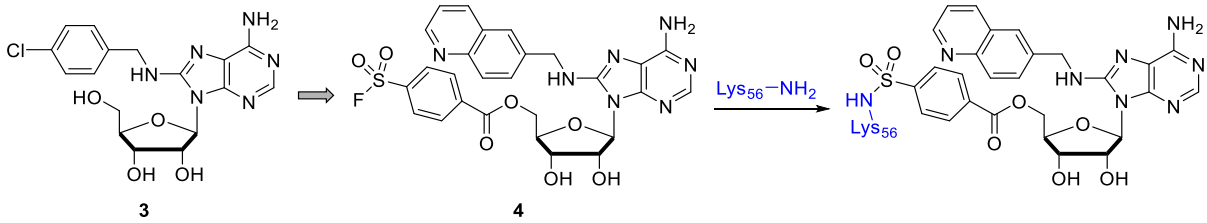

Scheme 11 Developed by Pettinger *et al.*, **4** is an irreversible inhibitor targeting HSP72 derived from reversible analogue **3**.[194] The sulfonyl fluoride at the 5' position reacts with non-catalytic Lys56.

Overexpression of eukaryotic translation initiation factor 4E (eIF4E), a part of the eIF4F protein complex, results in the stimulation of protein translation implicated in several types of cancer.[195,196] Taunton *et al.* generated a small library of aryl sulfonyl fluorides targeting the non-catalytic Lys162 proximal to the m7GTP binding pocket.[197] Guided by their virtual library, molecular docking, and co-crystal structures, compound **5** was synthesised as part of the study (Scheme 12). Compared to previously known inhibitors, which were inactive in cells because of a lack of cell permeability,[198–200] **5** was found to label eIF4E efficiently both as a purified protein and in Jurkat and HEK239T cells.

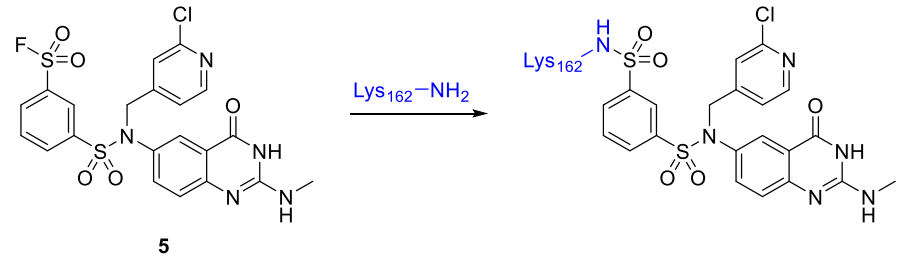

5

Scheme 12 Aryl sulfonyl fluoride **5** was developed by Wan *et al*. as an eIF4E covalent inhibitor targeting non-catalytic Lys162 near the binding site.[197]

2.3.4.4. Targeting solvent-exposed lysine residues

The most challenging Lys residues to target are those that are solvent-exposed as their pK_a values would be largely unperturbed, thus possessing little nucleophilicity.[172] Mcl-1 is an anti-apoptotic protein that binds to BH3-only proteins, preventing the activation of pro-apoptotic proteins, and is overexpressed in several refractory cancers, making it a validated target for cancer treatment.[201–203] Akçay *et al*.[204] developed the pseudo-irreversible covalent inhibitor **7** by appending a boronic acid–aldehyde warhead to the indole–acid in the non-covalent inhibitor **6** (Scheme 13).[205] The pyrazole and phenol rings were used as spacers to place the electrophilic warhead within 3 Å of the solvent-exposed Lys234. A boronic acid group was incorporated to stabilise the bound imine product **8** against hydrolysis. Compound **7** was shown to gain a 5-fold increase in cellular activity compared to its non-covalent version.

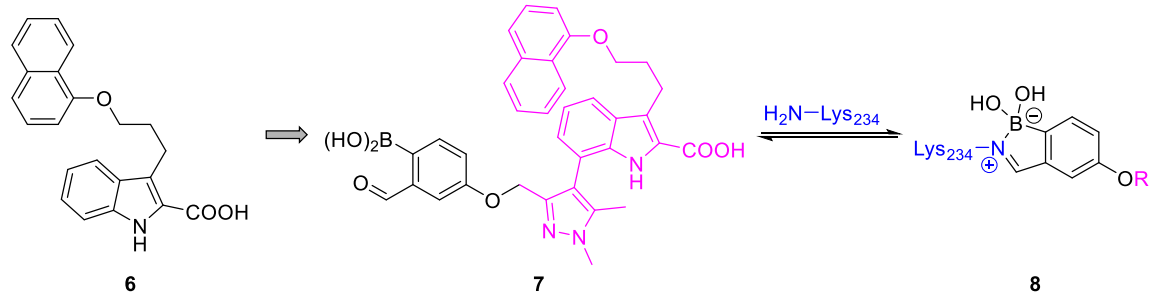

6 7 8

Scheme 13 Based on the indole-acid **6**, the boronic acid–aldehyde **7** is a pseudo-irreversible covalent inhibitor targeting Mcl-1. Lys234 covalently binds **7** through the formation of boronic acid–stabilised imine **8**.

The inhibitors of apoptosis proteins (IAPs) are a protein family that plays a crucial role in regulating cell survival and death processes.[206–208] XIAP, cIAP1, and cIAP2, three of the eight members, are overexpressed in many human tumour tissues, leading to poor prognosis.[209–213] Pellecchia research group disclosed successive reports of Lys-targeted pan-IAP and XIAP-selective covalent inhibitors.[214–216] Based on the tetrapeptide AVPF, which was known to interact with several IAPs, they conducted a series of screening campaigns and molecular docking studies that led to sulfonyl fluoride **9** and fluorosulfates **10**–**11** (Figure 9). Compounds **9** and **10** were designed to target surface-exposed Lys311 of XIAP.[214,216] Subsequently developed as a pan-IAP inhibitor, the fluorosulfate **11** can react with Lys297 of

XIAP and Lys291 of both cIAP1 and cIAP2.[215] The fluorosulfate **11** displayed 9–14 nM IC_{50} values for the three IAPs after six hours of incubation.

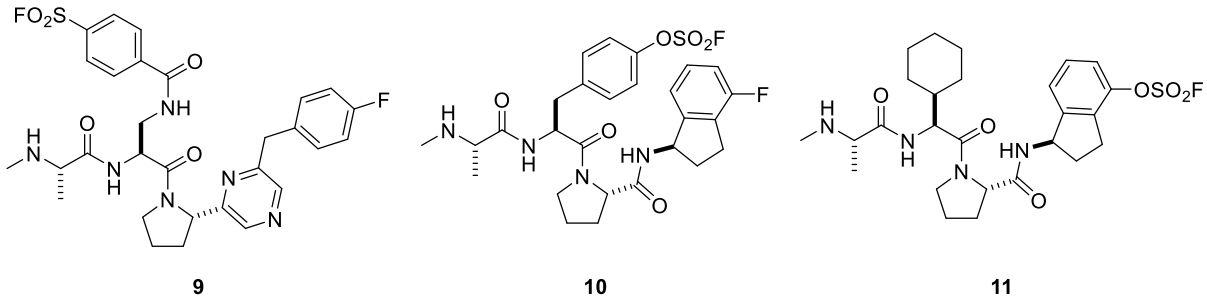

9 **10** **11**

Figure 9 Developed by Pellechia and co-workers, the aryl sulfonyl fluoride **9** and the fluorosulfates **10-11** were used as IAP inhibitors targeting surfaced-exposed lysines.[214–216]

Overall, covalent inhibitors have re-emerged as an extremely powerful tool in therapeutics. Using rational design and a broad range of electrophiles available, they have gained ground in oncology and are likely to develop into other fields.[140] While initially, cysteinyl thiols were the primary target for TCIs, targeting the ε-NH_2 in lysines has been shown to also be a viable strategy. With the ever-increasing interest in TCIs,[145,147] we have gained more insight into this field, and the future for covalent inhibitors is promising.

2.3.5. Combining stapled peptides and covalent inhibition

Given the outlined advantages of covalent inhibition (section 2.3.2), its combination with stapled peptide can be considered as a progression towards a more effective drugging of PPIs. The merging of the two modalities was exemplified by the work of Hoppmann and Wang, which inspired the work described in Chapter 4 of this thesis. They described the incorporation of an aryl sulfonyl fluoride–bearing amino acid into a stapled peptide sequence, mSF-SAH, for irreversible inhibition of p53–MDM2/4 PPI.[134] The sulfonyl fluoride group was placed close to histidines and surfaced-exposed lysines of both MDM2 and MDM4. While no significant improvement to binding against MDM2 was achieved, mSF-SAH gained a 10-fold improvement in MDM4 binding relative to SAHp53-8, the unmodified stapled peptide (Figure 10).[99,134] The formation of a covalent complex of MDM4–mSF-SAH was confirmed by ESI-MS of MDM4 incubated with mSF-SAH, but studies to confirm the reacting residue were not performed.

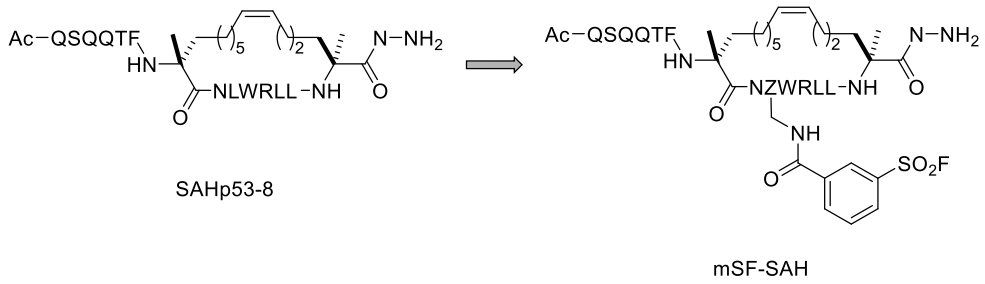

Figure 10 SAHp53-8 (by Bernal *et al.*)[99] was used as a basis for MDM4 inhibitor mSF-SAH developed by Hoppmann and Wang.[134]

Currently, research into combining stapled peptides and covalent inhibitors is still in its infancy, with scarce examples in the literature.[134,217] All instances feature one-component hydrocarbon stapling, which lacks a functionalisable handle; hence an electrophilic moiety must be placed on a side-chain or the *N*-terminus, making its incorporation and optimisation more laborious than via stapling. Thus, there is an opportunity to improve the process by switching the stapling procedure to 2C-PS. The utilisation of external linkers would accelerate the screening and open up the field for more exploration towards inhibiting PPIs covalently.

Chapter 3 — Antibody–Drug Conjugates

3.1. Description and mechanism of action of antibody–drug conjugates

The concept of targeted cancer therapeutics is not new. In fact, Paul Ehrlich (1854–1915), a German physician, developed the concept of "Zauberkugel" or "magic bullet" which can specifically target microbes or tumour cells.[218] Ehrlich's ground-breaking work opened up the field of chemotherapy and eventually led to the conception of antibody–drug conjugates (ADCs).

ADCs consist of three parts: a monoclonal antibody acting as a delivery motif, a cytotoxic drug (also called "payload" or "warhead") for killing target cells, and a chemical linker covalently connecting the two parts (Figure 11). While each component has its own role in the ADC, they can exert influences on one another. Thus, designing an ADC requires careful consideration of all components.

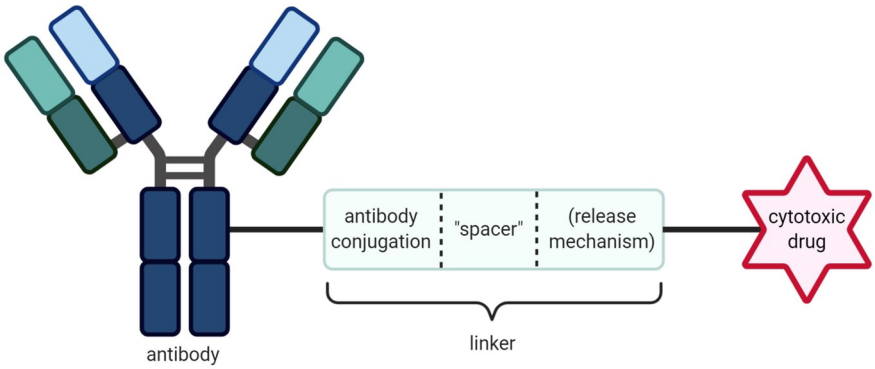

Figure 11 General structure of ADCs. The "spacer" can be used for physicochemical property modulation. The release mechanism is not present in some ADCs. Created with BioRender.com.

ADCs utilise the exquisite targeting ability of the antibody to specifically bind to the chosen antigen.[219,220] After recognising and binding to the cell-surface receptor, the ADC-antigen complexes are internalised via receptor-mediated endocytosis.[219,220] Subsequent trafficking inside the cell liberates the payload either in the endosome or the lysosome, dependent upon the release mechanism. The payload is then able to execute its mechanism of action and cause cell death (Figure 12).[221–224]

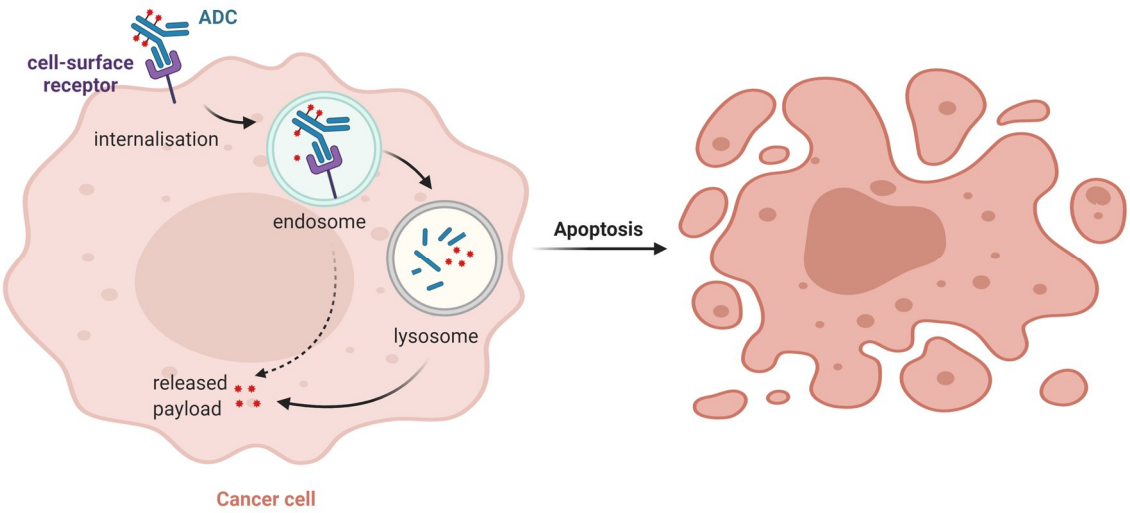

Figure 12 Mechanism of action of ADCs. Payloads may be liberated in the endosome or the lysosome depending on the release mechanism. Created with BioRender.com.

The use of targeting motif like an antibody to guide cytotoxic drugs results in a larger percentage of drugs reaching the target cells, decreasing a minimum effective dose (MED). Also, as fewer drug molecules enter healthy cells, the toxicity decreases, hence increasing a maximum tolerated dose (MTD). Overall, the therapeutic window is expanded (Figure 13).[225]

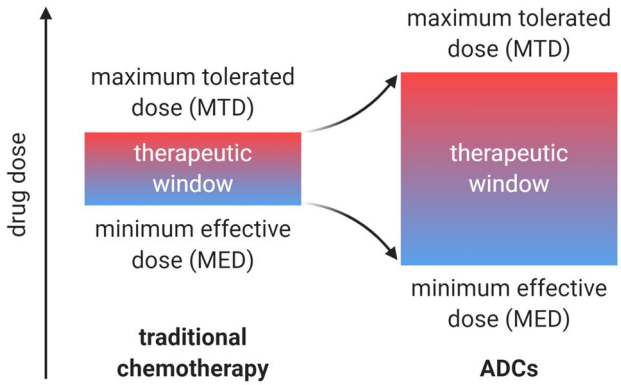

Figure 13 Expansion of therapeutic window through the use of ADCs. Created with BioRender.com.

3.2. Marketed ADCs

The first ADC, reported in 1958 by Mathé *et al*., was constructed from a hamster-derived IgG antibody conjugated with the anti-cancer drug methotrexate.[226,227] The ADC was found to be superior in killing leukaemia cells in mice compared to methotrexate alone or co-administration of the immunoglobulin and methotrexate. While Mathé's ADC did not reach clinical application, it provided a proof of principle for this now rapidly growing area of immunoconjugates.

The field had to wait over 40 years for the first ADC to arrive on the market. In 2000, Gemtuzumab ozogamicin (Mylotarg®) was approved by the FDA for the treatment of acute myeloid leukaemia (AML).[228] However, Mylotarg® was voluntarily withdrawn by Pfizer in 2010 after results from the confirmatory trial showed no clear benefit over standard of care and associated toxicity.[229,230] Mylotarg® was re-introduced in 2017 after an adjustment in its dosing regimen and employed for a restricted subset of CD33-positive AML patients.[53,231,232]

The setback from the withdrawal of Mylotarg® did not remain for long and was quickly turned around by the approval of brentuximab vedotin (Adcetris®) in 2011 for treatment of relapsed or refractory Hodgkin lymphoma and anaplastic large cell lymphoma.[233] Since then, the number of ADCs in the market has increased to nine—five of these were approved by the FDA in the last two years (Table 2).[53] Furthermore, over 80 ADCs are currently being evaluated in clinical trials.

Table 2 Currently FDA-approved ADCs (up to 31 October 2020).

Name	Trade name	Maker	Antibody type	Linker	Conjugation†	Payload	Treatment	Year approved by the FDA	References
Gemtuzumab ozogamicin	Mylotarg	Pfizer/Wyeth	Humanised IgG4κ	Cleavable hydrazone	Lys, NHS ester	*N*-acetyl calicheamicin γ_1^I	Acute myeloid leukaemia	2000,* 2017	228, 229, 231, 232
Brentuximab vedotin	Adcetris	Seattle Genetics	Chimaeric IgG1	Cleavable Val-Cit	Interchain Cys, MC	MMAE	Relapsed or refractory Hodgkin lymphoma, anaplastic large cell lymphoma	2011	233
Trastuzumab emtansine	Kadcyla	Genentech, Roche	Humanised IgG1κ	Non-cleavable thioether	Lys, NHS ester	DM1	HER2-positive metastatic breast cancer	2013	234–236
Inotuzumab ozogamicin	Besponsa	Pfizer/Wyeth	Humanised IgG4	Cleavable hydrazone	Lys, NHS ester	*N*-acetyl calicheamicin γ_1^I	B-cell acute lymphoblastic leukaemia	2017	237
Polatuzumab vedotin-piiq	Polivy	Genentech, Roche	Humanised IgG1κ	Cleavable Val-Cit	Interchain Cys, MC	MMAE	Relapsed or refractory diffuse large B-cell lymphoma	2019	238, 239
Enfortumab vedotin	Padcev	Astellas/Seattle Genetics	Human IgG1κ	Cleavable Val-Cit	Interchain Cys, MC	MMAE	Locally advanced or metastatic urothelial cancer	2019	240, 241
Trastuzumab deruxtecan	Enhertu	Daiichi Sankyo	Humanised IgG1κ	Cleavable GGFG	Interchain Cys, MC	exatecan (DXd)	HER2-positive unresectable or metastatic breast cancer	2019	242–245
Sacituzumab govitecan	Trodelvy	Immunomedics	Humanised IgG1κ	Cleavable carbonate	Interchain Cys, MC	SN-38	Metastatic triple-negative breast cancer	2020	246–249
Belantamab mafodotin	Blenrep	GlaxoSmithKline	Afucosylated humanised IgG1	Non-cleavable amide	Interchain Cys, MC	MMAF	Multiple myeloma	2020	250, 251

†Conjugation refers to the amino acid used for linker attachment and followed by the method of attachment. *Withdrawn in 2010 and re-approved in 2017. Abbreviations: Val-Cit = valine-citrulline; GGFG = glycyn-glycyn-phenylalanyn-glycyn; NHS = *N*-hydroxysuccinimide; MC = maleimidocaproyl; MMAE = monomethyl auristatin E; DM1 = emtansine; MMAF = monomethyl auristatin F

3.3. Monoclonal antibodies

Antibodies or immunoglobulins (Ig) are large, Y-shaped glycoproteins, which are secreted by B-cells upon activation of the immune system (Figure 14).[252] They consist of four polypeptide chains, namely, two identical heavy chains (HCs) and two identical light chains (LCs). For IgG_1, which is the most commonly used antibody subtype in ADCs, the chains are connected via four disulfide bonds in the hinge region.[253] Each HC contains three constant domains (C_H1, C_H2, and C_H3) and one variable domain (V_H), while each LC contains one constant domain (C_L) and one variable domain (V_L). All constant domains constitute the constant region, which is highly conserved across each antibody subtype. In contrast, the variable region, containing V_H and V_L domains, are much more diverse in structure and sequence. The two Fab (fragment, antigen-binding) arms, which are the antigen-binding region, comprise the entire LCs and the V_H and C_H1 domains of HCs. The rest of the HCs form the Fc (fragment, crystallisable) stems, which are responsible for binding to other receptors or immune molecules, ensuring appropriate immune responses for each antigen.[254] IgG, the most abundant antibody in human, also contains a conserved glycosylation pattern at Asp297 in the C_H2 domains.[252,255]

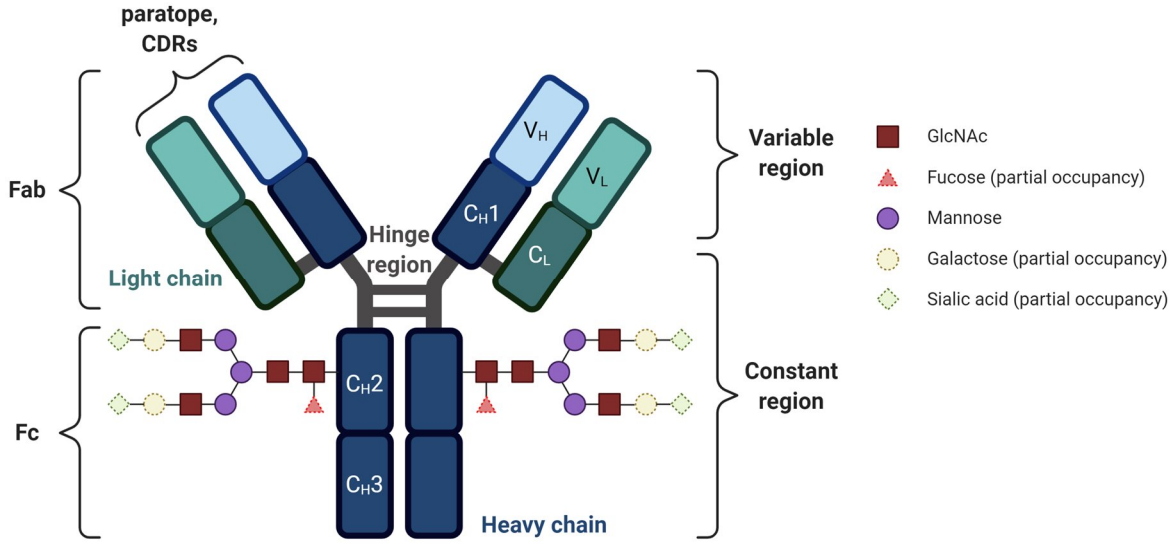

Figure 14 General structure of an immunoglobulin G_1 (IgG_1) antibody. Created with BioRender.com.

Antibodies have two main functions. First, they recognise foreign pathogens by the binding of complementary binding regions (CDRs) at their paratopes (the amino acids at the tip of the Fab region) to specific cell-surface antigens.[256] Upon recognition, antibodies then perform their second function by recruiting effector cells like phagocytes or natural killer (NK) cells to destroy the bound cells, the specifics of which depend on a particular Fc region. This process can also invoke antibody-dependent cell-mediated cytotoxicity (ADCC) for eliminating pathogens through the interaction of the Fc region with Fc-gamma receptors (FcγRs) on immune cells such as NK cells.[256,257]

The selection of antibodies for constructing ADCs requires them to pass the following criteria.[258,259] Firstly, ADCs should specifically target a receptor that is highly expressed on

cancer cells and has significantly lower expression on healthy cells, thereby ensuring the delivery of the cytotoxin to the malignant cells. Secondly, they should possess an excellent target-binding affinity to allow for efficient internalisation. Thirdly, the antibodies should have long circulating half-life as it may take days or weeks before they can bind to the target. In addition, they should have low immunogenicity, i.e. the immune system should not recognise the antibodies as foreign and hence does not prematurely remove them from the body.

3.4. Linkers

Linkers are heterobifunctional molecules, having two orthogonal functionalities for connecting a mAb to a drug molecule. The properties of these chemical linkages can directly influence the performance of ADCs, including their stability, pharmacodynamics (PD), pharmacokinetics (PK), and therapeutic window.[258,260–262] Absolute requirements for ADC linkers are stability in circulation to avoid premature cleavage of the payload, which can contribute to systemic toxicity, and an ability to release the payload upon internalisation in a traceless fashion (i.e. unmodified drug) or such that there is no detrimental effect on the performance of the drug if a remnant of the linker remains. Apart from these criteria, low hydrophobicity is also desired to reduce aggregation of the resulting ADCs; high aggregation can cause faster clearance, hepatotoxicity, and an undesired immune response.[262]

3.4.1. Antibody attachment site

The sites of linker-antibody conjugation can have a large effect on the pharmacology of an ADC. The potency and PK are primarily controlled by the drug-to-antibody ratio (DAR). While a greater DAR can elicit a better efficacy (with limitation), too high DAR may cause aggregation and poor PK profile due to the hydrophobic nature of most warheads.[262] The sites of attachment can also have a significant impact to the stability of the linkage and the binding affinity of the antibody—e.g. conjugation in the Fab region may negatively affect the antigen recognition ability of the antibody.[263,264]

Most ADCs in the clinic use either native surface Lys side chains or reduced Cys in the hinge region for conjugation (Scheme 14). For Lys conjugation, amide coupling using NHS ester as the reagent is currently the main method which is used, such as in the synthesis of gemtuzumab ozogamicin, trastuzumab emtansine, and inotuzumab ozogamicin.[53] However, as there are approximately 80 lysine residues, with approximately 40 of them chemically accessible,[265] a heterogeneous mixture of ADC species with varying DARs are inevitably obtained.[262] To address the problem of heterogeneity, cysteines can be modified instead. The four interchain disulfides can first be reduced to reveal free thiols, without affecting the

structural integrity of the antibody. These liberated thiols can then be modified through a variety of chemical means with maleimides being the most commonly used alkylating reagents; six of the nine approved ADCs utilise this reagent.[53]

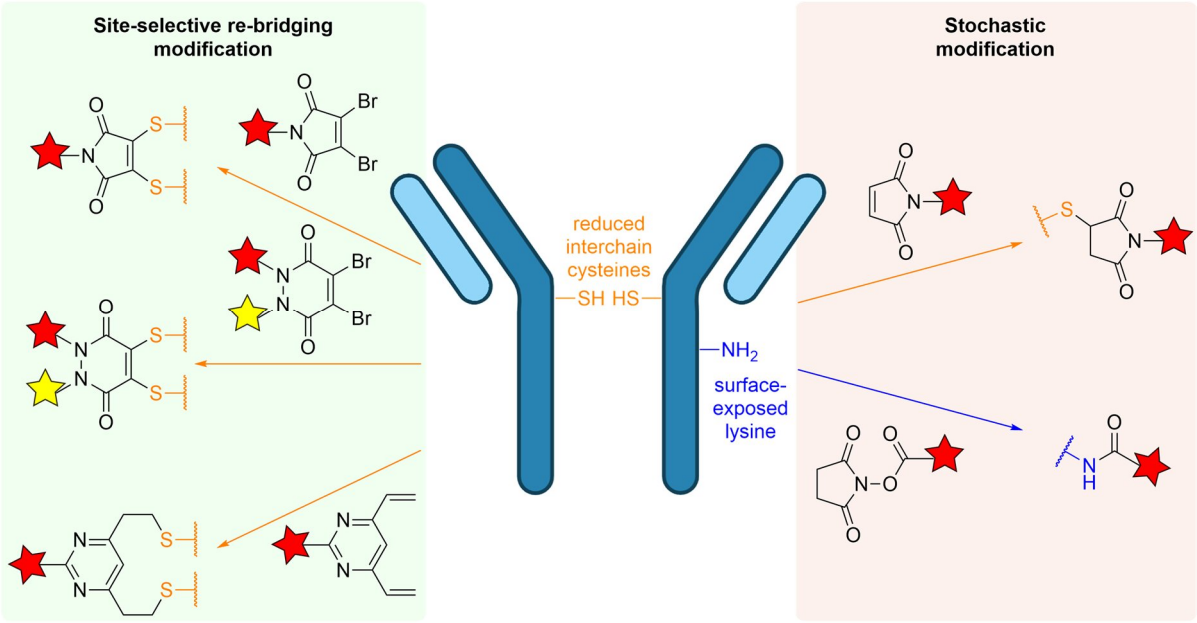

Scheme 14 Selected examples of antibody modification using native lysine or cysteines. Examples of stochastic modification include the use of NHS ester and maleimide reagents for lysine and cysteine conjugations, respectively. For site-selective re-bridging modification, dibromomaleimide, dibromopyridazinedione, and divinylpyrimidine (DVP) reagents are shown. Stars refer to payloads.

To further improve the homogeneity of the resultant ADCs, site-selective modification strategies have been invented. An example is re-bridging reactions of native cysteines (Scheme 14). By re-bridging pairs of cysteines, precise installation of a controlled number of payloads (typically four per antibody) can be achieved. Examples of such reagents include dibromomaleimide,[266,267] dibromopyridazinedione,[268] and divinylpyrimidine (DVP).[269] Other approaches to site-selective modification include antibodies engineered with unnatural amino acids for bioorthogonal conjugations, non-natural cysteines, and enzymatic modification of amino acids or the antibody glycan.[261,262]

3.4.2. Release mechanism

The second role of linkers is to release the drug when ADCs have arrived in the target cells. Depending on the release mechanisms, the linkers can be broadly categorised into either cleavable or non-cleavable.

3.4.2.1. Non-cleavable linkers

Non-cleavable linkers contain stable bonds that do not suffer breakage in a cellular environment.[262] Therefore, the warheads are released when the ADCs undergo lysosomal degradation and will have the conjugation amino acid attached to the active warhead.[262] Thus, the success of this strategy requires that the drug molecule is not affected by the extra appendage. Non-cleavable linkers are currently used in two marketed ADCs, trastuzumab emtansine a0nd belantamab mafodotin. In the former ADC, conjugation was achieved using succinimidyl 4-(*N*-maleimidomethyl)cyclohexane-1-carboxylate (SMCC) resulting in final thioether linkage,[235] while the latter contains a maleimidocaproyl (MC) amide linkage (Scheme 15).[251] It has been demonstrated that the modified DM1 (from trastuzumab emtansine) and MMAF (from belantamab mafodotin) retain their cytotoxicity with these appendages.[235,270]

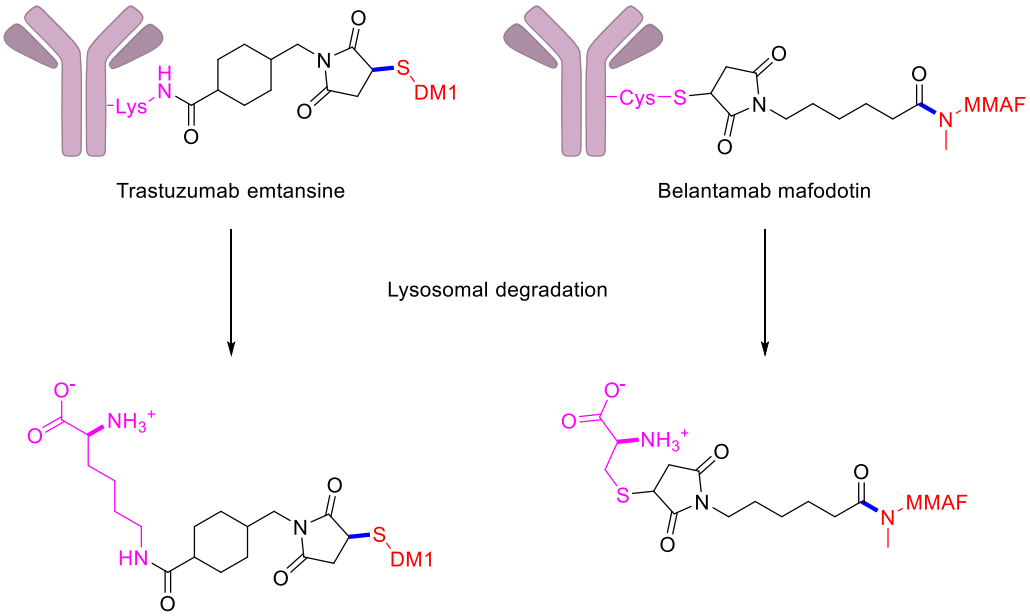

Scheme 15 Non-cleavable linkers of trastuzumab emtansine and belantamab mafodotin. Lysosomal degradation of both ADCs results in amino acid–linker modification to the payloads. Bold blue bond indicates payload-linker bond; red refers to payload; pink atoms are part of an antibody.

3.4.2.2. Cleavable linkers

An alternative strategy is to utilise the unique environment in the malignant cells to release an unmodified payload from the antibody, e.g. low pH in the endosomes and lysosomes, reducing environment, or intracellular enzymes. The first two examples are termed "chemically cleavable", while the last is called "enzyme cleavable".

As the ADCs are internalised via receptor-mediated endocytosis, they are trafficked through endosomes and lysosomes. These cellular compartments are significantly more acidic (pH 5.0-6.0 for endosomes, pH 4.8 for lysosomes) than in plasma (pH 7.4).[262] Chemists exploit this

difference by using acid-labile functional groups like acyl hydrazones and carbonates for intracellular drug release (Scheme 16). Gemtuzumab ozogamicin and inotuzumab ozogamicin contain the acyl hydrazone linkage,[228,237] whereas sacituzumab govitecan bears the acid-sensitive carbonate moiety.[249] Alternatively, a high concentration of free thiols such as GSH in cells can be exploited to release payloads from disulfide linkages.[271,272] This strategy is used mainly in maytansinoid-containing ADCs but is also a part of the double release mechanism in calicheamicin-based ADCs, Mylotarg® and Besponsa® (Scheme 16).[228,237,273]

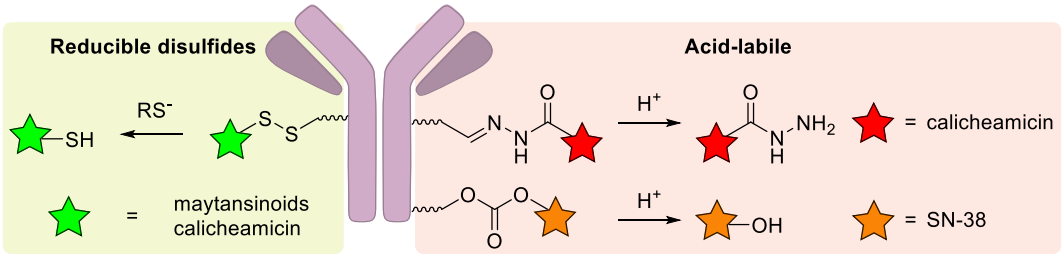

Scheme 16 Chemically cleavable linkers. Two main types are reducible disulfides and acid-labile linkage.

Internalised ADCs are often trafficked to lysosomes, which contain several unique hydrolytic enzymes that can be exploited for intracellular release of unmodified cytotoxins.[274] One heavily targeted enzyme is cathepsin B, a lysosomal protease overexpressed in many cancer types.[275] Cathepsin B can recognise certain short dipeptide sequences such as valine-citrulline (Val-Cit), valine-alanine (Val-Ala), or phenylalanine-lysine (Phe-Lys), cleaving the *C*-terminal amide bond (Scheme 17).[276–278] The installation of a self-immolative spacer such as *p*-aminobenzyloxycarbonyl (PABC) allows the enzyme room to access the peptide bond and a traceless release of the payload (Scheme 17).[277] Val-Cit-PABC linkers are successfully used in three marketed ADCs, all of which use MMAE as the payload: brentuximab vedotin, polatuzumab vedotin-piiq, and enfortumab vedotin.[53] The tetrapeptide sequence glycine-glycine-phenylalanine-glycine (GGFG) has also recently been exploited for constructing cathepsin B–cleavable ADC, trastuzumab deruxtecan.[242] Other moiety like cyclobutane-1,1-dicarboxamide-citrulline (*c*Bu-Cit) was developed for greater specificity towards cathepsin B.[279]

Because cytotoxic warheads tend to be lipophilic, the use of abovementioned peptidic linkers contributes to the formation of undesired aggregates.[280,281] Thus, several hydrophilic, cleavable linkers have been invented to reduce this issue (Scheme 17). Examples include the use of sugars such as glucuronic acid or galactose, cleavable by their corresponding glycosidases,[282,283] and anionic linkages like aryl sulfates and pyrophosphates, cleavable by arylsulfatase and phosphatase, respectively.[284,285]

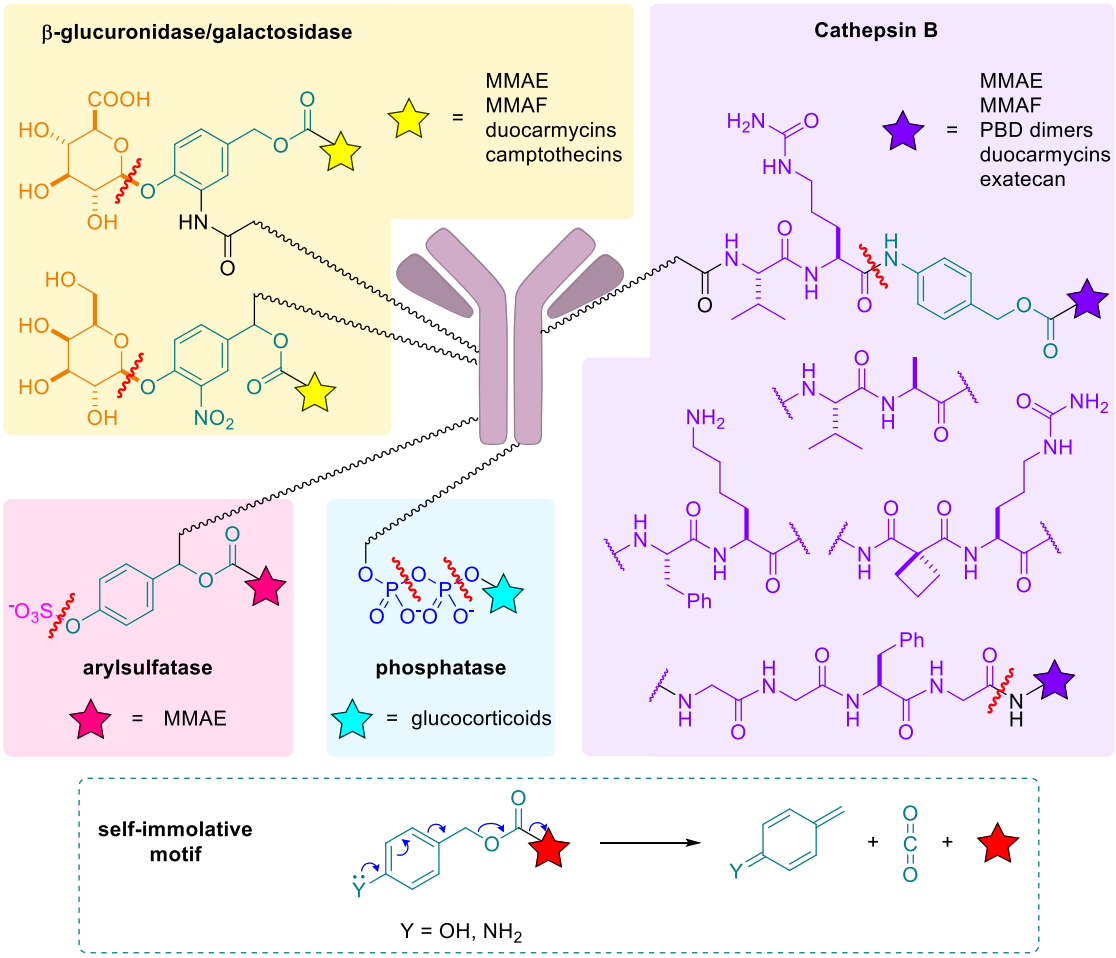

Scheme 17 Enzyme-cleavable linkers used in ADC constructions. The endogenous enzymes include cathepsin B, β-glucuronidase, β-galactosidase, arylsulfatase, and phosphatase. Cleavage sites are shown with red bold wavy lines. Stars indicate payloads. The self-immolative motif *p*-aminobenzyloxycarbonyl (PABC) or *p*-hydroxybenzyloxycarbonyl is frequently used as a spacer.

With a wide variety of linker technologies, each with its advantages and disadvantages, production of ADCs can now be done with better and more precise pharmacological properties.

3.5. Payloads

Cytotoxic drugs, usually called payloads or warheads, are an integral part of ADCs and responsible for killing the target cells. Early ADCs utilise traditional chemotherapeutic agents such as methotrexate and doxorubicin (Figure 15).[226,227,286] The Lewis-Y specific chimaeric mAb–doxorubicin immunoconjugate (BMS-182248) reached phase II clinical trials but was discontinued due to the lack of efficacy.[287] The failure to reach full clinical applications of these first-generation ADCs can be attributed to several factors, key amongst them being the low cytotoxicity of the payloads.[288]

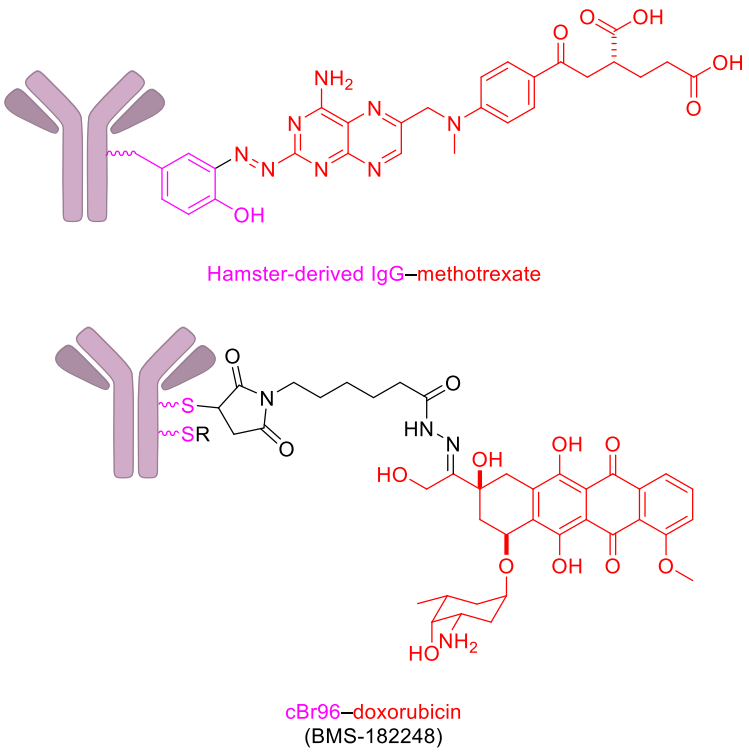

Figure 15 Early ADCs used traditional chemotherapeutic agents as payloads (red). R in BMS-182248 indicates the same modification on cysteine. Antibodies and linkers are shown in pink and black, respectively.

As it has been shown that only a tiny fraction of the administered ADC binds to the tumour cells (approximately 0.001–0.01%), extreme cytotoxicity of the payloads is of great importance.[289] Currently, it is recognised that payloads with a sub-nM *in vitro* IC_{50} values are generally required to produce effective ADCs.[225,290] While high cytotoxicity is critical to the ADC construction, there are also other important criteria to be fulfilled: a known mechanism of action, stability in plasma, amenability to linker attachment, moderate aqueous solubility, and acceptable lipophilicity.[291]

Due to the stringent prerequisites, only a limited number of compounds are being employed as ADC payloads. There are two main classes of drugs currently employed in ADC fields: microtubule disruptors and DNA-damaging agents (including topoisomerase I inhibitors).[291] Alternative payload classes such as RNA polymerase II inhibitors, Bcl-X_L inhibitors, and spliceosome inhibitors are also being investigated to a lesser extent.[291] In the following sections, focus will be placed on payloads used in marketed ADCs or those that are in late-stage clinical trials.

3.5.1. DNA-damaging agents

DNA integrity is critical to proper cellular functions and cell survival.[292] Thus, damaging DNA in tumour cells constitutes an attractive strategy to afford cell death. DNA-damaging agents

can be categorised into four broad types: DNA alkylators, DNA cross-linkers, DNA intercalators, and DNA double-strand breakers.[291]

3.5.1.1. Calicheamicins

Calicheamicins are a family of enediyne anti-tumour antibiotics first isolated from a bacterium *Micromonospora echinospora* subsp. *calichensis* in caliche clay soil.[293–296] The enediyne natural products kill tumour cells by binding to DNA minor groove and cause a scission in DNA double-strands through a reaction with reactive 1,4-dehydrobenzene diradical (Scheme 18).[297] Calicheamicin γ_1^I, the most abundant calicheamicin family member, is known to be the most potent cytotoxin of the family and was found to be highly active against leukaemia in a P388 murine model.[298] Although it was later found that the calicheamicins were too toxic to be used as chemotherapy,[298] its potential in targeted therapy was recognised. Currently, two marketed ADCs, Mylotarg® and Besponsa®, are equipped with *N*-acetyl calicheamicin γ_1^I, a semi-synthetic derivative.[228,237]

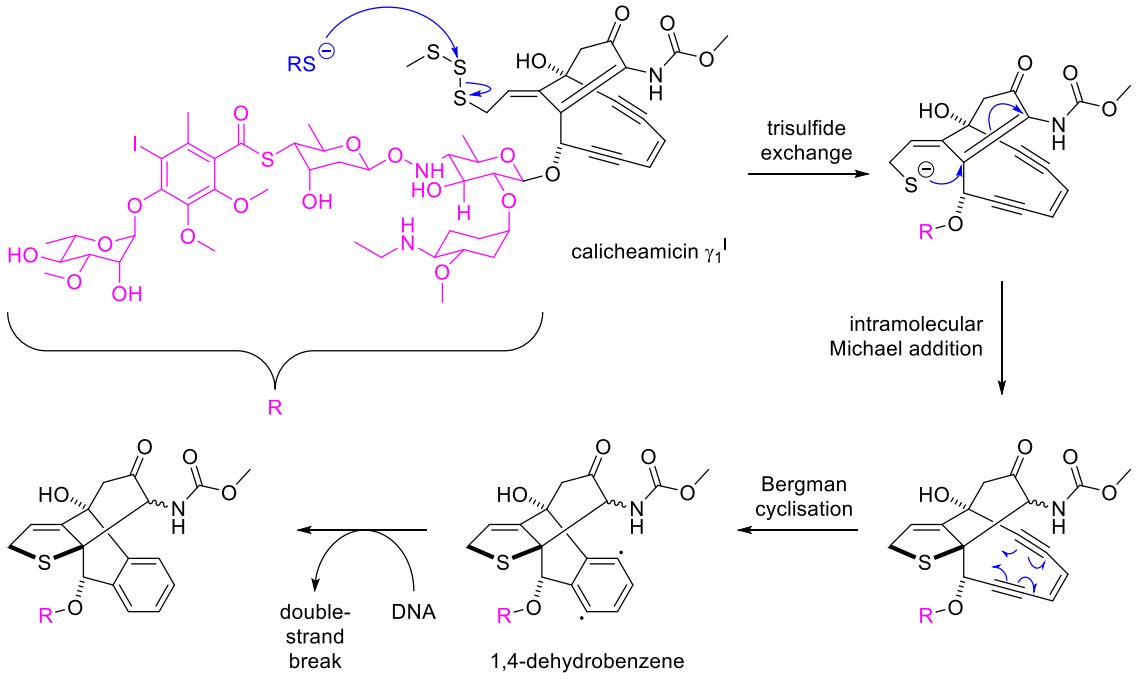

Scheme 18 Mechanism of action of calicheamicin γ_1^I. After trisulfide exchange with free thiols, intramolecular cyclisation follows. Consequent conformational shift triggers Bergman cyclisation to produce the diradical 1,4-dehydrobenzene which cleaves the bound DNA strand.

Its intriguing structure and elegant mode of action prompted organic chemists to synthesise calicheamicin γ_1^I, first accomplished by Nicolaou and co-workers in 1992,[299] followed by Danishefsky and co-workers in 1994.[300] Owing to the complexity of this natural product, both total syntheses were long and arduous, with over 50 total steps, resulting in minimal yield of the final product. Thus, the industrial manufacture of calicheamicin γ_1^I is by fermentation.[298] Modification of this fermentation product was performed by installing an *N*-acetyl group to improve stability, followed by disulfide exchange with 3-mercapto-3-methylbutyryl hydrazide (DMH), hydrazone formation with 4-(4'-acetylphenoxy)butanoic acid (AcBut), and

final NHS ester formation to give the desired linker–drug, ready for bioconjugation with an antibody (Scheme 19).[227,298]

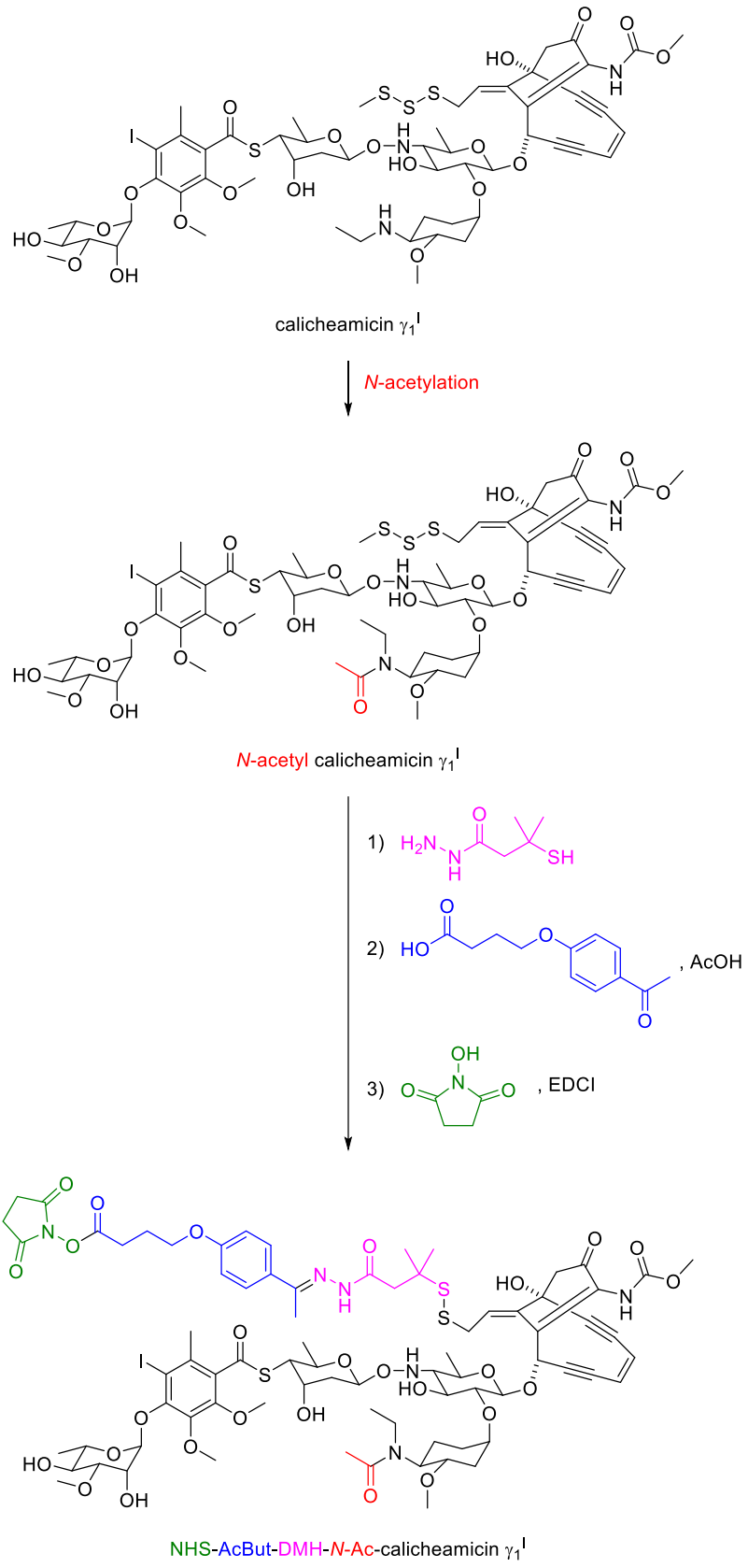

Scheme 19 Semi-synthesis of linker–drug NHS-AcBut-DMH-*N*-Ac-calicheamicin γ_1^I.

3.5.1.2. Pyrrolobenzodiazepines

The first member of the pyrrolobenzodiazepine (PBD) monomer natural product family, anthramycin, was first isolated from the *Streptomyces refunius* bacterium in 1965 (Figure 16).[301] PBD monomers were found to be potent anti-tumour antibiotics, and several other members of the family such as tomaymycin were soon discovered afterwards (Figure 16).

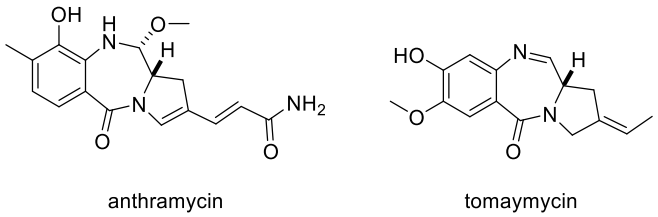

Figure 16 Anthramycin and tomaymycin, two members of the PBD monomer family.

PBDs are sequence-selective DNA minor-groove binders. After a PBD binds to a DNA sequence, the C2-amino group of guanine can attack the C11 imine in the PBD core (Scheme 20).[302] The resulting covalent PBD–DNA adduct can cause various biological effects, including the inhibition of transcription or DNA repair, leading to cell death.[303,304]

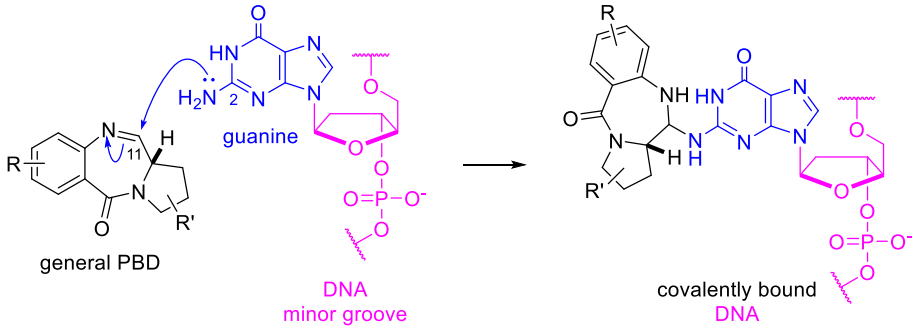

Scheme 20 Mechanism of action of PBDs. After its insertion into DNA minor groove, C2-amino group of guanine attacks the electrophilic imine in PBD to form aminal linkage.

A study by Bose *et al*. in the 1990s found that linking two PBD monomers can dramatically increase its *in vitro* potency, as demonstrated by connecting two DC-81 molecules via a propane diether linker at C8-alkoxy group to form the PBD dimer DSB-120 (Figure 17a).[305] Subsequently, many PBD dimers have been developed, including SJG-136 (Figure 17b), which displayed an *in vitro* IC_{50} of 0.27 pM against the A2780 human ovarian carcinoma cell line.[306] SJG-136 advanced to phase II clinical trials for the treatment of advanced chronic lymphocytic leukaemia (CLL) and AML.[304]

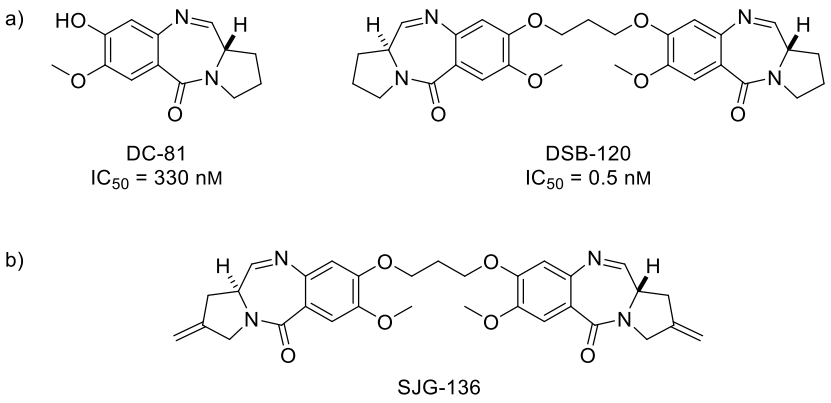

Figure 17 a) Dimerisation of PBD monomer DC-81 improved IC_{50} in murine AJD/PC6 plasmacytoma cell line by more than 600 folds. Data were taken from Bose *et al*.[305] b) Structure of PBD dimers SJG-136.

PBD dimers are attractive as ADC payloads because of their distinct mechanism of action and extreme potency. Two prominent examples are SGD1882 (payload of linker–drug talirine) and SG3199 (payload of linker–drug tesirine; Figure 18). Both payloads are highly potent anti-cancer agents with low-pM *in vitro* IC_{50} values, but SG3199 is significantly less hydrophobic due to the removal of the pyrroline-linked phenyl rings.[307] They are used in vadastuximab talirine (phase III for treatment of AML, terminated due to higher rate of deaths)[53] and loncastuximab tesirine (phase III for treatment of relapsed or refractory diffuse large B-cell lymphoma clinical trials).[308]

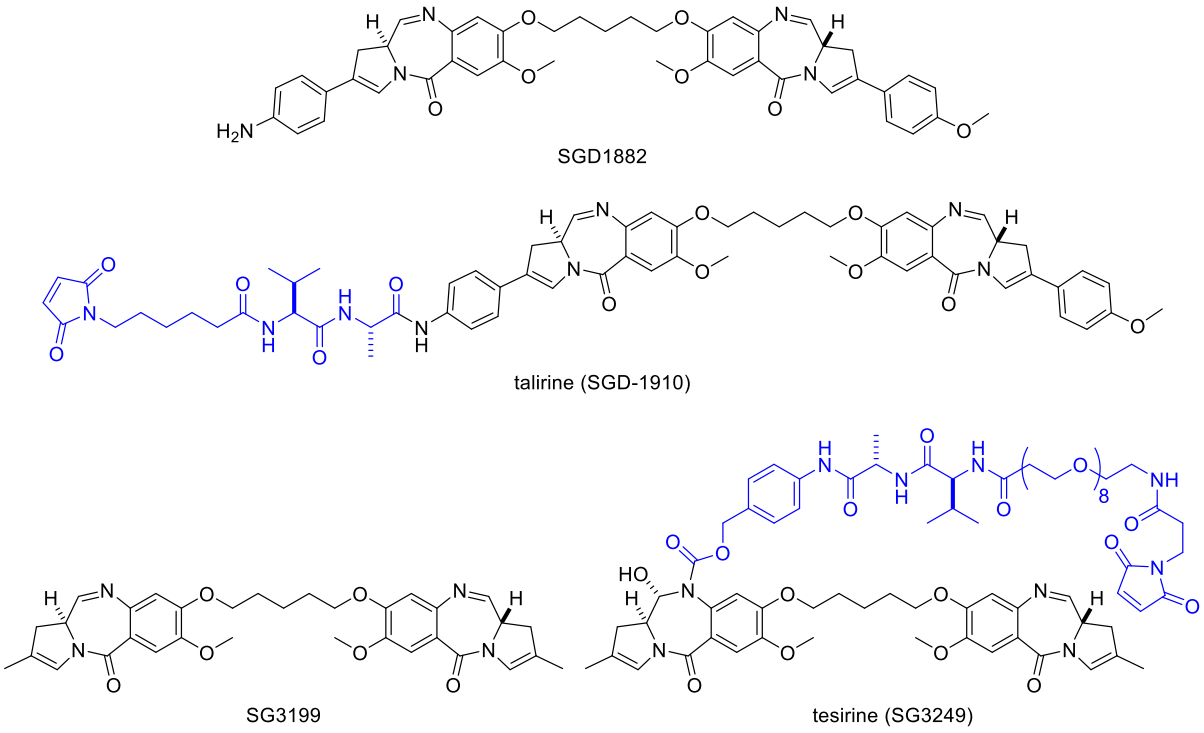

Figure 18 Two PBD dimers, SGD1882 and SG3199, and their respective linker–drugs, talirine and tesirine. Both compounds are used in ADCs which are being investigated in clinical trials. Linker portions are indicated in blue.

The synthesis of tesirine was disclosed by researchers at Spirogen in 2016 (Scheme 21).[309] Starting from benzylvanillin (**12**), one PBD monomer was synthesised with Val-Ala-PABC

attached (**19**) and another without the linker (**21**); the key step was the formation of the central seven-membered ring via a spontaneous cyclisation between the carbamate nitrogen and the aldehyde formed after Swern oxidation. The heterodimerisation was then achieved using diiodopentane, giving PBD dimer **22**. Removal of all protecting groups and incorporation of maleimide-PEG unit produced tesirine in 0.54% overall yield over 30 steps.

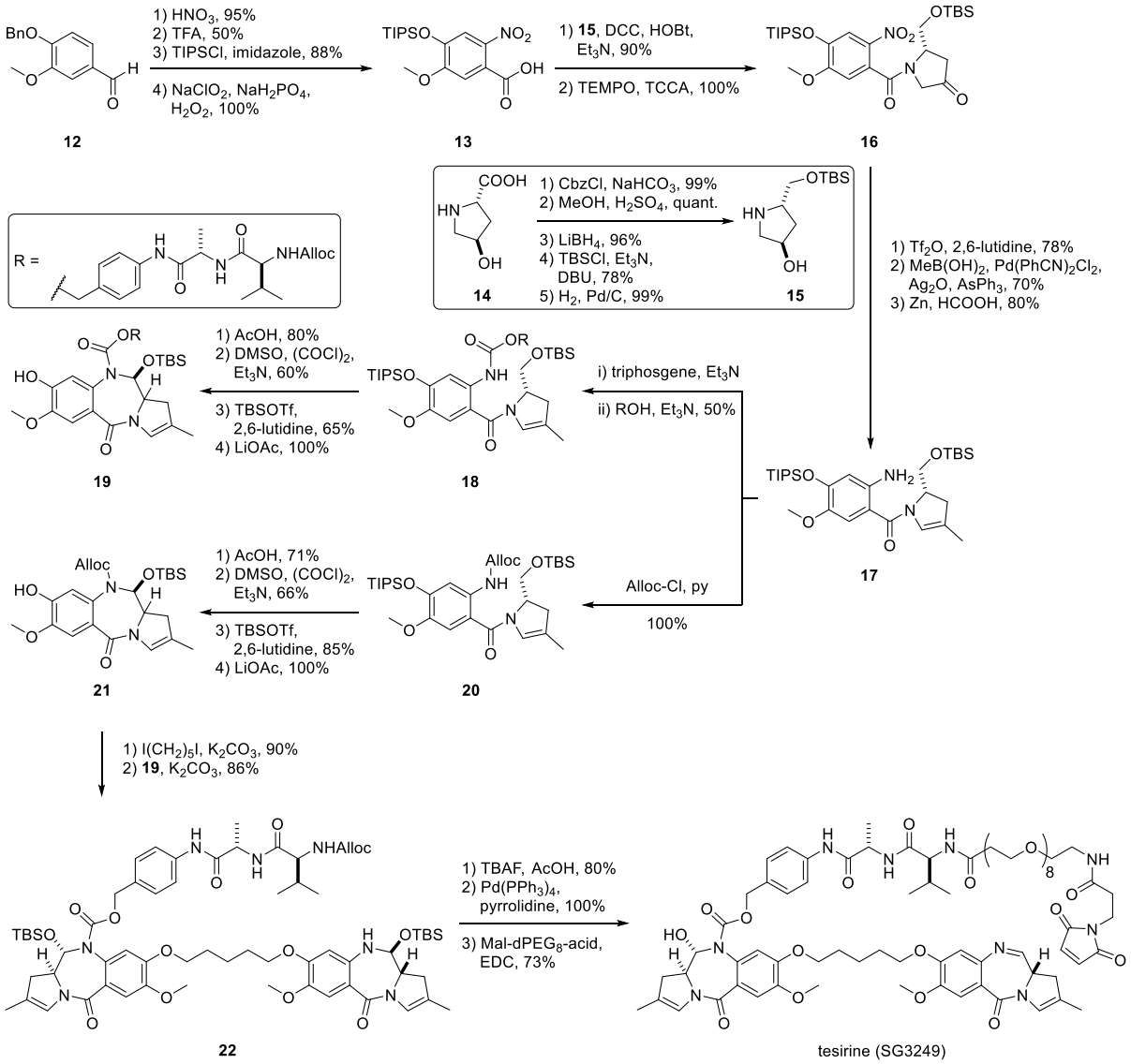

Scheme 21 Total synthesis of tesirine (SG3249) starting from benzylvanillin (**12**) by Tiberghien *et al.*[309] DCC = *N*,*N*'-dicyclohexylcarbodiimide, HOBt = 1-hydroxybenzotriazole, TEMPO = (2,2,6,6-tetramethylpiperidin-1-yl)oxyl, TCCA = trichloroisocyanuric acid, DBU = 1,8-diazabicyclo[5.4.0]undec-7-ene, TBAF = tetrabutylammonium fluoride, Mal = maleimide, dPEG = discrete poly(ethylene glycol), EDC = *N*-(3-(dimethylamino)propyl)-*N*'-ethylcarbodiimide hydrochloride.

3.5.1.3. Duocarmycins

Duocarmycins are a family of natural product anti-cancer antibiotics featuring a reactive spirocyclopropane motif. Its first member, CC-1065, was isolated from a *Streptomyces*

bacterium in the 1970s (Scheme 22a).[310,311] Duocarmycins are known to bind the DNA minor groove in A-T-rich regions and selectively alkylate N3 of adenine, providing mid-pM *in vitro* cytotoxicity (Scheme 22b).[312] CC-1065 was extremely potent *in vitro*, but its lacklustre activity and irreversible hepatotoxicity *in vivo* hampered its therapeutic development.[310,313] Thus, other synthetic analogues have been investigated to improve the biological properties of duocarmycins. In particular, halogen-containing *seco* analogues were developed as prodrugs, which require cyclisation for cytotoxicity. *Seco*-duocarmycin-hydroxybenzamide-azaindole (*seco*-DUBA, Scheme 22b), developed by Synthon Biopharmaceuticals, is being used as an ADC payload in trastuzumab duocarmazine, currently in phase III clinical trial for the treatment of metastatic breast cancer.[53,314–316]

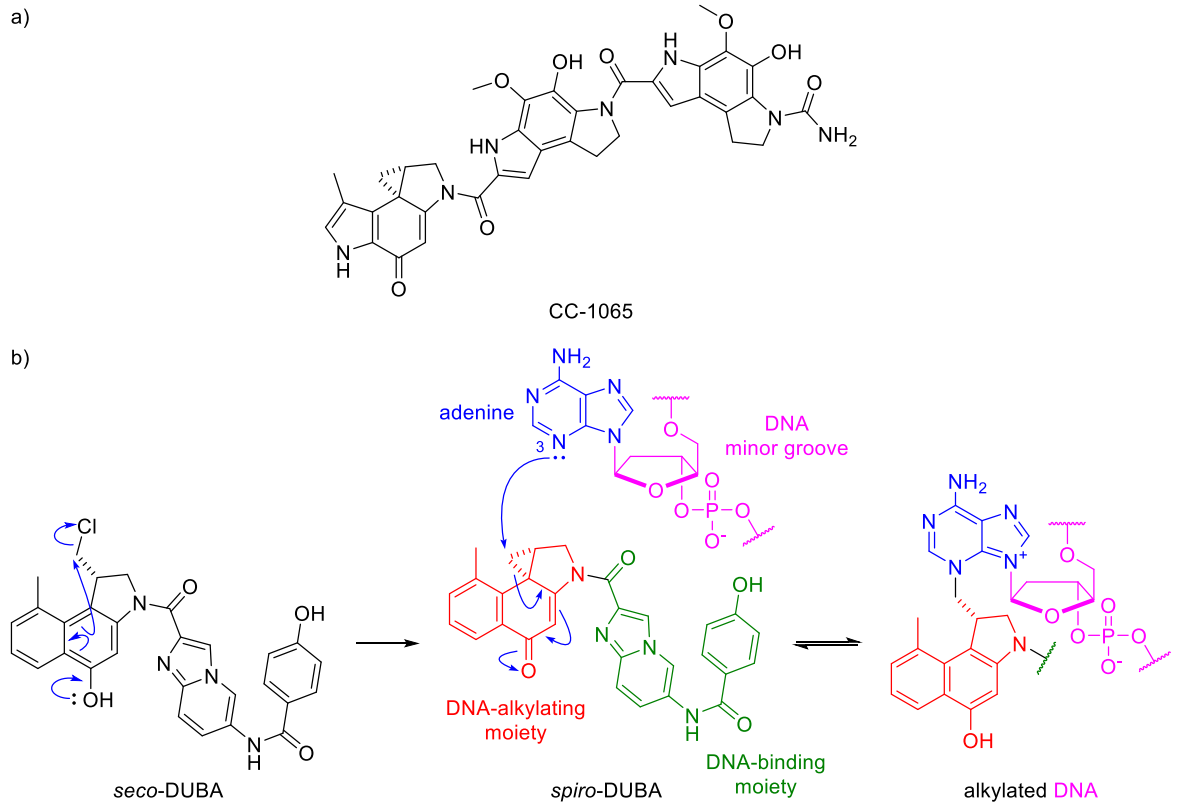

Scheme 22 a) Structure of CC-1065, first isolated duocarmycin. b) Activation of *seco*-duocarmycin-hydroxybenzamide-azaindole (*seco*-DUBA) via Winstein-Baird spirocyclisation and its mechanism of action.

The synthesis of *seco*-DUBA was disclosed by Elgersma *et al*. in 2015 (Scheme 23). The DNA-binding moiety **25** (indicated by green in Scheme 22b) was synthesised in four steps from 5-nitropyridin-2-amine (**23**) via a Chichibabin cyclisation. Separately, the synthesis of the DNA-alkylating unit **30** (indicated by red in Scheme 22b) was achieved in ten steps via the key incorporation of an epoxide to form intermediate **29**, which allowed subsequent intramolecular cyclisation, via lithium-halogen exchange, to form the five-membered ring portion. The two units were then coupled using EDC, and then the removal of benzyl and MOM protecting groups gave *seco*-DUBA in 18 synthetic steps.

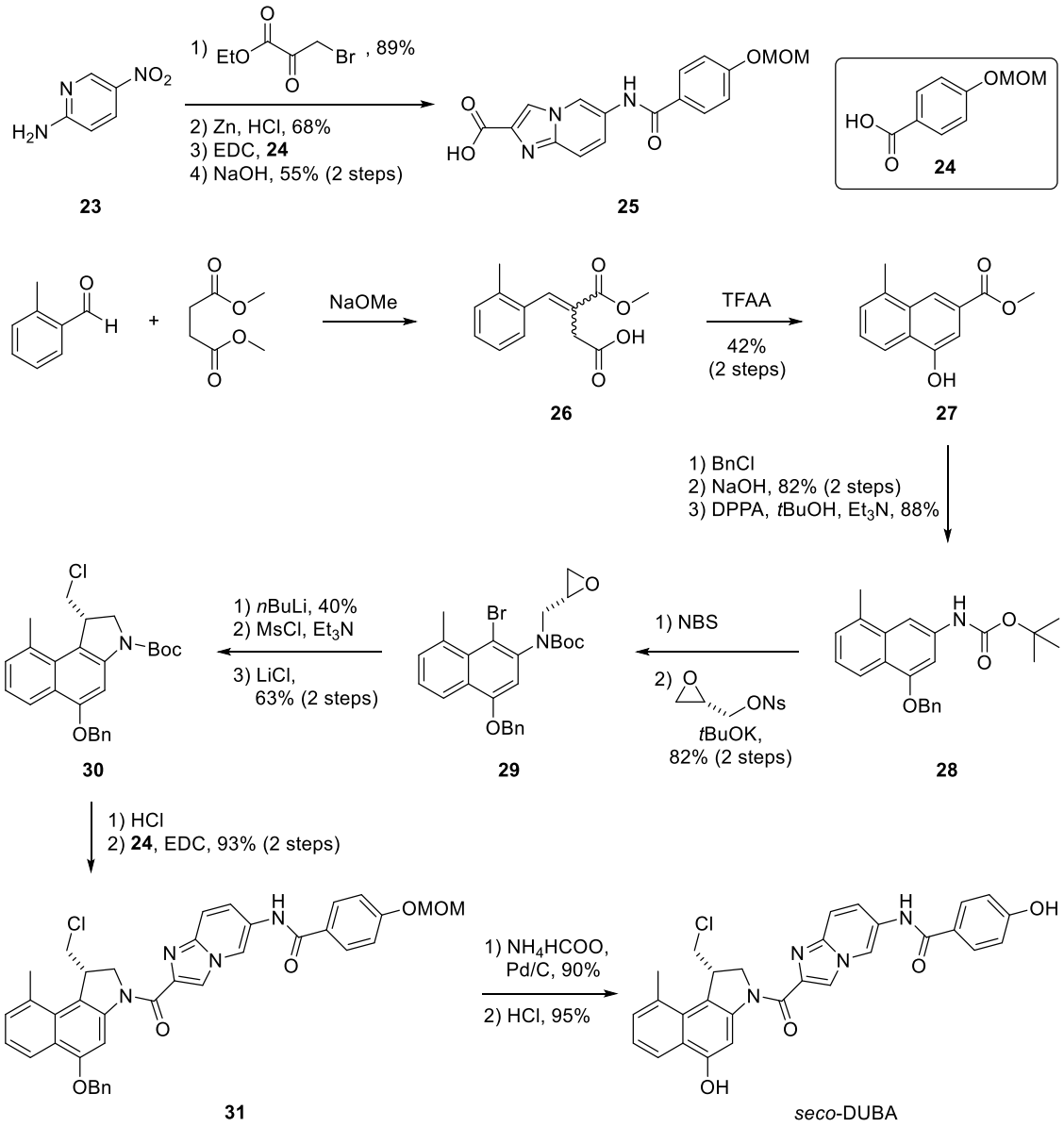

Scheme 23 Synthesis of *seco*-DUBA by Elgersma *et al*.[315] TFAA = trifluoroacetic anhydride, DPPA = diphenylphosphoryl azide, Ns = nosyl

3.5.1.4. Camptothecins

Camptothecin is an alkaloid natural product first isolated from the Chinese plant *Camptotheca acuminata* in the 1960s (Figure 19).[317] It acts as a potent anti-cancer agent by binding to a topoisomerase I–DNA cleavage complex, preventing DNA religation, subsequently causing DNA double-strand breaks and apoptosis.[318] Whereas camptothecin showed good *in vitro* anti-cancer activity, it suffered from poor solubility and severe side effects *in vivo*.[318] Analogues with better pharmacological profiles have been developed, and two (irinotecan and topotecan) are approved by the US FDA for cancer treatment (Figure

19).[319] Furthermore, two other camptothecin derivatives are successfully used as payloads in marketed ADCs: SN-38 and exatecan.[319]

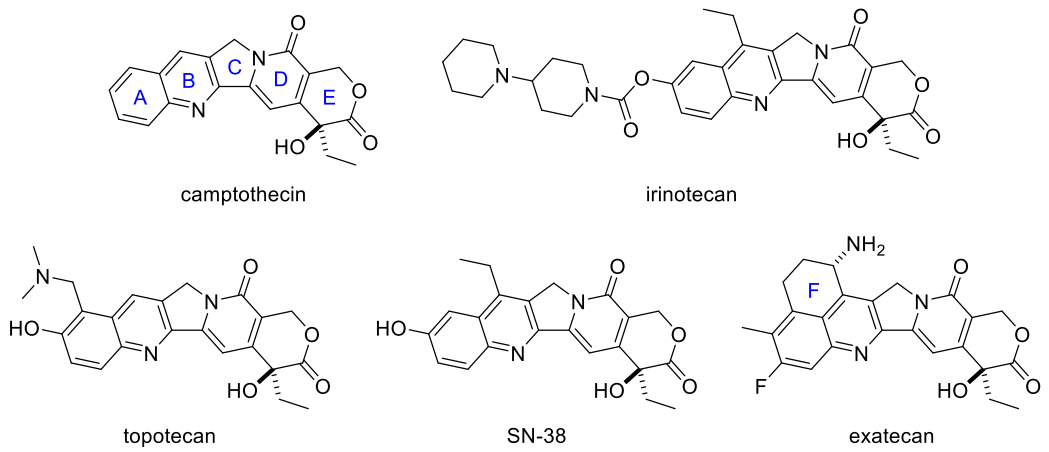

Figure 19 Structure of camptothecin and its four analogues: irinotecan and topotecan (used in chemotherapy), SN-38 (the active metabolite of irinotecan), and exatecan. The last two are used in marketed ADCs. Blue capital letters denote ring names.

SN-38 is the active metabolite of the prodrug irinotecan.[320] While SN-38 is 2-3 orders of magnitude more potent than irinotecan, it has low aqueous solubility and so cannot be administered on its own.[319,321] On the contrary, as SN-38 has *in vitro* IC_{50} in the low nanomolar range,[322] it has generated widespread interest in targeted therapeutics and is used as the payload in sacituzumab govitecan (Trodelvy®).[247] Reported by Sawada *et al.*, SN-38 can be accessed semi-synthetically from camptothecin in three steps (Scheme 24).[323] Ethylation at the 7-position of camptothecin was effected by Minisci-type reaction using propionaldehyde and ferrous sulfate to give intermediate **32**. Compound **32** was then oxidised to *N*-oxide **33** with hydrogen peroxide and following irradiation with mercury lamp in the presence of sulfuric acid gave SN-38 in 30-35% overall yield. It is also possible to obtain SN-38 via a total synthesis, accomplished in 17 steps in 2011 by Yao *et al.*[324]

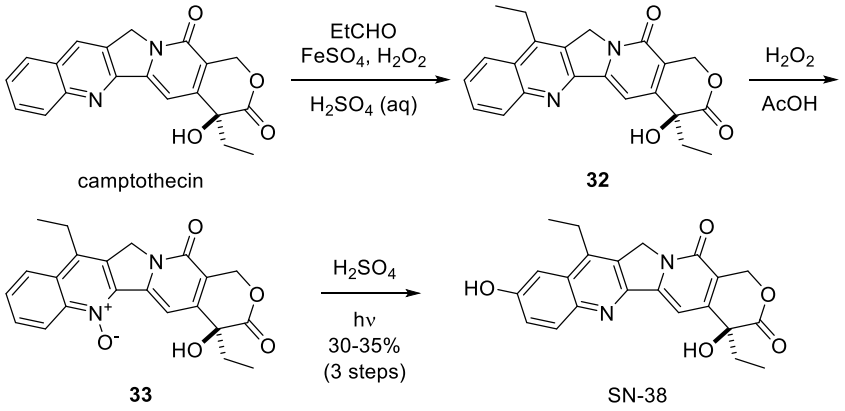

Scheme 24 Semi-synthesis of SN-38 from camptothecin by Sawada *et al.*[323]

Exatecan (DS-8201) is a more potent camptothecin derivative compared to SN-38, exhibiting sub-nM cytotoxicity towards several cancer cell lines.[325–328] Exatecan contains the amine-substituted six-membered F ring bridging the A and B rings which increases its stability and

aqueous solubility.[319] The latest total synthesis of exatecan mesylate was disclosed in a patent filed by Daiichi Sankyo's scientists in 2019 (Scheme 25a).[329] Starting from commercially available 2-fluoro-4-nitrotoluene (**34**) as the template for the A-ring, the F-ring was installed through appending the carbon chain to compound **35** using a Heck reaction and cyclised via a Friedel-Crafts-type acylation. Annulation to form the B-ring was achieved with the Friedländer reaction between aminoaryl ketone **37** and compound **38**, which already contains C-, D-, and E-rings, to give protected exatecan **39**. Removal of the remaining acetyl group with methanesulfonic acid then gave exatecan as a mesylate salt in a total of 10 steps, not counting those required for the synthesis of the building block **38**. Amongst other procedures, a multi-decagram-scale asymmetric synthesis of the tricyclic compound **38** was reported by Henegar *et al.*, which comprised of a total of 18 steps and is summarised in Scheme 25b.[330]

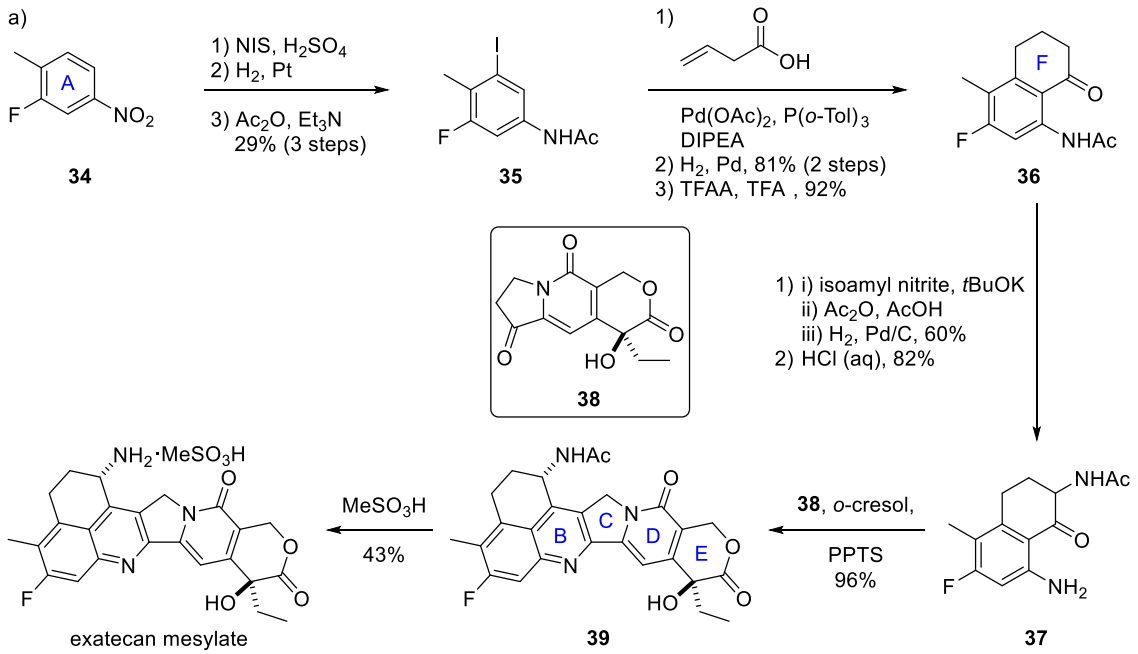

Scheme 25 Total synthesis of exatecan mesylate and its building block **38** a) Total synthesis of exatecan mesylate from a patent filed by Nishi *et al.*[329] NIS = *N*-iodosuccinimide, PPTS = pyridinium *p*-toluenesulfonate.

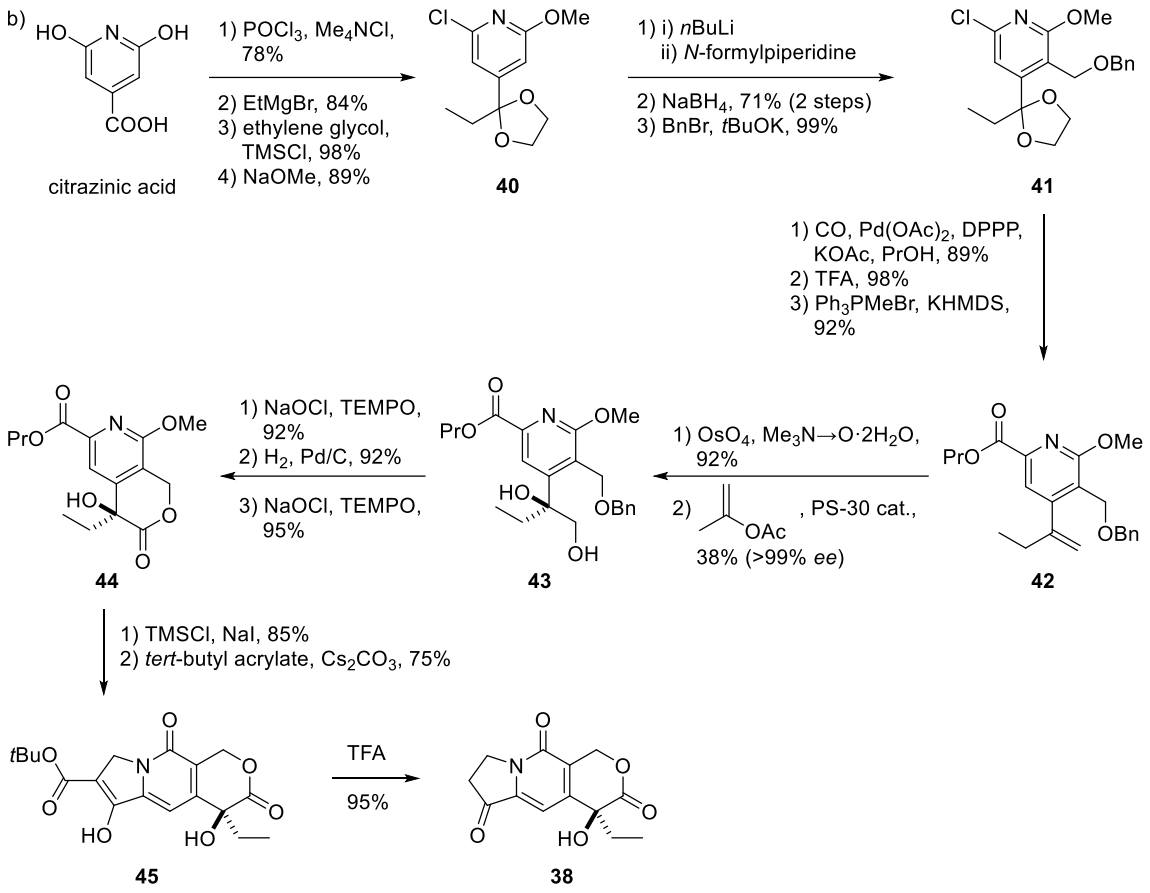

Scheme 25 (continued) b) Asymmetric synthesis of compound **38**, an important building block for the synthesis of camptothecin and its analogues, was published by Henegar *et al.*[330] DPPP = 1,3-bis(diphenylphosphino)propane.

3.5.2. Tubulin inhibitors

Microtubules are dynamic protein polymers with a cylindrical shape consisting of heterodimers of α- and β-tubulins.[23] These filaments are a major component of the cytoskeleton, essential to all eukaryotic cells. The highly dynamic polymerisation-depolymerisation of microtubules is vital to a myriad of cellular processes, including intracellular transport, structural integrity maintenance, cell division, and mitosis.[331] Thus, inhibition of tubulin biology has been a very effective strategy to target rapidly proliferating cancer cells. Many traditional chemotherapeutic agents, such as vincristine, vinblastine, and paclitaxel are anti-tubulin compounds.[27]

Tubulin inhibitors can be divided into two broad classes according to their effects on the microtubule polymer; microtubule stabilisers enhance polymerisation, while microtubule destabilisers impede polymerisation.[332] The former class includes the vinca alkaloids, colchicines, and dolastatins, while the latter class contain compounds such as the taxanes and discodermolide.[332] Of the tubulin inhibitors, the auristatins and maytansines are amongst the most potent with sub-nM *in vitro* cytotoxicity, and so are attractive as ADC payloads.

3.5.2.1. Auristatins

Auristatins are a class of synthetic peptides originated from anti-mitotic marine natural product dolastatin 10 isolated from *Dolabella* sea hares.[276,333,334] Dolastatins and auristatins are highly cytotoxic with sub-nM *in vitro* IC_{50} values.[270,276,335] They exert their cell-killing effects through the inhibition of tubulin polymerisation by binding near the Vinca alkaloid site, resulting in cell cycle arrest. However, auristatins are more water-soluble than their parent dolastatins.[291,332,336,337] Combined, monomethyl auristatin E (MMAE) and monomethyl auristatin F (MMAF) are the most widely used cytotoxins in ADC development (Figure 20).[291,337]

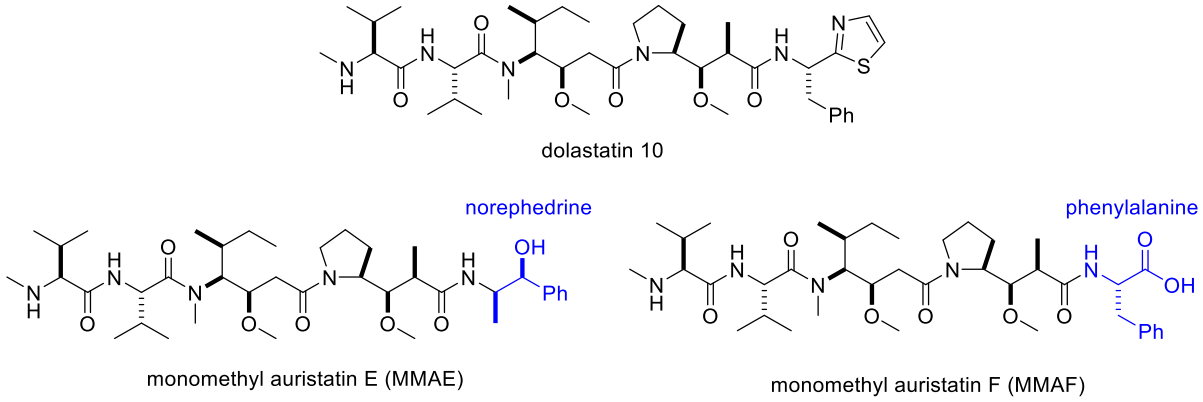

Figure 20 Structures of dolastatin 10, monomethyl auristatin E (MMAE), and monomethyl auristatin F (MMAF).

MMAE contains a norephedrine moiety at the "*C*-terminus" of the molecule, and its neutral charge gives it good membrane permeability.[338] This auristatin analogue is currently used in three marketed ADCs, Adcetris®, Polivy®, and Padcev®.[53] The total synthesis of MMAE was developed and licenced by Seattle Genetics,[339] while Pettit *et al*. had earlier developed the synthesis of the constituent non-canonical β-methoxy-γ-amino acids, dolaproine (Dap) and dolaisoleuine (Dil) (Scheme 26).[340,341] The total synthesis of MMAE centred on a stereoselective aldol reaction utilising boron enolate and Evans' oxazolidinone to produce Dap and Dil. The two γ-amino acids were then elaborated to give fragment **50** and the tripeptide Fmoc-MeVal-Val-Dil-O*t*Bu, which were then united using diethyl phosphorocyanidate (DEPC). The final Fmoc-deprotection then gave MMAE in a total of 23 steps.

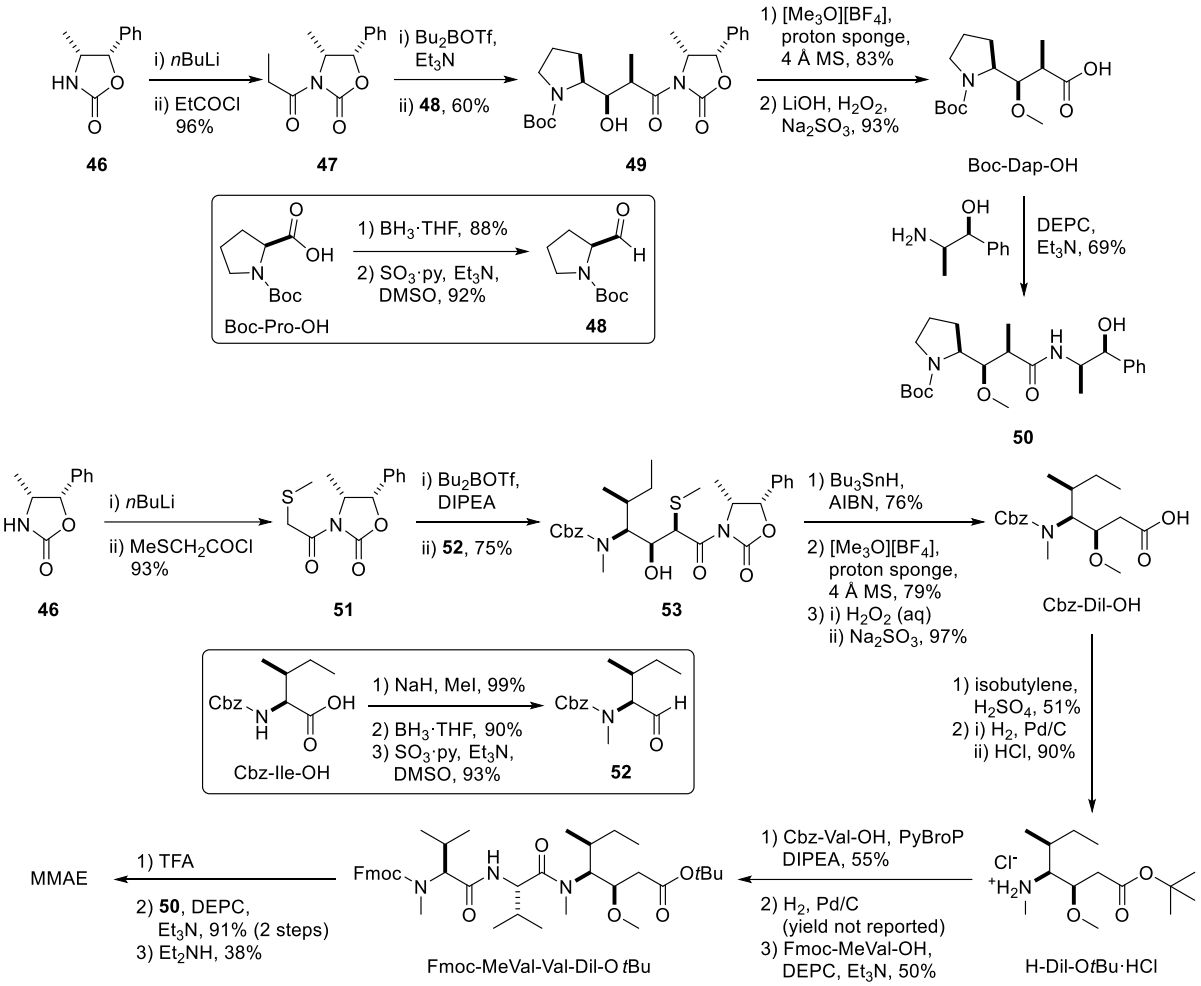

Scheme 26 Total synthesis of monomethyl auristatin E (MMAE) in a patent filed by Seattle Genetics.[339] Synthesis of Boc-Dap-OH and H-Dil-O*t*Bu·HCl was according to Pettit *et al*.[340,341] Proton sponge = 1,8-bis(dimethylamino)naphthalene, Dap = dolaproine, MS = molecular sieves, DEPC = diethyl phosphorocyanidate, DIPEA = *N*,*N*-diisopropylethylamine, Dil = dolaisoleuine, MeVal = *N*-methylvaline, AIBN = azobisisobutyronitrile.

MMAF differs from MMAE by replacing the norephedrine unit with phenylalanine. This change causes the generation of a charged terminal carboxylate at physiological pH, impairing its membrane permeability and lowering its potency in its free form.[270] The decreased permeability can be seen as beneficial when used with targeted therapy against haematological cancers as seen in one marketed MMAF-containing ADC, Blenrep® for treatment of multiple myeloma.[250,251] Doronina *et al*. reported the synthesis of MMAF using an Fmoc solid-phase peptide synthesis strategy on 2-chlorotrityl resin (Scheme 27).[270] Resin-bound phenylalanine was elongated with Dap, and then with tripeptide MeVal-Val-Dil. Final cleavage from the resin with TFA gave MMAF.

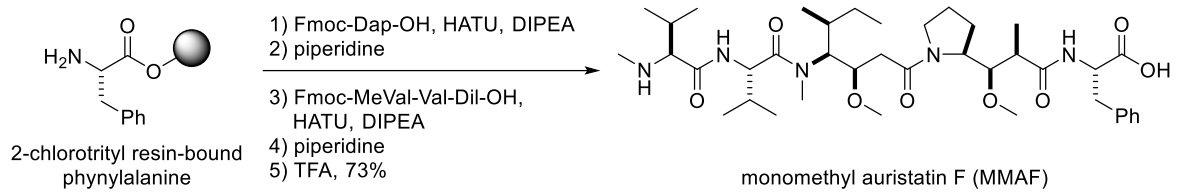

Scheme 27 Total synthesis of monomethyl auristatin F (MMAF) by Doronina *et al*.[270] See Scheme 26 for structures of Dap and MeVal-Val-Dil.

3.5.2.2. Maytansinoids

Maytansine is a benzoansamacrolide first isolated from the bark of the Ethiopian shrub *Maytenus ovatus* in 1972 (Figure 21).[342] Maytansine is a microtubule destabiliser that binds tubulin near the Vinca alkaloid binding site and has sub-nM potency against several cancer cell lines.[343,344] Because of its high cytotoxicity, maytansine was evaluated as single-agent chemotherapy, but clinical benefits were not observed.[345] Later, attention was focussed on using maytansine or its derivatives, maytansinoids, in targeted therapeutics.[346] SAR study of maytansine by Widdison *et al*. found that while the ester side chain at C3 is required for bioactivity, its exact nature is variable without negatively affecting its cytotoxicity, except for the essential (*S*)-configuration at C2'.[344] Thus, thiol-bearing maytansinoids DM1 and DM4 were developed to facilitate their conjugation to an antibody.[344] Currently, DM1 is used in Kadcyla® for treatment of HER2-positive metastatic breast cancer,[234–236] and DM4 is a payload of mirvetuximab soravtansine, an ADC being examined in phase III clinical trial for folate receptor α–positive epithelial, primary peritoneal, or fallopian tube cancers.[53,347,348]

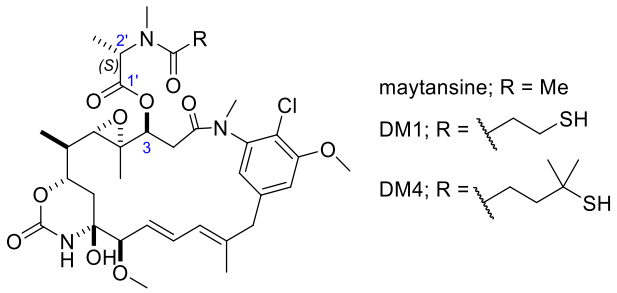

Figure 21 Structures of maytansine and maytansinoids DM1 and DM4.

The total synthesis of maytansine was accomplished by Corey *et al*. in 1980 over 30 steps.[349] Due to the complexity of the total synthesis, on industrial scale, maytansinoids are instead accessed semi-synthetically from a mixture of ansamitocins, obtained from fermentation of *Actinosynnema pretiosum* bacterium (Scheme 28).[235] The acyl group at C3-hydroxyl was removed by reduction with $LiAlH(OMe)_3$ to afford maytansinol. The obtained alcohol was then coupled with disulfide-containing acids **54** using EDC and $ZnCl_2$ to give intermediates **55** whose disulfide was reduced with dithiothreitol (DTT) to give DM1 and DM4.

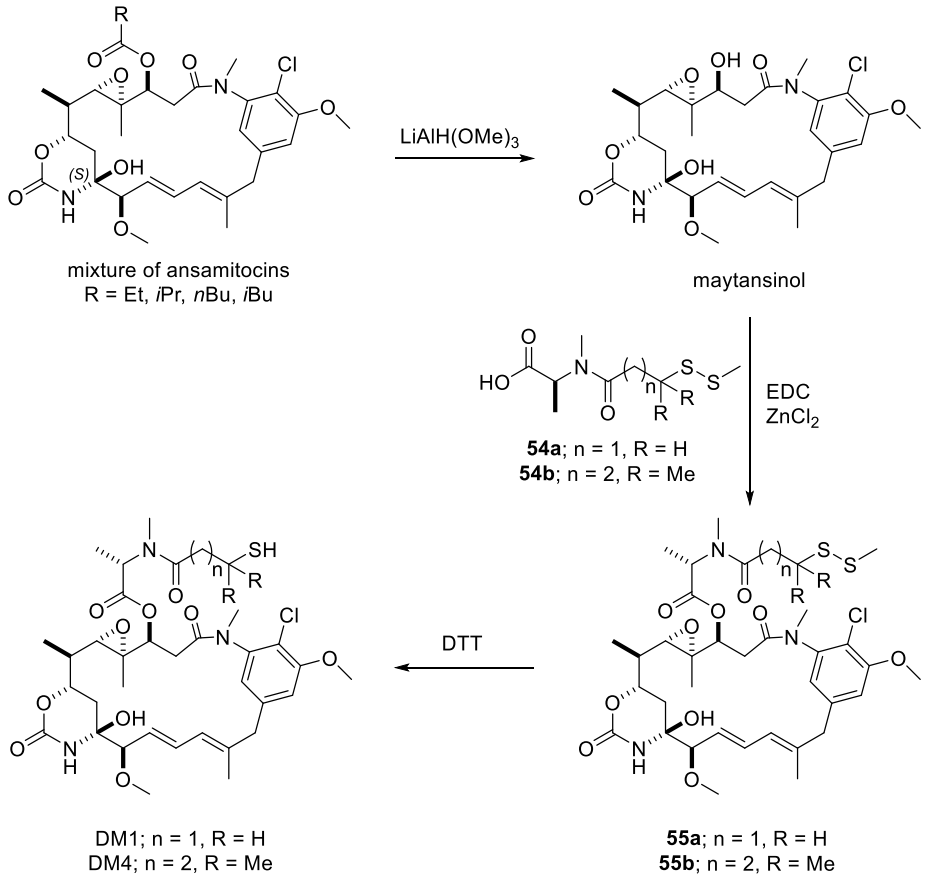

Scheme 28 Semi-synthesis of DM1 and DM4 from ansamitocin mixture by Lambert and Chari.[235] DTT = dithiothreitol.

3.5.3. Other payloads

Apart from the abovementioned payloads, there are also other classes of compounds currently under investigation for use in ADCs (Figure 22): the anti-tubulin tubulysins,[350,351] DNA-alkylating agent indolinobenzodiazepine dimers (IGNs),[352] RNA polymerase II–inhibitor amatoxins,[353] and spliceosome inhibitors.[354] All these compounds are extremely potent cytotoxins *in vitro*, except for the amatoxins which suffer from poor membrane permeability due to its hydrophilicity. The syntheses of these payloads are not presented here as they are used significantly less in the ADC field.

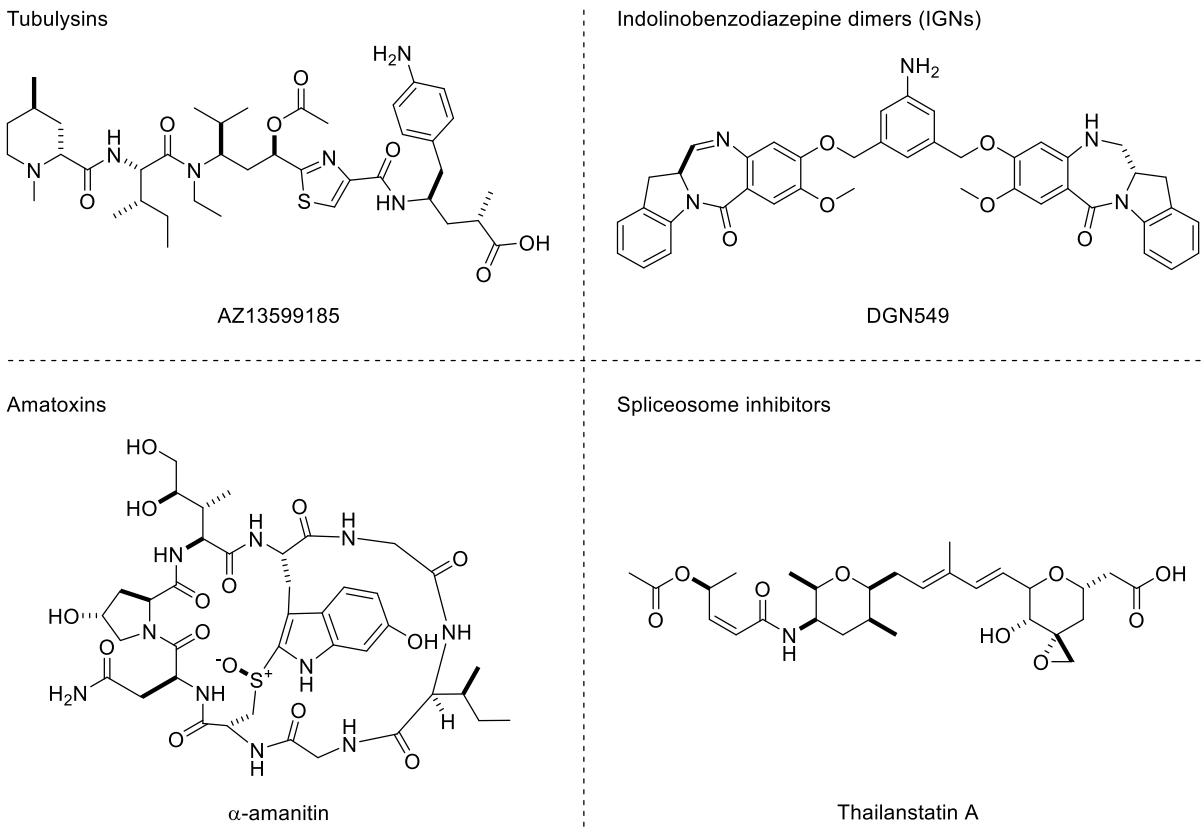

Figure 22 Other classes of cytotoxins under investigation for the use as ADC payloads.

3.5.4. Summary

The introduced payloads with their *in vitro* cytotoxicities are summarised in Figure 23. Most payloads require laborious total synthesis or are derived semi-synthetically from fermentation products. All current payloads have low- or sub-nM IC_{50} values (cf. earlier-generation payloads which have mid-nM to sub-µM IC_{50} values), with some PBDs exhibiting sub-pM cytotoxicity.

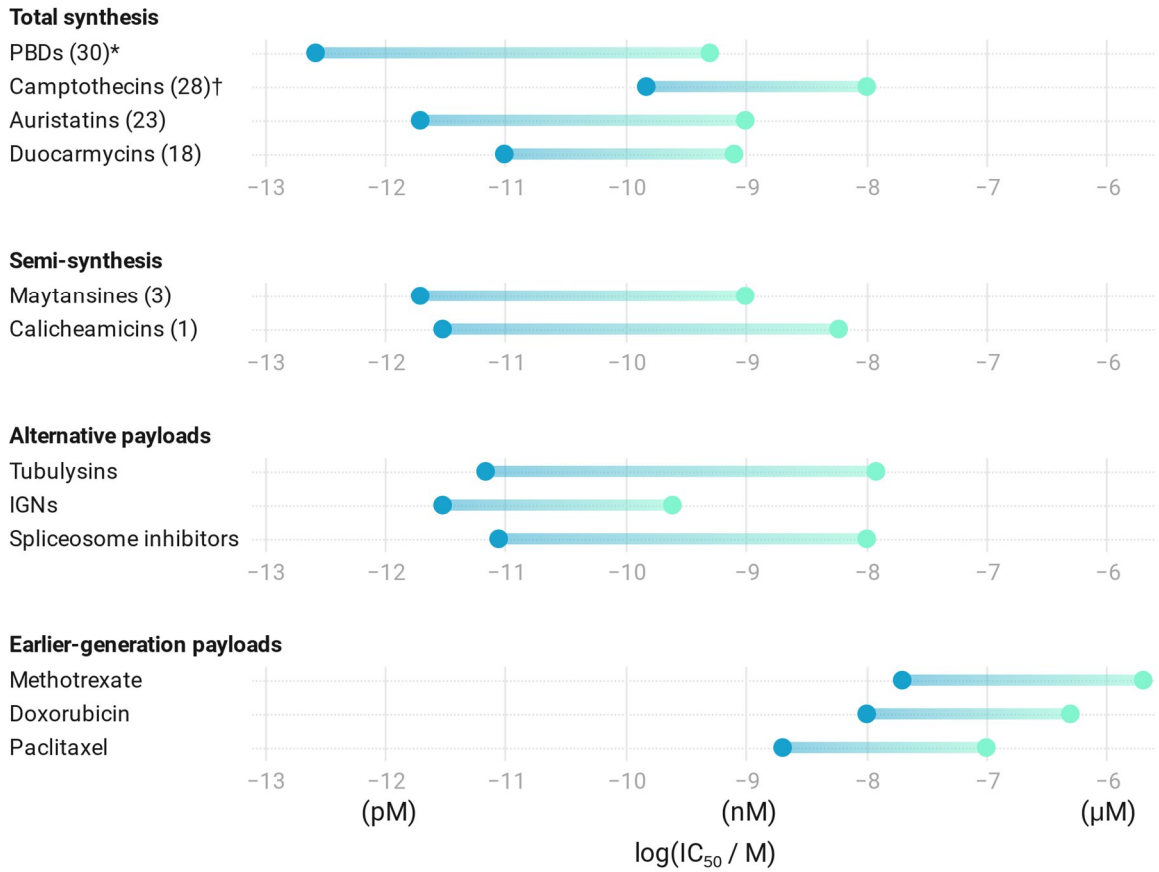

Figure 23 Summary of *in vitro* cytotoxicity of various payloads. Numbers in parentheses after the payload class indicate a representative number of total steps for the synthesis or semi-synthesis. Amatoxins are not included in this chart as their *in vitro* IC_{50} values do not reflect their actual cytotoxicity. *The number of steps includes the incorporation of a linker. †May also be accessed semi-synthetically in three steps.

3.6. Hemiasterlin

Hemiasterlin (**56**, Figure 24), first discovered in the marine sponge *Hemiasterella minor*, is a member of a family of marine cytotoxic tripeptides and is a microtubule destabiliser.[355,356] The tripeptide binds in the vinca domain, disrupting microtubule dynamics, and causes apoptosis with low- to sub-nM IC_{50} for several cancer cell lines.[357,358]

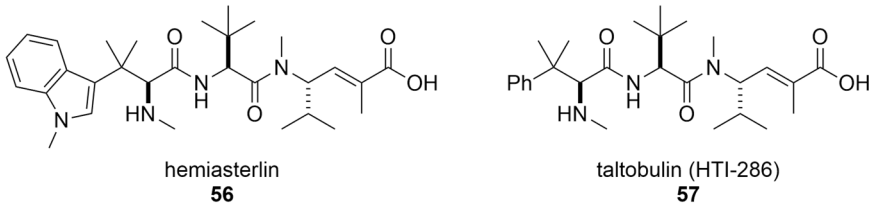

Figure 24 Structures of hemiasterlin (**56**) and taltobulin (HTI-286, **57**).

Extensive SAR studies by Nieman *et al*. and Zask *et al*. revealed taltobulin (HTI-286, **57**) to be a similarly potent hemiasterlin analogue, by replacing the indole ring with a phenyl ring

(Figure 24).[359,360] It was reported that taltobulin, although slightly less cytotoxic than hemiasterlin, would be more synthetically tractable.[358] Hence, taltobulin was investigated clinically as a treatment for NSCLC and advanced to phase II clinical trial.[361] However, the development was terminated by Wyeth for business reasons.[362]

There have been three published total syntheses of hemiasterlin to date. Each route is described in brief in the following paragraphs.*

The first total synthesis of hemiasterlin was published by Andersen *et al*. in 1997 via the use of Evans' oxazolidinone (Scheme 29).[363] First, indole **58** was trimethylated with MeI using KHMDS as a base in two steps giving indole **60**. Next, a five-step procedure, in a sequence of DIBAL-H reduction to alcohol, Ley-Griffith oxidation to aldehyde, Wittig reaction to install an enol ether, followed by acid hydrolysis and Pinnick oxidation, for homologation of the carboxylate was used to generate carboxylic acid **61**. Subsequent installation of a chiral oxazolidinone via a reactive mixed anhydride was followed by azidation with 2,4,6-triisopropylbenzenesulfonyl azide (TPS-N_3) resulting in a chiral azide which was reduced to an amine with $SnCl_2$ and then Boc-protected to give compound **63**. The chiral auxiliary was then removed by treating compound **63** with LiOOH. Finally, double methylation followed by LiOH-mediated hydrolysis gave the Boc-protected amino acid **64**.

The synthesis of the dipeptide fragment began with the derivatisation of Boc-protected *N*-methylvaline (Boc-MeVal-OH) to a Weinreb amide which was reduced to an aldehyde with $LiAlH_4$, followed by a Wittig reaction and deprotection with TFA to give unsaturated γ-amino ester **65**. The amine **65** was extended to dipeptide **66** by coupling with Boc-*tert*-leucine (Boc-Tle-OH) and subsequent deprotection. The two fragments, **64** and **66**, were joined using PyBroP and DMAP. Finally, ester hydrolysis and Boc-group removal gave hemiasterlin in a total of 23 steps with a longest linear sequence (LLS) of 17 steps and an overall yield of 13%.

* The overall yields are reported based on the longest linear sequence in each synthesis.

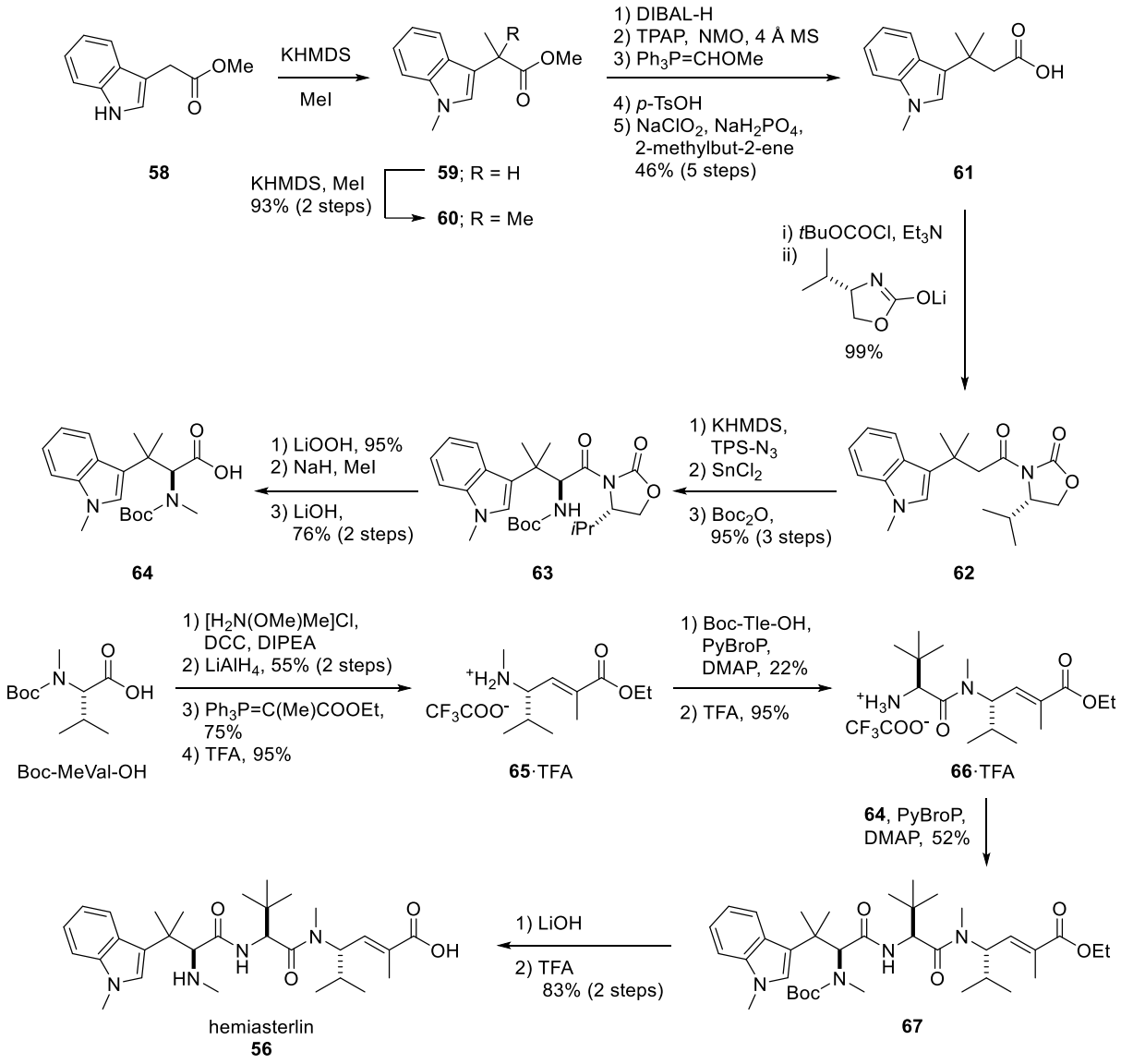

Scheme 29 Total synthesis of hemiasterlin by Andersen *et al.*[363] KHMDS = potassium hexamethyldisilazide, DIBAL-H = diisobutylaluminium hydride, TPAP = tetrapropylammonium perruthenate, MS = molecular sieves, NMO = *N*-methylmorpholine, TPS-N_3 = 2,4,6-triisopropylbenzenesulfonyl azide, DCC = dicyclohexylcarbodiimide, Tle = *tert*-leucine, PyBroP = bromotripyrrolidinophosphonium hexafluorophosphate, DMAP = *N*,*N*-dimethyl-4-aminopyridine.

In 2001, Vedejs and Kongkittingam reported their total synthesis of hemiasterlin using a benzothiazol-2-sulfonyl (Bts) protecting group and asymmetric Strecker synthesis strategy (Scheme 30). The synthesis of dipeptide **66** started with the protection of the amino group of (*S*)-valinol with Bts chloride, followed by *N*-methylation, Swern oxidation and Wittig reaction to give Bts-protected amino ester **68**. Ensuing removal of Bts group was effected using thiophenol and K_2CO_3 to reveal a free amine which was then coupled with the Bts-protected acyl chloride of *tert*-leucine—prepared from *tert*-leucine in two steps. Subsequent removal of the Bts group gave dipeptide **66**.

The synthesis of a chiral tetramethyltryptophan motif started with scandium(III)-catalysed asymmetric Strecker reaction via an imine generated from aldehyde **69** (prepared in four steps

according to Andersen *et al.*)[363] and (*R*)-2-phenylglycinol (**70**) with Bu_3SnCN as the cyanide source to give amino nitrile **71**. The nitrile was hydrolysed with hydrogen peroxide and potassium carbonate, and the chiral auxiliary was removed via hydrogenolysis to give amino amide **72**. The amino group in **72** was protected with BtsCl and methylated with MeI, and the amide was converted to a reactive bis-Boc derivative **73** by treatment with Boc_2O and DMAP. Amine **66** and compound **73** were united by treatment with DMAP; final Bts-deprotection and ester hydrolysis gave hemiasterlin in a total of 20 steps (LLS 13 steps, overall yield 30%).*

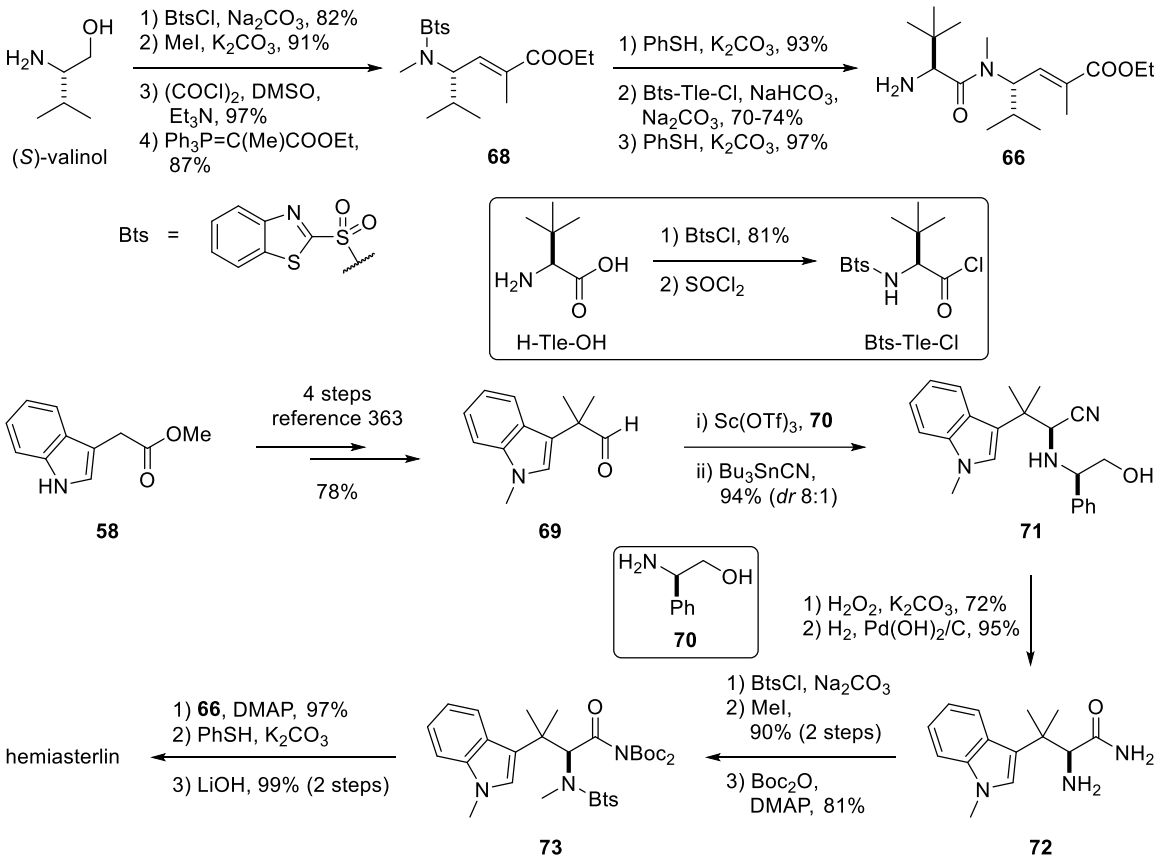

Scheme 30 Total synthesis of hemiasterlin by Vedejs and Kongkittingam.[364] Bts = *N*-benzothiazol-2-sulfonyl.

The most recent total synthesis of hemiasterlin was reported by Lang, Jones, and Lindel in 2017 via an organocatalysed α-hydrazination (Scheme 31).[365] First, 3-*tert*-prenylation on 1*H*-indole was performed under modified Tamaru's conditions[366] and then followed by *N*-methylation giving compound **74**. Hydroboration-oxidation of the terminal alkene with .9-BBN and oxidation of the resulting alcohol by IBX gave aldehyde **75**. The α-hydrazine was installed enantiomerically through an enamine-catalysed process using D-proline-derived tetrazole analogue (prepared from Cbz-D-proline in four steps as summarised in Scheme 31) with dibenzyl azodicarboxylate, followed by $NaBH_4$ reduction to give alcohol **77**. Subsequent hydrogenolysis simultaneously removed the Cbz protecting group and reduced the N-N bond

* The yield for the transformation of compound 58 to compound 69 was based on reference 359 as yields were not reported in reference 363 for the last two individual steps of this transformation.

to give an amine which was then protected with Boc_2O to give amino alcohol **78**. Conversion of compound **78** to amino ester **79** was carried out by Parikh-Doering oxidation of the alcohol and Pinnick oxidation of the resulting aldehyde to form a carboxylic acid which was methylated concurrently with the amine using methyl iodide and sodium hydride. To perform peptide coupling with dipeptide **66** (prepared according to Andersen *et al*. in six steps)[363], the methyl ester **79** was first hydrolysed using barium hydroxide. The coupling was then effected using 2-bromo-*N*-ethylpyridinium tetrafluoroborate (BEP) as the activating agent to give protected hemiasterlin **67**. Finally, removal of the Boc group and the ethyl ester gave hemiasterlin in a total of 21 steps (LLS 15 steps, overall yield 17%).

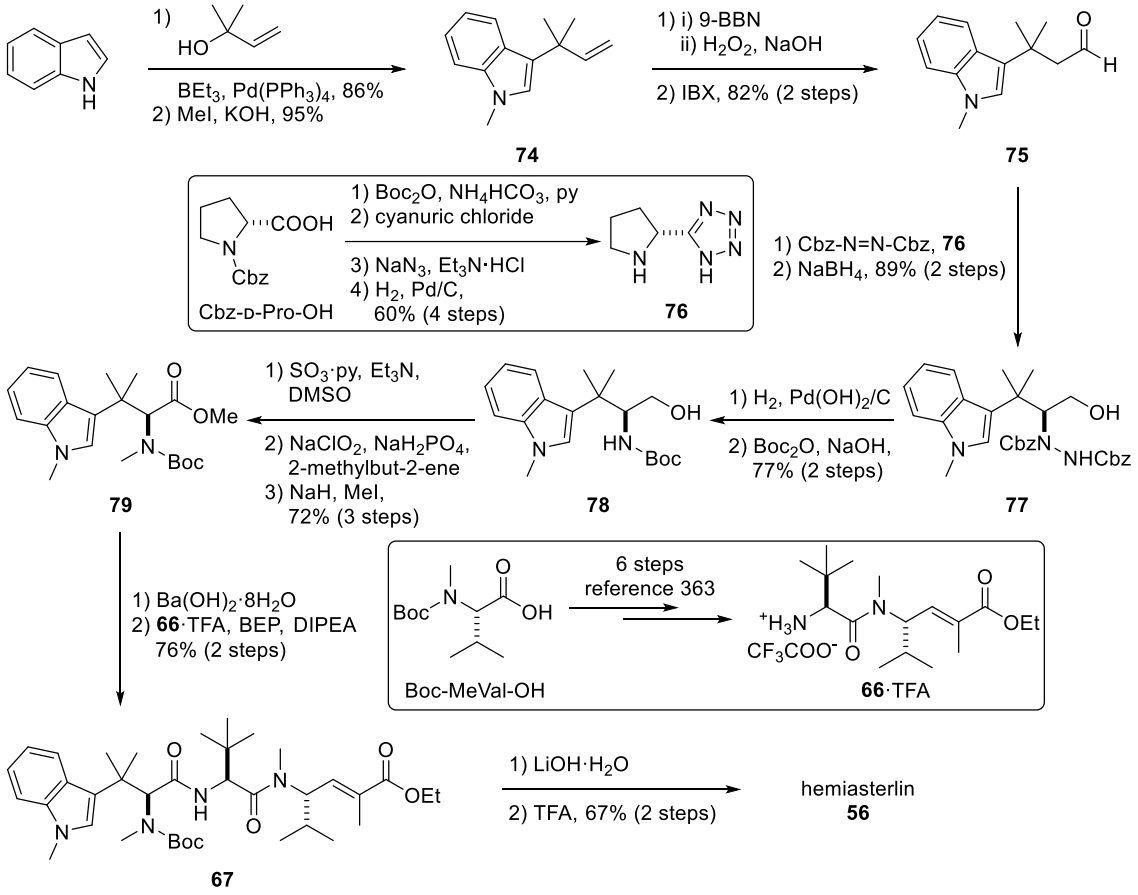

Scheme 31 Total synthesis of hemiasterlin by Lang, Jones, and Lindel.[365] 9-BBN = 9-borabicyclo[3.3.1]nonane, IBX = 2-iodoxybenzoic acid, BEP = 2-bromo-*N*-ethylpyridinium tetrafluoroborate.

With its high cytotoxicity and relatively short and accessible synthesis, hemiasterlin has the potential to become a widely used payload in ADCs. Indeed, STRO-002, an ADC developed by Sutro Biopharma, Inc. and currently in phase I clinical trial for the treatment of ovarian and endometrial cancers, uses 3-aminophenylhemiasterlin as its payload.[367]

Section II:

Results and Discussion

Chapter 4 — Development of Stapled Peptide–Targeted Covalent Inhibitors of p53–MDM2 PPI*

4.1. Project aims and overview

The aim of this project was to develop a series of novel stapled peptides carrying dialkynyl linkers with an electrophilic functionality to covalently bind to MDM2 and hence inhibit the p53–MDM2 PPI. The stapled peptides, mimicking p53, would be synthesised using the two-component CuAAC peptide stapling developed in the Spring Group and the electrophile will be added onto the staple. In such a way, the peptide and the staple could be optimised separately and merged in the click reaction. Upon binding of the peptide, we envisioned that the electrophile would be able to covalently bind to a nucleophilic residue (i.e. Lys) located in the proximity of the binding site of MDM2 and thus improving the overall binding efficiency (Scheme 32).[134]

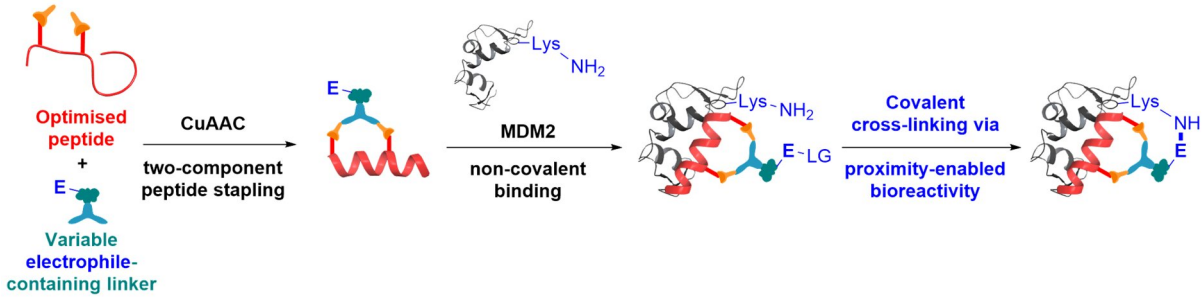

Scheme 32 Utilising two-component peptide stapling to generate electrophile-bearing stapled peptides and their proximity-enabled bioreactivity. E = electrophile, LG = leaving group.

The ideal electrophile used on the linker should be stable in water, preferentially attacked by Lys over other nucleophilic amino acids, and compatible with our CuAAC stapling methodology. Initially, efforts were focussed on incorporating a sulfonyl fluoride—an electrophilic moiety that has already been reported in the literature to increase the inhibitory activities of peptides via covalent cross-linking—on the dialkynyl linker.[134,369] This functionality displays desirable properties for biological applications, such as resistance to reduction and hydrolysis, and cleavage being exclusively heterolytic.[370] Several examples that employed sulfonyl fluorides for targeting Lys are shown in Section 2.3.4. The linker would then be tested for its suitability for stapling by studying its stability under both CuAAC and physiological conditions, along with its reactivity towards Lys.

Concurrent to the study of the electrophilic motif and dialkynyl linker, the design and synthesis of the peptides to be stapled were carried out. Based on previous work in the Spring Group, peptides PDI-E (Ac-LTFXEYWAQLXS-NH_2, X = Orn(N_3)) and PMI (H-

* The work described in this chapter has been published in Charoenpattarapreeda, *et al.*, *ChemComm*, 2019.[368] Part of the text and figures were adapted from this publication.

TSFAEYWNLLSP-OH) were chosen as the starting point for our investigations, since both showed high affinity in binding MDM2.[103] Stapling positions, sequence mutations and the type of linkers were investigated under the guidance of computational simulations (performed by our collaborator Dr Yaw Sing Tan at the Bioinformatics Institute, A*STAR, Singapore).

Suitable electrophilic linkers were then used for stapling appropriate peptide sequences using the double-click stapling (Scheme 32).[115] The binding of the obtained stapled peptides to MDM2 was examined using fluorescence polarisation (FP) and mass spectrometry (MS) experiments.

4.2. Peptide and linker design

Close to the p53 binding surface of MDM2, there are two potential lysine residues that can be targeted with a sulfonyl fluoride group: Lys51 and Lys94 (Figure 25).

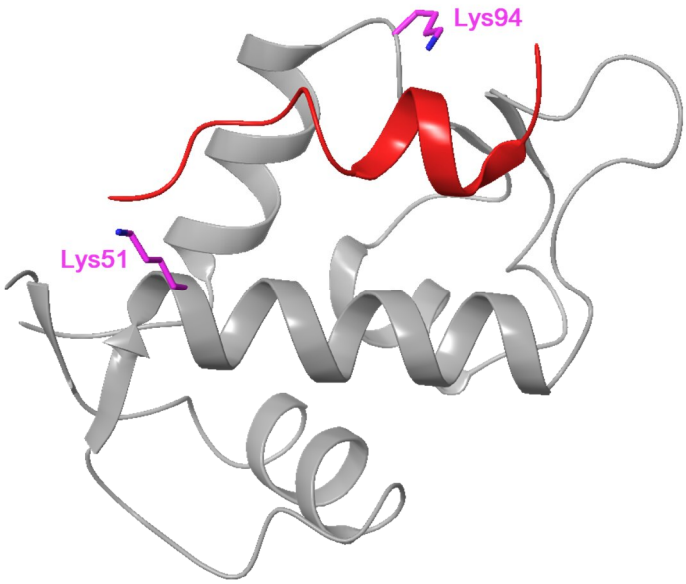

Figure 25 MDM2 shown with the two potential lysine residue targets (purple). p53 is shown in red and MDM2 in grey. (PDB ID: 1YCR)[82]

Molecular modelling, conducted by Dr Yaw Sing Tan, suggested two different linkers that could be used to staple the p53 peptide while enabling access to the two lysine residues:

- Strategy (1): the prediction to reach Lys51 showed peptide **PDI-E** stapled with compound **80**, an aryl sulfonyl fluoride analogue of the strained diyne SWD (Scheme 33a).
- Strategy (2): 3,5-diethynylbenzene sulfonyl fluoride (**81**) was anticipated as the optimal staple to target Lys94. (Scheme 33b).

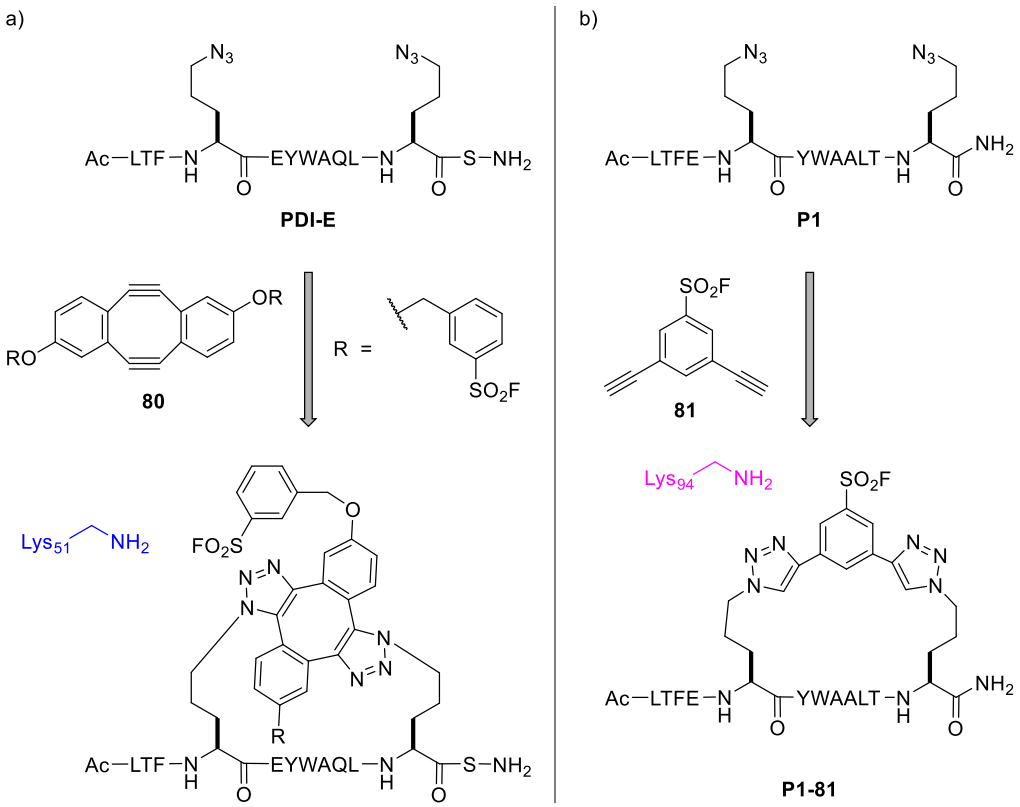

Scheme 33 Two proposed strategies for reaching lysines close to MDM2 binding site. a) Stapling **PDI-E** with the aryl sulfonyl fluoride **80** for targeting Lys51 (blue). b) Stapling **P1** with **81** for targeting Lys94 (pink).

Previous work in the Spring Group indicated that **80** is not readily available, due to long and challenging synthesis.[120] Thus, it was decided to prioritise the second strategy.

To pursue this strategy, several changes to the peptide sequence in **PDI-E** were needed. In order to obtain an optimal distance between the aryl sulfonyl fluoride group of **81** and Lys94 (1.63 Å),[371] it was necessary to move the position of the staple from what was previously published by the Spring group. In particular, the azido amino acids replaced Glu5 and Ser12 of **PDI-E**, and the mutation Q9A was also introduced to minimise the steric clash between the side chains of the peptide and the linker **81**. Orn(N_3) was chosen as the azido amino acid for stapling as its side chain showed the optimum length to reach Lys94 and increased helicity according to computational modelling (Figure 26).[102]

According to the design, the synthesis of linker **81** and peptide **P1** was commenced to obtain the stapled peptide **P1-81**.

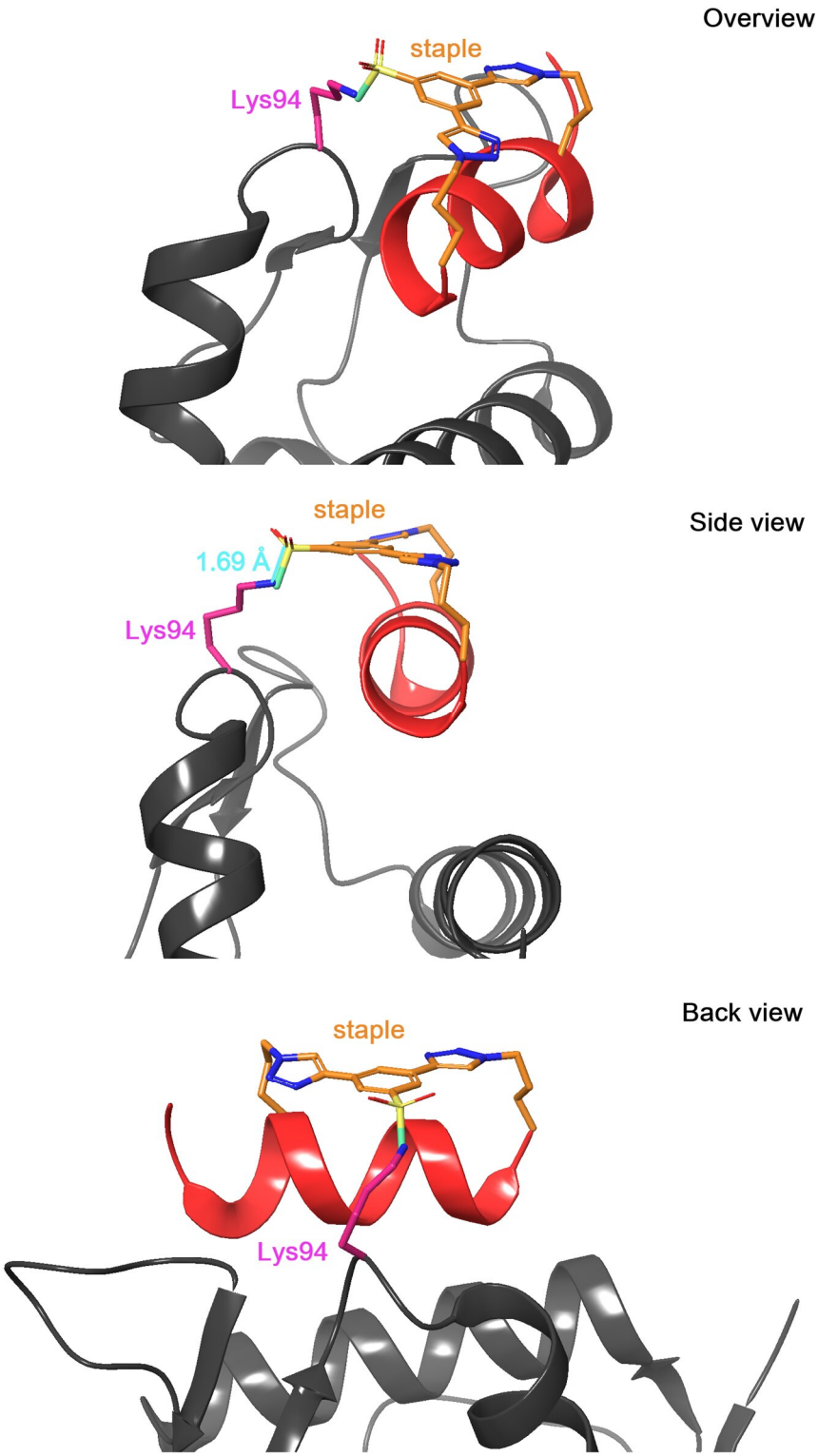

Figure 26 Molecular modelling of stapled peptide **P1-81** (shown in red and orange) bound with MDM2 (shown in grey) based on the crystal structure of the stapled peptide "**E1**" bound to MDM2 (PDB ID: 5AFG).[103] Distance between the nitrogen atom of Lys94 and the sulphur atom of the sulfonyl fluoride (1.69 Å) is shown by the cyan line in the side view.

4.3. Synthesis of 3,5-diethynylbenzenesulfonyl fluoride

The initial retrosynthetic route for the synthesis of sulfonyl fluoride **81** is outlined below (Scheme 34).

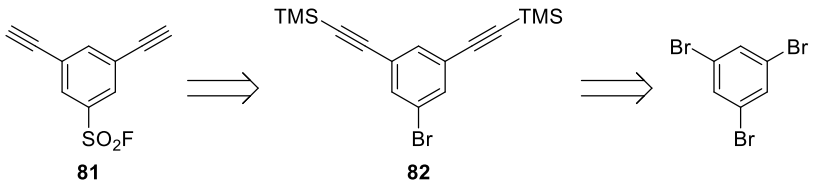

Scheme 34 Initial retrosynthetic route for the synthesis of **81**

We envisioned the formation of the dialkynylbromobenzene **82** from 1,3,5-tribromobenzene via Sonogashira coupling[372] in the presence of (trimethylsilyl)acetylene. Dialkyne **82** could then be converted into the desired product **81** via palladium-catalysed fluorosulfonylation[373,374] followed by the removal of the trimethylsilyl group.

The Sonogashira coupling of 1,3,5-tribromobenzene with 2.2 equivalents of (trimethylsilyl)acetylene gave **82** in moderate yield (Scheme 35). Flash column chromatography was not sufficient for purification of **82** as several unidentified by-products co-eluted with the desired product regardless of the solvent system used. Further purification by preparative TLC afforded pure **82**.

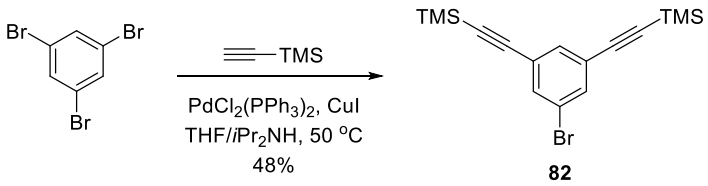

Scheme 35 Synthesis of **82** via Sonogashira coupling

The fluorosulfonylation reaction utilises 1,4-diazabicyclo[2.2.2]octane–bis(sulfur dioxide) (DABSO) as a source of sulfur dioxide to first form a sulfinate salt via a Pd-catalysed process. The addition of an electrophilic fluorine source then provides the sulfonyl fluoride. The different conditions tried are shown in Table 3. The first attempt at this reaction used $PdCl_2(APhos)_2$ as the catalyst and *N*-fluorobenzenesulfonimide (NFSI) as the fluorine source (Table 3 Entry 1).[373] The reaction gave a complex mixture, but the presence of F could not be observed in the NMR of the crude, while peaks corresponding to terminal alkyne were seen. It was speculated that the trimethylsilyl group might have interfered with the reaction. Thus, a reaction with five equiv. of NFSI was attempted, but the desired product was not obtained (Table 3 Entry 2). Consequently, a different condition reported in the literature, using $Pd(OAc)_2$ as the Pd-source with CataCXium A as the ligand and Selectfluor™ as the fluorine source was tried (Table 3 Entry 3).[374] Unfortunately, this condition gave little conversion. Considering the lack of alternative conditions in the literature for direct fluorosulfonylation, this synthetic route was abandoned.

Table 3 Conditions employed in attempts at fluorosulfonylation of **82**

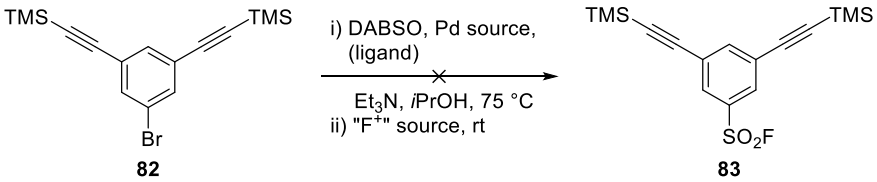

Entry	Pd source	Ligand	F^+ source	Yield (%)
1	$PdCl_2(APhos)_2$	(APhos pre-complexed with Pd)	NFSI (1.5 equiv.)	0[a]
2	$PdCl_2(APhos)_2$	(APhos pre-complexed with Pd)	NFSI (5 equiv.)	0[b]
3	$Pd(OAc)_2$	cataCXium® A (8 mol%)	Selectfluor™ (3 equiv.)	0[c]

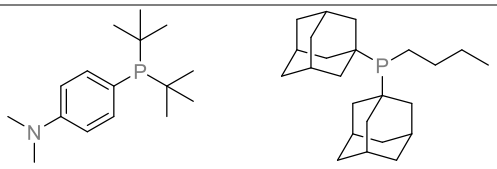

Conditions: DABSO (0.6 equiv.), Pd source (5 mol%), Et_3N (3 equiv.). [a]Complex mixture and alkyne deprotection; [b]complex mixture; [c]unreacted starting material recovered. NFSI = *N*-fluorobenzenesulfonimide, Selectfluor™ = 1-chloromethyl-4-fluoro-1,4-diazoniabicyclo[2.2.2]octane bis(tetrafluoroborate).

Since literature evidence suggested that fluorination via the sulfonyl chloride intermediate **84** would be more convenient,[370] we envisioned an alternative route to synthesise this key intermediate (Scheme 36). Sulfonyl fluoride **81** could be constructed by nucleophilic substitution at the sulfonyl centre from sulfonyl chloride **84**. It was then envisaged that nitrobenzene **86** could be used as the precursor to compound **84** via a reduction to aniline **85** and a Sandmeyer-type reaction with SO_2 and a chloride source. Finally, nitrobenzene **86** could be obtained from commercially available 2,6-dibromo-4-nitroaniline (**88**) through Sonogashira coupling for installation of the dialkyne and a removal of the amino group.

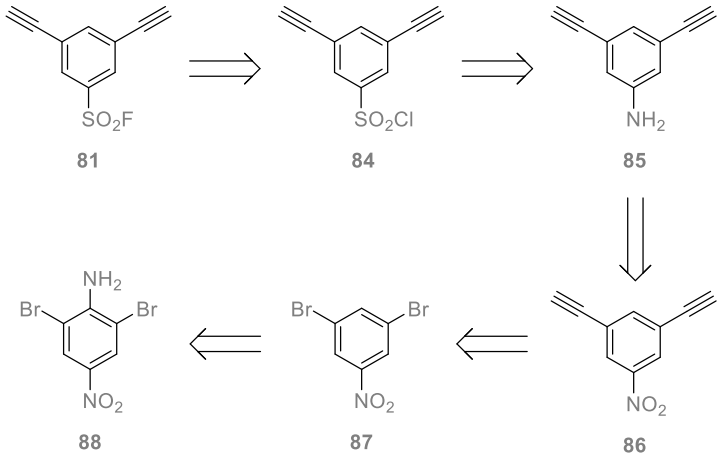

Scheme 36 Alternative retrosynthetic analysis for the synthesis of **81**

The forward synthesis of **81** began with the removal of the amino group in aniline **88** via formation of a diazonium salt followed by a reduction to form **87** in good yield. Subsequent Sonogashira coupling of **87** with (trimethylsilyl)acetylene followed by *in situ* TMS

deprotection afforded **86** in 68% yield. **86** was then reduced to the corresponding aniline **85** using $SnCl_2$ in 85% yield (Scheme 37).

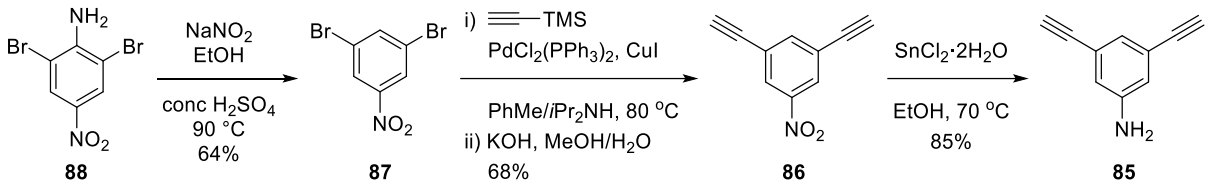

Scheme 37 Synthesis of aniline intermediate **85**.

The conversion of aniline **85** to sulfonyl chloride **84** was performed via diazotisation followed by a Sandmeyer-type reaction. Initially, the procedure from Hogan *et al.*[375] was employed because of its practicality—as it does not involve the use of SO_2 gas—but the reaction was unsuccessful, yielding an unidentified product (found m/z = 447.4 (ES^-); NMR showed a substitution at the amino group) (Scheme 38).

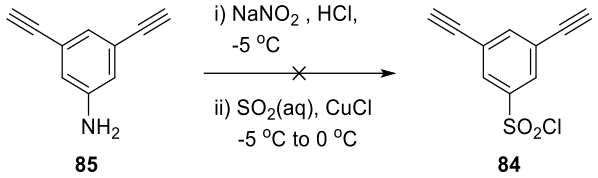

Scheme 38 Attempted chlorosulfonylation via the use of aqueous sulfur dioxide.

Alternative literature conditions, which used SO_2 gas and a copper(II) salt as a catalyst to attenuate the reaction rate,[376] were used to afford the key intermediate **84** in good yield (Scheme 39). The identity of sulfonyl chloride **84** was confirmed by elemental analysis and high-resolution mass spectrometry, as the compound suffered from hydrolysis during the LCMS.

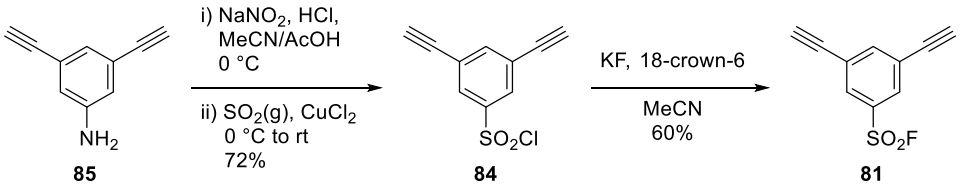

Scheme 39 Conversion of **85** to the aryl sulfonyl fluoride **81**

Sulfonyl chloride **84** was subsequently treated with excess KF and 18-crown-6 as the catalyst to afford the desired 3,5-diethynylbenzenesulfonyl fluoride (**81**) in good yield (Scheme 39).

4.4. Stability and reactivity of aryl sulfonyl fluoride 81

4.4.1. Stability in CuAAC reaction condition

Since aryl sulfonyl fluorides have never been used in CuAAC stapling and considering the ease of hydrolysis of the related sulfonyl chloride, it was essential to test its compatibility to the reaction condition.

To determine the stability of the sulfonyl fluoride moiety, *p*-toluenesulfonyl fluoride, compound **81** and 1,3-diethynylbenzene were subjected to the generic CuAAC reaction condition (condition a). Stability tests were also performed in the presence of the solvents *t*BuOH/H_2O only (condition b). Results of the stability tests are shown in Table 4.

Table 4 Stability test conditions: Condition a: *t*BuOH/H_2O (1:1), 1.1 equiv. of the compound (0.73 mM concentration), $CuSO_4 \cdot 5H_2O$ (1 equiv.), THPTA (1 equiv.) and Na-L-ascorbate (3 equiv.) Condition b: *t*BuOH/ H_2O (1:1), 1.1 equiv. of the compound (0.73 mM concentration).

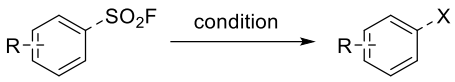

Entry	Compound	Condition	Result
1	*p*-toluenesulfonyl fluoride	a	No decomposition after two days
2	*p*-toluenesulfonyl fluoride	b	No decomposition after two days
3	**81**	a	Approximately 85% decomposition after 24 hours. See Figure 27.
4	**81**	b	No decomposition after two days
5	1,3-diethynylbenzene	a	No decomposition after two days

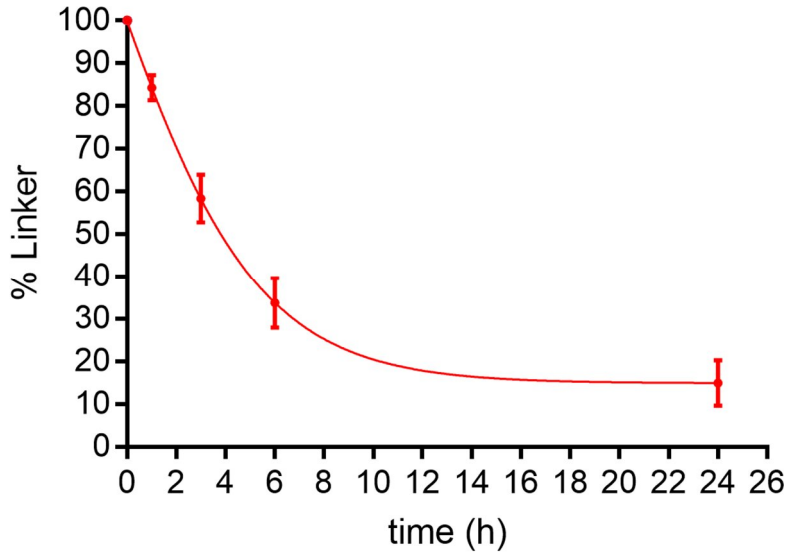

Figure 27 Decomposition of **81** under CuAAC condition showing approximately 85% decomposition after 24 hours. Caffeine was used as an internal standard. Decomposition was monitored by analytical HPLC. The results are an average of two repeats and the errors shown as standard errors of mean.

No decomposition was observed for *p*-toluenesulfonyl fluoride. In contrast, **81** decomposed under CuAAC reaction condition within approximately 24 h but was stable in *t*BuOH/H_2O (Table 3 Entries 3 and 4). 1,3-diethynylbenzene was also stable under the click conditions employed in this study (Table 3 Entry 5).

This observation suggested that the presence of both alkyne and sulfonyl fluoride is essential for the decomposition reaction to occur. The decomposition products could be tentatively identified via LCMS analysis (Figure 28). One decomposition product (peak 15, *m/z* = 205.2 (ES^-)) may correspond to the hydrolysed product of **81** to its corresponding sulfonic acid (calcd *m/z* for $[M-H]^-$ = 205.0) and the other product (peak 16, *m/z* = 189.3 (ES^-)) may correspond to the sulfinic acid (calcd *m/z* for $[M-H]^-$ = 189.0).

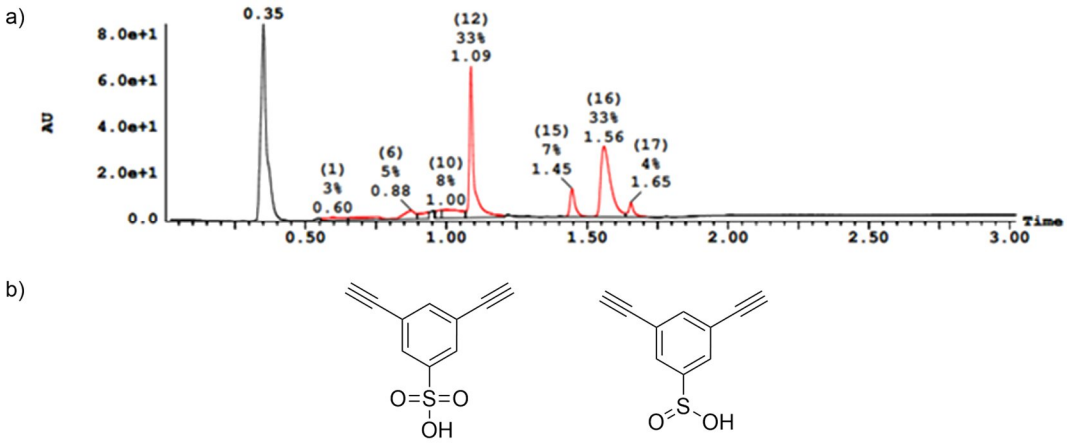

Figure 28 a) UV trace of LCMS analysis of the reaction mixture of linker **81** in Cu-click condition after 23 hours. Peak 12 corresponds to caffeine. b) The two possible decomposition products.

These results suggested that, albeit the decomposition reaction is almost complete in 24 hours, only 40% of the material is decomposed in the first 3 hours. Since the CuAAC reaction has an average reaction completion time of 1 hour,[115] we hypothesised that this could outcompete the undesired decomposition pathway, leading to the formation of the stapled peptide product. Thus, we decided to continue our studies on **81** as candidate staple.

4.4.2. Stability in aqueous media

Next, linker **81** was subjected to stability tests in aqueous media at physiological pH and temperature, with MeCN as a co-solvent to aid dissolution (Figure 29). This experiment was performed to check whether the electrophile would be stable under physiological environment. It was found that the sulfonyl fluoride has a half-life of approximately 24 hours under these conditions.

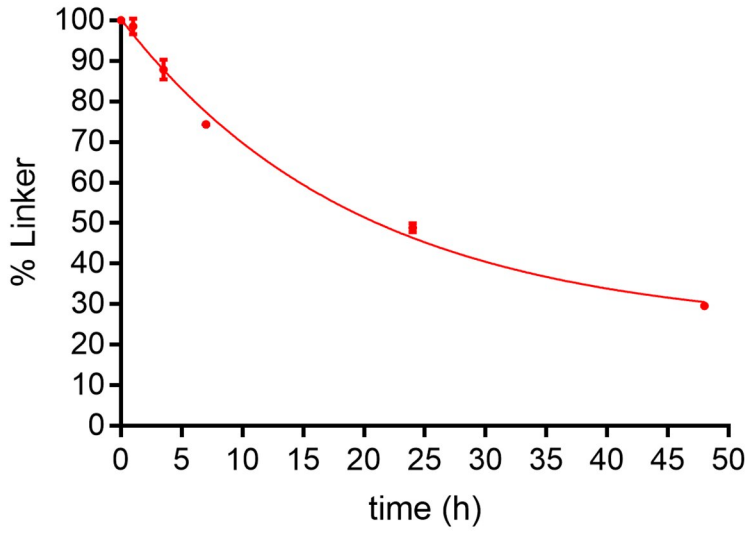

Figure 29 Stability test of linkers **81** in PBS (1x)/MeCN (1.94:1) at 37 °C. Caffeine was used as an internal standard. Decomposition was monitored by analytical HPLC. The results are an average of two repeats and the errors shown as standard errors of mean. For some data points, the error bars are smaller than the markers.

4.4.3. Reactivity against lysine

To assess the ability of the linker to react with Lys, **81** was incubated with *N*α-Ac-Lys-OH in PBS (1x): MeCN at 37 °C (Figure 30). Fifty equivalents of Lys were employed to mimic the high local concentration of the Lys side chain when the electrophile is in close proximity. Under these conditions, the aryl sulfonyl fluoride was found to undergo conjugation and hydrolysis at a similar rate. Approximately 46% of **81-Lys** and 49% of **81-OH** were detected after 23 hours.

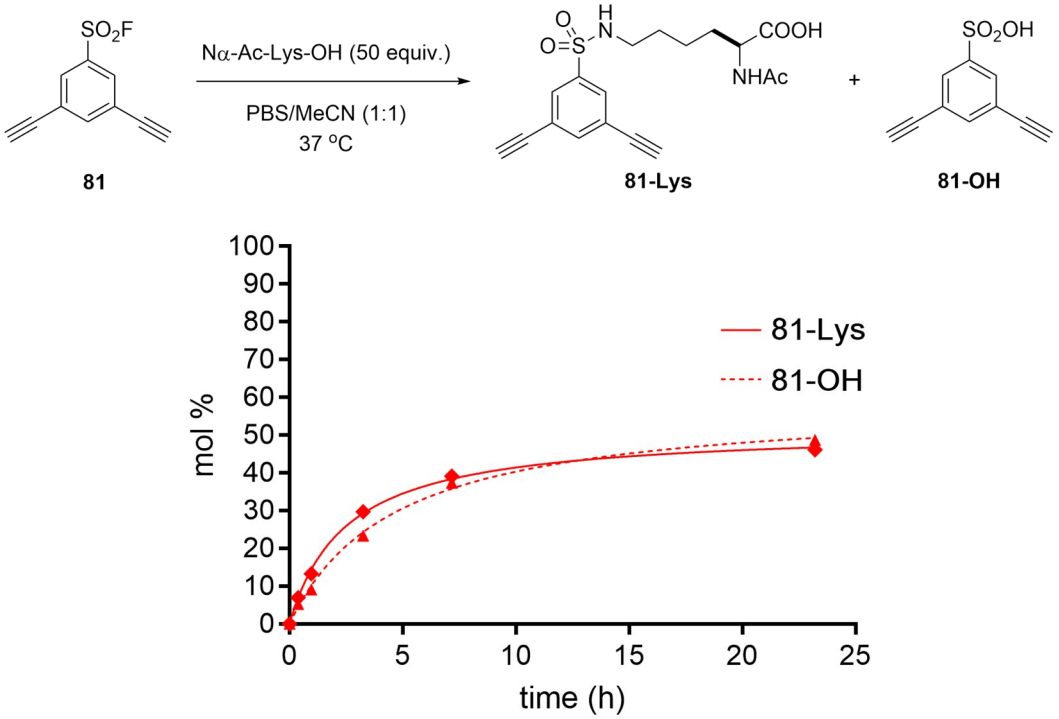

Figure 30 Reactivity of linker **81** against *N*α-Ac-Lys-OH. Conditions: PBS (1x)/MeCN (1:1), 37 °C, linker at 1 mM concentration, *N*α-Ac-Lys-OH (50 equiv.). Caffeine was used as an internal standard. Reactions were monitored by LCMS. The results are the average of two repeats. For all data points, the error bars are smaller than the markers.

While the reactivity of the sulfonyl fluoride was not ideal, its good stability in aqueous media prompted us to further investigate this linker. To evaluate whether these results correlate to the ability to form a covalent complex with MDM2, we decided that a stapled peptide with compound **81** as a linker would be synthesised.

4.5. Synthesis of linear and stapled peptides

4.5.1. Synthesis of unnatural azido amino acid

Synthesis of the proposed peptide **P1** required the synthesis of the azido amino acid ornithine **90**, which was carried out as previously reported in the literature (Scheme 40).[102] The first step was the Boc-deprotection of the commercially available Fmoc-Orn(Boc)-OH, followed by copper-catalysed diazo transfer reaction to afford **90** in a moderate yield.

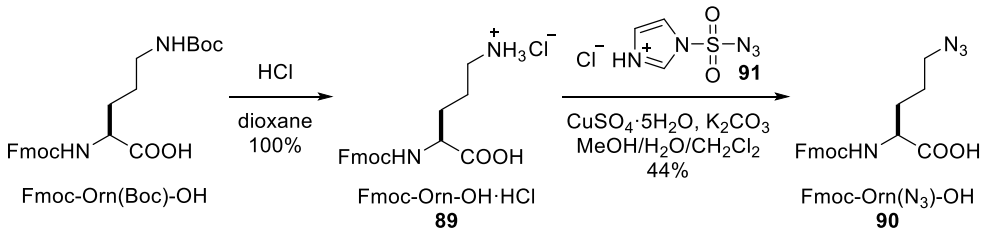

Scheme 40 Synthesis of Fmoc-protected azido ornithine **90**

The diazo-transfer reagent **91** used in the above reaction was synthesised in large scale following a literature procedure giving **91** in moderate yield (Scheme 41).[377]

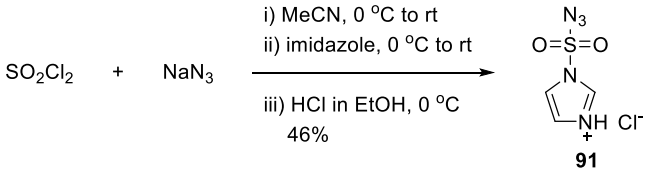

Scheme 41 Synthesis of diazo-transfer reagent **91**.

4.5.2. Initial click reactions

The peptide Ac-LTFEXYWAALTX-NH_2 (**P1**) was synthesised by standard Fmoc solid-phase peptide synthesis (SPPS) protocol on LL Rink Amide resin (0.40 mmol/g) using DIPEA and HATU in DMF as the base and the coupling reagent respectively. The amount of **P1** obtained was very low, possibly because of its high lipophilicity, causing a loss of material during the HPLC purification process. Evidencing this lipophilicity, **P1** showed poor solubility in *t*BuOH/H_2O (1:1), which we hypothesised that could be caused by the lack of positively charged residues in the sequence. The incorporation of nucleophilic amino acids was avoided due to the presence of the sulfonyl fluoride on the linker. MeOH, DMF, DMSO or further addition of *t*BuOH did not dissolve **P1**. Regardless of this issue, the click reaction between **P1** and linker **81** was attempted in DMSO/H_2O/*t*BuOH (2:1:1), expecting that the small amount of **P1** in solution would undergo stapling and push the solid–aqueous equilibrium of **P1** towards the aqueous phase. After four days, no stapled product was observed through LCMS, so stapling of **P1** was abandoned.

4.5.3. Attempts to improve the solubility of the linear peptide

Peptide **P1** was based on the **PDI-E** sequence[103] with its staple position moved from the 4th and 11th to the 5th and 12th positions. Thus, 4th and 11th positions were reverted to Glu and Thr from the original PDI sequence. Sawyer and co-workers found that the H5E and H5A mutations on the PDI sequence lead to a four-fold increase and four-fold decrease in aqueous media solubility, respectively.[100] Therefore, the H5X mutation may have had a deleterious

effect on the solubility. However, our target peptide requires those particular staple positions to efficiently target the Lys94 of MDM2. Thus, we decided to synthesise two variants: **P2** with A8S mutation and **P3** with L1E and A8S mutations based on the sequence **PDI-Q** published by Chen *et al*. (Table 5).

Table 5 Diazidopeptides based on phage display peptide **PDI** and their variants.

Peptide	Sequence
PDI	H-LTFEHYWAQLTS-OH
PDI-E	Ac-LTFXEYWAQLXS-NH_2
PDI-Q	H-ETFEHWWSQLLS-NH_2
P2	Ac-LTFEXYWSALTX-NH_2
P3	Ac-ETFEXYWSALTX-NH_2

However, the single mutation in **P2** did not improve the solubility. Prior to purification, dissolution of crude **P2** was done in DMSO as its solubility in MeCN/H_2O (the solvent system used on the HPLC) was low. In DMSO, peptide **P2** formed a jelly-like semi-solid. Further addition of DMSO and sonication turned it into a cloudy suspension. As a result, the purification of **P2** was not attempted.

While pure **P3** had a noticeably better solubility in DMSO, it could not be dissolved completely in *t*BuOH/H_2O (1:1) despite the use of a small amount of DMSO. Nonetheless, the CuAAC reaction in the presence of **81** and **92** (a non-electrophilic linker; to be used as a negative control peptide) was again attempted (Scheme 42).

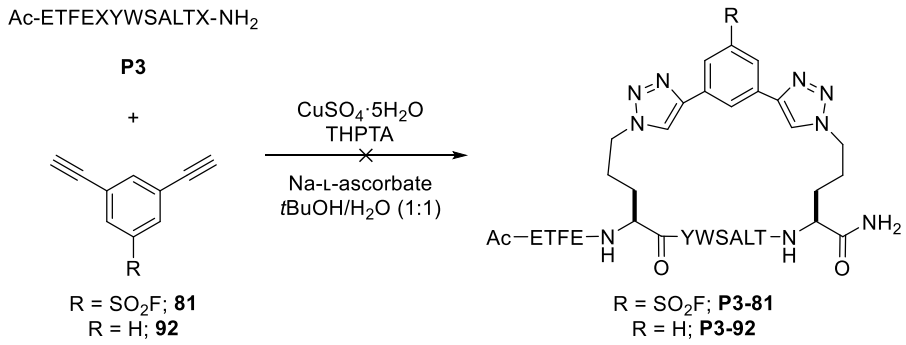

Scheme 42 CuAAC reaction between **P3** and the linkers **81** and **92**

After three days, the reactions showed the presence of insoluble material, so it was decided to warm the reaction to 37 °C to aid the solubility. However, no visual change was observed after three hours. The reaction was therefore worked up, and the presence of traces of the desired product were found via LCMS analysis in both the reaction mixture and the crude product, with no purification possible.

Altogether, further alternatives to improve solubility were explored. In the literature, several ways of improving the solubility of polypeptides included fusion with solubilising proteins such as maltose-binding protein (MBP),[378] *N*-utilisation substance A (NusA),[379] thioredoxin,[380] glycosylation,[381,382] PEGylation,[383] and *N*-terminal capping with trimethylglycine (betaine).[384]

Most of the aforementioned methods require the addition of large masses to the peptide, whereas the *N*-terminal capping with trimethylglycine only required the addition of one amino acid and looked the most feasible for our purpose.

Additionally, the *C*-terminal amide was replaced with carboxylic acid, and an A8N mutation (**P5**) was included as asparagine should be more solubilising than serine. A variant with an uncapped *N*-terminus (**P4**) was also synthesised (Table 6).

Table 6 Second generation of peptides with additional solubilising components. The sequence of **P3** is also shown, and changes are highlighted in red.

Peptide	Sequence
P3	Ac-ETFEXYWSALTX-NH_2
P4	H-ETFXEYWNALTX-OH
P5	Tmg-ETFXEYWNALTX-OH

Tmg = 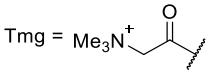

In order to obtain the *C*-terminal carboxylic acid, 2-chlorotrityl resin was used for the synthesis of **P4** and **P5**. The 2-chlorotrityl resin was chosen over Wang resin because of its milder conditions for attaching the first amino acid, which lowers the possibility of racemisation. Although pre-loaded Wang resins are commercially available, the first amino acid needed in this study was the unnatural azido amino acids; none of the commercially available pre-loaded resins features that specific amino acid. The 2-chlorotrityl resin is a high loading resin (1.22 mmol/g); therefore, it was only partially loaded to reduce steric hindrance later on in the synthesis, and the rest of the sites capped with MeOH. The substitution rate was determined by UV absorbance at 301 nm (for the release of the Fmoc group in deprotection), and it was found to be at 0.22 mmol/g. Most of the amino acids required double coupling during the peptide synthesis.

The *N*-terminal capping of **P5** with trimethylglycine proved to be problematic. Owing to its zwitterionic character, trimethylglycine has poor solubility in DMF and could not be dissolved to 0.4 M concentration (the usual concentration for manual SPPS). However, a 0.2 M solution could be made. Even with the use of excess trimethylglycine, longer coupling times and repeated couplings, full conversion was not observed (both **P4** and **P5** were observed on LCMS from trial cleavage). Coupling with PyBOP, an alternative coupling reagent, was also attempted but did not give full conversion. Although the reaction did not proceed to full conversion, the peptide was cleaved from the solid support and purified. **P5** was not obtained in a pure form due to the retention time on the HPLC being very similar to **P4**. In addition, another impurity with very close retention time, which may be a deletion sequence of **P5** where an Ala residue was missing (m/z = 1579.1 (ES^-)), was observed.

Despite the solubility-enhancing modifications, **P4** and **P5** still only showed partial solubility at 1 mg/mL concentration in *t*BuOH/H_2O (1:1). The CuAAC reactions of **P4** with 1,3-diethynylbenzene (**92**) and the linker **81** were attempted. The stapled products were detected on the LCMS, but purification was not attempted due to the small amount of material.

Thereafter, we decided to explore the solvent system used in the click reaction. While DMF and MeCN, either neat or as a mixture with water, failed to dissolve **P4** and **P5**, it was found that DMSO/H_2O (11:4) could give a complete dissolution of both peptides. Therefore, the CuAAC reactions were performed using this solvent system (Table 7).

Table 7 Isolated yields for stapled peptides from CuAAC reactions DMSO/H_2O (11:4)

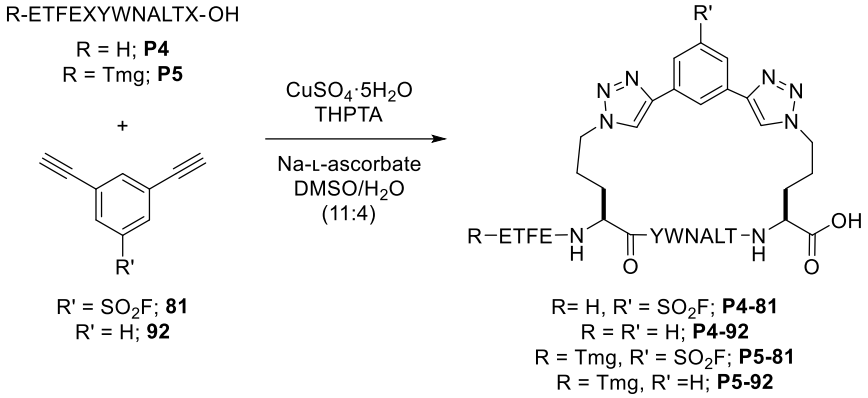

Peptide	Isolated yield (%)
P4-81	0[a]
P4-92	0[a]
P5-81	7[b]
P5-92	trace

[a]Chromatogram turned complicated upon solvent removal, thus no product could be isolated. [b]64% purity.

At first, **P4** and **P5** were reacted with 1.1 equivalents of **92** at a concentration of 1.0 mg/mL. The reaction proceeded to completion within 30 minutes, but a significant proportion of 1:2 peptide-linker linear clicked peptide was formed (Figure 31 and 32). The 1:1 peptide linker complex was confirmed to be the stapled product by further addition of 1,3-diethynylbenzene (**92**) and the Cu-click reagent, at which no changes were observed.

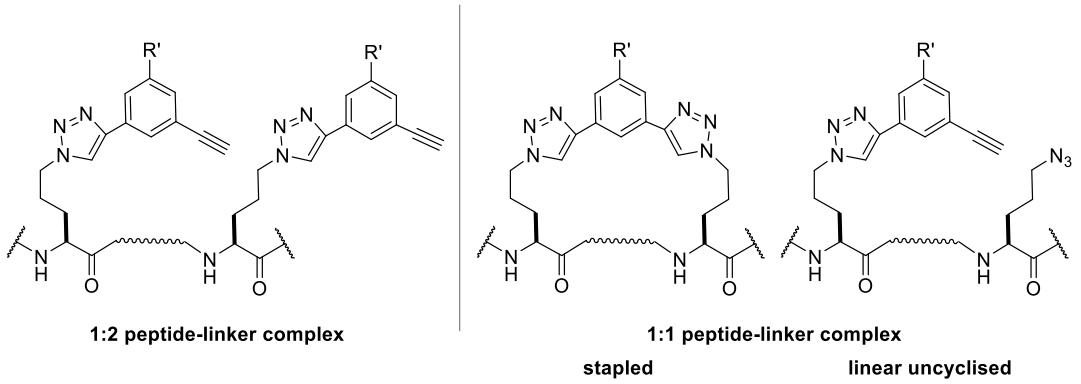

Figure 31 General possible products from CuAAC reaction between a diazidopeptide and a dialkynyl linker

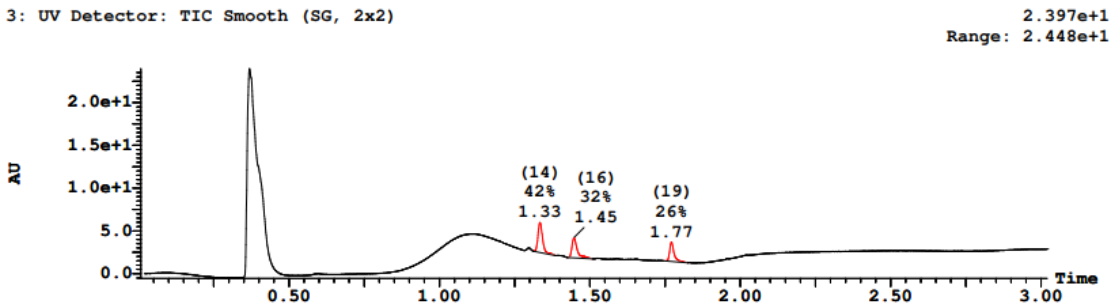

Figure 32 LCMS UV trace from reaction between **P4** and 1,3-diethynylbenzene (**92**). Peak (14), (16), (19) correspond to 1:1 peptide linker complex (*m/z* = 841.0, $[M+2H]^+$), 1:2 linear peptide linker complex (*m/z* = 1807.4, $[M+H]^+$), and 1,3-diethynylbenzene, respectively.

The purification of **P4-92** was unsuccessful due to chromatogram turning complicated after solvent removal. On the other hand, **P5-92** was purified by HPLC, but the obtained stapled peptide was impure and only available in a small amount due to the significant loss caused by the formation of the 1:2 peptide linker complex.

To reduce the formation of the 1:2 linear peptide linker complex in the click reaction, the peptide concentration was reduced to 0.8 mg/mL (0.5 mM) and the number of equivalents of the linker reduced to 1 equivalent. Under these conditions, the reactions of **P4** and **P5** with linker **81** showed the desired product in their respective reaction mixtures via LCMS analysis (Figure 33).

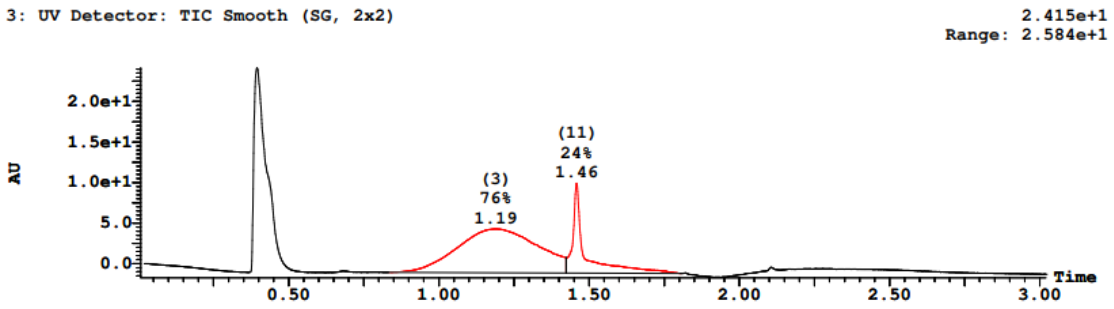

Figure 33 LCMS UV trace from reaction between **P4** and linker **81**. Peak (11) corresponds to 1:1 peptide-linker complex (*m/z* = 1763.2, $[M+H]^+$).

Unfortunately, similar to **P4-92**, the purification of **P4-81** was not possible due to chromatogram turning complicated after solvent removal. On the other hand, **P5-81** could be obtained, albeit with only 64% purity.

4.5.4. Refinement of the peptide sequence

The difficult synthesis of the linear peptide **P5**, its corresponding stapled peptides, and the low solubility of PDI-derived peptides led to a reconsideration of a different peptide sequence. PMI (H-TSFAEYWNLLSP-OH) was shown to be a potent MDM2-binding peptide from a phage display library and therefore represented an excellent alternative.[385] PMI was reported to be more soluble in an aqueous environment and equipotent to PDI.[385]

A hydrocarbon-stapled PMI and double-click-stapled PMI have been made previously in the Lane[101] and Spring groups respectively.[103] In both cases, the 4th and 11th positions were used as the stapling positions, and Pro12 was removed from the sequence as it was not critical for the binding.[101]

Similar to the initial design, the 5th and 12th positions of the peptide appeared to be the best residues for replacement by the azido amino acids to allow the staple to be in the correct position—close to the target Lys94. In addition, molecular dynamics simulation of covalent peptide–MDM2 complex that used 3,5-diethynylbenzenesulfonyl fluoride (**81**) as the staple showed that an L9G mutation was necessary to avoid Leu10 from pulling away from the binding pocket (Figure 34). Therefore, the sequence Ac-TSFAXYWNGLSX-NH_2 (**P6**) was adopted as the new linear and more soluble sequence.

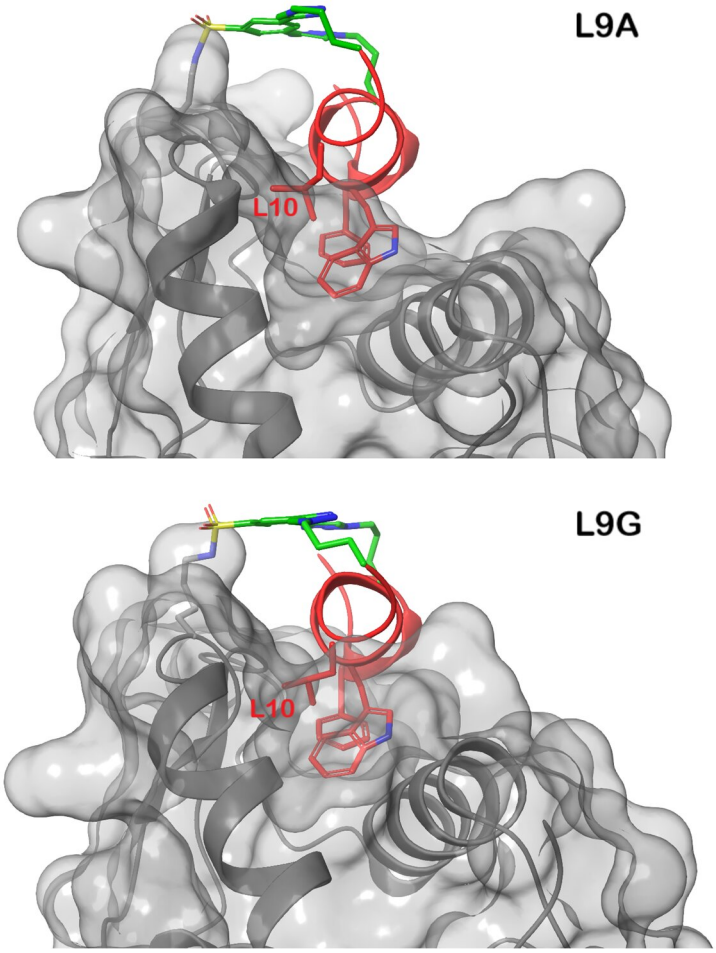

Figure 34 Molecular dynamics simulation of PMI stapled peptide (red) covalently linked with MDM2 (grey) via a sulfonamide linkage. L9A mutation resulted in Leu10 pulling away from the pocket, whereas L9G did not.

P6 was then synthesised by automatic SPPS and was found to be more soluble in *t*BuOH/H_2O (1:1) than the previously synthesised PDI-based peptides.

4.6. Synthesis and biological evaluation of sulfonyl fluoride–bearing stapled peptide

With the optimised peptide sequence and the staple for covalent targeting of Lys in hand, we decided to merge the two motifs and assess the binding of the stapled peptides.

4.6.1. Computational binding energy for non-covalent binding of PMI stapled peptides

To assess the non-covalent binding of the peptides to MDM2, molecular dynamics simulations were performed for the linear peptide **P6** and the stapled peptide **P6-81** (dialkyne **81** as the linker). Data for the wild-type p53 peptide was also obtained for comparison (Table 10). The simulations were performed by Dr Yaw Sing Tan.

Table 8 Calculated binding energy data from molecular dynamics simulation for linear peptide **P6**, the stapled peptides **P6-28** and **P6-15**, and p53 peptide. Computation was performed by Dr Yaw Sing Tan.

Peptide	ΔH / kcal mol^{-1}	TΔS / kcal mol^{-1}	ΔG / kcal mol^{-1}
P6	−53.67 ± 2.42	−37.47 ± 1.65	−16.20 ± 2.92
P6-81	−47.66 ± 0.82	−35.34 ± 2.51	−12.32 ± 1.96
p53 peptide[†]	−56.8 ± 0.9	−44.1 ± 2.9	−12.7 ± 3.8

[†]The sequence is Ac-ETFSDLWKLLPEN-NH_2. The energies were obtained from Tan *et al*. for comparison purposes.[386]

The simulation indicated that the linear peptide **P6** would be a better binder than the p53 peptide. However, the stapling appeared to weaken the binding by approximately 4 kcal mol^{-1}. Whilst this was not favourable, the stapled peptide should still be able to compete with the p53 peptide, and the covalent linkage should permanently inhibit MDM2.

4.6.2. Synthesis of stapled peptides

The stapled peptide **P6-81** and its negative control for covalent attachment, **P6-92**, were successfully synthesised by CuAAC reactions (Scheme 43). A small amount of DMSO was used to pre-dissolve **P6** to ensure full solubility in *t*BuOH/H_2O (1:1). The stapled peptides were purified by RP-HPLC and characterised by analytical HPLC and LCMS.

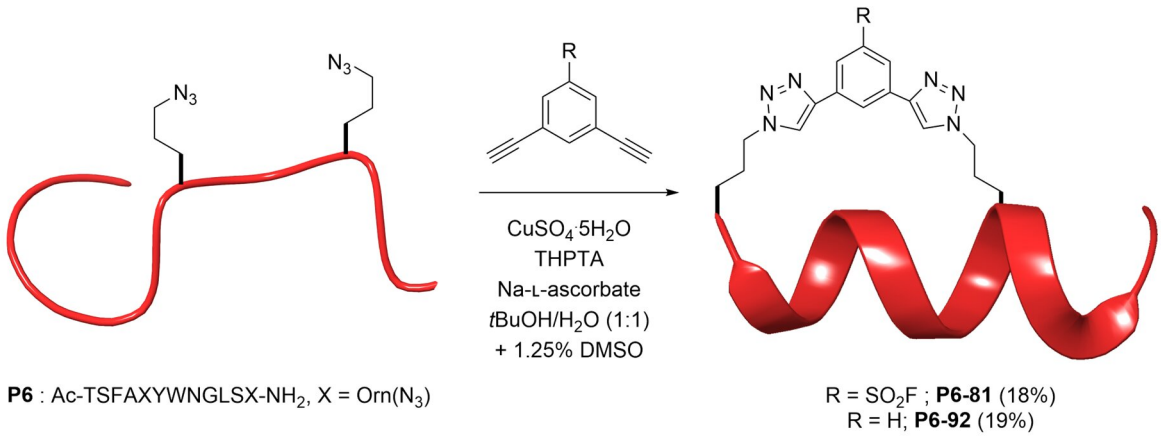

Scheme 43 Two-component CuAAC stapling between peptide **P6** and staples **81** and **92**.

4.6.3. Biological testing

With the isolated stapled peptides in hand, we first verified their ability to covalently bind the target protein. The stapled peptides were incubated with MDM2 in PBS buffer 37 °C for 1 hour. The mixture was then analysed for any covalent cross-linking using mass spectrometry. The assay was performed in collaboration with Dr Stephen Walsh from the Spring Group.

The incubation of MDM2 with **P6-81** resulted only in a small amount of the sulfonamide covalent complex formed (mass 15380 Da) (Figure 35b). For the incubation of MDM2 with **P6-92**, the non-electrophilic control stapled peptide, detection of a peptide–MDM2 complex was not observed under the same assay condition (Figure 35c).

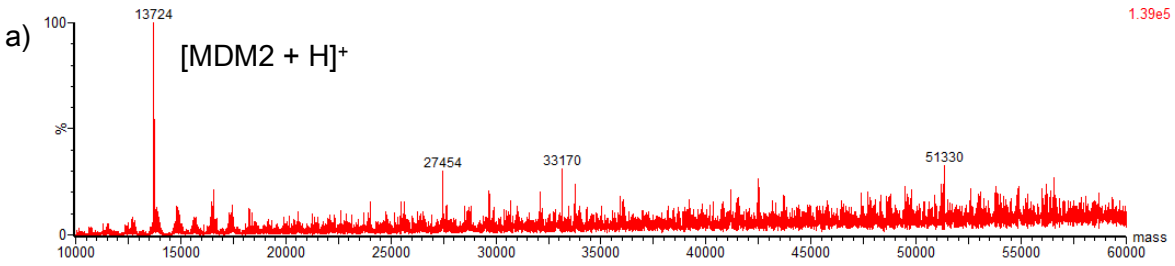

Figure 35 a) ESI-MS spectrum of unmodified MDM2 (6–125), showing its mass at 13724 Da.

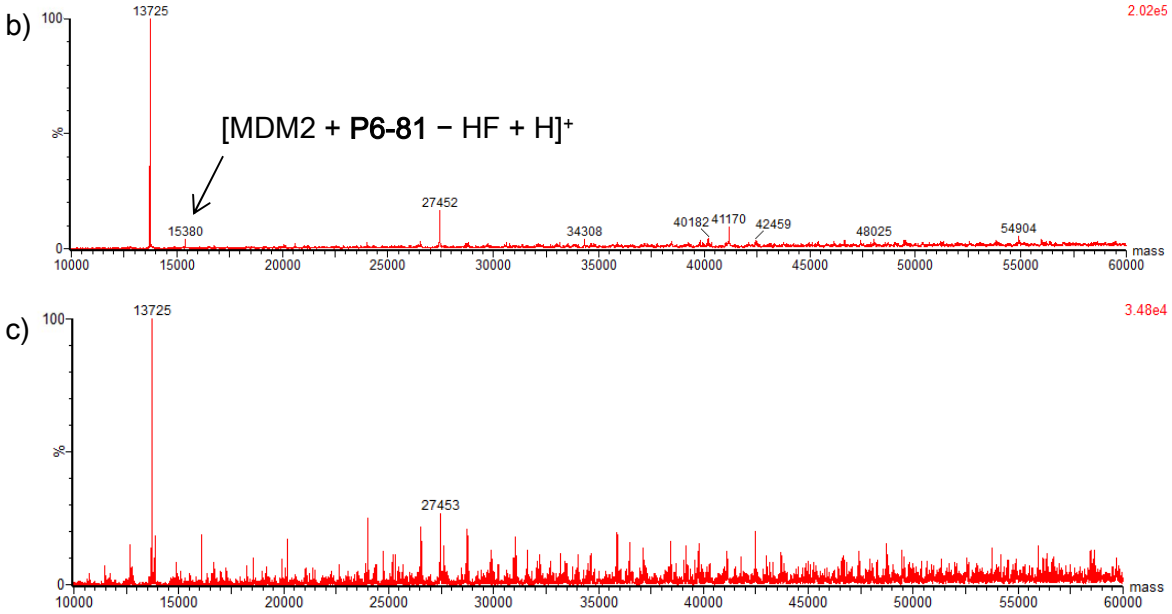

Figure 35 (continued) b) **P6-81** (2 μM) was incubated with MDM2 (1 μM) in PBS buffer (+ 0.01% Tween + 3% DMSO) at 37 °C for 1 hour.* The ESI-MS spectrum showed only a small amount of MDM2 was modified. [MDM2 + **P6-81** − HF + H]$^+$ = 15380 Da. c) Non-electrophilic **P6-92** was incubated with MDM2 under the same condition as in b). Unmodified MDM2 was observed.

Next, the apparent dissociation constant ($K_{d,app}$) of **P6-81** to MDM2 was examined and compared to the non-covalent peptides using a competitive fluorescence polarisation (FP) assay (Table 9 and Figure 36).[101,102] The assay was performed by Dr Rohan Eapen from the Itzhaki Group, Department of Pharmacology. The linear diazidopeptide **P6** was found to have an attenuated affinity for MDM2 (K_d = 47.8 ± 1.5 nM) compared to the wild-type (WT) PMI (K_d = 16.6 ± 0.2 nM).[385] Pleasingly, the stapled peptide **P6-92** showed an affinity comparable to the WT (K_d = 19.3 ± 0.3 nM). Crucially, over the course of 120 minutes,† these dissociation constants did not change significantly (Figure 36a–c). **P6-81**, which contains the aryl sulfonyl fluoride moiety, displayed a diminished binding affinity (K_d = 112.9 ± 4.2 nM), in agreement with the predicted lower binding energy compared to **P6**. In addition, in line with the observation from the mass spectrometry experiment, no appreciable changes in its binding affinity were found throughout the assay (Figure 46d). Hence, this confirmed that the sulfonyl fluoride–bearing stapled peptide does not exhibit substantial covalent binding to MDM2.

* The conditions for the incubation between P6-81 and MDM2 were different from further experiments as a preliminary result. No further mass spectrometry experiments were conducted with P6-81.

† Due to the instability of MDM2 in the assay, no data from time-points beyond 120 minutes were obtained.

Table 9 Binding affinities of linear and stapled peptides from competitive FP assays, conducted by Dr Rohan Eapen.

Peptide	K_d (nM)†
WT PMI	16.6 ± 0.2
P6	47.8 ± 1.5
P6-81‡	112.9 ± 4.2
P6-92	19.3 ± 0.3

†The K_d values are the average of every time point, and the errors are standard errors of mean. ‡Quoted as K_d as no significant changes were observed over the course of the assay.

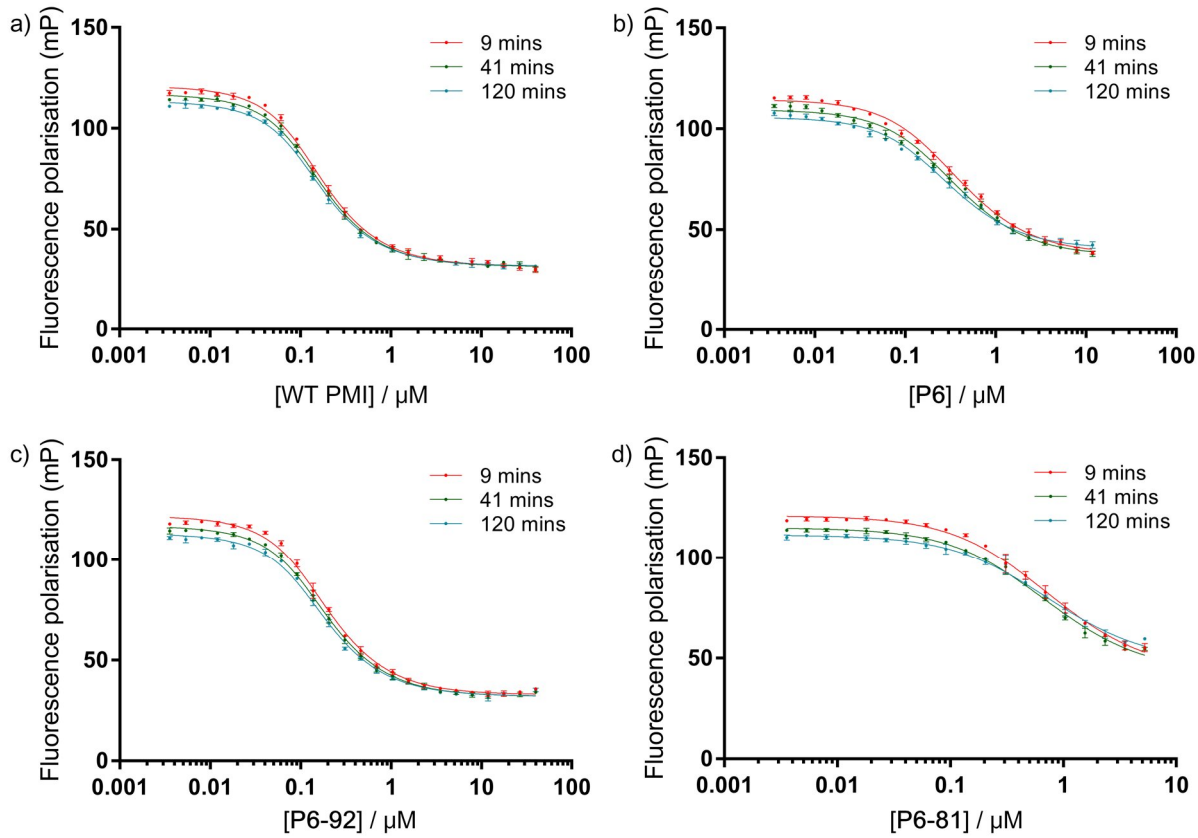

Figure 36 Competitive FP assay binding curves over two hours of a) WT PMI b) **P6** c) **P6-92** d) **P6-81**. The four peptides show no change in the binding curves over the course of the assay; Each curve represents one time point: 9 min (red), 41 min (green), and 120 min (blue). Each data point is arithmetic mean of triplicate, and the errors shown are standard errors of mean.

Considering the low reactivity and unsatisfactory MS and FP results of **P6-81**, we decided to explore alternative electrophilic moieties for the linker.

4.7. Exploring alternative electrophiles for covalent bond formation

A recent study by Cravatt and co-workers has shown that each lysine residue has its own unique reactivity and preference towards different electrophiles depending on its function

and location.[387] This prompted us to expand the electrophiles pool to improve the chance of successfully achieving the covalent interaction on the MDM2.

Two potential alternative electrophilic linkers, chosen based on the precedent of reactive functionalities used for lysine modification in the literature, comprised sulfotetrafluorophenyl ester (STP) ester **93** and 2,4-dinitrophenyl ester **94** (Figure 37). These activated esters were selected for their harder electrophilic character, which would make them more selective towards an amine attack as well as more stable towards GSH. Indeed, similar compounds with dinitrophenoxide and tetrafluorophenoxide as leaving groups have been used as a probe for proteomic profiling for lysine reactivity.[387]

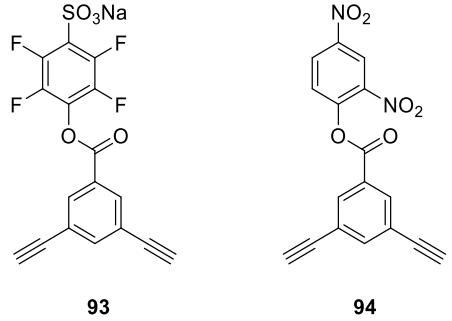

93 **94**

Figure 37 Two candidates as new electrophilic moieties.

We envisioned that activated esters **93** and **94** could be made from a coupling between 3,5-diethynylbenzoic acid and the corresponding phenols which are commercially available (Scheme 44).

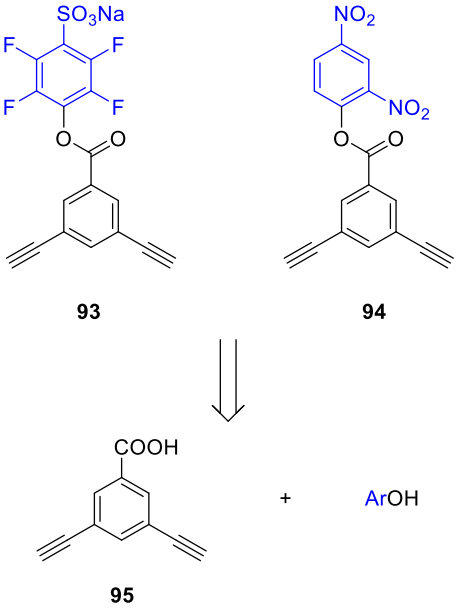

93 **94**

95

Scheme 44 Retrosynthetic analysis of the activated esters **93** and **94**.

The synthesis of **93** and **94** started from the synthesis of 3,5-diethynylbenzoic acid (**95**), which was carried out as previously reported by Lau *et al.*[102] (Scheme 45). Commercially available methyl 3,5-dibromobenzoate underwent a double Sonogashira coupling with

trimethylsilylacetylene to form compound **96** in good yield. Ester **96** was hydrolysed, and its TMS group simultaneously deprotected with the treatment of aqueous 6 M KOH in THF to form the desired benzoic acid **95** in moderate yield.

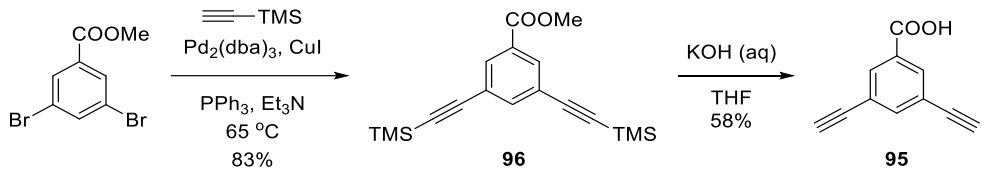

Scheme 45 Synthesis of 3,5-diethynylbenzoic acid (**95**). dba = dibenzylideneacetone.

Benzoic acid **95** was then coupled with the corresponding phenols to form the activated esters **93** and **94** (Scheme 46). Following literature procedures for similar compounds,[388] **93** was formed via the use of DCC, while **94** was generated through an acid chloride intermediate.

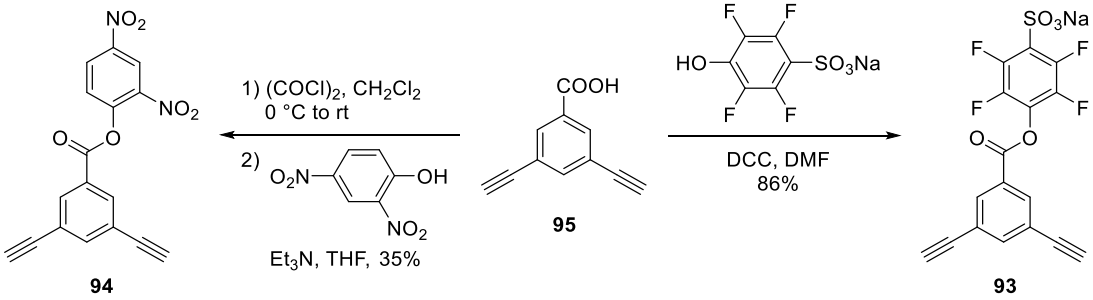

Scheme 46 Synthesis of activated esters **93** and **94**.

4.8. Reactivity and stability of the activated ester linkers

To enable a comparison of aqueous stability and reactivity to aryl sulfonyl fluoride **81**, kinetic studies of the activated esters **93** and **94** were performed.

4.8.1. Stability in CuAAC reaction condition for the activated esters

Stability test of **93** in CuAAC reaction condition was conducted to determine its compatibility with our Cu-click stapling (Figure 38). Linker **93** decomposed to benzoic acid **95** by approximately 15% after 24 hours. In comparison, about 85% of aryl sulfonyl fluoride **81** decomposed in the same period of time.

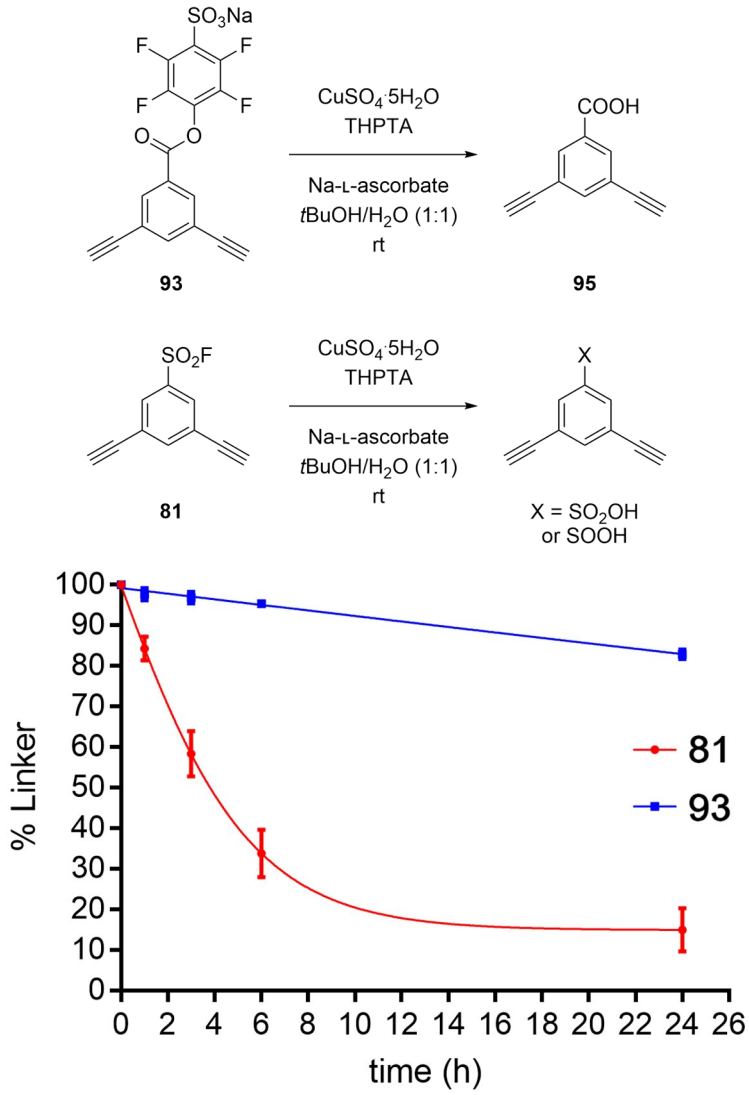

Figure 38 Decomposition of **93** and **81** under CuAAC condition. Stability test condition: *t*BuOH/H_2O (1:1), 1.1 equiv. of the compound (0.73 mM concentration), $CuSO_4 \cdot 5H_2O$ (1 equiv.), THPTA (1 equiv.) and Na-L-ascorbate (3 equiv.) at rt. Caffeine was used as an internal standard. Reactions were monitored by analytical HPLC. The results are average of two repeats and the errors shown as standard errors of mean. For some data points, the error bars are smaller than the markers.

Linker **94** proved to be only partially soluble in *t*BuOH/H_2O (1:1). Moreover, it was observed that linker **94** in *t*BuOH/H_2O (1:1) underwent hydrolysis, confirmed by the appearance of **95** on the LCMS ($[M-H]^-$ found m/z = 169.1, calcd m/z = 169.0). Considering this evidence, linker **94** was excluded from further investigation.

4.8.2. Stability in aqueous media

Linker **93** was also subjected to stability tests in aqueous media at physiological pH and temperature, the same as previously described in section 4.4.2. Results are shown, together with data of linker **81** for comparison, in Figure 39. The STP ester **93** was found to have

comparable stability to the sulfonyl fluoride **81** under the test condition. Both compounds underwent hydrolysis by approximately 50% after 24 hours.

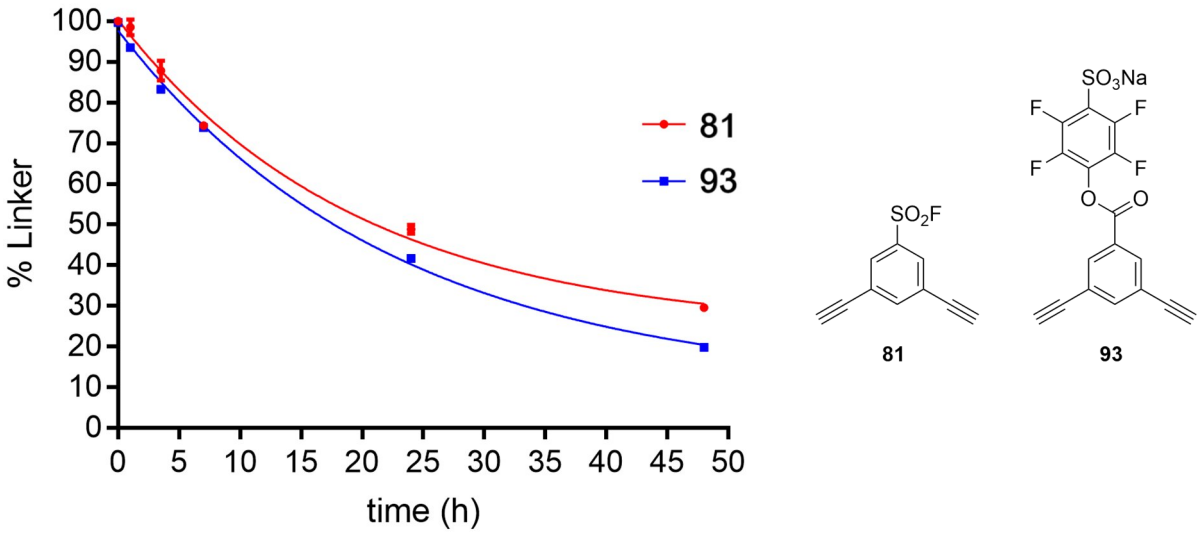

Figure 39 Stability test of linkers **81** and **93** in PBS (1x)/MeCN (1.94:1) at 37 °C. Caffeine was used as an internal standard. Reactions were monitored by analytical HPLC. The results are an average of two repeats and the errors shown as standard errors of mean. For some data points, the error bars are smaller than the markers.

4.8.3. Reactivity against nucleophilic amino acids

To compare the reactivities of the two linkers towards Lys, **81** and **93** were subjected to reactions against *N*α-Ac-Lys-OH in PBS (1x)/MeCN at 37 °C. Similarly to section 4.4.3, 50 equivalents of Lys were initially employed to mimic the high local concentration of the Lys side chain when the electrophile is in close proximity. In contrast to linker **81**, the reaction with linker **93** was very fast (over 30% conversion under 5 minutes), making the reaction monitoring difficult. Thus, the amount was decreased to 2 equivalents (Figure 40).

The STP ester **93** showed a faster reactivity against Lys compared to the sulfonyl fluoride **81** (5% conjugation for **81** vs 95% conjugation for **93** after four hours). Remarkably, a negligible amount of **93** underwent hydrolysis, in contrast with **81** which hydrolysed significantly.

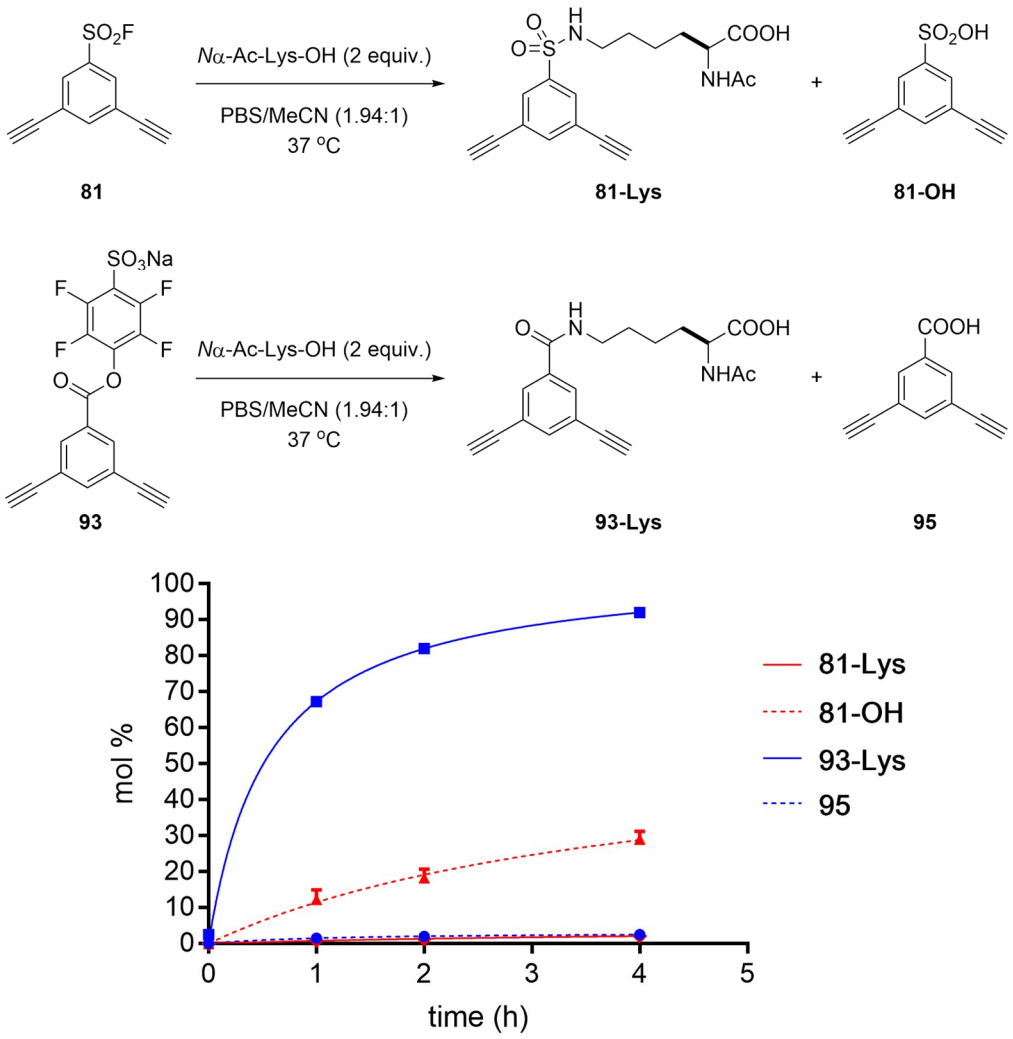

Figure 40 Reactivity comparison between linkers **81** and **93** against *N*α-Ac-Lys-OH. Conditions: PBS (1x)/MeCN (1.94:1), 37 °C, linker at 1 mM concentration, *N*α-Ac-Lys-OH (2 equiv.). Caffeine was used as an internal standard. Reactions were monitored by analytical HPLC. The results are average of two repeats and the errors shown as standard errors of mean. For some data points, the error bars are smaller than the markers.

Given these data, we could establish that the activated ester **93** is a superior electrophile for our purpose. Whilst the STP ester is similarly stable to sulfonyl fluoride **81**, its much higher reactivity towards Lys makes it a more suitable electrophile for targeting Lys residues.

To shed light on the selectivity of linker **93** against other nucleophilic side chains, the STP ester was also reacted with *N*α-Ac-Cys-OH. However, it was observed that the rate of reaction of **93** against Cys is almost identical to that against Lys under the same conditions (Figure 41).

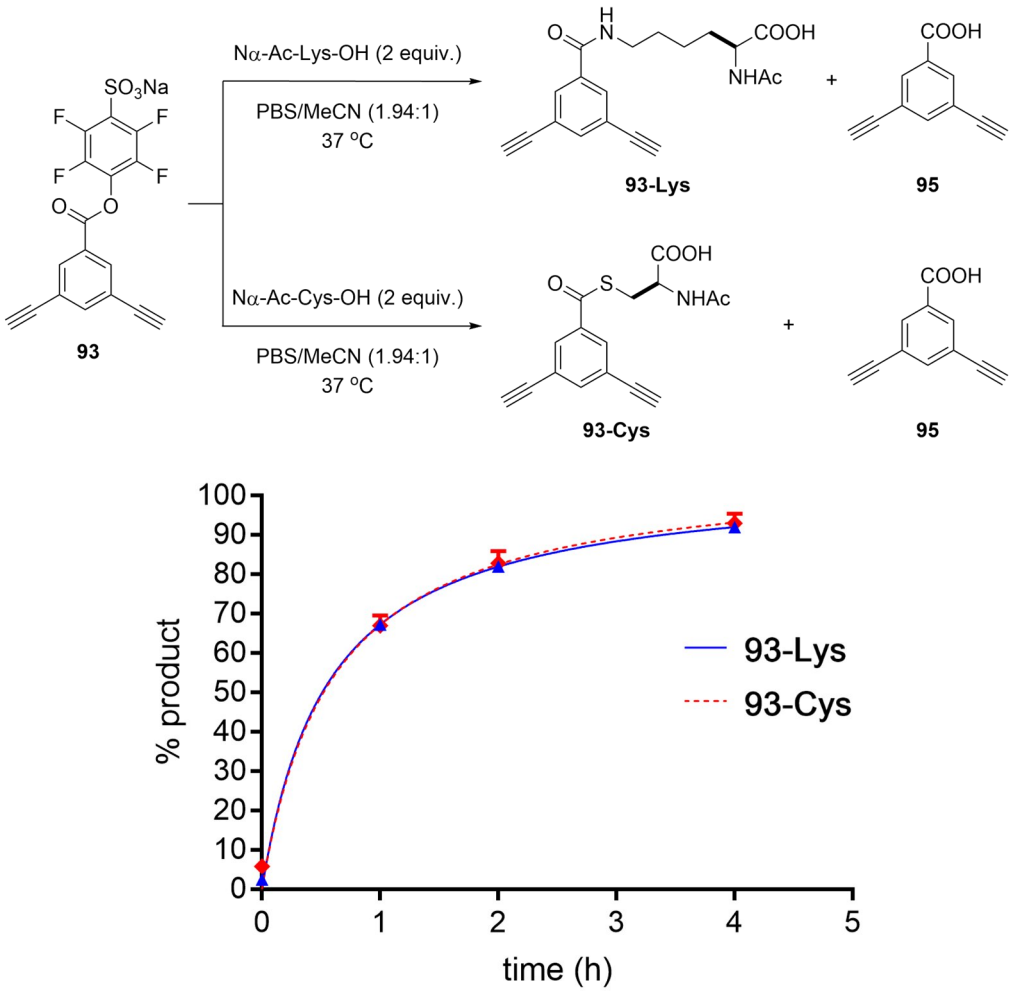

Figure 41 Comparison between the reactivity of linker **93** against *N*α-Ac-Lys-OH and *N*α-Ac-Cys-OH. The amount of hydrolysed products were negligible and thus not shown. Conditions: PBS (1x)/MeCN (1.94:1), 37 °C, linker at 1 mM concentration, amino acid (2 equiv.). Caffeine was used as an internal standard. Reactions were monitored by analytical HPLC. For some data points, the error bars are smaller than the markers. The results are an average of two repeats and the errors shown as standard errors of mean.

Even though these results imply that the activated ester may not be as selective towards an attack by amines in physiological conditions as initially hypothesised, the good reactivity towards Lys attack and the lack of Cys residues near the binding site could still be capitalised upon. Validation of this linker as a viable way to introduce and deliver an electrophile to bind a target lysine selectively and covalently would be a powerful proof of principle. In addition, such validation would establish a solid starting point for further optimisation of the electrophilic moiety to tackle the issues underlined by the tests described in this chapter. For these reasons, we decided to synthesise a stapled peptide with linker **93**.

4.9. Synthesis and biological evaluation of STP ester–bearing stapled peptide

4.9.1. Computational binding energy for non-covalent binding of STP ester–bearing stapled peptide

Before proceeding to the synthesis, a computational assessment of stapled peptide **P6-93** was performed. The simulations were performed by Dr Yaw Sing Tan. The calculation yielded a similar result to **P6-81** (Table 10). As the change in the electrophilic moiety did not appear to negatively impact the non-covalent binding ability of the stapled peptide, we decided to proceed to synthesise **P6-93**.

Table 10 Calculated binding energy data from molecular dynamics simulation for the stapled peptides **P6-81** and **P6-93**. Computation was performed by Dr Yaw Sing Tan.

Peptide	ΔH / kcal mol^{-1}	TΔS / kcal mol^{-1}	ΔG / kcal mol^{-1}
P6-81	−47.66 ± 0.82	−35.34 ± 2.51	−12.32 ± 1.96
P6-93	−52.56 ± 2.32	−40.50 ± 1.33	−12.05 ± 1.23

4.9.2. Synthesis of STP ester–bearing stapled peptide

The stapled peptide **P6-93** was successfully synthesised by the CuAAC reaction, using the same conditions described in section 4.6.2 (Scheme 47). **P6-93** was purified by RP-HPLC and characterised by analytical HPLC and LCMS.

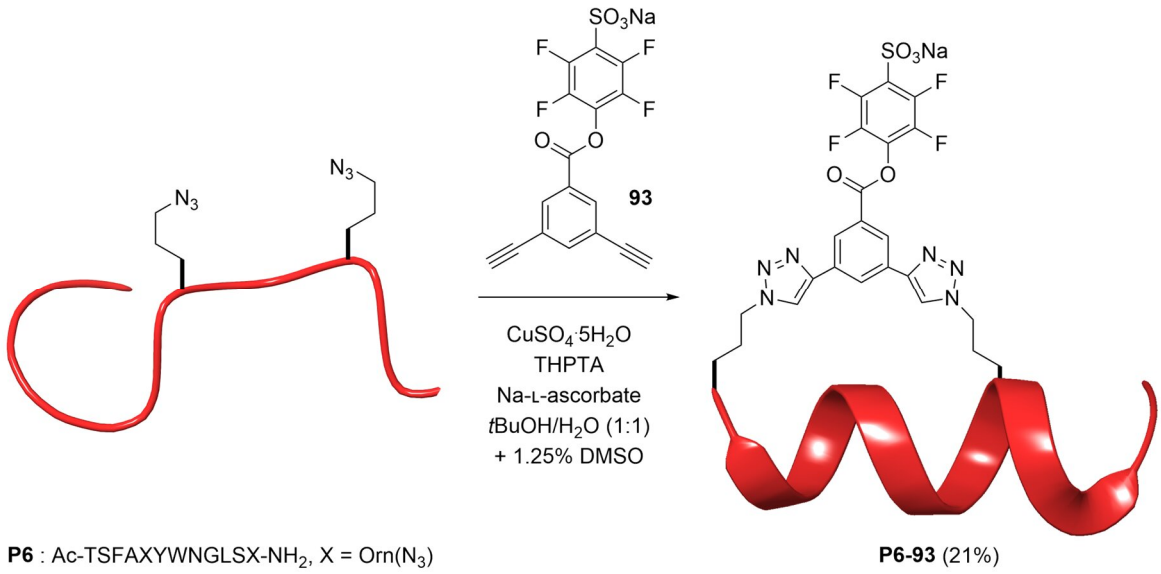

P6 : Ac-TSFAXYWNGLSX-NH_2, X = Orn(N_3)

P6-93 (21%)

Scheme 47 Two-component CuAAC stapling between peptide **P6** and staple **93**.

4.9.3. Biological testing

With **P6-93** in hand, its covalent binding was first verified using an MS experiment. The assay was performed in collaboration with Dr Stephen Walsh from the Spring Group. After the incubation of **P6-93** with MDM2, the mass corresponding to the covalent peptide–MDM2 complex (15400 Da) was observed with a negligible amount of unmodified MDM2 (13783 Da) remained (Figure 42). This observation signified a complete modification of MDM2 by the stapled peptide **P6-93**. The covalent complex formation resulted in a loss of sodium 2,3,5,6-tetrafluoro-4-hydroxybenzenesulfonate (STPOH). This result contrasted to the less reactive sulfonyl fluoride stapled peptide **P6-81**, which gave a meagre amount of the peptide–MDM2 covalent complex (Figure 35).

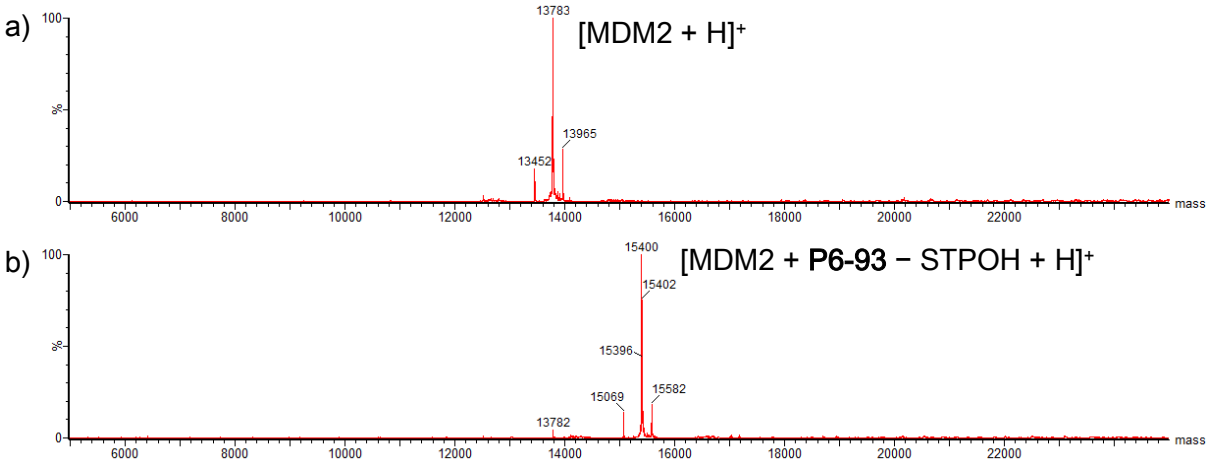

Figure 42 ESI-MS spectra for reactions with MDM2 a) the unmodified MDM2.* [MDM2 + H]$^+$ = 13783 Da. b) **P6-93** (25 µM) was incubated with MDM2 (25 µM) in PBS buffer (+10% DMSO)† at 37 °C for 1 hour. ESI-MS spectrum of the reaction indicated the complete covalent binding of the stapled peptide. [MDM2 + **P6-93** − STPOH + H]$^+$ = 15400 Da; STPOH = sodium 2,3,5,6-tetrafluoro-4-hydroxybenzenesulfonate.

MDM2 was also incubated with **P6-92**, the non-electrophilic control stapled peptide. Pleasingly, no change in the mass of MDM2 was observed. (Figure 43)

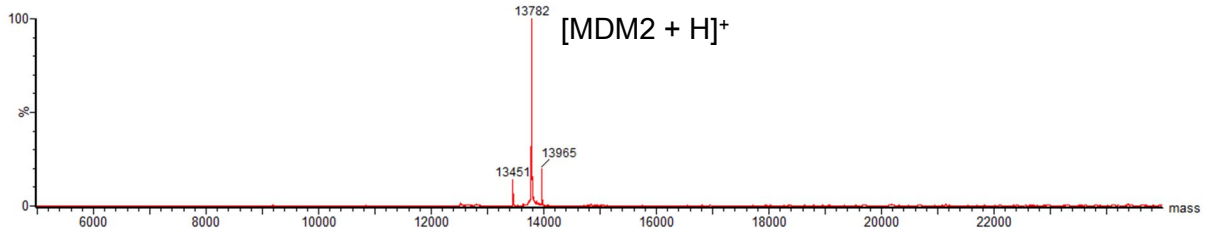

Figure 43 ESI-MS spectrum of MDM2 incubated with **P6-92**, the control peptide, which possessed no electrophilic moieties resulted in no change in the mass of MDM2. Condition: **P6-92** (25 µM) was incubated with MDM2 (25 µM) in PBS buffer (+10% DMSO) at 37 °C for 1 hour. [MDM2 + H]$^+$ = 13782 Da.

* MDM2 for experiments in this section contains extra GGS amino acids attached at the N-terminus.

† Extra DMSO was added to accommodate greater assay concentration for obtaining MS spectra with higher quality.

Under the same conditions, mass spectrometry results of the STP ester **93** alone (i.e. without peptide) with MDM2 resulted in only a small amount of the protein being modified, therefore highlighting the importance of the specific non-covalent binding of **P6-93** to MDM2 for the cross-linking event to occur (Figure 44).

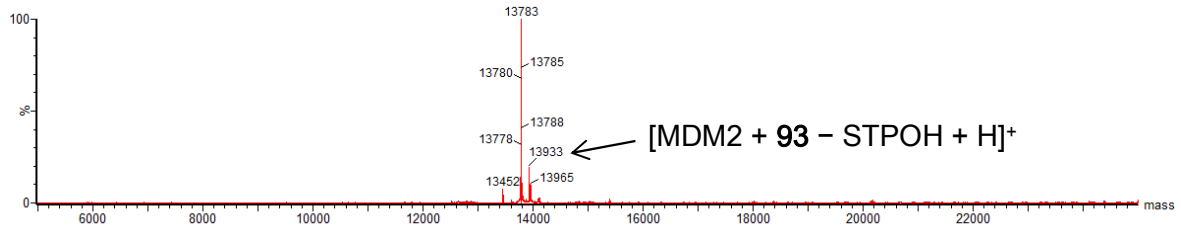

Figure 44 The same incubation as in Figure 43 but with **P6-93** replaced with compound **93**. ESI-MS spectrum showed low reactivity of the electrophile linker, with most MDM2 unreacted. [MDM2 + **93** − STPOH + H]$^+$ = 13933 Da.

The selectivity of the stapled peptide was further investigated by the addition of human lysozyme (Lyz) to the incubation. Lyz contains five highly solvent-accessible lysine residues out of which, one is particularly active.[389] Following the incubation, the formation of the peptide–lysozyme covalent complex was not detected, indicating that **P6-93** selectively binds MDM2 (Figure 45).

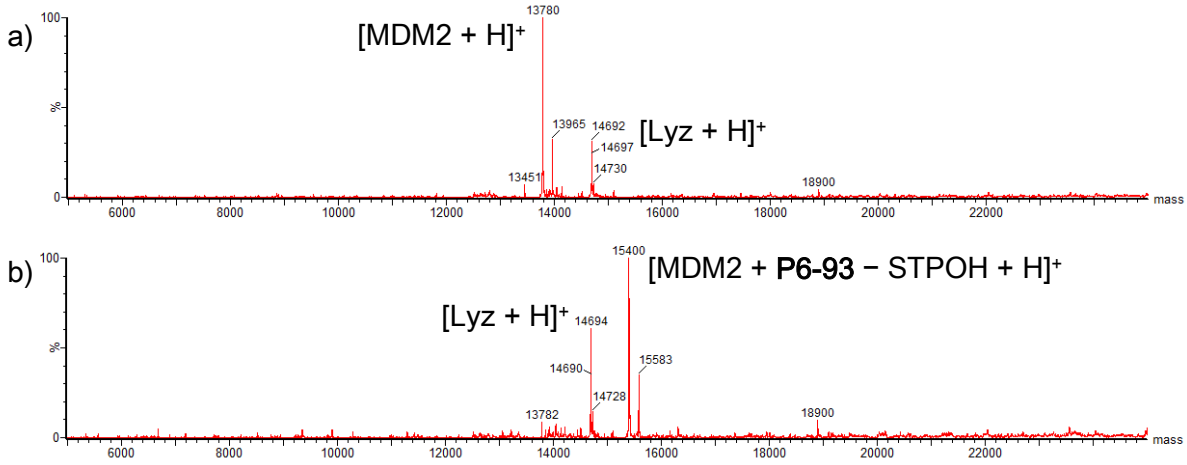

Figure 45 STP ester–functionalised stapled peptide was selective towards binding MDM2 covalently. a) ESI-MS spectrum of MDM2 and lysozyme (Lyz). [Lyz + H]$^+$ = 14694 Da. b) **P6-93** (25 μM) was incubated with MDM2 (25 μM) and lysozyme (25 μM) in PBS buffer (+10% DMSO) at 37 °C for 1 hour. ESI-MS spectrum of the reaction showed the exclusive attack on MDM2 with no modified lysozyme observed.

Next, the apparent dissociation constant ($K_{d,app}$) of **P6-93** to MDM2 was examined using a competitive FP assay (Figure 46).[101,102] The assay was performed by Dr Rohan Eapen from the Itzhaki Group, Department of Pharmacology. In contrast to the non-covalent peptides described in section 4.6.3, as expected for a TCI, the $K_{d,app}$ of **P6-93** improved over time as the covalent bond was formed, ultimately resulting in a potent MDM2 inhibition after two hours ($K_{d,app}$ = 30.0 ± 9.2 nM at 9 minutes, decreasing to 7.1 ± 2.1 nM at 120 minutes, Figure 46).[139]

a)

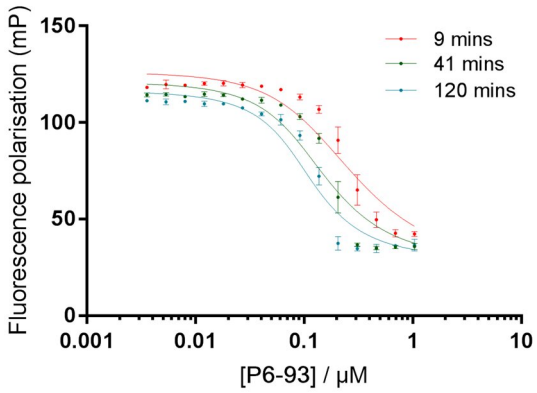

b)

Time (min)	$K_{d,app}$ (nM)
9	30.0 ± 9.2
41	12.9 ± 4.1
120	7.1 ± 2.1

Figure 46 Competitive FP assays of **P6-93**. a) Binding curves for **P6-93** over two hours. **P6-93** showed a decrease of the apparent dissociation constant over time. Each curve represents one time point: 9 min (red), 41 min (green), and 120 min (blue). Each data point is arithmetic mean of triplicate, and the errors shown are standard errors of mean. b) Apparent dissociation constant ($K_{d,app}$) of **P6-93** at each time point. The errors shown are standard errors of mean.

Finally, circular dichroism (CD) analysis was used to measure the helicity of the stapled peptide (Figure 47). Pleasingly, CD measurements confirmed that the staple used was able to enhance the helicity of the peptide (12% for **P6** vs 22% for **P6-93**, Figure 47b). The CD experiments were performed by Dr Jessica Iegre from the Spring Group.

a)

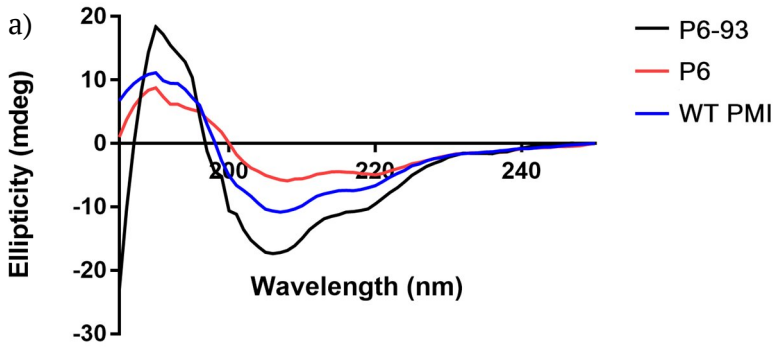

b)

Peptide	%helicity
WT PMI	15
P6	12
P6-93	22

Figure 47 a) Circular dichroism (CD) spectra for peptides **P6**, **P6-93**, and wild-type (WT) PMI. The graph shows higher helicity for the stapled peptide **P6-93** compared to the linear diazidopeptide **P6** and WT PMI. The peptides were dissolved in MQ water/MeCN (1:1) at a concentration of 100 μM. The measurements were performed at 25 °C by Dr Jessica Iegre. b) % helicity for the three peptides. Stapling increased the helicity of the peptide compared to both wild-type and the linear diazidopeptide.

4.10. Conclusion and future work

In conclusion, we developed a strategy for covalent binding of a stapled p53-like peptide to MDM2, leading to increased apparent binding with respect to the unstapled peptide. Expanding on the two-component CuAAC peptide stapling developed previously in the Spring Group, the dialkynyl linker was functionalised with an electrophilic moiety for targeted covalent inhibition of a solvent-exposed lysine residue near the binding site.

The investigation started from using aryl sulfonyl fluoride **81** as the electrophilic motif. However, through reactivity studies against lysine, the activated ester **93** (Figure 48) was found to be a more suitable option due to its superior kinetics. Linker **93** was then used to staple a peptide sequence adapted from PMI, a known MDM2 binder.[385] The stapled peptide **P6-93** exhibited complete and selective covalent binding to MDM2 with nanomolar inhibition demonstrated through a series of mass spectrometry and competitive FP assay experiments.

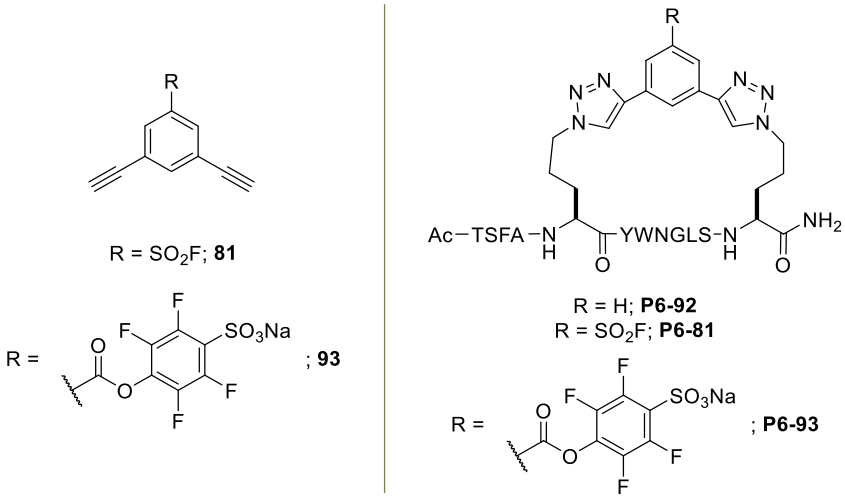

Figure 48 Structures of linkers and stapled peptides.

These results represent an initial proof-of-concept study towards the development of stapled peptide–targeted covalent inhibitors (SPTCIs) using two-component peptide stapling. Further optimisation of the electrophile-bearing staple is required for a more modulated electrophilic warhead since this study showed that the reactivity of **93** against Cys was comparable to that of Lys. Thus, future work will focus on screening alternative electrophiles, e.g. vinyl sulfones **97** and **98** (Figure 49). Vinyl sulfones have been used successfully in the development of a lysine-targeted covalent inhibitor for inhibiting CDK2.[188] It was also reported that this functional group is more selective towards an attack by amine than thiol .[390] As vinyl sulfones were found to be very reactive, adding a methyl group would decrease its activity and should make it more stable.

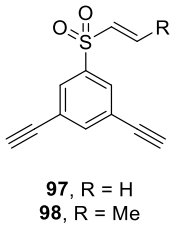

Figure 49 Structure of vinyl sulfones **97** and **98**.

It is envisioned that the concept herein developed, of careful design of an electrophilic moiety for selective covalent binding (Scheme 48), will be valuable for further development of this class of inhibitors for relevant PPI targets. Especially, target proteins with slow re-synthesis rate would gain the most benefit from using this approach.

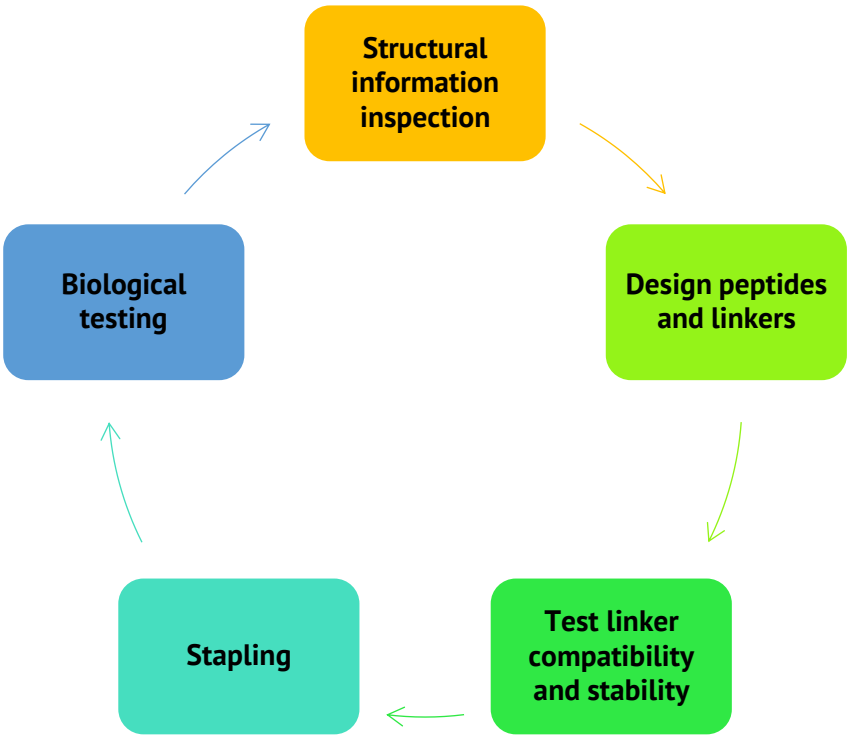

Scheme 48 Development cycle for SPTCIs.

Future work will focus on applying the whole strategy to a different PPI for further validation. One interesting protein target is β-catenin (CTNNB1), a central hub in Wnt signalling pathway.[391,392] Aberrant accumulation of β-catenin is implicated in several types of cancers.[391–393] The accumulated β-catenin then shuttles into the nucleus where it associates with T-cell factor/lymphoid enhancer factor-1 (TCF/Lef1). This key downstream interaction results in subsequent cell proliferation.[391] Thus, inhibition of this PPI serves as an attractive target for cancer therapeutics. As β-catenin has a longer half-life ($t_{1/2}$ = 5-6 hours)[394] compared to MDM2 ($t_{1/2}$ < 30 minutes),[395,396] the inhibition should also reap more benefits from the covalent cross-linking.

Verdine and co-workers have developed, aStAx-35, a hydrocarbon-stapled peptide inhibitor of β-catenin.[397] Crystal structure of the complex shows the presence of a solvent-exposed lysine in proximity to the binding site, which can potentially be targeted using a TCI (Figure 50). Using the concept developed in this thesis (Scheme 48) and the available structural information,[397] the development of SPTCIs for β-catenin will start from molecular modelling to find an appropriate point of stapling and linker with aStAx-35 as a starting peptide. The process will then progress to kinetics studies of the linkers, peptide stapling, and biological testing. Depending on the results, the cycle can be re-iterated for further optimisation of the SPTCIs.

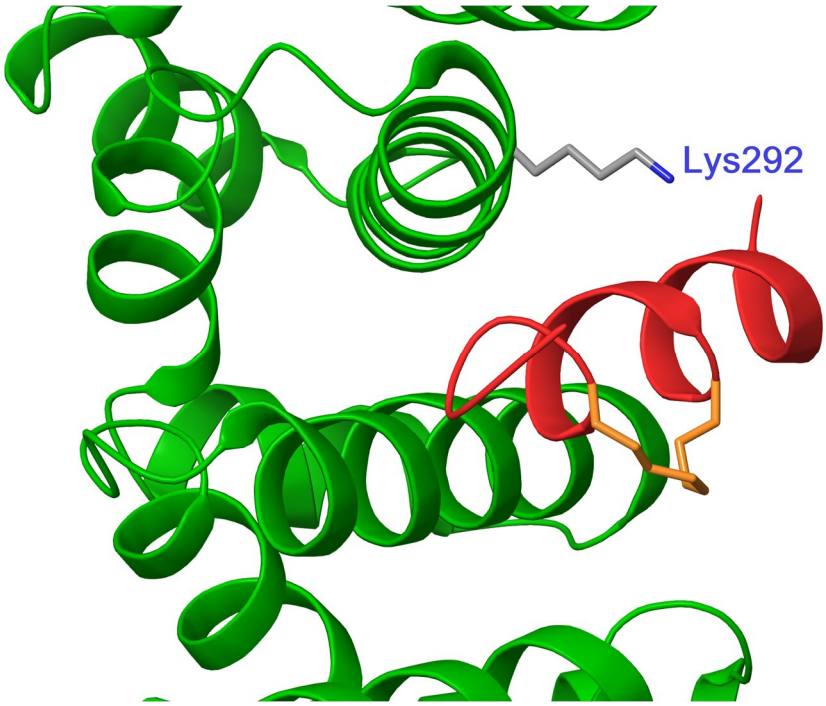

Figure 50 Close-up of the crystal structure of aStAx-35 (red with the staple in orange) bound to β-catenin (green) showing nearby Lys292 (PDB ID: 4DJS).[397]

Chapter 5 — Novel Total Synthesis of Hemiasterlin and Its Application in Antibody–Drug Conjugate*

5.1. Project aims and overview

Payloads used in the ADC field, as described in section 3.5, must be highly potent and thus, have complex structures, requiring lengthy synthesis or semi-synthesis relying on scarce natural products or fermentation. Despite its relatively simple structure, hemiasterlin (**56**),[355–357,359,360,399–401] introduced in section 3.6, has a level of cytotoxicity that is similar to other ADC payloads; therefore, it is an ideal candidate for a widespread application in the ADC area. Nevertheless, only one ADC, STRO-002, has been described to employ a hemiasterlin analogue called 3-aminophenylhemiasterlin as its payload.[367]

As mentioned in section 3.6, three previous total syntheses have been reported: Andersen *et al*. (17 LLS, 23 total steps),[363] Vedejs and Kongkittingam (13 LLS, 20 steps),[364] and Lang *et al*. (15 LLS, 21 total steps).[365] In addition, Lesma *et al.* reported the use of four-component Ugi reaction (Ugi-4CR) to synthesise analogues of hemiasterlin with the L-*tert*-leucine central amino acid replaced by L-valine (Scheme 49).[402] Hence, it was envisaged that a similar Ugi-4CR could be used to simplify the route to hemiasterlin and thereby allow easy access to its analogues. This simpler synthesis would potentially enable widespread use of hemiasterlin or its analogues as an ADC payload.

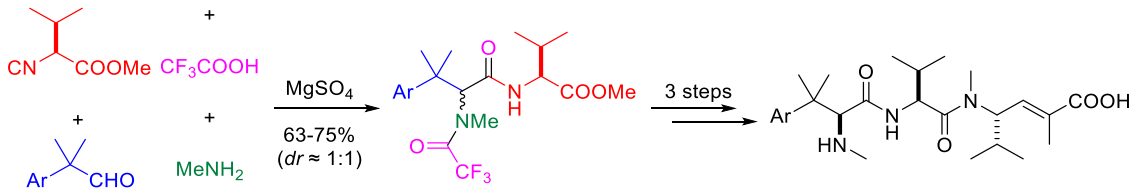

Scheme 49 Synthesis of hemiasterlin analogues using Ugi-4CR by Lesma *et al*.[402] The central L-*tert*-leucine was replaced by L-valine.

The project will be executed with the following aims.

1) Synthesis of the key building blocks for Ugi-4CR for the synthesis of hemiasterlin.
2) Optimisation of the Ugi-4CR step.
3) Total synthesis of hemiasterlin using the optimised procedure in aim 2.
4) Generation of an exemplary analogue, taltobulin (HTI-286, **57**), according to aims 1 and 2.
5) Synthesis of linker–drug compounds with hemiasterlin and taltobulin.
6) Synthesis of ADCs containing the linker–drugs in aim 5.

* The work described in this chapter has been published in Charoenpattarapreeda, *et al*., *Angew. Chem. Intl. Ed.*, 2020.[398] Part of the text and figures were adapted from this publication.

7) Investigation of cytotoxicity of the ADCs, comparing them to the parent small molecules.

5.2. Synthesis of hemiasterlin and taltobulin

5.2.1. Initial route design

To commence the investigation, a retrosynthetic analysis of hemiasterlin was performed (Scheme 49). It was hypothesised that Ugi-4CR could be used to generate the dipeptide **99** from four simple starting materials. Coupling of this dipeptide with unsaturated γ-amino ester **100**, which would be accessible from Boc-*N*-methylvaline through a literature route,[359] followed by a global deprotection of the resulting amide, would then reveal hemiasterlin.

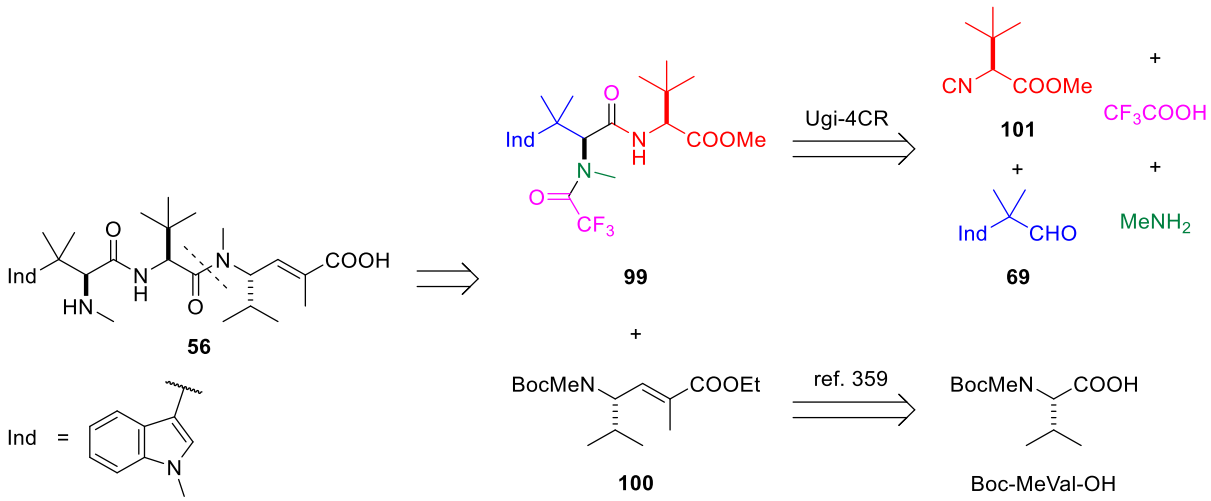

Scheme 50 Retrosynthetic analysis of hemiasterlin (**56**).

5.2.2. First-generation route

With a proposed synthetic route to hemiasterlin in place, the synthesis of isonitrile **101** was undertaken. Commercially available L-*tert*-leucine methyl ester was heated under reflux in ethyl formate and triethylamine to give formamide **102** in excellent yield (Scheme 51).[403] While numerous reagents (phosgene,[404–407] diphosgene,[408] triphosgene,[409,410] and $POCl_3$[411]) in combination with tertiary amines (Et_3N and *N*-methylmorpholine (NMM)) have been employed for the dehydration of formamides to generate isonitriles, many of these conditions can cause substrate racemisation. Zhu *et al*. reported the use of triphosgene with NMM as a base at low temperature to accomplish the dehydration without racemisation.[410] Thus, these conditions were chosen, and formamide **102** was converted to the desired isonitrile **101** in 94% yield.

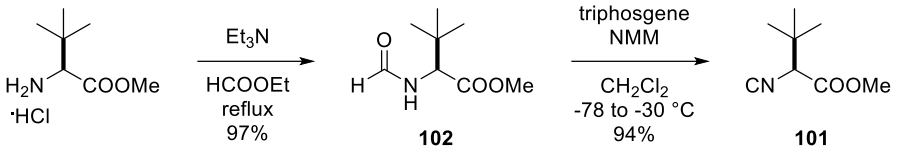

Scheme 51 Synthesis of isonitrile **101**.

Synthesis of the aldehyde building block **69** was initially attempted via a two-step procedure from *N*-methylindole (Scheme 52).[402] Accordingly, treatment of *N*-methylindole (**103**) with elemental bromine in DMF generated 3-bromo-*N*-methylindole (**104**) in 65% yield.[412] However, the brominating agent was later switched to 1,3-dibromo-5,5-dimethylhydantoin (DBDMH), a safer and easier-to-handle alternative, which resulted in a similar yield (Scheme 52).[413] Unfortunately, Pd-catalysed C(sp^3)-H α-arylation of isobutyraldehyde with bromoindole **104** using Q-Phos as the ligand gave the desired aldehyde **69** in poor yield,[414] with debrominated starting material obtained as the major product. No significant improvement was achieved after a screening of reaction conditions (Table 11). Literature reports also suggested that alteration of the Pd catalyst would not improve conversion to the desired product.[415–417] Owing to the low yield of this step and the instability of bromoindole **104**, this route was abandoned.

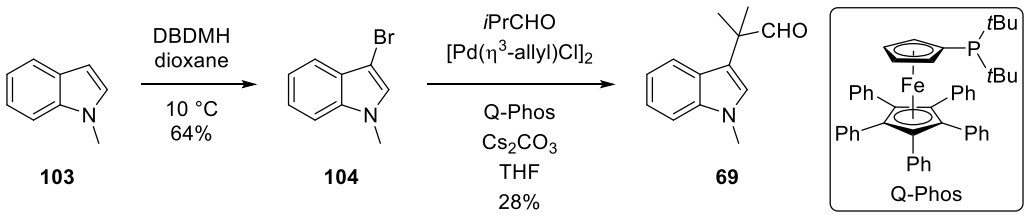

Scheme 52 Synthesis of aldehyde **69** via bromination and Pd-catalysed α-arylation of isobutyraldehyde.

Table 11 Screening of conditions for Pd-catalysed C(sp^3)-H α-arylation of isobutyraldehyde with **104**.

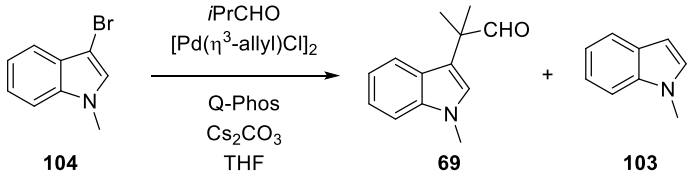

Entry*	*i*PrCHO (equiv.)	[Pd] (mol%)	Q-Phos (mol%)	Cs_2CO_3 (equiv.)	T (°C)	Yield† (%)	Ratio of 69:103‡
1	1.17	0.5	1	2	80	25	1:4
2	2.33	1	2	4	80	23	1:2.2
3	2.33	0.5	1	4	80	-	1:2.4
4	1.17	0.5	2	2	80	28	1:1.5
5	1.17	0.5	1	2	60	-	1:2.5
6	2.33	0.5	1	4	60	-	1:2.9

*All reactions were stirred for 18 h. †Isolated yield. ‡Ratios were calculated from ^{1}H-NMR of the crude product.

Nieman *et al*. have previously reported a four-step synthesis of aldehyde **69**.[359] Although requiring more synthetic steps than the original route, it was hypothesised that this route would provide access to the required aldehyde in better yield. Accordingly, starting from indole **58**, simultaneous *N*- and α-methylation was performed using KHMDS and MeI (Scheme 53). Next, the second α-methylation was performed under the same conditions to give indole **60** in excellent yield. The ester was then reduced using diisobutylalumimium hydride (DIBAL-H), giving alcohol **105**, which was then oxidised under Ley-Griffith conditions[418] to afford aldehyde **69** in 70% yield over four steps.

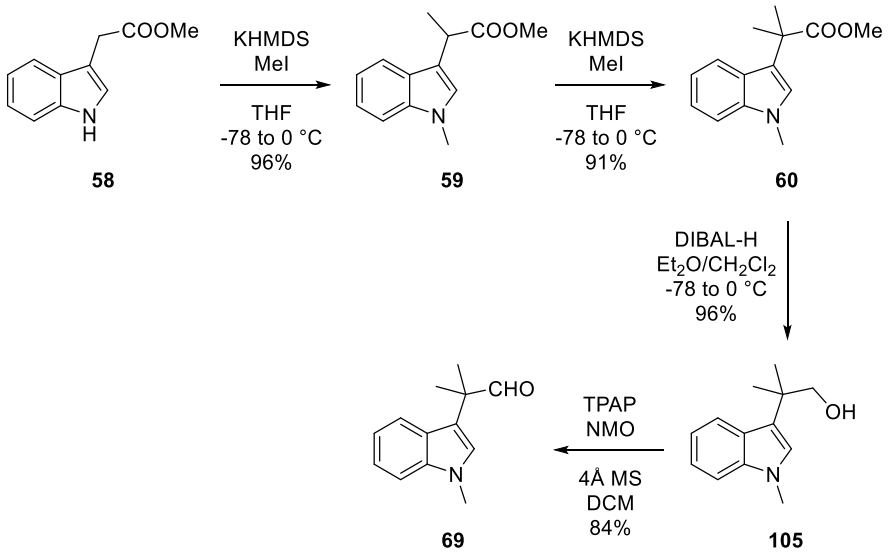

Scheme 53 Synthesis of aldehyde **69** using the four-step procedure by Nieman *et al*.[359]

With all the components in hand, the Ugi-4CR of isonitrile **101**, aldehyde **69**, methylamine, and trifluoroacetic acid was first attempted with conditions published by Lesma *et al*. using anhydrous $MgSO_4$ as the drying agent (Table 12 Entry 1). Trifluoroacetic acid was used as the acid component because the resulting *N*-trifluoroacetamide is stable towards mild ester hydrolysis conditions at room temperature, but it can be hydrolysed under elevated temperature or chemoselectively reduced, leaving the ester group intact.[419,420] Under these conditions, separable mixtures of **99a** and **99b** were obtained in 41% combined yield (*dr* = 1:1.2), but a significant amount of free amine product **106** (23%) was isolated. It was hypothesised that inefficient drying was responsible for this lower than desired yield (Scheme 54). Pleasingly, switching to 3 Å molecular sieves eliminated the side-product formation, and the products **99** were obtained in 70% total yield (*dr* 1:1.3, Table 12 Entry 2). Their absolute stereochemistries were confirmed by X-ray crystallography analysis (see Appendix B for crystal structures).

Table 12 Ugi-4CR of aldehyde **69**, isonitrile **101**, methylamine, and trifluoroacetic acid.

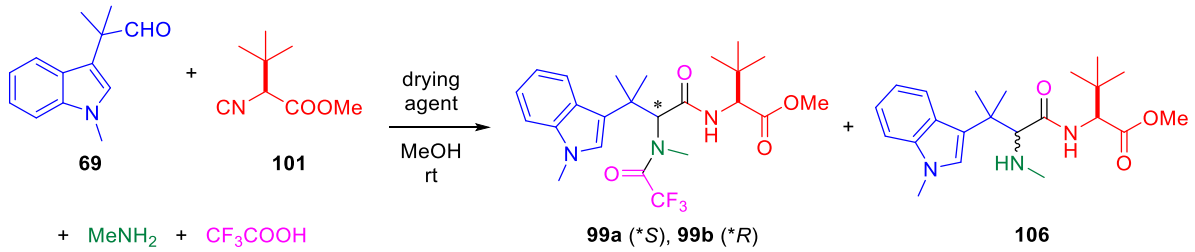

Entry	Drying agent	%99 (*dr* = 99a:99b)*	%106*,†
1	anhydrous $MgSO_4$	41% (*dr* 1:1.2)	23%
2	3 Å molecular sieves	70% (*dr* 1:1.3)	0%

*Yields refer to isolated yield. †Isolated as a mixture of diastereomers with undetermined *dr*.

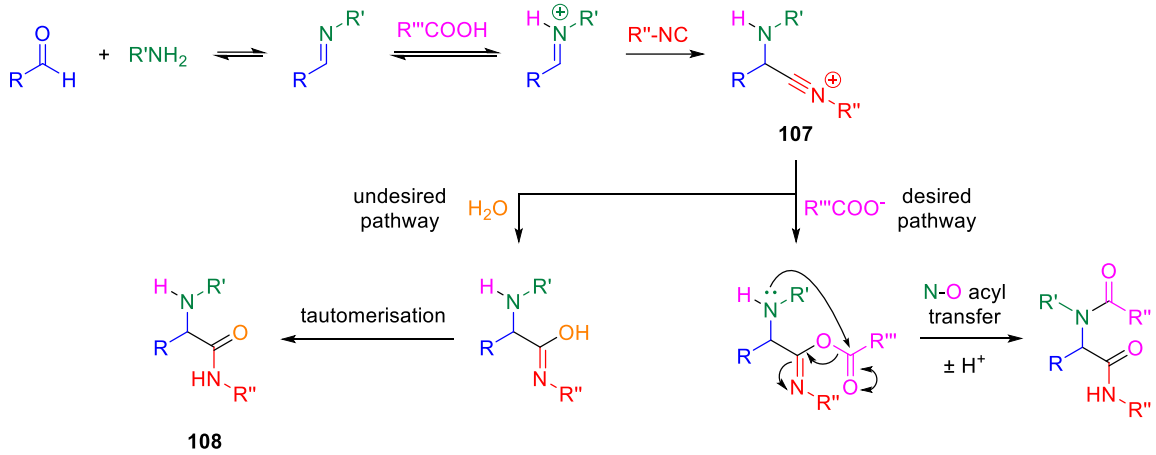

Scheme 54 The mechanism of Ugi reaction leading to the undesired free amine **108** if H_2O attacks the nitrilium ion intermediate **107** instead.

Prior to amide coupling for assembling the full carbon skeleton of hemiasterlin, hydrolysis of the methyl ester in esters **99a** and **99b** was achieved using lithium hydroxide to produce acids **109a** and **109b** (Scheme 55).

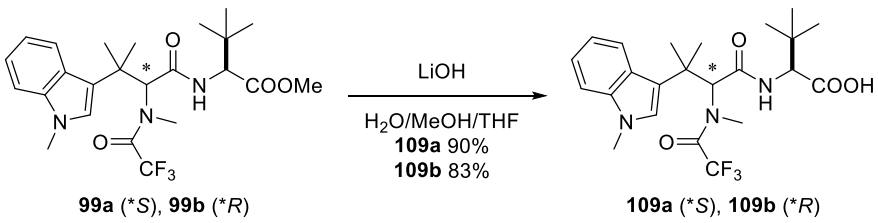

Scheme 55 Ester hydrolysis of compounds **99**.

Next, the amino ester **100** was synthesised according to literature procedures (Scheme 56).[359] Amide coupling of Boc-protected *N*-methylvaline with *N*,*O*-dimethylhydroxylamine hydrochloride was achieved using benzotriazol-1-yl-oxytripyrrolidinophosphonium hexafluorophosphate (PyBOP) as the activating agent to afford Weinreb amide **110** in 88% yield. Reduction of Weinreb amide **110** to the corresponding aldehyde **111** was conducted using lithium aluminium hydride ($LiAlH_4$) and was directly reacted with ylid **112** to give

amino ester **100** in 53% yield over two steps. The Boc group was then removed with HCl in dioxane to give amine **65** in 90% yield.

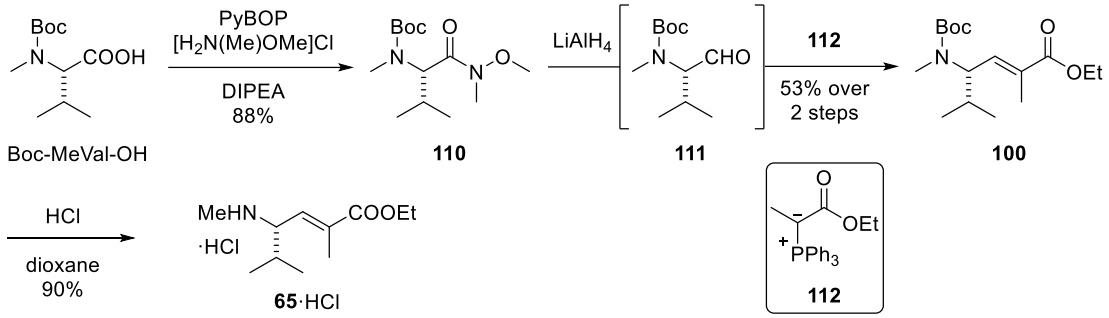

Scheme 56 Synthesis of amino ester **65**.[359]

With the required amine and acid in hand, the fragment amide coupling was first attempted using 2-(1*H*-benzotriazol-1-yl)-1,1,3,3-tetramethyluronium hexafluorophosphate (HBTU) as the activating agent (Table 13 Entry 1). Unfortunately, the formation of protected hemiasterlin **113** was not observed in this reaction. Instead, undesired oxazolone **114** was isolated in 59% yield. The formation of an oxazolone is a common problem in fragment amide couplings as the nucleophilic amide oxygen can attack the activated ester intermediate to form a 5-membered heterocycle, which may also easily epimerise.[421–425] This was somewhat surprising as Lesma and co-workers reported good yields for the fragment amide coupling with HBTU to generate their tripeptide library.[402] Several other conditions were then attempted, which featured different active intermediate species including *O*-acylurea (Table 13 Entries 4–5) and acyl fluoride (Table 13 Entries 6–7). $CuCl_2$ was reported to reduce epimerisation and so employed in hope to suppress oxazolone formation (Table 13 Entry 4–5).[426] Fluoro-*N*,*N*,*N*',*N*'-bis(tetramethylene)formamidinium hexafluorophosphate (BTFFH) was used to form an acyl fluoride intermediate which was reported to be suitable for amide coupling of sterically hindered secondary amines (Table 13 Entry 6–7).[427] Unfortunately, all conditions resulted in either complex crude mixture or formation of oxazolone **114**.

Table 13 Screening of conditions for fragment amide coupling of acid **109** with amine **65**.

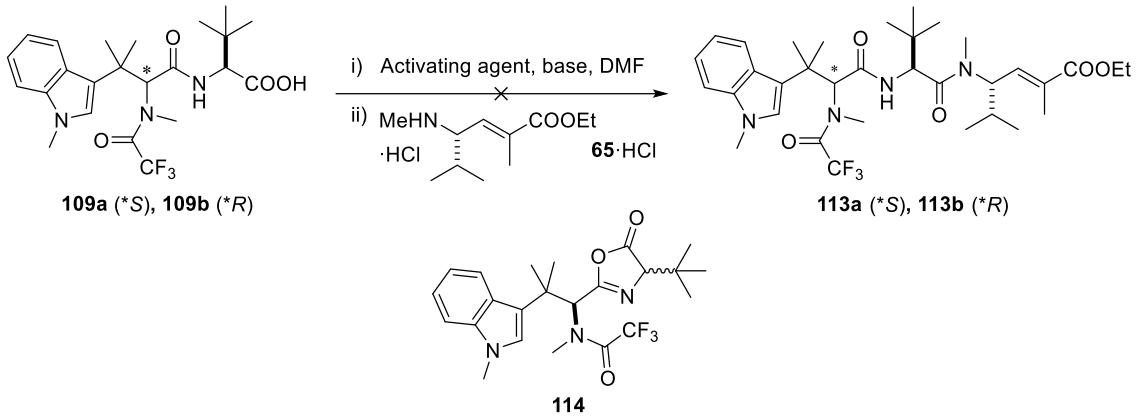

Entry	Conditions	%yield
1	HBTU, DIPEA, CH_2Cl_2[402,a]	0[c]
2	HATU, DIPEA, DMF[428,a]	0
3	EDC, HOAt, NMM, DMF[429,a]	0
4	DIC, HOAt, $CuCl_2$, DIPEA, DMF[426,b]	0
5	DIC, NMM, $CuCl_2$, DMF[426,b]	0
6	BTFFH, DIPEA, CH_2Cl_2, 80 °C (sealed tube)[427,b]	0
7	BTFFH, DIPEA, CH_2Cl_2, 80 °C (microwave)[427,b]	0

Unless otherwise stated, all reactions were conducted at room temperature. [a]**109a** was used; [b]**109b** was used; [c]Oxazolone **114** (59% yield) was isolated. HOAt = 1-hydroxy-7-azabenzotriazole, DIC = diisopropylcarbodiimide.

5.2.3. Second-generation route

Given the success of the Ugi-4CR, it was hypothesised that an analogous Ugi reaction could be used to assemble the full hemiasterlin scaffold with more elaborated components, in place of the fragment amide coupling in the final step. Favourably, isonitrile **117** was identified as the key component required for the proposed Ugi reaction and was potentially accessible from valine-derived amino ester **100**, synthesised in the previous route.

As such, Boc-deprotection of **100** was effected via treatment with hydrochloric acid in dioxane and followed by a HATU-mediated amide coupling with Boc-Tle-OH to give dipeptide **115** in excellent yield (Scheme 57). Subsequent Boc-removal, followed by formamide formation, and triphosgene-mediated dehydration afforded the required isonitrile **117** in 81% yield over three steps. The conditions for the dehydration step was adjusted according to Zhu *et al*. for a peptide substrate, whereby the base was switched to 2,6-lutidine and the temperature was lowered to −50 °C.[410] No justification for this modification was given in the original paper.

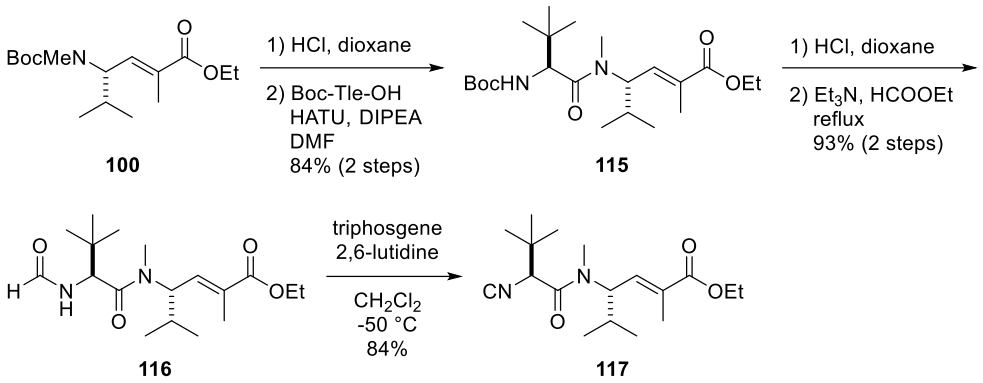

Scheme 57 Synthesis of isonitrile **117**.

With the isonitrile component in hand, the Ugi reaction between aldehyde **69**, isonitrile **117**, methylamine and TFA, using the same conditions as previously, was then attempted. Unfortunately, this reaction resulted in only 20% overall yield of diastereomeric mixtures of **113a** and **113b** (Table 14 Entry 1). A significant amount of oxazole by-product **118** was tentatively identified by LCMS analysis ($[M+H]^+$ found m/z = 537.8, calcd m/z = 537.4, Scheme 58). Isonitrileacetamides have previously been used in three-component Ugi-type reaction to generate oxazoles due to favourable conformation and higher basicity of the amide oxygen which promotes intramolecular cyclisation (Scheme 58).[430] It was hypothesised that by increasing the concentration of the trifluoroacetate anion in the reaction, it might be possible to outcompete the intramolecular pathway. While the addition of extra TFA resulted in a complex mixture (Table 14 Entry 2), pleasingly, the addition of CF_3COONa increased the overall yield to 73% (*dr* 1:1.4, Table 14 Entry 3).

Table 14 Optimisation for the second attempt at Ugi-4CR.

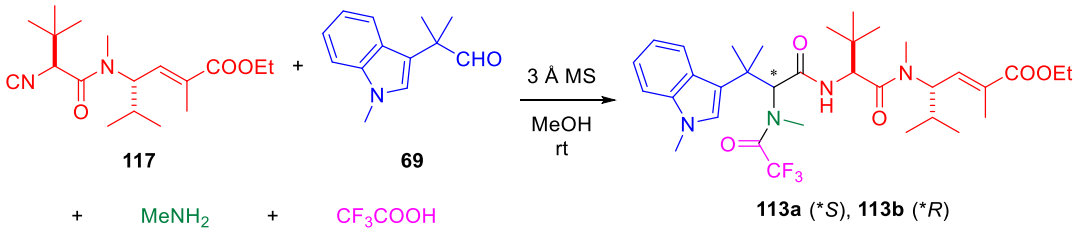

Entry	TFA equiv.	Additive	Isolated yield (*dr* = 113a:b)*	Remarks
1	1.2	-	20% (*dr* 1:1.3)	Oxazole side-product observed
2	2.5	-	-	Complex mixture
3	1.2	CF_3COONa (1.2 equiv.)	73% (*dr* 1:1.4)	-

*Diastereomeric ratios were determined from ^{19}F-NMR of the crude product.

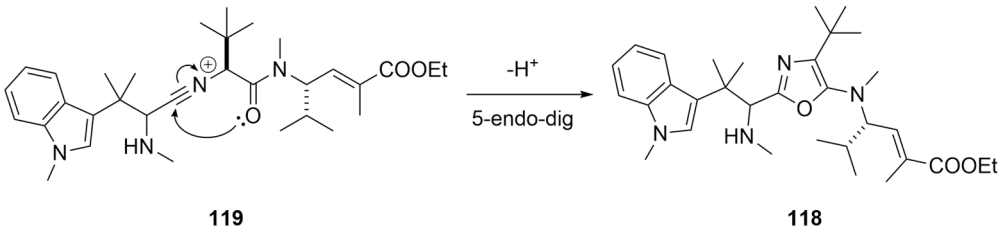

119 118

Scheme 58 Proposed cyclisation of the nitrilium intermediate **119** to form a tentative undesired oxazole side-product **118**.

X-ray crystallography analysis of **113a** was used to determine its absolute stereochemistry which corresponded to that of hemiasterlin (Figure 51).

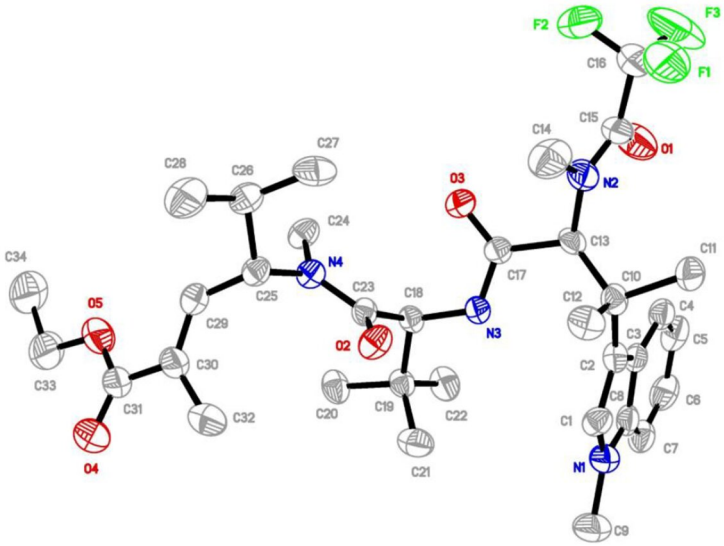

Figure 51 X-ray crystal structure of **113a**.

A commonly observed issue with Ugi-4CR and isocyanide-based multi-component reactions (IMCRs) in natural product total syntheses is the low diastereoselectivity of the reactions.[431–435] A notable exception to this problem is when cyclic imines are used instead of aldehyde and amine components.[436,437] Consequently, several enantioselective IMCRs have been developed which utilise chiral phosphoric acids (CPAs) catalysts to control the enantioselectivity.[438–440] Thus, an attempt was made to improve the diastereoselectivity by screening several CPAs (Table 15). **CPA2-4** were synthesised by Guillermo Caballero-Garcia, the Goodman Group, Department of Chemistry, University of Cambridge.

Table 15 Screening of conditions for improving diastereoselectivity of the Ugi reaction for generating **113**.

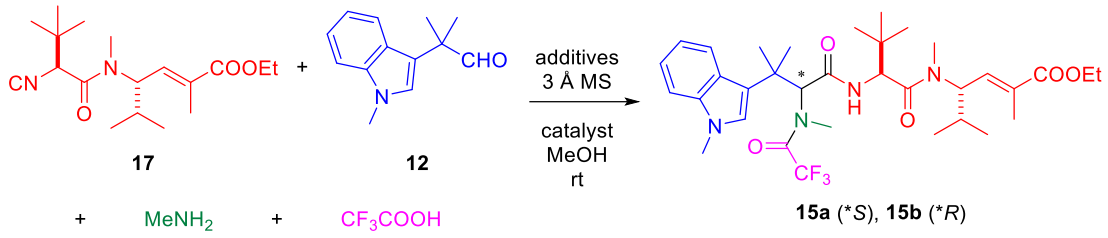

Entry	Solvent (0.05 M)	Additives (1.2 equiv.)	Catalyst (5 mol%)	%yield (NMR)*	*dr*† = (*S*):(*R*)
1‡	MeOH (0.5 M)	CF_3COONa	-	73§	1:1.4
2	MeOH	CF_3COONa	-	20	1:1.3
3	MeOH	CF_3COONa	**CPA1**	15	1:1.4
4	CH_2Cl_2	CF_3COONa	-	7	1:1.5
5	CH_2Cl_2	CF_3COOH, Et_3N	-	58	1:1.4
6	CH_2Cl_2	CF_3COOH, Et_3N	**CPA1**	15	1:1.3
7	CH_2Cl_2	CF_3COOH, Et_3N	**CPA2**	31	1:1.3
8	CH_2Cl_2	CF_3COOH, Et_3N	**CPA3**	22	1:1.3
9	CH_2Cl_2	CF_3COOH, Et_3N	**CPA4**	6	1:1.4

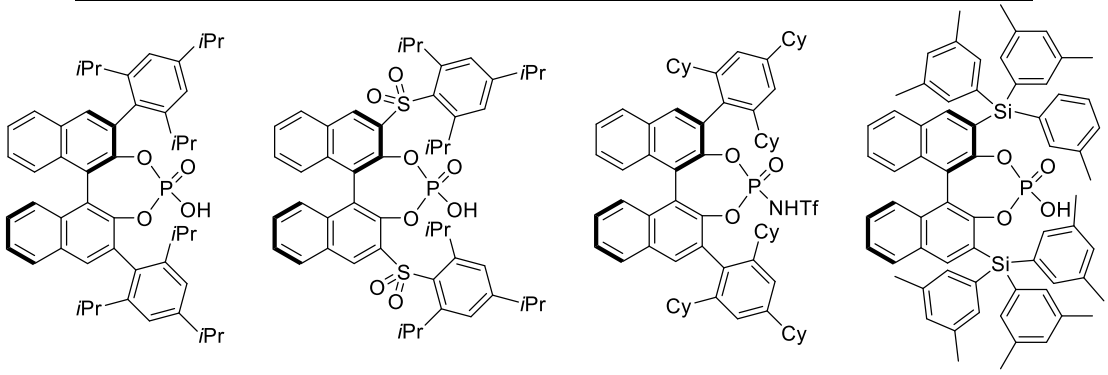

CPA1 **CPA2** **CPA3** **CPA4**

Unless noted otherwise, all reactions were performed at 0.05 mmol scale of **69** with 1.1 equiv. of **117**, 1.1 equiv. of $MeNH_2$, and 1.2 equiv. of CF_3COOH. *Analysed by ^{19}F-NMR using 4,4'-difluorobenzophenone as the internal standard. †Determined with ^{19}F-NMR of the crude product. ‡1.2 equiv. of **117** and at 0.1 mmol scale. §Isolated yield.

The original, optimised Ugi conditions (Table 15 Entry 1) involved performing the reaction at 0.5 M of aldehyde. However, reported diastereoselective Ugi reactions are performed at significantly lower reaction concentrations (about 0.05–0.1 M).[438,439] As such, it was decided to perform the initial attempts to increase the diastereoselectivity of the reaction at this lower concentration (0.05 M). While this resulted in lower yield (Table 15 Entry 2), it was thought that initially, *dr* improvement was a priority. No change in the diastereoselectivity was observed when **CPA1** was added (Table 15 Entry 3), which was an expected outcome. While polar protic solvents, e.g. MeOH or TFE, are preferred for Ugi-4CR as they can stabilise the

polar intermediates through H-bonding,[441] the stereoinduction step requires H-bonding between the CPA and imine intermediate; these protic solvents would prevent this interaction from forming.[439] Therefore, the solvent was switched to aprotic CH_2Cl_2, which was also used in an enantioselective Ugi-4CR.[439] As seen previously (Table 14), to effectively form the products **113**, extra trifluoroacetate anion was required in the reaction mixture. However, the insolubility of CF_3COONa in CH_2Cl_2 was detrimental to reaction progression (Table 15 Entry 4). Thus, an equimolar mixture of CF_3COOH and Et_3N was used to generate the anion instead, (Table 15 Entry 5) affording the desired products **113** in 58% yield by NMR. With CPA-compatible conditions in hand, four BINOL-based CPAs were screened using these conditions (Table 15 Entries 6–9).[440] In all cases, the *dr* changes were negligible. Further screenings of other CPAs, e.g. SPINOL-based CPAs,[439] are required to verify whether the stereoselectivity can be improved. However, it was decided that further investigation of the diastereoselective Ugi-4CR would be suspended as it was deemed a priority to finish the total synthesis of hemiasterlin and investigate its capabilities as an ADC payload. In addition, the non-diastereoselective Ugi-4CR was able to generate sufficient material to continue the synthesis.

To complete the synthesis, the Ugi products **113** were subjected to lithium hydroxide monohydrate at 60 °C to simultaneously hydrolyse the methyl ester and the trifluoroacetamide group, producing hemiasterlin **56** and *epi*-hemiasterlin **56b** in 86% and 78% yield, respectively (Scheme 59).

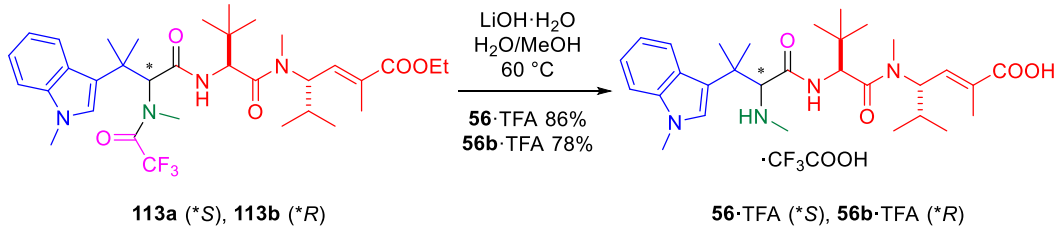

Scheme 59 Hydrolysis of **113** to give hemiasterlin (**56**) and its epimer (**56b**).

To demonstrate the amenability of the developed synthetic route for the synthesis of hemiasterlin analogues, taltobulin was also synthesised from 2-methyl-2-phenylpropanal (**120**). This aldehyde was made from its corresponding acid by reduction to an alcohol using $LiAlH_4$ and subsequent re-oxidation using Ley-Griffith conditions (Scheme 60). The Ugi-4CR of aldehyde **120** with isocyanide **117**, methylamine, and TFA produced a partially separable diastereomeric mixture of **121** by flash column chromatography. The diastereomeric mixture was obtained in good yield and carried forward onto the final step. Treatment with lithium hydroxide monohydrate generated the desired compounds **57** and **57b**, each in 20% yield after RP-HPLC purification (Scheme 60).

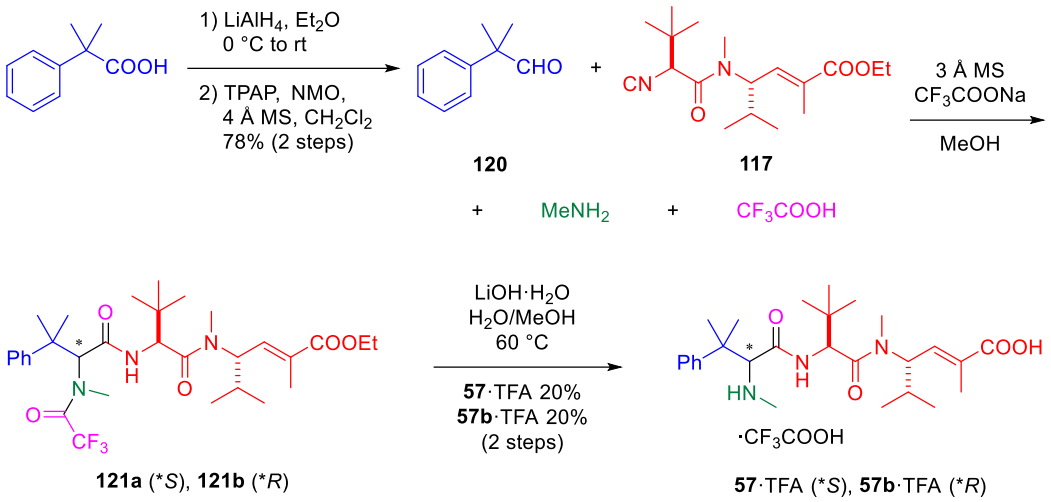

Scheme 60 Synthesis of taltobulin (**57**) and its epimer (**57b**).

In summary, hemiasterlin (**56**) and taltobulin (**57**) were synthesised via a convergent strategy involving a multi-component Ugi-4CR in 14 and 12 total steps (both with an LLS of 10 steps), in 11% and 6% overall yield, respectively.

5.3. Synthesis of linker–drugs for bioconjugation

After successfully developing a superior synthetic route to hemiasterlin and taltobulin, their utility as ADC payloads was investigated. First, it was necessary to modify the natural product with bioconjugation linkers to facilitate their attachment to an antibody.

5.3.1. Design and selection of the linkers

Divinylpyrimidine (DVP) reagents, previously developed in the Spring Group,[113,269] were chosen as the bioconjugation motif due to their efficient conjugation and excellent stability under physiological conditions (Scheme 61). IgG antibodies contain four interchain disulfide bonds, which can be reduced to reveal eight reactive cysteine thiols (other buried disulfide bonds are not reduced). DVP linkers react with these eight selectively reduced cysteines, “rebridging” (or cross-linking) the reduced disulfides. In doing so, each antibody can be modified with four payloads to give a consistent DAR of four. The cathepsin-cleavable Val-Ala-PABC was incorporated into the linker design on the payload attachment side as it was deemed essential to release an unmodified drug from the antibody.[278] Finally, to enable a convergent synthesis, it was hypothesised that modification of the payload with an azide and the DVP linker with an alkyne would allow the use of a CuAAC reaction to assemble the complete linker–drug in the final step (Scheme 61).

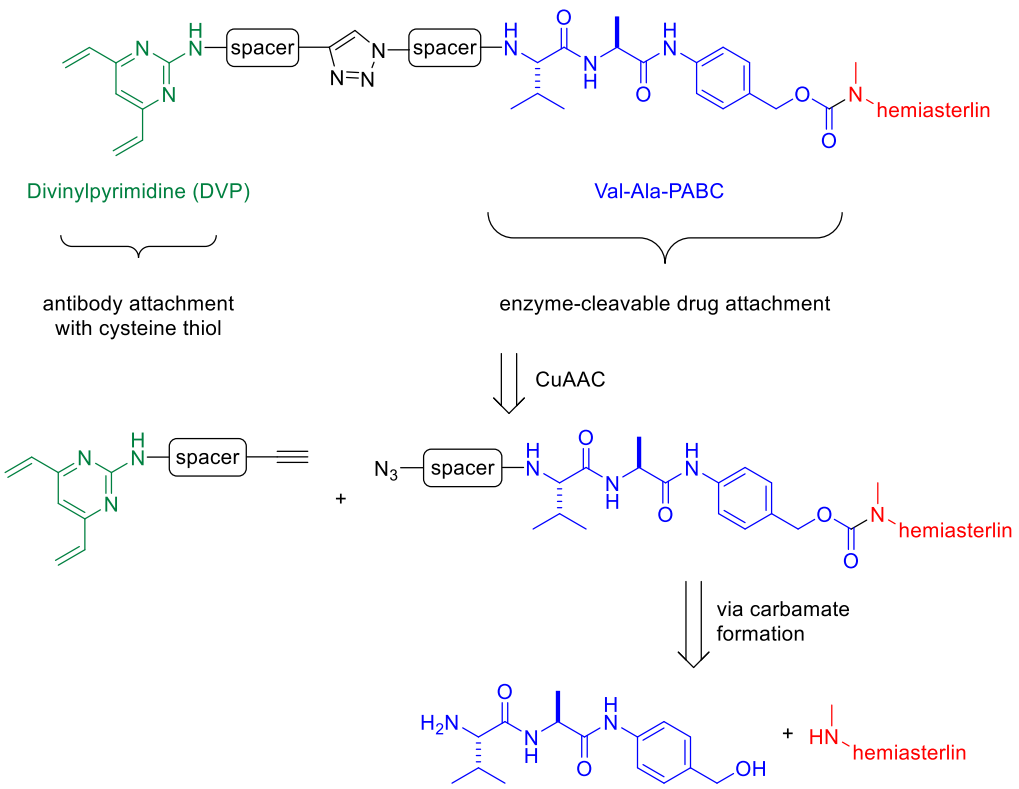

Scheme 61 Design of the linker–drug for bioconjugation.

5.3.2. Carbamate formation optimisation

It was anticipated that the carbamate formation step would be the most challenging in this strategy as hemiasterlin possesses a sterically hindered secondary amine. To assess the viability of this route, it was decided that test reactions to form simpler carbamates were to be carried out first. For this purpose, reactive mixed carbonate Alloc-Val-Ala-PABC-*p*-nitrophenoxy (OPNP; **123**) was synthesised by a reaction between Alloc-Val-Ala-PABA (**122**) and bis(*p*-nitrophenyl)carbonate in the presence of DIPEA in excellent yield (Scheme 62).

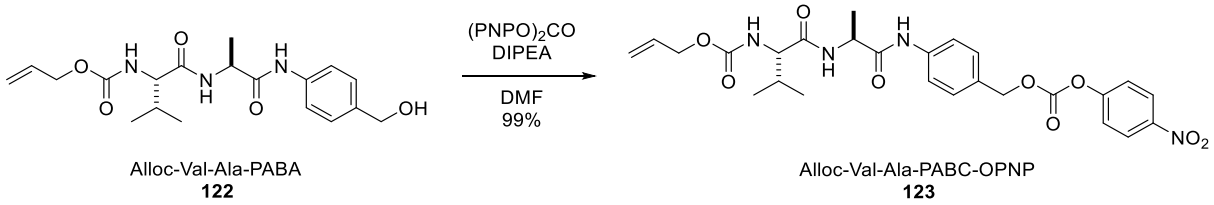

Scheme 62 Synthesis of mixed carbonate **123**.

Initially, the widely used protocol for carbamate formation between the trifluoroacetate salt of hemiasterlin (**56**·TFA) and *p*-nitrophenyl carbonate **123** with 1-hydroxy-7-azabenzotriazole (HOAt) and DIPEA was used; however, the desired product **124** could not be detected (Scheme 63).[285] Additional carbonate, raising the temperature, or addition of

catalytic DMAP did not result in the formation of the desired product. In all cases, only unreacted hemiasterlin was observed by LCMS analysis.

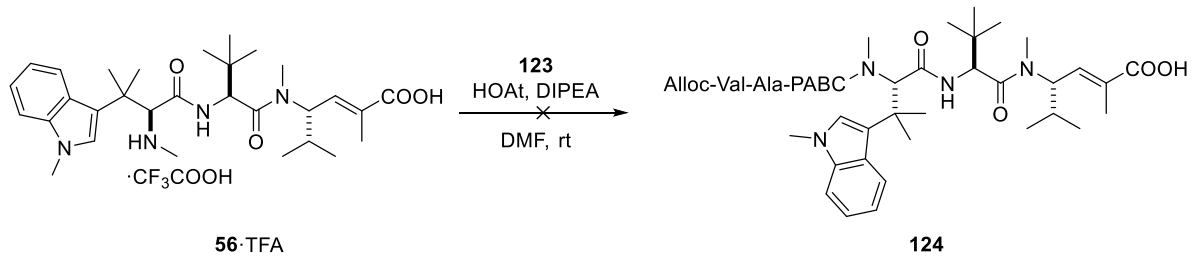

56·TFA **124**

Scheme 63 Attempted carbamate formation using hemiasterlin trifluoroacetate salt (**56**·TFA), carbonate **123**, HOAt, and DIPEA.

It was hypothesised that a more reactive electrophile was required for the reaction to proceed. Therefore, the synthesis of chloroformate **125** was attempted by reacting alcohol **122** with triphosgene (Scheme 64). Unfortunately, the chloroformate could not be isolated; instead, benzyl chloride **126** was tentatively detected ($[M+H]^+$ found m/z = 396.5, calcd m/z = 396.2) in the crude product via LCMS analysis.

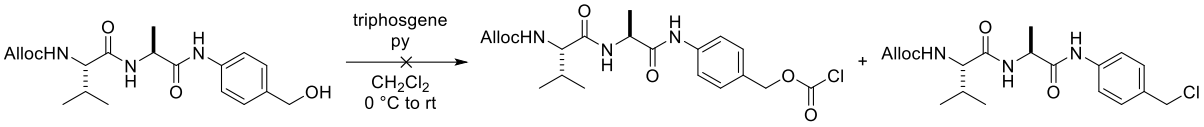

122 **125** not detected **126** *m/z* found

Scheme 64 Attempt at synthesising chloroformate **125**. None could be isolated with chloride **126** tentatively found instead.

To preserve the precious hemiasterlin, a model substrate was sought to replace the natural product. It was thought that available *N*-protected dipeptides **109** from the first-generation route (see Scheme 55) were ideally suited to this purpose. By hydrolysing compounds **109**, the obtained products can be used as the model substrate. Thus, dipeptide **127a** was synthesised from hydrolysis of trifluoroacetamide **109a** at 60 °C in good yield (Scheme 65). As chloroformate **125** may be too unstable for isolation, *in situ* generation of intermediate **125** and direct reaction with **127a** in a one-pot fashion was carried out, but was unsuccessful (Scheme 65).

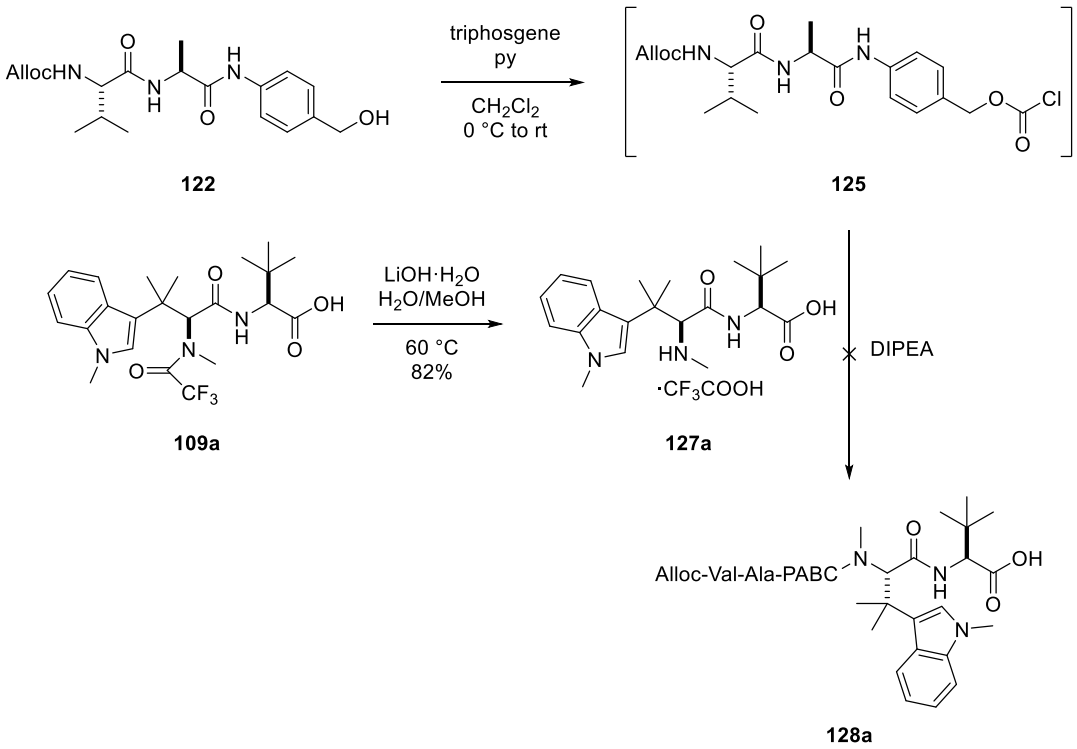

Scheme 65 Synthesis of **127a** and attempt at making **128a**.

As the activation on the alcohol side proved ineffective, it was thought that the polarity of the carbamate formation reaction could be reversed by activation of the secondary amine followed by treatment with the benzyl alcohol Alloc-Val-Ala-PABA. To prevent interference from the acid moiety, dipeptide **127a** was esterified using thionyl chloride in MeOH to give methyl ester **129a** in moderate yield (Scheme 66). First, conversion of amine **127a** to the corresponding carbamoyl chloride **130** was attempted via a reaction with triphosgene (Scheme 66).[442] While some carbamoyl chlorides are stable, attempts to isolate intermediate **130** were unsuccessful. To detect whether compound **130** was being formed, an aliquot was removed from the reaction mixture and quenched with MeOH. No methyl carbamate was detected via LCMS analysis and an *m/z* corresponding to hydantoin **131** was observed ($[M+H]^+$ found *m/z* = 414.5, calcd *m/z* = 414.2). The second proposed strategy involved the use of 1,1'-carbonyldiimidazole (CDI) to first form a carbamoylimidazole which would then be further activated by methylation to a carbamoylimidazolium before conversion to a carbamate.[443] Unfortunately, amine **129a** was unreactive towards CDI, and no carbamoylimidazole **132** formation was observed.

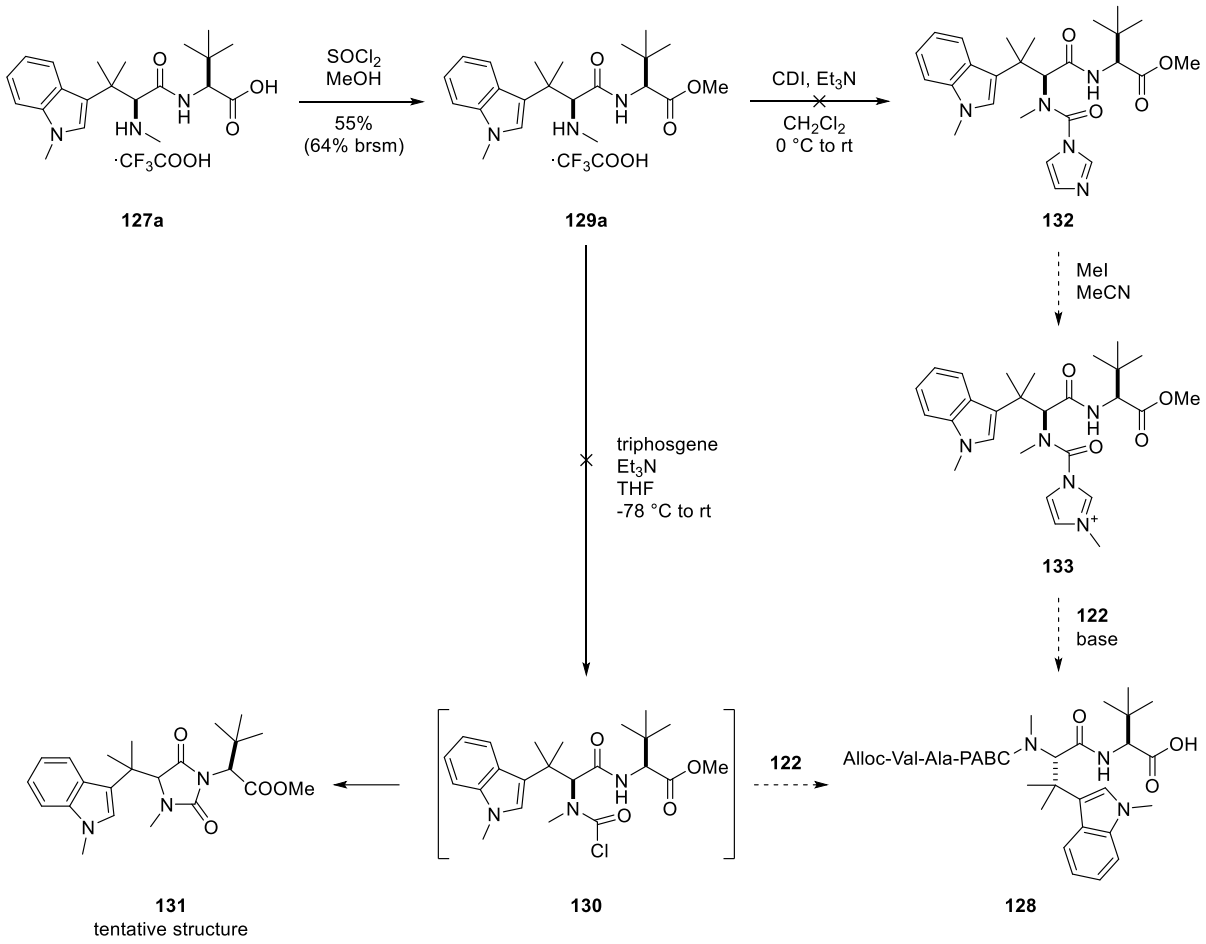

Scheme 66 Synthesis of amino ester **129a** and attempts at making carbamate **128a** through activation on the amine side. CDI = 1,1'-carbonyldiimidazole.

It was thought that the zwitterionic nature of hemiasterlin (or its model substrate) might have hindered its reaction with Alloc-Val-Ala-PABC-OPNP (**123**), and that protection of the acid as an alkyl ester would potentially aid reactivity. A method for the synthesis of carbamates employing *p*-nitrophenyl carbonate was thus revisited with the use of an ester substrate. A patent by Kim *et al*. reported the reaction between taltobulin ethyl ester and a *p*-nitrophenyl mixed carbonate with DIPEA and a catalytic amount of HOAt to form its corresponding carbamate in 43% yield.[444] Under these literature conditions, a reaction between amine **129a** and reactive carbonate **123** was performed (Scheme 67). Excitedly, a product which had an *m/z* corresponded to **128a** was observed via LCMS analysis ($[M+Na]^+$ found *m/z* = 813.5, calcd *m/z* = 813.4) affording 8% conversion.

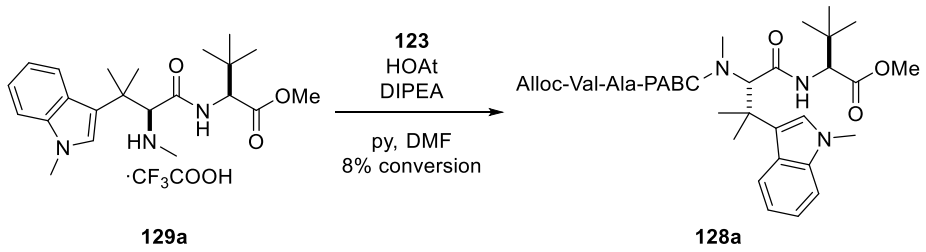

Scheme 67 Carbamate formation between **129a** and **123**. Conditions: **123** (1 equiv.), HOAt (0.2 equiv.), py:DMF (1:6), rt.

Encouraged by this result, it was decided to conduct an optimisation based on these conditions. Given the low availability of **129a** at the time, it was thought that using its epimer **129b**, which could be obtained from amply available precursor **99b**, as the model substrate instead would not cause a significant change to the reactivity of the amine. Thus, the epimer **129b** was synthesised via a $NaBH_4$ reduction of trifluoroacetamide **99b** in quantitative yield (Scheme 68).

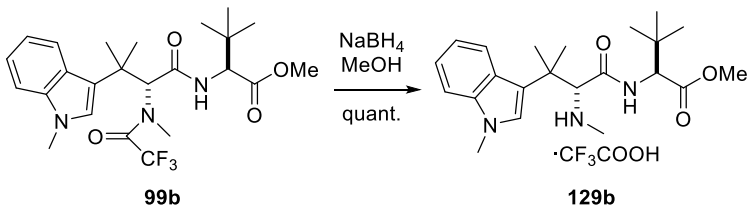

Scheme 68 Synthesis of amine **129b**.

With the model substrate in hand, an optimisation for the carbamate reaction was carried out (Table 16). It was found that the increase in HOAt and carbonate was critical for greater conversion (Table 16 Entries 2–3) while doubling the amount of pyridine stopped the reaction entirely (Table 16 Entry 4). Leaving the reactions for seven days, instead of 17 hours, approximately doubled the conversion (Table 16 Entries 5–7). However, changing the base to Et_3N or pre-activation of the carbonate did not give any appreciable change (Table 16 Entries 6–7).

Table 16 Optimisation for the synthesis of carbamate **128b**

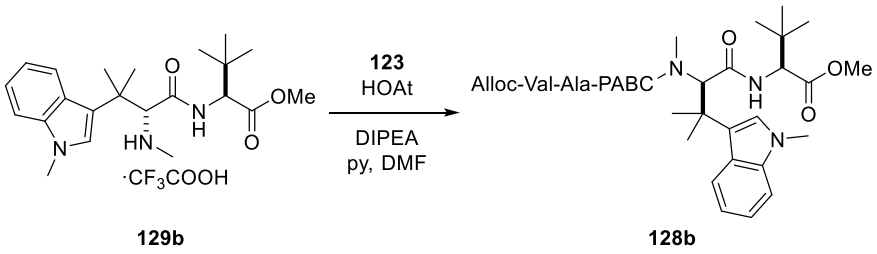

129b **128b**

Entry	123 (equiv.)	HOAt (equiv.)	DIPEA (equiv.)	py:DMF[a]	%conv.[b]
1[c]	1.1	0.2	2	1:6	8
2	2	1	2	1:6	35
3	2	0.2	4	1:6	10
4	2	0.2	2	1:3	0
5	2	1	4	1:6	54[d]
6	2	1	4[e]	1:6	53[d]
7[f]	2	1	4	1:6	55[d]

All reactions were conducted at room temperature. [a]Volumetric ratio. [b]Estimated by LCMS analysis after 17 h of reaction time. [c] **129a** was used to form **128a**, and no changes were observed after heating to 50 °C. [d]After seven days of reaction time. [e]Et_3N was used. [f]Carbonate **123** was pre-activated with HOAt before amine **129b** was added.

With feasible conditions in hand and to validate the reaction, carbamate **128b** was synthesised and isolated in 25% yield (47% brsm, Scheme 69). Its identity was confirmed by high-temperature ^{1}H-NMR; as at room temperature, a complex rotameric mixture was observed (see Appendix B for the spectra).

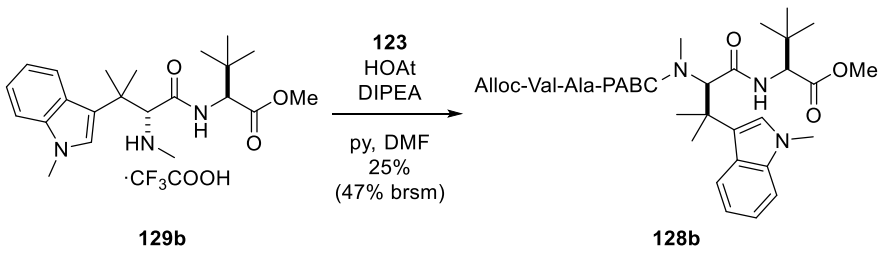

129b **128b**

Scheme 69 Synthesis of carbamate **128b**.

5.3.3. Preparation of the linker–drugs

With confirmed reaction conditions for modifying hemiasterlin with a cleavable dipeptide, synthesis of an azide-functionalised Val-Ala-PABC-hemiasterlin (and Val-Ala-PABC-taltobulin), to facilitate bioconjugation to an antibody was commenced (Scheme 70). First,

removal of the Alloc group from dipeptide **122** using $Pd(PPh_3)_4$ proceeded in excellent yield. The revealed free amine **134** was then amide coupled with N_3-PEG_4-COOH, giving azide **135**. Subsequent treatment with bis(*p*-nitrophenyl)carbonate afforded mixed carbonate **136** in 76% yield (Scheme 70a). Chemoselective removal of the trifluoroacetamide group from protected hemiasterlin **113a** and taltobulin **121a** was achieved using $NaBH_4$ (59% yield for **137** and 99% yield for **138**). Finally, the free amines were reacted with activated carbonate **136** to give azides **139** and **140** in moderate yields (Scheme 70b).

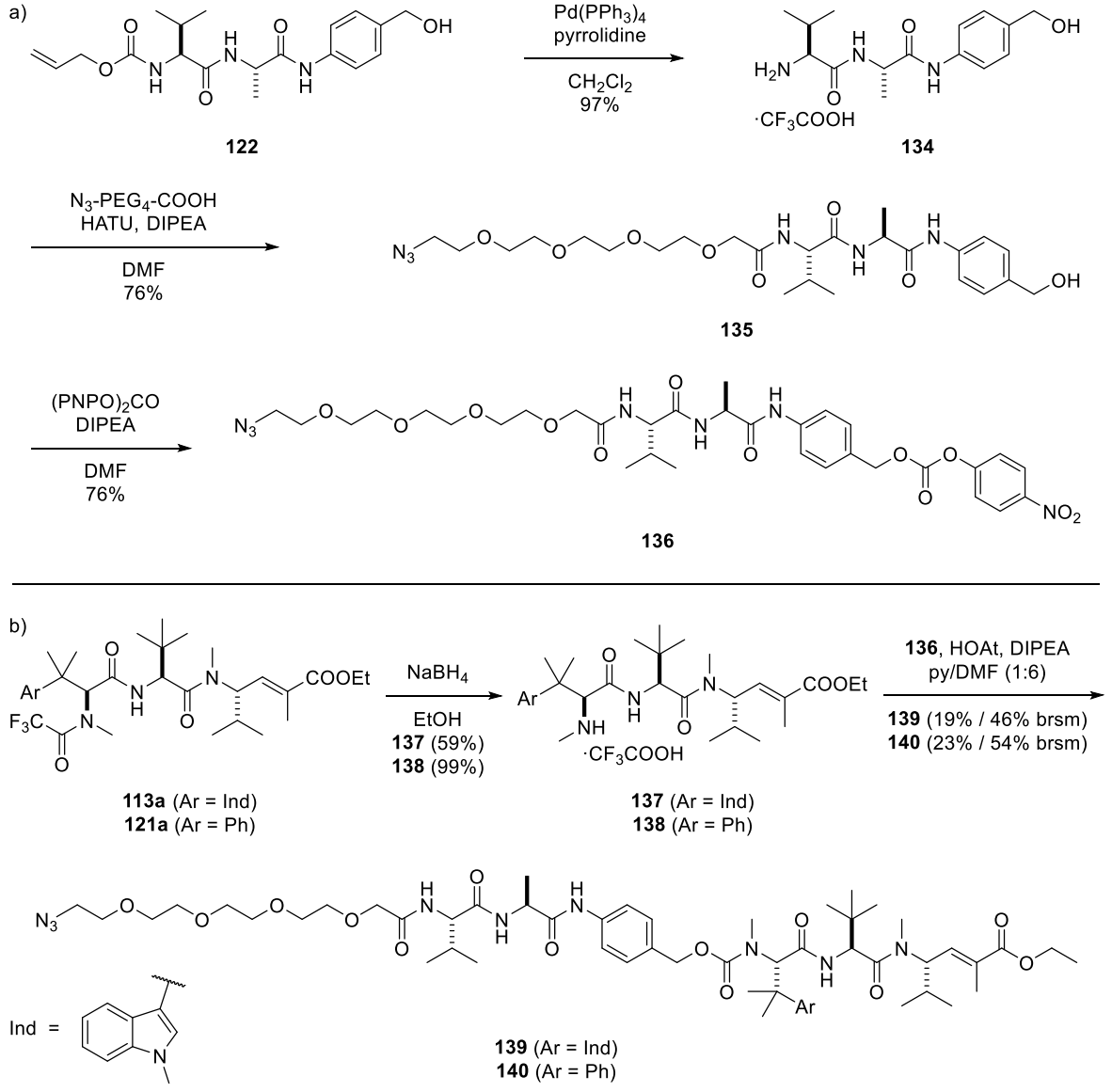

Scheme 70 a) Synthesis of *p*-nitrophenyl mixed carbonate **136**. b) Synthesis of azides **139** and **140**.

It was hypothesised that an alkynyl DVP could be prepared via a strategy resembling solid-phase peptide synthesis.[113] Introduction of a reactive alkyne could be achieved through the incorporation of propargylglycine (propargylGly) into the peptide-like chain. Furthermore, simultaneous incorporation of polyethylene glycol (PEG) chains and glutamic acid residues would improve the aqueous solubility of the linker–drug and decrease the hydrophobicity and aggregation propensity of the resultant ADCs. Thus, peptidomimetic H-PEG_2-Glu_3-PEG_2-

propargylGly-NH_2⊠TFA (**141**) was synthesised using a standard Fmoc-protecting group protocol on LL Rink Amide resin (Scheme 71). Following cleavage from the resin and RP-HPLC purification, amide coupling of amine **141** with DVP–carboxylic acid **142** (synthesised by Hikaru Seki, Spring Group, Department of Chemistry, University of Cambridge) produced the desired linker **143**. CuAAC reaction of DVP–alkyne **143** with azides **139** and **140** was followed by ester hydrolysis to give the final linker–drug compounds **144** and **145** after reverse-phase flash chromatography purification, which were characterised by analytical HPLC and HRMS.

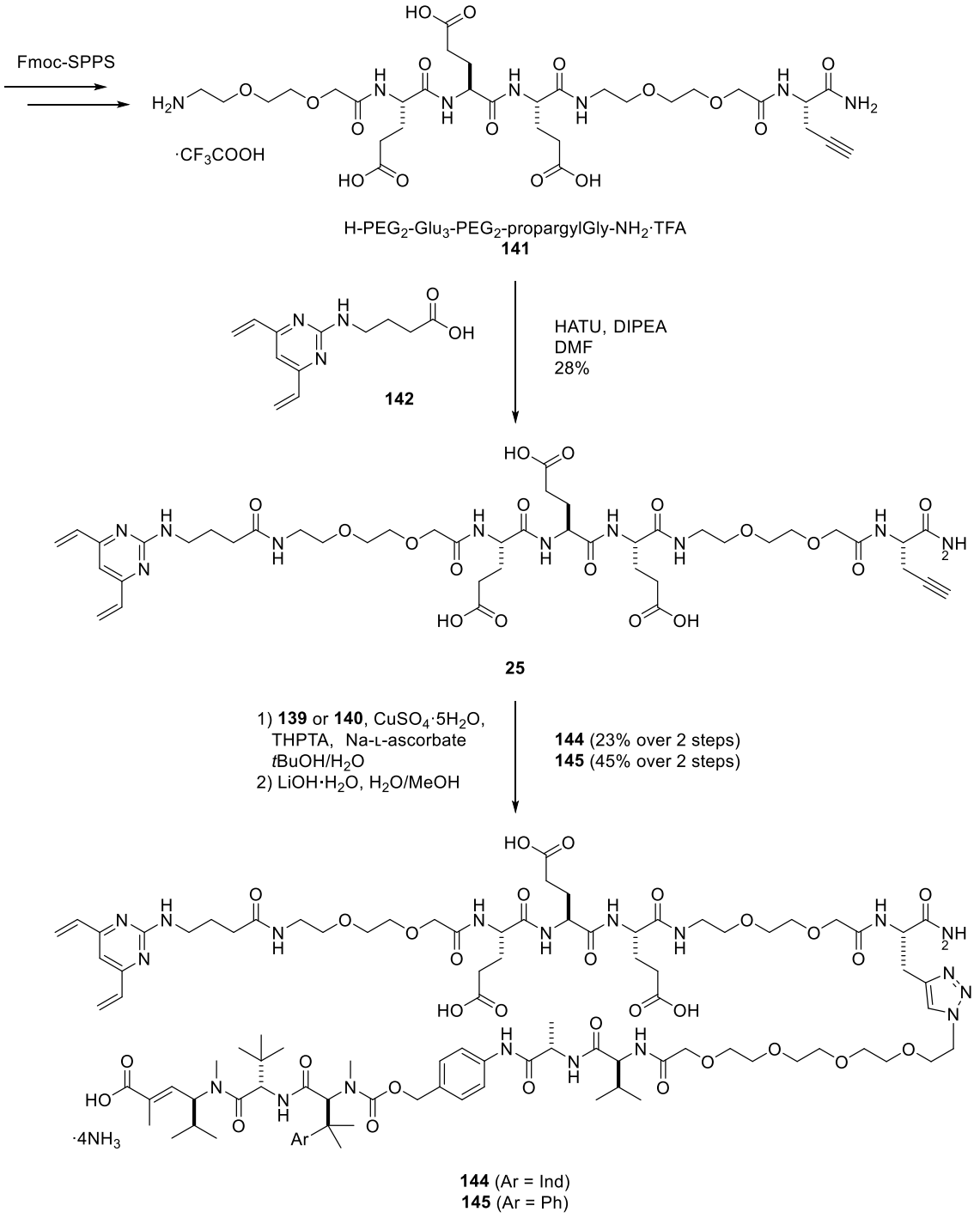

Scheme 71 Synthesis of linker–drugs **144** and **145**.

5.4. Synthesis of antibody–drug conjugates

With the desired linker–drugs in hand, synthesis of ADCs was undertaken. Trastuzumab is an FDA-approved mAb targeting human epidermal growth factor receptor 2 (HER2), a transmembrane receptor that is overexpressed in 20–30% of breast cancers.[445] The mAb also constitutes the antibody component of two marketed ADC drugs, Kadcyla® and Enhertu®.[235,242] Trastuzumab was chosen for this study to enable a comparison of hemiasterlin-based ADCs against other reported ADCs loaded with alternative cytotoxins.

To commence ADC synthesis, the four interchain disulfides in trastuzumab were reduced via treatment with tris(2-carboxyethyl)phosphine hydrochloride (TCEP) for 1 hour at 37 °C, revealing eight reactive thiols. The reduced antibody was then reacted with the DVP linker–drug compounds **144** and **145** for 4 hours at 37 °C (Scheme 72a). Pleasingly, LCMS and sodium dodecylsulfate–polyacrylamide gel electrophoresis (SDS-PAGE) analysis revealed >95% conversion to the rebridged antibody species **ADC 1** and **ADC 2** with a loading of four drug molecules per antibody (Scheme 72b–f). The SDS-PAGE analysis also showed significant formation of the half-antibody species whereby the hinge disulfides did not undergo interchain rebridging, which would have resulted in forming the full-antibody species; instead, non-native intrachain cross-linking of the reduced heavy chain cysteines occurred (Scheme 72b). This observation is in line with the usage of DVP as a rebridging linker, noting that the structural integrity and the ability of half-antibodies to bind to their cell-surface receptor is not impacted.[269] The LCMS and SDS-PAGE analysis was performed by Dr Stephen Walsh, Spring Group, Department of Chemistry, University of Cambridge.

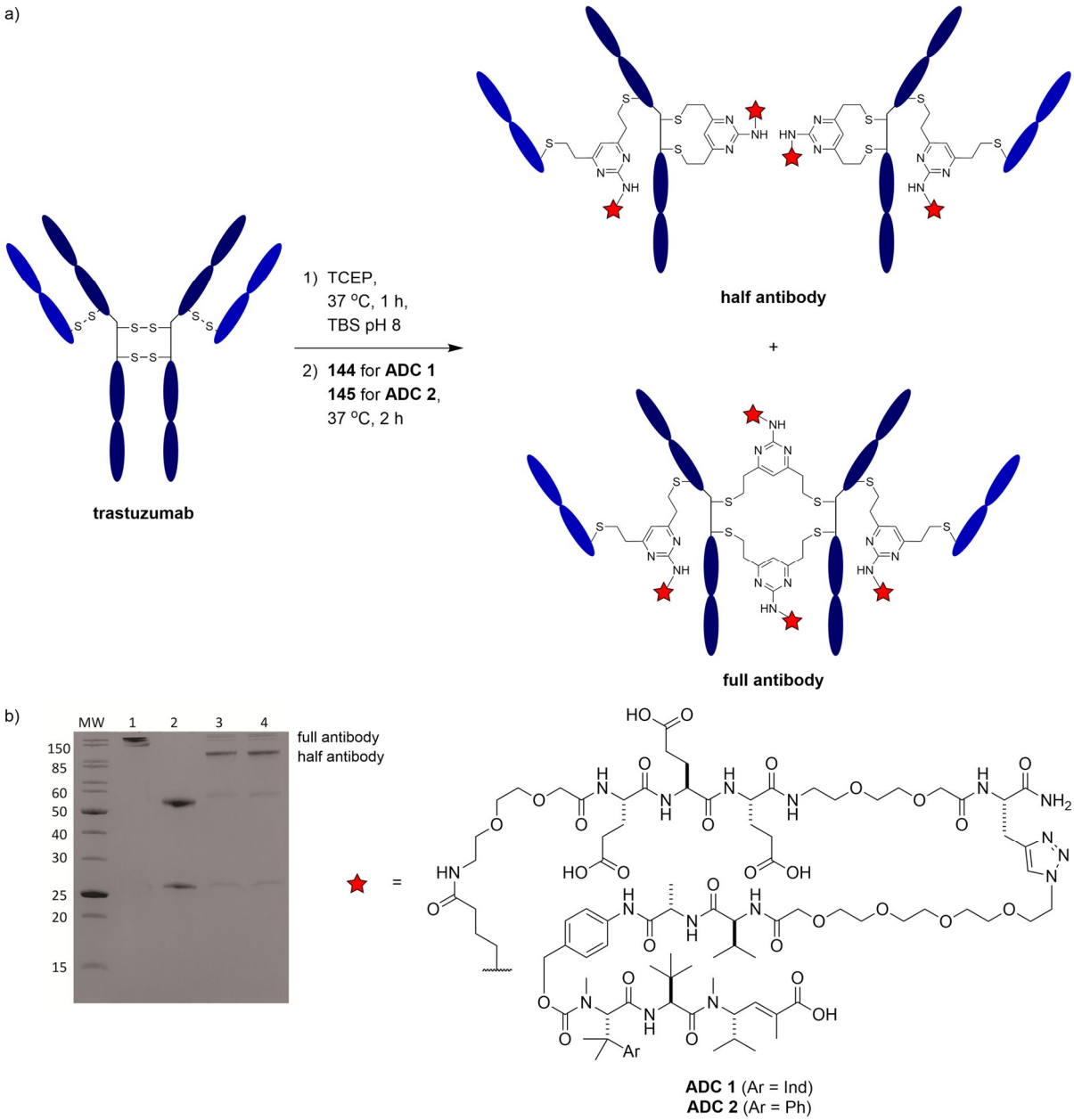

Scheme 72 a) Synthesis of **ADC 1** and **ADC 2**. b) SDS-PAGE analysis of the two ADCs; lane 1 is non-reducing, lanes 2–4 are reducing; lanes: MW = molecular weight marker, (1) trastuzumab, (2) reduced trastuzumab, (3) **ADC 1**, (4) **ADC 2**. TCEP = tris(2-carboxyethyl)phosphine hydrochloride, TBS = Tris-buffered saline (Tris·HCl 25 mM, NaCl, 25 mM, EDTA 0.5 mM pH 8).

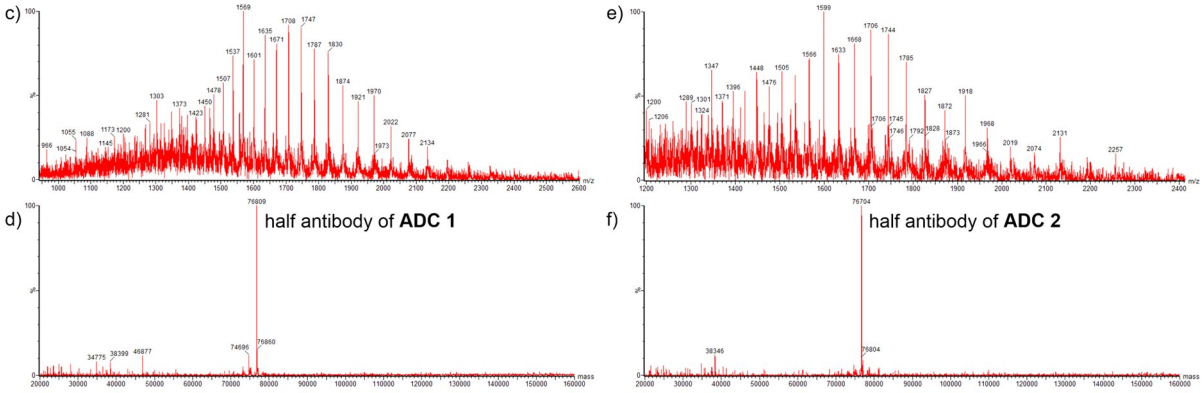

Scheme 72 (continued) c) Non-deconvoluted MS of **ADC 1**. d) Deconvoluted MS of **ADC 1**, expected for the half antibody 76806 Da, found 76809 Da e) Non-deconvoluted MS of **ADC 2**. f) Deconvoluted MS of **ADC 2**, expected for the half antibody 76700 Da, found 76704 Da. TCEP = tris(2-carboxyethyl)phosphine hydrochloride, TBS = Tris-buffered saline (Tris·HCl 25 mM, NaCl, 25 mM, EDTA 0.5 mM pH 8).

To investigate the aggregation propensity of the ADCs, size-exclusion chromatography (SEC) analysis was carried out. This analysis demonstrated that both ADCs had ⩾99.5% monomeric content, confirming minimal aggregation propensity with this linker–payload (Figure 52). The SEC analysis was performed by Teodors Pantelejevs, Hyvönen Group, Department of Biochemistry, University of Cambridge.

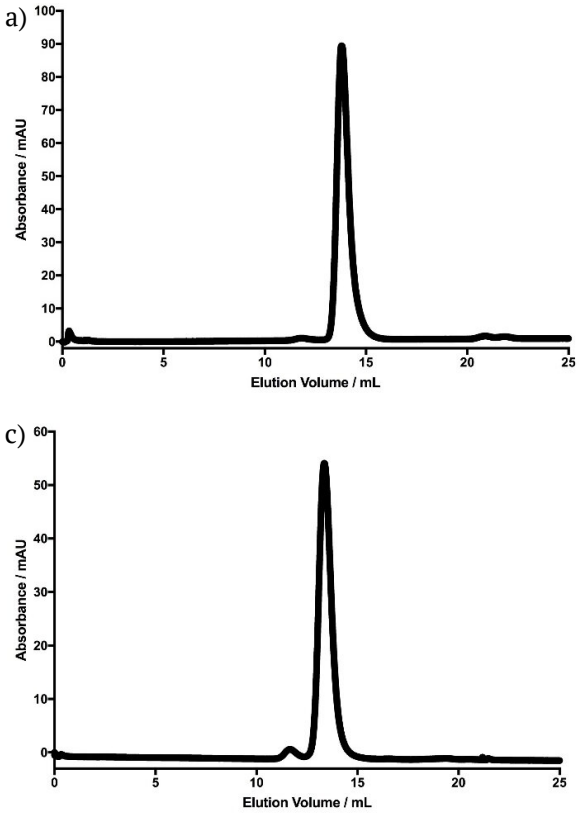

d)

ADC	% monomeric content
Trastuzumab	99.9
ADC 1	99.9
ADC 2	99.5

Figure 52 Size-exclusion chromatography (SEC) of trastuzumab and the two synthesised ADCs. Chromatograms from SEC analysis of a) trastuzumab b) **ADC 1** c) **ADC 2**. d) Monomeric content of trastuzumab, **ADC 1**, and **ADC 2**.

5.5. Biological evaluation of the ADCs and the small molecules

To investigate the biological activity of hemiasterlin, taltobulin, and their corresponding ADCs, their effect on the cell viability of both HER2-positive (SKBR3, BT474) and HER2-negative (MCF7) cell lines was determined (Table 17 and Figure 53). The cellular assays were performed by Dr Stephen Walsh, Spring Group, Department of Chemistry, University of Cambridge. Hemiasterlin exhibited sub-nanomolar cytotoxicity against all cell lines, whilst the potency of taltobulin was approximately one order of magnitude lower.[360] Pleasingly, both **ADC 1** and **ADC 2** displayed exquisite cytotoxicity against SKBR3 and BT474 cells, comparable to that reported for an analogous cathepsin-cleavable trastuzumab–MMAE ADC.[113,285] Moreover, both ADCs had negligible activity against MCF7 cells at the concentrations tested. These combined data suggest that both hemiasterlin and taltobulin have the potential to serve as cytotoxic payloads in the development of ADCs and other targeted therapeutics, and that they can generate equivalent potency as clinically validated payloads.

Table 17 *In vitro* cellular evaluation of **56**, **57**, **ADC 1** and **ADC 2** in comparison with MMAE and Tras–MMAE.

IC_{50} (nM)†	SKBR3 (HER2+)	BT474 (HER2+)	MCF7 (HER2-)
Hemiasterlin (**56**)	0.18	0.15	0.37
Taltobulin (**57**)	1.12	1.40	3.00
MMAE*	0.08	0.12	0.2
ADC 1	0.086	0.27	>50
ADC 2	0.25	0.45	>50
Tras–MMAE*	0.041	0.092	>30

†Each data point is an average of independent triplicates. *Data from Walsh *et al.*[269] and Bargh *et al.*[285]

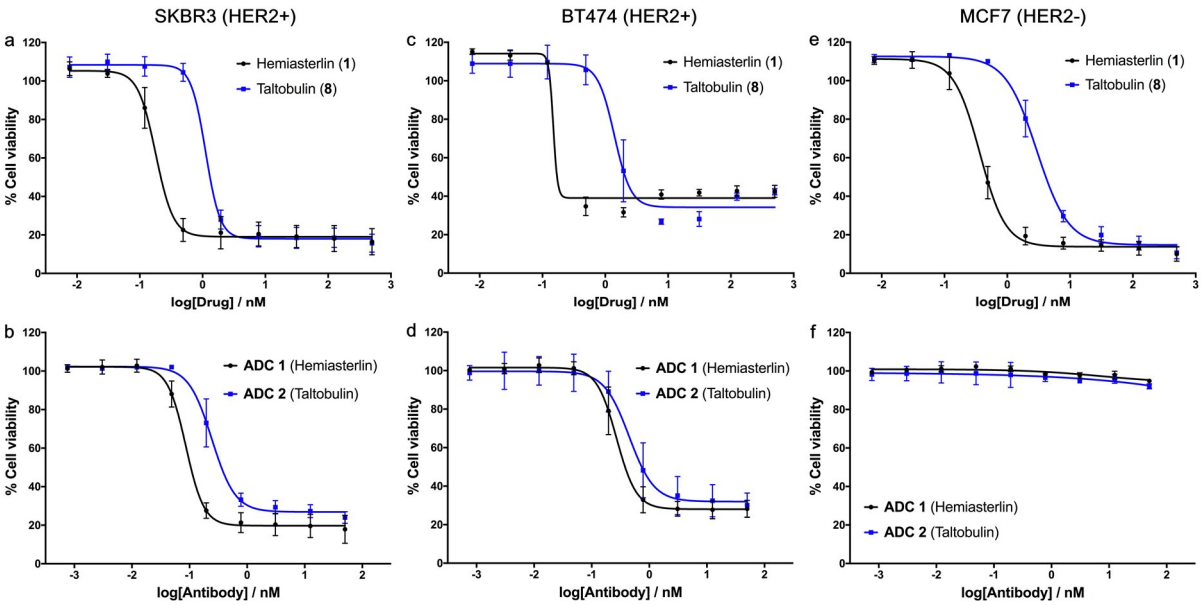

Figure 53 Cellular viability assays of **56**, **57**, **ADC 1**, and **ADC 2** in a), b) HER2-positive SKBR3 cells, c), d) HER2-positive BT474 cells, and e), f) HER2-negative MCF7 cells.

5.6. Conclusion and future work

In conclusion, the total synthesis of hemiasterlin (**56**) has been accomplished via a four-component Ugi reaction with a longest linear sequence of 10 steps, in 11% overall yield. The improved synthetic approach allows for simple analogue exploration on the *N*-terminus of the molecule, which was demonstrated by the synthesis of taltobulin (**57**), a synthetic derivative of hemiasterlin. ADCs synthesised from the two compounds, **ADC 1** and **ADC 2**, showed exceptionally potent and selective bioactivity, similar to that of an analogous MMAE ADC. With its relatively short synthesis and high cytotoxicity, this study paves the way for the future use of hemiasterlin and its analogues as payloads in ADC therapeutics. Furthermore, this represents the first documented use of hemiasterlin and its ADC in the treatment of breast cancer, showcasing its potential in the treatment of this disease.

Future work will first focus on improving the Ugi-4CR step. While the overall yield of the reaction was satisfactory, the low diastereoselectivity can still be enhanced. Further catalyst exploration can be done with other available CPAs. Another two interesting CPAs are the octahydro-BINOL-based **CPA5** and the SPINOL-based **CPA6** which have been reported to induce enantioselectivity in Ugi reactions (Figure 54).[438,439]

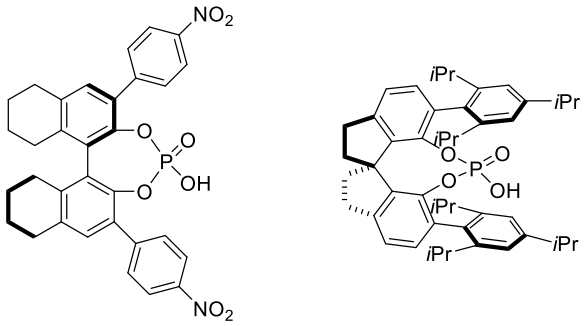

CPA5 **CPA6**

Figure 54 Structures of **CPA5** and **CPA6**.

Another issue that was encountered during the synthesis of hemiasterlin was the poor scalability of the Ugi-4CR for generating protected hemiasterlin **113**. It was noticed that the yield dropped significantly in larger-scale reactions (down to 24% at 100 mg scale with respect to aldehyde **69**). In contrast, the Ugi-4CR in the first-generation route was not impacted (up to 400 mg scale with respect to aldehyde **69**). Thus, it is hypothesised that using a convertible isonitrile, to avoid the formation of oxazole entirely may solve this problem (Scheme 73). Convertible isonitriles are isonitriles which can be easily replaced by various functional groups after IMCRs.[446–449] One suitable candidate is compound **146**, developed by Kobayashi and co-workers.[450] Wessjohann *et al.* reported the application of this isonitrile for peptide ligation and macrocyclisation.[451] Following their report, it is hypothesised that upon treatment of the Ugi products **147** with camphorsulfonic acid (CSA), the activated *N*-acylindole is obtained which can then be converted to the desired peptide **113** via a reaction with free amine **66**.

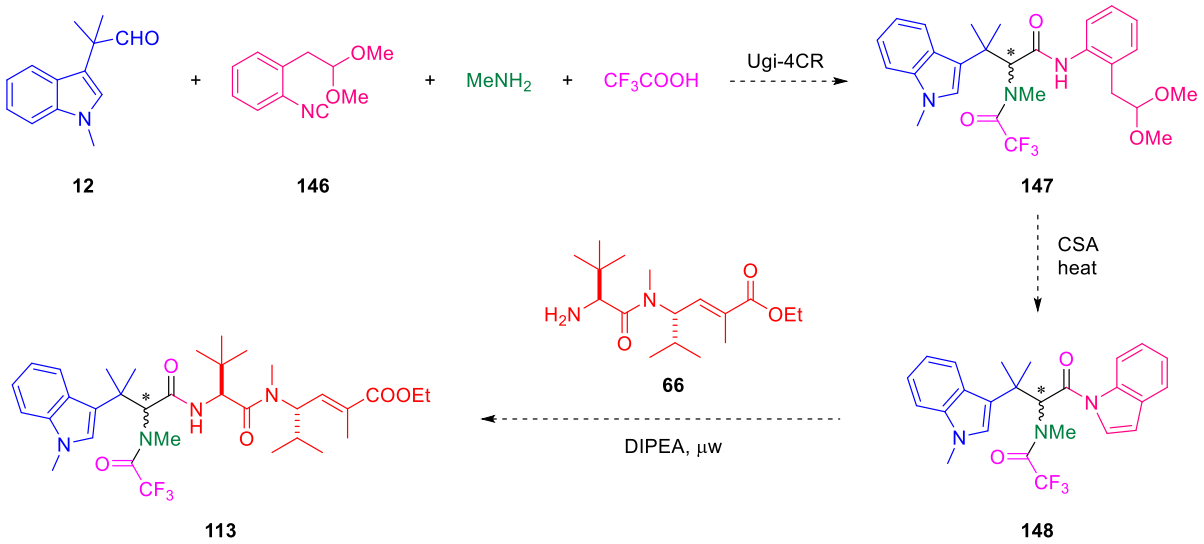

Scheme 73 Proposed new route for the synthesis of analogues of hemiasterlin via the use of convertible isonitrile **146**.

Further work will also include synthesis of hemiasterlin analogues with the indole ring functionalised with an amino group. It was proposed that the steric bulk around the secondary amine of hemiasterlin was hindering the carbamate formation resulting in low

yield. To provide an alternative vector for a linker attachment, installation of an amino group on the indole ring will therefore be explored. The aldehydes **151** are thought to be accessible through commercially available aminoindoles **149** via a Ru-catalysed C3-alkylation of indole (Scheme 74).[452] The amino group in **149** will first be protected and then alkylated at the C3 position to give indoles **150**. The alkylated indoles will then be *N*-methylated and transformed to aldehydes **151** using the same synthetic strategy as described in section 5.2.2. The generated aldehydes can then be used in the Ugi-4CR to produce other hemiasterlin analogues. The synthesised amino-substituted hemiasterlin analogues will then be tested in cytotoxicity assays to determine the most active regioisomer. Finally, this isomer will be investigated for the synthesis of corresponding linker–drug compound and ADC.

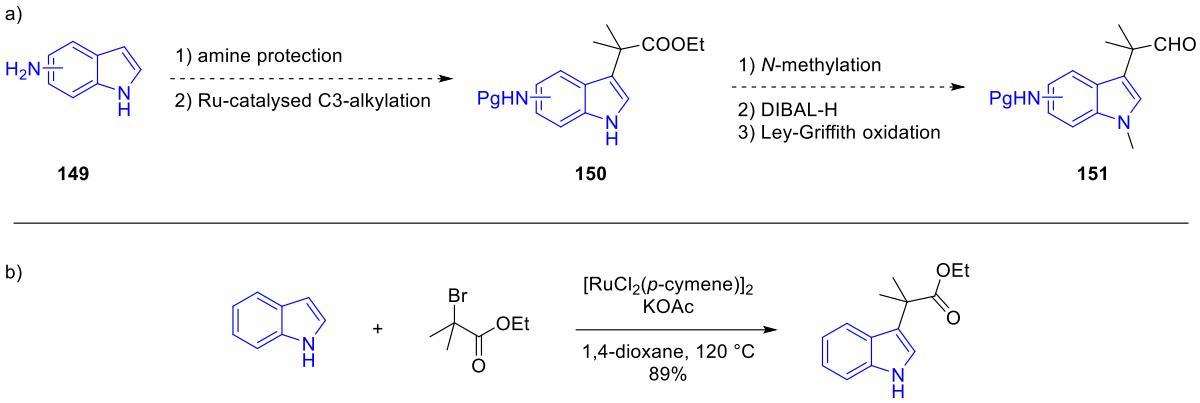

Scheme 74 a) Proposed synthesis of amine-functionalised indoles **151** for the generation of hemiasterlin analogues. b) Ru-catalysed C3-alkylation of 1*H*-indole.[452] Pg = protecting group.

Section III:

Experimental

Chapter 6 — Experimental

6.1. General experimental

General methods: All reactions were carried out under nitrogen atmosphere using oven-dried glassware at rt unless otherwise stated. Temperatures of −78 °C were maintained using a dry ice–acetone bath. Temperatures of 0 °C were maintained using an ice-water bath. Room temperature (rt) refers to ambient temperature.

Solvents: Dichloromethane (CH_2Cl_2), methanol (MeOH) and toluene were distilled from calcium hydride. Tetrahydrofuran (THF) was dried using sodium wire and distilled from a mixture of calcium hydride and lithium aluminium hydride with triphenylmethane as an indicator. Diethyl ether (Et_2O) was distilled from a mixture of calcium hydride and lithium aluminium hydride. Ethyl acetate (EtOAc) was distilled before use. 40–60 petroleum ether was distilled before use and refers to the fraction between 40–60 °C. Acetonitrile (MeCN), anhydrous dimethylformamide (DMF) and *tert*-butyl alcohol (*t*BuOH) were purchased from commercial sources and used without further purification.

Reagents: Unless otherwise stated, all reagents were used as received from commercial sources or prepared as described in the literature. The chemicals were handled in accordance with COSHH regulations.

Yield: Refer to chromatographically and spectroscopically pure compounds unless otherwise stated.

Flash column chromatography: Carried out using slurry-packed Merck 9385 Kieselgel 60 SiO_2 (230–400 mesh) or Combiflash Rf200 automated chromatography system with Redisep® normal-phase silica flash columns (35–70 μm) or Redisep® reverse-phase C18-silica flash columns (20–40 μm). Yields refer to chromatographically and spectroscopically pure compounds unless otherwise stated.

Analytical thin-layer chromatography (TLC): Carried out on glass plates coated with silica (0.2 mm, Merck Kieselgel 60 F254). Visualisation was done using UV irradiation (254 nm and 365 nm) or staining with potassium permanganate, ninhydrin, or vanillin dips made using standard procedures. Retardation factors (R_f) are quoted to the nearest 0.01.

Preparative thin-layer chromatography: Carried out on glass plates coated with silica (1 mm, Merck Kieselgel 60 F254). Visualisation was done using UV fluorescence (254 nm and 365 nm).

Melting points (mp): Measured using a Büchi melting point B545 apparatus or Gallenkamp MPD350.BM2.5 melting point apparatus and are uncorrected.

Optical rotations ($[\alpha]_D$): Recorded on an Anton-Paar MCP polarimeter and are reported in deg dm^{-1} cm^3 g^{-1} at 589 nm. Concentrations (c) are given in g $(100\ mL)^{-1}$.

General nuclear magnetic resonance spectroscopy: Processed using TopSpin v. 3.5 or 4.0 (Bruker). An aryl, quaternary, or two or more possible assignments were given when signals could not be distinguished by any means. Measured coupling constants are reported for mutually coupled signals; coupling constants are labelled apparent (app) in the absence of an observed mutual coupling, or multiplet (m) when none can be determined.

Proton magnetic resonance (^{1}H-NMR) spectroscopy: Recorded using an internal deuterium lock (at ambient temperature unless stated otherwise) on Bruker Avance III HD (400 MHz, Smart Probe), Bruker Avance III HD (400 MHz, BBO Probe), Bruker Neo Prodigy (400 MHz, Prodigy Cryoprobe), Bruker Avance III (400 MHz, QNP Cryoprobe), Bruker Avance III (500 MHz; DCH Cryoprobe), Bruker Avance (600 MHz, BBI probe), or Bruker Avance II+ (700 MHz, TBO Cryoprobe) spectrometers. Proton assignments are supported by ^{1}H–^{1}H COSY, ^{1}H–^{13}C HSQC or ^{1}H–^{13}C HMBC spectra, or by analogy. Chemical shifts (δ_H) are quoted in ppm to the nearest 0.01 ppm and are referenced to the residual non-deuterated solvent peak.[453] Discernible coupling constants (*J*) are reported as measured values in Hz, rounded to the nearest 0.1 Hz. Data are reported as: chemical shift, multiplicity (br, broad; s, singlet; d, doublet; t, triplet; q, quartet; qn, quintet; m, multiplet; ABq, AB quartet; or a combination thereof), coupling constants, number of nuclei, and assignment.

Carbon nuclear magnetic resonance (^{13}C-NMR) spectroscopy: Recorded using an internal deuterium lock at ambient temperature on Bruker Avance III HD (101 MHz, Smart Probe), Bruker Avance III HD (101 MHz, BBO Probe), Bruker Neo Prodigy (101 MHz, Prodigy Cryoprobe), Bruker Avance III (101 MHz, QNP Cryoprobe), Bruker Avance III (126 MHz; DCH Cryoprobe), or Bruker Avance II+ (176 MHz, TBO Cryoprobe) spectrometers with broadband proton decoupling. Carbon spectra assignments are supported by DEPT editing, ^{1}H–^{13}C HSQC or ^{1}H–^{13}C HMBC spectra, or by analogy. Chemical shifts (δ_C) are quoted in ppm to the nearest 0.1 ppm and are referenced to the deuterated solvent peak.[453] Coupling constants between carbon and other nuclei (X) over *n* bonds ($^{n}J_{C\text{-}X}$) are reported as measured values in Hz, rounded to the nearest 0.1 Hz. Data are reported as: chemical shift, multiplicity (if not a singlet), coupling constants, number of nuclei (if not one), and assignment.

Fluorine nuclear magnetic resonance (^{19}F-NMR) spectroscopy: Recorded on Bruker Avance III (376 MHz; QNP Cryoprobe) or Bruker Avance III HD (376 MHz; Smart probe) spectrometers. Chemical shifts (δ_F) are quoted in ppm to the nearest 0.1 ppm, from $CFCl_3$, and are uncorrected. Data are reported as: chemical shift, multiplicity (if not a singlet), and coupling constants.

Infrared spectroscopy (IR): Recorded neat on a Perkin Elmer Spectrum One FT-IR spectrometer fitted with an attenuated total reflectance (ATR) sampling accessory. Selected absorption maxima ($\tilde{\nu}_{max}$) are quoted in wavenumbers (cm^{-1}) with the following abbreviations: w, weak; m, medium; s, strong; vs, very strong; br, broad.

Ultraviolet–visible spectroscopy (UV-Vis): Recorded on a NanoDrop™ One spectrophotometer. The absorption maxima (λ_{max}) are reported in nanometres (nm).

Liquid chromatography–mass spectrometry (LCMS): Chromatographs were recorded using a Waters ACQUITY H-Class UPLC with an ESCi Multi-Mode Ionisation Waters SQ Detector 2 spectrometer using MassLynx 4.1 software; ESI refers to the electrospray ionisation technique; LC system: solvent A: 2 mM NH_4OAc in H_2O/MeCN (95:5); solvent B: MeCN; solvent C: 2% formic acid; column: ACQUITY UPLC® CSH C18 (2.1 mm × 50 mm, 1.7 µm, 130 Å) at 40 °C; gradient: 5–95 % B with constant 5 % C over 1 min at flow rate of 0.6 mL/min; detector: PDA eλ Detector 220–800 nm, interval 1.2 nm

High-resolution mass spectrometry (HRMS): Recorded using Waters LCT Premier Time of Flight (ToF), ThermoFinnigan Orbitrap Classic, Waters Vion IMS Qtof, or Micromass Q-TOF mass spectrometers using electrospray ionisation (ESI) or atmospheric solids analysis probe (ASAP) techniques. Reported mass values are within the error limits of ±5 ppm mass units.

High-performance liquid chromatography (HPLC): Analytical chromatographs were obtained on an Agilent 1260 Infinity using a Supercosil ABZ+PLUS column (150 mm × 4.6 mm, 3 µm) eluting with a linear gradient system (solvent A: 0.05% (v/v) TFA in H_2O, solvent B: 0.05% (v/v) TFA in MeCN) over 15 min at a flow rate of 1 mL/min. Retention times (t_R) are quoted in minutes to 2 decimal places. Semi-preparative HPLC was carried out on an Agilent 1260 Infinity using a Supercosil ABZ+PLUS column (250 mm × 21.2 mm, 5 µm) eluting with a linear gradient system (solvent A: 0.1% (v/v) TFA in H_2O, solvent B: 0.05% (v/v) TFA in MeCN) over 20 min at a flow rate of 20 mL/min. HPLC was monitored by UV absorbance at 220 and 254 nm.

Elemental analysis: Performed by the University of Cambridge Microanalytical Laboratory in the Department of Chemistry and are quoted to the nearest 0.01% for all elements.

Protein liquid chromatography–mass spectrometry (Protein LCMS): Performed on a Xevo G2-S TOF mass spectrometer coupled to an Acquity UPLC system using an Acquity UPLC BEH300 C4 column (1.7 µm, 2.1 × 50 mm). H_2O with 0.1% formic acid (solvent A) and 95% MeCN and 5% H_2O with 0.1% formic acid (solvent B), were used as the mobile phase at a flow rate of 0.2 mL/min. The gradient was programmed as follows: 95% A for 0.93 min, then a gradient to 100% B over 4.28 min, then 100% B for 1.04 min, then a gradient to 95% A over 1.04 min. The electrospray source was operated with a capillary voltage of 2.0 kV and a cone voltage of 150 V. Nitrogen was used as the desolvation gas at a total flow of 850 L h^{-1}. Total mass spectra were reconstructed from the ion series using the MaxEnt algorithm preinstalled on MassLynx software (v4.1 from Waters) according to the manufacturer's instructions. Trastuzumab samples were deglycosylated with PNGase F (New England Biolabs) prior to LCMS analysis. The analyses were performed by Dr Stephen Walsh, Spring Group, Department of Chemistry, University of Cambridge.

6.2. Chapter 4 Experimental

6.2.1. Molecular modelling

Molecular modelling was performed by Dr Yaw Sing Tan, Verma Group, A*STAR Institute, Singapore.

Initial molecular models of the covalent *i*, *i*+7 stapled peptide were created using the Builder module in PyMOL.[454]

Preparation of structures

The structure of MDM2 in complex with a stapled peptide (PDB code 5AFG)[103] was used as the initial structure for molecular dynamics (MD) simulations. The stapled peptide (LTFXEYWAQLXS, in which X are the stapled residues) was mutated to the PMI peptide (TSFAEYWNLLSP) using the LEaP module of AMBER 14.[455] The point mutations E69A and K70A in MDM2 were reversed. PMI was modified into stapled peptides **P6-81** and **P6-93** (Ac-TSFAXYWNGLSX-NH_2) by replacing residues 5 and 12 with a two-component triazole staple, formed by a double-click reaction between two azido-ornithine residues and 3,5-diethynylbenzenesulfonyl fluoride (**81**), and between two azido-ornithine residues and 4-((3,5-diethynylbenzoyl)oxy)-2,3,5,6-tetrafluorobenzenesulfonate (**93**), respectively. Leu9 was mutated to Gly in these stapled peptides to avoid steric clashing of the side chain with the staple. The respective sulfonamide and ester covalent complexes of these stapled peptides with Lys94 of MDM2 were further generated. MDM2 was capped at its *N*- and *C*-termini by acetyl and N-methyl groups respectively while the peptides were capped at their *N*- and *C*-termini by acetyl and amide groups, respectively. PDB2PQR[456] was used to determine the protonation states of residues. Each MDM2 complex was solvated with TIP3P water molecules[457] in a periodic truncated octahedron box, such that its walls were at least 9 Å away from the complex, and neutralised with sodium ions.

Molecular dynamics

Energy minimisations and MD simulations were performed with the sander and PMEMD modules of AMBER 14,[455] respectively. Three independent MD simulations were carried out on each of the complexes using the ff14SB[458] and generalised AMBER force fields (GAFF).[459] Atomic charges for the stapled residues were derived using the R.E.D. Server,[460] which fits restrained electrostatic potential (RESP) charges[461] to a molecular electrostatic potential (MEP) computed by the Gaussian 09 program[462] at the HF/6-31G* theory level. All bonds involving hydrogen atoms were constrained by the SHAKE algorithm,[463] allowing for a time step of 2 fs. Nonbonded interactions were truncated at 9 Å, while the particle mesh Ewald method[464] was used to account for long-range electrostatic interactions under periodic

boundary conditions. Weak harmonic positional restraints with a force constant of 2.0 kcal mol^{-1} $Å^{-2}$ were placed on the protein and peptide non-hydrogen atoms during the minimisation and equilibration steps. Energy minimisation was carried out using the steepest descent algorithm for 500 steps, followed by the conjugate gradient algorithm for another 500 steps. The systems were then heated gradually to 300 K over 50 ps at constant volume before equilibration at a constant pressure of 1 atm for another 50 ps. Subsequent unrestrained equilibration (2 ns) and production (100 ns) runs were carried out at 300 K using a Langevin thermostat[465] with a collision frequency of 2 ps^{-1}, and 1 atm using a Berendsen barostat[466] with a pressure relaxation time of 2 ps.

6.2.2. Synthetic procedures

6.2.2.1. Synthesis of staple 81

((5-Bromo-1,3-phenylene)bis(ethyne-2,1-diyl))bis(trimethylsilane) (82)

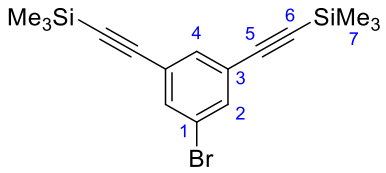

$PdCl_2(PPh_3)_2$ (362 mg, 0.516 mmol), PPh_3 (271 mg, 1.03 mmol), *i*Pr_2NH (10 mL), (trimethylsilyl)acetylene (3.21 mL, 22.7 mmol), and CuI (98.3 mg, 0.516 mmol) were added to a solution of 1,3,5-tribromobenzene (3.25 g, 10.3 mmol) in THF (30 mL). After stirring at 50 °C for 20 h, the reaction mixture was allowed to cool to rt, filtered through Celite®, and concentrated *in vacuo*. H_2O and $CHCl_3$ were added, the phases separated, and the aqueous phase was extracted further with $CHCl_3$ (3 × 25 mL). The combined organic phase was dried over Na_2SO_4, filtered, and the solvent removed *in vacuo* to give a brown liquid. The crude product was purified by column chromatography (100% hexane) and further purified by preparative thin-layer chromatography (100% hexane) to give compound **82** as a colourless liquid (1.75 g, 5.01 mmol, 48%).

R_f = 0.34 (hexane)

^{1}H NMR (400 MHz, $CDCl_3$): δ_H = 7.54 (d, *J* = 1.2 Hz, 2 H, H-2), 7.50 (t, *J* = 1.4 Hz, 1 H, H-4), 0.25 (s, 18 H, H-7)

^{13}C NMR (101 MHz, $CDCl_3$): δ_C = 134.6 (C-2), 134.1 (C-4), 125.2 (C-1), 121.8 (C-3), 102.6 (C-5), 96.7 (C-6), −0.1 (C-7)

IR (ATR): $\tilde{\nu}_{max}$ / cm^{-1} = 2959 (m, -C-H), 2157 (m, C≡C), 1738 (m), 1550 (m, C=C)

HRMS (ASAP$^+$): *m/z* $[M]^+$ calcd for $C_{16}H_{21}BrSi_2$: 348.0365; found: 348.0352 (Δ = −3.7 ppm)

Prepared according to Hirose *et al.*[467] Spectroscopic data are in accordance with the literature.[467]

3,5-Dibromonitrobenzene (87)

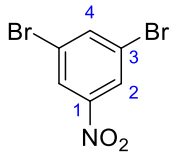

To an ice-cooled solution of 2,6-dibromo-4-nitroaniline (11.8 g, 40.0 mmol) in ethanol (250 mL), was added drop-wise concentrated H_2SO_4 (21.3 mL, 0.383 mol) over 30 min. The reaction mixture was heated to 60 °C, and $NaNO_2$ (8.83 g, 0.128 mol) was added portion-wise. The reaction was then heated to reflux at 90 °C for 3 h. The mixture was allowed to cool to rt before being poured into ice-water. The resulting brown solid was filtered and washed with H_2O. The crude product was purified by column chromatography (eluting gradient hexane:CH_2Cl_2 from 40:1 to 6:1) to give 3,5-dibromonitrobenzene as a pale yellow solid (7.19 g, 25.6 mmol, 64%).

$\boldsymbol{R_f}$ = 0.25 (hexane:CH_2Cl_2 = 6:1)

mp = 104–106 °C (lit.[468] 104 °C)

^{1}H NMR (400 MHz, $CDCl_3$): δ_H = 8.33 (d, *J* = 1.7 Hz, 2 H, H-2), 8.01 (t, *J* = 1.7 Hz, 1 H, H-4)

^{13}C NMR (101 MHz, $CDCl_3$): δ_C = 149.2 (C-1), 140.2 (C-4), 125.7 (C-2), 123.6 (C-3)

IR (ATR): $\tilde{\nu}_{max}$ / cm^{-1} = 3076 (s, =C-H), 1802 (w, =C-H), 1763 (w, =C-H), 1528 (s, N-O), 1334 (s, N-O)

HRMS (ASAP$^+$): *m/z* [M]$^+$ calcd for $C_6H_3{}^{79}Br_2NO_2$: 278.8531; found: 278.8526 (Δ = −1.8 ppm)

Prepared according to Görl *et al.*[469] Spectroscopic data are in accordance with the literature.[469]

1,3-Diethynyl-5-nitrobenzene (86)

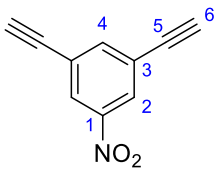

3,5-Dibromonitrobenzene **87** (1.18 g, 4.20 mmol), $Pd(PPh_3)Cl_2$ (884 mg, 1.26 mmol), CuI (40.0 mg, 0.210 mmol) and PPh_3 (110 mg, 0.419 mmol) were dissolved in *i*Pr_2NH (4 mL) and toluene (12 mL). The mixture was stirred at rt for 5 min before (trimethylsilyl)acetylene (2.37 mL, 16.8 mmol) was added. The reaction mixture was stirred at 80 °C for 17 h. It was then allowed to

cool to rt, and a solution of KOH (943 mg, 16.8 mmol) in H_2O (0.7 mL) and MeOH (2.8 mL) was added in one portion. The mixture was stirred for another 3 h, quenched with saturated aqueous NH_4Cl solution (80 mL) and then extracted with CH_2Cl_2 (3 × 70 mL). The combined organic phases were filtered through Celite®, washed with aqueous HCl (2 M, 70 mL), H_2O (70 mL), and brine (70 mL), dried over $MgSO_4$, and the solvent was removed *in vacuo*. The crude product was purified by column chromatography (eluting gradient hexane:CH_2Cl_2 from 40:1 to 6:1) to give 1,3-diethynyl-5-nitrobenzene as a grey solid (488 mg, 2.85 mmol, 68%).

R_f = 0.13 (hexane:CH_2Cl_2 = 6:1)

mp = 115–117 °C (lit.[470] 113.5–115 °C)

^{1}H NMR (400 MHz, $CDCl_3$): δ_H = 8.29 (d, *J* = 1.4 Hz, 2 H, H-2), 7.87 (t, *J* = 1.4 Hz, 1 H, H-4), 3.26 (s, 2 H, H-6)

^{13}C NMR (101 MHz, $CDCl_3$): δ_C = 148.1 (C-1), 140.9 (C-4), 127.0 (C-2), 124.4 (C-3), 80.8 (C-6), 80.4 (C-5)

IR (ATR): $\tilde{\nu}_{max}$ / cm^{-1} = 3287 (m, ≡C-H), 3269 (s, ≡C-H), 3075 (w, =C-H), 2112 (m, C≡C), 1738 (s), 1535 (vs, N-O), 1352 (vs, N-O)

HRMS (ASAP$^+$): *m/z* $[M]^+$ calcd for $C_{10}H_5NO_2$: 171.0320; found: 171.0319 (Δ = −0.6 ppm)

Procedure adapted from Severin *et al.*[471] Spectroscopic data are in accordance with the literature.[471]

3,5-Diethynylaniline (85)

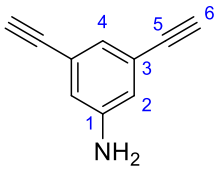

A solution of 1,3-diethynyl-5-nitrobenzene **86** (771 mg, 4.50 mmol) and $SnCl_2{\cdot}2H_2O$ (5.08 g, 22.5 mmol) in EtOH (45 mL) was heated to 70 °C for 1.5 h. The reaction mixture was allowed to cool to rt and quenched with addition of aqueous NaOH solution (2 M) to pH 9. The aqueous phase was extracted with Et_2O (3 × 50 mL), and the combined organic phases were dried over Na_2SO_4 and solvent removed *in vacuo* to give 3,5-diethynylaniline as a brown solid (538 mg, 3.81 mmol, 85%). This compound was used in the next step without further purification.

R_f = 0.15 (hexane:EtOAc = 5:1)

mp = 56–57 °C (lit.[472] 125–127 °C)

^{1}H NMR (400 MHz, $CDCl_3$): δ_H = 7.03 (t, *J* = 1.3 Hz, 1 H, H-4), 6.78 (d, *J* = 1.3 Hz, 2 H, H-2), 3.72 (br s, 2 H, NH_2), 3.03 (s, 2 H, H-6)

^{13}C NMR (101 MHz, $CDCl_3$): δ_C = 146.4 (C-1), 126.2 (C-4), 123.2 (C-3), 119.0 (C), 83.0 (C-5), 77.3 (C-6)

IR (ATR): $\tilde{\nu}_{max}$ / cm^{-1} = 3414 (m, N-H), 3331 (m, N-H), 3278 (s, ≡C-H), 2110 (w, C≡C), 1737 (s), 1587 (vs)

HRMS (ASAP$^+$): *m/z* $[M]^+$ calcd for $C_{10}H_7N$: 141.0578; found: 141.0576 (Δ = −1.4 ppm)

Spectroscopic data are in accordance with the literature.[473]

3,5-Diethynylbenzenesulfonyl chloride (84)

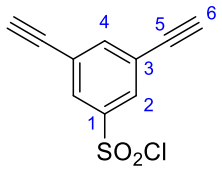

Acetic acid (2.80 mL) and concentrated aqueous HCl (1.40 mL) were added to an ice-cooled solution of 3,5-diethynylaniline **85** (494 mg, 3.50 mmol) in MeCN (28 mL). A solution of $NaNO_2$ (289 mg, 4.20 mmol) in H_2O (525 µL) was added over 10 min at 0 °C. After stirring for further 20 min, SO_2 was bubbled in over 40 min at 0 °C. A solution of $CuCl_2$ (592 mg, 4.40 mmol) in H_2O (875 µL) was added, and the mixture was allowed to warm to rt and stirred for further 16 h. The solvent was removed *in vacuo* and the residue re-dissolved in H_2O (20 mL) and CH_2Cl_2 (30 mL). The two phases were separated; the aqueous phase was extracted with CH_2Cl_2 (3 × 25 mL). The combined organic phases were dried over Na_2SO_4, filtered and the solvent removed *in vacuo*. The red-brown oily residue was purified by column chromatography (eluting gradient hexane:CH_2Cl_2 from 40:1 to 5:1) to give 3,5-diethynylbenzenesulfonyl chloride as a beige solid (566 mg, 2.52 mmol, 72%).

R_f = 0.27 (hexane:CH_2Cl_2 = 5:1)

mp = 69–71 °C

^{1}H NMR (400 MHz, $CDCl_3$): δ_H = 8.09 (d, *J* = 1.4 Hz, 2H, H-2), 7.89 (t, *J* = 1.4 Hz, 1H, H-4), 3.30 (s, 2H, H-6)

^{13}C NMR (101 MHz, $CDCl_3$): δ_C = 144.9 (C-1), 141.4 (C-4), 130.1 (C-2), 124.9 (C-3), 81.6 (C-6), 80.1 (C-5)

IR (ATR): $\tilde{\nu}_{max}$ / cm^{-1} = 3292 (s, ≡C-H), 3268 (s, ≡C-H), 3072 (m, =C-H), 2111 (w, C≡C), 1590 (m, C=C), 1434 (s), 1375 (vs, S=O), 1172 (vs, S=O)

HRMS (ASAP$^+$): *m/z* $[M]^+$ calcd for $C_{10}H_5{}^{35}ClO_2S$: 223.9699; found: 223.9694 (Δ = −2.2 ppm)

Elemental analysis: calcd for $C_{10}H_5ClO_2S$: C 53.46%, H 2.24%, Cl 15.78%, O 14.24%, S 14.27%; found: C 53.38% H 2.04%, Cl 14.90%, S 12.14%

3,5-Diethynylbenzenesulfonyl fluoride (81)

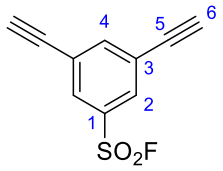

Potassium fluoride (87.2 mg, 1.50 mmol) and 18-crown-6 (3.96 mg, 0.0150 mmol) were added to a solution of 3,5-diethynylbenzenesulfonyl chloride **84** (67.4 mg, 0.300 mmol) in MeCN (1.5 mL), under a N_2 atmosphere. The reaction mixture was stirred at rt for 3 days and the solvent removed *in vacuo*. EtOAc (10 mL) was added to the residue, and the organic phase washed with H_2O (3 × 5 mL), and brine (5 mL), dried over Na_2SO_4, filtered, and the solvent removed *in vacuo* to give 3,5-diethynylbenzenesulfonyl fluoride as a white solid (37.3 mg, 0.179 mmol, 60%).

R_f = 0.20 (hexane:CH_2Cl_2 = 5:1)

mp = 77–79 °C

^{1}H NMR (400 MHz, $CDCl_3$): δ_H = 8.06 (d, J = 1.5 Hz, 2H, H-2), 7.92 (t, J = 1.4 Hz, 1H, H-4), 3.30 (s, 2H, H-6)

^{13}C NMR (101 MHz, $CDCl_3$): δ_C = 141.8 (C-4), 134.2 (d, $^2J_{C\text{-}F}$ = 26.2 Hz, C-1), 131.5 (C-2), 124.9 (C-3), 81.6 (C-6), 80.0 (C-5)

^{19}F NMR (376 MHz, $CDCl_3$): δ_F = 65.8

IR (ATR): $\tilde{\nu}_{max}$ / cm^{-1} = 3287 (s, ≡C-H), 2111 (w, C≡C), 1592 (w, C=C), 1434 (s), 1407 (s, S=O), 1202 (vs, S=O)

HRMS (ASAP$^+$): *m/z* [M]$^+$ calcd for $C_{10}H_5FO_2S$: 207.9994; found: 207.9992 (Δ = −1.0 ppm)

6.2.2.2. Synthesis of staples 93 and 94

Methyl 3,5-bis((trimethylsilyl)ethynyl)benzoate (96)

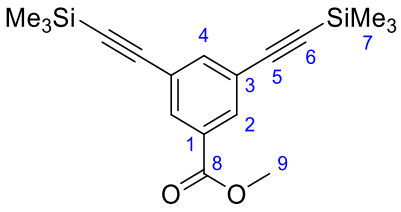

Methyl 3,5-dibromobenzoate (1.52 g, 5.17 mmol), $Pd_2(dba)_3$ (89.7 mg, 0.0980 mmol), CuI (19.1 mg, 0.100 mmol) and PPh_3 (129 mg, 0.492 mmol) were added to Et_3N (25 mL), followed by trimethylsilylacetylene (9.94 mL, 70.3 mmol). The reaction mixture was stirred at 65 °C for 20 h, then concentrated *in vacuo*. The residue was re-dissolved in CH_2Cl_2 (30 mL), filtered

through Celite®, then solvent removed *in vacuo*. The crude product was purified by flash column chromatography (hexane:EtOAc = 99:1) to give compound **96** as a yellow solid (1.41 g, 4.29 mmol, 83%)

R_f = 0.31 (hexane:EtOAc = 20:1)

mp = 73–76 °C (lit.[102] 71–73 °C)

^{1}H NMR (400 MHz, $CDCl_3$): δ_H = 8.05 (d, *J* = 1.6 Hz, 2H, H-2), 7.74 (t, *J* = 1.6 Hz, 1H, H-4), 3.92 (s, 3H, H-9), 0.25 (s, 18H, H-7)

^{13}C NMR (101 MHz, $CDCl_3$): δ_C = 165.8 (C-8), 139.2 (C-4), 132.8 (C-2), 130.7 (C-1), 124.0 (C-3), 103.1 (C-5), 96.3 (C-6), 52.5 (C-9), −0.1 (C-7)

IR (ATR): $\tilde{\nu}_{max}$ / cm^{-1} = 2957 (m, -C-H), 2900 (w, -C-H), 2157 (m, C≡C), 1729 (s, C=O), 1588 (m)

HRMS (ASAP$^+$): *m/z* $[M+H]^+$ calcd for $C_{18}H_{25}O_2Si_2$: 329.1393; found: 329.1383 (Δ = −3.0 ppm)

Procedure adapted from Lau *et al.*[102] Spectroscopic data are in accordance with the literature.[102]

3,5-Diethynylbenzoic acid (95)

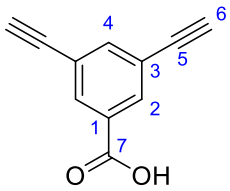

Aqueous KOH (6.00 M, 2.50 mL, 15.0 mmol) was added to a solution of methyl 3,5-bis((trimethylsilyl)ethynyl)benzoate **96** (850 mg, 2.59 mmol) in THF (15 mL). The reaction mixture was stirred at rt for 18 h, and the volatiles were removed *in vacuo*. The remaining aqueous mixture was acidified with aqueous HCl (2 M, 40 mL) and extracted with Et_2O (3 × 40 mL). The combined organic phases were dried over $MgSO_4$ and the solvent removed *in vacuo*. The crude product was recrystallised from $CHCl_3$ to give 3,5-diethynylbenzoic acid as a deep beige fine powder (255 mg, 1.50 mmol, 58%)

mp = 173 °C (dec) (lit. 173 °C[474]; 250 °C (dec)[102])

^{1}H NMR (400 MHz, $CDCl_3$): δ_H = 8.19 (d, *J* = 1.6 Hz, 2 H, H-2), 7.82 (t, *J* = 1.6 Hz, 1 H, H-4), 3.17 (s, 2 H, H-6)

^{13}C NMR (101 MHz, $CDCl_3$): δ_C = 169.3 (C-7), 140.2 (C-4), 133.9 (C-2), 130.0 (C-1), 123.4 (C-3), 81.5 (C-5), 79.3 (C-6)

IR (ATR) : $\tilde{\nu}_{max}$ / cm^{-1} = 3285 (m, ≡C-H), 2600 (br m, O-H), 1682 (vs, C=O), 1588 (s)

HRMS (ASAP$^+$): *m/z* $[M+H]^+$ calcd for $C_{11}H_7O_2$: 171.0446; found: 171.0448 (Δ = 1.2 ppm)

Procedure adapted from Lau *et al.*[102] Spectroscopic data are in accordance with the literature.[102]

Sodium 4-((3,5-diethynylbenzoyl)oxy)-2,3,5,6-tetrafluorobenzenesulfonate (93)

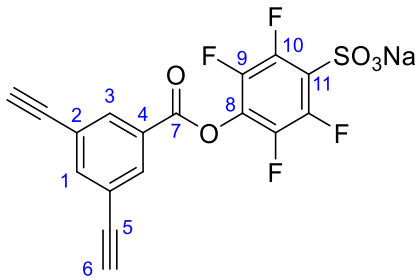

To the solution of sodium 2,3,5,6-tetrafluoro-4-hydroxybenzenesulfonate (134 mg, 0.500 mmol) and 3,5-diethynylbenzoic acid **95** (85.1 mg, 0.500 mmol) in DMF (1.25 mL) was added DCC (103 mg, 0.500 mmol), under a N_2 atmosphere. The reaction mixture was stirred at rt for 21 h, then stirred at 0 °C for 1 h, filtered and washed with DMF (80 µL). The product was triturated from the filtrate using Et_2O then filtered to give sodium 4-((3,5-diethynylbenzoyl)oxy)-2,3,5,6-tetrafluorobenzenesulfonate as a beige powder (181 mg, 0.431 mmol, 86%).

mp = 150 °C (dec)

^{1}H NMR (500 MHz, DMSO-d_6): δ_H = 8.20 (d, J = 1.5 Hz, 2 H, H-3), 8.00 (t, J = 1.5 Hz, 1 H, H-1), 4.50 (s, 2 H, H-6)

^{13}C NMR (126 MHz, DMSO-d_6): δ_C = 160.8 (C-7), 143.0 (d, $^1J_{C\text{-}F}$ = 249.3 Hz, C-9 or 10), 140.4 (C-1), 140.0 (dd, J = 249.5, 19.3 Hz, C-10 or 9), 133.3 (C-3), 127.9 (t, $^2J_{C\text{-}F}$ = 14.5 Hz, C-8 or 11), 127.6 (C-4), 125.0 (t, $^2J_{C\text{-}F}$ = 18.7 Hz, C-11 or 8), 123.7 (C-2), 83.7 (C-6), 80.8 (C-5)

^{19}F NMR (376 MHz, DMSO-d_6): δ_F = −140.0 (dd, J = 25.5, 9.7 Hz), −154.4 (dd, J = 25.5, 9.8 Hz)

IR (ATR): $\tilde{\nu}_{max}$ / cm^{-1} = 3282 (m, ≡C-H), 1756 (s, C=O), 1646 (m, C=C), 1480 (vs), 1184 (vs, S=O)

HRMS (ESI$^-$): m/z $[M-Na]^-$ calcd for $C_{17}H_5F_4O_5S$: 396.9799; found: 396.9795 (Δ = −1.2 ppm)

2,4-Dinitrophenyl 3,5-diethynylbenzoate (94)

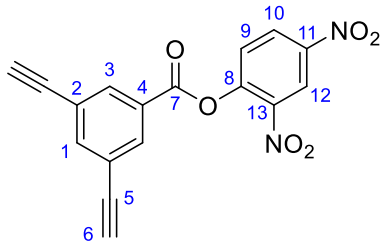

DMF (20 µL) was added to a suspension of 3,5-diethynylbenzoic acid **95** (85.1 mg, 0.500 mmol) in CH_2Cl_2 (2.5 mL) and the mixture was then cooled to 0 °C. Oxalyl chloride (64.3 µL, 0.750 mmol) was added and the reaction mixture stirred at rt for 5 h. The solvent was removed *in vacuo* to give the crude acid chloride.

The crude acid chloride was re-dissolved in THF (1 mL) and added to a solution of 2,4-dinitrophenol (138 mg, 0.750 mmol) and Et_3N (69.7 µL, 0.500 mmol) in THF (1 mL) at 0 °C. The reaction mixture was stirred at rt for 21 h, then quenched by adding saturated $NaHCO_3$ (5 mL). The mixture was extracted with Et_2O (3 × 10 mL). The combined organic phases were dried over $MgSO_4$, filtered, and the solvent removed *in vacuo*. The crude product was purified by column chromatography (eluting gradient hexane:EtOAc from 40:1 to 5:1) to give 2,4-dinitrophenyl 3,5-diethynylbenzoate as an off-white powder (59.2 mg, 0.176 mmol, 35%).

$\boldsymbol{R_f}$ = 0.21 (hexane:EtOAc = 5:1)

mp = 155 °C (dec)

^{1}H NMR (500 MHz, $CDCl_3$): δ_H = 9.05 (s, 1 H, H-12), 8.60 (d, *J* = 8.9 Hz, 1 H, H-10), 8.26 (s, 2 H, H-3), 7.90 (s, 1 H, H-1), 7.65 (d, *J* = 8.9 Hz, 1 H, H-9), 3.22 (s, 2H, H-6)

^{13}C NMR (126 MHz, $CDCl_3$): δ_C = 162.2 (C-7), 148.6 (C-8, 11 or 13), 145.5 (C-8, 11 or 13), 141.8 (C-8, 11 or 13), 141.1 (C-1), 134.2 (C-3), 129.3 (C-10), 128.4 (C-4), 126.8 (C-9), 123.9 (C-2), 122.1 (C-12), 81.1 (C-6), 80.0 (C-5)

IR (ATR): $\tilde{\nu}_{max}$ / cm^{-1} = 3285 (m, ≡C-H), 3082 (w, =C-H), 1750 (s, C=O), 1611 (m, C=C), 1532 (vs, N-O), 1348 (vs, N-O)

LCMS (ESI$^+$): *m/z* $[M+NH_4]^+$ calcd for $C_{17}H_{12}N_3O_6$: 354.1; found: 354.5

6.2.2.3. Synthesis of azido amino acid

Fmoc-Orn-OH·HCl (89)

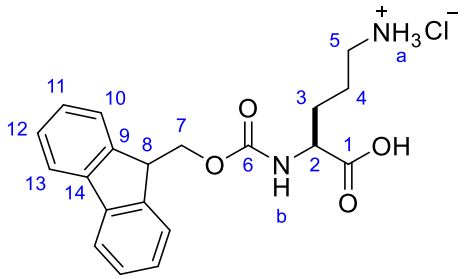

To a stirred solution of Fmoc-Orn(Boc)-OH (3.98 g, 8.76 mmol) in dioxane (14 mL) was added a solution of HCl in dioxane (4 M, 14 mL) in a single portion. The reaction mixture was stirred at rt for 16 h. The mixture was then diluted with Et_2O (150 mL) and the white precipitate collected under filtration and washed with Et_2O (4 × 25 mL) to give compound **89** as a white powder (3.42 g, 8.75 mmol, quant.)

mp = 150 °C (dec) (lit. 179 °C (dec))[475]

$[\alpha]_D^{25}$ = −4.7° (c = 1.0, DMSO, lit.[475] $[\alpha]_D^{27}$ = −2.3°)

^{1}H NMR (400 MHz, DMSO-d_6): δ_H = 12.71 (br s, 1 H, COOH), 7.99 (br s, 3H, H-N^a), 7.90 (d, *J* = 7.5 Hz, 2 H, H-13), 7.73 (d, *J* = 7.8 Hz, 1 H, H-10), 7.70 (d, *J* = 8.3 Hz, 1 H, H-N^b), 7.42 (t, *J* = 7.4 Hz, 2 H, H-12), 7.34 (t, *J* = 7.4 Hz, 2 H, H-11), 4.32–4.21 (m, 3H, H-7 and 8), 3.98–3.93 (m, 1H, H-2), 2.77 (br s, 2H, H-5), 1.85-1.58 (m, 4H, H-3 and 4)

^{13}C NMR (101 MHz, DMSO-d_6): δ_C = 173.5 (C-1), 156.2 (C-6), 143.8 (C-9), 140.7 (C-14), 127.7 (C-12), 127.1 (C-11), 125.3 (C-10), 120.2 (C-13), 65.7 (C-7), 53.4 (C-2), 46.6 (C-8), 38.4 (C-5), 27.7 (C-3), 24.0 (C-4)

IR (ATR): $\tilde{\nu}_{max}$ / cm^{-1} = 3333 (m, O-H), 3039 (br m, N-H), 1726 (s, C=O), 1690 (vs, C=O), 1531 (s, C=C), 1477 (m, C=C), 1451 (m, C=C)

HRMS (ESI$^+$): *m/z* $[M-Cl]^+$ calcd for $C_{20}H_{23}N_2O_4$: 355.1652; found: 355.1643 (Δ = −2.5 ppm)

Spectroscopic data are in accordance with the literature.[475]

Fmoc-Orn(N_3)-OH (90)

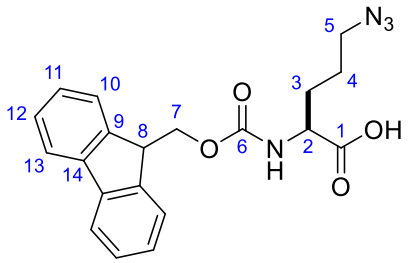

Fmoc-Orn-OH·HCl **89** (3.28 g, 8.39 mmol) was dissolved in a biphasic mixture of H_2O (48 mL), methanol (96 mL) and CH_2Cl_2 (80 mL). $CuSO_4 \cdot 5H_2O$ (17.0 mg, 0.0681 mmol) and 1-(azidosulfonyl)-1*H*-imidazol-3-ium chloride **91** (6.46 g, 30.8 mmol) were added to the mixture. The pH was adjusted to 9 with saturated aqueous K_2CO_3 solution followed by vigorous stirring at rt for 23 h. The reaction was diluted with CH_2Cl_2 (105 mL), then the two phases were separated. The organic phase was extracted with saturated $NaHCO_3$ solution (2 × 140 mL). The combined aqueous phases were washed with Et_2O (2 × 140 mL), acidified to pH 2 with concentrated HCl and extracted with Et_2O (3 × 160 mL). The combined organic extracts were dried with $MgSO_4$, filtered and the solvent removed *in vacuo* to give an oily residue. The residue was re-dissolved in EtOAc and the volatile removed under a stream of N_2 to give compound **90** as a white solid (1.40 g, 3.68 mmol, 44%)

mp = 131–133 °C (lit. 132–134 °C)[102]

$[\alpha]_D^{25}$ = −3.7° (c = 1.0, MeOH, lit.[476] $[\alpha]_D$ = −2.3°)

^{1}H NMR (400 MHz, $CDCl_3$): δ_H = 7.78 (d, *J* = 7.8 Hz, 2 H, H-13), 7.63–7.52 (m, 2 H, H-10), 7.41 (t, *J* = 7.5 Hz, 2 H, H-12$_c$), 7.32 (app tt, *J* = 7.4, 0.7 Hz, 2 H, H-11), 5.34 (d, *J* = 8.0 Hz, 1 H, H-N), 4.63–4.40 (m, 3 H, H-2 and 7), 4.23 (t, *J* = 6.7 Hz, 1 H, H-8), 3.39–3.10 (m, 2 H, H-5), 2.06–1.42 (m, 4 H, H-3 and 4)

^{13}C NMR (101 MHz, $CDCl_3$): δ_C = 175.8 (C-1), 156.2 (C-6), 143.9 (C-9), 143.7 (C-9'), 141.5 (C-14), 127.9 (C-12), 127.2 (C-11), 125.2 (C-10), 120.2 (C-13), 67.3 (C-7), 53.3 (C-8), 50.9 (C-5), 47.3 (C-2), 29.8 (C-3), 25.0 (C-4)

IR (ATR): $\tilde{\nu}_{max}$ / cm^{-1} = 3335 (m, O-H), 2960 (br w, N-H), 2087 (s, N=N=N), 1709 (s, C=O), 1678 (s, C=O), 1530 (s, C=C), 1450 (m, C=C)

HRMS (ESI^+): *m/z* $[M+Na]^+$ calcd for $C_{20}H_{20}N_4O_4{}^{23}Na$: 403.1377; found: 403.1369 (Δ = −2.0 ppm)

Prepared according to Lau *et al.*[102] Spectroscopic data are in accordance with the literature.[102]

1-(azidosulfonyl)-1*H*-imidazol-3-ium chloride (91)

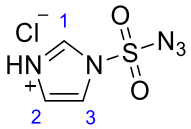

Sulfuryl chloride (16.1 mL, 200 mmol) was added dropwise to an ice-cooled suspension of NaN_3 (13.0 g, 200 mmol) in MeCN (200 mL) and the mixture stirred overnight at rt. The mixture was then cooled to 0°C and imidazole (25.9 g, 380 mmol) was added portion-wise. The resulting slurry was allowed to warm to rt and stirred for 5 h. The mixture was diluted with EtOAc (400 mL) and then separated. The organic phase was washed with H_2O (2 × 400 mL), saturated $NaHCO_3$ solution (2 × 400 mL), dried over $MgSO_4$ and filtered. A solution of HCl in EtOH [obtained by the dropwise addition of AcCl (21.3 mL, 300 mmol) to ice-cooled dry ethanol (75 mL)] was added dropwise to the ice-cooled filtrate while stirring. The precipitate was collected under filtration, washed with EtOAc (3 × 100 mL) to give compound **91** as white needles (19.3 g, 92.1 mmol, 46%).

mp = 101–102°C (lit. 100–102°C)[377]

^{1}H NMR (400 MHz, D_2O): δ_H = 9.31 (t, *J* = 1.3 Hz, 1 H, H-1), 8.01 (t, *J* = 1.8 Hz, 1 H, H-3), 7.60 (t, *J* = 1.6 Hz, 1 H, H-2)

^{13}C NMR (101 MHz, D_2O): δ_C = 137.7 (C-1), 124.1 (C-2), 119.9 (C-3)

IR (ATR): $\tilde{\nu}_{max}$ / cm^{-1} = 3102 (m, C-H), 3057 (m, C-H), 2169 (s, N=N=N), 1581 (s, C=C), 1298 (m, S=O), 1137 (vs, S=O)

Procedure adapted from Goddard-Borger *et al.*[377] Spectroscopic data are in accordance with the literature.[377]

6.2.2.4. Linear peptide syntheses

Peptide synthesis was carried out on solid-phase using Fmoc-protecting group strategy on a CEM LibertyBlue Automated Microwave Peptide Synthesizer using Rink Amide MBHA LL resin (0.33 mmol/g) (Merck Millipore). Fmoc-protected amino acids were made up as a solution of 0.2 M in DMF to give 5 equivalents relative to resin loading. Oxyma Pure was made up as a 1 M solution in DMF to give 5 equivalents relative to resin and *N*,*N*'-diisopropylcarbodiimide as a 1 M solution in DMF to give 10 equivalents relative to the resin. All amino acid couplings were double coupled and heated to 90 °C for two mins, except for Fmoc-Orn(N_3)-OH which was single coupled and heated to 90 °C for 270 s for each coupling. Fmoc deprotection was carried out using 20 % (v/v) piperidine in DMF and heated to 90 °C for 60 s twice. The Ac capping of the *N*-terminus was carried out using 20 % (v/v) Ac_2O in DMF and heated to 40 °C for 10 min.

6.2.2.5. Peptide stapling

Under a N_2 atmosphere, a solution of diazidopeptide in DMSO (1 equiv., 0.4 mg/μL) was added to a degassed *t*BuOH/H_2O (1:1) making the concentration of the peptide to 1 mg/mL. A dialkynyl linker (1.1 equiv.) was then added to the peptide solution. Sodium L-ascorbate (3 equiv.) was added to a degassed aqueous solution of $CuSO_4 \cdot 5H_2O$ (1 equiv.) and THPTA (1 equiv.) under N_2. The copper solution was added to the reaction mixture, stirred at rt, and monitored by HPLC until its completion. The mixture was lyophilised and then purified by semi-preparative HPLC.

6.2.2.6. LCMS data and analytical HPLC traces for peptides

Peptide	Sequence[a]	Exact Mass	*m/z* found	*m/z* calcd	Species	t_R (min)[b]
P1	Ac-LTFEXYWAALTX-NH_2	1534.77	766.9	766.4	$[M-2H]^{2-}$	10.57[c]
P3	Ac-ETFEXYWSALTX-NH_2	1566.72	783.2	782.4	$[M-2H]^{2-}$	10.82[d]
P4	H-ETFEXYWNALTX-OH	1552.71	1552.2	1551.7	$[M-H]^-$	9.82[e]
P5	Tmg-ETFEXYWNALTX-OH	1652.78	1653.4	1652.8	$[M]^+$	10.21[e]
P6	Ac-TSFAXYWNGLSX-NH_2	1465.69	734.5	733.9	$[M+2H]^{2+}$	8.97
WT PMI	Ac-TSFAEYWNNLSP-NH_2	1467.70	735.0	734.9	$[M+2H]^{2+}$	9.16
P5-81		1860.78	929.8	929.4	$[M-2H]^-$	10.90[e]
P6-81		1673.68	838.6	837.8	$[M+2H]^{2+}$	9.38
P6-92		1591.73	797.6	796.9	$[M+2H]^{2+}$	8.76
P6-93		1885.66	933.5	932.9	$[M-Na+3H]^{2+}$	8.71

[a]Shown for linear peptides only; X = Orn(N_3); Tmg = trimethylglycyl which contains a permanent +1 charge. [b]Obtained from analytical HPLC runs with 5-95%B over 15 min gradient (an x-y gradient signifies the amount of solvent B being x % at the start and y% at the end of the run, respectively.). [c]30-80%B over 15 min gradient used. [d]10-80%B over 15 min gradient used. [e]20-60%B over 15 min gradient used.

6.2.2.7. Circular dichroism

Circular dichroism measurements were performed by Dr Jessica Iegre, Spring Group, Department of Chemistry, University of Cambridge.

CD spectra of selected peptides were recorded on an AVIV 410 circular dichroism spectropolarimeter using a 1 mm path length quartz cuvette. CD measurements were performed at 298 K over a range of 185–260 nm using a response time of 0.5 s, 1 nm pitch and 0.5 nm bandwidth. Peptides were dissolved in 1:1 MQ water/acetonitrile to a final

concentration of 100 µM. The recorded spectra represent a smoothed average of three scans, zero-corrected at 260 nm. The %helicity was calculated from mean residue ellipticity ($[\theta]_{222}$) and compared to the theoretical maximum value (θ_{222}^{∞} = -39,500 deg cm^2 dmol^{-1}) according to the following equation:[477]

$$\%helicity = \frac{[\theta]_{222}}{\theta_{222}^{\infty}\left[1 - \frac{ik}{n}\right]}$$

where *i* is the number of helices in the sample, *k* is the wavelength specific constant (2.57 at 222 nm), and *n* is the number of amino acid residues in the peptide.

6.2.3. Stability and reactivity test protocols

6.2.3.1. Stability tests in CuAAC peptide stapling condition

Sodium L-ascorbate (3 equiv.) was added to a degassed aqueous solution of $CuSO_4 \cdot 5H_2O$ (1 equiv.) and THPTA (1 equiv.) under nitrogen. The mixture was then added to a solution of a dialkynyl linker (1.1 equiv., 0.73 mM) and caffeine (0.3 equiv.) in degassed *t*BuOH/H_2O (1:1) at rt under nitrogen. The reactions were monitored by analytical HPLC, and conversions were calculated by comparing the integrations of the area under the chromatogram peaks of the linker with the internal standard (caffeine) at 254 nm.

6.2.3.2. Stability tests in aqueous media for linkers

At 37 °C, PBS (1 mL) was added caffeine solution in MeCN (0.75 mM, 200 µL) and linker solution in 3:2 MeCN/PBS (2.5 mM, 800 µL). The mixture was incubated at 37 °C, and the reactions were monitored by analytical HPLC. Conversions were calculated by comparing the integrations of the area under the chromatogram peaks of the remaining linker and the internal standard (caffeine) determined by analytical HPLC at 254 nm.

6.2.3.3. Reactivity tests with lysine for linkers

At 37 °C, a stock solution of *N*α-Ac-Lys-OH in PBS (4 mM, 1 mL) was added caffeine solution in MeCN (0.75 mM, 200 µL) and linker solution in 3:2 MeCN/PBS (2.5 mM, 800 µL). The reactions were monitored by analytical HPLC. Conversions were calculated by comparing the integrations of the area under the chromatogram peaks of the products and the internal standard (caffeine) determined by analytical HPLC at 254 nm.

6.2.4. Biological experiments

6.2.4.1. Expression and purification of MDM2 (6–125)

The protein expression and purification were performed by Dr Elaine Fowler from the Spring Group, Department of Chemistry, University of Cambridge and Dr Rohan Eapen from the Itzhaki Group, Department of Pharmacology, University of Cambridge.

Coding region of MDM2, residues 6–125 were cloned into a pRSET vector with an *N*-terminal 6His-tag and TEV protease cleavage site via BamHI & KpnI restriction sites. The plasmid was transformed into C41 cells and expressed in 2xYT medium supplemented with 100 µg/mL ampicillin. Cultures were grown in baffled 2 L flasks to an OD600 = 0.6, prior to induction with 0.3 mM IPTG at 18 °C for around 16 h. Cells were harvested by centrifugation at 7000 × g at 4 °C and were resuspended in 50 mM Tris-HCl, 300 mM NaCl, 15 mM imidazole, 1 mM DTT, SigmaFAST EDTA-free protease inhibitor cocktail tablet (Sigma) and DNaseI (Sigma), pH 8.0. Resuspended cells were lysed using a C5-emulsiflex (Avestin). The lysate was then clarified by centrifugation at 45,000 × g at 4 °C. His-tagged proteins were bound to a 5 mL HisTrap Excel column using an AKTA PURE chromatography system and washed with 20 CV of 50 mM Tris-HCl, 300 mM NaCl, 15 mM imidazole, 1 mM DTT, pH 8.0. Proteins were eluted with 5 CV of 50 mM Tris-HCl, 300 mM NaCl, 300 mM imidazole, 1 mM DTT, pH 8.0, directly into a pre-equilibrated 26/10 desalting column of 20 mM Tris-HCl, 180 mM NaCl, 1 mM DTT, pH 8.0. Eluent fractions containing 6His-tagged MDM2 were pooled and 6His-TEV protease (S219V) was added to cleave overnight at 4 °C. Cleaved proteins were then run over a 5 mL HisTrap Excel column, collecting the flow through. Proteins were diluted in 20 mM Bis-Tris, 1 mM DTT, pH 6.5 to approximately 20 mM NaCl. MonoS 10/100 GL column was then equilibrated in 20 mM Bis-Tris, 30 mM NaCl, 1 mM DTT, pH 6.5 before loading protein samples onto the column. Proteins were then eluted in a linear gradient with 20 mM Bis-Tris, 1 M NaCl, 1 mM DTT, pH 6.5 over 20 CV. Elution fractions were run on a 15% SDS PAGE gel to assess purity (>90%), before concentrating using a Vivaspin 20, 5K MWCO centrifugal concentrator (Sartorius Stedim). Proteins were snap-frozen in liquid nitrogen and stored at -80 °C for long-term storage.

6.2.4.2. Covalent cross-linking determination

The LCMS analyses were performed by Dr Stephen Walsh from the Spring Group, Department of Chemistry, University of Cambridge.

MDM2 protein stock solution (195 µM) was diluted in PBS buffer to 55.6 µM. PBS (5 µL) was added to the diluted MDM2 solution (5 µL) in a 500 µL-centrifuge tube. DMSO (0.556 µL) and the peptide solution (0.556 µL, 500 µM in DMSO) were then added successively and the mixture incubated at 37 °C for 1 h. The negative control used DMSO in place of peptide solution. Lysozyme solution (55.6 µM) was used instead of PBS for selectivity assay. The mass

of the protein was detected by protein LCMS as described in the general experimental except that the electrospray source was operated with a cone voltage of 40 V.

6.2.4.3. MDM2 competitive fluorescence polarisation assay

The assay was conducted by Dr Rohan Eapen from the Itzhaki Group, Department of Pharmacology, University of Cambridge.

Competitive fluorescence polarisation was carried out using MDM2 and a 5-TAMRA-labelled FP tracer peptide in a similar fashion as previously described.[101,102] The dissociation constant was previously described by Lau *et al*.[102] Stock solutions of peptide inhibitors in DMSO (10 mM) were diluted in assay buffer (1 × PBS + 0.05% (v/v) Tween-20 + 3% (v/v) DMSO) to a top concentration of 80 µM (final assay concentration of 40 µM). 1.5-fold serial dilutions were performed by multichannel pipette, in the assay plate (OptiPlate™ -384 F, Perkin Elmer) to produce a 24-point titration with a volume of 20 µL. An equal volume of MDM2 and fluorescent tracer peptide were then added to each well, by multichannel pipette for a final concentration of 95 nM and 50 nM, respectively. All titrations were conducted in triplicate. Fluorescence polarisation was measured using a BMG ClarioStar plate reader using an excitation filter at 540 nm and an emission filter at 590 nm, with a 20 nm bandwidth. Plates were read at time points indicated. Graphs were plotted using GraphPad Prism 7.0 and analysed using the equations below.[478] The equations described by Wang describe competitive binding, where neither protein nor ligand was depleted. However, in the case of a covalent ligand (**P6-93**), both the target protein and covalent ligand were depleted in a stoichiometric manner over the course of the incubation, resulting in a deviation from the model fit over time. Nonetheless, the system could still illustrate the time-dependent nature of a covalent ligand's interaction with the target protein and thus an apparent dissociation constant, $K_{d,app}$, was quoted.

Here, r = anisotropy measured, r_0 = anisotropy of free peptide, r_b = anisotropy of MDM2:5-TAMRA peptide complex, K_{d1} = dissociation constant of 5-TAMRA peptide to MDM2, K_{d2} = (apparent) dissociation constant of non-labelled ligand to MDM2, $[P]_t$ = MDM2 concentration, $[L]_t$ = non-labelled ligand concentration and $[L]_{st}$ = 5-TAMRA peptide concentration.

$$r = r_0 + (r_b + r_0) \times \frac{2\sqrt{(d^2 - 3e)}\cos(\theta/3) - 9}{3K_{d1} + 2\sqrt{(d^2 - 3e)}\cos(\theta/3) - d}$$

$$d = K_{d1} + K_{d2} + [L]_{st} + [L]_t - [P]_t$$

$$e = K_{d1}([L]_t - [P]_t) + K_{d2}([L]_{st} - [P]_t) + K_{d1}K_{d2}$$

$$\theta = \cos^{-1}\left(\frac{-2d^3 + 9de - 27f}{2\sqrt{(d^2 - 3e)^3}}\right)$$

$$f = -K_{d1}K_{d2}[P]_t$$

6.3. Chapter 5 Experimental

6.3.1. Synthesis of hemiasterlin and taltobulin

Methyl (*S*)-2-formamido-3,3-dimethylbutanoate (102)

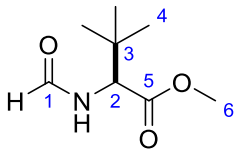

Triethylamine (1.53 mL, 11.0 mmol) was added to a suspension of methyl (*S*)-*tert*-leucinate hydrochloride (1.82 g, 10.0 mmol) in ethyl formate (15 mL). The reaction mixture was refluxed for 20 h, allowed to cool to rt, then filtered through a short silica plug. The solvent was removed *in vacuo* to give formamide **102** as a white solid (1.68 g, 9.70 mmol, 97%). The product was used in the next step without further purification.

R_f = 0.52 (EtOAc)

$[\alpha]_D^{20}$ = +13.4° (c = 1.06, $CHCl_3$, lit.[403] +14.2°, c = 1.0)

^{1}H NMR (400 MHz, $CDCl_3$): Major rotamer δ_H = 8.24 (d, *J* = 0.8 Hz, 1 H, H-1), 6.23 (br s, 1 H, H-N), 4.57 (dd, *J* = 9.6, 0.7 Hz, 1 H, H-2), 3.74 (s, 3 H, H-6), 0.99 (s, 9 H, H-4); Minor rotamer (observed peaks) δ_H = 7.99 (d, *J* = 11.7 Hz, 1 H, H-1), 3.79 (d, *J* = 10.6 Hz, 1 H, H-2), 3.76 (s, 3 H, H-6)

^{13}C NMR (101 MHz, $CDCl_3$): Major rotamer δ_C = 171.9 (C-5), 160.8 (C-1), 58.6 (C-2), 52.1 (C-6), 34.9 (C-3), 26.6 (C-4); Minor rotamer δ_C = 170.7 (C-5), 163.6 (C-1), 63.7 (C-2), 52.2 (C-6), 34.8 (C-3), 26.3 (C-4)

HRMS (ESI): *m/z* $[M+H]^+$ calcd for $C_8H_{16}NO_3$: 174.1130; found: 174.1128 (Δ = −1.1 ppm)

Prepared according to Ackermann *et al.*[403] Spectroscopic data are in accordance with the literature.[403]

Methyl (*S*)-2-isocyano-3,3-dimethylbutanoate (101)

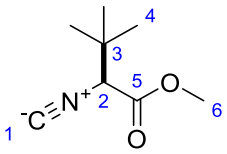

To a solution of methyl (*S*)-2-formamido-3,3-dimethylbutanoate **102** (866 mg, 5.00 mmol) in anhydrous CH_2Cl_2 (50 mL) was added *N*-methylmorpholine (1.10 mL, 10.0 mmol). The mixture was then cooled to −78 °C. Triphosgene (519 mg, 1.75 mmol) was then added in a single portion and the reaction mixture stirred at −78 °C for 5 min before being slowly warmed to -

30 °C and then stirred at this temperature for 3 h. The reaction was then quenched with H_2O (50 mL) and the phases separated. The aqueous phase was then extracted with Et_2O (3 × 50 mL). The combined organic phases were dried with Na_2SO_4, and the solvent was removed *in vacuo* (the bath temperature was kept below 15 °C). The crude product was purified by flash column chromatography (eluting gradient Et_2O:30–40 petroleum ether from 0:1 to 1:4) to give isocyanide **101** as a clear colourless liquid (731 mg, 4.71 mmol, 94%).

R_f = 0.64 (EtOAc:hexane = 1:1)

$[\alpha]_D^{20}$ = +33.3° (c = 0.990, $CHCl_3$, lit.[403] +39.7°, c = 1.0)

^{1}H NMR (400 MHz, $CDCl_3$): δ_H = 4.00 (s, 1 H, H-2), 3.81 (s, 3 H, H-6), 1.10 (s, 9 H, H-4)

^{13}C NMR (101 MHz, $CDCl_3$): δ_C = 166.3 (C-5), 160.0 (C-1), 66.4 (t, *J* = 7.0 Hz, C-2), 52.8 (C-6), 35.2 (C-3), 26.2 (C-4)

HRMS (ESI): *m/z* $[M+H]^+$ calcd for $C_8H_{14}NO_2$: 156.1025; found: 156.1022 (Δ = −1.9 ppm)

Procedure adapted from Zhu *et al.*[410] Spectroscopic data are in accordance with the literature.[403]

3-Bromo-1-methyl-1*H*-indole (104)

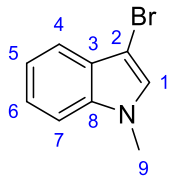

DBDMH (157 mg, 0.550 mmol) was added in five portions to a solution of *N*-methylindole (125 µL, 1.00 mmol) in dioxane (10 mL) at 10 °C over 2 min. The reaction mixture was stirred at this temperature for 10 min before being poured into saturated aqueous $NaHCO_3$ (10 mL). The mixture was extracted with EtOAc (2 × 15 mL), the combined organic phases were dried over anhydrous Na_2SO_4, and the solvent removed *in vacuo*. The resulting crude oil was purified by flash column chromatography (eluting gradient EtOAc:40–60 petroleum ether from 0:1 to 1:15) to give indole **104** as a colourless oil (134 mg, 0.638 mmol, 64%), which was prone to decomposition to a dark solid over time.

R_f = 0.37 (EtOAc:40–60 petroleum ether = 1:10)

^{1}H NMR (400 MHz, $CDCl_3$): δ_H = 7.59 (dt, *J* = 8.0, 0.9 Hz, 1 H, H-4), 7.33 (dt, *J* = 8.3, 0.9 Hz, 1 H, H-7), 7.29 (ddd, *J* = 8.2, 6.9, 1.2 Hz, 1 H, H-6), 7.22 (ddd, *J* = 8.0, 6.8, 1.2 Hz, 1 H, H-5), 7.09 (s, 1 H, H-1), 3.79 (s, 3 H, H-9)

^{13}C NMR (101 MHz, $CDCl_3$): δ_C = 136.4 (C-8), 127.8 (C-1), 127.4 (C-3), 122.7 (C-6), 120.2 (C-5), 119.4 (C-4), 109.6 (C-7), 89.5 (C-2), 33.2 (C-9)

HRMS (ESI): *m/z* $[M+H]^+$ calcd for C_9H_9BrN: 209.9918; found: 209.9908 (Δ = −4.8 ppm)

Procedure adapted from Yan *et al.*[413] Spectroscopic data are in accordance with the literature.[479]

(±)-Methyl 2-(1-methyl-1*H*-indol-3-yl)propanoate (59)

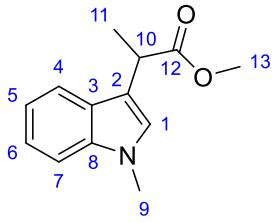

A solution of KHMDS in THF (0.91 M, 33.0 mL, 30.0 mmol) was diluted with freshly distilled THF (100 mL) and then cooled to −78 °C. A solution of methyl 2-(1*H*-indol-3-yl)acetate **58** (1.89 g, 10.0 mmol) in THF (46 mL) was then added slowly. The reaction mixture was warmed to 0 °C and stirred for 1 h before re-cooling to −78 °C. Methyl iodide (5.0 mL, 80 mmol) was then added slowly to the reaction mixture which was then warmed to 0 °C and stirred for 1 h before being placed in a freezer (−30 °C) for 17 h. The reaction was then quenched with H_2O (135 mL) and then extracted with Et_2O (3 × 135 mL). The combined organic phases were washed with brine (135 mL), dried with anhydrous $MgSO_4$, and the solvent removed *in vacuo*. The resulting crude oil was purified by flash column chromatography (eluting gradient Et_2O:40–60 petroleum ether from 0:1 to 1:4) to give indole **59** as a viscous yellow oil (2.08 g, 9.57 mmol, 96%).

$\boldsymbol{R_f}$ = 0.17 (Et_2O:40–60 petroleum ether = 1:4)

^{1}H NMR (500 MHz, $CDCl_3$): δ_H = 7.68 (dt, *J* = 8.0, 0.9 Hz, 1 H, H-4), 7.31 (dt, *J* = 8.2, 0.8 Hz, 1 H, H-7), 7.25 (ddd, *J* = 8.2, 7.0, 1.1 Hz, 1 H, H-6), 7.14 (ddd, *J* = 8.0, 7.0, 1.1 Hz, 1 H, H-5), 7.02 (s, 1 H, H-1), 4.05 (q, 1 H, *J* = 7.1 Hz, H-10), 3.77 (s, 3 H, H-9), 3.69 (s, 3 H, H-13), 1.62 (d, *J* = 7.2 Hz, 3 H, H-11)

^{13}C NMR (126 MHz, $CDCl_3$): δ_C = 175.8 (C-12), 137.1 (C-8), 126.9 (C-3), 126.4 (C-1), 121.9 (C-6), 119.4 (C-4), 119.2 (C-5), 114.1 (C-2), 109.4 (C-7), 52.1 (C-13), 36.9 (C-10), 32.9 (C-9), 18.2 (C-11)

HRMS (ESI): *m/z* $[M+H]^+$ calcd for $C_{13}H_{16}NO_2$: 218.1176; found: 218.1181 (Δ = −2.3 ppm)

Procedure adapted from Nieman *et al.*[359] Spectroscopic data are in accordance with the literature.[359]

Methyl 2-methyl-2-(1-methyl-1*H*-indol-3-yl)propanoate (60)

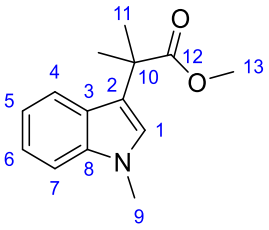

A solution of KHMDS in THF (0.91 M, 13.2 mL, 12.0 mmol) was diluted with freshly distilled THF (94 mL) and then cooled to −78 °C. A solution of (±)-methyl 2-(1-methyl-1*H*-indol-3-yl)propanoate **59** (1.74 g, 8.00 mmol) in THF (38 mL) was then added slowly. The reaction mixture was warmed to 0 °C and stirred for 1 h before re-cooling to −78 °C. Methyl iodide (3.0 mL, 48 mmol) was then added slowly to the reaction mixture which was then warmed to 0 °C and stirred for 45 min. The reaction was then quenched with H_2O (80 mL) and then extracted with Et_2O (3 × 80 mL). The combined organic phases were washed with brine (80 mL), dried with anhydrous $MgSO_4$, and the solvent removed *in vacuo*. The resulting crude product was purified by flash column chromatography (eluting gradient Et_2O:40–60 petroleum ether from 0:1 to 1:4) to give indole **60** as a white solid (1.69 g, 7.31 mmol, 91%).

$\boldsymbol{R_f}$ = 0.21 (Et_2O:40–60 petroleum ether = 1:4)

^{1}H NMR (500 MHz, $CDCl_3$): δ_H = 7.65 (dt, *J* = 8.0, 0.9 Hz, 1 H, H-4), 7.31 (dt, *J* = 8.3, 0.9 Hz, 1 H, H-7), 7.23 (ddd, *J* = 8.2, 7.0, 1.1 Hz, 1 H, H-6), 7.10 (ddd, *J* = 8.0, 7.0, 1.1 Hz, 1 H, H-5), 6.95 (s, 1 H, H-1), 3.77 (s, 3 H, H-9), 3.65 (s, 3 H, H-13), 1.71 (s, 6 H, H-11)

^{13}C NMR (126 MHz, $CDCl_3$): δ_C = 177.8 (C-12), 137.6 (C-8), 126.2 (C-3), 125.4 (C-1), 121.7 (C-6), 120.4 (C-4), 119.3 (C-2), 119.1 (C-5), 109.5 (C-7), 52.3 (C-13), 42.1 (C-10), 32.8 (C-9), 26.4 (C-11)

HRMS (ESI): *m/z* $[M+H]^+$ calcd for $C_{14}H_{18}NO_2$: 232.1329; found: 232.1332 (Δ = −1.3 ppm)

Procedure adapted from Nieman *et al.*[359] Spectroscopic data are in accordance with the literature.[359]

2-Methyl-2-(1-methyl-1H-indol-3-yl)propan-1-ol (105)

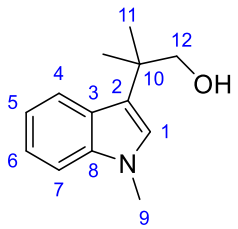

Methyl 2-methyl-2-(1-methyl-1*H*-indol-3-yl)propanoate **60** (1.27 g, 5.50 mmol) was dissolved in Et_2O (60 mL) and CH_2Cl_2 (16 mL) and cooled to −78 °C. A solution of DIBAL-H in

THF (1.0 M, 19.3 mL, 19.3 mmol) was then added slowly, and the reaction mixture was warmed to 0 °C and stirred for 3 h. The reaction was then quenched with H_2O (12 mL), allowed to warm to rt, and saturated aqueous solution of potassium sodium tartrate (28 mL) was added. The phases were separated, and the aqueous phase was extracted with Et_2O (2 × 60 mL). The combined organic phases were washed with brine (60 mL), dried with anhydrous $MgSO_4$, and the solvent removed *in vacuo*. The resulting crude product was purified by flash column chromatography (eluting gradient Et_2O:40–60 petroleum ether from 1:20 to 1:1) to give alcohol **105** as a white solid (1.07 g, 5.26 mmol, 96%).

R_f = 0.24 (Et_2O:40–60 petroleum ether = 1:1)

^{1}H NMR (400 MHz, $CDCl_3$): δ_H = 7.79 (d, *J* = 8.0 Hz, 1 H, H-4), 7.34 (d, *J* = 8.2 Hz, 1 H, H-7), 7.28–7.22 (m, 1 H, H-6), 7.12 (ddd, *J* = 8.0, 7.0, 1.0 Hz, 1 H, H-5), 6.92 (s, 1 H, H-1), 3.81 (s, 2 H, H-12), 3.78 (s, 3 H, H-9), 1.47 (s, 6 H, H-11)

^{13}C NMR (101 MHz, $CDCl_3$): δ_C = 138.0 (C-8), 127.2 (C-1), 126.1 (C-3), 121.6 (C-6), 121.1 (C-4), 119.5 (C-2), 118.8 (C-5), 109.7 (C-7), 71.6 (C-12), 37.7 (C-10), 32.8 (C-9), 25.6 (C-11)

HRMS (ESI): *m/z* $[M+H]^+$ calcd for $C_{13}H_{18}NO$: 204.1383; found: 204.1377 (Δ = −2.9 ppm)

Procedure adapted from Nieman *et al*.[359] Spectroscopic data are in accordance with the literature.[359]

2-Methyl-2-(1-methyl-1*H*-indol-3-yl)propanal (69)

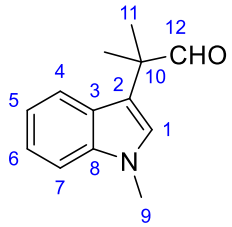

To a mixture of 2-methyl-2-(1-methyl-1*H*-indol-3-yl)propan-1-ol **105** (1.02 g, 5.00 mmol), *N*-methylmorpholine *N*-oxide (1.05 g, 9.00 mmol), and 4 Å powdered molecular sieves (1.09 g) in dry CH_2Cl_2 (36 mL) were added tetrapropylammonium perruthenate (87.9 mg, 0.250 mmol). The black reaction mixture was stirred at rt for 20 h, filtered through Celite®, and concentrated *in vacuo*. The crude black oil was purified by flash column chromatography (eluting gradient Et_2O:40–60 petroleum ether from 0:1 to 1:5) to give aldehyde **69** as a pale-yellow solid (846 mg, 4.20 mmol, 84%).

R_f = 0.21 (Et_2O:40–60 petroleum ether = 1:4)

^{1}H NMR (400 MHz, $CDCl_3$): δ_H = 9.50 (s, 1 H, H-12), 7.57 (d, *J* = 8.1 Hz, 1 H, H-4), 7.34 (d, *J* = 8.2 Hz, 1 H, H-7), 7.26 (t, *J* = 8.0 Hz, 1 H, H-6), 7.11 (t, *J* = 7.5 Hz, 1 H, H-5), 6.98 (s, 1 H, H-1), 3.80 (s, 3 H, H-9), 1.56 (s, 6 H, H-11)

^{13}C NMR (101 MHz, $CDCl_3$): δ_C = 202.4 (C-12), 137.8 (C-8), 126.8 (C-1), 126.3 (C-3), 122.0 (C-6), 120.4 (C-4), 119.4 (C-5), 115.2 (C-2), 109.7 (C-7), 46.6 (C-10), 33.0 (C-9), 22.1 (C-11)

HRMS (ESI): *m/z* $[M+H]^+$ calcd for $C_{13}H_{16}NO$: 202.1232; found: 202.1228 (Δ = −2.0 ppm)

Procedure adapted from Nieman *et al*.[359] Spectroscopic data are in accordance with the literature.[359]

Methyl (*S*)-3,3-dimethyl-2-((*S*)-3-methyl-3-(1-methyl-1*H*-indol-3-yl)-2-(2,2,2-trifluoro-*N*-methylacetamido)butanamido)butanoate (99a)

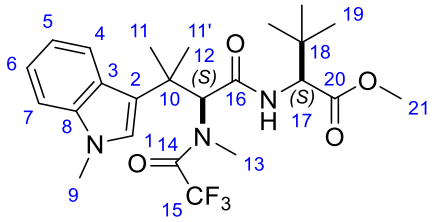

and **methyl (*S*)-3,3-dimethyl-2-((*R*)-3-methyl-3-(1-methyl-1*H*-indol-3-yl)-2-(2,2,2-trifluoro-*N*-methylacetamido)butanamido)butanoate (99b)**

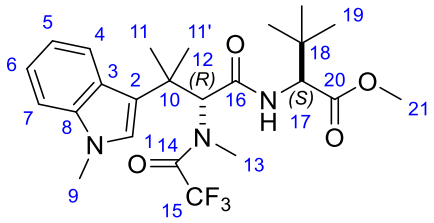

Methylamine solution in MeOH (2 M, 1.10 mL. 2.20 mmol) was added to a solution of 2-methyl-2-(1-methyl-1*H*-indol-3-yl)propanal **69** (403 mg, 2.00 mmol) in dry MeOH (5.1 mL). 3 Å molecular sieves (1.8 g) were then added, and the reaction was stirred at rt for 2 h before TFA (184 µL, 2.40 mmol) was added. The reaction mixture was stirred for a further 20 min before methyl (*S*)-2-isocyano-3,3-dimethylbutanoate **101** (373 mg, 2.4 mmol) was added. The reaction was stirred at rt for a further 19 h, filtered through Celite®, and the solvent removed *in vacuo*. The crude product was purified by flash column chromatography (eluting gradient EtOAc:40–60 petroleum ether from 0:1 to 1:3) to give amide **99a** as a white solid (291 mg, 0.602 mmol, 30%) and **99b** as a white solid (382 mg, 0.790 mmol, 40%). A small amount of both isomers was re-crystallised from hexane/Et_2O for X-ray crystallography.

99a

***R**$_f$* = 0.23 (EtOAc:40–60 petroleum ether = 1:3)

mp = 150–157 °C

[α]$_D^{25}$ = −21.7° (c = 1.44, $CHCl_3$)

^{1}H NMR (400 MHz, $CDCl_3$): δ_H = 8.27 (d, *J* = 8.0 Hz, 1 H, H-4), 7.33 (d, *J* = 7.6 Hz, 1 H, H-7), 7.31–7.26 (m, 1 H, H-6), 7.22 (ddd, *J* = 8.0, 6.8, 1.4 Hz, 1 H, H-5), 7.09 (s, 1 H, H-1), 6.33 (s, 1 H, H-12), 5.91 (d, *J* = 8.5 Hz, 1 H, N-H), 4.04 (d, *J* = 8.6 Hz, 1 H, H-17), 3.77 (s, 3 H, H-9), 3.67 (s, 3 H, H-21), 3.46 (q, $^{5}J_{H\text{-}F}$ = 1.9 Hz, 3 H, H-13), 1.69 (s, 3 H, H-11 or 11'), 1.50 (s, 3 H, H-11' or 11), 0.45 (s, 9 H, H-19)

^{13}C NMR (101 MHz, $CDCl_3$): δ_C = 171.9 (C-20), 168.4 (C-16), 159.4 (app d, $^{2}J_{C\text{-}F}$ = 35.6 Hz, C-14), 138.2 (C-8), 127.1 (C-1), 124.7 (C-3), 122.6 (C-6), 121.1 (C-4), 120.7 (C-2), 120.2 (C-5), 117.0 (app d, $^{1}J_{C\text{-}F}$ = 288.3 Hz, C-15), 109.8 (C-7), 63.0 (C-12), 60.4 (C-17), 51.7 (C-21), 39.3 (C-10), 35.0 (q, $^{4}J_{C\text{-}F}$ = 4.2 Hz, C-13), 33.6 (C-18), 32.9 (C-9), 27.5 (C-11' or 11), 26.0 (C-19), 24.5 (C-11 or 11')

^{19}F NMR (376 MHz, $CDCl_3$): δ_F = −69.5

IR (ATR): $\tilde{\nu}_{max}$ / cm^{-1} = 3358 (w, N-H), 2972 (w, C-H), 1738 (m, C=O), 1673 (s, C=O)

HRMS (ESI): *m/z* $[M+Na]^+$ calcd for $C_{24}H_{32}F_3N_3{}^{23}NaO_4$: 506.2237; found: 506.2238 (Δ = 0.2 ppm)

99b

R_f = 0.35 (EtOAc:40–60 petroleum ether = 1:3)

mp = 94–97 °C

$[\alpha]_D^{25}$ = +60.4° (c = 0.747, $CHCl_3$)

IR (ATR): $\tilde{\nu}_{max}$ / cm^{-1} = 3347 (w, N-H), 2967 (w, C-H), 1743 (m, C=O), 1690 (m, C=O), 1673 (s, C=O)

^{1}H NMR (400 MHz, $CDCl_3$): δ_H = 8.16 (dd, *J* = 7.0, 1.2 Hz, 1 H, H-4), 7.32 (dd, *J* = 7.5, 1.7 Hz, 1 H, H-7), 7.28–7.19 (m, 2 H, H-6 and 5), 6.91 (s, 1 H, H-1), 6.12 (s, 1 H, H-12), 5.63 (d, *J* = 9.3 Hz, 1 H, N-H), 4.07 (d, *J* = 9.0 Hz, 1 H, H-17), 3.72 (s, 3 H, H-9), 3.51 (s, 3 H, H-21), 3.47 (q, $^{5}J_{H\text{-}F}$ = 1.9 Hz, 3 H, H-13), 1.74 (s, 3 H, H-11 or 11'), 1.49 (s, 3 H, H-11' or 11), 0.44 (s, 9 H, H-19)

^{13}C NMR (101 MHz, $CDCl_3$): δ_C = 170.7 (C-20), 167.6 (C-16), 159.2 (app d, $^{2}J_{C\text{-}F}$ = 36.0 Hz, C-14), 138.0 (C-8), 126.5 (C-1), 125.1 (C-3), 122.1 (C-6), 120.7 (C-4), 120.1 (C-5), 119.9 (C-2), 116.8 (q, $^{1}J_{C\text{-}F}$ = 288.2 Hz, C-15), 109.8 (C-7), 62.6 (C-12), 60.1 (C-17), 51.6 (C-21), 39.7 (C-10), 34.0-33.9 (m, C-13), 33.9 (C-18), 32.6 (C-9), 27.2 (C-11' or 11), 25.8 (C-19), 24.4 (C-11 or 11')

^{19}F NMR (376 MHz, $CDCl_3$): δ_F = −69.5

HRMS (ESI): *m/z* $[M+H]^+$ calcd for $C_{24}H_{33}F_3N_3O_4$: 484.2418; found: 484.2397 (Δ = −4.3 ppm)

(*S*)-*N*$^{\alpha}$-*tert*-butoxycarbonyl-*N*$^{\alpha}$-methylvalin-*N*-methoxy-*N*-methylamide (110)

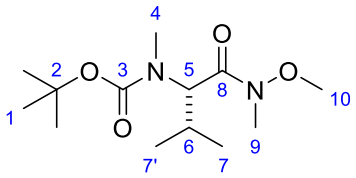

N-Boc-*N*-methylvaline (3.70 g, 16.0 mmol), *N*,*O*-dimethylhydroxylamine hydrochloride (2.03 g, 20.8 mmol), and PyBOP (8.74 g, 16.8 mmol) were dissolved in dry CH_2Cl_2 (16 mL). The mixture was cooled to 0 °C before DIPEA (8.36 mL, 48.0 mmol) was added and stirred at this temperature for 1 min. The reaction was allowed to warm to rt and stirred for a further 2.5 h. Et_2O (100 mL) was then added and the mixture was washed successively with aqueous HCl (3 M, 3 × 35 mL), saturated aqueous $NaHCO_3$ (3 × 35 mL), and brine (3 × 35 mL). The organic phase was then dried with anhydrous $MgSO_4$, and the solvent was removed *in vacuo*. The crude product was then purified by flash column chromatography (eluting gradient Et_2O:40–60 petroleum ether from 0:1 to 1:1) to give Weinreb amide **110** as a slightly yellow oil (3.86 g, 14.1 mmol, 88%)

R_f = 0.50 (EtOAc:40–60 petroleum ether = 1:1)

$[\alpha]_D^{25}$ = −128.7° (c = 1.07, $CHCl_3$, lit.[480] $[\alpha]_D^{20}$ = −163.6°, c = 1.3)

^{1}H NMR (400 MHz, $CDCl_3$): Major rotamer δ_H = 5.00 (br d, *J* = 9.6 Hz, 1 H, H-5), 3.72 (s, 3 H, H-10), 3.20* (br s, 3 H, H-9), 2.83 (s, 3 H, H-4), 2.35–2.17* (m, 1 H, H-6), 1.46 (s, 9 H, H-1); Minor rotamer δ_H = 4.70 (br s, 1 H, H-5), 3.68 (s, 3 H, H-10), 3.20* (br s, 3 H, H-9), 2.80 (s, 3 H, H-4), 2.35–2.17* (m, 1 H, H-6), 1.49 (s, 9 H, H-1); Unassigned† δ_H = 0.90 (d, *J* = 6.8 Hz, 2 H, H-7 and 7'), 0.88 (d, *J* = 6.8 Hz, 4 H, H-7 or 7')

^{13}C NMR (101 MHz, $CDCl_3$): Major rotamer δ_C = 172.3 (C-8), 156.3 (C-3), 80.0 (C-2), 61.9 (C-10), 58.1 (C-5), 32.1 (C-9), 29.8 (C-4), 28.5 (C-1), 27.3 (C-6); Minor rotamer δ_C = 171.2 (C-8), 155.7 (C-3), 79.7 (C-2), 61.8 (C-10), 59.9 (C-5), 32.0 (C-9), 29.2 (C-4), 28.6 (C-1), 27.1 (C-6); Unassigned† δ_C = 19.9 (C-7 or 7'), 19.4 (C-7 or 7'), 18.5 (C-7 or 7')

*These signals appear as single signals and belong to both rotamers.

†Unassigned signals cannot be unambiguously assigned to either rotamers. The numbers of proton nuclei quoted are with respect to the sum of both rotamers.

HRMS (ESI): *m/z* $[M+Na]^+$ calcd for $C_{13}H_{26}N_2{}^{23}NaO_4$: 297.1785; found: 297.1784 (Δ = −0.3 ppm)

Procedure adapted from Nieman *et al.*[359] Spectroscopic data are in accordance with the literature.[359]

Ethyl (2*E*,4*S*)-*N*-*tert*-butoxycarbonyl-*N*-methyl-4-amino-2,5-dimethylhex-2-enoate (100)

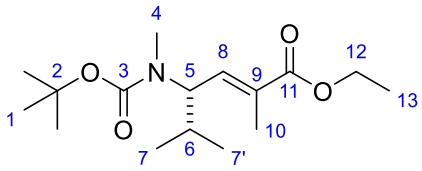

Lithium aluminium hydride (190 mg, 5.00 mmol) was added to the solution of Weinreb amide **110** (1.37 g, 5.00 mmol) in dry THF (5 mL) in one portion at −78 °C. The reaction mixture was then warmed to 0 °C and stirred for 15 min. The mixture was then poured into a stirring ice-cold aqueous solution of $KHSO_4$ (0.25 M, 40 mL), and the phases were separated. The aqueous phase was then extracted with Et_2O (3 × 30 mL). The combined organic phases were quickly washed with aqueous HCl (1 M, 2 × 30 mL), saturated aqueous $NaHCO_3$ (2 × 30 mL), and brine (30 mL), dried with anhydrous $MgSO_4$, and concentrated *in vacuo* (the bath temperature was kept below 20 °C) to give the crude aldehyde **111** as a clear volatile liquid which was used in the next step without further purification.

The crude aldehyde obtained was dissolved in dry CH_2Cl_2 (5 mL) and [(1-ethoxycarbonyl)ethylidene]triphenylphosphorane (2.72 g, 7.50 mmol) was added. The reaction mixture was stirred at rt for 20 h. The reaction was quenched with addition of H_2O (15 mL), and the phases were separated. The aqueous phase was extracted with Et_2O (3 × 30 mL), and the combined organic phases were washed with brine (30 mL), dried with anhydrous $MgSO_4$, and the solvent was removed *in vacuo*. The crude product was purified by flash column chromatography (eluting gradient Et_2O:40–60 petroleum ether from 0:1 to 1:4) to give unsaturated ester **100** as a colourless oil (798 mg, 2.67 mmol, 53% over two steps).

R_f = 0.21 (EtOAc:40–60 petroleum ether = 1:4)

$[\alpha]_D^{25}$ = −83.5° (c = 1.00, $CHCl_3$, lit.[359] +61.1°, c = 9.1)

^{1}H NMR (400 MHz, $CDCl_3$): Rotameric mixtures* δ_H = 6.66 (br d, *J* = 9.2 Hz, 1 H, H-8), 4.64–4.50 (m, 0.5 H, H-5), 4.38–4.26 (m, 0.5 H, H-5), 4.21 (q, *J* = 7.1 Hz, 2 H, H-12), 2.73 (br s, 3 H, H-4), 1.94–1.81 (m, 1 H, H-6), 1.91 (s, 3 H, H-10), 1.47 (s, 9 H, H-1), 1.31 (t, *J* = 7.1 Hz, 3 H, H-13), 0.92 (d, *J* = 6.6 Hz, 3 H, H-7 or 7'), 0.86 (d, *J* = 6.3 Hz, 3 H, H-7' or 7)

^{13}C NMR (126 MHz, $CDCl_3$): Rotameric mixtures* δ_C = 168.1 (br, C-11), 155.9 (C-3), 155.7 (C-3), 139.0 (C-8), 138.9 (C-8), 131.9 (C-9), 131.1 (C-9), 79.9 (C-2), 79.5 (C-2), 61.2 (C-12), 60.9 (C-12), 59.8 (C-5), 58.1 (C-5), 30.5 (C-6), 29.3 (C-4), 29.1 (C-4), 28.6 (C-1), 19.7 (C-7 or 7'), 19.3 (C-7' or 7), 19.0 (C-7' or 7), 14.4 (C-13), 14.1 (C-13), 13.3 (br, C-10)

*Signals are unassigned to individual rotamers as most protons give the same signals in both rotamers.

HRMS (ESI): *m/z* $[M+Na]^+$ calcd for $C_{16}H_{29}N^{23}NaO_4$: 322.1989; found: 322.1984 (Δ = −1.6 ppm)

Procedure adapted from Nieman *et al*.[359] Spectroscopic data are in accordance with the literature.[359]

Ethyl (*S*,*E*)-4-((*S*)-2-((*tert*-butoxycarbonyl)amino)-*N*,3,3-trimethylbutanamido)-2,5-dimethylhex-2-enoate (115)

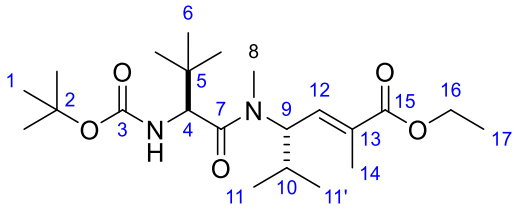

To a solution of ethyl (2*E*,4*S*)-*N*-*tert*-butoxycarbonyl-*N*-methyl-4-amino-2,5-dimethylhex-2-enoate **100** (2.29 g, 7.65 mmol) in dioxane (19 mL) was added a solution of HCl in dioxane (4 M, 19.1 mL, 76.5 mmol). The reaction mixture was then stirred at rt for 15 h before Et_2O (100 mL) was added. The white precipitate formed was filtered under reduced pressure and washed with a copious amount of Et_2O to give the HCl salt of ethyl (2*E*,4*S*)-*N*-methyl-4-amino-2,5-dimethylhex-2-enoate as a white powder (1.61 g, 6.83 mmol, 90%). The product was used in the next step without further purification.

To a solution of (*S*)-*N*-*tert*-butoxycarbonyl-*tert*-leucine (3.15 g, 13.6 mmol) and HATU (5.17 g, 13.6 mmol) in DMF (30 mL) at 0 °C was added DIPEA (2.37 mL, 13.6 mmol). The reaction mixture was stirred for 5 min before a solution of the HCl salt of ethyl (2*E*,4*S*)-*N*-methyl-4-amino-2,5-dimethylhex-2-enoate (1.59 g, 6.7 mmol) and DIPEA (2.37 mL, 13.6 mmol) in DMF (15 mL) was added over 2 min. The reaction mixture was stirred for 18 h before EtOAc (500 mL) was added. The mixture was then successively washed with aqueous HCl (1 M, 3 × 100 mL), saturated aqueous $NaHCO_3$ (3 × 100 mL), and brine (100 mL). The organic phase was then dried with anhydrous $MgSO_4$, and the solvent was removed *in vacuo*. The crude product was purified by flash column chromatography (eluting gradient EtOAc:40–60 petroleum ether from 0:1 to 1:5) to give amide **115** as a white solid (2.59 g, 6.28 mmol, 93%).

R_f = 0.48 (EtOAc:40–60 petroleum ether = 1:3)

$[\alpha]_D^{25}$ = −126.9° (c = 0.864, $CHCl_3$, lit.[359] −76.9°, c = 2.43)

^{1}H NMR (400 MHz, $CDCl_3$): δ_H = 6.63 (app dd, *J* = 9.3, 1.4 Hz, 1 H, H-12), 5.20 (d, *J* = 10.0 Hz, 1 H, N-H), 5.09 (t, *J* = 9.9 Hz, 1 H, H-9), 4.41 (d, *J* = 10.2 Hz, 1 H, H-4), 4.18 (q, *J* = 7.1 Hz, 2 H, H-16), 2.97 (s, 3 H, H-8), 1.93–1.82 (m, 4 H, H-10 and H-14), 1.40 (s, 9 H, H-1), 1.29 (t, *J* = 7.1 Hz, 3 H, H-17), 0.94 (s, 9 H, H-6), 0.86 (d, *J* = 6.6 Hz, 3 H, H-11 or 11'), 0.82 (d, *J* = 6.6 Hz, 3 H, H-11' or 11)

^{13}C NMR (101 MHz, $CDCl_3$): δ_C = 172.5 (C-7), 167.9 (C-15), 156.2 (C-3), 138.7 (C-12), 132.7 (C-13), 79.6 (C-2), 60.9 (C-16), 56.4 (C-4), 56.0 (C-9), 35.0 (C-5), 31.1 (C-8), 30.2 (C-10), 28.4 (C-1), 26.5 (C-6), 19.6 (C-11 or 11'), 18.7 (C-11' or 11), 14.3 (C-17), 13.9 (C-14)

LCMS (ESI): *m/z* $[M+H]^+$ calcd for $C_{22}H_{41}N_2O_5$: 413.3; found: 413.4

Spectroscopic data are in accordance with the literature.[359]

Ethyl (*S*,*E*)-4-((*S*)-2-formamido-*N*,3,3-trimethylbutanamido)-2,5-dimethylhex-2-enoate (116)

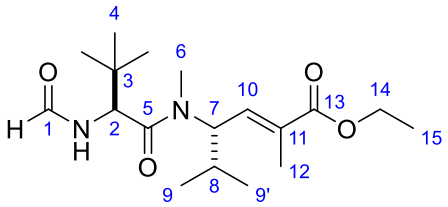

To a solution of ethyl (*S*,*E*)-4-((*S*)-2-((*tert*-butoxycarbonyl)amino)-*N*,3,3-trimethylbutanamido)-2,5-dimethylhex-2-enoate **115** (744 mg, 1.80 mmol) in dioxane (4.5 mL) was added a solution of HCl in dioxane (4 M, 4.50 mL, 18.0 mmol). The reaction mixture was then stirred at rt for 14 h before volatiles were removed *in vacuo* to give the crude deprotected amine. Ethyl formate (60 mL) and triethylamine (276 µL, 1.98 mmol) were added, and the reaction mixture was refluxed for 20 h. The mixture was then filtered through a short silica gel plug and eluted with EtOAc. The volatiles were removed *in vacuo* to give formamide **116** as a colourless viscous oil which solidified into white needles under a stream of N_2 over several days (569 mg, 1.67 mmol, 93% over two steps). This compound was used in the next step without further purification.

R_f = 0.50 (EtOAc)

mp = 71–75 °C

$[\alpha]_D^{25}$ = −129.3° (c = 0.760, $CHCl_3$)

^{1}H NMR (400 MHz, $CDCl_3$): δ_H = 8.21 (d, *J* = 1.0 Hz, 1 H, H-1), 6.64 (app dd, *J* = 9.4, 1.3 Hz, 1 H, H-10), 6.46 (br d, *J* = 9.3 Hz, 1 H, N-H), 5.09 (t, *J* = 10.0 Hz, 1 H, H-7), 4.94 (d, *J* = 9.7 Hz, 1 H, H-2), 4.20 (q, *J* = 7.1 Hz, 2 H, H-14), 2.99 (s, 3 H, H-6), 1.97–1.83 (m, 4 H, H-8 and H-12),1.31 (t, *J* = 7.1 Hz, 3 H, H-15), 0.97 (s, 9 H, H-4), 0.88 (d, *J* = 6.5 Hz, 3 H, H-9 or 9'), 0.82 (d, *J* = 6.5 Hz, 3 H, H-9' or 9)

^{13}C NMR (101 MHz, $CDCl_3$): δ_C = 171.3 (C-5), 167.8 (C-13), 160.8 (C-1), 138.3 (C-10), 132.9 (C-11), 61.0 (C-14), 56.3 (C-7), 53.3 (C-2), 35.7 (C-3), 31.3 (C-6), 30.1 (C-8), 26.6 (C-4), 19.5 (C-9 or 9'), 18.9 (C-9' or 9), 14.3 (C-15), 14.0 (C-12)

IR (ATR): $\tilde{\nu}_{max}$ / cm^{-1} = 3264 (w, N-H), 2965 (m, C-H), 1713 (m, C=O), 1674 (m, C=O), 1633 (s, C=O)

HRMS (ESI): *m/z* $[M+Na]^+$ calcd for $C_{18}H_{32}N_2{}^{23}NaO_4$: 363.2254; found: 363.2261 (Δ = 1.9 ppm)

Ethyl (*S*,*E*)-4-((*S*)-2-isocyano-*N*,3,3-trimethylbutanamido)-2,5-dimethylhex-2-enoate (117)

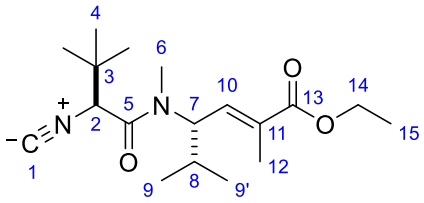

To a solution of ethyl (*S*,*E*)-4-((*S*)-2-formamido-*N*,3,3-trimethylbutanamido)-2,5-dimethylhex-2-enoate **116** (529 mg, 1.55 mmol) in CH_2Cl_2 (31 mL) at −50 °C was added 2,6-lutidine (812 µL, 6.98 mmol) and triphosgene (276 mg, 0.93 mmol) in one portion. The reaction mixture was stirred at −50 °C for 21 h before quenching by addition of saturated aqueous $NaHCO_3$ (45 mL) and diluting with CH_2Cl_2 (45 mL). The phases were then separated. The organic phase was then washed successively with aqueous HCl (1 M, 30 mL), saturated aqueous $NaHCO_3$ (30 mL), and brine (30 mL), dried with anhydrous Na_2SO_4, filtered, and the solvent removed *in vacuo*. The crude oil was purified by flash column chromatography (eluting gradient EtOAc:40–60 petroleum ether from 0:1 to 1:5) to give isocyanide **117** as a white solid (423 mg, 1.31 mmol, 84%).

R_f = 0.38 (EtOAc:40–60 petroleum ether = 1:3)

mp = 102–104 °C

$[\alpha]_D^{25}$ = −86.9° (c = 0.452, $CHCl_3$)

^{1}H NMR (400 MHz, $CDCl_3$): δ_H = 6.63 (app dd, *J* = 9.2, 1.4 Hz, 1 H, H-10), 5.10 (t, *J* = 9.9 Hz, 1 H, H-7), 4.21 (q, *J* = 7.2 Hz, 2 H, H-14), 4.19 (s, 1 H, H-2), 2.94 (s, 3 H, H-6), 2.01–1.90 (m, 1 H, H-8), 1.89 (d, *J* = 1.4 Hz, 3 H, H-12),1.31 (t, *J* = 7.1 Hz, 3 H, H-15), 1.12 (s, 9 H, H-4), 0.94 (d, *J* = 6.7 Hz, 3 H, H-9 or 9'), 0.91 (d, *J* = 6.5 Hz, 3 H, H-9' or 9)

^{13}C NMR (101 MHz, $CDCl_3$): δ_C = 167.7 (C-13), 164.9 (C-5), 158.4 (br, C-1) 137.7 (C-10), 133.4 (C-11), 61.7 (C-2), 61.1 (C-14), 56.7 (C-7), 35.7 (C-3), 31.1 (C-6), 30.5 (C-8), 26.2 (C-4), 19.6 (C-9 or 9'), 18.8 (C-9' or 9), 14.3 (C-15), 13.8 (C-12)

IR (ATR): $\tilde{\nu}_{max}$/ cm^{-1} = 2964 (m, C-H), 2153 (m, C≡N), 1715 (s, C=O), 1646 (s, C=O)

HRMS (ESI): *m/z* $[M+Na]^+$ calcd for $C_{18}H_{30}N_2{}^{23}NaO_3$: 345.2149; found: 345.2153 (Δ = 1.2 ppm)

***N*-trifluoroacetyl hemiasterlin ethyl ester (113a)**

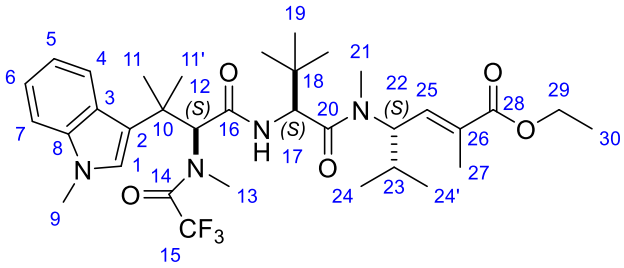

and ***N*-trifluoroacetyl *epi*-hemiasterlin ethyl ester (113b)**

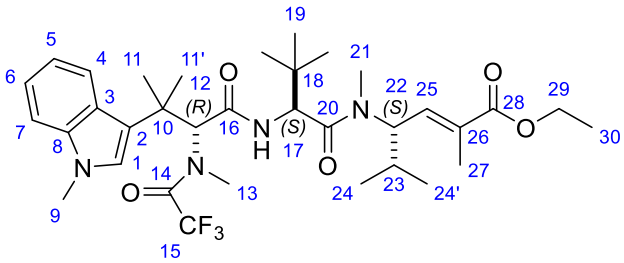

Methylamine solution in MeOH (2 M, 55 µL, 0.11 mmol) was added to a solution of 2-methyl-2-(1-methyl-1*H*-indol-3-yl)propanal **69** (20.1 mg, 0.100 mmol) in dry MeOH (0.2 mL). 3 Å molecular sieves (100 mg) were then added and the reaction was stirred at rt for 2 h before TFA (9.78 µL, 0.120 mmol) and sodium trifluoroacetate (16.3 mg, 0.120 mmol) were added. The reaction mixture was stirred for a further 30 min before ethyl (*S*,*E*)-4-((*S*)-2-isocyano-*N*,3,3-trimethylbutanamido)-2,5-dimethylhex-2-enoate **117** (38.7 mg, 0.120 mmol) was added. The reaction was stirred at rt for a further 19 h, filtered through Celite®, and the solvent was removed *in vacuo*. The crude product was purified by flash column chromatography (eluting gradient EtOAc:40–60 petroleum ether from 0:1 to 1:3) to give protected hemiasterlin **113a** as a white solid (26.5 mg, 0.0407 mmol, 41%) and protected *epi*-hemiasterlin **113b** as a white solid (20.8 mg, 0.0320 mmol, 32%). A small amount of **113a** was re-crystallised using the slow evaporation method with EtOAc/hexane (1:5) as a solvent for X-ray crystallographic analysis.

113a (*S*,*S*,*S*)

***R*$_f$** = 0.24 (EtOAc:40–60 petroleum ether = 1:3)

mp = 181–184 °C

[α]$_D^{25}$ = −103.8° (c = 0.212, $CHCl_3$)

^{1}H NMR (400 MHz, $CDCl_3$): δ_H = 8.28 (d, *J* = 8.1 Hz, 1 H, H-4), 7.33 (d, *J* = 8.3 Hz, 1 H, H-7), 7.28 (ddd, *J* = 8.1, 6.9, 1.0, 1 H, H-6), 7.21 (ddd, *J* = 8.0, 6.9, 1.3 Hz, 1 H, H-5), 7.18 (s, 1 H, H-1), 6.64 (dq, *J* = 9.2, 1.5 Hz, 1 H, H-25), 6.38 (s, 1 H, H-12), 6.32 (br d, *J* = 8.7 Hz, 1 H, N-H), 5.07 (dd, *J* = 10.5, 9.5 Hz, 1 H, H-22), 4.42 (d, *J* = 8.8 Hz, 1 H, H-17), 4.20 (q, *J* = 7.1 Hz, 2 H, H-29), 3.78 (s, 3 H, H-9), 3.37 (q, $^5J_{H\text{-}F}$ = 1.9 Hz, 3 H, H-13), 2.97 (s, 3 H, H-21), 1.97-1.87 (m, 4 H,

H-23 and H-27), 1.61 (s, 3 H, H-11 or 11'), 1.47 (s, 3 H, H-11' or 11), 1.30 (t, *J* = 7.1 Hz, 3 H, H-30), 0.91 (d, *J* = 6.6 Hz, 3 H, H-24 or 24'), 0.87 (d, *J* = 6.6 Hz, 3 H, H-24' or 24), 0.44 (s, 9 H, H-19)

^{13}C NMR (101 MHz, $CDCl_3$): δ_C = 171.3 (C-20), 168.6 (C-16), 167.8 (C-28), 159.3 (q, $^2J_{C\text{-}F}$ = 35.5 Hz, C-14), 138.9 (C-25), 138.3 (C-8), 132.7 (C-26), 127.0 (C-1), 124.7 (C-3), 122.6 (C-6), 121.2 (C-4), 120.9 (C-2), 120.1 (C-5), 117.0 (app d, $^1J_{C\text{-}F}$ = 288.1 Hz, C-15), 109.7 (C-7), 63.2 (C-12), 61.0 (C-29), 56.2 (C-22), 55.5 (C-17), 39.2 (C-10), 35.1 (q, $^4J_{C\text{-}F}$ = 4.1 Hz, C-13), 34.0 (C-18), 32.8 (C-9), 31.3 (C-21), 30.2 (C-23), 27.7 (C-11' or 11), 26.0 (C-19), 24.3 (C-11 or 11'), 19.6 (C-24 or 24'), 19.0 (C-24' or 24), 14.3 (C-30), 14.0 (C-27)

^{19}F NMR (376 MHz, $CDCl_3$): δ_F = −69.5

IR (ATR): $\tilde{\nu}_{max}$ / cm^{-1} = 3359 (m, N-H), 2967 (m, C-H), 2925 (m, C-H), 1706 (m, C=O), 1686 (m, C=O), 1663 (m, C=O), 1634 (m, C=O)

HRMS (ESI): *m/z* $[M+Na]^+$ calcd for $C_{34}H_{49}F_3N_4{}^{23}NaO_5$: 673.3547; found: 673.3564 (Δ = 2.5 ppm)

113b (*R*,*S*,*S*)

R_f = 0.18 (EtOAc:40–60 petroleum ether = 1:3)

mp = 150–153 °C

$[\alpha]_D^{25}$ = −16.2° (c = 0.222, $CHCl_3$)

^{1}H NMR (400 MHz, $CDCl_3$): δ_H = 8.07 (d, *J* = 7.4 Hz, 1 H, H-4), 7.29 (dd, *J* = 7.5, 1.3 Hz, 1 H, H-7), 7.24–7.15 (m, 2 H, H-6 and 5), 6.90 (s, 1 H, H-1), 6.54 (dq, *J* = 9.0, 1.5 Hz, 1 H, H-25), 5.98 (s, 1 H, H-12), 5.95 (d, *J* = 9.5 Hz, 1 H, N-H), 4.91 (dd, *J* = 10.5, 9.2 Hz, 1 H, H-22), 4.49 (d, *J* = 9.6 Hz, 1 H, H-17), 4.17 (q, *J* = 7.1 Hz, 2 H, H-29), 3.71 (s, 3 H, H-9), 3.39 (q, $^5J_{H\text{-}F}$ = 1.9 Hz, 3 H, H-13), 2.82 (s, 3 H, H-21), 1.79 (d, *J* = 1.4 Hz, 3 H, H-27), 1.78–1.70 (m, 4 H, H-23 and H-11 or 11'), 1.49 (s, 3 H, H-11' or 11), 1.28 (t, *J* = 7.1 Hz, 3 H, H-30), 0.81 (d, *J* = 6.6 Hz, 3 H, H-24 or 24'), 0.55 (d, *J* = 6.6 Hz, 3 H, H-24' or 24), 0.40 (s, 9 H, H-19)

^{13}C NMR (101 MHz, $CDCl_3$): δ_C = 170.9 (C-20), 167.8 (C-28), 167.4 (C-16), 159.0 (q, $^2J_{C\text{-}F}$ = 35.6 Hz, C-14), 138.6 (C-25), 138.1 (C-8), 133.0 (C-26), 126.6 (C-1), 125.5 (C-3), 122.1 (C-6), 120.8 (C-4), 120.0 (C-5), 119.9 (C-2), 116.8 (q, $^1J_{C\text{-}F}$ = 288.3 Hz, C-15), 109.9 (C-7), 62.9 (C-12), 60.9 (C-29), 55.6 (C-22), 54.3 (C-17), 39.8 (C-10), 34.5 (C-18), 33.7 (q, $^4J_{C\text{-}F}$ = 4.1 Hz, C-13), 32.8 (C-9), 30.9 (C-21), 30.3 (C-23), 27.3 (C-11' or 11), 25.7 (C-19), 24.5 (C-11 or 11'), 19.4 (C-24 or 24'), 18.0 (C-24' or 24), 14.3 (C-30), 13.8 (C-27)

^{19}F NMR (376 MHz, $CDCl_3$): δ_F = −69.7

IR (ATR): $\tilde{\nu}_{max}$ / cm^{-1} = 3316 (m, N-H), 2960 (m, C-H), 1687 (s, C=O), 1672 (s, C=O), 1634 (s, C=O)

HRMS (ESI): *m/z* $[M+Na]^+$ calcd for $C_{34}H_{49}F_3N_4{}^{23}NaO_5$: 673.3547; found: 673.3562 (Δ = 2.2 ppm)

Hemiasterlin trifluoroacetate salt (56·TFA)

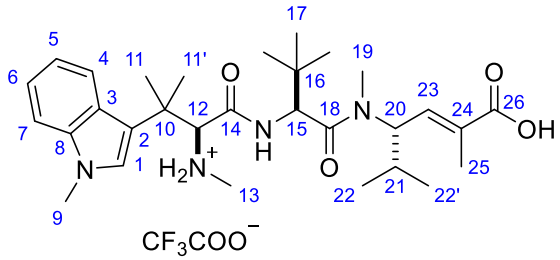

LiOH·H_2O (16.0 mg, 0.381 mmol) was added to a solution of *N*-trifluoroacetyl hemiasterlin ethyl ester **113a** (15.5 mg, 23.8 µmol) in H_2O/MeOH (1:1, 2 mL). The reaction was heated to 60 °C and stirred for 8 days. The mixture was then purified by reverse-phase semi-preparative HPLC (30–46%B over 16 min) to give the trifluoroacetate salt of hemiasterlin **56**·TFA as a white powder (13.1 mg, 20.4 µmol, 86%).

t_R / min = 10.14 (5–95%B over 15 min)

$[\alpha]_D^{25}$ = −24.1° (c = 0.108, MeOH, lit.[359] −76°, c = 0.7, MeOH)

^{1}H NMR (700 MHz, DMSO-d_6): δ_H = 12.48 (br s, 1 H, COO-H), 8.96–8.78 (m, 2 H, CON-H, NH_2^+), 8.11 (br s, 1 H, H-4), 7.46 (d, *J* = 8.1 Hz, 1 H, H-7), 7.35 (br s, 1 H, NH_2^+), 7.21 (t, *J* = 7.5 Hz, 1 H, H-6), 7.17 (s, 1 H, H-1), 7.09 (t, *J* = 7.3 Hz, 1 H, H-5), 6.68 (d, *J* = 9.4 Hz, 1 H, H-23), 4.94 (t, *J* = 10.0 Hz, 1 H, H-20), 4.86 (d, *J* = 8.2 Hz, 1 H, H-15), 4.43 (br s, 1 H, H-12), 3.76 (s, 3 H, H-9), 3.03 (s, 3 H, H-19), 2.23 (br s, 3 H, H-13), 2.07–1.96 (m, 1 H, H-21), 1.80 (s, 3 H, H-25), 1.41 (s, 3 H, H-11 or 11'), 1.38 (s, 3 H, H-11' or 11), 1.00 (s, 9 H, H-17), 0.81 (d, *J* = 6.6 Hz, 3 H, H-22 or 22'), 0.79 (d, *J* = 6.2 Hz, 3 H, H-22' or 22)

^{13}C NMR (176 MHz, DMSO-d_6): δ_C = 170.1 (C-18), 168.6 (C-26), 165.7 (C-14), 157.7 (q, $^2J_{C\text{-}F}$ = 30.9 Hz, CF_3**C**OO^-), 138.4 (C-23), 137.8 (C-8), 131.8 (C-24), 128.8 (C-1), 125.0 (C-3), 121.3 (C-6), 120.4 (C-4), 118.5 (C-5), 117.4 (q, $^1J_{C\text{-}F}$ = 300.7 Hz, **C**F_3COO^-), 116.3 (C-2), 110.2 (C-7), 67.4 (C-12), 56.3 (C-20), 55.6 (C-15), 37.6 (C-10), 34.8 (C-16), 33.5 (C-13), 32.5 (C-9), 31.1 (C-19), 28.8 (C-21), 27.0 (C-11' or 11), 26.4 (C-17), 22.4 (C-11 or 11'), 19.4 (C-22 or 22'), 18.9 (C-22' or 22), 13.6 (C-25)

^{19}F NMR (376 MHz, DMSO-d_6): δ_F = −73.4

IR (ATR): $\tilde{\nu}_{max}$ / cm^{-1} = 2967 (m, C-H), 1673 (s, C=O)

UV-Vis: λ_{max} / nm = 229, 287 (1 mM in MeCN/H_2O (1:4), lit.[359] 216, 273 in MeOH)

HRMS (ESI): *m/z* $[M+H]^+$ calcd for $C_{30}H_{47}N_4O_2$: 527.3592; found: 527.3606 (Δ = 2.7 ppm)

Spectroscopic data are in accordance with the literature.[359]

epi-hemiasterlin trifluoroacetate salt (56b·TFA)

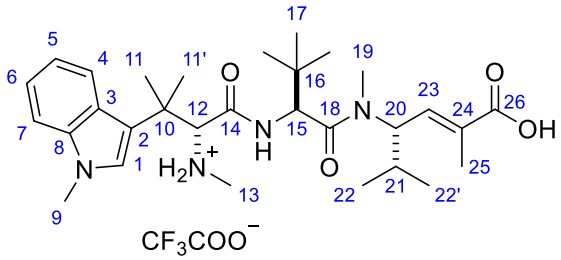

LiOH·H_2O (256.2 mg, 0.624 mmol) was added to a solution of *N*-trifluoroacetyl *epi*-hemiasterlin ethyl ester **113b** (25.4 mg, 39.0 µmol) in H_2O/MeOH (1:1, 3 mL). The reaction was heated to 60 °C and stirred for 7 days. The mixture was then purified by reverse-phase semi-preparative HPLC (30–46%B over 16 min) to give the trifluoroacetate salt of *epi*-hemiasterlin **56b**·TFA as a white powder (19.5 mg, 30.9 µmol, 78%).

t_R / min = 10.06 (5–95%B over 15 min)

$[\alpha]_D^{25}$ = −101.8° (c = 0.108, MeOH)

^{1}H NMR (700 MHz, DMSO-d_6): δ_H = 12.51 (br s, 1 H, COO-H), 9.00 (br s, 1 H, CON-H or NH_2^+), 8.89 (br s, 1 H, CON-H or NH_2^+), 8.09 (d, *J* = 7.8 Hz, 1 H, H-4), 7.54 (br s, 1 H, CON-H or NH_2^+), 7.44 (d, *J* = 8.2 Hz, 1 H, H-7), 7.20 (t, *J* = 7.8 Hz, 1 H, H-6), 7.18 (s, 1 H, H-1), 7.08 (t, *J* = 7.5 Hz, 1 H, H-5), 6.66 (d, *J* = 9.5 Hz, 1 H, H-23), 4.90 (t, *J* = 10.0 Hz, 1 H, H-20), 4.76 (d, *J* = 9.0 Hz, 1 H, H-15), 4.53 (d, *J* = 9.7 Hz, 1 H, H-12), 3.75 (s, 3 H, H-9), 3.02 (s, 3 H, H-19), 2.17 (s, 3 H, H-13), 2.05–1.95 (m, 1 H, H-21), 1.78 (s, 3 H, H-25), 1.51 (s, 3 H, H-11 or 11'), 1.47 (s, 3 H, H-11' or 11), 0.89 (s, 9 H, H-17), 0.79 (d, *J* = 6.6 Hz, 3 H, H-22 or 22'), 0.72 (d, *J* = 6.5 Hz, 3 H, H-22' or 22)

^{13}C NMR (176 MHz, DMSO-d_6): δ_C = 170.7 (C-18), 168.6 (C-26), 166.5 (C-14), 157.7 (q, $^2J_{C\text{-}F}$ = 30.4 Hz, CF_3**C**OO^-), 138.4 (C-23), 137.8 (C-8), 131.9 (C-24), 128.6 (C-1), 125.0 (C-3), 121.3 (C-6), 120.6 (C-4), 118.5 (C-5), 117.5 (app d, $^1J_{C\text{-}F}$ = 303.6 Hz, **C**F_3COO^-), 116.3 (C-2), 110.1 (C-7), 67.6 (C-12), 56.2 (C-20), 55.6 (C-15), 37.1 (C-10), 34.2 (C-16), 33.1 (C-13), 32.5 (C-9), 31.1 (C-19), 28.8 (C-21), 26.6 (C-11' or 11), 26.3 (C-17), 23.1 (C-11 or 11'), 19.4 (C-22 or 22'), 18.8 (C-22' or 22), 13.6 (C-25)

^{19}F NMR (376 MHz, DMSO-d_6): δ_F = −73.4

IR (ATR): $\tilde{\nu}_{max}$ / cm^{-1} = 2970 (m, C-H), 1671 (s, C=O)

UV-Vis: λ_{max} / nm = 229, 288 (1 mM in MeCN/H_2O (1:4))

HRMS (ESI): *m/z* $[M+H]^+$ calcd for $C_{30}H_{47}N_4O_2$: 527.3592; found: 527.3620 (Δ = 5.3 ppm)

2-Methyl-2-phenylpropanal (120)

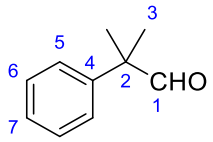

2-Methyl-2-phenylpropanoic acid (657 mg, 4.00 mmol) was dissolved in dry Et_2O (80 mL) and cooled to 0 °C. $LiAlH_4$ (493 mg, 13.0 mmol) was added to the mixture in 3 portions over 10 min. The reaction was allowed to warm to rt and stirred for 90 min before being cooled to 0 °C. The reaction was quenched by the slow addition of aqueous HCl (1 M, 10 mL) and the phases separated. The aqueous phase was extracted with Et_2O (3 × 25 mL), and the combined organic phases were dried with anhydrous $MgSO_4$. The solvent was removed *in vacuo* to give the crude alcohol which was then re-dissolved in dry CH_2Cl_2 (29 mL). *N*-methylmorpholine *N*-oxide (844 mg, 7.20 mmol), 4 Å powdered molecular sieves (870 mg), and tetrapropylammonium perruthenate (70.3 mg, 0.200 mmol) were added to the solution. The black reaction mixture was stirred at rt for 20 h, filtered through Celite®, and concentrated *in vacuo* (the bath temperature was kept below 20 °C). The crude black oil was purified by flash column chromatography (eluting gradient Et_2O:30–40 petroleum ether from 0:1 to 1:50) to give aldehyde **120** as a colourless liquid (460 mg, 3.11 mmol, 78% over two steps).

$\boldsymbol{R_f}$ = 0.53 (Et_2O:40–60 petroleum ether = 1:5)

^{1}H NMR (400 MHz, $CDCl_3$): δ_H = 9.52 (s, 1 H, H-1), 7.40 (t, *J* = 7.5 Hz, 2 H, H-6 or 7), 7.33-7.27 (m, 3 H, H-5 and 7 or 6), 1.48 (s, 6 H, H-3)

^{13}C NMR (101 MHz, $CDCl_3$): δ_C = 202.4 (C-1), 141.3 (C-4), 129.0 (C-5, 6, or 7), 127.4 (C-5, 6, or 7), 126.8 (C-5, 6, or 7), 50.6 (C-2), 22.6 (C-3)

Spectroscopic data are in accordance with the literature.[481]

Taltobulin trifluoroacetate salt (57·TFA)

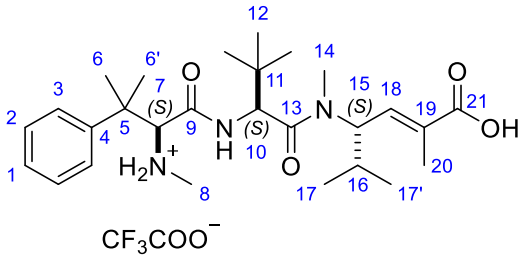

and ***epi*-Taltobulin trifluoroacetate salt (57b·TFA)**

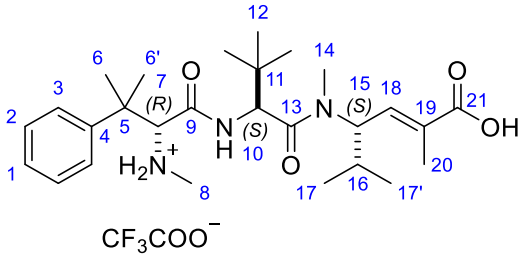

Methylamine solution in MeOH (2 M, 110 µL, 0.220 mmol) was added to a mixture of 2-methyl-2-phenylpropanal **120** (29.6 mg, 0.200 mmol) and 3 Å molecular sieves (200 mg) in dry MeOH (0.4 mL), and the reaction was stirred at rt for 2 h. TFA (18.4 µL, 0.240 mmol) and sodium trifluoroacetate (81.6 mg, 0.600 mmol) were added. The reaction mixture was stirred for a further 25 min before ethyl (*S*,*E*)-4-((*S*)-2-isocyano-*N*,3,3-trimethylbutanamido)-2,5-dimethylhex-2-enoate **117** (65.0 mg, 0.202 mmol) was added. The reaction was stirred at rt for a further 19 h, filtered through Celite®, and the solvent removed *in vacuo*. The crude product was purified by flash column chromatography (eluting gradient EtOAc:40–60 petroleum ether from 0:1 to 1:3) to give a partially separable diastereomeric mixture of protected taltobulin **121a** (80% purity, 28.1 mg, 47.0 µmol, 24%) and protected *epi*-taltobulin **121b** (80% purity, 38.5 mg, 64.4 µmol, 32%) which were used in the next step without further purification.

The protected taltobulin **121a** and **121b** were dissolved separately in H_2O/MeOH (1:1, 3 mL). LiOH·H_2O (16 equiv.) was added to each reaction. The reaction mixtures were heated to 60 °C and stirred for 8 days. The mixtures were then purified by reverse-phase semi-preparative HPLC (5–38%B over 70 min for **57a**, 5–36%B over 76 min for **57b**) to give the trifluoroacetate salt of taltobulin **57**·TFA as a white powder (23.0 mg, 39.1 µmol, 20% over two steps) and the trifluoroacetate salt of *epi*-taltobulin **57b**·TFA as a white powder (24.0 mg, 40.8 µmol, 20% over two steps).

57·TFA (*S*,*S*,*S*)

t_R / min = 9.19 (5–95%B over 15 min)

$[\alpha]_D^{25}$ = −26.5° (c = 0.102, MeOH, lit.[359] $[\alpha]_D^{22}$ = −21.7°, c = 0.23)

^{1}H NMR (700 MHz, CD_3OD): δ_H = 7.54 (d, *J* = 7.5 Hz, 2 H, H-3), 7.45 (t, *J* = 7.7 Hz, 2 H, H-2), 7.35 (t, *J* = 7.3 Hz, 1 H, H-1), 6.78 (app dd, *J* = 9.7, 1.4 Hz, 1 H, H-18), 5.05 (t, *J* = 10.1 Hz, 1 H, H-15), 4.92 (s, 1 H, H-10), 4.36 (s, 1 H, H-7), 3.14 (s, 3 H, H-14), 2.50 (s, 3 H, H-8), 2.08–2.01 (m, 1 H, H-16), 1.91 (d, *J* = 1.4 Hz, 3 H, H-20), 1.47 (s, 3 H, H-6 or 6'), 1.38 (s, 3 H, H-6' or 6), 1.07 (s, 9 H, H-12), 0.92–0.88 (m, 6 H, H-17 and 17')

^{13}C NMR (176 MHz, CD_3OD): δ_C = 172.3 (C-13), 170.8 (C-21), 167.1 (C-9), 145.0 (C-4), 139.7 (C-18), 133.6 (C-19), 130.4 (C-2), 128.9 (C-1), 127.4 (C-3), 71.3 (C-7), 58.5 (C-15), 57.8 (C-10), 42.1 (C-5), 36.0 (C-11), 34.2 (C-8), 31.9 (C-14), 30.8 (C-16), 29.8 (C-6' or C-6), 26.9 (C-12), 21.5 (C-6 or 6'), 19.8* (C-17 or 17'), 19.8* (C-17' or 17), 14.2 (C-20)

*Denoted signals with equal chemical shifts to 1 decimal place appear as two distinguishable signals.

^{19}F NMR (376 MHz, DMSO-d_6): δ_F = −76.9

IR (ATR): $\tilde{\nu}_{max}$ / cm^{-1} = 2966 (m, C-H), 1669 (s, C=O), 1625 (s, C=O)

UV-Vis: λ_{max} / nm = 206, 212 (1 mM in MeCN/H_2O (1:4))

HRMS (ESI): *m/z* $[M+H]^+$ calcd for $C_{27}H_{44}N_3O_6$: 474.3326; found: 474.3344 (Δ = 3.8 ppm)

Spectroscopic data are in accordance with the literature.[359]

57b (**R,S,S*)

t_R / min = 9.32 (5–95%B over 15 min)

$[\alpha]_D^{25}$ = −89.7° (c = 0.107, MeOH, lit.[359] $[\alpha]_D^{22}$ = −96.7°, c = 2.4)

^{1}H NMR (700 MHz, CD_3OD): δ_H = 7.51 (d, *J* = 7.5 Hz, 2 H, H-3), 7.44 (t, *J* = 7.8 Hz, 2 H, H-2), 7.32 (t, *J* = 7.3 Hz, 1 H, H-1), 6.75 (app dd, *J* = 9.7, 1.3 Hz, 1 H, H-18), 5.03 (t, *J* = 10.2 Hz, 1 H, H-15), 4.55 (s, 1 H, H-10), 4.33 (s, 1 H, H-7), 3.12 (s, 3 H, H-14), 2.47 (s, 3 H, H-8), 2.06–1.98 (m, 1 H, H-16), 1.88 (d, *J* = 1.3 Hz, 3 H, H-20), 1.54 (s, 3 H, H-6 or 6'), 1.48 (s, 3 H, H-6' or 6), 0.91 (s, 9 H, H-12), 0.90–0.86 (m, 6 H, H-17 and 17')

^{13}C NMR (176 MHz, CD_3OD): δ_C = 173.1 (C-13), 170.8 (C-21), 167.7 (C-9), 145.0 (C-4), 139.8 (C-18), 133.6 (C-19), 130.3 (C-2), 128.8 (C-1), 127.4 (C-3), 71.3 (C-7), 58.7 (C-10), 58.5 (C-15), 41.5 (C-5), 35.0 (C-11), 34.0 (C-8), 31.8 (C-14), 30.8 (C-16), 27.1 (C-6' or C-6), 27.0 (C-12), 24.0 (C-6 or 6'), 19.8 (C-17 or 17'), 19.6 (C-17' or 17), 14.1 (C-20)

^{19}F NMR (376 MHz, DMSO-d_6): δ_F = −76.9

IR (ATR): $\tilde{\nu}_{max}$ / cm^{-1} = 2975 (m, C-H), 1669 (s, C=O)

UV-Vis: λ_{max} / nm = 206, 214.5 (1 mM in MeCN/H_2O (1:4))

HRMS (ESI): *m/z* $[M+H]^+$ calcd for $C_{27}H_{44}N_3O_6$: 474.3326; found: 474.3343 (Δ = 3.6 ppm)

6.3.2. Linker–drug synthesis

H-Val-Ala-PABA·TFA (134)

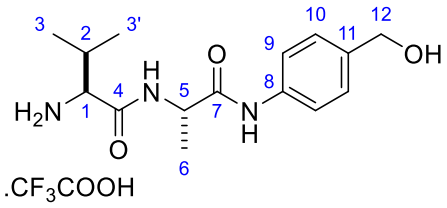

Pyrrolidine (83.5 µL, 1.00 mmol) was added to a solution of Alloc-Val-Ala-PABA **122** (189 mg, 0.500 mmol) and $Pd(PPh_3)_4$ (28.9 mg, 0.0250 mmol) in CH_2Cl_2/DMF (7:1, 20 mL). The reaction mixture was stirred at rt for 20 h and the volatiles were removed *in vacuo*. The crude mixture was then purified with reverse-phase semi-preparative HPLC (5–36%B over 8 min) to give the trifluoroacetate salt of amine **134** as a white powder (198 mg, 0.486 mmol, 97%)

t_R / min = 4.79 (5–95%B over 15 min)

$[\alpha]_D^{25}$ = −31.3° (c = 0.668, MeOH)

^{1}H NMR (400 MHz, CD_3OD): δ_H = 7.53 (d, *J* = 8.2 Hz, 2 H, H-9), 7.30 (d, *J* = 8.2 Hz, 2 H, H-10), 4.56 (s, 2 H, H-12), 4.57–4.49 (m, 1 H, H-5), 3.71 (d, *J* = 5.7 Hz, 1 H, H-1), 2.23 (octet, *J* = 6.7 Hz, 1 H, H-2), 1.47 (d, *J* = 7.1 Hz, 3 H, H-6), 1.09 (d, *J* = 6.9 Hz, 3 H, H-3 or 3'), 1.05 (d, *J* = 6.9 Hz, H-3' or 3)

^{13}C NMR (101 MHz, CD_3OD): δ_C = 172.6 (C-7), 169.3 (C-4), 138.7* (C-8 or 11), 138.7* (C-11 or 8), 128.6 (C-10), 121.1 (C-9), 64.8 (C-12), 59.6 (C-1), 51.2 (C-5), 31.6 (C-2), 18.9 (C-3 or 3'), 18.1 (C-6), 17.8 (C-3' or 3)

*Denoted signals with equal chemical shifts to 1 decimal place appear as two distinguishable signals.

^{19}F NMR (376 MHz, CD_3OD): δ_F = −77.0

IR (ATR): $\tilde{\nu}_{max}$ / cm^{-1} = 3281 (br m, O-H, N-H), 2971 (m, C-H), 1658 (s, C=O), 1606 (m)

HRMS (ESI): *m/z* $[M+H]^+$ calcd for $C_{15}H_{24}N_3O_5$: 294.1812; found: 294.1808 (Δ = −1.4 ppm)

N_3-PEG_4-Val-Ala-PABA (135)

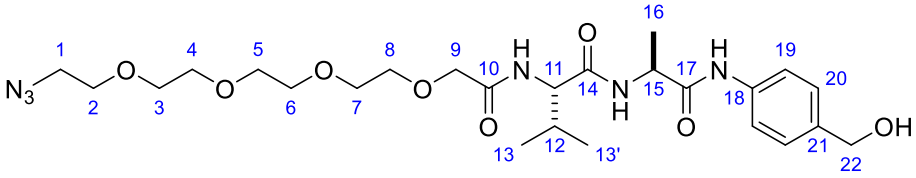

HATU (47.9 mg, 0.126 mmol) was added to a solution of 14-azido-3,6,9,12-tetraoxatetradecanoic acid (0.5 M in TBME, 264 µL, 0.132 mmol) and DIPEA (25.1 µL, 0.144

mmol) in DMF (1 mL) and the mixture was stirred at rt for 1 min. The activated acid solution was then added to the mixture of H-Val-Ala-PABA·TFA **134** (48.9 mg, 0.120 mmol) and DIPEA (41.8 µL, 0.240 mmol) in DMF (1 mL). The reaction mixture was stirred for 16 h, and then EtOAc (40 mL) was added. The mixture was washed successively with saturated aqueous NH_4Cl (2 × 10 mL), saturated aqueous $NaHCO_3$ (2 × 10 mL), and brine (10 mL), then dried over anhydrous Na_2SO_4. The solvent was removed *in vacuo* and the crude product purified using reverse-phase semi-preparative HPLC (10–70%B over 20 min) to give N_3-PEG_4-Val-Ala-PABA **135** as a white solid (50.1 mg, 90.7 µmol, 76%).

t_R / min = 8.17 (5–95%B over 15 min)

^{1}H NMR (400 MHz, CD_3OD): δ_H = 7.54 (d, *J* = 8.6 Hz, 2 H, H-19), 7.30 (d, *J* = 8.7 Hz, 2 H, H-20), 4.56 (s, 2 H, H-22), 4.48 (q, *J* = 7.1 Hz, 1 H, H-15), 4.31 (d, *J* = 6.9 Hz, 1 H, H-11), 4.06 (s, 2 H, H-9), 3.76–3.60 (m, 14 H, H-2 to 8), 3.35 (t, *J* = 4.9 Hz, 2 H, H-1), 2.14 (octet, *J* = 6.8 Hz, 1 H, H-12), 1.44 (d, *J* = 7.1 Hz, 3 H, H-16), 1.00 (d, *J* = 7.1 Hz, 3 H, H-13 or 13'), 0.97 (d, *J* = 6.8 Hz, 3 H, H-13' or 13)

^{13}C NMR (101 MHz, CD_3OD): δ_C = 173.0 (C-14), 172.9 (C-17), 172.7 (C-10), 138.8 (C-18 or 21), 138.6 (C-21 or 18), 128.6 (C-20), 121.1 (C-19), 72.2, 71.6, 71.6, 71.5, 71.4, 71.1 (C-2 to C-9)*, 64.8 (C-22), 59.4 (C-11), 51.8 (C-1), 51.1 (C-15), 32.4 (C-12), 19.8 (C-13 or 13'), 18.7 (C-13' or 13), 18.0 (C-16)

*Signals from 72.2 to 71.1 ppm (inclusive) overlap greatly and only six distinguishable signals for C-2 to C-9 were observed.

IR (ATR): $\tilde{\nu}_{max}$ / cm^{-1} = 3282 (m, N-H, O-H), 2873 (m, C-H), 2098 (m, N=N=N), 1662 (m, C=O), 1630 (m, C=O)

HRMS (ESI): *m/z* $[M+Na]^+$ calcd for $C_{25}H_{40}N_6{}^{23}NaO_8$: 575.2800; found: 575.2809 (Δ = 1.6 ppm)

N_3-PEG_4-Val-Ala-PABC-OPNP (136)

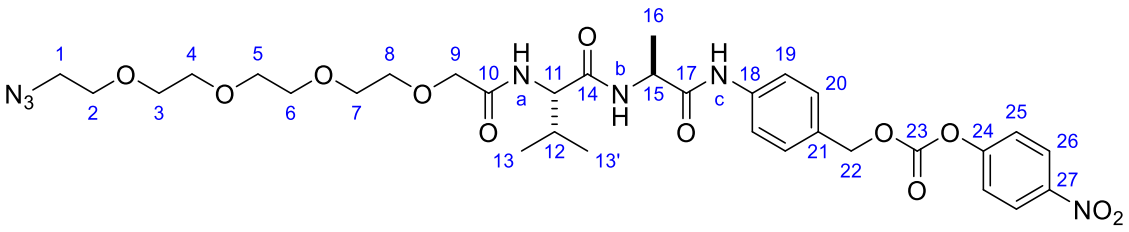

DIPEA (176 µL, 1.01 mmol) was added to a solution of N_3-PEG_4-Val-Ala-PABA **135** (112 mg, 0.202 mmol) and bis(4-nitrophenyl)carbonate (92.2 mg, 0.303 mmol) in DMF (1 mL) and the reaction mixture was stirred at rt for 16 h before EtOAc (50 mL) was added. The mixture was washed with saturated aqueous solution of Na_2CO_3 (6 × 15 mL), dried over anhydrous $MgSO_4$, and the solvent was removed *in vacuo*. The crude product was purified by flash column chromatography (eluting gradient MeOH:CH_2Cl_2 from 0:1 to 1:20) to give N_3-PEG_4-Val-Ala-

PABC-OPNP **136** as a colourless oil which solidified under a stream of N_2 over several days (110 mg, 0.153 mmol, 76%).

$\boldsymbol{R_f}$ = 0.19 (MeOH/CH_2Cl_2 = 1:20)

^{1}H NMR (400 MHz, $CDCl_3$): δ_H = 8.90 (s, 1 H, H-N^c), 8.28–8.23 (m, 2 H, H-26), 7.63–7.58 (m, 2 H, H-19), 7.41–7.34 (m, 5 H, H-20, H-25, H-N^a), 7.19 (br d, J = 7.2 Hz, 1 H, H-N^b), 5.23 (s, 2 H, H-22), 4.64 (qn, J = 7.1 Hz, 1 H, H-15), 4.33 (dd, J = 7.9, 7.0 Hz, 1 H, H-11), 4.11, 4.04 (ABq, J_{AB} = 15.8 Hz, 2 H, H-9), 3.76–3.61 (m, 14 H, H-2 to 8), 3.37 (t, J = 5.0 Hz, 2 H, H-1), 2.21 (octet, J = 6.7 Hz, 1 H, H-12), 1.45 (d, J = 7.1 Hz, 3 H, H-16), 0.99 (d, J = 6.8 Hz, 3 H, H-13 or 13'), 0.98 (d, J = 6.8 Hz, 3 H, H-13' or 13)

^{13}C NMR (101 MHz, $CDCl_3$): δ_C = 171.7 (C-14), 171.1 (C-10), 170.4 (C-17), 155.6 (C-27 or 24), 152.5 (C-23), 145.5 (C-24 or C-27), 138.9 (C-18), 129.9 (C-21), 129.8 (C-20), 125.4 (C-26), 121.9 (C-25), 120.0 (C-19), 71.3, 70.8, 70.8, 70.7, 70.7, 70.7, 70.4, 70.4, 70.1 (C-2 to C-9, and C-22)*, 58.8 (C-11), 50.8 (C-1), 49.9 (C-15), 30.6 (C-12), 19.4 (C-13 or 13'), 18.4 (C-13' or 13), 17.2 (C-16)

*Signals from 71.3 to 70.1 ppm (inclusive) which have the same chemical shifts to 1 decimal place are distinguishable.

IR (ATR): $\tilde{\nu}_{max}$ / cm^{-1} = 3273 (m, N-H), 2871 (m, C-H), 2097 (m, N=N=N), 1759 (m, C=O), 1665 (m, C=O), 1633 (s, C=O)

HRMS (ESI): *m/z* [M+Na]$^+$ calcd for $C_{32}H_{43}N_7{}^{23}NaO_{12}$: 740.2862; found: 740.2871 (Δ = 1.2 ppm)

Hemiasterlin ethyl ester trifluoroacetate salt (137)

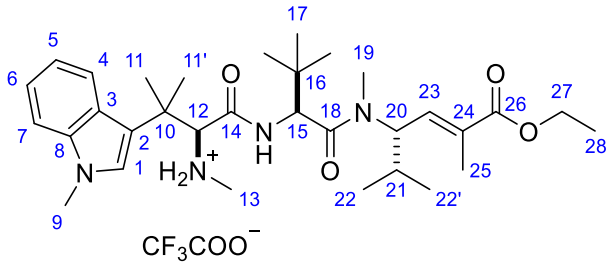

$NaBH_4$ (11.8 mg, 0.310 mmol) was added to a solution of *N*-trifluoroacetyl hemiasterlin ethyl ester **113a** (37.0 mg, 56.9 µmol) in EtOH (5 mL) and the reaction mixture was stirred at rt for 24 h. The reaction was quenched by an addition of H_2O (10 mL) and then extracted with CH_2Cl_2 (4 × 10 mL). The combined organic phases were dried over anhydrous $MgSO_4$, and the solvent was removed *in vacuo*. The crude product was purified by reverse-phase semi-preparative HPLC (5–45%B over 20 min) to give the trifluoroacetate salt of amine **137** as a white powder (22.6 mg, 33.8 µmol, 59%).

$\boldsymbol{t_R}$ / min = 11.51 (5–95%B over 15 min)

$[\alpha]_D^{25}$ = −33.8° (c = 0.346, MeOH)

^{1}H NMR (400 MHz, CD_3OD): δ_H = 8.09 (d, *J* = 8.1 Hz, 1 H, H-4), 7.44 (d, *J* = 8.2 Hz, 1 H, H-7), 7.26 (ddd, *J* = 8.1, 7.1, 0.9 Hz, 1 H, H-6), 7.15 (ddd, *J* = 8.0, 7.0, 0.9 Hz, 1 H, H-5), 7.14 (s, 1 H, H-1), 6.77 (app dd, *J* = 9.7, 1.5 Hz, 1 H, H-23), 5.07 (t, *J* = 10.6 Hz, 1 H, H-20), 4.95 (s, 1 H, H-15), 4.54 (s, 1 H, H-12), 4.21 (q, *J* = 7.1 Hz, 2 H, H-27), 3.81 (s, 3 H, H-9), 3.15 (s, 3 H, H-19), 2.45 (s, 3 H, H-13), 2.12–2.00 (m, 1 H, H-21), 1.93 (d, *J* = 1.4 Hz, 3 H, H-25), 1.58 (s, 3 H, H-11 or 11'), 1.47 (s, 3 H, H-11' or 11), 1.30 (t, *J* = 7.1 Hz, 3 H, H-28), 1.05 (s, 9 H, H-17), 0.91 (d, *J* = 6.7 Hz, 3 H, H-22 or 22'), 0.90 (d, *J* = 6.7 Hz, 3 H, H-22' or 22)

^{13}C NMR (101 MHz, CD_3OD): δ_C = 172.4 (C-18), 169.1 (C-26), 167.1 (C-14), 140.0 (C-8), 139.7 (C-23), 133.5 (C-24), 129.5 (C-1), 126.2 (C-3), 123.1 (C-6), 121.0 (C-4), 120.4 (C-5), 117.5 (C-2), 111.2 (C-7), 69.8 (C-12), 62.1 (C-27), 58.3 (C-20), 57.9 (C-15), 39.4 (C-10), 35.9 (C-16), 34.3 (C-13), 33.0 (C-9), 32.0 (C-19), 30.8 (C-21), 27.4 (C-11' or 11), 26.9 (C-17), 23.2 (C-11 or 11'), 19.8* (C-22 or 22'), 19.8* (C-22' or 22), 14.5 (C-28), 14.2 (C-25)

*Denoted signals with equal chemical shifts to 1 decimal place appear as two distinguishable signals.

^{19}F NMR (376 MHz, CD_3OD): δ_F = −77.1

IR (ATR): $\tilde{\nu}_{max}$ / cm^{-1} = 2966 (m, C-H), 1670 (s, C=O)

HRMS (ESI): *m/z* $[M+H]^+$ calcd for $C_{32}H_{51}N_4O_4$: 555.3905; found: 555.3907 (Δ = 0.4 ppm)

N_3-PEG_4-Val-Ala-PABC-hemiasterlin-OEt (139)

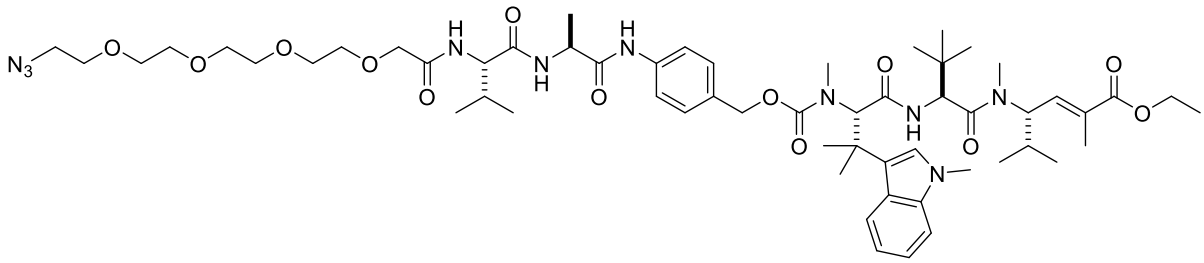

To a solution of hemiasterlin ethyl ester trifluoroacetate salt **137** (18.9 mg, 28.3 µmol), N_3-PEG_4-Val-Ala-PABC-OPNP **136** (43.1 mg, 60.0 µmol), and HOAt (4.08 mg, 30.0 µmol) in DMF (540 µL) was added pyridine (90 µL, 1.1 mmol) and DIPEA (20.9 µL, 120 µmol). The reaction was stirred at rt for 7 days before the volatiles were removed under a stream of N_2. The crude mixture was purified by reverse-phase semi-preparative HPLC (20–95%B over 20 min) to give carbamate **139** as a white solid (6.1 mg, 5.4 µmol, 19%, 46%brsm) and the starting material hemiasterlin ethyl ester trifluoroacetate salt was recovered (11.1 mg, 16.6 µmol, 59%).

t_R / min = 14.68 (5–95%B over 15 min)

^{1}H NMR (400 MHz, $CDCl_3$): Unassigned due to complex rotameric mixture.

HRMS (ESI): *m/z* $[M+H]^+$ calcd for $C_{58}H_{89}N_{10}O_{13}$: 1133.6611; found: 1133.6606 (Δ = −0.4 ppm)

Taltobulin ethyl ester trifluoroacetate salt (138)

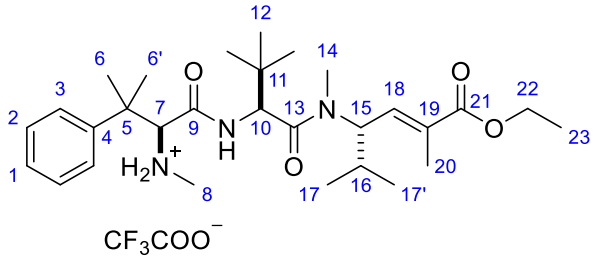

$NaBH_4$ (25.5 mg, 0.670 mmol) was added to a solution of *N*-trifluoroacetyl taltobulin ethyl ester **121a** (3.35:1 *dr*, 80.3 mg, 0.134 mmol) in EtOH (10 mL) and the reaction mixture was stirred at rt for 24 h. The reaction was quenched by an addition of H_2O (15 mL) and then extracted with CH_2Cl_2 (4 × 15 mL). The combined organic phases were dried over anhydrous $MgSO_4$, and the solvent was removed *in vacuo*. The crude product was purified by reverse-phase semi-preparative HPLC (5–45%B over 75 min) to give amine **138** as a white powder (62.8 mg, 0.102 mmol, 99% w.r.t. the desired isomer).

t_R / min = 10.87 (5–95%B over 15 min)

$[\alpha]_D^{25}$ = −43.5° (c = 0.524, MeOH)

^{1}H NMR (400 MHz, CD_3OD): δ_H = 7.54 (d, *J* = 8.0 Hz, 2 H, H-3), 7.45 (t, *J* = 7.6 Hz, 2 H, H-2), 7.35 (t, *J* = 7.2 Hz, 1 H, H-1), 6.76 (d, *J* = 9.7 Hz, 1 H, H-18), 5.05 (t, *J* = 10.1 Hz, 1 H, H-15), 4.91 (s, 1 H, H-10), 4.36 (s, 1 H, H-7), 4.21 (q, *J* = 7.2 Hz, 2 H, H-22), 3.14 (s, 3 H, H-14), 2.50 (s, 3 H, H-8), 2.11–1.99 (m, 1 H, H-16), 1.93 (s, 3 H, H-20), 1.47 (s, 3 H, H-6 or 6'), 1.38 (s, 3 H, H-6' or 6), 1.30 (t, *J* = 7.1 Hz, 3 H, H-23), 1.06 (s, 9 H, H-12), 0.90 (d, *J* = 6.5 Hz, 6 H, H-17 and 17')

^{13}C NMR (101 MHz, CD_3OD): δ_C = 172.3 (C-13), 169.1 (C-21), 167.0 (C-9), 145.0 (C-4), 139.7 (C-18), 133.5 (C-19), 130.4 (C-2), 128.9 (C-1), 127.4 (C-3), 71.2 (C-7), 62.1 (C-22), 58.3 (C-15), 57.8 (C-10), 42.1 (C-5), 35.9 (C-11), 34.2 (C-8), 31.9 (C-14), 30.8 (C-16), 29.8 (C-6' or C-6), 26.9 (C-12), 21.5 (C-6 or 6'), 19.8* (C-17 or 17'), 19.8* (C-17' or 17), 14.5 (C-23), 14.2 (C-20)

*Denoted signals with equal chemical shifts to 1 decimal place appear as two distinguishable signals.

^{19}F NMR (376 MHz, CD_3OD): δ_F = −77.2

IR (ATR): $\tilde{\nu}_{max}$ / cm^{-1} = 2970 (m, C-H), 1713 (m, C=O), 1669 (s, C=O), 1627 (s, C=O)

HRMS (ESI): *m/z* $[M+H]^+$ calcd for $C_{29}H_{48}N_3O_4$: 502.3639; found: 502.3648 (Δ = 1.8 ppm)

Spectroscopic data are in accordance with the literature.[359]

N_3-PEG_4-Val-Ala-PABC-taltobulin-OEt (140)

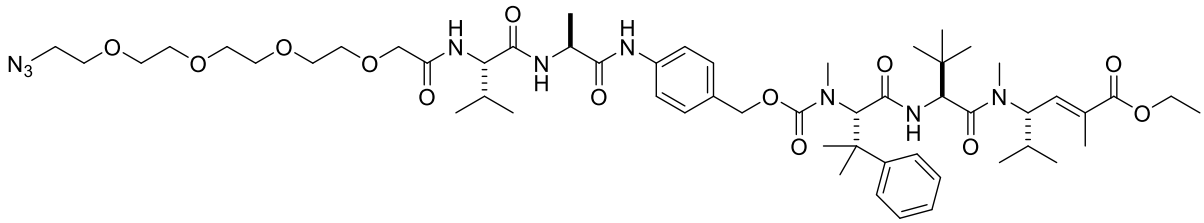

To a solution of taltobulin ethyl ester trifluoroacetate salt **138** (24.6 mg, 40.0 µmol), N_3-PEG_4-Val-Ala-PABC-OPNP **136** (57.4 mg, 60.0 µmol), and HOAt (5.44 mg, 40.0 µmol) in DMF (720 µL) was added pyridine (120 µL, 1.48 mmol) and DIPEA (27.9 µL, 160 µmol). The reaction was stirred at rt for 7 days before the volatiles were removed under a stream of N_2. The crude mixture was purified by reverse-phase semi-preparative HPLC (20–95%B over 20 min) to give carbamate **140** as a yellow solid (10.1 mg, 9.35 µmol, 23%, 54%brsm) and the starting material taltobulin ethyl ester trifluoroacetate salt **138** was recovered (14.0 mg, 22.7 µmol, 57%).

t_R / min = 14.70 (5–95%B over 15 min)

^{1}H NMR (600 MHz, $CDCl_3$): Unassigned due to complex rotameric mixture.

HRMS (ESI): *m/z* $[M+Na]^+$ calcd for $C_{55}H_{85}N_9{}^{23}NaO_{13}$: 1102.6159; found: 1102.6146 (Δ = −1.2 ppm)

H-PEG_2-Glu_3-PEG_2-propargylGly-NH_2·TFA (141)

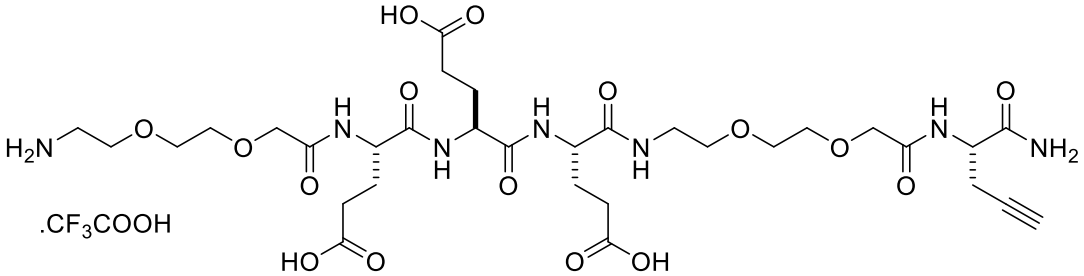

The peptide was synthesised by standard manual Fmoc solid-phase peptide synthesis (Fmoc-SPPS) on LL Rink Amide resin (0.51 mmol/g, 1.00 g). Fmoc-deprotection was performed using 20% piperidine solution in DMF (1 × 1 min, 2 × 5 min).

The coupling was performed by the following: Fmoc-protected amino acids (4 equiv.) were activated with HATU (4 equiv.) and DIPEA (8 equiv.) in DMF (0.4 M of amino acid) for 10 s. The mixture was then added to the resin and agitated by a stream of N_2 for 5 min. The *t*Bu protecting group was used for the side chain of Glu.

Completion of peptide couplings was monitored using chloranil test. To a small amount of resin swelled in CH_2Cl_2 was added acetaldehyde (200 µL) then followed by saturated chloranil solution in toluene (50 µL). The mixture was shaken for 5 min at rt. Resin beads remaining

colourless indicated a complete coupling whereas green colouration indicated an incomplete coupling. Any incomplete couplings were subjected to a second round of coupling.

Peptide cleavage and global deprotection of all amino acid side chains were achieved by the treatment of the dried resin with TFA/CH_2Cl_2/H_2O/TIPS (92.5:2.5:2.5:2.5, 20 mL) at 42 °C for 40 min. The mixture was then filtered through cotton wool, and volatiles were removed under a stream of nitrogen. The crude peptides were triturated with Et_2O and then washed with Et_2O (3 × 15 mL) before purification by reverse-phase semi-preparative HPLC (5–25%B over 9 min) to give the peptide **141** as a hygroscopic white powder (285 mg, 0.315 mmol, 62% yield).

t_R / min = 5.06 (5–95%B over 15 min)

HRMS (ESI): *m/z* $[M-H]^-$ calcd for $C_{32}H_{50}N_7O_{16}$: 788.3314; found: 788.3320 (Δ = −0.8 ppm)

DVP-PEG$_2$-Glu$_3$-PEG$_2$-propargylGly-NH$_2$ (143)

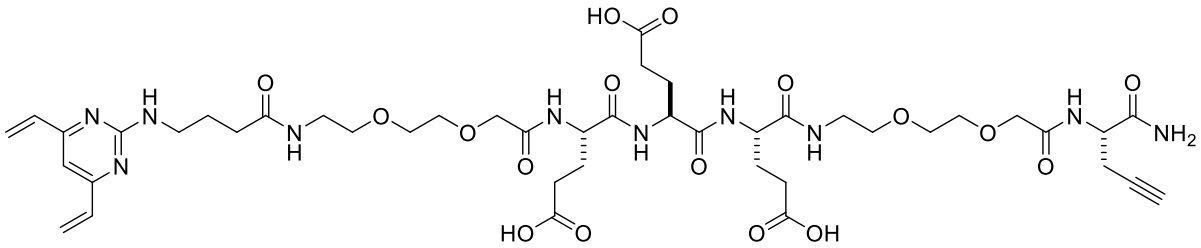

4-((4,6-divinylpyrimidin-2-yl)amino)butanoic acid[285] **142** was synthesised by Hikaru Seki from the Spring Group, Department of Chemistry, University of Cambridge.

DIPEA (11.0 µL, 63.0 µmol) was added to a solution of 4-((4,6-divinylpyrimidin-2-yl)amino)butanoic acid **142** (12.3 mg, 52.5 µmol) and HATU (19.0 mg, 50.0 µmol) in DMF (0.5 mL) and the solution was stirred at rt for 5 min. The activated acid solution was then added to a solution of peptide **141** (43.2 mg, 47.8 µmol) and DIPEA (69.7 µL, 400 µmol) in DMF (0.5 mL) and the reaction mixture was stirred at rt for 1 h before purification by automatic reverse-phase flash column chromatography to give alkynyl DVP **143** as a hygroscopic white powder (13.4 mg, 13.3 µmol, 28%).

t_R / min = 6.68 (5–95%B over 15 min)

HRMS (ESI): *m/z* $[M]^+$ calcd for $C_{44}H_{64}N_{10}O_{17}$: 1004.4409; found: 1004.4404 (Δ = 0.5 ppm)

DVP-PEG$_2$-Glu$_3$-PEG$_2$-triazole-PEG$_4$-Val-Ala-PABC-hemiasterlin ammonium salt (144)

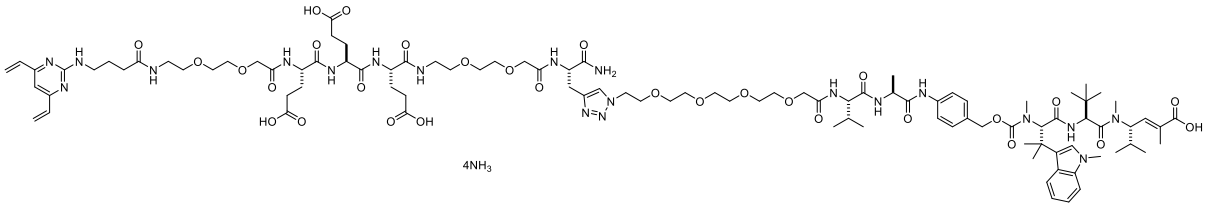

$CuSO_4 \cdot 5H_2O$ (0.29 mg, 1.2 µmol) and THPTA (0.84 mg, 1.9 µmol) were dissolved in a degassed mixture of H_2O/*t*BuOH (1:1, 0.5 mL) and stirred at rt for 1 min before Na-L-ascorbate (0.96 mg, 4.9 µmol) was added. The colourless copper solution was then added to a degassed solution of azide **139** (1.10 mg, 0.971 µmol) and alkyne **143** (1.95 mg, 1.94 µmol) in H_2O/*t*BuOH (0.5 mL). The reaction mixture was stirred at rt for 3 h before the solvent was removed by lyophilisation. The resulting crude triazole ester was re-dissolved in H_2O/MeOH (1:1, 1 mL). Aqueous $LiOH \cdot H_2O$ solution (0.357 M, 13.6 µL, 4.86 µmol) was added to the solution, and the reaction was stirred at rt for 6 days, during which extra $LiOH \cdot H_2O$ was added until the reaction went to completion. The volatiles were then removed *in vacuo*, and the resulting crude product was purified by automatic reverse-phase flash column chromatography to give linker–drug **144** as a white powder (0.49 mg, 0.22 µmol, 23% over two steps).

t_R / min = 10.66 (5–95%B over 15 min)

HRMS (ESI): *m/z* $[M+2H]^{2+}$ calcd for $C_{100}H_{150}N_{20}O_{30}$: 1055.5408; found: 1055.5422 (Δ = 1.3 ppm)

DVP-PEG$_2$-Glu$_3$-PEG$_2$-triazole-PEG$_4$-Val-Ala-PABC-taltobulin ammonium salt (145)

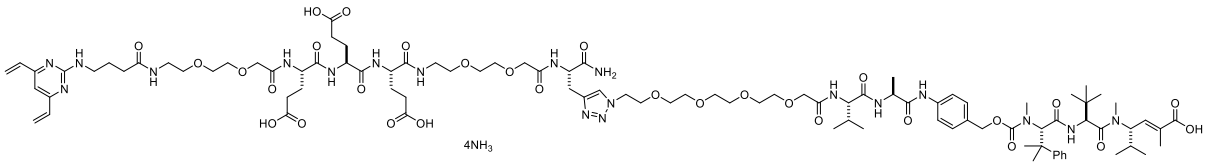

$CuSO_4 \cdot 5H_2O$ (0.53 mg, 2.1 µmol) and THPTA (1.53 mg, 3.52 µmol) were dissolved in a degassed mixture of H_2O/*t*BuOH (1:1, 0.9 mL) and stirred at rt for 1 min before Na-L-ascorbate (1.74 mg, 8.78 µmol) was added. The colourless copper solution was then added to a degassed solution of azide **140** (1.90 mg, 1.76 µmol) and alkyne **143** (3.54 mg, 3.52 µmol) in H_2O/*t*BuOH (0.9 mL). The reaction mixture was stirred at rt for 3 h before the solvent was removed by lyophilisation. The resulting crude triazole ester was re-dissolved in H_2O/MeOH (1:1, 2 mL). Aqueous $LiOH \cdot H_2O$ solution (0.357 M, 24.6 µL, 8.78 µmol) was added to the solution, and the reaction was stirred at rt for 5 days, during which extra $LiOH \cdot H_2O$ was added until the reaction went to completion. The volatiles were then removed *in vacuo*, and the resulting crude product was purified by automatic reverse-phase flash column chromatography to give linker–drug **145** as a white powder (1.70 mg, 0.800 µmol, 45% over two steps).

t_R / min = 10.63 (5–95%B over 15 min)

HRMS (ESI): *m/z* $[M+2H]^{2+}$ calcd for $C_{97}H_{147}N_{19}O_{30}$: 1029.0275; found: 1029.0275 (Δ = 0.0 ppm)

6.3.3. Reaction condition screening

6.3.3.1. Fragment amide coupling

(*S*)-3,3-Dimethyl-2-((*S*)-3-methyl-3-(1-methyl-1*H*-indol-3-yl)-2-(2,2,2-trifluoro-*N*-methylacetamido)butanamido)butanoic acid (109a)

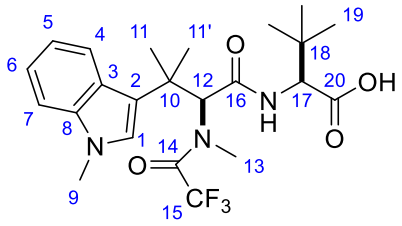

To a solution of ester **99a** (96.7 mg, 0.200 mmol) in MeOH/THF (1:1, 8 mL) was added an aqueous solution of LiOH (0.25 M, 4.00 mL, 1.00 mmol) which resulted in a cloudy reaction mixture. The reaction mixture was stirred at rt for 4 days before H_2O (12 mL) was added and then washed with Et_2O (2 × 10 mL). The aqueous phase was then acidified with 5% aqueous H_3PO_4 to pH 2-3 and was then extracted with EtOAc (3 × 10 mL). The combined organic phases were dried over anhydrous Na_2SO_4, and the solvent was removed *in vacuo* to give the crude acid **109a** as a white solid (84.4 mg, 0.180 mmol, 90%), which was used in the next step without further purification.

mp = 200 °C (dec)

$[\alpha]_D^{25}$ = −15.6° (c = 0.343, $CHCl_3$)

^{1}H NMR (400 MHz, $CDCl_3$): δ_H = 8.26 (d, *J* = 8.0 Hz, 1 H, H-4), 7.35–7.20 (m, 3 H, H-5 to H-7), 7.03 (s, 1 H, H-1), 6.35 (s, 1 H, H-12), 5.89 (d, *J* = 8.1 Hz, 1 H, N-H), 4.02 (d, *J* = 8.6 Hz, 1 H, H-17), 3.74 (s, 3 H, H-9), 3.49 (s, 3 H, H-13), 1.71 (s, 3 H, H-11 or 11'), 1.51 (s, 3 H, H-11' or 11), 0.50 (s, 9 H, H-19)

^{13}C NMR (101 MHz, $CDCl_3$): δ_C = 175.5 (C-20), 168.9 (C-16), 159.5 (app d, $^2J_{C\text{-}F}$ = 35.5 Hz, C-14), 138.2 (C-8), 127.0 (C-1), 124.7 (C-3), 122.7 (C-6), 121.0 (C-4), 120.6 (C-2), 120.3 (C-5), 117.0 (app d, $^1J_{C\text{-}F}$ = 287.5 Hz, C-15), 109.9 (C-7), 63.0 (C-12), 60.6 (C-17), 39.5 (C-10), 35.0 (q, $^4J_{C\text{-}F}$ = 3.8 Hz, C-13), 33.3 (C-18), 32.8 (C-9), 27.5 (C-11' or 11), 26.0 (C-19), 24.5 (C-11 or 11')

^{19}F NMR (376 MHz, $CDCl_3$): δ_F = −69.5

IR (ATR): $\tilde{\nu}_{max}$ / cm^{-1} = 2965 (m, C-H), 1663 (s, C=O)

HRMS (ESI): *m/z* $[M-H]^-$ calcd for $C_{23}H_{29}F_3N_3O_4$: 468.2116; found: 468.2106 (Δ = −2.1 ppm)

(*S*)-3,3-Dimethyl-2-((*R*)-3-methyl-3-(1-methyl-1*H*-indol-3-yl)-2-(2,2,2-trifluoro-*N*-methylacetamido)butanamido)butanoic acid (109b)

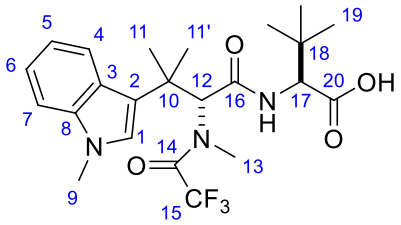

To a solution of ester **99b** (96.7 mg, 0.200 mmol) in MeOH/THF (1:1, 8 mL) was added an aqueous solution of LiOH (0.25 M, 4.00 mL, 1.00 mmol) which resulted in a cloudy reaction mixture. The reaction mixture was stirred at rt for 4 days before H_2O (12 mL) was added and then washed with Et_2O (2 × 10 mL). The aqueous phase was then acidified with 5% aqueous H_3PO_4 to pH 2-3 and was then extracted with EtOAc (3 × 10 mL). The combined organic phases were dried over anhydrous Na_2SO_4 and the solvent was removed *in vacuo* to give the crude acid **109b** as a white solid (78.4 mg, 0.167 mmol, 83%), which was used in the next step without further purification.

mp = 104–108 °C

$[\alpha]_D^{25}$ = +55.0° (c = 0.420, $CHCl_3$)

^{1}H NMR (400 MHz, $CDCl_3$): δ_H = 8.13 (d, *J* = 7.5 Hz, 1 H, H-4), 7.29–7.12 (m, 3 H, H-5 to H-7), 6.92 (s, 1 H, H-1), 6.15 (s, 1 H, H-12), 5.94 (d, *J* = 8.7 Hz, 1 H, N-H), 4.06 (d, *J* = 8.7 Hz, 1 H, H-17), 3.71 (s, 3 H, H-9), 3.45 (s, 3 H, H-13), 1.74 (s, 3 H, H-11 or 11'), 1.50 (s, 3 H, H-11' or 11), 0.50 (s, 9 H, H-19)

^{13}C NMR (101 MHz, $CDCl_3$): δ_C = 174.8 (C-20), 167.8 (C-16), 159.4 (app d, $^2J_{C\text{-}F}$ = 35.8 Hz, C-14), 138.2 (C-8), 126.5 (C-1), 125.2 (C-3), 122.3 (C-6), 120.7 (C-4), 120.2 (C-2), 120.0 (C-5), 116.9 (app d, $^1J_{C\text{-}F}$ = 288.2 Hz, C-15), 110.0 (C-7), 63.1 (C-12), 60.1 (C-17), 39.8 (C-10), 34.2 (q, $^4J_{C\text{-}F}$ = 4.3 Hz, C-13), 34.1 (C-18), 32.8 (C-9), 27.4 (C-11' or 11), 26.0 (C-19), 24.6 (C-11 or 11')

^{19}F NMR (376 MHz, $CDCl_3$): δ_F = −69.6

IR (ATR): $\tilde{\nu}_{max}$ / cm^{-1} = 2968 (m, C-H), 1738 (m, C=O), 1665 (s, C=O)

HRMS (ESI): *m/z* $[M-H]^-$ calcd for $C_{23}H_{29}F_3N_3O_4$: 468.2116; found: 468.2107 (Δ = −1.9 ppm)

***N*-((1*S*)-1-(4-(*tert*-Butyl)-5-oxo-4,5-dihydrooxazol-2-yl)-2-methyl-2-(1-methyl-1*H*-indol-3-yl)propyl)-2,2,2-trifluoro-1*N*-methylacetamide (114, as an inseparable diastereomeric mixture of 1.7:1 *dr*)**

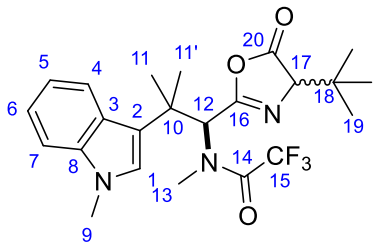

A white solid.

R$_f$ = 0.28 (EtOAc:40–60 petroleum ether = 1:5)

^{1}H NMR (400 MHz, $CDCl_3$): Major diastereomer δ_H = 7.97 (d, *J* = 8.0 Hz, 1 H, H-4), 6.29 (d, *J* = 1.1 Hz, 1 H, H-12), 3.80 (d, *J* = 1.4 Hz, 1 H, H-17), 1.83 (s, 3 H, H-11 or 11'), 1.60 (s, 3 H, H-11' or 11), 0.78 (s, 9 H, H-19); Minor diastereomer δ_H = 7.93 (d, *J* = 8.1 Hz, 1 H, H-4), 6.22 (d, *J* = 1.4 Hz, 1 H, H-12), 1.80 (s, 3 H, H-11 or 11'), 1.62 (s, 3 H, H-11' or 11), 0.87 (s, 9 H, H-19); Overlapping / indistinguishable signals* δ_H = 7.30–7.26 (m, 1 H, H-7), 7.25–7.18 (m, 1 H, H-6), 7.17–7.11 (m, 1 H, H-5), 6.93–6.90 (m, 1 H, H-1), 3.75–3.72 (m, 3.4 H, H-9 and H-17 of minor diastereomer), 3.21–3.17 (m, 3 H, H-13)

*The numbers of proton nuclei quoted are with respect to the sum of both diastereomers.

^{13}C NMR (101 MHz, $CDCl_3$): Major diastereomer δ_C = 175.9 (C-20), 160.6 (C-16), 158.7 (app d, $^2J_{C\text{-}F}$ = 36.1 Hz, C-14), 137.6 (C-8), 127.1 (C-1), 125.6 (C-3), 121.7‡ (C-6), 120.9 (C-4), 119.5 (C-5), 119.4‡ (C-2), 116.6† (app d, $^1J_{C\text{-}F}$ = 287.6 Hz, C-15), 109.6‡ (C-7), 73.4 (C-17), 59.6 (C-17), 39.7 (C-10), 35.5 (C-18), 33.8 (q, $^4J_{C\text{-}F}$ = 4.4 Hz, C-13), 32.8 (C-9), 27.4 (C-11' or 11), 25.8 (C-19), 25.4 (C-11 or 11'); Minor diastereomer δ_C = 176.1 (C-20), 161.2 (C-16), 158.5 (app d, $^2J_{C\text{-}F}$ = 36.1 Hz, C-14), 137.7 (C-8), 127.0 (C-1), 125.9 (C-3), 121.7‡ (C-6), 121.0 (C-4), 119.4‡ (C-5), 119.0‡ (C-2), 116.6† (app d, $^1J_{C\text{-}F}$ = 287.6 Hz, C-15), 109.6‡ (C-7), 73.1 (C-17), 60.4 (C-17), 39.8 (C-10), 35.4 (C-18), 33.9 (q, $^4J_{C\text{-}F}$ = 3.9 Hz, C-13), 32.7 (C-9), 27.4‡ (C-11' or 11), 26.2 (C-11 or 11'), 26.1 (C-19)

‡Denoted signals with equal chemical shifts to 1 decimal place appear as two distinguishable signals.

†Appear as a single signal.

^{19}F NMR (376 MHz, $CDCl_3$): Major diastereomer δ_F = −70.8; Minor diastereomer δ_F = −70.7

IR (ATR): $\tilde{\nu}_{max}$ / cm^{-1} = 2977 (m, C-H), 1822 (s, C=O), 1676 (s, C=N)

HRMS (ESI): *m/z* $[M+H]^+$ calcd for $C_{23}H_{29}F_3N_3O_3$: 452.2161 ; found: 452.2158 (Δ = −0.7 ppm)

6.3.3.2. Attempts at improving diastereoselectivity of the Ugi reaction

Methylamine solution in MeOH or THF (2 M, 27.5 µL, 0.0550 mmol) was added to a mixture of 2-methyl-2-(1-methyl-1*H*-indol-3-yl)propanal **69** (10.1 mg, 0.0500 mmol) and 3 Å molecular sieves (200 mg) in dry solvent (1 mL). The reaction was stirred at rt for 2 h before TFA (4.59 µL, 0.0600 mmol), additives, and a chiral phosphoric acid (2.5 µmol) were added. The reaction mixture was stirred for a further 30 min before isocyanide **17** (17.7 mg, 0.0550 mmol) was added. The reaction was stirred at rt for a further 19 h, filtered through Celite®, eluted with a copious amount of MeOH, and the solvent removed *in vacuo*. The crude product was analysed by ^{19}F-NMR using 4,4'-difluorobenzophenone as an internal standard.

6.3.3.3. Carbamate formation screening

(*S*)-3,3-Dimethyl-2-((*S*)-3-methyl-3-(1-methyl-1*H*-indol-3-yl)-2-(methylamino)butanamido)butanoic acid trifluoroacetate salt (127a)

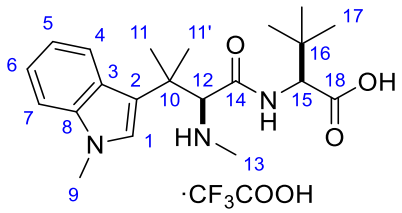

To a solution of trifluoroacetamide **109a** (70.4 mg, 0.150 mmol) in H_2O/MeOH (1:1, 10 mL) was LiOH·H_2O (101 mg, 2.40 mmol). The reaction mixture was stirred at 60 °C for 10 days before MeOH was removed *in vacuo*. The remaining aqueous solution was acidified to pH 3 with TFA and then extracted with EtOAc (4 × 5 mL). The combined organic phases were dried over anhydrous Na_2SO_4 and the solvent was removed *in vacuo* to give the crude product which was purified by reverse-phase semi-preparative HPLC (10–50%B over 16 min) to give amine **127a** as a white powder (60.3 mg, 0.124 mmol, 82%).

t_R / min = 8.45 (5–95%B over 15 min)

$[\alpha]_D^{25}$ = 38.6° (c = 0.220, MeOH)

^{1}H NMR (400 MHz, CD_3OD): δ_H = 8.06 (d, *J* = 8.1 Hz, 1 H, H-4), 7.43 (d, *J* = 8.2 Hz, 1 H, H-7), 7.25 (t, *J* = 7.6 Hz, 1 H, H-6), 7.18–7.11 (m, 2 H, H-1 and H-5), 4.50 (s, 1 H, H-12), 4.41 (s, 1 H, H-15), 3.81 (s, 3 H, H-9), 2.46 (s, 3 H, H-13), 1.65 (s, 3 H, H-11 or 11'), 1.52 (s, 3 H, H-11' or 11), 1.08 (s, 9 H, H-17)

^{13}C NMR (101 MHz, CD_3OD): δ_C = 173.2 (C-18), 167.2 (C-14), 139.9 (C-8), 129.4 (C-1), 126.3 (C-3), 123.1 (C-6), 121.0 (C-4), 120.4 (C-5), 117.6 (C-2), 111.2 (C-7), 70.2 (C-12), 62.8 (C-15), 39.4 (C-10), 34.7 (C-16), 34.3 (C-13), 33.0 (C-9), 27.2 (C-17), 27.1 (C-11' or 11), 23.5 (C-11 or 11')

^{19}F NMR (376 MHz, CD_3OD): δ_F = −77.0

IR (ATR): $\tilde{\nu}_{max}$ / cm^{-1} = 2965 (m, C-H), 1663 (s, C=O)

HRMS (ESI): *m/z* $[M+H]^+$ calcd for $C_{21}H_{32}N_3O_3$: 374.2438; found: 374.2439 (Δ = 0.3 ppm)

Methyl (*S*)-3,3-dimethyl-2-((*S*)-3-methyl-3-(1-methyl-1*H*-indol-3-yl)-2-(methylamino)butanamido)butanoate trifluoroacetate salt (129a)

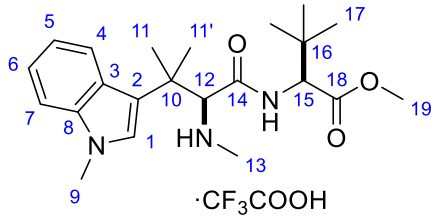

To a solution of acid **127a** (37.0 mg, 0.0759 mmol) in dry MeOH (1 mL) was added thionyl chloride (16.5 µL, 0.228 mmol) at 0 °C. The reaction mixture was then allowed to warm to rt and stirred for 19 h before extra thionyl chloride (16.5 µL, 0.228 mmol) was added. The reaction mixture was stirred for a further 5 days before the volatiles were removed *in vacuo*. The crude product was purified by reverse-phase semi-preparative HPLC (5–95%B over 20 min) to give amine **129a** as a white powder (21.0 mg, 0.0418 mmol, 55%, 64% brsm) and the starting material (5.20 mg, 0.0107 mmol, 14%) was recovered.

t_R / min = 9.52 (5–95%B over 15 min)

$[\alpha]_D^{25}$ = +28.0° (c = 0.236, MeOH)

^{1}H NMR (400 MHz, CD_3OD): δ_H = 8.04 (d, *J* = 8.1 Hz, 1 H, H-4), 7.43 (d, *J* = 8.3 Hz, 1 H, H-7), 7.25 (ddd, *J* = 8.2, 7.2, 1.0 Hz, 1 H, H-6), 7.15 (s, 1 H, H-1), 7.14 (ddd, *J* = 8.1, 7.1, 1.0 Hz, 1 H, H-5), 4.49 (s, 1 H, H-12), 4.41 (s, 1 H, H-15), 3.81 (s, 3 H, H-9), 3.73 (s, 3 H, H-19), 2.47 (s, 3 H, H-13), 1.65 (s, 3 H, H-11 or 11'), 1.52 (s, 3 H, H-11' or 11), 1.04 (s, 9 H, H-17)

^{13}C NMR (101 MHz, CD_3OD): δ_C = 172.2 (C-18), 167.4 (C-14), 139.9 (C-8), 129.5 (C-1), 126.3 (C-3), 123.1 (C-6), 121.0 (C-4), 120.4 (C-5), 117.6 (C-2), 111.2 (C-7), 70.2 (C-12), 63.0 (C-15), 52.3 (C-19), 39.4 (C-10), 35.0 (C-16), 34.3 (C-13), 33.0 (C-9), 27.1 (C-17), 26.8 (C-11' or 11), 23.7 (C-11 or 11')

HRMS (ESI): *m/z* $[M+H]^+$ calcd for $C_{22}H_{34}N_3O_3$: 388.2595; found: 388.2601 (Δ = 1.5 ppm)

Methyl (*S*)-3,3-dimethyl-2-((*R*)-3-methyl-3-(1-methyl-1*H*-indol-3-yl)-2-(methylamino)butanamido)butanoate trifluoroacetate salt (129b)

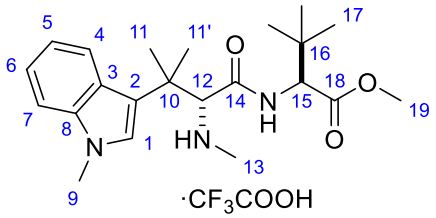

$NaBH_4$ (47.5 mg, 1.25 mmol) was added to a solution of trifluoroacetamide **99b** (121 mg, 0.250 mmol) in MeOH (20 mL) at 0 °C. The reaction mixture was allowed to warm to rt and stirred for 18 h. The reaction was quenched by an addition of H_2O (20 mL) and then extracted with CH_2Cl_2 (3 × 30 mL). The combined organic phases were dried over anhydrous $MgSO_4$, and the solvent was removed *in vacuo*. The crude product was re-dissolved in MeCN/H_2O and acidified by TFA and then lyophilised to give amine **129b** as a white powder (125 mg, 0.250 mmol, quant.).

t_R / min = 9.91 (5–95%B over 15 min)

$[\alpha]_D^{25}$ = −50.8° (c = 0.500, MeOH)

^{1}H NMR (400 MHz, CD_3OD): δ_H = 7.99 (d, *J* = 8.1 Hz, 1 H, H-4), 7.42 (d, *J* = 8.2 Hz, 1 H, H-7), 7.25 (ddd, *J* = 8.2, 7.1, 1.0 Hz, 1 H, H-6), 7.16 (ddd, *J* = 8.1, 7.0, 1.1 Hz, 1 H, H-5), 7.15 (s, 1 H, H-1), 4.52 (s, 1 H, H-12), 4.16 (s, 1 H, H-15), 3.79 (s, 3 H, H-9), 3.71 (s, 3 H, H-19), 2.49 (s, 3 H, H-13), 1.64 (s, 3 H, H-11 or 11'), 1.57 (s, 3 H, H-11' or 11), 0.91 (s, 9 H, H-17)

^{13}C NMR (101 MHz, CD_3OD): δ_C = 172.8 (C-18), 168.2 (C-14), 139.9 (C-8), 129.2 (C-1), 126.4 (C-3), 123.1 (C-6), 121.1 (C-4), 120.5 (C-5), 117.7 (C-2), 111.2 (C-7), 70.2 (C-12), 63.7 (C-15), 52.3 (C-19), 39.0 (C-10), 34.14 (C-13), 34.06 (C-16), 32.9 (C-9), 27.1 (C-17), 26.5 (C-11' or 11), 24.3 (C-11 or 11')

^{19}F NMR (376 MHz, CD_3OD): δ_F = −77.0

IR (ATR): $\tilde{\nu}_{max}$ / cm^{-1} = 2968 (m, C-H), 1738 (m, C=O), 1665 (s, C=O)

HRMS (ESI): *m/z* $[M+H]^+$ calcd for $C_{22}H_{34}N_3O_3$: 388.2595; found: 388.2599 (Δ = 1.0 ppm)

Alloc-Val-Ala-PABC-OPNP (123)

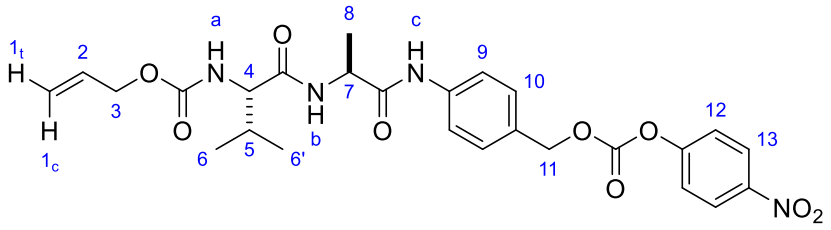

DIPEA (122 µL, 0.700 mmol) was added to the solution of Alloc-Val-Ala-PABA **122** (52.8 mg, 0.140 mmol) and bis(4-nitrophenyl)carbonate (63.9 mg, 0.210 mmol) in DMF (0.5 mL) and the reaction mixture was stirred at rt for 18 h. The volatiles were then removed under a stream of N_2, and the residue was re-partitioned in CH_2Cl_2 (10 mL) and saturated aqueous $NaHCO_3$ (10 mL). The phases were separated, and the aqueous layer was extracted with CH_2Cl_2 (3 × 15 mL). The combined organic phases were washed with saturated aqueous $NaHCO_3$ (3 × 15 mL) and saturated aqueous K_2CO_3 (3 × 15 mL), dried over anhydrous $MgSO_4$, and the solvent was removed *in vacuo* to give Alloc-Val-Ala-PABC-OPNP **123** as a pale yellow solid (75.5 mg, 0.139 mmol, 99%), which was used in the next step without further purification.

R_f = 0.08 (MeOH:CH_2Cl_2 = 1:20)

^{1}H NMR (600 MHz, $CDCl_3$): δ_H = 8.68 (br s, 1 H, H-N^c), 8.29-8.25 (m, 2 H, H-13), 7.61 (br d, *J* = 8.3 Hz , 2 H, H-9, H-10, or H-12), 7.41–7.35 (m, 4 H, H-9, H-10, or H-12), 6.71 (br d, *J* = 8.3 Hz, 1 H, H-N^a or H-N^b), 5.96–5.87 (m, 1 H, H-1$_t$, 1$_c$ or 2), 5.35–5.29 (m, 2 H), 5.27–5.21 (m, 3 H), 4.67 (qn, *J* = 7.2 Hz, 1 H, H-7), 4.64–4.56 (m, 2 H, H-3), 4.05 (t, *J* = 6.5 Hz, 1 H, H-4), 2.19 (octet, *J* = 6.8 Hz, 1 H, H-5), 1.48 (d, *J* = 7.0 Hz, 3 H, H-8), 0.99 (d, *J* = 6.8 Hz, 3 H, H-6 or 6'), 0.95 (d, *J* = 6.8 Hz, 3 H, H-6' or 6)

LCMS (ESI): *m/z* $[M+H]^+$ calcd for $C_{26}H_{31}N_4O_9$: 543.2; found: 543.4

Prepared according to Walsh.[482] Spectroscopic data are in accordance with the literature.[482]

Carbamate 128b

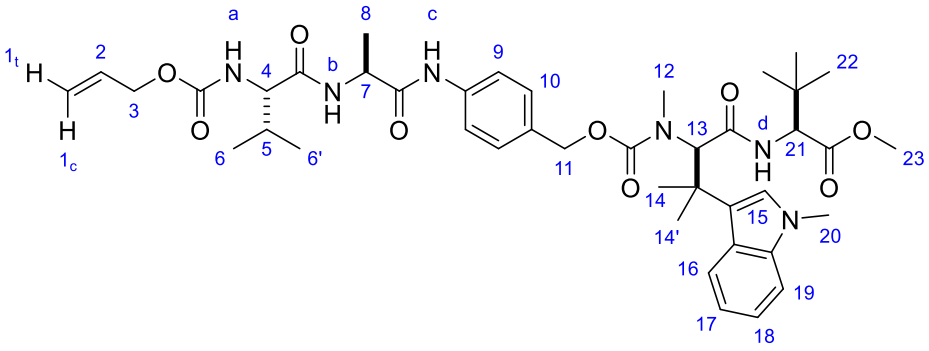

To a solution of methyl (*S*)-3,3-dimethyl-2-((*R*)-3-methyl-3-(1-methyl-1*H*-indol-3-yl)-2-(methylamino)butanamido)butanoate trifluoroacetate salt **129b** (25.1 mg, 50.0 µmol), Alloc-Val-Ala-PABC-OPNP **123** (54.3 mg, 0.100 mmol), and HOAt (6.80 mg, 50.0 µmol) in DMF (900 µL) was added pyridine (150 µL) and DIPEA (34.8 µL, 0.200 mmol). The reaction was stirred at rt for 4 days before the volatiles were removed under a stream of N_2. The residue was re-partitioned in EtOAc (5 mL) and H_2O (5 mL), and the phases were separated. The aqueous phase was extracted with EtOAc (3 × 5 mL). The combined organic phases were dried over anhydrous $MgSO_4$, and the solvent was removed *in vacuo*. The crude product was purified by reverse-phase semi-preparative HPLC (5–95%B over 20 min) to give carbamate **128b** as a white solid (10.0 mg, 12.6 µmol, 25%, 47%brsm) and the starting material **129b** was recovered (11.6 mg, 23.1 µmol, 46%).

t_R / min = 10.58 (35–95%B over 15 min)

$[\alpha]_D^{25}$ = −14.5° (c = 0.200, $CHCl_3$)

^{1}H NMR (400 MHz, DMSO-d_6): Room temperature NMR was unassigned due to complex rotameric mixtures.

^{1}H NMR (500 MHz, DMSO-d_6, 130 °C): δ_H = 9.47 (s, 1 H, H-N^c), 7.83 (br d, *J* = 7.9 Hz, 1 H, H-16 or H-N), 7.69 (br d, *J* = 7.2 Hz, 1 H, H-N or H-16), 7.58–7.54 (m, 2 H, H-9 or H-10), 7.35 (d, *J* = 8.3 Hz, 1 H, H-19), 7.30 (d, *J* = 8.6 Hz, 2 H, H-10 or H-9), 7.13 (ddd, *J* = 8.2, 7.1, 0.9 Hz, 1 H, H-18), 7.08 (s, 1 H, H-15), 6.97 (t, *J* = 7.5 Hz, 1 H, H-17), 6.56 (br d, *J* = 8.1 Hz, 1 H, H-N), 6.14 (br d, *J* = 8.1 Hz, 1 H, H-N), 5.92 (ddt, *J* = 17.3, 10.7, 5.3 Hz, 1 H, H-2), 5.55 (s, 1 H, H-13), 5.30 (dq, *J* = 17.3, 1.7 Hz, 1 H, H-1'), 5.17 (dq, *J* = 10.6, 1.5 Hz, 1 H, H-1), 5.11, 5.05 (ABq, J_{AB} = 12.4 Hz, 2 H, H-11), 4.56–4.47 (m, 3 H, H-3 and H-7), 4.01 (d, *J* = 8.8 Hz, 1 H, H-21), 3.94 (dd, *J* = 8.7, 6.4 Hz, 1 H, H-4), 3.70 (s, 3 H, H-20), 3.49 (s, 3 H, H-23), 3.03 (s, 3 H, H-12), 2.07 (octet, *J* = 6.7 Hz, 1 H, H-5), 1.65 (s, 3 H, H-14 or 14'), 1.45 (s, 3 H, H-14' or 14), 1.36 (d, *J* = 7.0 Hz, 3 H, H-8), 0.99 (d, *J* = 6.8 Hz, 3 H, H-6 or 6'), 0.91 (d, *J* = 6.9 Hz, 3 H, H-6' or 6), 0.60 (s, 9 H, H-22)

^{13}C NMR (101 MHz, $CDCl_3$): Unassigned due to complex rotameric mixtures.

HRMS (ESI): *m/z* $[M+Na]^+$ calcd for $C_{42}H_{58}N_6{}^{23}NaO_9$: 813.4157; found: 813.4161 (Δ = 0.5 ppm)

6.3.4. ADC synthesis

The ADCs were synthesised following literature procedure:[269]

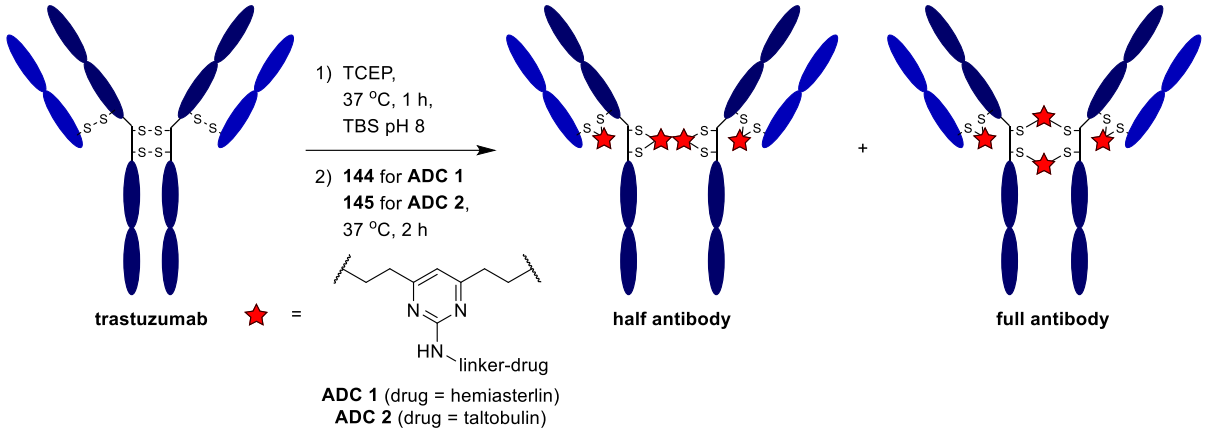

To a solution of trastuzumab (50 µL, 17 µM, 2.5 mg/mL) in TBS buffer (25 mM Tris·HCl pH 8, 25 mM NaCl, 0.5 mM EDTA) was added TCEP solution (5 mM, 10 equiv.). The reaction mixture was vortexed and incubated at 37 °C for 1 h. The linker-drug stock solution in DMSO (20 mM, 60 equiv.) was added (final DMSO percentage at 10% v/v), and the reaction mixture was vortexed and incubated at 37 °C for 4 h. The excess reagents were removed using a Zeba™ Spin desalting column (40,000 MWCO, 0.5 mL, ThermoFisher) pre-equilibrated with PBS. The reaction product was completely buffer exchanged into PBS by repeated diafiltration using an Amicon-Ultra centrifugal filter (10,000 MWCO, Merck Millipore). LCMS and SDS-PAGE analysis demonstrated >95% conversion to the desired conjugate.

6.3.4.1. SDS-PAGE analysis

Non-reducing Tris-Glycine SDS-PAGE with 12% acrylamide with 4% stacking gel was performed as standard. Broad range molecular weight marker (10–200 kDa, New England BioLabs) was run in all gels. Samples (10 µL of 0.4 mg/mL) were prepared with reducing loading dye (10 µL, containing β-mercaptoethanol) and heated to 95 °C for 5 min. Gels were run at constant voltage (160 V) for 60 min in 1x Laemmli running buffer (LRB). All gels were stained with Coomassie dye and imaged on a Syngene gel imaging system.

6.3.4.2. Size exclusion chromatography (SEC) analysis

SEC was performed on an ÄKTA Pure chromatography system using a Superdex 200 10/300 gel filtration column equilibrated with PBS. The protein was eluted using PBS and the UV trace measured at 280 nm. SEC analysis was performed by Teodors Pantelejevs, Hyvönen Group, Department of Biochemistry, University of Cambridge.

6.3.5. Biological assays

The biological assays were performed by Dr Stephen Walsh from the Spring Group, Department of Chemistry, University of Cambridge.

6.3.5.1. Cells Lines

HER2-positive SKBR3 and BT474 cells were obtained from the American Type Culture Collection (ATCC), and HER2-negative MCF7 cells were obtained from the European Collection of Authenticated Cell Cultures (ECACC). SKBR3 cells were maintained in high glucose McCoy's 5A medium, supplemented with 10% heat-inactivated foetal-bovine serum (FBS), 50 U/mL penicillin and 50 µg/mL streptomycin. MCF7 cells were maintained in Dulbecco's Modified Eagle Medium (DMEM) supplemented with 10% heat-inactivated FBS, 2 mM L-glutamine, 50 U/mL penicillin and 50 µg/mL streptomycin. BT474 cells were maintained in RPMI-1640 medium supplemented with 10% heat-inactivated FBS, 2 mM L-glutamine, 50 U/mL penicillin and 50 µg/mL streptomycin. All cell lines were incubated at 37 °C with 5% CO_2.

6.3.5.2. Cellular viability assays

Cells were seeded in 96-well plates for 24 h at 37 °C with 5% CO_2. SKBR3 cells were seeded at 20,000 cells/well, BT474 cells were seeded at 20,000 cells/well and MCF7 cells were seeded at 7,500 cells/well. Serial dilutions of **ADC 1**, **ADC 2**, **56**, **57**, and trastuzumab were added to the cells in complete growth medium and incubated at 37 °C with 5% CO_2 for 96 h. Cell viability was measured using CellTiter-Glo viability assay (Promega) according to the manufacturer's instructions. Cell viability was plotted as a percentage of untreated cells. Each measurement was taken in triplicate, and three independent repeats were performed.

References

1 World Health Organization, *WHO report on cancer: setting priorities, investing wisely and providing care for all*, Geneva, 2020.

2 D. Hanahan and R. A. Weinberg, *Cell*, 2000, **100**, 57–70.

3 D. Hanahan and R. A. Weinberg, *Cell*, 2011, **144**, 646–674.

4 C. B. Blackadar, *World J. Clin. Oncol.*, 2016, **7**, 54.

5 P. S. Moore and Y. Chang, *Nat. Rev. Cancer*, 2010, **10**, 878–889.

6 World Health Organization, International Classification of Diseases 11th Revision (ICD-11), https://icd.who.int/en, (accessed 18 September 2020).

7 A. Urruticoechea, R. Alemany, J. Balart, A. Villanueva, F. Vinals and G. Capella, *Curr. Pharm. Des.*, 2010, **16**, 3–10.

8 C. Kleisiaris, S. Ch and I. Papathanasiou, *J. Med. Ethics Hist. Med.*, 2014, **7**, 6.

9 G. B. Faguet, *Int. J. Cancer*, 2015, **136**, 2022–2036.

10 S. I. Hajdu, *Cancer*, 2004, **100**, 2048–2051.

11 W. C. Röntgen, *Science*, 1896, **3**, 227–231.

12 E. H. Grubbé, *Radiology*, 1933, **21**, 156–162.

13 V. T. DeVita and E. Chu, *Cancer Res.*, 2008, 68, 8643–8653.

14 B. A. Chabner and T. G. Roberts, *Nat. Rev. Cancer*, 2005, **5**, 65–72.

15 L. S. Goodman, M. M. Wintrobe, W. Dameshek, M. J. Goodman, A. Gilman and M. T. Mclennan, *J. Am. Med. Assoc.*, 1946, **132**, 126–132.

16 J. E. Fenn and R. Udelsman, *J. Am. Coll. Surg.*, 2011, **212**, 413–417.

17 J. G. Bennette, *Br. J. Cancer*, 1952, **6**, 377–388.

18 C. Heidelberger, N. K. Chaudhuri, P. Danneberg, D. Mooren, L. Griesbach, R. Duschinsky, R. J. Schnitzer, E. Pleven and J. Scheiner, *Nature*, 1957, **179**, 663–666.

19 G. B. Elion, S. Singer and G. H. Hitchings, *J. Biol. Chem.*, 1954, **208**, 477–488.

20 G. H. Hitchings and G. B. Elion, *Ann. N. Y. Acad. Sci.*, 1954, **60**, 195–199.

21 I. S. Johnson, J. G. Armstrong, M. Gorman and J. P. Burnett, *Cancer Res.*, 1963, **23**, 1390–1427.

22 M. A. Jordan, D. Thrower and L. Wilson, *Cancer Res.*, 1991, **51**, 2212–22.

23 M. A. Jordan, *Curr. Med. Chem. - Anti-Cancer Agents*, 2002, **2**, 1–17.

24 L. Kelland, *Nat. Rev. Cancer*, 2007, **7**, 573–584.

25 M. C. Wani, H. L. Taylor, M. E. Wall, P. Coggon and A. T. McPhail, *J. Am. Chem. Soc.*, 1971, **93**, 2325–2327.

26 O. M. Friedman and A. M. Seligman, *J. Am. Chem. Soc.*, 1954, **76**, 655–658.

27 G. M. Cragg and D. J. Newman, *J. Nat. Prod.*, 2004, **67**, 232–244.

28 R. V. J. Chari, M. L. Miller and W. C. Widdison, *Angew. Chem. Int. Ed.*, 2014, **53**, 3796–3827.

29 J. Zhang, P. L. Yang and N. S. Gray, *Nat. Rev. Cancer*, 2009, **9**, 28–39.

30 R. Kannaiyan and D. Mahadevan, *Expert Rev. Anticancer Ther.*, 2018, **18**, 1249–1270.

31 K. S. Bhullar, N. O. Lagarón, E. M. McGowan, I. Parmar, A. Jha, B. P. Hubbard and H. P. V. Rupasinghe, *Mol. Cancer*, 2018, **17**, 48.

32 B. J. Druker, M. Talpaz, D. J. Resta, B. Peng, E. Buchdunger, J. M. Ford, N. B. Lydon, H. Kantarjian, R. Capdeville, S. Ohno-Jones and C. L. Sawyers, *N. Engl. J. Med.*, 2001, **344**, 1031–1037.

33 M. Sattler and J. D. Griffin, *Int. J. Hematol.*, 2001, **73**, 278–291.

34 M. Deininger, E. Buchdunger and B. J. Druker, *Blood*, 2005, **105**, 2640–2653.

35 M. Muhsin, J. Graham and P. Kirkpatrick, *Nat. Rev. Cancer*, 2003, **3**, 556–557.

36 N. P. Shah, F. Y. Lee, R. Luo, Y. Jiang, M. Donker and C. Akin, *Blood*, 2006, **108**, 286–291.

37 J. Das, P. Chen, D. Norris, R. Padmanabha, J. Lin, R. V. Moquin, Z. Shen, L. S. Cook, A. M. Doweyko, S. Pitt, S. Pang, D. R. Shen, Q. Fang, H. F. De Fex, K. W. McIntyre, D. J. Shuster, K. M. Gillooly, K. Behnia, G. L. Schieven, J. Wityak and J. C. Barrish, *J. Med. Chem.*, 2006, **49**, 6819–6832.

38 R. Y. Tsang, S. Sadeghi and R. S. Finn, *Clin. Med. Insights Ther.*, 2011, **3**, 1–13.

39 K. T. Flaherty, J. R. Infante, A. Daud, R. Gonzalez, R. F. Kefford, J. Sosman, O. Hamid, L. Schuchter, J. Cebon, N. Ibrahim, R. Kudchadkar, H. A. Burris, G. Falchook, A. Algazi, K. Lewis, G. V. Long, I. Puzanov, P. Lebowitz, A. Singh, S. Little, P. Sun, A. Allred, D. Ouellet, K. B. Kim, K. Patel and J. Weber, *N. Engl. J. Med.*, 2012, **367**, 1694–1703.

40 R. A. Ward, S. Fawell, N. Floc'h, V. Flemington, D. Mckerrecher and P. D. Smith, *Chem. Rev.*, 2020, DOI:10.1021/acs.chemrev.0c00383.

41 R. Pisa and T. M. Kapoor, *Nat. Chem. Biol.*, 2020, **16**, 817–825.

42 R. B. Mokhtari, T. S. Homayouni, N. Baluch, E. Morgatskaya, S. Kumar, B. Das and H. Yeger, *Oncotarget*, 2017, **8**, 38022–38043.

43 R. J. Deshaies, *Nat. Chem. Biol.*, 2015, **11**, 634–635.

44 H. Pei, Y. Peng, Q. Zhao and Y. Chen, *RSC Adv.*, 2019, **9**, 16967–16976.

45 X. Sun, H. Gao, Y. Yang, M. He, Y. Wu, Y. Song, Y. Tong and Y. Rao, *Signal Transduct. Target. Ther.*, 2019, **4**, 64.

46 X. Li and Y. Song, *J. Hematol. Oncol.*, 2020, **13**, 50.

47 V. S. Rodrik-Outmezguine, M. Okaniwa, Z. Yao, C. J. Novotny, C. McWhirter, A. Banaji,

H. Won, W. Wong, M. Berger, E. de Stanchina, D. G. Barratt, S. Cosulich, T. Klinowska, N. Rosen and K. M. Shokat, *Nature*, 2016, **534**, 272–276.

48 Z. Zhao and P. E. Bourne, *Drug Discov. Today*, 2018, **23**, 727–735.

49 S. Khozin, C. Weinstock, G. M. Blumenthal, J. Cheng, K. He, L. Zhuang, H. Zhao, R. Charlab, I. Fan, P. Keegan and R. Pazdur, *Clin. Cancer Res.*, 2017, **23**, 2131–2135.

50 J. Engel, J. Lategahn and D. Rauh, *ACS Med. Chem. Lett.*, 2016, **7**, 2–5.

51 H. Kaplon, M. Muralidharan, Z. Schneider and J. M. Reichert, *MAbs*, 2020, **12**, e1703531.

52 R.-M. Lu, Y.-C. Hwang, I.-J. Liu, C.-C. Lee, H.-Z. Tsai, H.-J. Li and H.-C. Wu, *J. Biomed. Sci.*, 2020, **27**, 1.

53 L. Gauzy-Lazo, I. Sassoon and M. P. Brun, *SLAS Discov.*, 2020, **25**, 843–868.

54 A. L. Garner and K. D. Janda, *Curr. Top. Med. Chem.*, 2011, **11**, 258–280.

55 A. A. Ivanov, F. R. Khuri and H. Fu, *Trends Pharmacol. Sci.*, 2013, **34**, 393–400.

56 Y. H. Lau, P. de Andrade, Y. Wu and D. R. Spring, *Chem. Soc. Rev.*, 2015, **44**, 91–102.

57 J. Iegre, J. S. Gaynord, N. S. Robertson, H. F. Sore, M. Hyvönen and D. R. Spring, *Adv. Ther.*, 2018, **1**, 1800052.

58 L. McDougall and A. G. Jamieson, *eLS*, 2019, 1–9.

59 A. M. Ali, J. Atmaj, N. Van Oosterwijk, M. R. Groves and A. Dömling, *Comput. Struct. Biotechnol. J.*, 2019, **17**, 263–281.

60 D. P. Ryan and J. M. Matthews, *Curr. Opin. Struct. Biol.*, 2005, **15**, 441–446.

61 E. Valeur, S. M. Guéret, H. Adihou, R. Gopalakrishnan, M. Lemurell, H. Waldmann, T. N. Grossmann and A. T. Plowright, *Angew. Chem. Int. Ed.*, 2017, **56**, 10294–10323.

62 D. E. Scott, A. R. Bayly, C. Abell and J. Skidmore, *Nat. Rev. Drug Discov.*, 2016, **15**, 533–550.

63 G. L. Verdine and L. D. Walensky, *Clin. Cancer Res.*, 2007, **13**, 7264–7270.

64 A. D. Thompson, A. Dugan, J. E. Gestwicki and A. K. Mapp, *ACS Chem. Biol.*, 2012, **7**, 1311–1320.

65 J. A. Wells and C. L. McClendon, *Nature*, 2007, **450**, 1001–1009.

66 H. Yin and A. D. Hamilton, *Angew. Chem. Int. Ed.*, 2005, **44**, 4130–4163.

67 A. E. Modell, S. L. Blosser and P. S. Arora, *Trends Pharmacol. Sci.*, 2016, **37**, 702–713.

68 M. R. Arkin, Y. Tang and J. A. Wells, *Chem. Biol.*, 2014, **21**, 1102–1114.

69 G. Zinzalla and D. E. Thurston, *Future Med. Chem.*, 2009, 1, 65–93.

70 M. Bakail and F. Ochsenbein, *Comptes Rendus Chim.*, 2016, **19**, 19–27.

71 G. D. Hartman, M. S. Egbertson, W. Halczenko, W. L. Laswell, M. E. Duggan, R. L. Smith, A. M. Naylor, P. D. Manno, R. J. Lynch, G. Zhang, C. T. C. Chang and R. J. Gould, *J. Med.*

Chem., 1992, **35**, 4640–4642.

72 D. Bojadzic and P. Buchwald, *Curr. Top. Med. Chem.*, 2018, **18**, 674–699.

73 H.-S. Cho, K. Mason, K. X. Ramyar, A. M. Stanley, S. B. Gabelli, D. W. Denney and D. J. Leahy, *Nature*, 2003, **421**, 756–760.

74 C. L. Vogel, M. A. Cobleigh, D. Tripathy, J. C. Gutheil, L. N. Harris, L. Fehrenbacher, D. J. Slamon, M. Murphy, W. F. Novotny, M. Burchmore, S. Shak, S. J. Stewart and M. Press, *J. Clin. Oncol.*, 2002, **20**, 719–726.

75 F. Saab, C. Ionescu and M. J. Schweiger, *Expert Opin. Drug Saf.*, 2012, **11**, 315–324.

76 A. Kelekar, B. S. Chang, J. E. Harlan, S. W. Fesik and C. B. Thompson, *Mol. Cell. Biol.*, 1997, **17**, 7040–7046.

77 A. Burgess, K. M. Chia, S. Haupt, D. Thomas, Y. Haupt and E. Lim, *Front. Oncol.*, 2016, **6**, 1–7.

78 B. Vogelstein, D. Lane and A. J. Levine, *Nature*, 2000, **408**, 307–310.

79 M. Hollstein, D. Sidransky, B. Vogelstein and C. Harris, *Science*, 1991, **253**, 49–53.

80 Y. Haupt, R. Maya, A. Kazaz and M. Oren, *Nature*, 1997, **387**, 296–299.

81 R. Honda, H. Tanaka and H. Yasuda, *FEBS Lett.*, 1997, **420**, 25–27.

82 P. H. Kussie, S. Gorina, V. Marechal, B. Elenbaas, J. Moreau, A. J. Levine and N. P. Pavletich, *Science*, 1996, **274**, 948–953.

83 H. Kawai, D. Wiederschain and Z.-M. Yuan, *Mol. Cell. Biol.*, 2003, **23**, 4939–4947.

84 E. Meulmeester, R. Frenk, R. Stad, P. de Graaf, J.-C. Marine, K. H. Vousden and A. G. Jochemsen, *Mol. Cell. Biol.*, 2003, **23**, 4929–4938.

85 M. Argentini, N. Barboule and B. Wasylyk, *Oncogene*, 2001, **20**, 1267–1275.

86 G. W. Yu, M. D. Allen, A. Andreeva, A. R. Fersht and M. Bycroft, *Protein Sci.*, 2006, **15**, 384–389.

87 S. Fang, J. P. Jensen, R. L. Ludwig, K. H. Vousden and A. M. Weissman, *J. Biol. Chem.*, 2000, **275**, 8945–8951.

88 T. Iwakuma and G. Lozano, *Mol. Cancer Res.*, 2003, **1**, 993–1000.

89 F. S. Leach, T. Tokino, P. Meltzer, M. Burrell, J. D. Oliner, S. Smith, D. E. Hill, D. Sidransky, K. W. Kinzler and B. Vogelstein, *Cancer Res.*, 1993, **53**, 2231–2234.

90 J. D. Oliner, K. W. Kinzler, P. S. Meltzer, D. L. George and B. Vogelstein, *Nature*, 1992, **358**, 80–83.

91 Y. Fang, G. Liao and B. Yu, *Acta Pharm. Sin. B*, 2020, **10**, 1253–1278.

92 G. Sanz, M. Singh, S. Peuget and G. Selivanova, *J. Mol. Cell Biol.*, 2019, **11**, 586–599.

93 M. Konopleva, G. Martinelli, N. Daver, C. Papayannidis, A. Wei, B. Higgins, M. Ott, J. Mascarenhas and M. Andreeff, *Leukemia*, 2020, **34**, 2858–2874.

94 V. Tisato, R. Voltan, A. Gonelli, P. Secchiero and G. Zauli, *J. Hematol. Oncol.*, 2017, **10**, 133.

95 D. Nguyen, W. Liao, S. X. Zeng and H. Lu, *Pharmacol. Ther.*, 2017, **178**, 92–108.

96 A. Aguilar, J. Lu, L. Liu, D. Du, D. Bernard, D. McEachern, S. Przybranowski, X. Li, R. Luo, B. Wen, D. Sun, H. Wang, J. Wen, G. Wang, Y. Zhai, M. Guo, D. Yang and S. Wang, *J. Med. Chem.*, 2017, **60**, 2819–2839.

97 Q. Ding, Z. Zhang, J. J. Liu, N. Jiang, J. Zhang, T. M. Ross, X. J. Chu, D. Bartkovitz, F. Podlaski, C. Janson, C. Tovar, Z. M. Filipovic, B. Higgins, K. Glenn, K. Packman, L. T. Vassilev and B. Graves, *J. Med. Chem.*, 2013, **56**, 5979–5983.

98 L. A. Carvajal, D. Ben Neriah, A. Senecal, L. Benard, V. Thiruthuvanathan, T. Yatsenko, S.-R. Narayanagari, J. C. Wheat, T. I. Todorova, K. Mitchell, C. Kenworthy, V. Guerlavais, D. A. Annis, B. Bartholdy, B. Will, J. D. Anampa, I. Mantzaris, M. Aivado, R. H. Singer, R. A. Coleman, A. Verma and U. Steidl, *Sci. Transl. Med.*, 2018, **10**, eaao3003.

99 F. Bernal, A. F. Tyler, S. J. Korsmeyer, L. D. Walensky and G. L. Verdine, *J. Am. Chem. Soc.*, 2007, **129**, 2456–2457.

100 Y. S. Chang, B. Graves, V. Guerlavais, C. Tovar, K. Packman, K. H. To, K. A. Olson, K. Kesavan, P. Gangurde, A. Mukherjee, T. Baker, K. Darlak, C. Elkin, Z. Filipovic, F. Z. Qureshi, H. Cai, P. Berry, E. Feyfant, X. E. Shi, J. Horstick, D. A. Annis, A. M. Manning, N. Fotouhi, H. Nash, L. T. Vassilev and T. K. Sawyer, *Proc. Natl. Acad. Sci. U.S.A.*, 2013, **110**, E3445–E3454.

101 C. J. Brown, S. T. Quah, J. Jong, A. M. Goh, P. C. Chiam, K. H. Khoo, M. L. Choong, M. A. Lee, L. Yurlova, K. Zolghadr, T. L. Joseph, C. S. Verma and D. P. Lane, *ACS Chem. Biol.*, 2013, **8**, 506–512.

102 Y. H. Lau, P. de Andrade, S.-T. Quah, M. Rossmann, L. Laraia, N. Sköld, T. J. Sum, P. J. E. Rowling, T. L. Joseph, C. Verma, M. Hyvönen, L. S. Itzhaki, A. R. Venkitaraman, C. J. Brown, D. P. Lane and D. R. Spring, *Chem. Sci.*, 2014, **5**, 1804–1809.

103 Y. H. Lau, Y. Wu, M. Rossmann, B. X. Tan, P. de Andrade, Y. S. Tan, C. Verma, G. J. McKenzie, A. R. Venkitaraman, M. Hyvönen and D. R. Spring, *Angew. Chem. Int. Ed.*, 2015, **54**, 15410–15413.

104 K. Hu, F. Yin, M. Yu, C. Sun, J. Li, Y. Liang, W. Li, M. Xie, Y. Lao, W. Liang and Z.-G. Li, *Theranostics*, 2017, **7**, 4566–4576.

105 X. Li, W. D. Tolbert, H.-G. Hu, N. Gohain, Y. Zou, F. Niu, W.-X. He, W. Yuan, J.-C. Su, M. Pazgier and W. Lu, *Chem. Sci.*, 2019, **10**, 1522–1530.

106 N. S. Robertson and D. R. Spring, *Molecules*, 2018, **23**, 959.

107 L. D. Walensky and G. H. Bird, *J. Med. Chem.*, 2014, **57**, 6275–6288.

108 X. Li, S. Chen, W.-D. Zhang and H.-G. Hu, *Chem. Rev.*, 2020, **120**, 10079–10144.

109 L. Reguera and D. G. Rivera, *Chem. Rev.*, 2019, **119**, 9836–9860.

110 C. M. Grison, G. M. Burslem, J. A. Miles, L. K. A. Pilsl, D. J. Yeo, Z. Imani, S. L. Warriner, M. E. Webb and A. J. Wilson, *Chem. Sci.*, 2017, **8**, 5166–5171.

111 P. T. Tran, C. Ø. Larsen, T. Røndbjerg, M. De Foresta, M. B. A. Kunze, A. Marek, J. H. Løper, L.-E. Boyhus, A. Knuhtsen, K. Lindorff-Larsen and D. S. Pedersen, *Chem. - Eur. J.*, 2017, **23**, 3490–3495.

112 Y. Wu, L. B. Olsen, Y. H. Lau, C. H. Jensen, M. Rossmann, Y. R. Baker, H. F. Sore, S. Collins and D. R. Spring, *ChemBioChem*, 2016, **17**, 689–692.

113 S. J. Walsh, J. Iegre, H. Seki, J. D. Bargh, H. F. Sore, J. S. Parker, J. S. Carroll and D. R. Spring, *Org. Biomol. Chem.*, 2020, **18**, 4224–4230.

114 O. Torres, D. Yüksel, M. Bernardina, K. Kumar and D. Bong, *ChemBioChem*, 2008, **9**, 1701–1705.

115 Y. H. Lau, Y. Wu, P. De Andrade, W. R. J. D. Galloway and D. R. Spring, *Nat. Protoc.*, 2015, **10**, 585–594.

116 I. Kii, A. Shiraishi, T. Hiramatsu, T. Matsushita, H. Uekusa, S. Yoshida, M. Yamamoto, A. Kudo, M. Hagiwara and T. Hosoya, *Org. Biomol. Chem.*, 2010, **8**, 4051–4055.

117 N. J. Agard, J. A. Prescher and C. R. Bertozzi, *J. Am. Chem. Soc.*, 2004, **126**, 15046–15047.

118 J. Dommerholt, F. P. J. T. Rutjes and F. L. van Delft, *Top. Curr. Chem.*, 2016, **374**, 16.

119 H. N. C. Wong, P. J. Garratt and F. Sondheimer, *J. Am. Chem. Soc.*, 1974, **96**, 5604–5605.

120 K. Sharma, A. V. Strizhak, E. Fowler, W. Xu, B. Chappell, H. F. Sore, W. R. J. D. Galloway, M. N. Grayson, Y. H. Lau, L. S. Itzhaki and D. R. Spring, *ACS Omega*, 2020, **5**, 1157–1169.

121 G. K. Dewkar, P. B. Carneiro and M. C. T. Hartman, *Org. Lett.*, 2009, **11**, 4708–4711.

122 L. E. J. Smeenk, N. Dailly, H. Hiemstra, J. H. Van Maarseveen and P. Timmerman, *Org. Lett.*, 2012, **14**, 1194–1197.

123 G. J. J. Richelle, M. Schmidt, H. Ippel, T. M. Hackeng, J. H. van Maarseveen, T. Nuijens and P. Timmerman, *ChemBioChem*, 2018, **19**, 1934–1938.

124 D. E. Streefkerk, M. Schmidt, J. H. Ippel, T. M. Hackeng, T. Nuijens, P. Timmerman and J. H. Van Maarseveen, *Org. Lett.*, 2019, **21**, 2095–2100.

125 N. Assem, D. J. Ferreira, D. W. Wolan and P. E. Dawson, *Angew. Chem. Int. Ed.*, 2015, **54**, 8665–8668.

126 A. M. Spokoyny, Y. Zou, J. J. Ling, H. Yu, Y.-S. Lin and B. L. Pentelute, *J. Am. Chem. Soc.*, 2013, **135**, 5946–5949.

127 G. Lautrette, F. Touti, H. G. Lee, P. Dai and B. L. Pentelute, *J. Am. Chem. Soc.*, 2016, **138**, 8340–8343.

128 S. P. Brown and A. B. Smith, *J. Am. Chem. Soc.*, 2015, **137**, 4034–4037.

129 J. Guy, R. Castonguay, N. B. Campos-Reales Pineda, V. Jacquier, K. Caron, S. W. Michnick and J. W. Keillor, *Mol. Biosyst.*, 2010, **6**, 976–987.

130 Z. Li, R. Huang, H. Xu, J. Chen, Y. Zhan, X. Zhou, H. Chen and B. Jiang, *Org. Lett.*, 2017, **19**, 4972–4975.

131 N. S. Robertson, S. J. Walsh, E. Fowler, M. Yoshida, S. M. Rowe, Y. Wu, H. F. Sore, J. S. Parker and D. R. Spring, *Chem. Commun.*, 2019, **55**, 9499–9502.

132 M. T. J. Bluntzer, J. O'Connell, T. S. Baker, J. Michel and A. N. Hulme, *Pept. Sci.*, 2020, 1–17.

133 S. M. Q. Chee, J. Wongsantichon, Q. Soo Tng, R. Robinson, T. L. Joseph, C. Verma, D. P. Lane, C. J. Brown and F. J. Ghadessy, *PLoS One*, 2014, **9**, e104914.

134 C. Hoppmann and L. Wang, *Chem. Commun.*, 2016, **52**, 5140–5143.

135 Y. H. Lau, P. de Andrade, N. Sköld, G. J. McKenzie, A. R. Venkitaraman, C. Verma, D. P. Lane and D. R. Spring, *Org. Biomol. Chem.*, 2014, **12**, 4074–4077.

136 A. V. Strizhak, O. Babii, S. Afonin, I. Bakanovich, T. Pantelejevs, W. Xu, E. Fowler, R. Eapen, K. Sharma, M. O. Platonov, V. V. Hurmach, L. Itzhaki, M. Hyvönen, A. S. Ulrich, D. R. Spring and I. V. Komarov, *Org. Biomol. Chem.*, 2020, **18**, 5359–5369.

137 M. M. Madden, A. Muppidi, Z. Li, X. Li, J. Chen and Q. Lin, *Bioorg. Med. Chem. Lett.*, 2011, **21**, 1472–1475.

138 M. H. Potashman and M. E. Duggan, *J. Med. Chem.*, 2009, **52**, 1231–1246.

139 J. Singh, R. C. Petter, T. A. Baillie and A. Whitty, *Nat. Rev. Drug Discov.*, 2011, **10**, 307–317.

140 T. A. Baillie, *Angew. Chem. Int. Ed.*, 2016, **55**, 13408–13421.

141 R. Lonsdale and R. A. Ward, *Chem. Soc. Rev.*, 2018, **47**, 3816–3830.

142 M. Gehringer and S. A. Laufer, *J. Med. Chem.*, 2019, **62**, 5673–5724.

143 S. Ray and A. S. Murkin, *Biochemistry*, 2019, **58**, 5234–5244.

144 T. Zhang, J. M. Hatcher, M. Teng, N. S. Gray and M. Kostic, *Cell Chem. Biol.*, 2019, **26**, 1486–1500.

145 T. A. Baillie, *Med. Chem. Res.*, 2020, **29**, 1093–1104.

146 M. Gehringer, *Future Med. Chem.*, 2020, **12**, 1363–1368.

147 R. A. Bauer, *Drug Discov. Today*, 2015, **20**, 1061–1073.

148 D. C. Swinney, *Curr. Top. Med. Chem.*, 2006, **6**, 461–478.

149 T. Barf and A. Kaptein, *J. Med. Chem.*, 2012, **55**, 6243–6262.

150 G. Sachs, J. M. Shin and C. W. Howden, in *Alimentary Pharmacology and Therapeutics*, Blackwell Publishing Ltd, 2006, vol. 23, pp. 2–8.

151 J. M. Shin, Y. M. Cho and G. Sachs, *J. Am. Chem. Soc.*, 2004, **126**, 7800–7811.

152 E. L. Kwak, R. Sordella, D. W. Bell, N. Godin-Heymann, R. A. Okimoto, B. W. Brannigan, P. L. Harris, D. R. Driscoll, P. Fidias, T. J. Lynch, S. K. Rabindran, J. P. McGinnis, A. Wissner, S. V Sharma, K. J. Isselbacher, J. Settleman and D. A. Haber, *Proc. Natl. Acad. Sci. U.S.A.*, 2005, **102**, 7665–7670.

153 W. Pao, V. A. Miller, K. A. Politi, G. J. Riely, R. Somwar, M. F. Zakowski, M. G. Kris and H. Varmus, *PLoS Med.*, 2005, **2**, e73.

154 C.-H. Yun, K. E. Mengwasser, A. V Toms, M. S. Woo, H. Greulich, K.-K. Wong, M. Meyerson and M. J. Eck, *Proc. Natl. Acad. Sci. U.S.A.*, 2008, **105**, 2070–2075.

155 T. A. Carter, L. M. Wodicka, N. P. Shah, A. M. Velasco, M. A. Fabian, D. K. Treiber, Z. V Milanov, C. E. Atteridge, W. H. Biggs, P. T. Edeen, M. Floyd, J. M. Ford, R. M. Grotzfeld, S. Herrgard, D. E. Insko, S. A. Mehta, H. K. Patel, W. Pao, C. L. Sawyers, H. Varmus, P. P. Zarrinkar and D. J. Lockhart, *Proc. Natl. Acad. Sci. U.S.A.*, 2005, **102**, 11011–11016.

156 W. Zhou, D. Ercan, L. Chen, C.-H. Yun, D. Li, M. Capelletti, A. B. Cortot, L. Chirieac, R. E. Iacob, R. Padera, J. R. Engen, K.-K. Wong, M. J. Eck, N. S. Gray and P. A. Jänne, *Nature*, 2009, **462**, 1070–1074.

157 D. A. E. Cross, S. E. Ashton, S. Ghiorghiu, C. Eberlein, C. A. Nebhan, P. J. Spitzler, J. P. Orme, M. R. V Finlay, R. A. Ward, M. J. Mellor, G. Hughes, A. Rahi, V. N. Jacobs, M. Red Brewer, E. Ichihara, J. Sun, H. Jin, P. Ballard, K. Al-Kadhimi, R. Rowlinson, T. Klinowska, G. H. P. Richmond, M. Cantarini, D.-W. Kim, M. R. Ranson and W. Pao, *Cancer Discov.*, 2014, **4**, 1046–61.

158 T. A. Halgren, *J. Chem. Inf. Model.*, 2009, **49**, 377–389.

159 J. Y. Gauthier, N. Chauret, W. Cromlish, S. Desmarais, L. T. Duong, J.-P. Falgueyret, D. B. Kimmel, S. Lamontagne, S. Léger, T. LeRiche, C. S. Li, F. Massé, D. J. McKay, D. A. Nicoll-Griffith, R. M. Oballa, J. T. Palmer, M. D. Percival, D. Riendeau, J. Robichaud, G. A. Rodan, S. B. Rodan, C. Seto, M. Thérien, V.-L. Truong, M. C. Venuti, G. Wesolowski, R. N. Young, R. Zamboni and W. C. Black, *Bioorg. Med. Chem. Lett.*, 2008, **18**, 923–928.

160 R. D. Chapurlat, *Ther. Adv. Musculoskelet. Dis.*, 2015, **7**, 103–9.

161 M. R. McClung, M. L. O'Donoghue, S. E. Papapoulos, H. Bone, B. Langdahl, K. G. Saag, I. R. Reid, D. P. Kiel, I. Cavallari, M. P. Bonaca, S. D. Wiviott, T. de Villiers, X. Ling, K. Lippuner, T. Nakamura, J.-Y. Reginster, J. A. Rodriguez-Portales, C. Roux, J. Zanchetta, C. A. F. Zerbini, J.-G. Park, K. Im, A. Cange, L. T. Grip, N. Heyden, C. DaSilva, D. Cohn, R. Massaad, B. B. Scott, N. Verbruggen, D. Gurner, D. L. Miller, M. L. Blair, A. B. Polis, S. A. Stoch, A. Santora, A. Lombardi, A. T. Leung, K. D. Kaufman, M. S. Sabatine, C. A. Mautalén, Z. Man, J. R. Zanchetta, C. H. Magaril, P. Sambrook, J.-Y. Reginster, P. Geusens, S. Goemaere, B. H. Albergaria, C. A. de F. Zerbini, M. L. Castro, L. H. Gregorio, R. Stoilov, A.-M. I. Borissova, K. H. Hristozov, N. L. Temelkova, I. K. Daskalova, S. I. Kuzmanova, D. Yaneva-Bichovska, A. Z. Batalov, P. Riedemann, J. A. Rodriguez Portales, H. Tang, H. Zhu, Z. Zhang, A. Chao, Y. Hu, Z. Liu, J. Lu, M. Qiu, X. Gao, S. Zhang, L. Xu, W. Xia, E. Liao, W. Yang, W. Wu, K. Dai, R. Hu, H. Tang, J. J. Jaller, F. Cabal, J. F. Molina, C. A. Cure Cure, H. Yupanqui-Lozno, P. Chalem, J. Londono, M. Abello, E. D. Tobias, W. Otero, T. Nikolic, B. Miskic, J. Stepan, V. Vyskocil, L. Novosad, J. Slesinger, P. Novosad, E. Vlckova, L. Bortlik, E. Dokoupilova, T. Hala, J.-E. B. Jensen, K. T. Brixen, B. L. Langdahl, P. Schwarz, P. C. Eskildsen, P. A. Eiken, A. P. Hermann, J. Gram, M. B. Schou, P. Alexandersen, B. Nedergaard, D. M. Mejía, L. Estrella De Henriquez, N. Páez, C. Velazco, I. Valter, K.-L. Vahula, I. Kull, K. Maasalu, R. Chapurlat, P. Fardellone, C. L. Benhamou, C. Roux, G. Weryha, V. Herkt, R. Martz, R. Nischik, W. Spieler, C. Contzen, D. Felsenberg, I. Frieling, E. Frahm, H. Briones, B. Sandoval, P.

Barrios, A. García, C. Avendaño, M. González, J. Guerra, M. Tuna, O. M. Díaz, E. Samayoa, E. López, J. R. Barrera, M. Palencia, M. Cifuentes, G. Alvarado, M. López, N. Chavez, F. Haase, R. Rivera, C. González, K. Tan, P. C. Leung, S. Mandalam, S. U. Pitale, G. Bantwal, A. C. Ammini, S. S. A. Shaikh, P. K. Kanakatte Mylariah, M. Dharmalingam, S. Mukhopadhyay, A. Jain, P. Singh, N. Shetty, S. S. Sathyanarayana, N. Shah, M. D. Chadha, R. Bhandankar, K. Velayutham, S. Marwah, M. John, R. K. Sahay, S. Adami, R. Nuti, G. Bianchi, M. L. Brandi, S. Minisola, C. E. Fiore, A. Rubinacci, H. Miyajima, H. Yamane, Y. Nakatani, S. Okamoto, K. Kuroda, M. Fujimori, A. Itabashi, K. Katayama, S. Nakajo, Y. Somekawa, Y. Ohsawa, W. Tajima, K. Mizuno, S. Mori, T. Kanabuchi, H. Hashizume, N. Oka, K. Hamada, M. Yamaguchi, F. Hirahara, M. Atobe, Y. Ohtake, S. Ichikawa, T. Onishi, K. Matsumoto, T. Nakamura, E. Shirasawa, K. Katayama, M. Takahashi, T. Oguma, H. Matsui, Y. Katoh, K. Shigenobu, T. Onishi, M. Shibukawa, S. Ikeda, K. Osaka, R. Kanda, Y. Inobe, M. Shigenobu, M. Hasegawa, T. Yamaji, Y. Miyazaki, T. Ito, E. Nakamura, S. Nagai, S.-K. Lim, Y.-S. Chung, C.-S. Shin, Y.-K. Min, G. S. Kim, H. K. Yoon, M.-I. Kang, K.-H. Yang, H. M. Park, I. J. Kim, D. J. Chung, H. Y. Chung, S. Jaundzeikare, D. Andersone, A. Medne, Y. Yaghi, V. Alekna, V. Kasiulevicius, I. Purtokaite - Labutiniene, A. Krasauskiene, J. Varanaviciene, V. Basijokiene, A. Abraitiene, L. Radzeviciene, J. Walliser, P. A. García Hernández, M. F. Araujo, H. E. Avila Armengol, P. De la Peña, J. Tamayo, B. Zazueta, F. Cons, N. L. Gilchrist, I. R. Reid, R. Leikis, P. Jones, J. G. P. Singh, J. I. Halse, U. Syversen, H. O. Høivik, E. S. Øfjord, H. C. Gulseth, S. Elle, P. D. Norheim, A. A. Calvo Quiroz, P. A. Cesar Augusto, M. G. León Portocarrero, L. F. Vidal Neira, J. Chavez, B. Garro Barrera, R. Kuroiwa Sampei, B. V. Luis Fernando, R. Oquelis Cabredo, S. Castillo, A. M. G. Morales, P. P. Tan, L. A. C. Leagogo, E. H. Wang, J. T. Li-Yu, A. Z. Sawicki, B. Stasiuk, G. Kania, R. Lorenc, A. Sidorowicz-Bialynicka, L. Szczepanski, E. Franek, R. Filip, J. Sekula, T. Blicharski, P. Leszczynski, E. Sewerynek, T. Miazgowski, A. Milewicz, M. Dabrowska, J. Romaszko, W. Pluskiewicz, L. Wojnowski, C. Codreanu, H. Bolosiu, R. Ionescu, I. Zosin, L. Macovei, M. Bojinca, F. Radulescu, S. Pop, A. Sarbu, L. I. Benevolenskaya, E. L. Nasonov, L. Y. Rozhinskaya, R. G. Oganov, S. S. Rodionova, E. V. Shlyakhto, V. Trofimov, E. G. Zotkin, I. E. Zazerskaya, E. N. Grineva, O. Ershova, O. Lesnyak, O. D. Ostroumova, S. B. Malichenko, E. G. Pikhlak, V. G. Pilyaev, T. Raskina, E. V Zonova, V. S. Shirinsky, A. N. Dimic, G. Cobeljic, S. Vujovic, G. C. Ellis, S. Lipschitz, T. J. De Villiers, A. J. De Weerd, T. Vally, Y. Trinder, J. L. Coetsee, C. P. Davis, S. Nayiager, F. S. Hough, L. F. Oelofse, E. van der Walt, J. J. Lombaard, S. Blignaut, U. Govind, L. F. Fouche, D. S. Kruger, J. P. Dalmeyer, M. M. Ferreira, A. Escudero-Contreras, M. Muñoz Torres, F. Hawkins Carranza, J. L. Perez Castrillon, J. A. García Meijide, E. Jodar Gimeno, S. Palacios Gil-Antuñana, L. de Teresa Parreno, E. Martín Mola, C. Alvarez Sanchez, K. Lippuner, K.-S. Tsai, S.-T. Tu, J.-F. Chen, O. K.-S. Lee, W.-W. Hsu, N. V. Grygorieva, V. V. Povoroznyuk, M. O. Korzh, O. L. Loskutov, A. B. Chukov, R. Sarmiento, H. Thomas, H. Donnachie, I. Pavel-Knox, H. Shaw, H. Hassanin, E. E. A. Abdulhakim, N. Savani, G. A. Bachmann, E. Barrett-Connor, N. C. Binkley, H. G. Bone, D. M. Brandon, D. D. Checketts, N. J. Fraser, N. B. Watts, S. A. Geller, J. S. Gimbel, M. W. Greenwald, P. A. Holt, C. C. Johnston, C. Fang, D. P. Kiel, D. J. Klashman, E. M. Lewiecki, M. B. Lowenstein, M. R. McClung, S. M. Nattrass, A. Odio, J. Levengood, J. Romaguera, K. G. Saag, M. B. Sebai, B. Snyder, M. E. Kutner, D. Streja, E. P. Schwartz and M. G. Christiansen, *Lancet Diabetes Endocrinol.*, 2019, **7**, 899–911.

162 J. Canon, K. Rex, A. Y. Saiki, C. Mohr, K. Cooke, D. Bagal, K. Gaida, T. Holt, C. G.

Knutson, N. Koppada, B. A. Lanman, J. Werner, A. S. Rapaport, T. San Miguel, R. Ortiz, T. Osgood, J.-R. Sun, X. Zhu, J. D. McCarter, L. P. Volak, B. E. Houk, M. G. Fakih, B. H. O'Neil, T. J. Price, G. S. Falchook, J. Desai, J. Kuo, R. Govindan, D. S. Hong, W. Ouyang, H. Henary, T. Arvedson, V. J. Cee and J. R. Lipford, *Nature*, 2019, **575**, 217–223.

163 R. Lagoutte, R. Patouret and N. Winssinger, *Curr. Opin. Chem. Biol.*, 2017, **39**, 54–63.

164 S. Wu, H. Luo, H. Wang, W. Zhao, Q. Hu and Y. Yang, *Biochem. Biophys. Res. Commun.*, 2016, **478**, 1268–1273.

165 D. A. Shannon and E. Weerapana, *Curr. Opin. Chem. Biol.*, 2015, **24**, 18–26.

166 S. M. Marino and V. N. Gladyshev, *J. Mol. Biol.*, 2010, **404**, 902–916.

167 A. Cuesta and J. Taunton, *Annu. Rev. Biochem.*, 2019, **88**, 365–381.

168 S. E. Dalton and S. Campos, *ChemBioChem*, 2020, **21**, 1080–1100.

169 A. Keeley, L. Petri, P. Ábrányi-Balogh and G. M. Keserű, *Drug Discov. Today*, 2020, **25**, 983–996.

170 S.-S. Cheng, G.-J. Yang, W. Wang, C.-H. Leung and D.-L. Ma, *J. Hematol. Oncol.*, 2020, **13**, 26.

171 C. Chen and K.-W. Yang, *Eur. J. Med. Chem.*, 2020, **203**, 112573.

172 J. Pettinger, K. Jones and M. D. Cheeseman, *Angew. Chem. Int. Ed.*, 2017, **56**, 15200–15209.

173 G. Platzer, M. Okon and L. P. McIntosh, *J. Biomol. NMR*, 2014, **60**, 109–129.

174 P. W. Brian, P. J. Curtis, H. G. Hemming and G. L. F. Norris, *Trans. Br. Mycol. Soc.*, 1957, **40**, 365–368.

175 C. Drahl, B. F. Cravatt and E. J. Sorensen, *Angew. Chem. Int. Ed.*, 2005, **44**, 5788–5809.

176 E. H. Walker, M. E. Pacold, O. Perisic, L. Stephens, P. T. Hawkins, M. P. Wymann and R. L. Williams, *Mol. Cell*, 2000, **6**, 909–919.

177 M. P. Wymann, G. Bulgarelli-Leva, M. J. Zvelebil, L. Pirola, B. Vanhaesebroeck, M. D. Waterfield and G. Panayotou, *Mol. Cell. Biol.*, 1996, **16**, 1722–1733.

178 V. M. Bondar, B. Sweeney-Gotsch, M. Andreeff, G. B. Mills and D. J. McConkey, *Mol. Cancer Ther.*, 2002, **1**, 989–97.

179 B. Levy, A. Spira, D. Becker, T. Evans, I. Schnadig, D. R. Camidge, J. E. Bauman, D. Hausman, L. Walker, J. Nemunaitis, C. M. Rudin, B. Halmos and D. W. Bowles, *J. Thorac. Oncol.*, 2014, **9**, 1031–1035.

180 S. J. Hotte, A. M. Joshua, V. Torri, R. J. Macfarlane, N. S. Basappa, J. Powers, E. Winquist, S. Mukherjee, R. W. Gregg, C. K. Kollmannsberger, D. L. Finch, H. Xu, D. F. Hausman, L. Seymour, E. A. Eisenhauer and K. N. Chi, *J. Clin. Oncol.*, 2015, **33**, 279–279.

181 M. W. Pitz, E. A. Eisenhauer, M. V. MacNeil, B. Thiessen, J. C. Easaw, D. R. Macdonald, D. D. Eisenstat, A. S. Kakumanu, M. Salim, H. Chalchal, J. Squire, M. S. Tsao, S. Kamel-Reid, S. Banerji, D. Tu, J. Powers, D. F. Hausman and W. P. Mason, *Neuro. Oncol.*, 2015,

17, 1270–1274.

182 S. E. Dalton, L. Dittus, D. A. Thomas, M. A. Convery, J. Nunes, J. T. Bush, J. P. Evans, T. Werner, M. Bantscheff, J. A. Murphy and S. Campos, *J. Am. Chem. Soc.*, 2018, **140**, 932–939.

183 K. Down, A. Amour, I. R. Baldwin, A. W. J. Cooper, A. M. Deakin, L. M. Felton, S. B. Guntrip, C. Hardy, Z. A. Harrison, K. L. Jones, P. Jones, S. E. Keeling, J. Le, S. Livia, F. Lucas, C. J. Lunniss, N. J. Parr, E. Robinson, P. Rowland, S. Smith, D. A. Thomas, G. Vitulli, Y. Washio and J. N. Hamblin, *J. Med. Chem.*, 2015, **58**, 7381–7399.

184 N. N. Gushwa, S. Kang, J. Chen and J. Taunton, *J. Am. Chem. Soc.*, 2012, **134**, 20214–20217.

185 Y. Liu, A. Bishop, L. Witucki, B. Kraybill, E. Shimizu, J. Tsien, J. Ubersax, J. Blethrow, D. O. Morgan and K. M. Shokat, *Chem. Biol.*, 1999, **6**, 671–678.

186 A. E. Speers and B. F. Cravatt, *Chem. Biol.*, 2004, **11**, 535–546.

187 D. G. Isom, C. A. Castaneda, B. R. Cannon and B. Garcia-Moreno E., *Proc. Natl. Acad. Sci. U.S.A.*, 2011, **108**, 5260–5265.

188 E. Anscombe, E. Meschini, R. Mora-Vidal, S. R. Wedge, J. A. Endicott, R. J. Griffin, M. P. Martin, D. Staunton, M. Geitmann, U. H. Danielson, W. A. Stanley, L. Z. Wang, T. Reuillon, B. T. Golding, C. Cano, D. R. Newell and M. E. M. Noble, *Chem. Biol.*, 2015, **22**, 1159–1164.

189 M. Guha, *Nat. Rev. Drug Discov.*, 2012, **11**, 892–894.

190 T. G. Davies, J. Bentley, C. E. Arris, F. T. Boyle, N. J. Curtin, J. A. Endicott, A. E. Gibson, B. T. Golding, R. J. Griffin, I. R. Hardcastle, P. Jewsbury, L. N. Johnson, V. Mesguiche, D. R. Newell, M. E. M. Noble, J. A. Tucker, L. Wang and H. J. Whitfield, *Nat. Struct. Biol.*, 2002, **9**, 745–749.

191 F. U. Hartl, A. Bracher and M. Hayer-Hartl, *Nature*, 2011, **475**, 324–332.

192 E. Zorzi and P. Bonvini, *Cancers (Basel)*, 2011, **3**, 3921–3956.

193 J. Pettinger, Y. V. Le Bihan, M. Widya, R. L. M. van Montfort, K. Jones and M. D. Cheeseman, *Angew. Chem. Int. Ed.*, 2017, **56**, 3536–3540.

194 J. Pettinger, M. Carter, K. Jones and M. D. Cheeseman, *J. Med. Chem.*, 2019, **62**, 11383–11398.

195 N. Siddiqui and N. Sonenberg, *Biochem. Soc. Trans.*, 2015, **43**, 763–772.

196 W. Zhou, S. T. Quah, C. S. Verma, Y. Liu, D. P. Lane and C. J. Brown, *PLoS One*, 2012, **7**, e47235.

197 X. Wan, T. Yang, A. Cuesta, X. Pang, T. E. Balius, J. J. Irwin, B. K. Shoichet and J. Taunton, *J. Am. Chem. Soc.*, 2020, **142**, 4960–4964.

198 B. Ghosh, A. O. Benyumov, P. Ghosh, Y. Jia, S. Avdulov, P. S. Dahlberg, M. Peterson, K. Smith, V. A. Polunovsky, P. B. Bitterman and C. R. Wagner, *ACS Chem. Biol.*, 2009, **4**, 367–377.

199 P. Ghosh, C. Park, M. S. Peterson, P. B. Bitterman, V. A. Polunovsky and C. R. Wagner, *Bioorg. Med. Chem. Lett.*, 2005, **15**, 2177–2180.

200 X. Chen, D. J. Kopecky, J. Mihalic, S. Jeffries, X. Min, J. Heath, J. Deignan, S. Lai, Z. Fu, C. Guimaraes, S. Shen, S. Li, S. Johnstone, S. Thibault, H. Xu, M. Cardozo, W. Shen, N. Walker, F. Kayser and Z. Wang, *J. Med. Chem.*, 2012, **55**, 3837–3851.

201 G. Wei, A. A. Margolin, L. Haery, E. Brown, L. Cucolo, B. Julian, S. Shehata, A. L. Kung, R. Beroukhim and T. R. Golub, *Cancer Cell*, 2012, **21**, 547–562.

202 V. Palve, S. Mallick, G. Ghaisas, S. Kannan and T. Teni, *PLoS One*, 2014, **9**, e111927.

203 A. Ashkenazi, *Nat. Rev. Drug Discov.*, 2008, **7**, 1001–1012.

204 G. Akçay, M. A. Belmonte, B. Aquila, C. Chuaqui, A. W. Hird, M. L. Lamb, P. B. Rawlins, N. Su, S. Tentarelli, N. P. Grimster and Q. Su, *Nat. Chem. Biol.*, 2016, **12**, 931–936.

205 A. Friberg, D. Vigil, B. Zhao, R. N. Daniels, J. P. Burke, P. M. Garcia-Barrantes, D. Camper, B. A. Chauder, T. Lee, E. T. Olejniczak and S. W. Fesik, *J. Med. Chem.*, 2013, **56**, 15–30.

206 Q. L. Deveraux and J. C. Reed, *Genes Dev.*, 1999, **13**, 239–52.

207 G. S. Salvesen and C. S. Duckett, *Nat. Rev. Mol. Cell Biol.*, 2002, **3**, 401–410.

208 M. Hrdinka and M. Yabal, *Genes Immun.*, 2019, **20**, 641–650.

209 I. Tamm, S. M. Kornblau, H. Segall, S. Krajewski, K. Welsh, S. Kitada, D. A. Scudiero, G. Tudor, Y. H. Qui, A. Monks, M. Andreeff and J. C. Reed, *Clin. Cancer Res.*, 2000, **6**, 1796–1803.

210 Y. Nakagawa, S. Abe, M. Kurata, M. Hasegawa, K. Yamamoto, M. Inoue, T. Takemura, K. Suzuki and M. Kitagawa, *Am. J. Hematol.*, 2006, **81**, 824–831.

211 R. Mannhold, S. Fulda and E. Carosati, *Drug Discov. Today*, 2010, **15**, 210–219.

212 R. B. Lopes, R. Gangeswaran, I. A. McNeish, Y. Wang and N. R. Lemoine, *Int. J. Cancer*, 2007, **120**, 2344–2352.

213 Y. Mizutani, H. Nakanishi, Y. Li, H. Matsubara, K. Yamamoto, N. Sato, T. Shiraishi, T. Nakamura, K. Mikami, K. Okihara, N. Takaha, O. Ukimura, A. Kawauchi, N. Nonomura, B. Bonavida and T. Miki, *Int. J. Oncol.*, 2007, **30**, 919–925.

214 C. Baggio, L. Gambini, P. Udompholkul, A. F. Salem, A. Aronson, A. Dona, E. Troadec, F. Pichiorri and M. Pellecchia, *J. Med. Chem.*, 2018, **61**, 6350–6363.

215 C. Baggio, P. Udompholkul, L. Gambini, A. F. Salem, J. Jossart, J. J. P. Perry and M. Pellecchia, *J. Med. Chem.*, 2019, **62**, 9188–9200.

216 L. Gambini, C. Baggio, P. Udompholkul, J. Jossart, A. F. Salem, J. J. P. Perry and M. Pellecchia, *J. Med. Chem.*, 2019, **62**, 5616–5627.

217 A. J. Huhn, R. M. Guerra, E. P. Harvey, G. H. Bird and L. D. Walensky, *Cell Chem. Biol.*, 2016, **23**, 1123–1134.

218 R. S. Schwartz, *N. Engl. J. Med.*, 2004, **350**, 1079–1080.

219 R. V. J. Chari, *Acc. Chem. Res.*, 2008, **41**, 98–107.

220 S. Jaracz, J. Chen, L. V. Kuznetsova and I. Ojima, *Bioorg. Med. Chem.*, 2005, **13**, 5043–5054.

221 M. Ritchie, L. Tchistiakova and N. Scott, *MAbs*, 2013, **5**, 13–21.

222 S. Xu, *Pharm. Res.*, 2015, **32**, 3577–3583.

223 H. Bouchard, C. Viskov and C. Garcia-Echeverria, *Bioorg. Med. Chem. Lett.*, 2014, **24**, 5357–5363.

224 S. Sau, H. O. Alsaab, S. K. Kashaw, K. Tatiparti and A. K. Iyer, *Drug Discov. Today*, 2017, **22**, 1547–1556.

225 A. Beck, L. Goetsch, C. Dumontet and N. Corvaïa, *Nat. Rev. Drug Discov.*, 2017, **16**, 315–337.

226 G. Mathe, L. O. C. Tran Ba and J. Bernard, *C. R. Hebd. Seances Acad. Sci.*, 1958, **246**, 1626–1628.

227 K. C. Nicolaou and S. Rigol, *Angew. Chem. Int. Ed.*, 2019, **58**, 11206–11241.

228 P. F. Bross, J. Beitz, G. Chen, X. H. Chen, E. Duffy, L. Kieffer, S. Roy, R. Sridhara, A. Rahman, G. Williams and R. Pazdur, *Clin. Cancer Res.*, 2001, **7**, 1490–6.

229 S. H. Petersdorf, K. J. Kopecky, M. Slovak, C. Willman, T. Nevill, J. Brandwein, R. A. Larson, H. P. Erba, P. J. Stiff, R. K. Stuart, R. B. Walter, M. S. Tallman, L. Stenke and F. R. Appelbaum, *Blood*, 2013, **121**, 4854–4860.

230 P. Zhao, Y. Zhang, W. Li, C. Jeanty, G. Xiang and Y. Dong, *Acta Pharm. Sin. B*, 2020, **10**, 1589–1600.

231 F. R. Appelbaum and I. D. Bernstein, *Blood*, 2017, **130**, 2373–2376.

232 E. Y. Jen, C.-W. Ko, J. E. Lee, P. L. Del Valle, A. Aydanian, C. Jewell, K. J. Norsworthy, D. Przepiorka, L. Nie, J. Liu, C. M. Sheth, M. Shapiro, A. T. Farrell and R. Pazdur, *Clin. Cancer Res.*, 2018, **24**, 3242–3246.

233 N. W. C. J. van de Donk and E. Dhimolea, *MAbs*, 2012, **4**, 458–465.

234 P. F. Peddi and S. A. Hurvitz, *Futur. Oncol.*, 2013, **9**, 319–326.

235 J. M. Lambert and R. V. J. Chari, *J. Med. Chem.*, 2014, **57**, 6949–6964.

236 G. von Minckwitz, C.-S. Huang, M. S. Mano, S. Loibl, E. P. Mamounas, M. Untch, N. Wolmark, P. Rastogi, A. Schneeweiss, A. Redondo, H. H. Fischer, W. Jacot, A. K. Conlin, C. Arce-Salinas, I. L. Wapnir, C. Jackisch, M. P. DiGiovanna, P. A. Fasching, J. P. Crown, P. Wülfing, Z. Shao, E. Rota Caremoli, H. Wu, L. H. Lam, D. Tesarowski, M. Smitt, H. Douthwaite, S. M. Singel and C. E. Geyer, *N. Engl. J. Med.*, 2019, **380**, 617–628.

237 Y. N. Lamb, *Drugs*, 2017, **77**, 1603–1610.

238 H. Tilly, F. Morschhauser, N. L. Bartlett, A. Mehta, G. Salles, C. Haioun, J. Munoz, A. I. Chen, K. Kolibaba, D. Lu, M. Yan, E. Penuel, J. Hirata, C. Lee and J. P. Sharman, *Lancet Oncol.*, 2019, **20**, 998–1010.

239 L. H. Sehn, A. F. Herrera, M. J. Matasar, M. Kamdar, S. Assouline, M. Hertzberg, T. M. Kim, W.-S. Kim, A. McMillan, M. Özcan, J. M. Hirata, E. Penuel, J. Cheng, G. Ku and C. R. Flowers, *Blood*, 2018, **132**, 1683–1683.

240 P. M. Challita-Eid, D. Satpayev, P. Yang, Z. An, K. Morrison, Y. Shostak, A. Raitano, R. Nadell, W. Liu, D. R. Lortie, L. Capo, A. Verlinsky, M. Leavitt, F. Malik, H. Avina, C. I. Guevara, N. Dinh, S. Karki, B. S. Anand, D. S. Pereira, I. B. J. Joseph, F. Donate, K. Morrison and D. R. Stover, *Cancer Res.*, 2016, **76**, 3003–3013.

241 T. K. Burki, *Lancet Oncol.*, 2020, **21**, e133.

242 Y. Ogitani, T. Aida, K. Hagihara, J. Yamaguchi, C. Ishii, N. Harada, M. Soma, H. Okamoto, M. Oitate, S. Arakawa, T. Hirai, R. Atsumi, T. Nakada, I. Hayakawa, Y. Abe and T. Agatsuma, *Clin. Cancer Res.*, 2016, **22**, 5097–5108.

243 T. N. Iwata, C. Ishii, S. Ishida, Y. Ogitani, T. Wada and T. Agatsuma, *Mol. Cancer Ther.*, 2018, **17**, 1494–1503.

244 K. Shitara, Y.-J. Bang, S. Iwasa, N. Sugimoto, M.-H. Ryu, D. Sakai, H.-C. Chung, H. Kawakami, H. Yabusaki, J. Lee, K. Saito, Y. Kawaguchi, T. Kamio, A. Kojima, M. Sugihara and K. Yamaguchi, *N. Engl. J. Med.*, 2020, **382**, 2419–2430.

245 S. Modi, C. Saura, T. Yamashita, Y. H. Park, S.-B. Kim, K. Tamura, F. Andre, H. Iwata, Y. Ito, J. Tsurutani, J. Sohn, N. Denduluri, C. Perrin, K. Aogi, E. Tokunaga, S.-A. Im, K. S. Lee, S. A. Hurvitz, J. Cortes, C. Lee, S. Chen, L. Zhang, J. Shahidi, A. Yver and I. Krop, *N. Engl. J. Med.*, 2020, **382**, 610–621.

246 W. Dong, J. Shi, T. Yuan, B. Qi, J. Yu, J. Dai and L. He, *Eur. J. Med. Chem.*, 2019, **167**, 583–593.

247 T. M. Cardillo, S. V. Govindan, R. M. Sharkey, P. Trisal, R. Arrojo, D. Liu, E. A. Rossi, C.-H. Chang and D. M. Goldenberg, *Bioconjug. Chem.*, 2015, **26**, 919–931.

248 R. M. Sharkey, W. J. McBride, T. M. Cardillo, S. V. Govindan, Y. Wang, E. A. Rossi, C.-H. Chang and D. M. Goldenberg, *Clin. Cancer Res.*, 2015, **21**, 5131–5138.

249 D. M. Goldenberg and R. M. Sharkey, *Expert Opin. Biol. Ther.*, 2020, **20**, 871–885.

250 S. Lonial, H. C. Lee, A. Badros, S. Trudel, A. K. Nooka, A. Chari, A.-O. Abdallah, N. Callander, N. Lendvai, D. Sborov, A. Suvannasankha, K. Weisel, L. Karlin, E. Libby, B. Arnulf, T. Facon, C. Hulin, K. M. Kortüm, P. Rodríguez-Otero, S. Z. Usmani, P. Hari, R. Baz, H. Quach, P. Moreau, P. M. Voorhees, I. Gupta, A. Hoos, E. Zhi, J. Baron, T. Piontek, E. Lewis, R. C. Jewell, E. J. Dettman, R. Popat, S. D. Esposti, J. Opalinska, P. Richardson and A. D. Cohen, *Lancet Oncol.*, 2020, **21**, 207–221.

251 Y.-T. Tai, P. A. Mayes, C. Acharya, M. Y. Zhong, M. Cea, A. Cagnetta, J. Craigen, J. Yates, L. Gliddon, W. Fieles, B. Hoang, J. Tunstead, A. L. Christie, A. L. Kung, P. Richardson, N. C. Munshi and K. C. Anderson, *Blood*, 2014, **123**, 3128–3138.

252 V. Chudasama, A. Maruani and S. Caddick, *Nat. Chem.*, 2016, **8**, 114–119.

253 H. Liu and K. May, *MAbs*, 2012, **4**, 17–23.

254 B. Heyman, *Immunol. Lett.*, 1996, **54**, 195–199.

255 P. Agarwal and C. R. Bertozzi, *Bioconjug. Chem.*, 2015, **26**, 176–192.

256 C. Lo Nigro, M. Macagno, D. Sangiolo, L. Bertolaccini, M. Aglietta and M. C. Merlano, *Ann. Transl. Med.*, 2019, **7**, 105.

257 J. M. Woof and D. R. Burton, *Nat. Rev. Immunol.*, 2004, **4**, 89–99.

258 C. H. Chau, P. S. Steeg and W. D. Figg, *Lancet*, 2019, **394**, 793–804.

259 P. Khongorzul, C. J. Ling, F. U. Khan, A. U. Ihsan and J. Zhang, *Mol. Cancer Res.*, 2020, **18**, 3–19.

260 J. R. McCombs and S. C. Owen, *AAPS J.*, 2015, **17**, 339–351.

261 N. Jain, S. W. Smith, S. Ghone and B. Tomczuk, *Pharm. Res.*, 2015, **32**, 3526–3540.

262 K. Tsuchikama and Z. An, *Protein Cell*, 2018, **9**, 33–46.

263 B. Q. Shen, K. Xu, L. Liu, H. Raab, S. Bhakta, M. Kenrick, K. L. Parsons-Reponte, J. Tien, S. F. Yu, E. Mai, D. Li, J. Tibbitts, J. Baudys, O. M. Saad, S. J. Scales, P. J. McDonald, P. E. Hass, C. Eigenbrot, T. Nguyen, W. A. Solis, R. N. Fuji, K. M. Flagella, D. Patel, S. D. Spencer, L. A. Khawli, A. Ebens, W. L. Wong, R. Vandlen, S. Kaur, M. X. Sliwkowski, R. H. Scheller, P. Polakis and J. R. Junutula, *Nat. Biotechnol.*, 2012, **30**, 184–189.

264 T. H. Pillow, J. D. Sadowsky, D. Zhang, S. F. Yu, G. Del Rosario, K. Xu, J. He, S. Bhakta, R. Ohri, K. R. Kozak, E. Ha, J. R. Junutula and J. A. Flygare, *Chem. Sci.*, 2016, **8**, 366–370.

265 L. Wang, G. Amphlett, W. A. Blättler, J. M. Lambert and W. Zhang, *Protein Sci.*, 2005, **14**, 2436–2446.

266 F. Bryden, A. Maruani, H. Savoie, V. Chudasama, M. E. B. Smith, S. Caddick and R. W. Boyle, *Bioconjug. Chem.*, 2014, **25**, 611–617.

267 C. R. Behrens, E. H. Ha, L. L. Chinn, S. Bowers, G. Probst, M. Fitch-Bruhns, J. Monteon, A. Valdiosera, A. Bermudez, S. Liao-Chan, T. Wong, J. Melnick, J. W. Theunissen, M. R. Flory, D. Houser, K. Venstrom, Z. Levashova, P. Sauer, T. S. Migone, E. H. Van Der Horst, R. L. Halcomb and D. Y. Jackson, *Mol. Pharm.*, 2015, **12**, 3986–3998.

268 A. Maruani, M. E. B. Smith, E. Miranda, K. A. Chester, V. Chudasama and S. Caddick, *Nat. Commun.*, 2015, **6**, 2–10.

269 S. J. Walsh, S. Omarjee, W. R. J. D. Galloway, T. T.-L. Kwan, H. F. Sore, J. S. Parker, M. Hyvönen, J. S. Carroll and D. R. Spring, *Chem. Sci.*, 2019, **10**, 694–700.

270 S. O. Doronina, B. A. Mendelsohn, T. D. Bovee, C. G. Cerveny, S. C. Alley, D. L. Meyer, E. Oflazoglu, B. E. Toki, R. J. Sanderson, R. F. Zabinski, A. F. Wahl and P. D. Senter, *Bioconjug. Chem.*, 2006, **17**, 114–124.

271 G. Wu, Y.-Z. Fang, S. Yang, J. R. Lupton and N. D. Turner, *J. Nutr.*, 2004, **134**, 489–492.

272 B. J. Mills and C. A. Lang, *Biochem. Pharmacol.*, 1996, **52**, 401–406.

273 W. Widdison, S. Wilhelm, K. Veale, J. Costoplus, G. Jones, C. Audette, B. Leece, L. Bartle, Y. Kovtun and R. Chari, *Mol. Pharm.*, 2015, **12**, 1762–1773.

274 J. D. Bargh, A. Isidro-Llobet, J. S. Parker and D. R. Spring, *Chem. Soc. Rev.*, 2019, **48**,

4361–4374.

275 C. S. Gondi and J. S. Rao, *Expert Opin. Ther. Targets*, 2013, **17**, 281–291.

276 S. O. Doronina, B. E. Toki, M. Y. Torgov, B. A. Mendelsohn, C. G. Cerveny, D. F. Chace, R. L. DeBlanc, R. P. Gearing, T. D. Bovee, C. B. Siegall, J. A. Francisco, A. F. Wahl, D. L. Meyer and P. D. Senter, *Nat. Biotechnol.*, 2003, **21**, 778–784.

277 G. M. Dubowchik, R. A. Firestone, L. Padilla, D. Willner, S. J. Hofstead, K. Mosure, J. O. Knipe, S. J. Lasch and P. A. Trail, *Bioconjug. Chem.*, 2002, **13**, 855–869.

278 S. C. Jeffrey, M. T. Nguyen, J. B. Andreyka, D. L. Meyer, S. O. Doronina and P. D. Senter, *Bioorg. Med. Chem. Lett.*, 2006, **16**, 358–362.

279 B. Wei, J. Gunzner-Toste, H. Yao, T. Wang, J. Wang, Z. Xu, J. Chen, J. Wai, J. Nonomiya, S. P. Tsai, J. Chuh, K. R. Kozak, Y. Liu, S. F. Yu, J. Lau, G. Li, G. D. Phillips, D. Leipold, A. Kamath, D. Su, K. Xu, C. Eigenbrot, S. Steinbacher, R. Ohri, H. Raab, L. R. Staben, G. Zhao, J. A. Flygare, T. H. Pillow, V. Verma, L. A. Masterson, P. W. Howard and B. Safina, *J. Med. Chem.*, 2018, **61**, 989–1000.

280 Y. Wang, S. Fan, W. Zhong, X. Zhou and S. Li, *Int. J. Mol. Sci.*, 2017, **18**, 1860.

281 P. J. Burke, P. D. Senter, D. W. Meyer, J. B. Miyamoto, M. Anderson, B. E. Toki, G. Manikumar, M. C. Wani, D. J. Kroll and S. C. Jeffrey, *Bioconjug. Chem.*, 2009, **20**, 1242–1250.

282 S. Kolodych, C. Michel, S. Delacroix, O. Koniev, A. Ehkirch, J. Eberova, S. Cianférani, B. Renoux, W. Krezel, P. Poinot, C. D. Muller, S. Papot and A. Wagner, *Eur. J. Med. Chem.*, 2017, **142**, 376–382.

283 S. C. Jeffrey, J. B. Andreyka, S. X. Bernhardt, K. M. Kissler, T. Kline, J. S. Lenox, R. F. Moser, M. T. Nguyen, N. M. Okeley, I. J. Stone, X. Zhang and P. D. Senter, *Bioconjug. Chem.*, 2006, **17**, 831–840.

284 J. C. Kern, M. Cancilla, D. Dooney, K. Kwasnjuk, R. Zhang, M. Beaumont, I. Figueroa, S. C. Hsieh, L. Liang, D. Tomazela, J. Zhang, P. E. Brandish, A. Palmieri, P. Stivers, M. Cheng, G. Feng, P. Geda, S. Shah, A. Beck, D. Bresson, J. Firdos, D. Gately, N. Knudsen, A. Manibusan, P. G. Schultz, Y. Sun and R. M. Garbaccio, *J. Am. Chem. Soc.*, 2016, **138**, 1430–1445.

285 J. D. Bargh, S. J. Walsh, A. Isidro-Llobet, S. Omarjee, J. S. Carroll and D. R. Spring, *Chem. Sci.*, 2020, **11**, 2375–2380.

286 P. A. Trail, D. Willner, S. J. Lasch, A. J. Henderson, S. Hofstead, A. M. Casazza, R. A. Firestone, I. Hellström and K. E. Hellström, *Science*, 1993, **261**, 212–215.

287 L. Ducry and B. Stump, *Bioconjug. Chem.*, 2010, **21**, 5–13.

288 R. V. J. Chari, *Adv. Drug Deliv. Rev.*, 1998, **31**, 89–104.

289 A. A. Epenetos, D. Snook, H. Durbin, P. M. Johnson and J. Taylor-Papadimitriou, *Cancer Res.*, 1986, **46**, 3183–3191.

290 M. Abdollahpour-Alitappeh, M. Lotfinia, T. Gharibi, J. Mardaneh, B. Farhadihosseinabadi, P. Larki, B. Faghfourian, K. S. Sepehr, K. Abbaszadeh-Goudarzi,

G. Abbaszadeh-Goudarzi, B. Johari, M. R. Zali and N. Bagheri, *J. Cell. Physiol.*, 2019, **234**, 5628–5642.

291 S. Yaghoubi, M. H. Karimi, M. Lotfinia, T. Gharibi, M. Mahi-Birjand, E. Kavi, F. Hosseini, K. Sineh Sepehr, M. Khatami, N. Bagheri and M. Abdollahpour-Alitappeh, *J. Cell. Physiol.*, 2020, **235**, 31–64.

292 K. Cheung-Ong, G. Giaever and C. Nislow, *Chem. Biol.*, 2013, **20**, 648–659.

293 M. D. Lee, T. S. Dunne, C. C. Chang, M. M. Siegel, G. O. Morton, G. A. Ellestad, W. J. McGahren and D. B. Borders, *J. Am. Chem. Soc.*, 1992, **114**, 985–997.

294 M. D. Lee, T. S. Dunne, C. C. Chang, G. A. Ellestad, M. M. Siegel, G. O. Morton, W. J. Mcgahren and D. B. Borders, *J. Am. Chem. Soc.*, 1987, **109**, 3466–3468.

295 M. D. Lee, T. S. Dunne, M. M. Siegel, G. O. Morton, D. B. Borders and C. C. Chang, *J. Am. Chem. Soc.*, 1987, **109**, 3464–3466.

296 M. D. Lee, G. A. Ellestad and D. B. Borders, *Acc. Chem. Res.*, 1991, **24**, 235–243.

297 Y. Fu and M. Ho, *Antib. Ther.*, 2018, **1**, 43–53.

298 R. G. Dushin, in *Cytotoxic Payloads for Antibody–Drug Conjugates*, eds. D. E. Thurston and P. J. M. Jackson, Royal Society of Chemistry, 2019, pp. 259–278.

299 K. C. Nicolaou, C. W. Hummel, E. N. Pitsinos, M. Nakada, A. L. Smith, K. Shibayama and H. Saimoto, *J. Am. Chem. Soc.*, 1992, **114**, 10082–10084.

300 S. A. Hitchcock, S. H. Boyer, M. Y. Chu-Moyer, S. H. Olson and S. J. Danishefsky, *Angew. Chem. Int. Ed.*, 1994, **33**, 858–862.

301 W. Leimgruber, V. Stefanovic, F. Schenker, A. Karr and J. Berger, *J. Am. Chem. Soc.*, 1965, **87**, 5791–5793.

302 M. Smellie, D. S. Bose, A. S. Thompson, T. C. Jenkins, J. A. Hartley and D. E. Thurston, *Biochemistry*, 2003, **42**, 8232–8239.

303 D. Antonow and D. E. Thurston, *Chem. Rev.*, 2011, **111**, 2815–2864.

304 J. Mantaj, P. J. M. Jackson, K. M. Rahman and D. E. Thurston, *Angew. Chem. Int. Ed.*, 2017, **56**, 462–488.

305 D. S. Bose, A. S. Thompson, J. Ching, J. A. Hartley, M. D. Berardini, T. C. Jenkins, S. Neidle, L. H. Hurley and D. E. Thurston, *J. Am. Chem. Soc.*, 1992, **114**, 4939–4941.

306 S. M. Guichard, J. S. Macpherson, D. E. Thurston and D. I. Jodrell, *Eur. J. Cancer*, 2005, **41**, 1811–1818.

307 S. J. Gregson, A. C. Tiberghien, L. A. Masterson and P. W. Howard, in *Cytotoxic Payloads for Antibody–Drug Conjugates*, eds. D. E. Thurston and P. J. M. Jackson, 2019, pp. 296–331.

308 F. Zammarchi, S. Corbett, L. Adams, P. C. Tyrer, K. Kiakos, N. Janghra, T. Marafioti, C. E. Britten, C. E. G. Havenith, S. Chivers, F. D'Hooge, D. G. Williams, A. Tiberghien, P. W. Howard, J. A. Hartley and P. H. Van Berkel, *Blood*, 2018, **131**, 1094–1105.

309 A. C. Tiberghien, J.-N. Levy, L. A. Masterson, N. V. Patel, L. R. Adams, S. Corbett, D. G. Williams, J. A. Hartley and P. W. Howard, *ACS Med. Chem. Lett.*, 2016, **7**, 983–987.

310 L. J. Haňka, A. Dietz, S. A. Gerpheide, S. L. Kuentzel and D. G. Martin, *J. Antibiot.*, 1978, **31**, 1211–1217.

311 A. M. Beekman, M. M. D. Cominetti and M. Searcey, in *Cytotoxic Payloads for Antibody–Drug Conjugates*, eds. D. E. Thurston and P. J. M. Jackson, 2019, pp. 187–208.

312 D. L. Boger and D. S. Johnson, *Angew. Chem. Int. Ed.*, 1996, **35**, 1438–1474.

313 J. P. McGovren, G. L. Clarke, E. A. Pratt and T. F. Dekoning, *J. Antibiot.*, 1984, **37**, 63–70.

314 M. M. C. Van Der Lee, P. G. Groothuis, R. Ubink, M. A. J. Van Der Vleuten, T. A. Van Achterberg, E. M. Loosveld, D. Damming, D. C. H. Jacobs, M. Rouwette, D. F. Egging, D. Van Den Dobbelsteen, P. H. Beusker, P. Goedings, G. F. M. Verheijden, J. M. Lemmens, M. Timmers and W. H. A. Dokter, *Mol. Cancer Ther.*, 2015, **14**, 692–703.

315 R. C. Elgersma, R. G. E. Coumans, T. Huijbregts, W. M. P. B. Menge, J. A. F. Joosten, H. J. Spijker, F. M. H. de Groot, M. M. C. van der Lee, R. Ubink, D. J. van den Dobbelsteen, D. F. Egging, W. H. A. Dokter, G. F. M. Verheijden, J. M. Lemmens, C. M. Timmers and P. H. Beusker, *Mol. Pharm.*, 2015, **12**, 1813–1835.

316 M. Nadal-Serrano, B. Morancho, S. Escrivá-de-Romaní, C. Bernadó Morales, A. Luque, M. Escorihuela, M. Espinosa Bravo, V. Peg, F. A. Dijcks, W. H. A. Dokter, J. Cortés, C. Saura and J. Arribas, *Cancers (Basel)*, 2020, **12**, 670.

317 M. E. Wall, M. C. Wani, C. E. Cook, K. H. Palmer, A. T. McPhail and G. A. Sim, *J. Am. Chem. Soc.*, 1966, **88**, 3888–3890.

318 Y. Pommier, *Nat. Rev. Cancer*, 2006, **6**, 789–802.

319 S. V. Govindan, T. M. Cardillo and D. M. Goldenberg, in *Cytotoxic Payloads for Antibody–Drug Conjugates*, eds. D. E. Thurston and P. J. M. Jackson, 2019, pp. 166–186.

320 J. P. Armand, M. Ducreux, M. Mahjoubi, D. Abigerges, R. Bugat, G. Chabot, P. Herait, M. de Forni and P. Rougier, *Eur. J. Cancer*, 1995, **31**, 1283–1287.

321 Y. Kawato, M. Aonuma, Y. Hirota, H. Kuga and K. Sato, *Cancer Res.*, 1991, **51**, 4187–4191.

322 Y. Shimizu, H. Nagata, Y. Kikuchi, S. Umezawa, K. Hasumi and T. Yokokura, *Oncol. Rep.*, 1998, **5**, 99–101.

323 S. Sawada, S. Okajima, R. Aiyama, K. Nokata, T. Furuta, T. Yokokura, E. Sugino, K. Yamaguchi and T. Miyasaka, *Chem. Pharm. Bull. (Tokyo).*, 1991, **39**, 1446–1454.

324 Y.-S. Yao, J.-L. Liu, J. Xi, B. Miu, G.-S. Liu, S. Wang, L. Meng and Z.-J. Yao, *Chem. - Eur. J.*, 2011, **17**, 10462–10469.

325 M. Ishii, M. Iwahana, I. Mitsui, M. Minami, S. Imagawa, A. Tohgo and A. Ejima, *Anticancer. Drugs*, 2000, **11**, 353–362.

326 N. Joto, M. Ishii, M. Minami, H. Kuga, I. Mitsui and A. Tohgo, *Int. J. Cancer*, 1997, **72**,

680–686.

327 S. Takiguchi, E. Kumazawa, T. Shimazoe, A. Tohgo and A. Kono, *Japanese J. Cancer Res.*, 1997, **88**, 760–769.

328 I. Mitsui, E. Kumazawa, Y. Hirota, M. Aonuma, M. Sugimori, S. Ohsuki, K. Uoto, A. Ejima, H. Terasawa and K. Sato, *Japanese J. Cancer Res.*, 1995, **86**, 776–782.

329 WO 2019/044946 A1, 2019.

330 K. E. Henegar, S. W. Ashford, T. A. Baughman, J. C. Sih and R. L. Gu, *J. Org. Chem.*, 1997, **62**, 6588–6597.

331 M. A. Jordan and L. Wilson, *Nat. Rev. Cancer*, 2004, **4**, 253–265.

332 C. Dumontet and M. A. Jordan, *Nat. Rev. Drug Discov.*, 2010, **9**, 790–803.

333 S. O. Doronina and P. D. Senter, in *Cytotoxic Payloads for Antibody–Drug Conjugates*, eds. D. E. Thurston and P. J. M. Jackson, 2019, pp. 73–99.

334 G. R. Pettit, Y. Kamano, C. L. Herald, A. A. Tuinman, F. E. Boettner, H. Kizu, J. M. Schmidt, L. Baczynskyi, K. B. Tomer and R. J. Bontems, *J. Am. Chem. Soc.*, 1987, **109**, 6883–6885.

335 R. Bai, G. R. Petit and E. Hamel, *Biochem. Pharmacol.*, 1990, **39**, 1941–1949.

336 R. Bai, M. C. Roach, S. K. Jayaram, J. Barkoczy, G. R. Pettit, R. F. Luduena and E. Hamel, *Biochem. Pharmacol.*, 1993, **45**, 1503–1515.

337 N. Diamantis and U. Banerji, *Br. J. Cancer*, 2016, **114**, 362–367.

338 F. Li, K. K. Emmerton, M. Jonas, X. Zhang, J. B. Miyamoto, J. R. Setter, N. D. Nicholas, N. M. Okeley, R. P. Lyon, D. R. Benjamin and C. L. Law, *Cancer Res.*, 2016, **76**, 2710–2719.

339 WO 02/088172 A2, 2002.

340 G. R. Pettit, D. D. Burkett, J. Barkóczy, G. L. Breneman and W. E. Pettit, *Synthesis*, 1996, **1996**, 719–725.

341 G. R. Pettit, D. D. Burkett and M. D. Williams, *J. Chem. Soc., Perkin Trans. 1*, 1996, 853–858.

342 S. M. Kupchan, Y. Komoda, W. A. Court, G. J. Thomas, R. M. Smith, A. Karim, C. J. Gilmore, R. C. Haltiwanger and R. F. Bryan, *J. Am. Chem. Soc.*, 1972, **94**, 1354–1356.

343 E. Hamel, *Pharmacol. Ther.*, 1992, **55**, 31–51.

344 W. C. Widdison, S. D. Wilhelm, E. E. Cavanagh, K. R. Whiteman, B. A. Leece, Y. Kovtun, V. S. Goldmacher, H. Xie, R. M. Steeves, R. J. Lutz, R. Zhao, L. Wang, W. A. Blättler and R. V. J. Chari, *J. Med. Chem.*, 2006, **49**, 4392–4408.

345 R. H. Blum and T. Kahlert, *Cancer Treat. Rep.*, 1978, **62**, 435–438.

346 W. C. Widdison, in *Cytotoxic Payloads for Antibody–Drug Conjugates*, eds. D. E. Thurston and P. J. M. Jackson, 2019, pp. 100–116.

347 O. Ab, K. R. Whiteman, L. M. Bartle, X. Sun, R. Singh, D. Tavares, A. La Belle, G. Payne, R. J. Lutz, J. Pinkas, V. S. Goldmacher, T. Chittenden and J. M. Lambert, *Mol. Cancer Ther.*, 2015, **14**, 1605–1613.

348 D. M. O'Malley, U. A. Matulonis, M. J. Birrer, C. M. Castro, L. Gilbert, I. Vergote, L. P. Martin, G. M. Mantia-Smaldone, A. G. Martin, R. Bratos, R. T. Penson, K. Malek and K. N. Moore, *Gynecol. Oncol.*, 2020, **157**, 379–385.

349 E. J. Corey, L. O. Weigel, A. R. Chamberlin, H. Cho and D. H. Hua, *J. Am. Chem. Soc.*, 1980, **102**, 6613–6615.

350 J. Y. Li, S. R. Perry, V. Muniz-Medina, X. Wang, L. K. Wetzel, M. C. Rebelatto, M. J. M. Hinrichs, B. Z. Bezabeh, R. L. Fleming, N. Dimasi, H. Feng, D. Toader, A. Q. Yuan, L. Xu, J. Lin, C. Gao, H. Wu, R. Dixit, J. K. Osbourn and S. R. Coats, *Cancer Cell*, 2016, **29**, 117–129.

351 M. Pegram, E. Hamilton, A. R. Tan, A. M. Storniolo, N. Elgeioushi, S. Marshall, S. Abdullah and M. Patel, *Ann. Oncol.*, 2018, **29**, iii8.

352 M. L. Miller, M. Shizuka, A. Wilhelm, P. Salomon, E. E. Reid, L. Lanieri, S. Sikka, E. K. Maloney, L. Harvey, Q. Qiu, K. E. Archer, C. Bai, D. Vitharana, L. Harris, R. Singh, J. F. Ponte, N. C. Yoder, Y. Kovtun, K. C. Lai, O. Ab, J. Pinkas, T. A. Keating and R. V. J. Chari, *Mol. Cancer Ther.*, 2018, **17**, 650–660.

353 J. Ko, C. Breunig, V. Figueroa, N. Lehners, A. Baumann, A. Pálfi, C. Müller, C. Lutz, T. Hechler, M. Kulke, C. Müller-Tidow, H. Goldschmidt, A. Pahl and M. S. Raab, *Blood*, 2017, **130**, 3070.

354 S. Puthenveetil, F. Loganzo, H. He, K. Dirico, M. Green, J. Teske, S. Musto, T. Clark, B. Rago, F. Koehn, R. Veneziale, H. Falahaptisheh, X. Han, F. Barletta, J. Lucas, C. Subramanyam, C. J. O'Donnell, L. N. Tumey, P. Sapra, H. P. Gerber, D. Ma and E. I. Graziani, *Bioconjug. Chem.*, 2016, **27**, 1880–1888.

355 R. Talpir, Y. Benayahu, Y. Kashman, L. Pannell and M. Schleyer, *Tetrahedron Lett.*, 1994, **35**, 4453–4456.

356 H. J. Anderson, J. E. Coleman, R. J. Andersen and M. Roberge, *Cancer Chemother. Pharmacol.*, 1997, **39**, 223–226.

357 J. E. Coleman, E. Dilip de Silva, F. Kong, R. J. Andersen and T. M. Allen, *Tetrahedron*, 1995, **51**, 10653–10662.

358 F. Loganzo, C. M. Discafani, T. Annable, C. Beyer, S. Musto, M. Hari, X. Tan, C. Hardy, R. Hernandez, M. Baxter, T. Singanallore, G. Khafizova, M. S. Poruchynsky, T. Fojo, J. A. Nieman, S. Ayral-Kaloustian, A. Zask, R. J. Andersen and L. M. Greenberger, *Cancer Res.*, 2003, **63**, 1838–45.

359 J. A. Nieman, J. E. Coleman, D. J. Wallace, E. Piers, L. Y. Lim, M. Roberge and R. J. Andersen, *J. Nat. Prod.*, 2003, **66**, 183–199.

360 A. Zask, G. Birnberg, K. Cheung, J. Kaplan, C. Niu, E. Norton, R. Suayan, A. Yamashita, D. Cole, Z. Tang, G. Krishnamurthy, R. Williamson, G. Khafizova, S. Musto, R. Hernandez, T. Annable, X. Yang, C. Discafani, C. Beyer, L. M. Greenberger, F. Loganzo

and S. Ayral-Kaloustian, *J. Med. Chem.*, 2004, **47**, 4774–4786.

361 D. Williams, W. Strangman, M. Roberge, D. G. I. Kingston and D. J. Newman, in *Anticancer Agents from Natural Products, Second Edition*, eds. G. M. Cragg, D. G. I. Kingston and D. J. Newman, CRC Press, 2011, pp. 347–362.

362 D. J. Newman, *Mar. Drugs*, 2019, **17**, 324.

363 R. J. Andersen, J. E. Coleman, E. Piers and D. J. Wallace, *Tetrahedron Lett.*, 1997, **38**, 317–320.

364 E. Vedejs and C. Kongkittingam, *J. Org. Chem.*, 2001, **66**, 7355–7364.

365 J. H. Lang, P. G. Jones and T. Lindel, *Chem. - Eur. J.*, 2017, **23**, 12714–12717.

366 M. Kimura, M. Futamata, R. Mukai and Y. Tamaru, *J. Am. Chem. Soc.*, 2005, **127**, 4592–4593.

367 X. Li, C. Abrahams, S. Zhou, S. Krimm, R. Henningsen, H. Stephenson, J. Hanson, M. R. Masikat, K. Bajjuri, T. Heibeck, C. Tran, G. Yin, J. Zawada, G. Sarma, J. Chen, M. Bruhns, W. Solis, A. Steiner, A. Galan, T. Kline, R. Stafford, A. Yam, V. I. De Almeida, M. Lupher and T. Hallam, *Cancer Res.*, 2018, **78 (13 Suppl)**, 1782.

368 J. Charoenpattarapreeda, Y. S. Tan, J. Iegre, S. J. Walsh, E. Fowler, R. S. Eapen, Y. Wu, H. F. Sore, C. S. Verma, L. Itzhaki and D. R. Spring, *Chem. Commun.*, 2019, **55**, 7914–7917.

369 A. J. Brouwer, A. Jonker, P. Werkhoven, E. Kuo, N. Li, N. Gallastegui, J. Kemmink, B. I. Florea, M. Groll, H. S. Overkleeft and R. M. J. Liskamp, *J. Med. Chem.*, 2012, **55**, 10995–11003.

370 J. Dong, L. Krasnova, M. G. Finn and K. Barry Sharpless, *Angew. Chem. Int. Ed.*, 2014, **53**, 9430–9448.

371 F. H. Allen, O. Kennard, D. G. Watson, L. Brammer, A. G. Orpen and R. Taylor, *J. Chem. Soc., Perkin Trans. 2*, 1987, S1–S19.

372 K. Sonogashira, Y. Tohda and N. Hagihara, *Tetrahedron Lett.*, 1975, **16**, 4467–4470.

373 A. T. Davies, J. M. Curto, S. W. Bagley, M. C. Willis, U. P. Dahal, A. M. Gilbert, C. Li, J. Montgomery, S. R. Oppenheimer, T. Ryder, B. P. Schuff, D. P. Uccello, G. S. Walker, Y. Wu, M. F. Brown, J. M. Chen, M. M. Hayward, M. C. Noe, R. S. Obach, L. Philippe, V. Shanmugasundaram, M. J. Shapiro, J. Starr, J. Stroh and Y. Che, *Chem. Sci.*, 2017, **8**, 1233–1237.

374 A. L. Tribby, I. Rodríguez, S. Shariffudin and N. D. Ball, *J. Org. Chem.*, 2017, **82**, 2294–2299.

375 P. J. Hogan and B. G. Cox, *Org. Process Res. Dev.*, 2009, **13**, 875–879.

376 N. Ikemoto, J. Liu, K. M. . Brands, J. M. McNamara and P. J. Reider, *Tetrahedron*, 2003, **59**, 1317–1325.

377 E. D. Goddard-Borger and R. V. Stick, *Org. Lett.*, 2007, **9**, 3797–3800.

378 R. B. Kapust and D. S. Waugh, *Protein Sci.*, 1999, **8**, 1668–1674.

379 G. D. Davis, C. Elisee, D. M. Newham and R. G. Harrison, *Biotechnol. Bioeng.*, 1999, **65**, 382–388.

380 E. R. LaVallie, E. A. DiBlasio, S. Kovacic, K. L. Grant, P. F. Schendel and J. M. McCoy, *Biotechnology*, 1993, **11**, 187–193.

381 A. M. Sinclair, S. Elliott, A. J. Erslev, J. B. McCrea, P. H. Vlasses, F. Medina, J. Caro, E. Morris, L. Hesterberg, I. Teyssandier, B. Varet, P. Mayeux, H. Shimano, S. Kimura, R. Nagai, N. Yamada, F. Martin, R. Navarro, T. Osslund, G. Rogers, N. Rogers, G. Trail and J. Egrie, *J. Pharm. Sci.*, 2005, **94**, 1626–1635.

382 S. Cheng, X. Chang, Y. Wang, G. F. Gao, Y. Shao, L. Ma and X. Li, *J. Med. Chem.*, 2015, **58**, 1372–1379.

383 A. Basu, K. Yang, M. Wang, S. Liu, R. Chintala, T. Palm, H. Zhao, P. Peng, D. Wu, Z. Zhang, J. Hua, M. C. Hsieh, J. Zhou, G. Petti, X. Li, A. Janjua, M. Mendez, J. Liu, C. Longley, Z. Zhang, M. Mehlig, V. Borowski, M. Viswanathan and D. Filpula, *Bioconjug. Chem.*, 2006, **17**, 618–630.

384 J. Xiao, A. Burn and T. J. Tolbert, *Bioconjug. Chem.*, 2008, **19**, 1113–1118.

385 M. Pazgier, M. Liu, G. Zou, W. Yuan, C. Li, C. Li, J. Li, J. Monbo, D. Zella, S. G. Tarasov and W. Lu, *Proc. Natl. Acad. Sci. U.S.A.*, 2009, **106**, 4665–4670.

386 Y. S. Tan, J. Reeks, C. J. Brown, D. Thean, F. J. Ferrer Gago, T. Y. Yuen, E. T. L. Goh, X. E. C. Lee, C. E. Jennings, T. L. Joseph, R. Lakshminarayanan, D. P. Lane, M. E. M. Noble and C. S. Verma, *J. Phys. Chem. Lett.*, 2016, **7**, 3452–3457.

387 S. M. Hacker, K. M. Backus, M. R. Lazear, S. Forli, B. E. Correia and B. F. Cravatt, *Nat. Chem.*, 2017, **9**, 1181–1190.

388 S. Kolodych, O. Koniev, Z. Baatarkhuu, J.-Y. Bonnefoy, F. Debaene, S. Cianférani, A. Van Dorsselaer and A. Wagner, *Bioconjug. Chem.*, 2015, **26**, 197–200.

389 M. Ahn, E. De Genst, G. S. Kaminski Schierle, M. Erdelyi, C. F. Kaminski, C. M. Dobson and J. R. Kumita, *PLoS One*, 2012, **7**, e50192.

390 U. P. Dahal, A. M. Gilbert, R. S. Obach, M. E. Flanagan, J. M. Chen, C. Garcia-Irizarry, J. T. Starr, B. Schuff, D. P. Uccello and J. A. Young, *Med. Chem. Commun.*, 2016, **7**, 864–872.

391 S. G. Pai, B. A. Carneiro, J. M. Mota, R. Costa, C. A. Leite, R. Barroso-Sousa, J. B. Kaplan, Y. K. Chae and F. J. Giles, *J. Hematol. Oncol.*, 2017, **10**, 101.

392 H. Clevers and R. Nusse, *Cell*, 2012, **149**, 1192–205.

393 J. N. Anastas and R. T. Moon, *Nat. Rev. Cancer*, 2013, **13**, 11–26.

394 R. K. Bikkavilli and C. C. Malbon, *J. Cell Sci.*, 2010, **123**, 1352–1362.

395 Y. Pan and D. S. Haines, *Cancer Res.*, 1999, **59**, 2064–7.

396 C. Xu, C. D. Fan and X. Wang, *Oncogene*, 2015, **34**, 281–289.

397 T. N. Grossmann, J. T.-H. Yeh, B. R. Bowman, Q. Chu, R. E. Moellering and G. L. Verdine, *Proc. Natl. Acad. Sci. U.S.A.*, 2012, **109**, 17942–7.

398 J. Charoenpattarapreeda, S. J. Walsh, J. S. Carroll and D. R. Spring, *Angew. Chem. Int. Ed.*, 2020, DOI:10.1002/anie.202010090.

399 J. E. Coleman, B. O. Patrick, R. J. Andersen and S. J. Rettig, *Acta Crystallogr. Sect. C Cryst. Struct. Commun.*, 1996, **52**, 1525–1527.

400 W. R. Gamble, N. A. Durso, R. W. Fuller, C. K. Westergaard, T. R. Johnson, D. L. Sackett, E. Hamel, J. H. Cardellina II and M. R. Boyd, *Bioorg. Med. Chem.*, 1999, **7**, 1611–1615.

401 R. Bai, N. A. Durso, D. L. Sackett and E. Hamel, *Biochemistry*, 1999, **38**, 14302–14310.

402 G. Lesma, I. Bassanini, R. Bortolozzi, C. Colletto, R. Bai, E. Hamel, F. Meneghetti, G. Rainoldi, M. Stucchi, A. Sacchetti, A. Silvani and G. Viola, *Org. Biomol. Chem.*, 2015, **13**, 11633–11644.

403 S. Ackermann, H.-G. Lerchen, D. Häbich, A. Ullrich and U. Kazmaier, *Beilstein J. Org. Chem.*, 2012, **8**, 1652–1656.

404 I. Ugi, W. Betz, U. Fetzer and K. Offermann, *Chem. Ber.*, 1961, **94**, 2814–2816.

405 X. Li, Y. Yuan, W. F. Berkowitz, L. J. Todaro and S. J. Danishefsky, *J. Am. Chem. Soc.*, 2008, **130**, 13222–13224.

406 X. Li, Y. Yuan, C. Kan and S. J. Danishefsky, *J. Am. Chem. Soc.*, 2008, **130**, 13225–13227.

407 X. Li and S. J. Danishefsky, *J. Am. Chem. Soc.*, 2008, **130**, 5446–5448.

408 G. Skorna and I. Ugi, *Angew. Chem. Int. Ed.*, 1977, **16**, 259–260.

409 H. Eckert and B. Forster, *Angew. Chem. Int. Ed.*, 1987, **26**, 894–895.

410 J. Zhu, X. Wu and S. J. Danishefsky, *Tetrahedron Lett.*, 2009, **50**, 577–579.

411 R. Obrecht, R. Herrmann and I. Ugi, *Synthesis*, 1985, **1985**, 400–402.

412 V. Bocchi and G. Palla, *Synthesis*, 1982, **1982**, 1096–1097.

413 J. Yan, T. Ni and F. Yan, *Tetrahedron Lett.*, 2015, **56**, 1096–1098.

414 G. D. Vo and J. F. Hartwig, *Angew. Chem. Int. Ed.*, 2008, **47**, 2127–2130.

415 M. Jean, J. Renault and P. van de Weghe, *Tetrahedron Lett.*, 2009, **50**, 6546–6548.

416 R. Martín and S. L. Buchwald, *Org. Lett.*, 2008, **10**, 4561–4564.

417 R. Martín and S. L. Buchwald, *Angew. Chem. Int. Ed.*, 2007, **46**, 7236–7239.

418 W. P. Griffith, S. V. Ley, G. P. Whitcombe and A. D. White, *J. Chem. Soc., Chem. Commun.*, 1987, 1625–1627.

419 Z. H. Kudzin, P. Łyżwa, J. Łuczak and G. Andrijewski, *Synthesis*, 1997, **1997**, 44–46.

420 A. Homberg, D. Poggiali, M. Vishe, C. Besnard, L. Guénée and J. Lacour, *Org. Lett.*, 2019, **21**, 687–691.

421 F. Albericio and A. El-Faham, *Org. Process Res. Dev.*, 2018, **22**, 760–772.

422 T. I. Al-Warhi, H. M. A. Al-Hazimi and A. El-Faham, *J. Saudi Chem. Soc.*, 2012, **16**, 97–

116.

423 A. El-Faham and F. Albericio, *Chem. Rev.*, 2011, **111**, 6557–6602.

424 E. Valeur and M. Bradley, *Chem. Soc. Rev.*, 2009, **38**, 606–631.

425 C. A. G. N. Montalbetti and V. Falque, *Tetrahedron*, 2005, **61**, 10827–10852.

426 WO2013/135870, 2013.

427 M. E. Due-Hansen, S. K. Pandey, E. Christiansen, R. Andersen, S. V. F. Hansen and T. Ulven, *Org. Biomol. Chem.*, 2016, **14**, 430–433.

428 D. W. Carney, K. R. Schmitz, J. V. Truong, R. T. Sauer and J. K. Sello, *J. Am. Chem. Soc.*, 2014, **136**, 1922–1929.

429 W. Gong, G. Zhang, T. Liu, R. Giri and J. Q. Yu, *J. Am. Chem. Soc.*, 2014, **136**, 16940–16946.

430 A. V. Gulevich, A. G. Zhdanko, R. V. A. Orru and V. G. Nenajdenko, *Chem. Rev.*, 2010, **110**, 5235–5331.

431 B. B. Touré and D. G. Hall, *Chem. Rev.*, 2009, **109**, 4439–4486.

432 O. Pando, S. Stark, A. Denkert, A. Porzel, R. Preusentanz and L. A. Wessjohann, *J. Am. Chem. Soc.*, 2011, **133**, 7692–7695.

433 A. L. Brown, Q. I. Churches and C. A. Hutton, *J. Org. Chem.*, 2015, **80**, 9831–9837.

434 G. M. Ziarani, R. Moradi and L. Mahammadkhani, *Arkivoc*, 2019, **2019**, 18–40.

435 T. M. Vishwanatha, B. Giepmans, S. K. Goda and A. Dömling, *Org. Lett.*, 2020, **22**, 5396–5400.

436 A. Znabet, M. M. Polak, E. Janssen, F. J. J. De Kanter, N. J. Turner, R. V. A. Orru and E. Ruijter, *Chem. Commun.*, 2010, **46**, 7918–7920.

437 C. Lambruschini, L. Moni and L. Banfi, *Eur. J. Org. Chem.*, 2020, **2020**, 3766–3778.

438 Y. Zhang, Y.-F. Ao, Z.-T. Huang, D.-X. Wang, M.-X. Wang and J. Zhu, *Angew. Chem. Int. Ed.*, 2016, **55**, 5282–5285.

439 J. Zhang, P. Yu, S.-Y. Li, H. Sun, S.-H. Xiang, J. J. Wang, K. N. Houk and B. Tan, *Science*, 2018, **361**, eaas8707.

440 Q. Wang, D.-X. Wang, M.-X. Wang and J. Zhu, *Acc. Chem. Res.*, 2018, **51**, 1290–1300.

441 R. O. Rocha, M. O. Rodrigues and B. A. D. Neto, *ACS Omega*, 2020, **5**, 972–979.

442 Y. Yasui, S. Tsuchida, H. Miyabe and Y. Takemoto, *J. Org. Chem.*, 2007, **72**, 5898–5900.

443 J. A. Grzyb, M. Shen, C. Yoshina-Ishii, W. Chi, R. S. Brown and R. A. Batey, *Tetrahedron*, 2005, **61**, 7153–7175.

444 WO 2017/089895 A1, 2017.

445 C. A. Hudis, *N. Engl. J. Med.*, 2007, **357**, 39–51.

446 I. Ugi and F. K. Rosendahl, *Justus Liebigs Ann. Chem.*, 1963, **666**, 65–67.

447 T. A. Keating and R. W. Armstrong, *J. Am. Chem. Soc.*, 1995, **117**, 7842–7843.

448 T. A. Keating and R. W. Armstrong, *J. Am. Chem. Soc.*, 1996, **118**, 2574–2583.

449 G. van der Heijden, J. A. W. (Sjaak) Jong, E. Ruijter and R. V. A. Orru, *Org. Lett.*, 2016, **18**, 984–987.

450 C. B. Gilley, M. J. Buller and Y. Kobayashi, *Org. Lett.*, 2007, **9**, 3631–3634.

451 L. A. Wessjohann, M. C. Morejón, G. M. Ojeda, C. R. B. Rhoden and D. G. Rivera, *J. Org. Chem.*, 2016, **81**, 6535–6545.

452 J. A. Leitch, C. L. McMullin, M. F. Mahon, Y. Bhonoah and C. G. Frost, *ACS Catal.*, 2017, **7**, 2616–2623.

453 H. E. Gottlieb, V. Kotlyar and A. Nudelman, *J. Org. Chem.*, 1997, **62**, 7512–7515.

454 W. L. Delano, The PyMOL Molecular Graphics System, DeLano Scientific, San Carlos, CA, USA 2002.

455 D. A. Case, V. Babin, J. T. Berryman, R. M. Betz, Q. Cai, D. S. Cerutti, T. E. Cheatham III, T. A. Darden, R. E. Duke, H. Gohlke, A. W. Goetz, S. Gusarov, N. Homeyer, P. Janowski, J. Kaus, I. Kolossváry, A. Kovalenko, T. S. Lee, S. LeGrand, T. Luchko, R. Luo, B. Madej, K. M. Merz, F. Paesani, D. R. Roe, A. Roitberg, C. Sagui, R. Salomon-Ferrer, G. Seabra, C. L. Simmerling, W. Smith, J. Swails, R. C. Walker, J. Wang, R. M. Wolf, X. Wu and P. A. Kollman, AMBER 14, University of California, San Francisco, USA 2014.

456 T. J. Dolinsky, P. Czodrowski, H. Li, J. E. Nielsen, J. H. Jensen, G. Klebe and N. A. Baker, *Nucleic Acids Res.*, 2007, **35**, W522–W525.

457 W. L. Jorgensen, J. Chandrasekhar, J. D. Madura, R. W. Impey and M. L. Klein, *J. Chem. Phys.*, 1983, **79**, 926–935.

458 J. A. Maier, C. Martinez, K. Kasavajhala, L. Wickstrom, K. E. Hauser and C. Simmerling, *J. Chem. Theory Comput.*, 2015, **11**, 3696–3713.

459 J. Wang, R. M. Wolf, J. W. Caldwell, P. A. Kollman and D. A. Case, *J. Comput. Chem.*, 2004, **25**, 1157–1174.

460 E. Vanquelef, S. Simon, G. Marquant, E. Garcia, G. Klimerak, J. C. Delepine, P. Cieplak and F.-Y. Dupradeau, *Nucleic Acids Res.*, 2011, **39**, W511–W517.

461 W. D. Cornell, P. Cieplak, C. I. Bayly and P. A. Kollmann, *J. Am. Chem. Soc.*, 1993, **115**, 9620–9631.

462 M. J. Frisch, G. W. Trucks, H. B. Schlegel, G. E. Scuseria, M. A. Robb, J. R. Cheeseman, G. Scalmani, V. Barone, B. Mennucci, G. A. Petersson, H. Nakatsuji, M. Caricato, X. Li, H. P. Hratchian, A. F. Izmaylov, J. Bloino, G. Zheng, J. L. Sonnenberg, M. Hada, M. Ehara, K. Toyota, R. Fukuda, J. Hasegawa, M. Ishida, T. Nakajima, Y. Honda, O. Kitao, H. Nakai, T. Vreven, J. Montgomery, J. A. Montgomery Jr., J. E. Peralta, F. Ogliaro, M. Bearpark, J. J. Heyd, E. Brothers, K. N. Kudin, V. N. Staroverov, R. Kobayashi, J. Normand, K. Raghavachari, A. Rendell, J. C. Burant, S. S. Iyengar, J. Tomasi, M. Cossi, N. Rega, N. J. Millam, M. Klene, J. E. Knox, J. B. Cross, V. Bakken, C. Adamo, J. Jaramillo, R. Gomperts,

R. E. Stratmann, O. Yazyev, A. J. Austin, R. Cammi, C. Pomelli, J. W. Ochterski, R. L. Martin, K. Morokuma, V. G. Zakrzewski, G. A. Voth, P. Salvador, J. J. Dannenberg, S. Dapprich, A. D. Daniels, Ö. Farkas, J. B. Foresman, J. V. Ortiz, J. Cioslowski and D. J. Fox, Gaussian 09, Revision B.1, Gaussian, Inc., Wallingford, CT, USA 2009.

463 J.-P. Ryckaert, G. Ciccotti and H. J. C. Berendsen, *J. Comput. Phys.*, 1977, **23**, 327–341.

464 T. Darden, D. York and L. Pedersen, *J. Chem. Phys.*, 1993, **98**, 10089–10092.

465 J. A. Izaguirre, D. P. Catarello, J. M. Wozniak and R. D. Skeel, *J. Chem. Phys.*, 2001, **114**, 2090–2098.

466 H. J. C. Berendsen, J. P. M. Postma, W. F. van Gunsteren, A. DiNola and J. R. Haak, *J. Chem. Phys.*, 1984, **81**, 3684–3690.

467 T. Hirose, Y. Shibano, Y. Miyazaki, N. Sogoshi, S. Nakabayashi and M. Yasutake, *Mol. Cryst. Liq. Cryst.*, 2011, **534**, 81–92.

468 J. F. Corbett and P. F. Holt, *J. Chem. Soc.*, 1963, 2385–2387.

469 C. Görl, N. Beck, K. Kleiber and H. G. Alt, *J. Mol. Catal. A Chem.*, 2012, **352**, 110–127.

470 B. Traber, T. Oeser and R. Gleiter, *Eur. J. Org. Chem.*, 2005, 1283–1292.

471 R. Severin, J. Reimer and S. Doye, *J. Org. Chem.*, 2010, **75**, 3518–3521.

472 F. Chimenti, A. Bolasco, D. Secci, P. Chimenti and A. Granese, *Synth. Commun.*, 2004, **34**, 2549–2555.

473 J. B. Pollock, T. R. Cook and P. J. Stang, *J. Am. Chem. Soc.*, 2012, **134**, 10607–10620.

474 Y. Tobe, N. Utsumi, K. Kawabata, A. Nagano, K. Adachi, S. Araki, M. Sonoda, K. Hirose and K. Naemura, *J. Am. Chem. Soc.*, 2002, **124**, 5350–5364.

475 Y. Wu, University of Cambridge, 2016.

476 A. L. C. Isaad, F. Barbetti, P. Rovero, A. M. D'Ursi, M. Chelli, M. Chorev and A. M. Papini, *Eur. J. Org. Chem.*, 2008, **2008**, 5308–5314.

477 Y.-H. Chen, J. T. Yang and K. H. Chau, *Biochemistry*, 1974, **13**, 3350–3359.

478 Z. X. Wang, *FEBS Lett.*, 1995, **360**, 111–114.

479 L. Shi, D. Zhang, R. Lin, C. Zhang, X. Li and N. Jiao, *Tetrahedron Lett.*, 2014, **55**, 2243–2245.

480 I. Coldham, S. Raimbault, D. T. E. Whittaker, P. T. Chovatia, D. Leonori, J. J. Patel and N. S. Sheikh, *Chem. - Eur. J.*, 2010, **16**, 4082–4090.

481 X. Cai, A. Keshavarz, J. D. Omaque and B. J. Stokes, *Org. Lett.*, 2017, **19**, 2626–2629.

482 S. J. Walsh, University of Cambridge, 2019.

Appendix A — Crystallographic data

Methyl (*S*)-3,3-dimethyl-2-((*S*)-3-methyl-3-(1-methyl-1*H*-indol-3-yl)-2-(2,2,2-trifluoro-*N*-methylacetamido)butanamido)butanoate (99a)

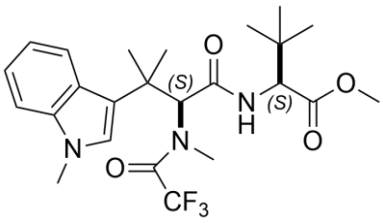

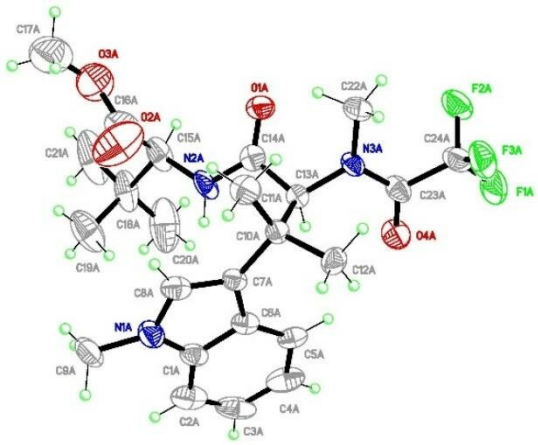

CCDC number	**2012415**
Crystal data	
Chemical formula	$C_{24}H_{32}F_3N_3O_4$
***M*$_r$**	483.52
Crystal system, space group	Monoclinic, $P2_1$
Temperature (K)	180
***a*, *b*, *c* (Å)**	18.9031 (7), 12.3366 (4), 21.0506 (7)
β (°)	90.002 (2)
***V* (Å^3)**	4909.0 (3)
Z	8
***F*(000)**	2048
***D*$_x$ (Mg m^{-3})**	1.308
Radiation type	Cu *K*α
No. of reflections for cell measurement	9656
θ range (°) for cell measurement	4.2–66.6
μ (mm^{-1})	0.88
Crystal shape	Lath
Crystal size (mm^3)	0.18 × 0.10 × 0.06
Data collection	
Diffractometer	Bruker D8-QUEST PHOTON-100
Scan method	ω and φ–scans
Absorption correction	Multi-scan *SADABS* (Bruker, 2014)
***T*$_{min}$, *T*$_{max}$**	0.661, 0.753
No. of measured, independent and observed [*I* > 2σ(*I*)] reflections	51831, 16567, 13315
***R*$_{int}$**	0.070

θ values (°)	θ_{max} = 67.2, θ_{min} = 2.3
(sin θ/λ)$_{max}$ (Å^{-1})	0.598
Refinement	
R*[*F*^{2} > 2σ(*F*^{2})], *wR*(*F*^{2}), *S	0.055, 0.126, 1.05
No. of reflections	16567
No. of parameters	1258
No. of restraints	541
H-atom treatment	H-atom parameters constrained
Δρ$_{max}$, Δρ$_{min}$ (e Å^{-3})	0.26, -0.29
Absolute structure	Flack x determined using 4819 quotients [(I+)-(I-)]/[(I+)+(I-)] (Parsons, Flack and Wagner, Acta Cryst. B69 (2013) 249-259).
Absolute structure parameter	-0.03 (9)

Methyl (*S*)-3,3-dimethyl-2-((*R*)-3-methyl-3-(1-methyl-1*H*-indol-3-yl)-2-(2,2,2-trifluoro-*N*-methylacetamido)butanamido)butanoate (99b)

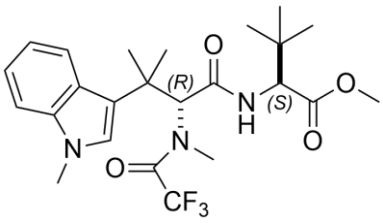

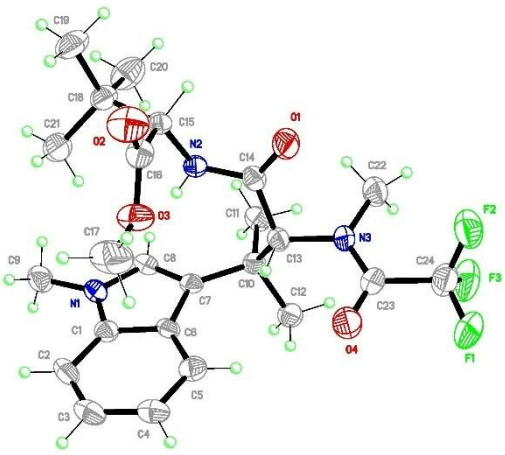

CCDC	**2012414**
Crystal data	
Chemical formula	$C_{24}H_{32}F_3N_3O_4$
***M*$_r$**	483.52
Crystal system, space group	Orthorhombic, $P2_12_12_1$
Temperature (K)	180
***a*, *b*, *c* (Å)**	10.2753 (4), 13.3147 (4), 17.9428 (5)
***V* (Å^3)**	2454.80 (14)
Z	4
***F*(000)**	1024
***D*$_x$ (Mg m^{-3})**	1.308
Radiation type	Cu *K*α
No. of reflections for cell measurement	4770
θ range (°) for cell measurement	4.1–66.6
μ (mm^{-1})	0.88
Crystal shape	Lath
Crystal size (mm^3)	0.16 × 0.10 × 0.04
Data collection	
Diffractometer	Bruker D8-QUEST PHOTON-100
Scan method	ω and φ–scans
Absorption correction	Multi-scan
	SADABS (Bruker, 2014)
***T*$_{min}$, *T*$_{max}$**	0.653, 0.753
No. of measured, independent and observed [*I* > 2σ(*I*)] reflections	12912, 4214, 3378
***R*$_{int}$**	0.055
θ values (°)	θ_{max} = 66.7, θ_{min} = 4.1
(sin θ/λ)$_{max}$ (Å^{-1})	0.596

Refinement	
$R[F^2 > 2\sigma(F^2)]$, $wR(F^2)$, S	0.045, 0.109, 1.03
No. of reflections	4214
No. of parameters	319
H-atom treatment	H atoms treated by a mixture of independent and constrained refinement
$\Delta\rho_{max}$, $\Delta\rho_{min}$ (e Å^{-3})	0.17, -0.17
Absolute structure	Flack x determined using 1196 quotients [(I+)-(I-)]/[(I+)+(I-)] (Parsons, Flack and Wagner, Acta Cryst. B69 (2013) 249-259).
Absolute structure parameter	0.04 (18)

N-trifluoroacetyl hemiasterlin ethyl ester (113a)

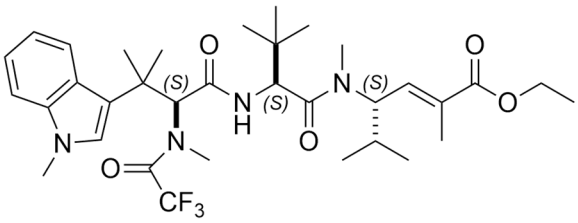

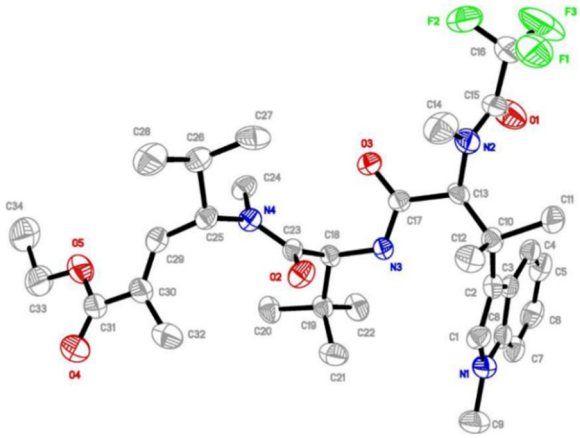

CCDC	**2012776**
Crystal data	
Chemical formula	$C_{34}H_{49}F_3N_4O_5$
***M*$_r$**	650.77
Crystal system, space group	Monoclinic, $P2_1$
Temperature (K)	180
***a*, *b*, *c* (Å)**	16.2983 (9), 6.1314 (4), 17.8581 (10)
β (°)	96.979 (3)
***V* (Å^3)**	1771.36 (18)
Z	2
***F*(000)**	696
***D*$_x$ (Mg m^{-3})**	1.220
Radiation type	Cu *K*α
No. of reflections for cell measurement	4141
θ range (°) for cell measurement	2.7–62.0
μ (mm^{-1})	0.77
Crystal shape	Needle
Crystal size (mm^3)	0.45 × 0.03 × 0.03
Data collection	
Diffractometer	Bruker D8-QUEST PHOTON-100
Scan method	ω and φ–scans
Absorption correction	Multi-scan *SADABS* (Bruker, 2014)
***T*$_{min}$, *T*$_{max}$**	0.608, 0.753
No. of measured, independent and observed [*I* > 2σ(*I*)] reflections	24424, 6173, 3784
***R*$_{int}$**	0.146
θ values (°)	θ_{max} = 66.7, θ_{min} = 2.5
(sin θ/λ)$_{max}$ (Å^{-1})	0.596
Refinement	
R*[*F*^{2} > 2s(*F*^{2})], *wR*(*F*^{2}), *S	0.073, 0.186, 1.01

No. of reflections	6173
No. of parameters	428
No. of restraints	1
H-atom treatment	H-atom parameters constrained
$\Delta\rho_{max}$, $\Delta\rho_{min}$ (e Å^{-3})	0.20, -0.21
Absolute structure	Classical Flack method preferred over Parsons because s.u. lower.
Absolute structure parameter	0.0 (5)

Appendix B — NMR spectra

B.1. Chapter 4

3,5-Dibromonitrobenzene (87)

^{1}H NMR

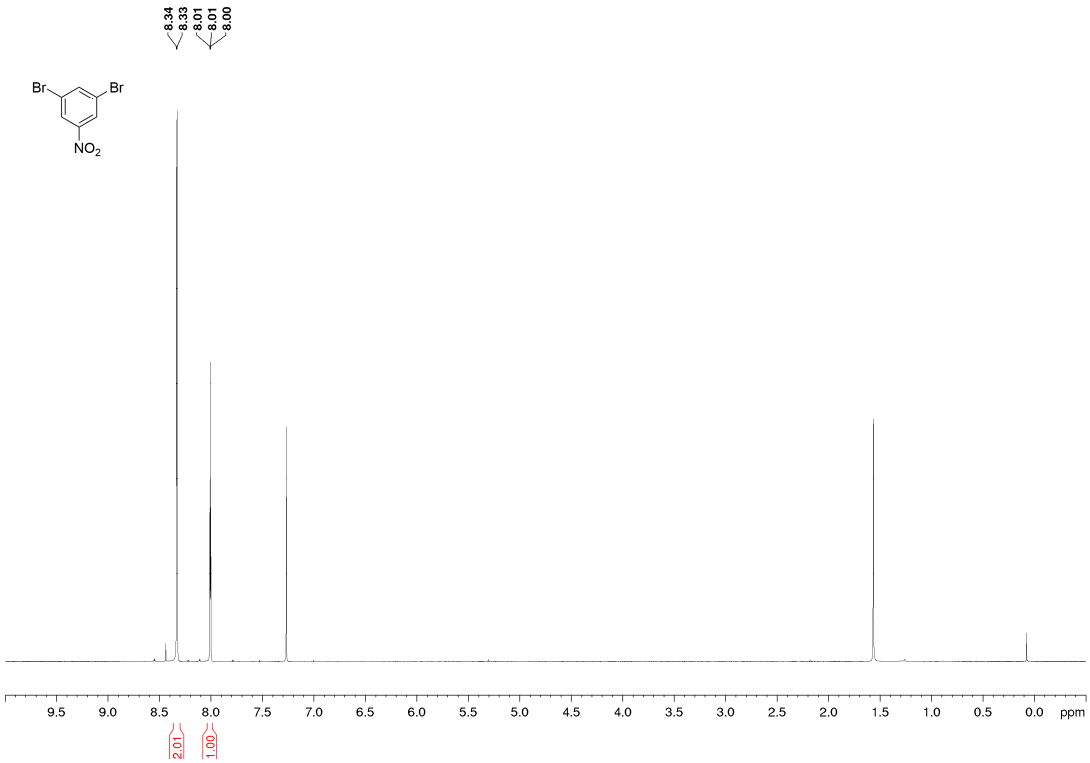

^{13}C NMR

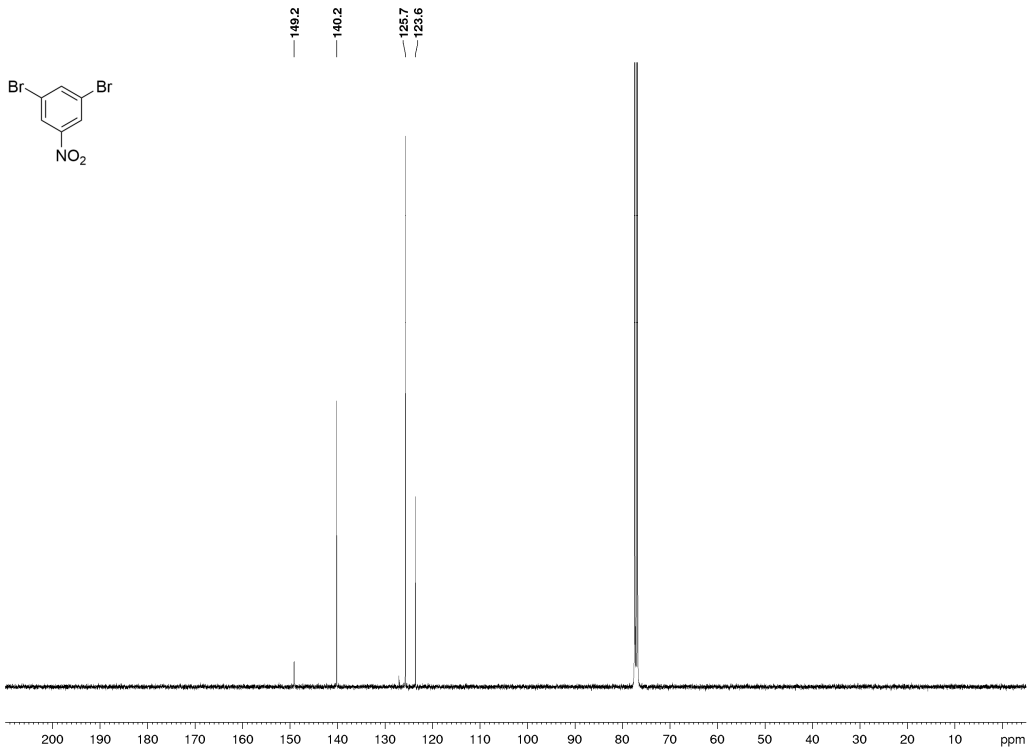

1,3-Diethynyl-5-nitrobenzene (86)

^{1}H NMR

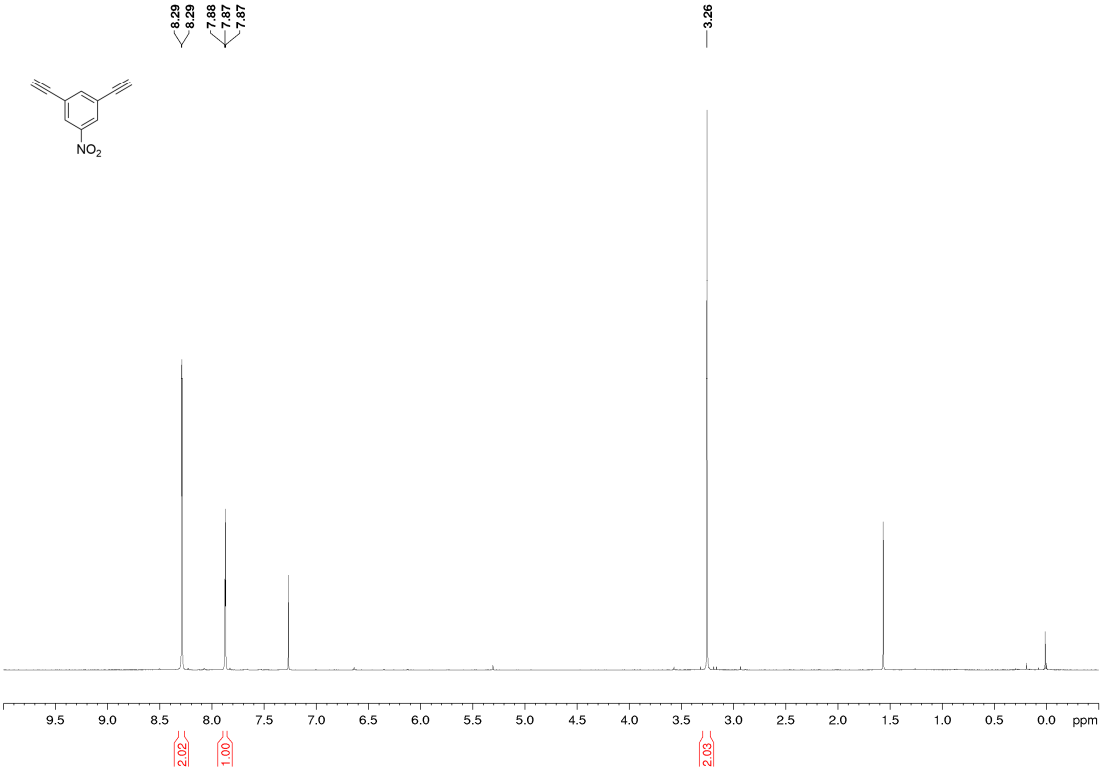

^{13}C NMR

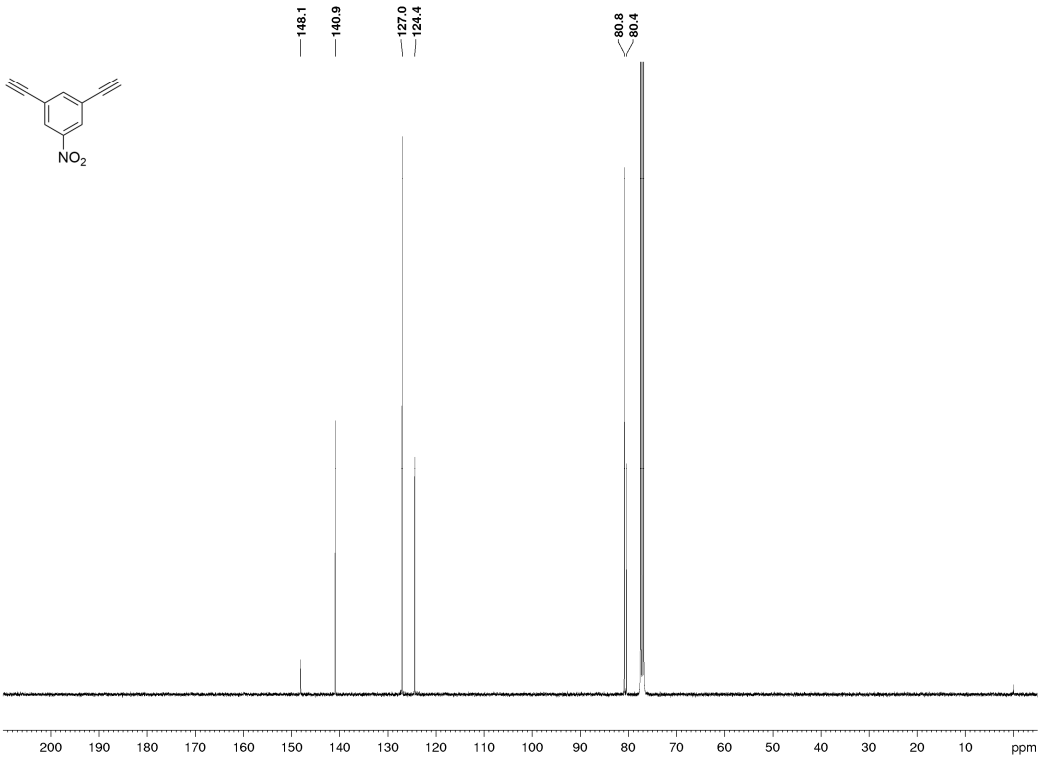

3,5-Diethynylaniline (85)

^{1}H NMR

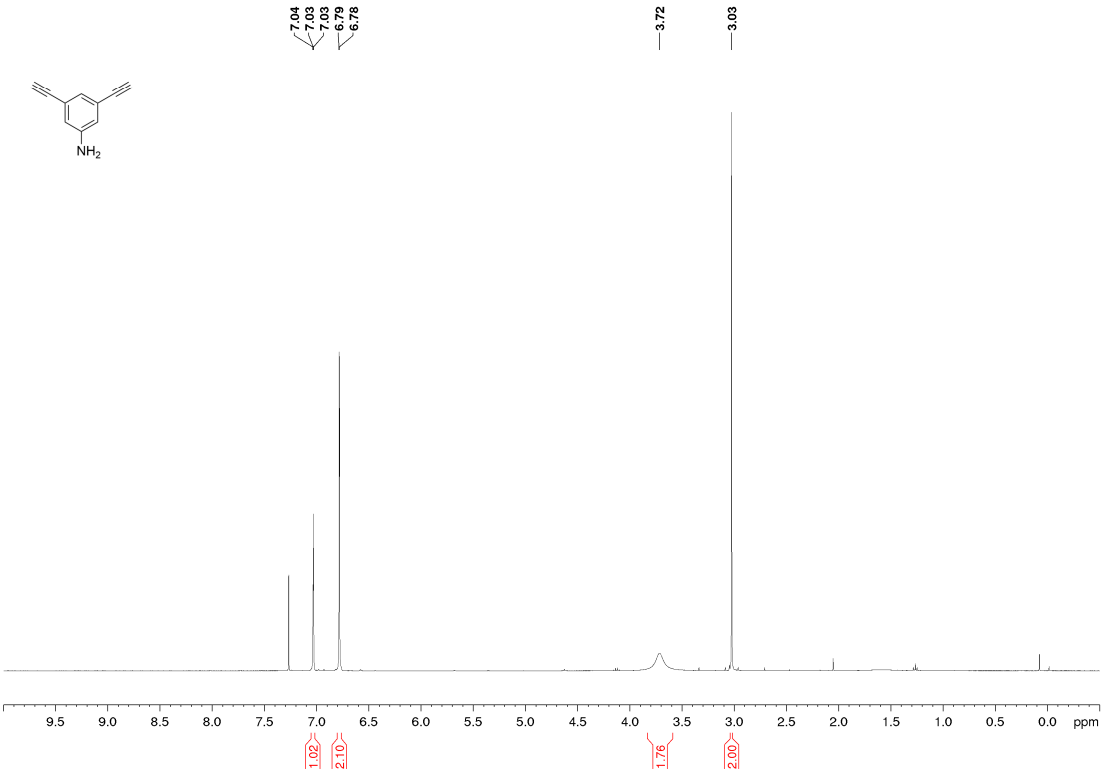

^{13}C NMR

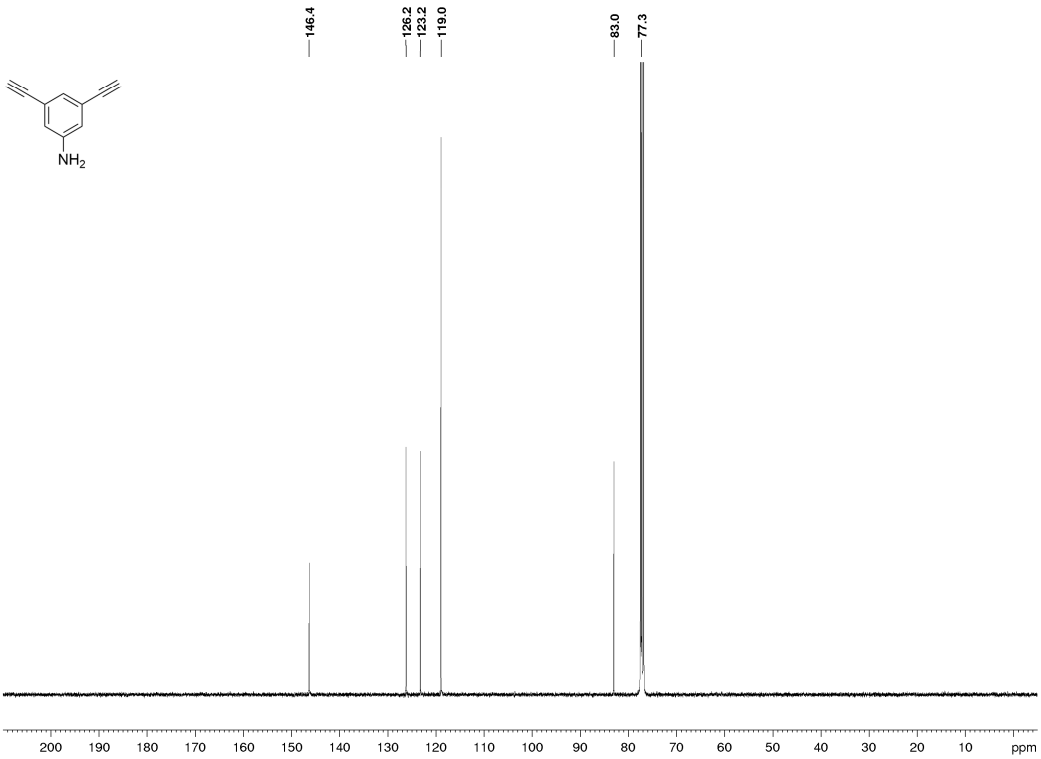

3,5-Diethynylbenzenesulfonyl chloride (84)

^{1}H NMR

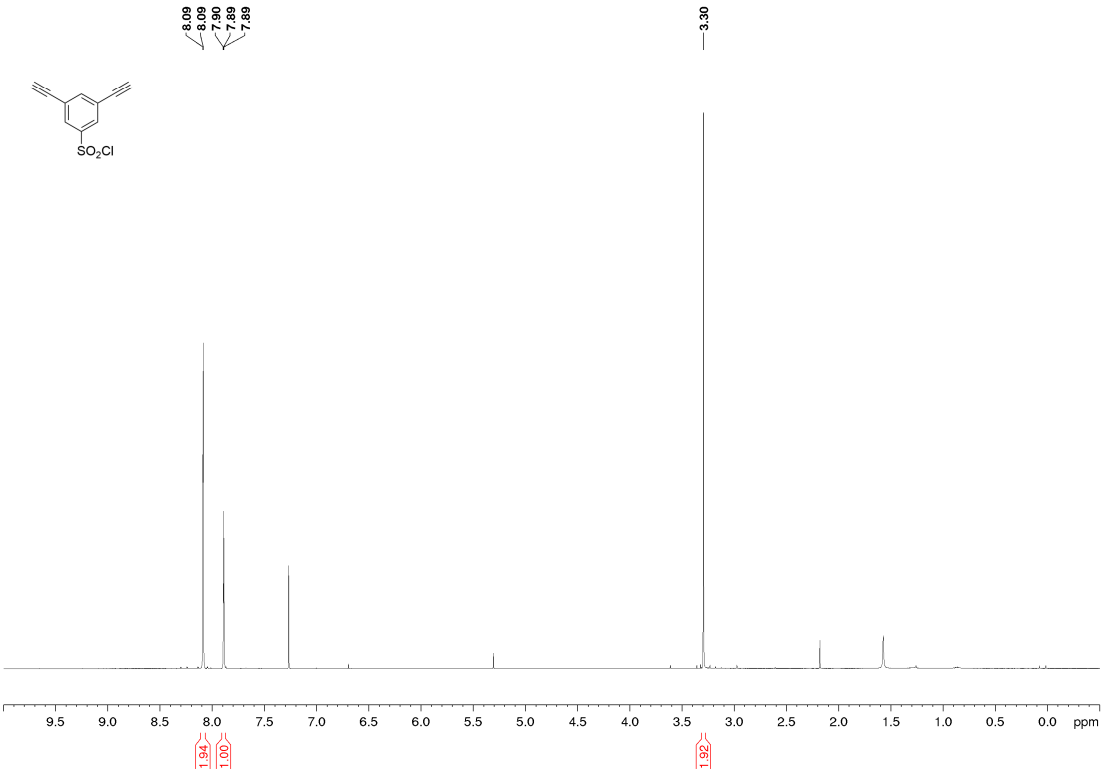

^{13}C NMR

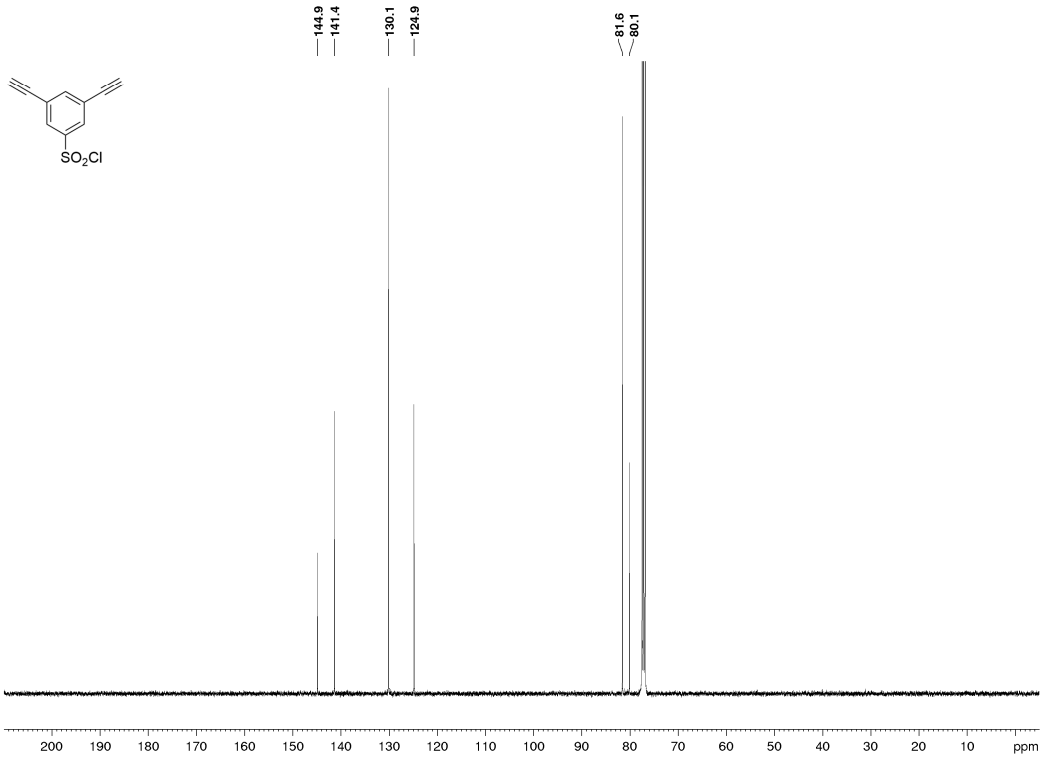

3,5-Diethynylbenzenesulfonyl fluoride (81)

^{1}H NMR

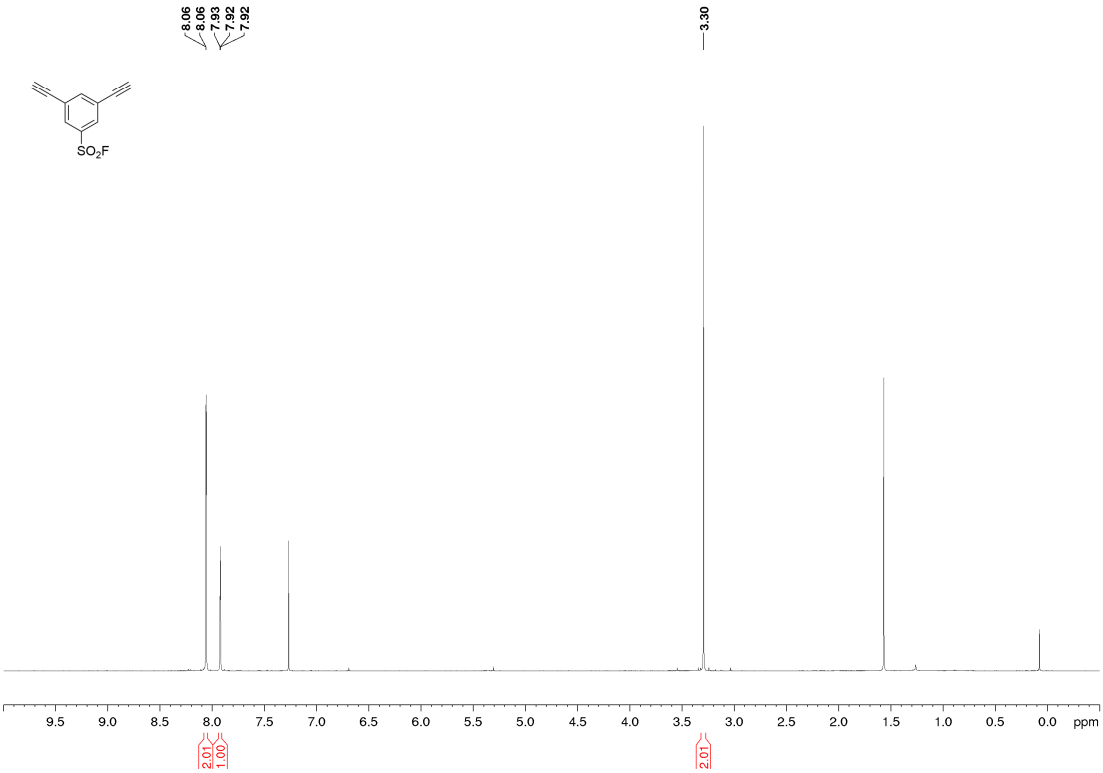

^{13}C NMR

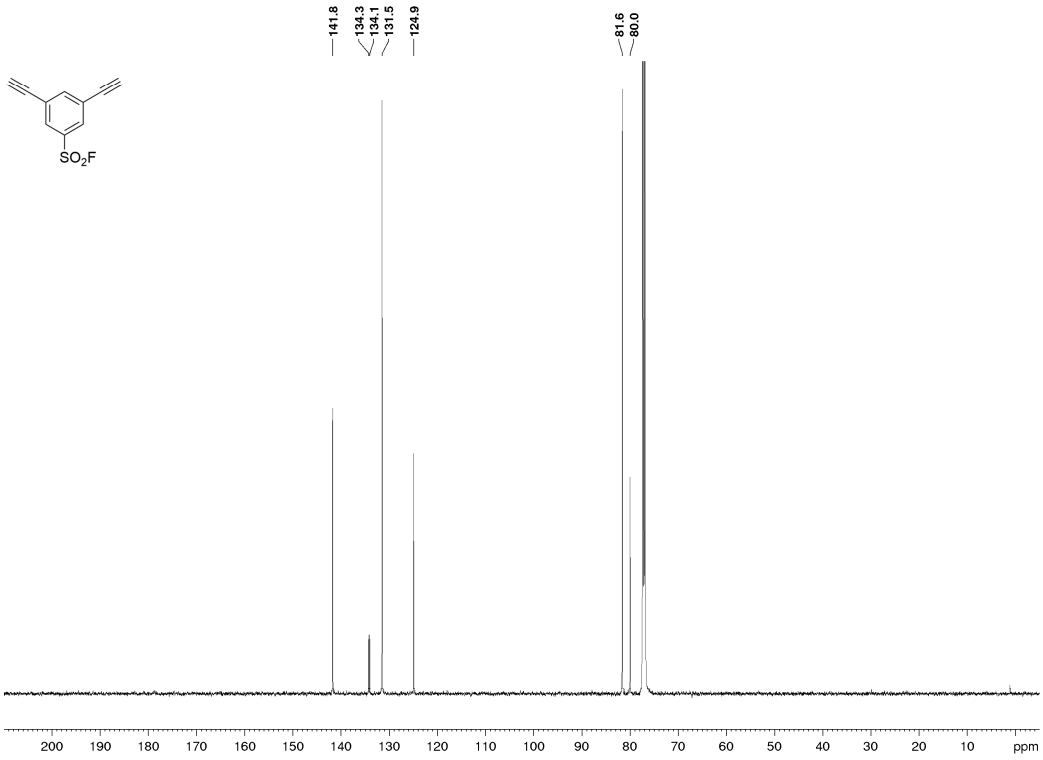

^{19}F NMR

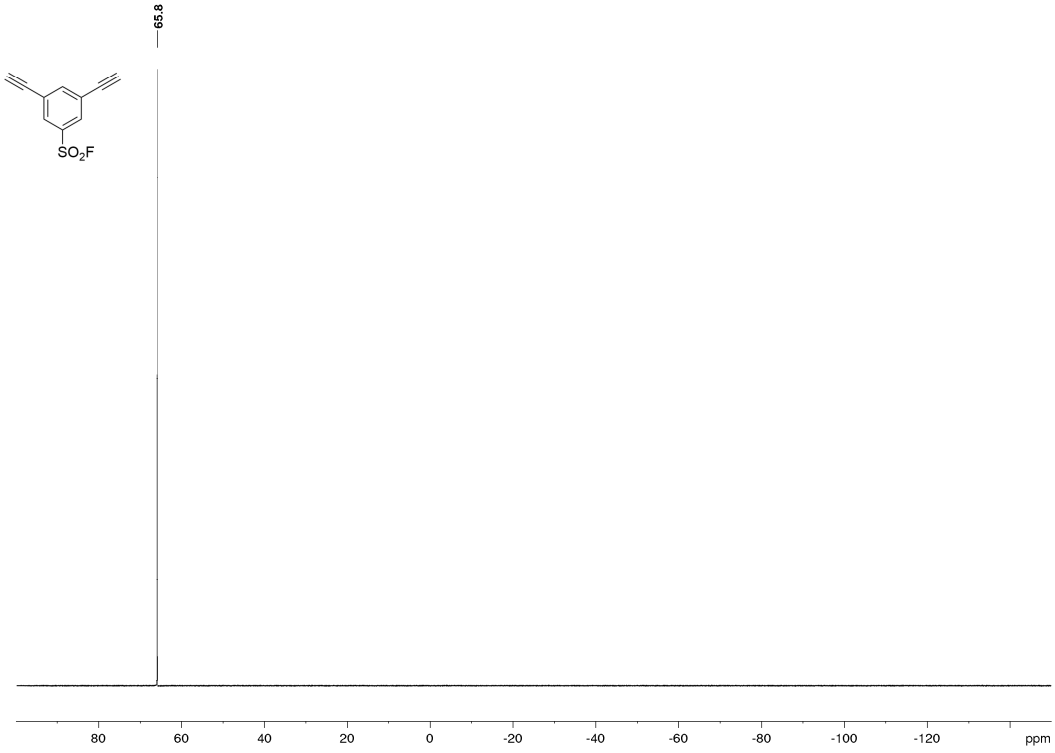

Sodium 4-((3,5-diethynylbenzoyl)oxy)-2,3,5,6-tetrafluorobenzenesulfonate (93)

^{1}H NMR

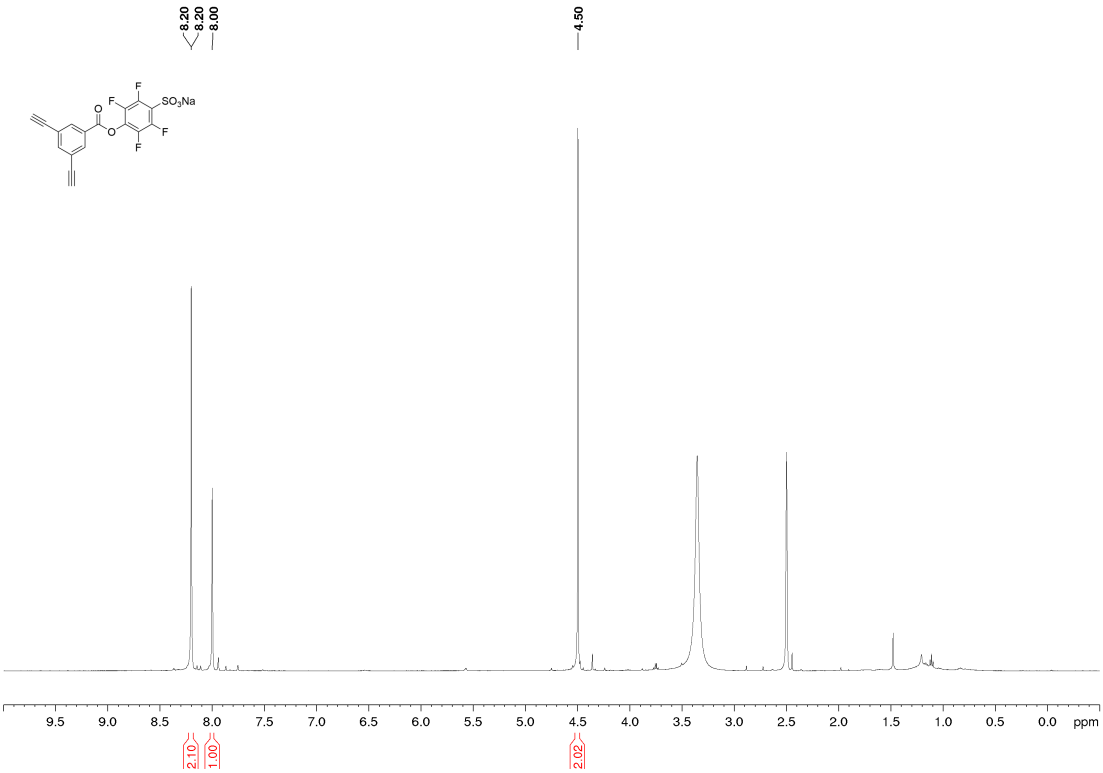

^{13}C NMR

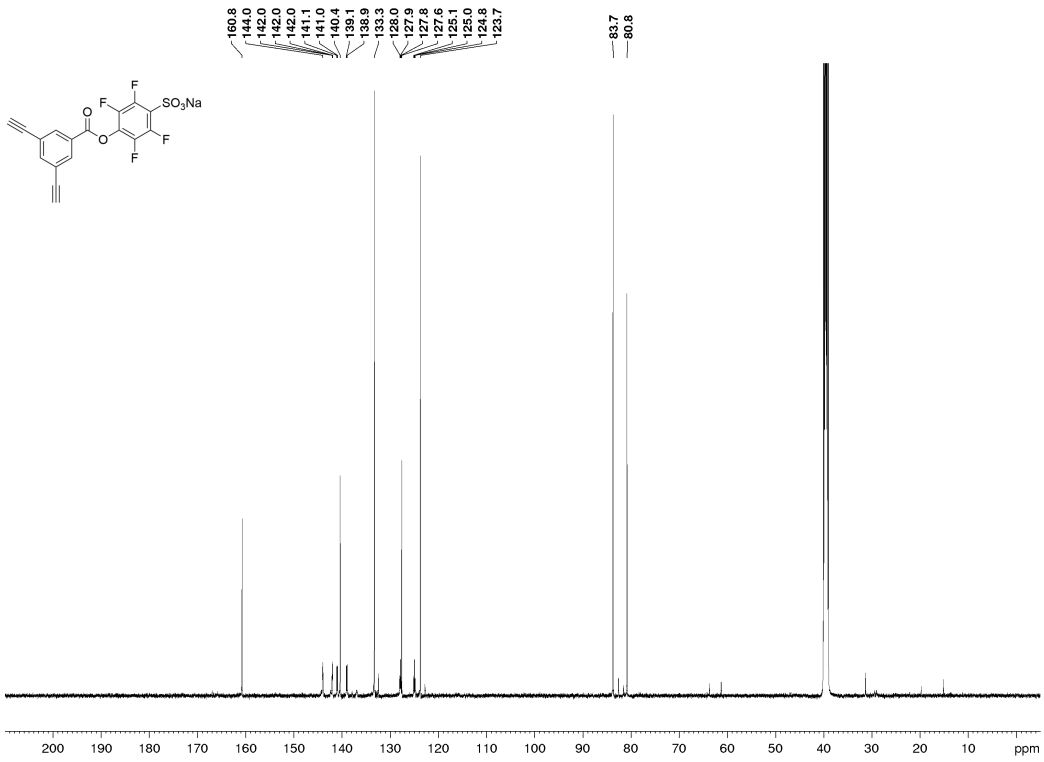

^{19}F NMR

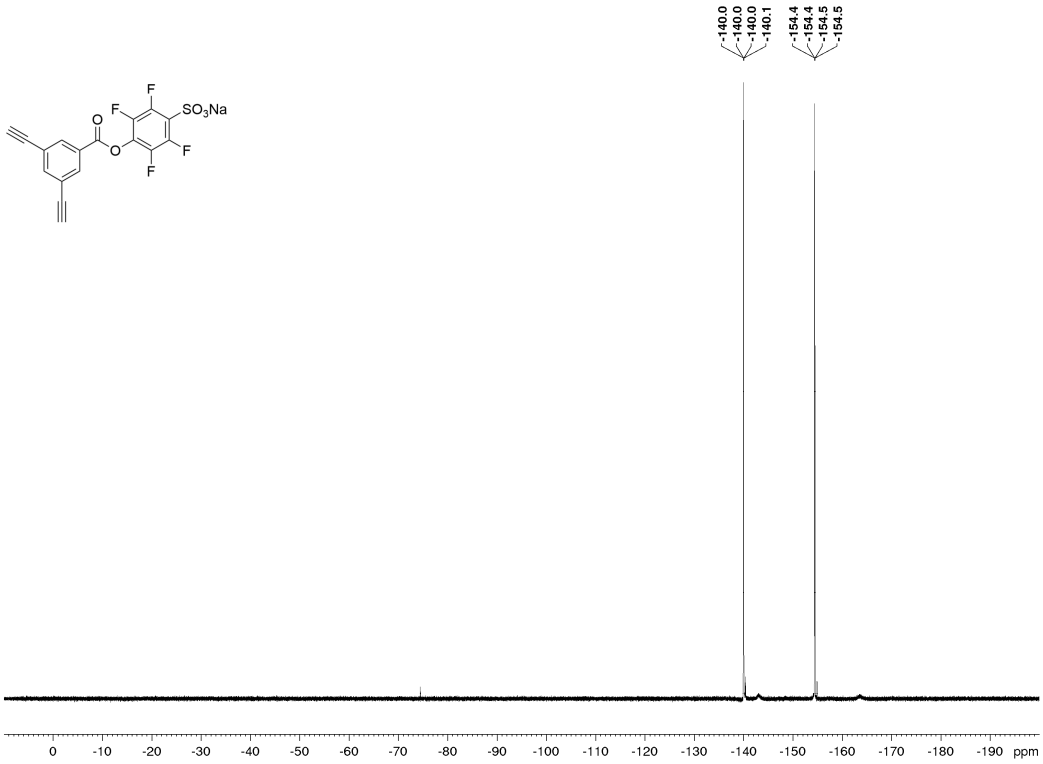
-140.0
-140.0
-140.0
-140.1
-154.4
-154.4
-154.5
-154.5
F
F
SO3Na
O
O
F
F
0
-10
-20
-30
-40
-50
-60
-70
-80
-90
-100
-110
-120
-130
-140
-150
-160
-170
-180
-190
ppm

2,4-Dinitrophenyl 3,5-diethynylbenzoate (94)

^{1}H NMR

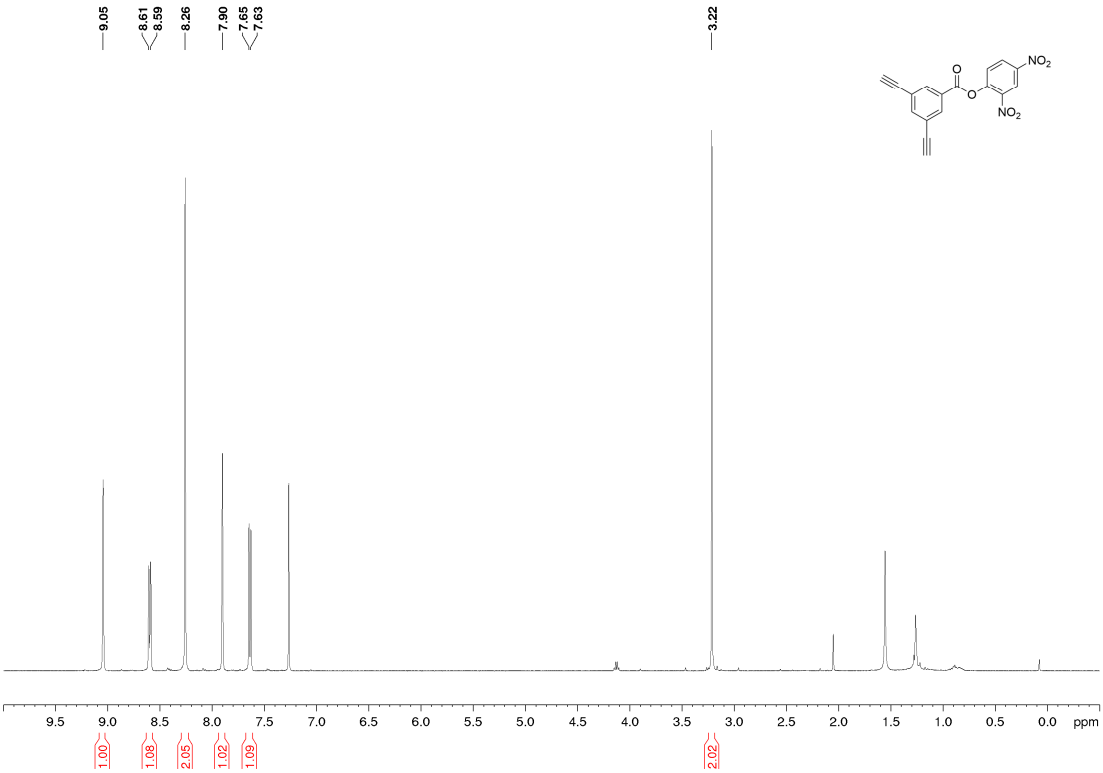

^{13}C NMR

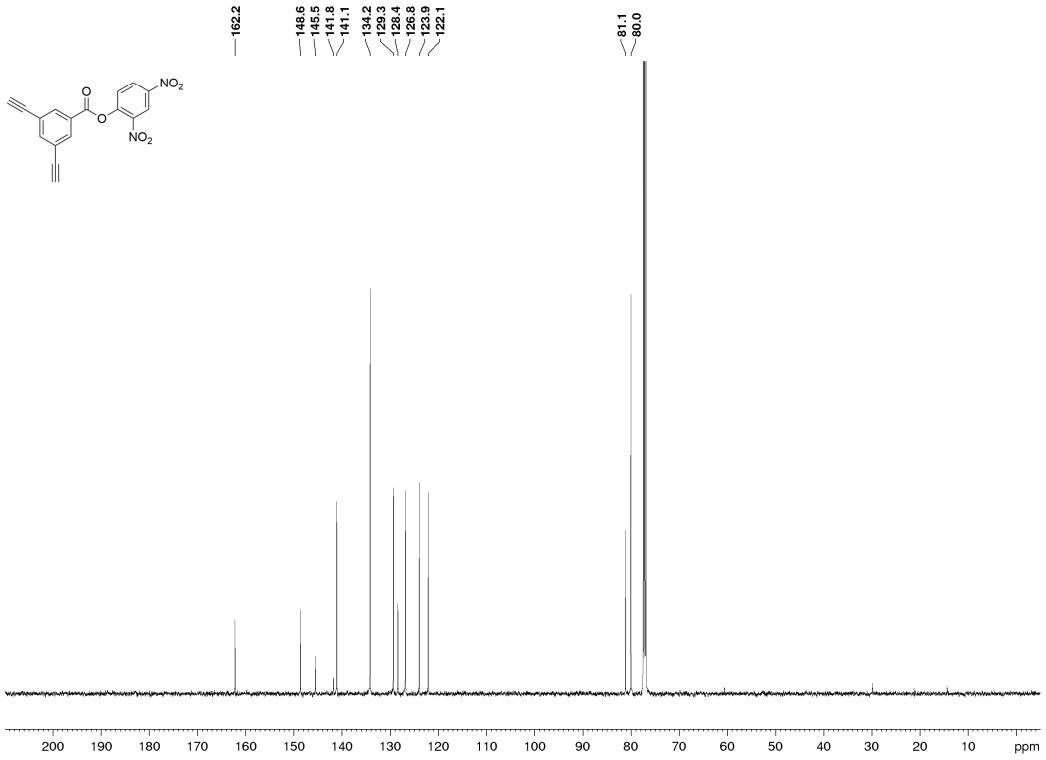

Fmoc-Orn-OH·HCl (89)

^{1}H NMR

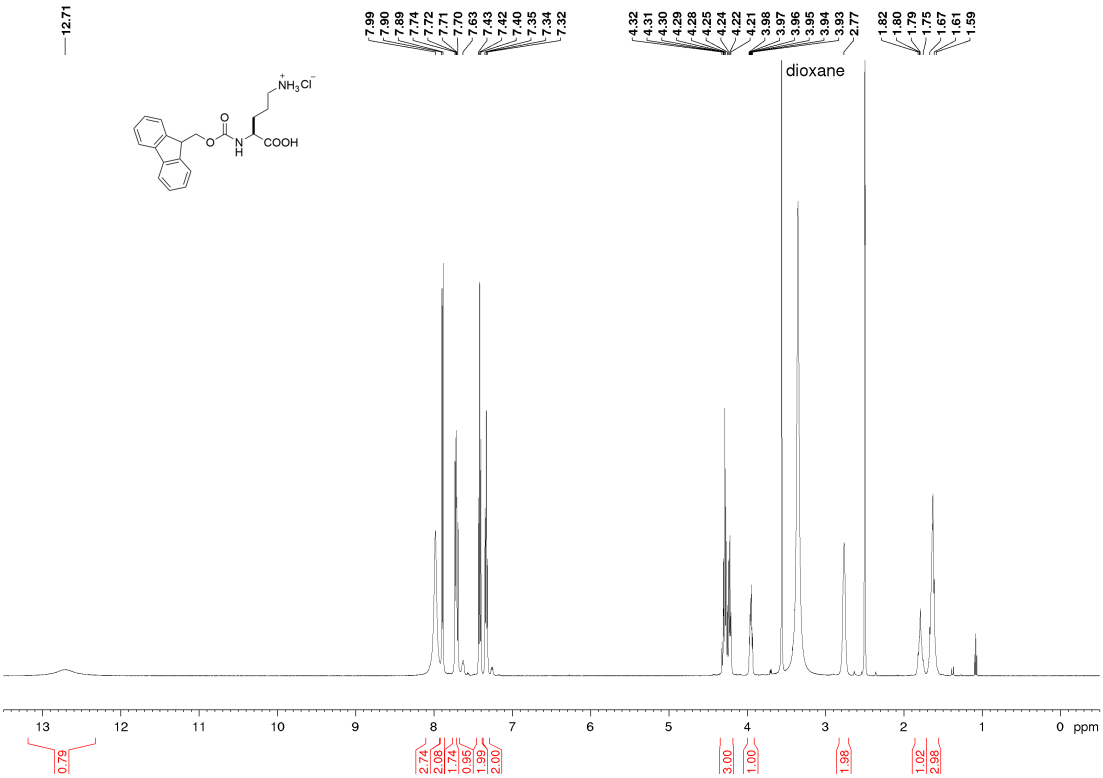

^{13}C NMR

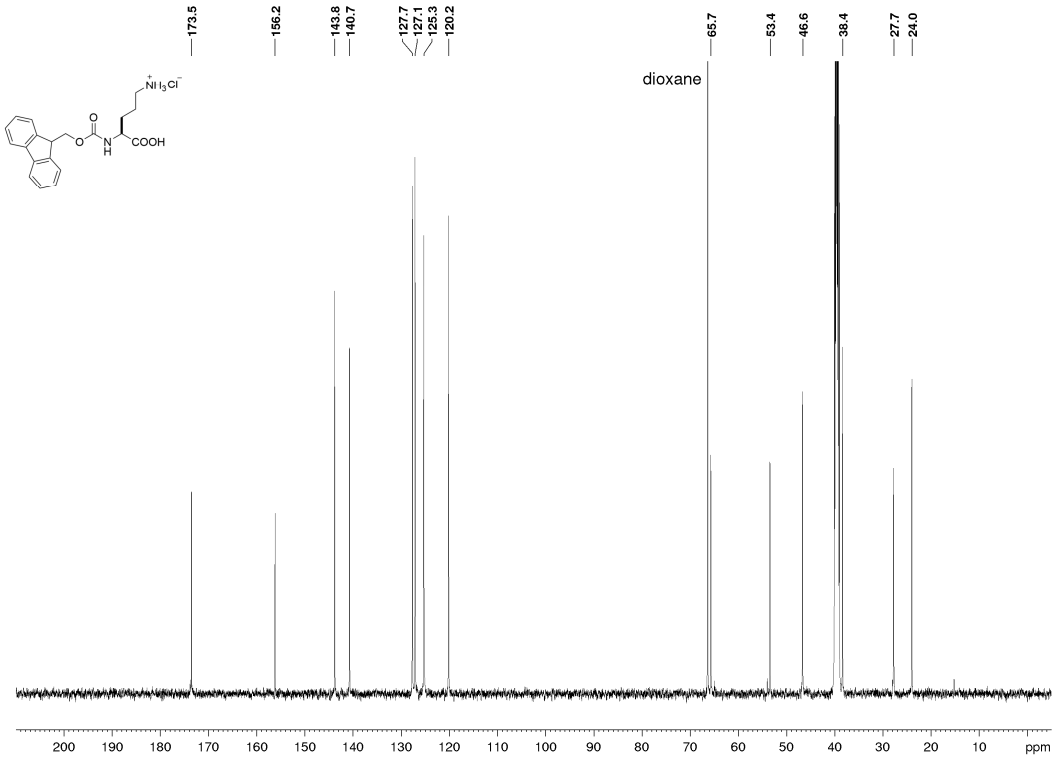

Fmoc-Orn(N_3)-OH (90)

^{1}H NMR

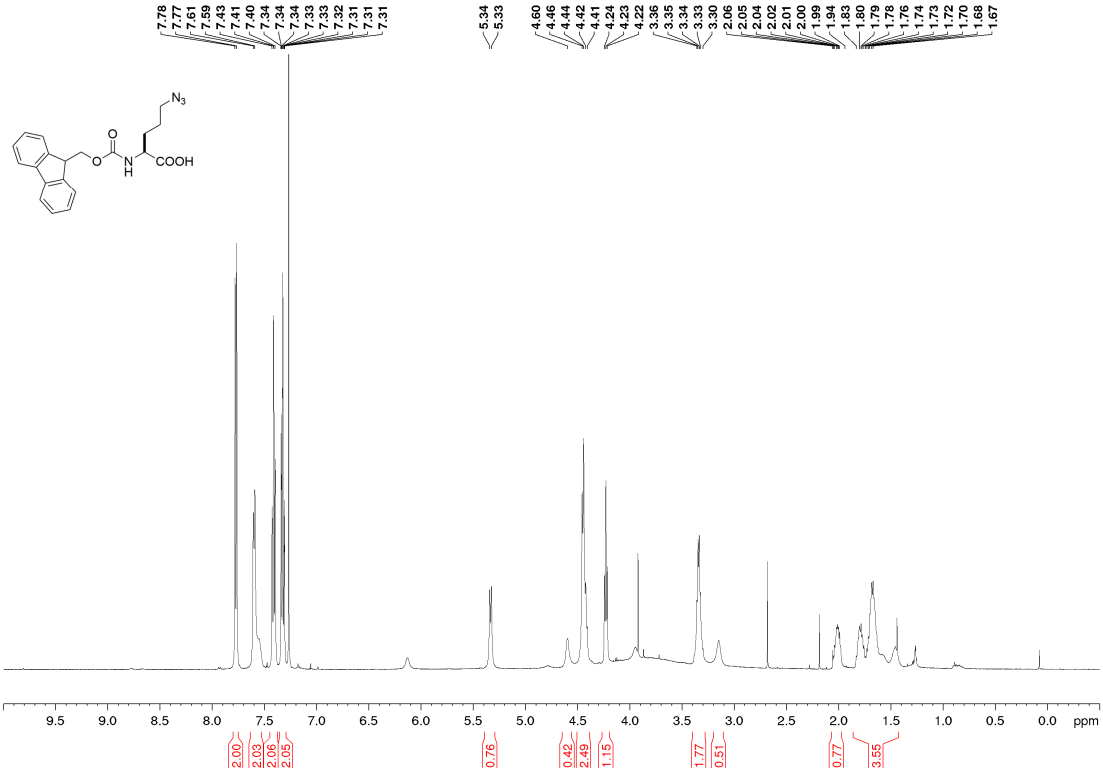

^{13}C NMR

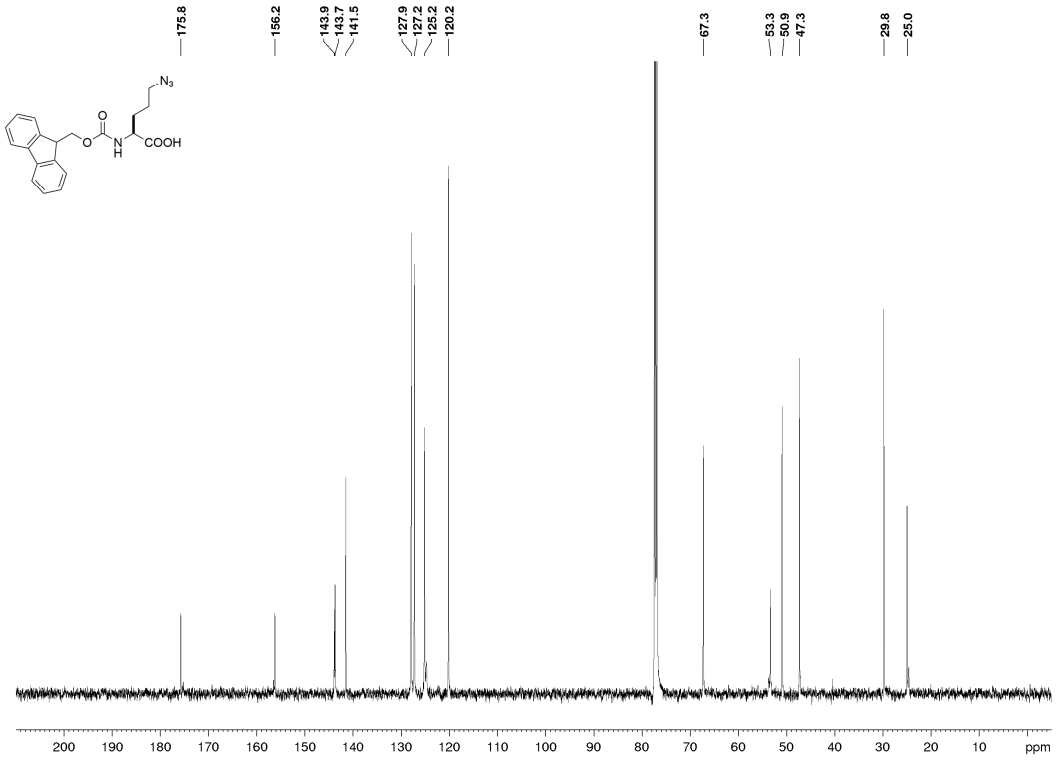

1-(Azidosulfonyl)-1*H*-imidazol-3-ium chloride (91)

^{1}H NMR

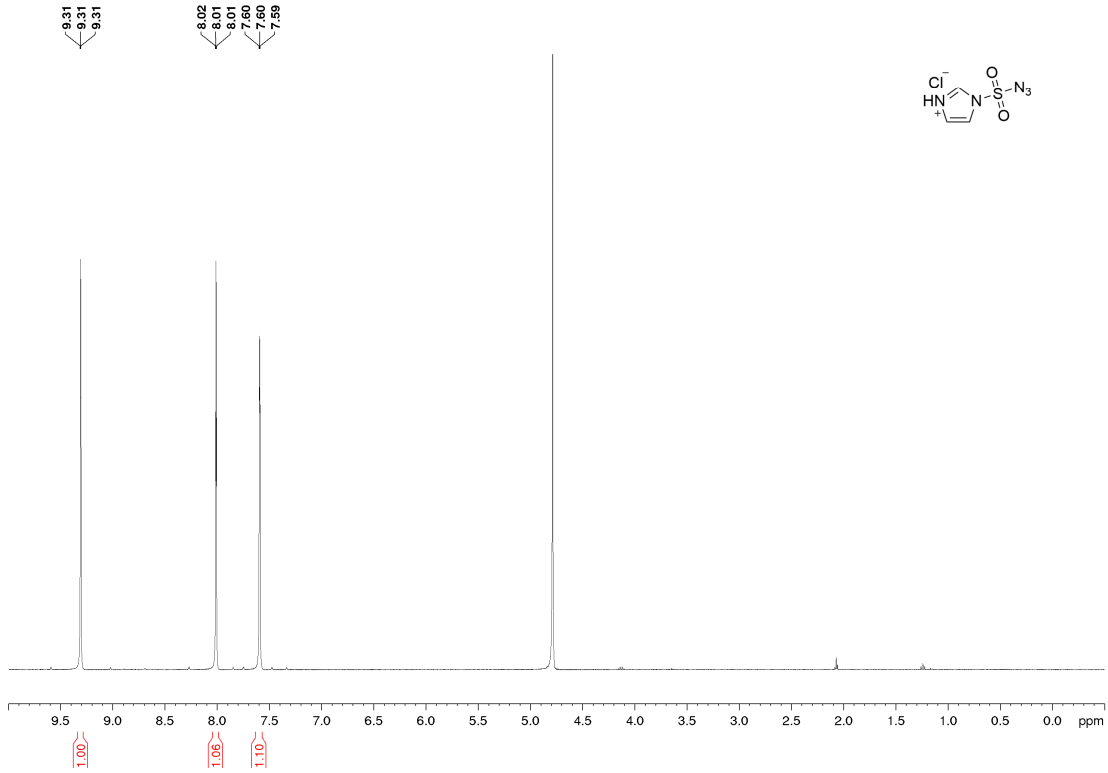

^{13}C NMR

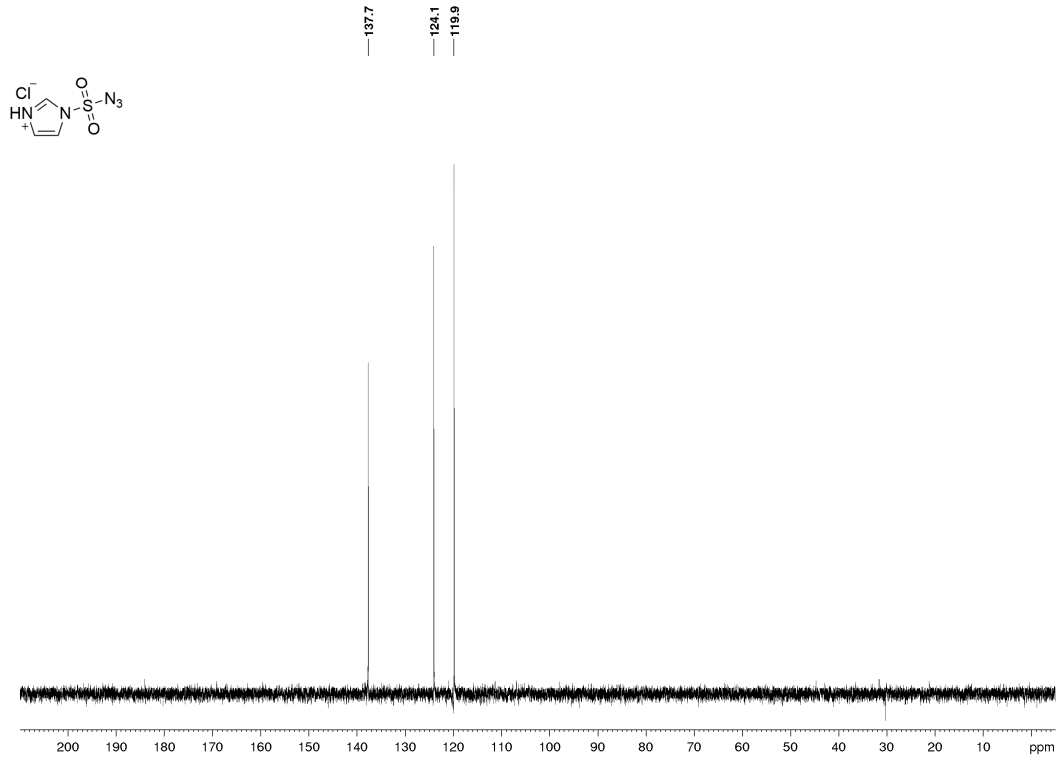

((5-Bromo-1,3-phenylene)bis(ethyne-2,1-diyl))bis(trimethylsilane) (82)

^{1}H NMR

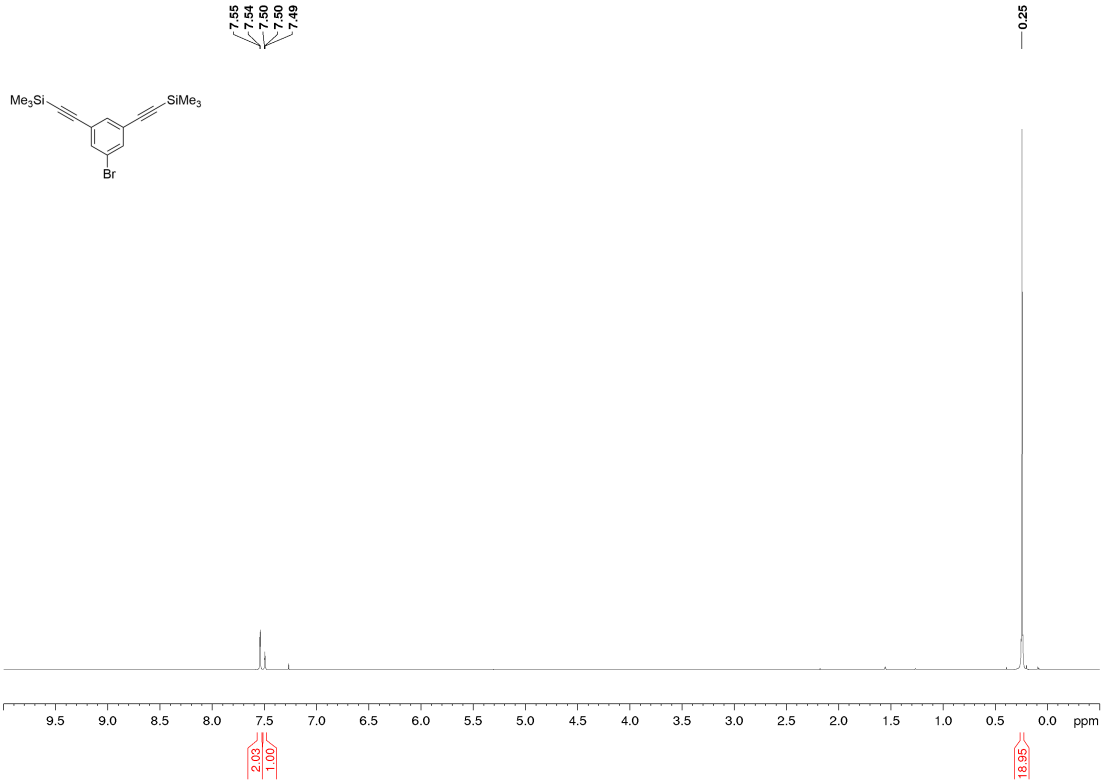

^{13}C NMR

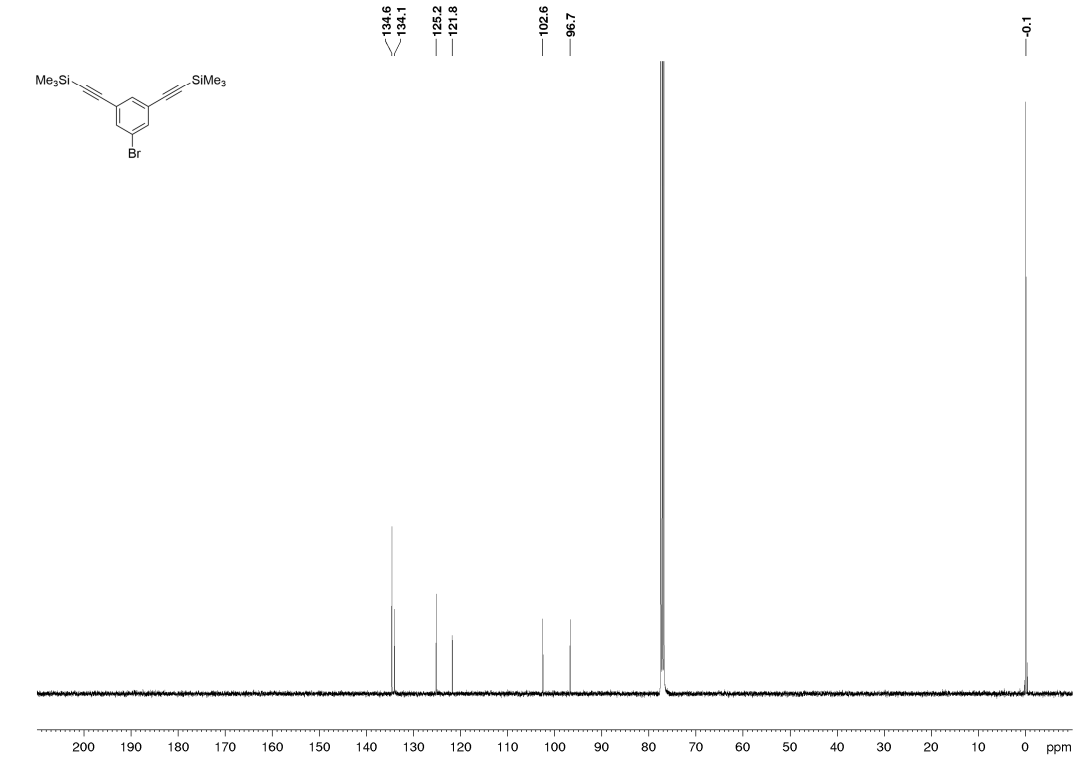

Methyl 3,5-bis((trimethylsilyl)ethynyl)benzoate (96)

^{1}H NMR

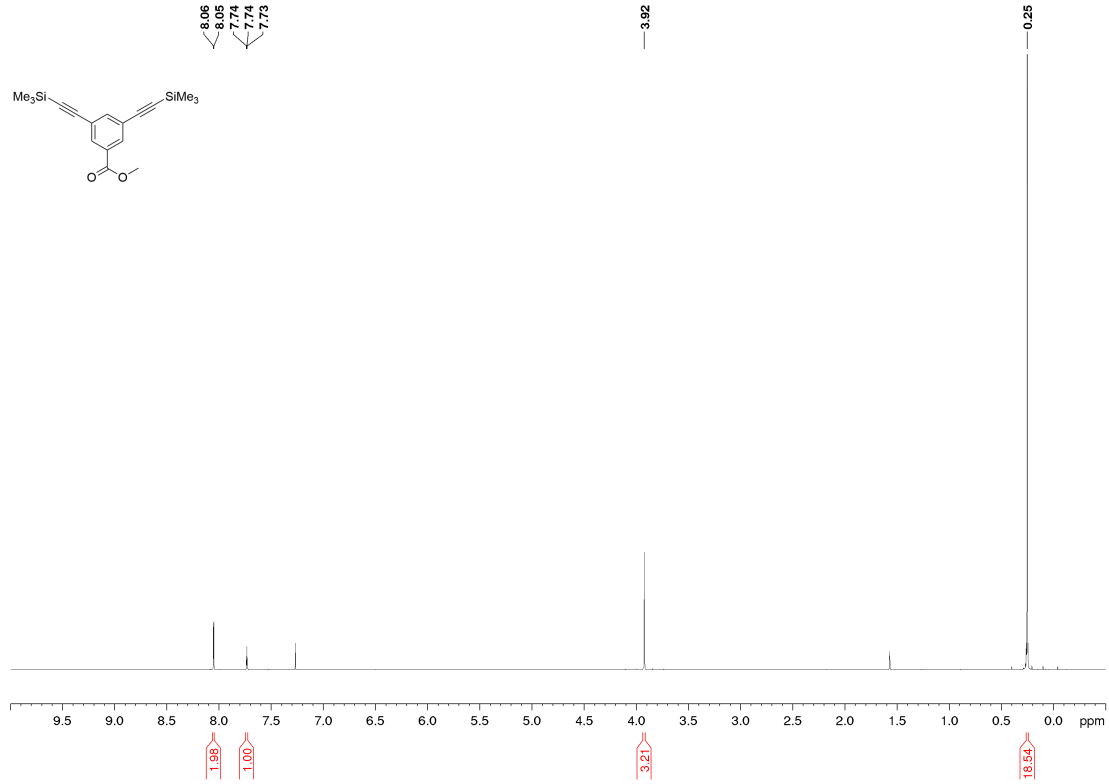

^{13}C NMR

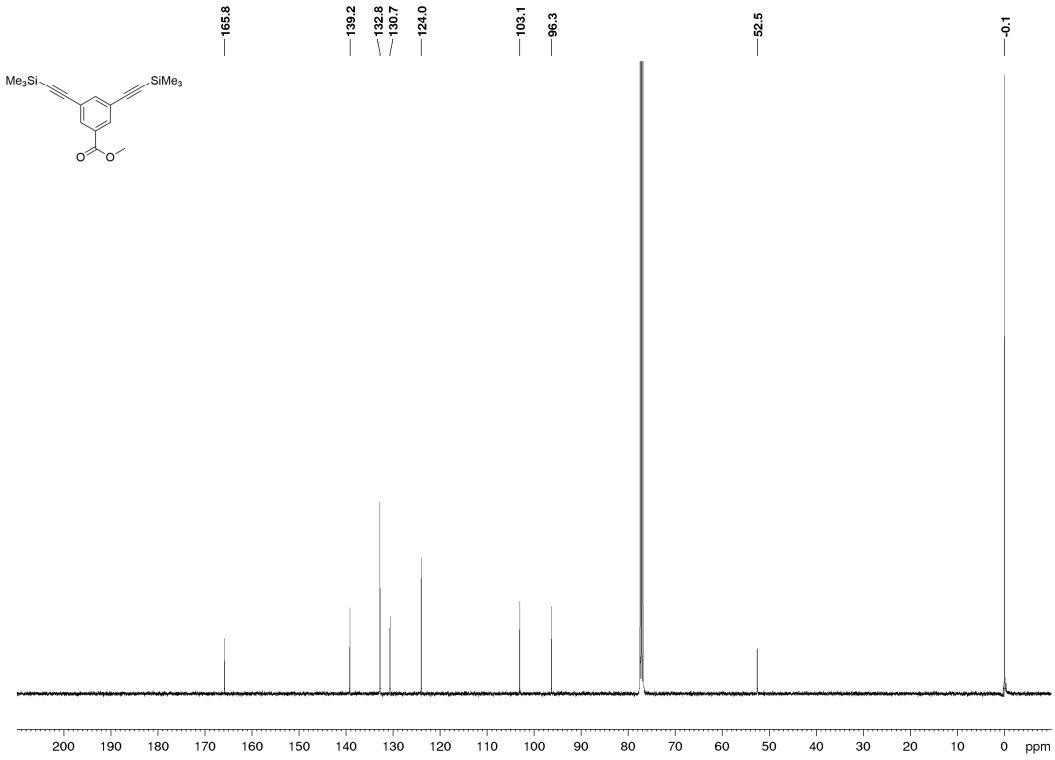

3,5-Diethynylbenzoic acid (95)

^{1}H NMR

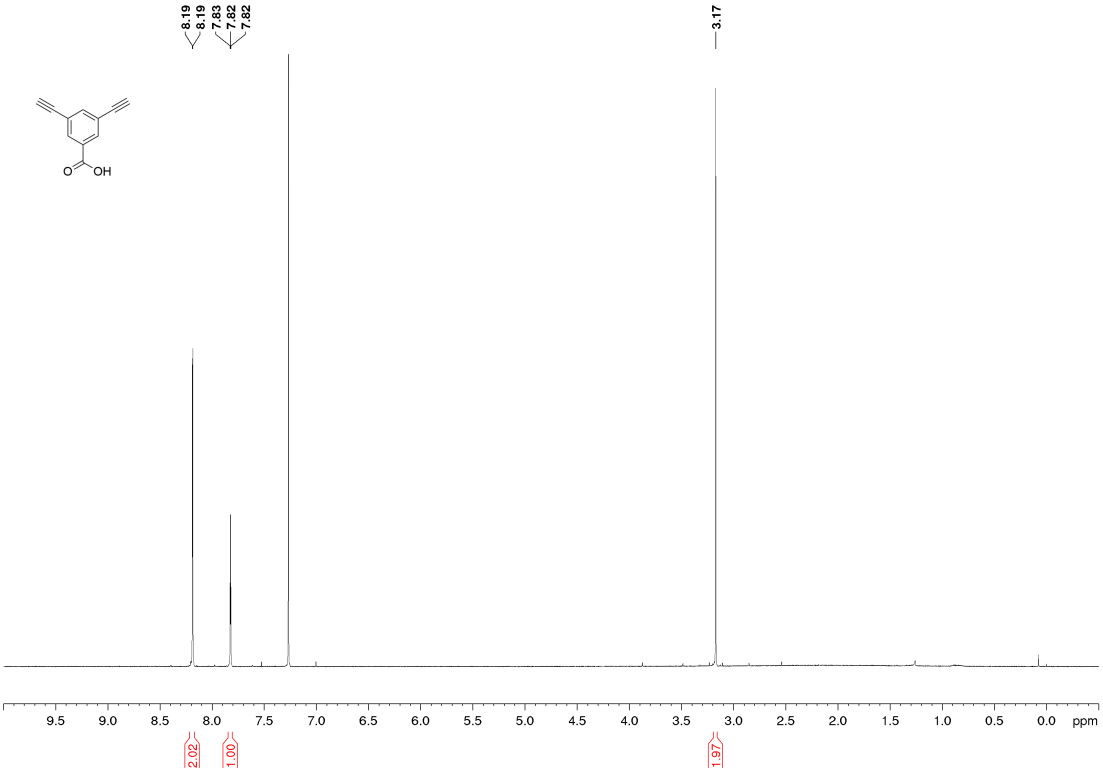

^{13}C NMR

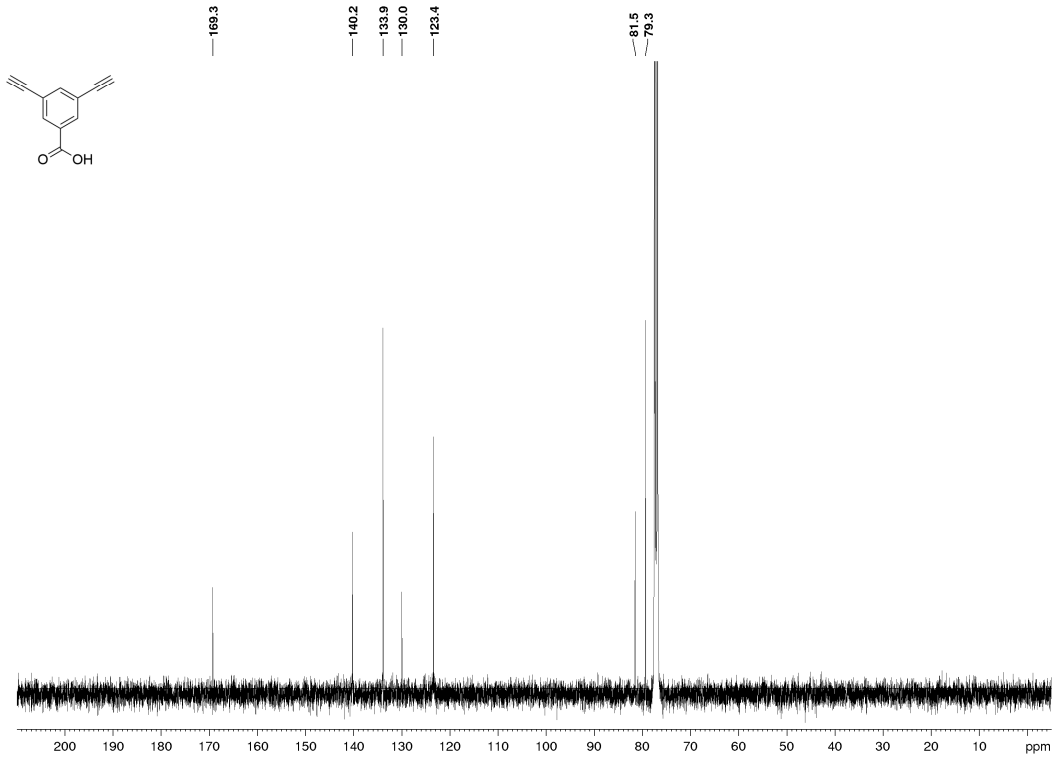

B.2. Chapter 5

Methyl (*S*)-2-formamido-3,3-dimethylbutanoate (102)

^{1}H-NMR

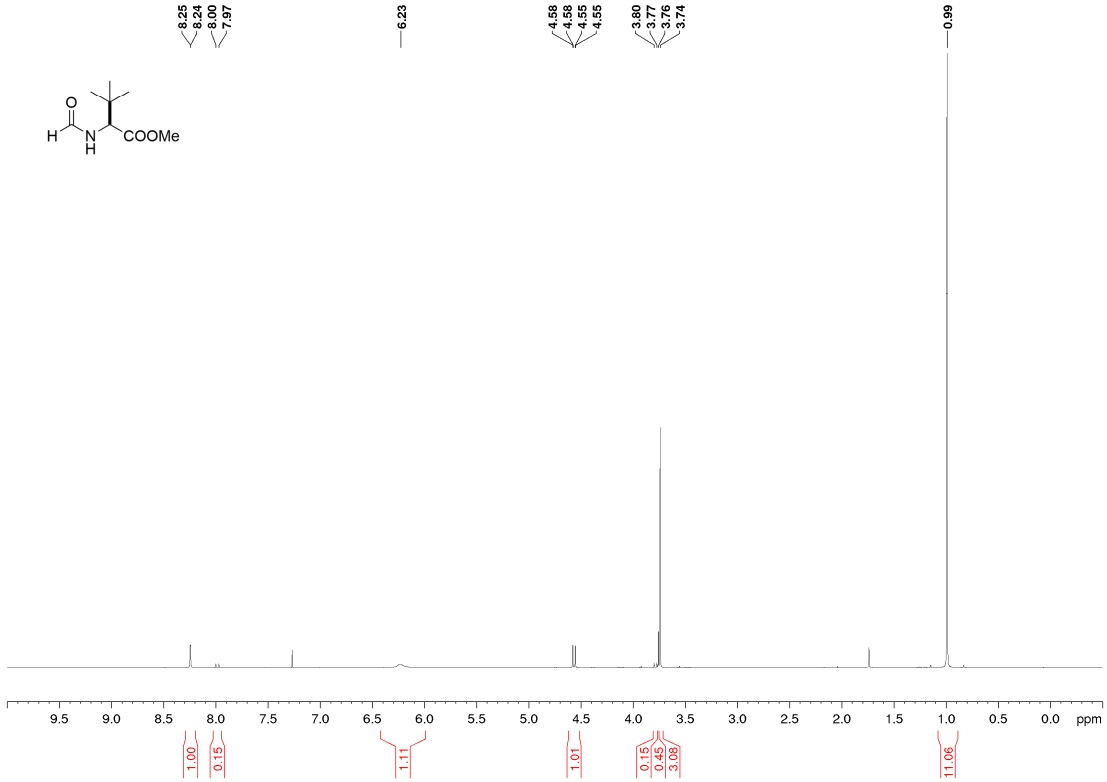

^{13}C-NMR

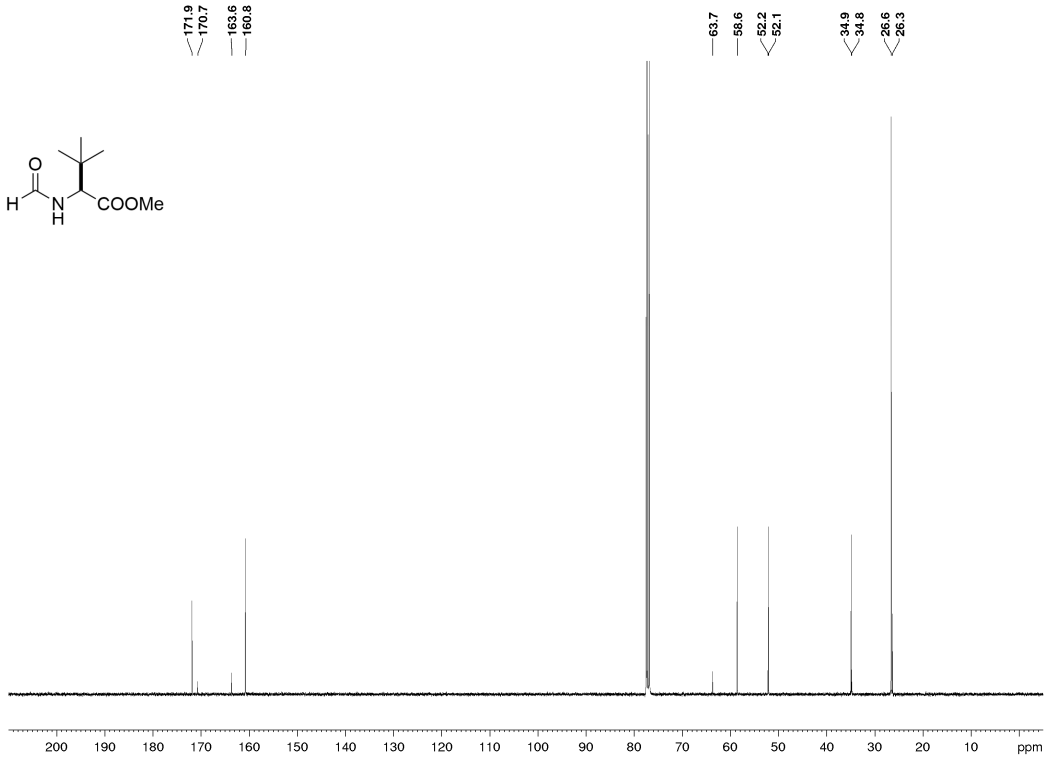

Methyl (*S*)-2-isocyano-3,3-dimethylbutanoate (101)

^{1}H-NMR

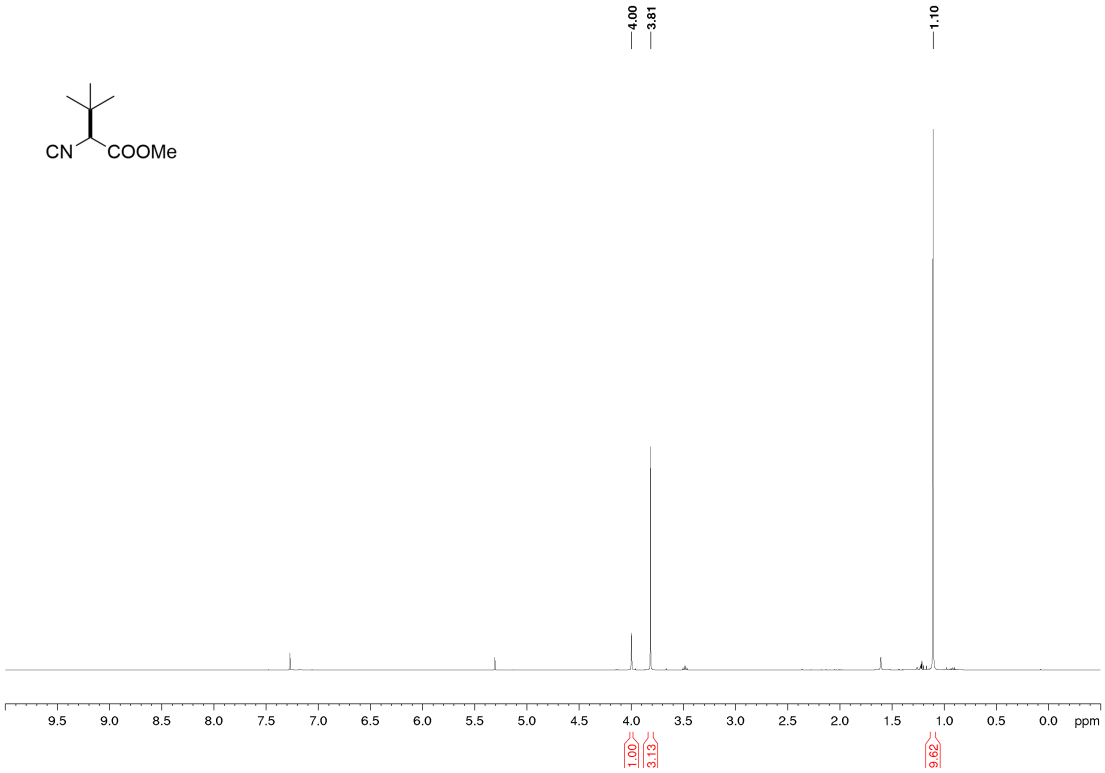

^{13}C-NMR

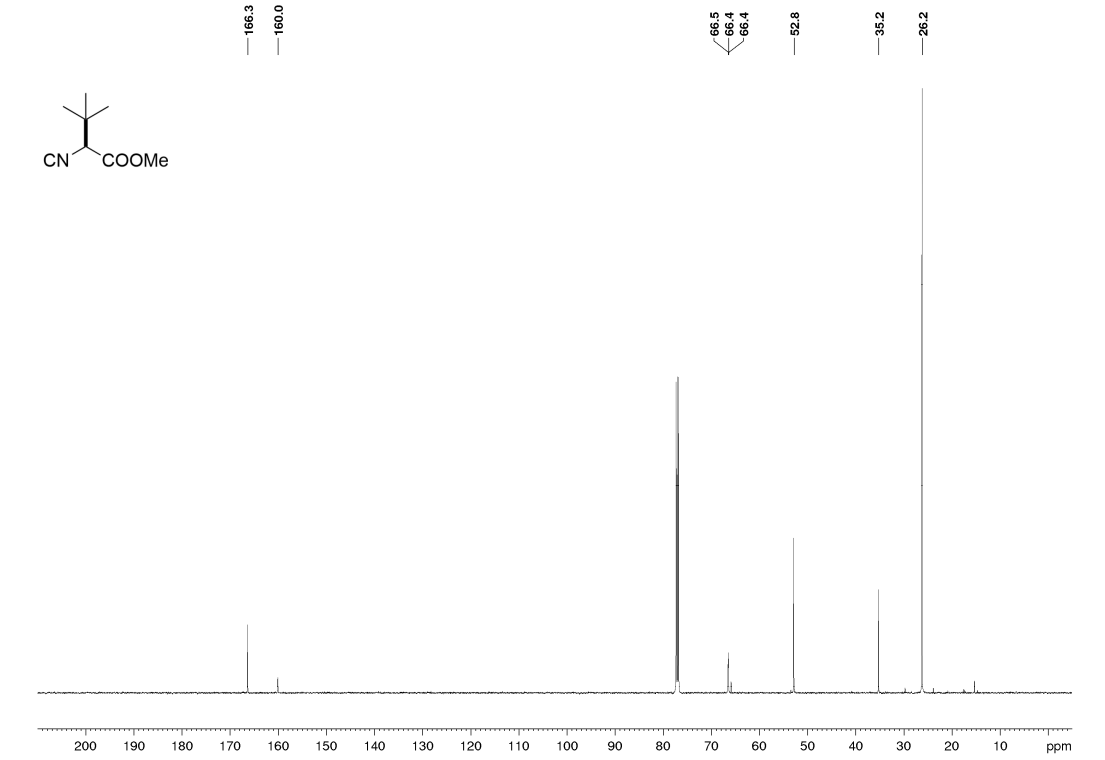

3-Bromo-1-methyl-1*H*-indole (104)

^{1}H-NMR

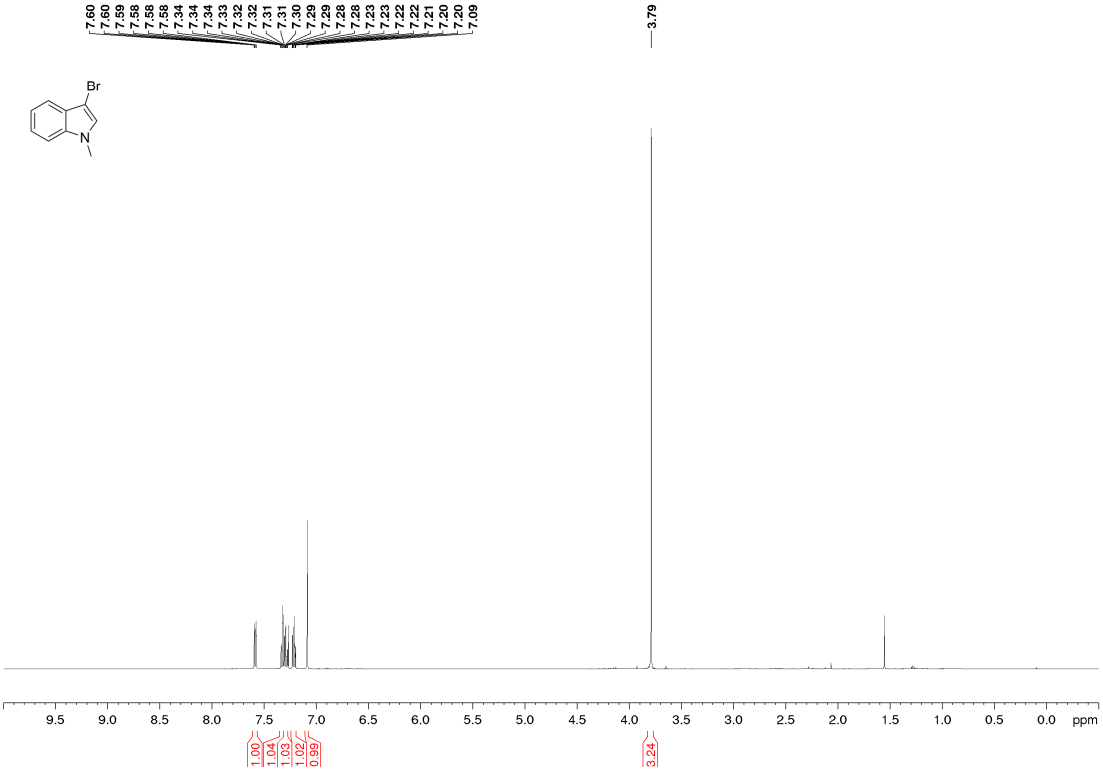

^{13}C-NMR

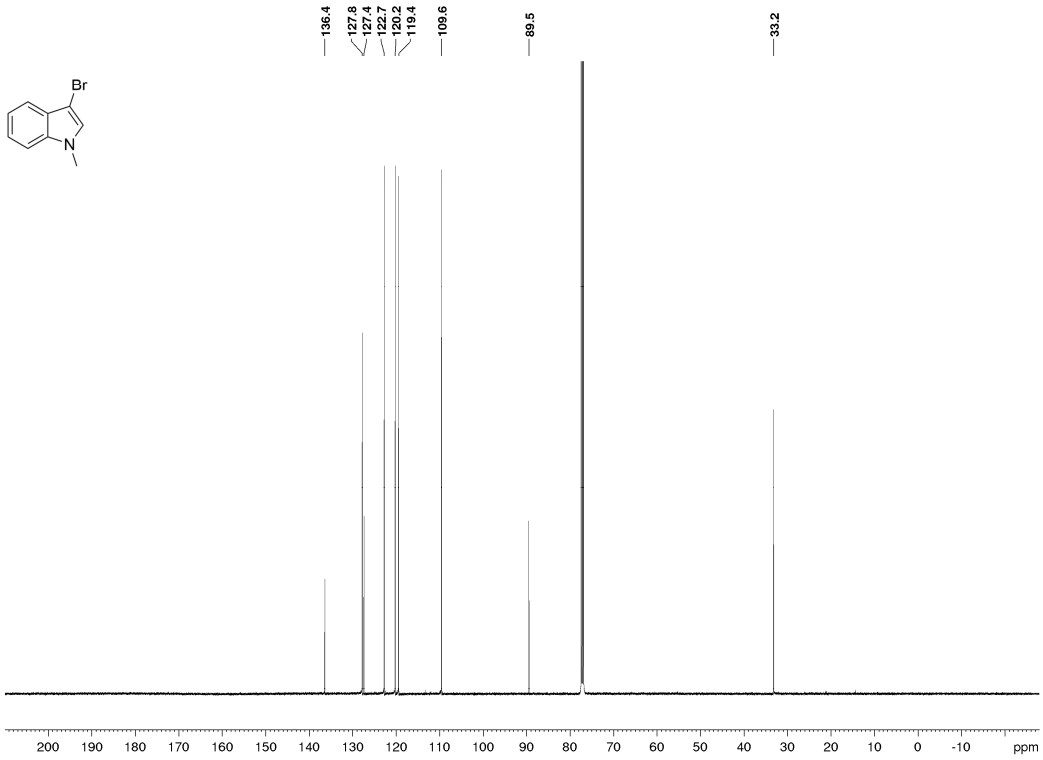

(±)-Methyl 2-(1-methyl-1*H*-indol-3-yl)propanoate (59)

^{1}H-NMR

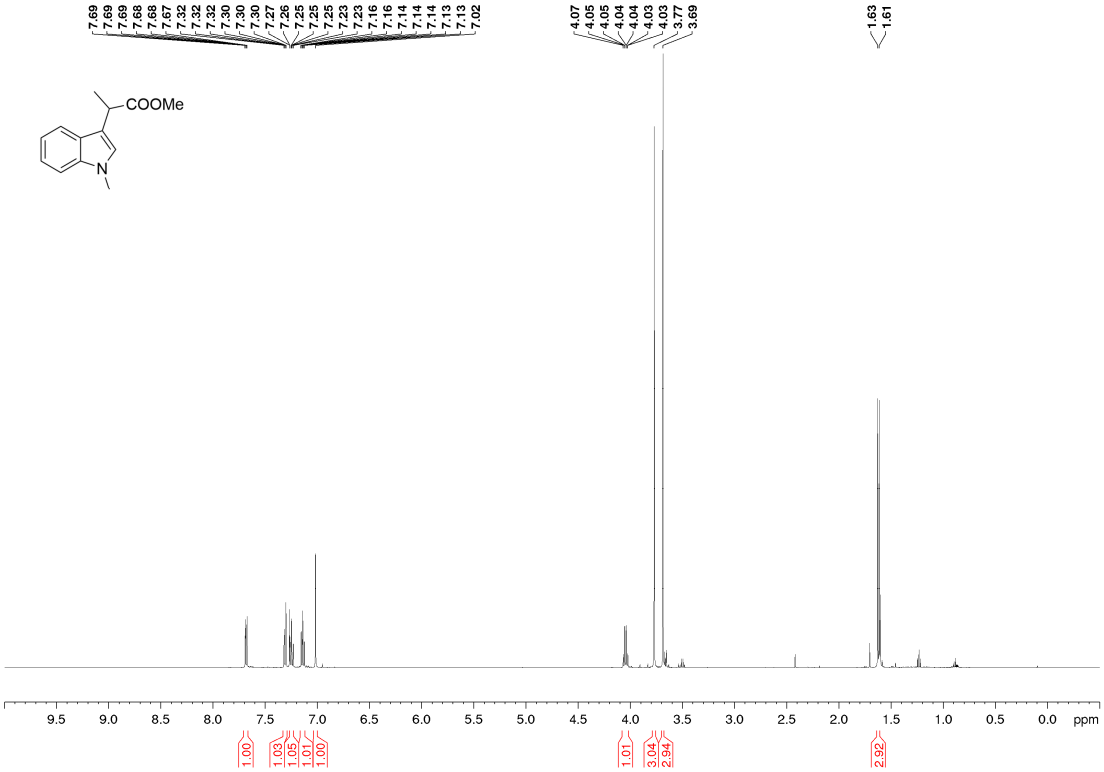

^{13}C-NMR

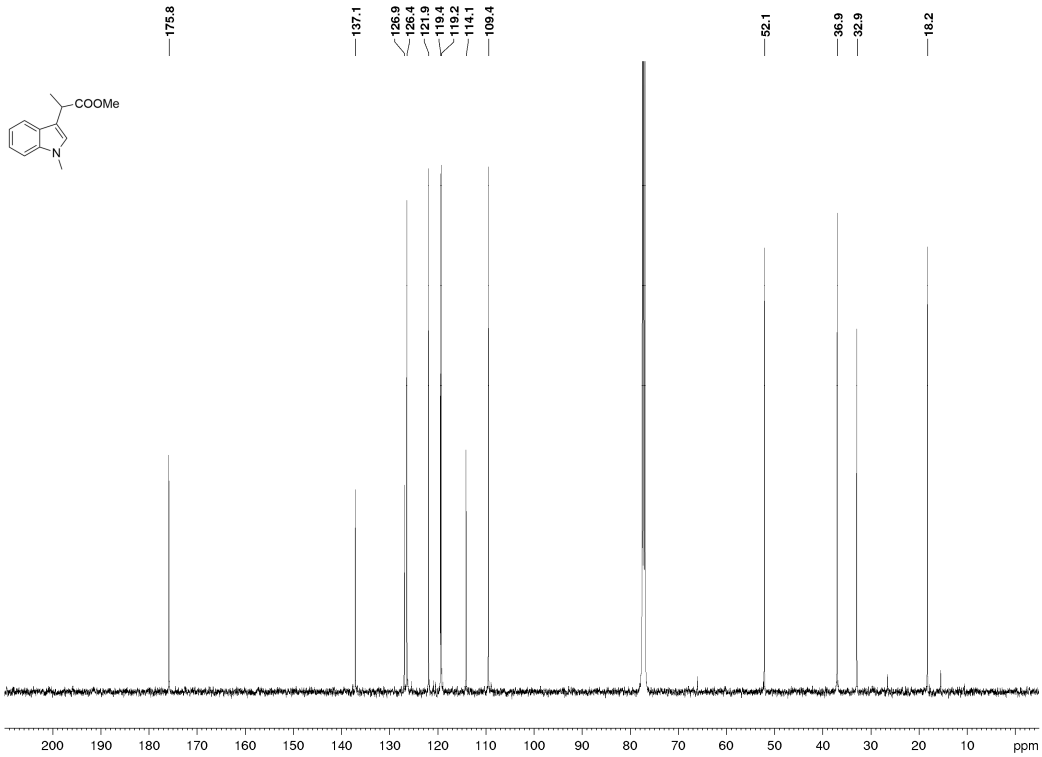

Methyl 2-methyl-2-(1-methyl-1*H*-indol-3-yl)propanoate (60)

^{1}H-NMR

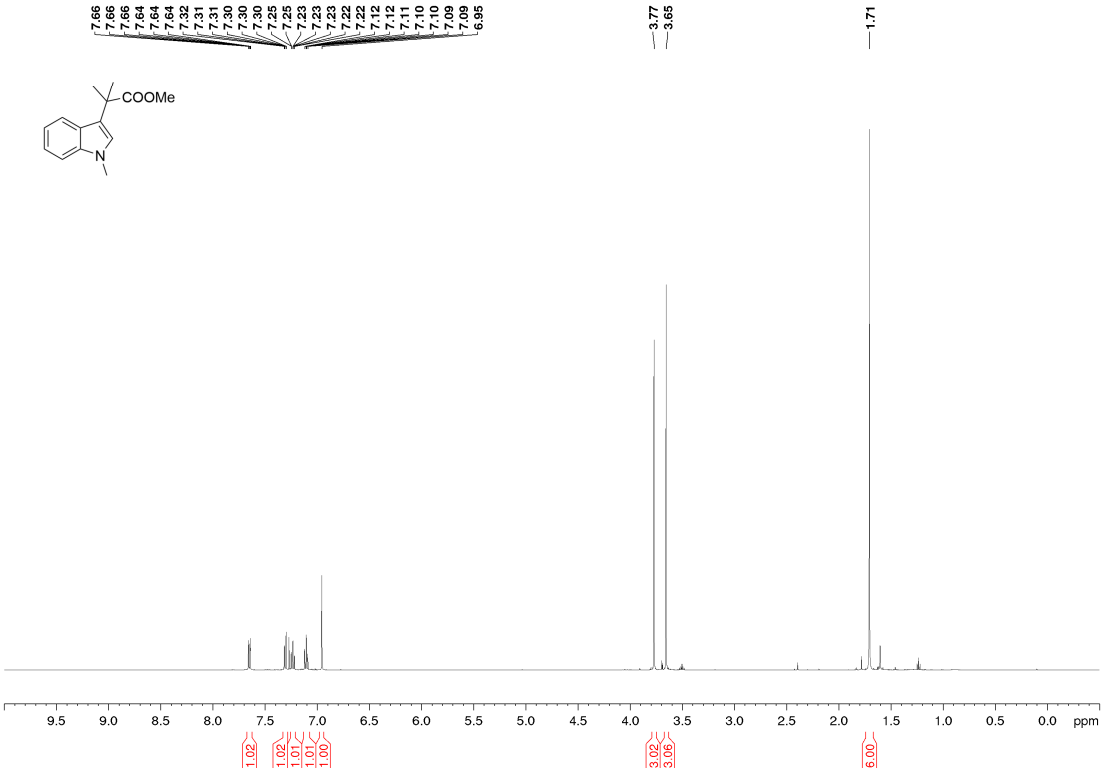

^{13}C-NMR

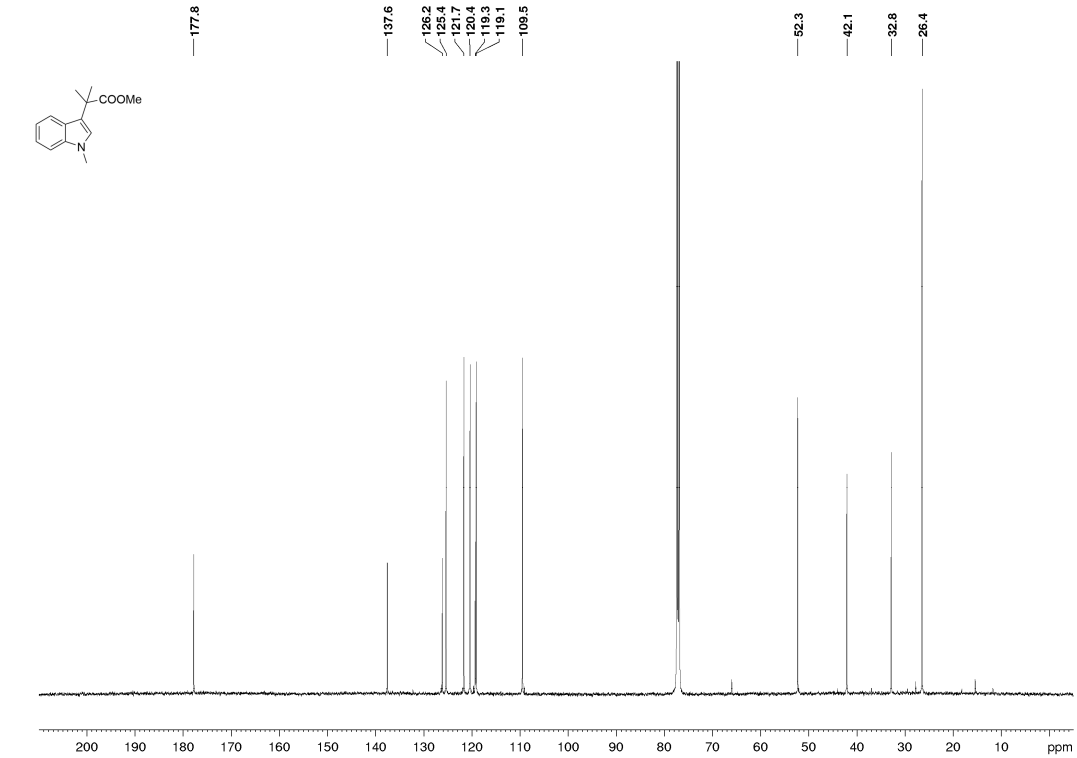

2-Methyl-2-(1-methyl-1*H*-indol-3-yl)propan-1-ol (105)

^{1}H-NMR

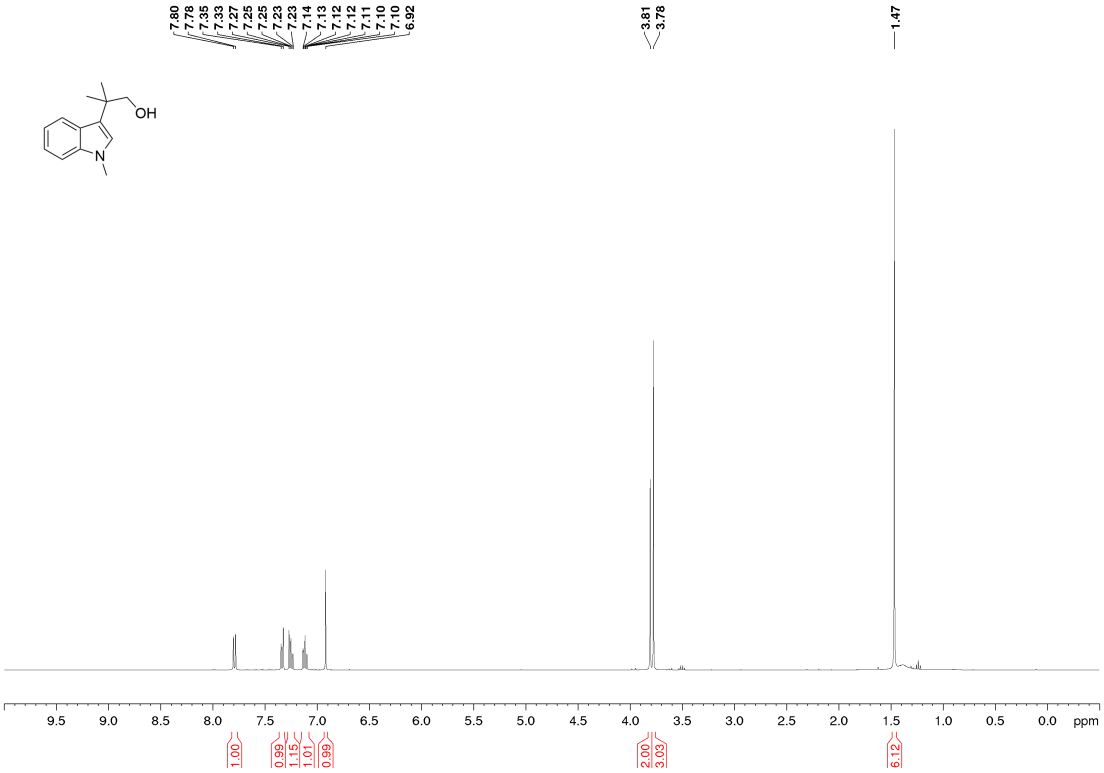

^{13}C-NMR

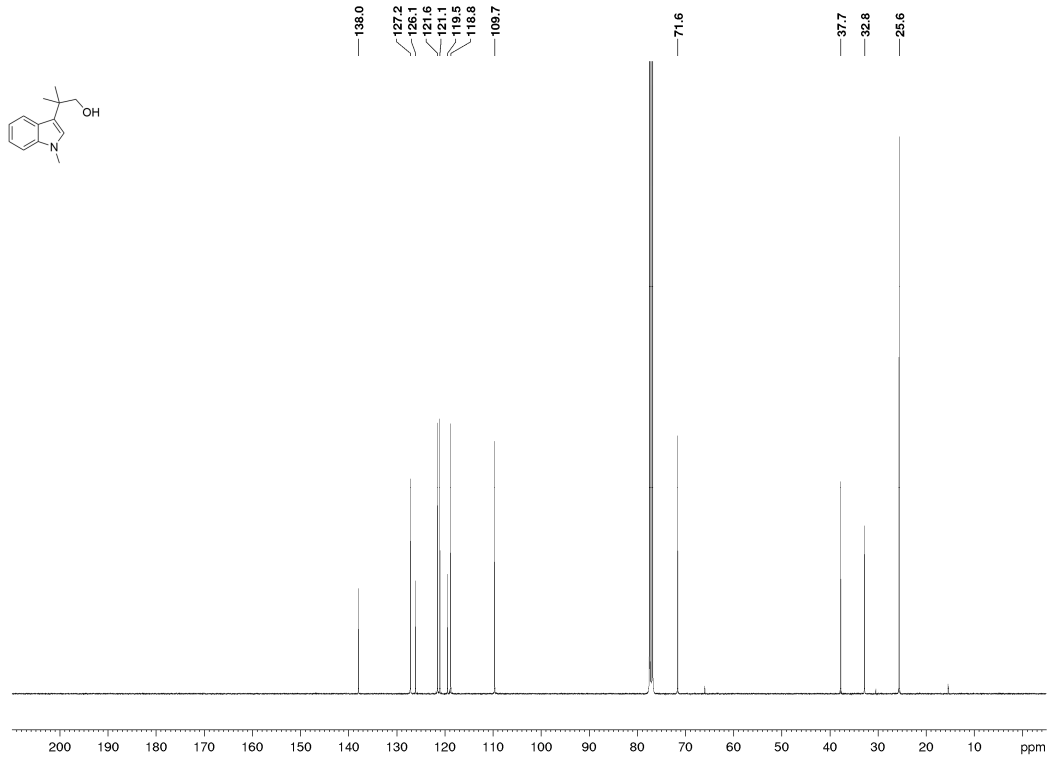

2-Methyl-2-(1-methyl-1*H*-indol-3-yl)propanal (69)

^{1}H-NMR

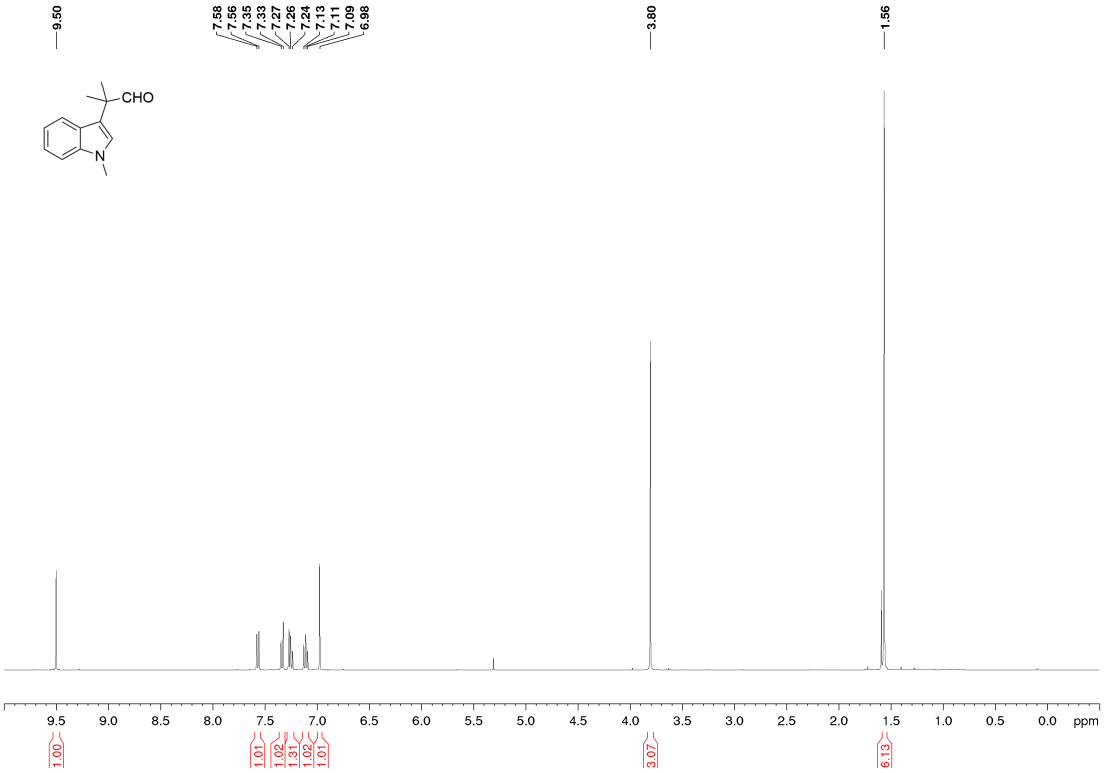

^{13}C-NMR

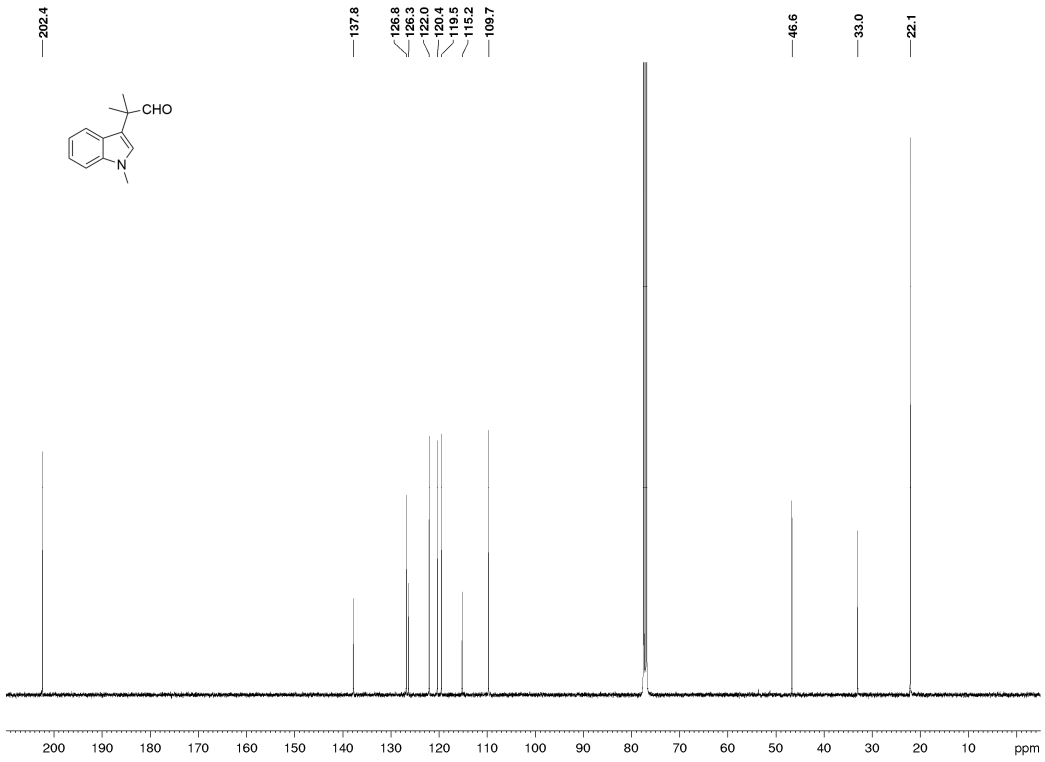

Methyl (*S*)-3,3-dimethyl-2-((*S*)-3-methyl-3-(1-methyl-1*H*-indol-3-yl)-2-(2,2,2-trifluoro-*N*-methylacetamido)butanamido)butanoate (99a)

^{1}H-NMR

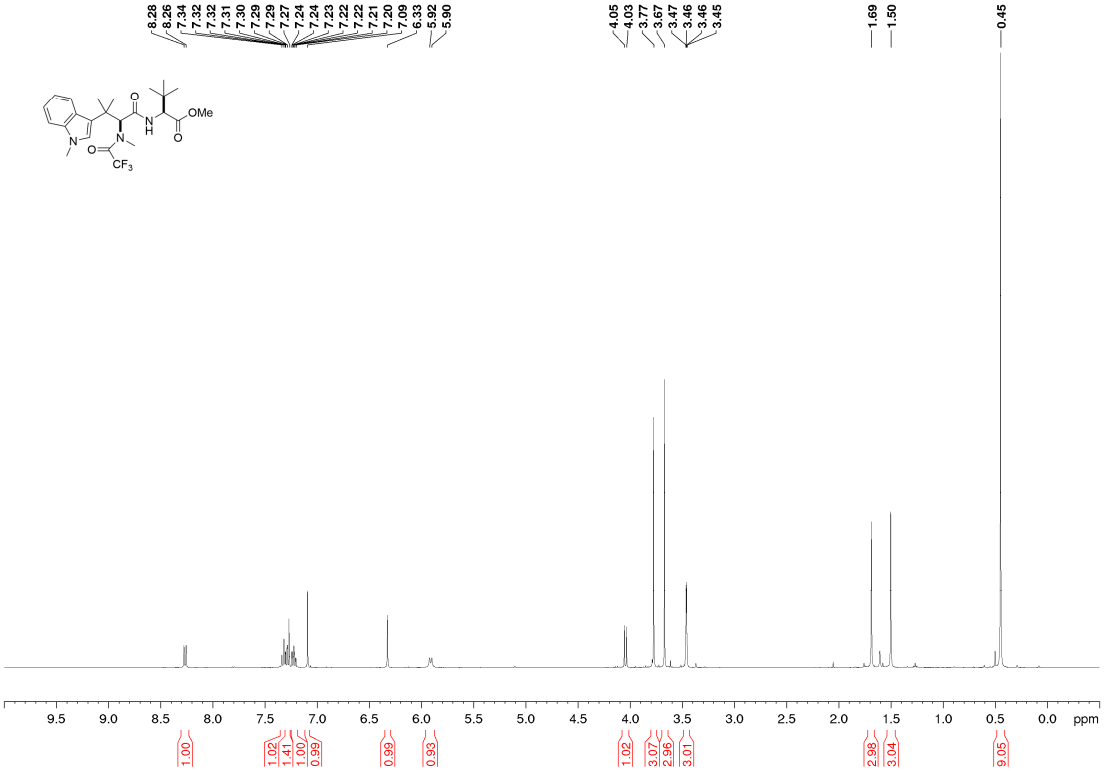

^{13}C-NMR

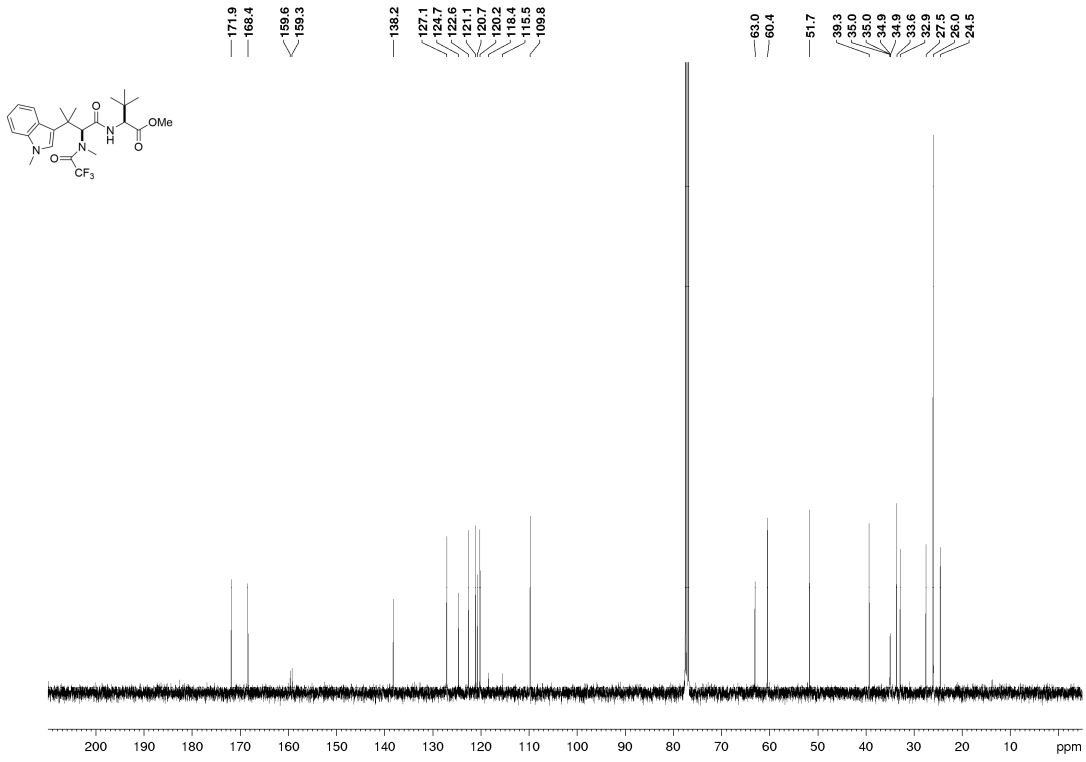

^{19}F-NMR

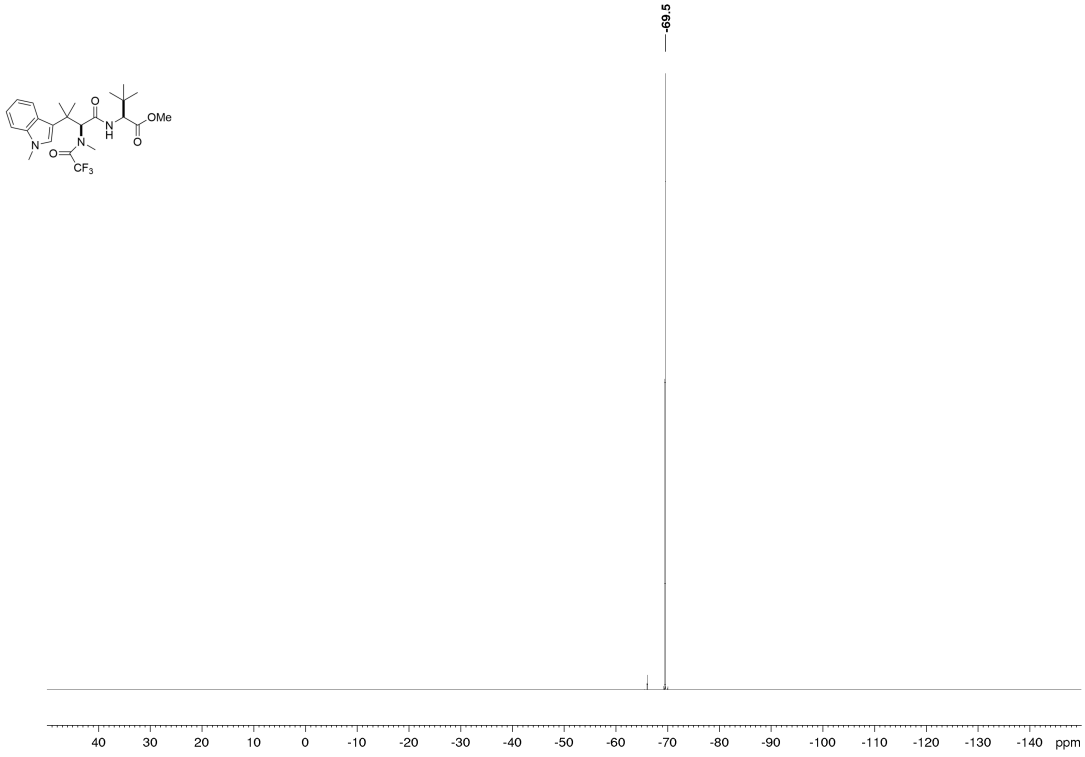

Methyl (*S*)-3,3-dimethyl-2-((*R*)-3-methyl-3-(1-methyl-1*H*-indol-3-yl)-2-(2,2,2-trifluoro-*N*-methylacetamido)butanamido)butanoate (99b)

^{1}H-NMR

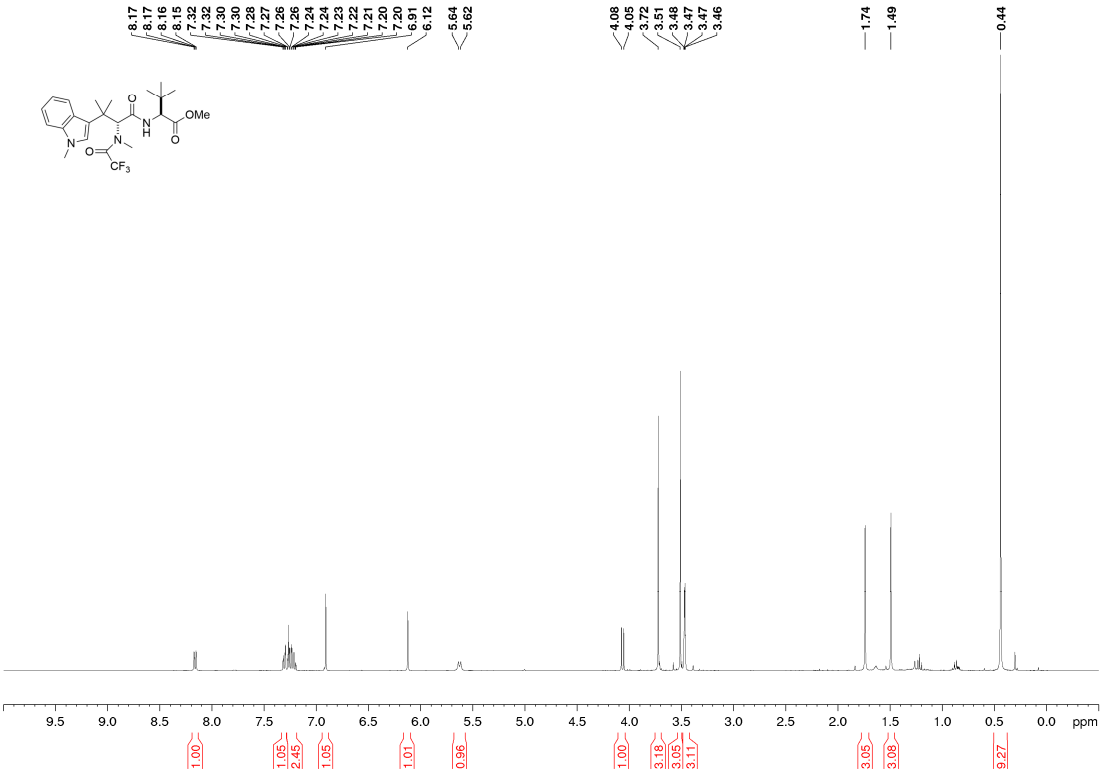

^{13}C-NMR

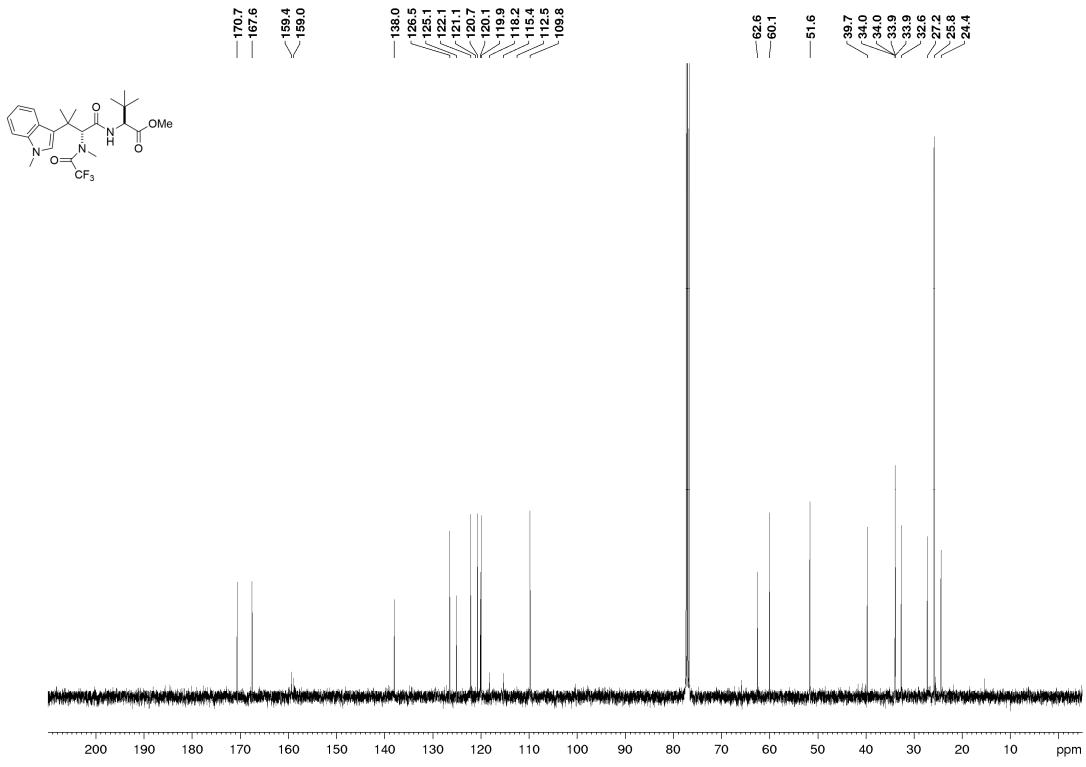

^{19}F-NMR

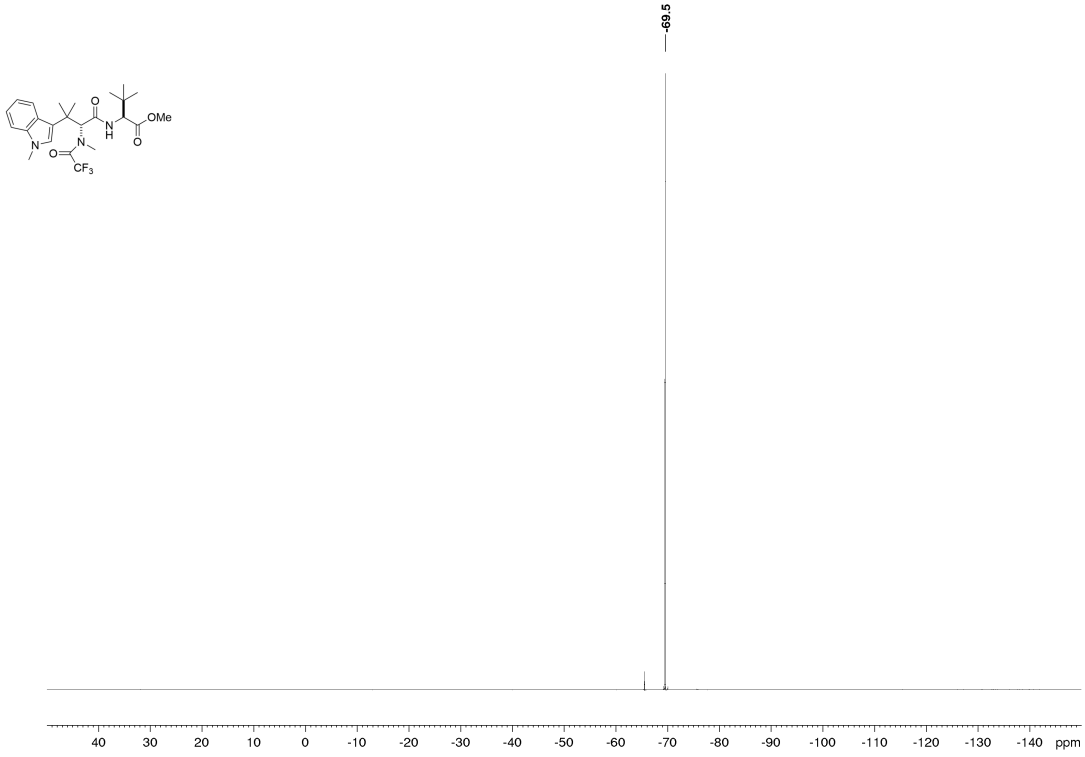

(*S*)-*N*$^{\alpha}$-*tert*-Butoxycarbonyl-*N*$^{\alpha}$-methylvalin-*N*-methoxy-*N*-methylamide (110)

^{1}H-NMR

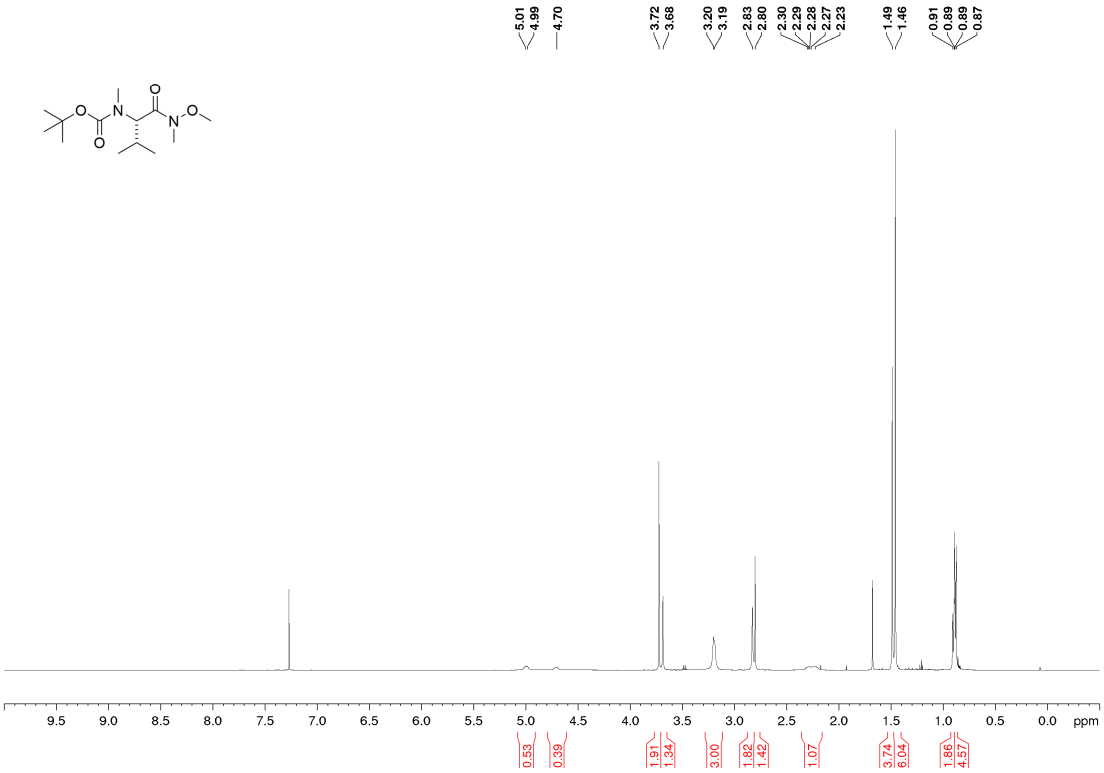

^{13}C-NMR

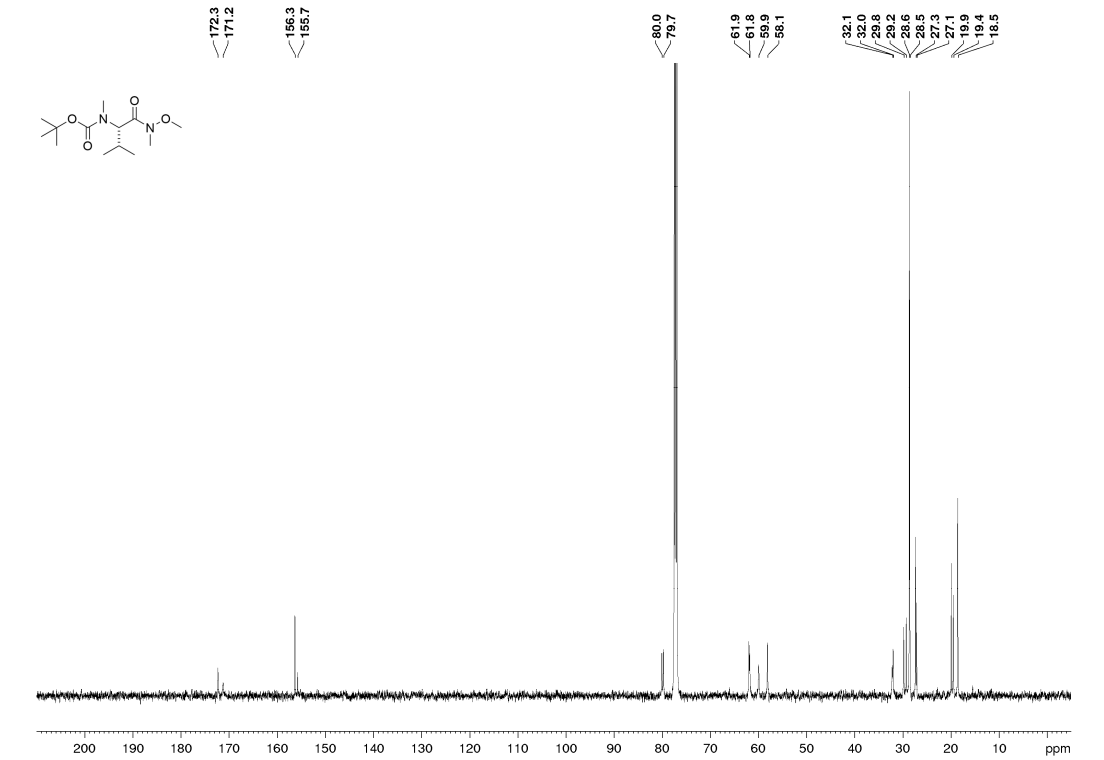

Ethyl (2*E*,4*S*)-*N*-*tert*-butoxycarbonyl-*N*-methyl-4-amino-2,5-dimethylhex-2-enoate (100)

^{1}H-NMR

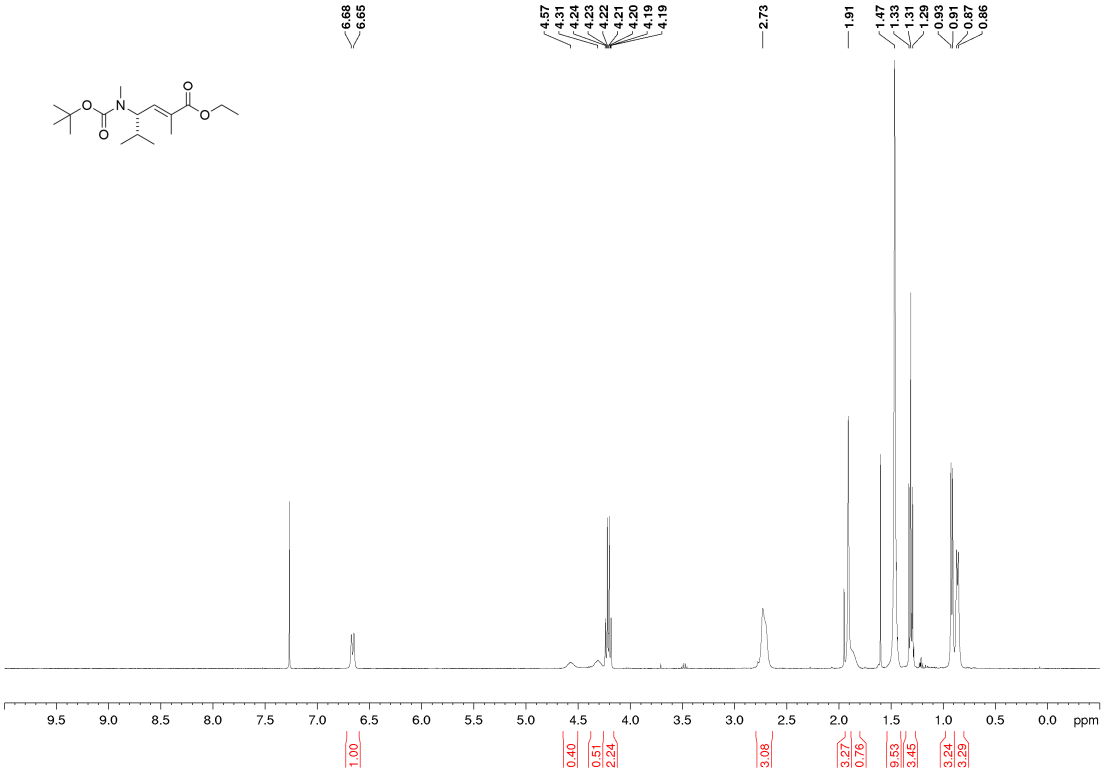

^{13}C-NMR

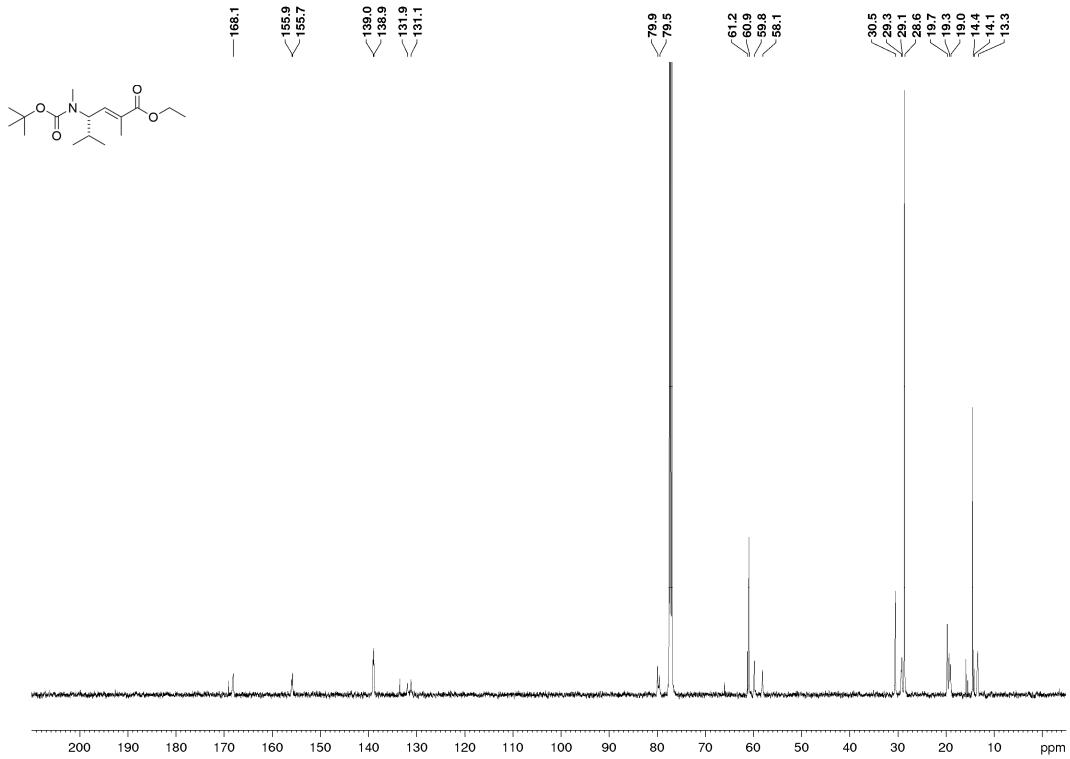

Ethyl (*S*,*E*)-4-((*S*)-2-((*tert*-butoxycarbonyl)amino)-*N*,3,3-trimethylbutanamido)-2,5-dimethylhex-2-enoate (115)

^{1}H-NMR

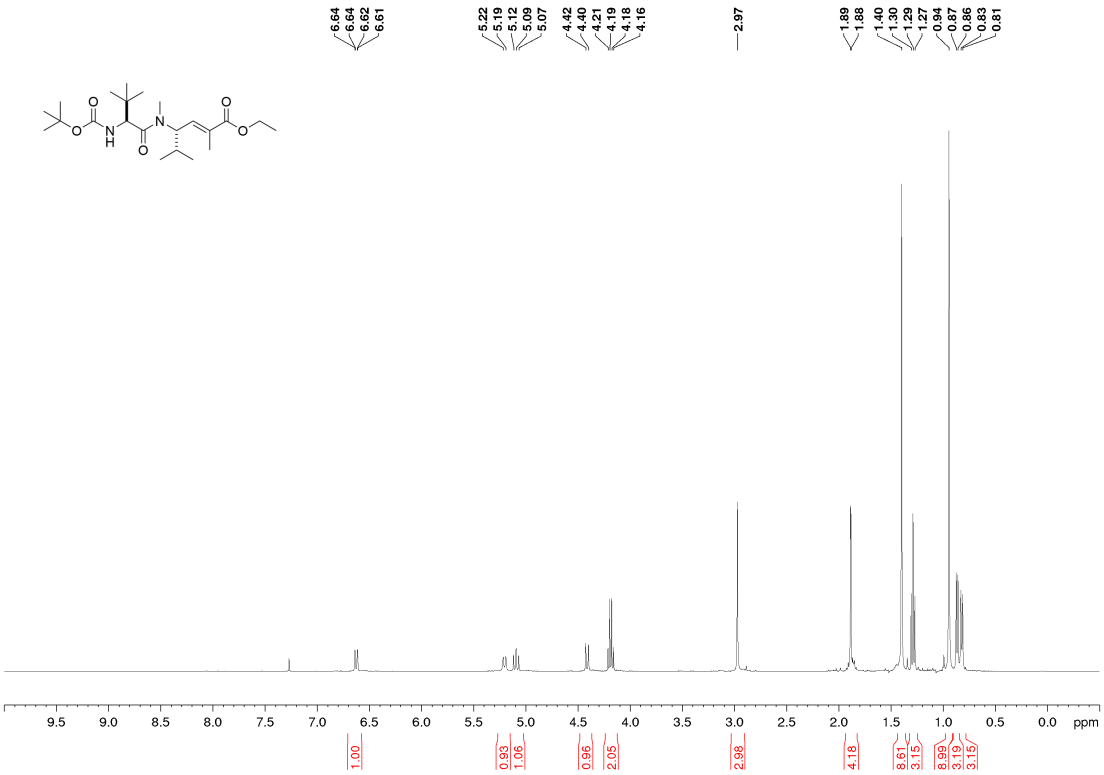

^{13}C-NMR

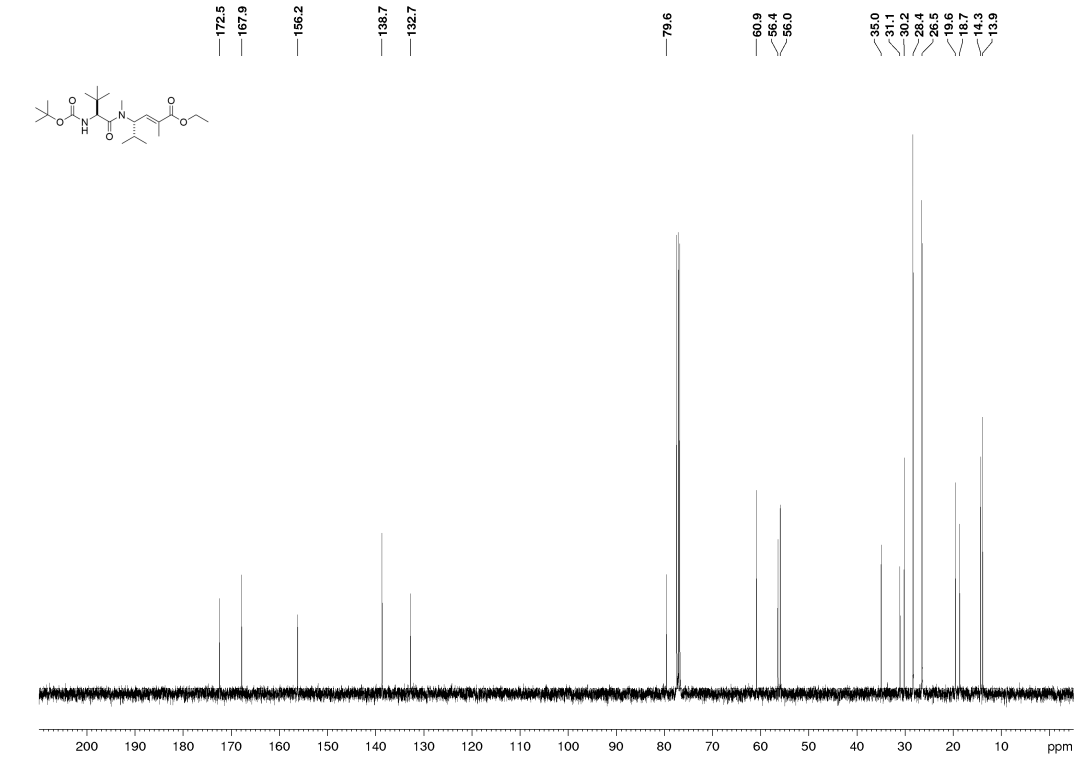

Ethyl (*S*,*E*)-4-((*S*)-2-formamido-*N*,3,3-trimethylbutanamido)-2,5-dimethylhex-2-enoate (116)

^{1}H-NMR

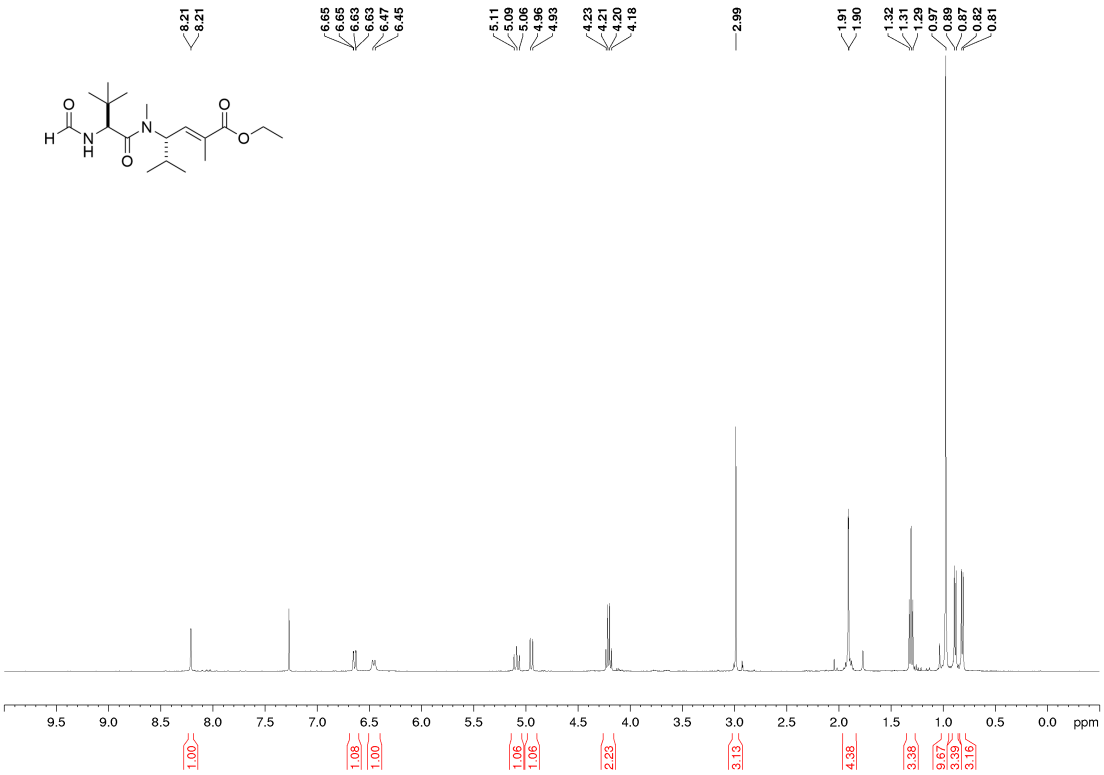

^{13}C-NMR

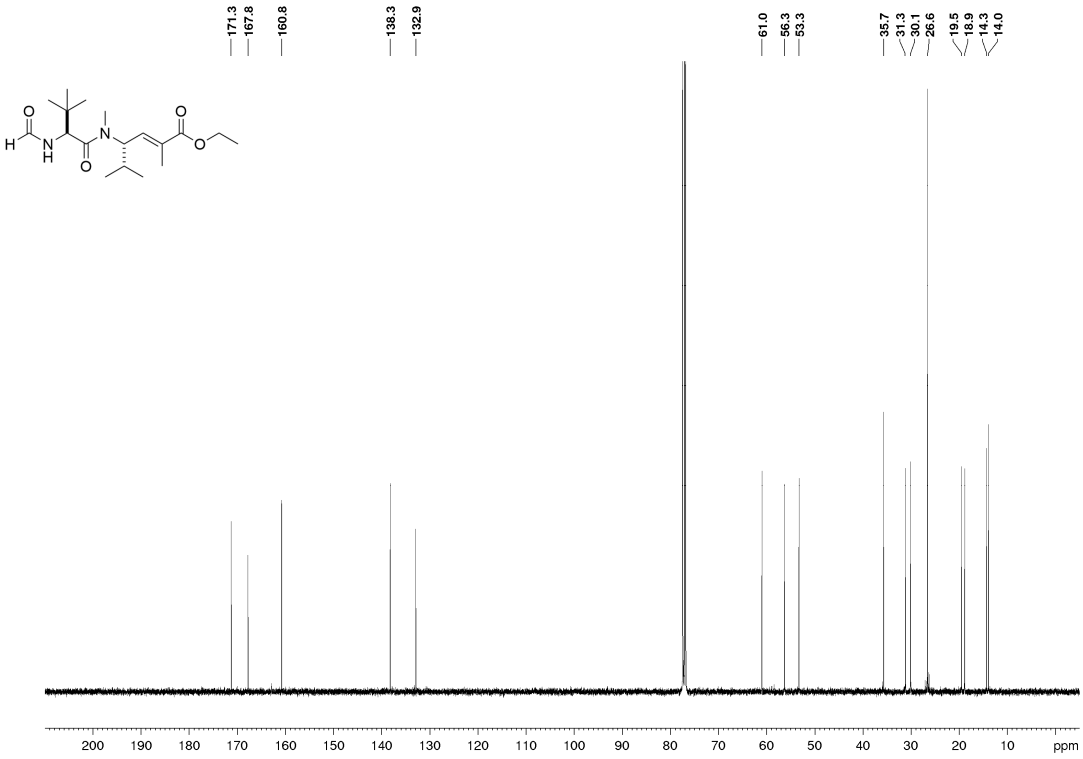

Ethyl (*S*,*E*)-4-((*S*)-2-isocyano-*N*,3,3-trimethylbutanamido)-2,5-dimethylhex-2-enoate (117)

^{1}H-NMR

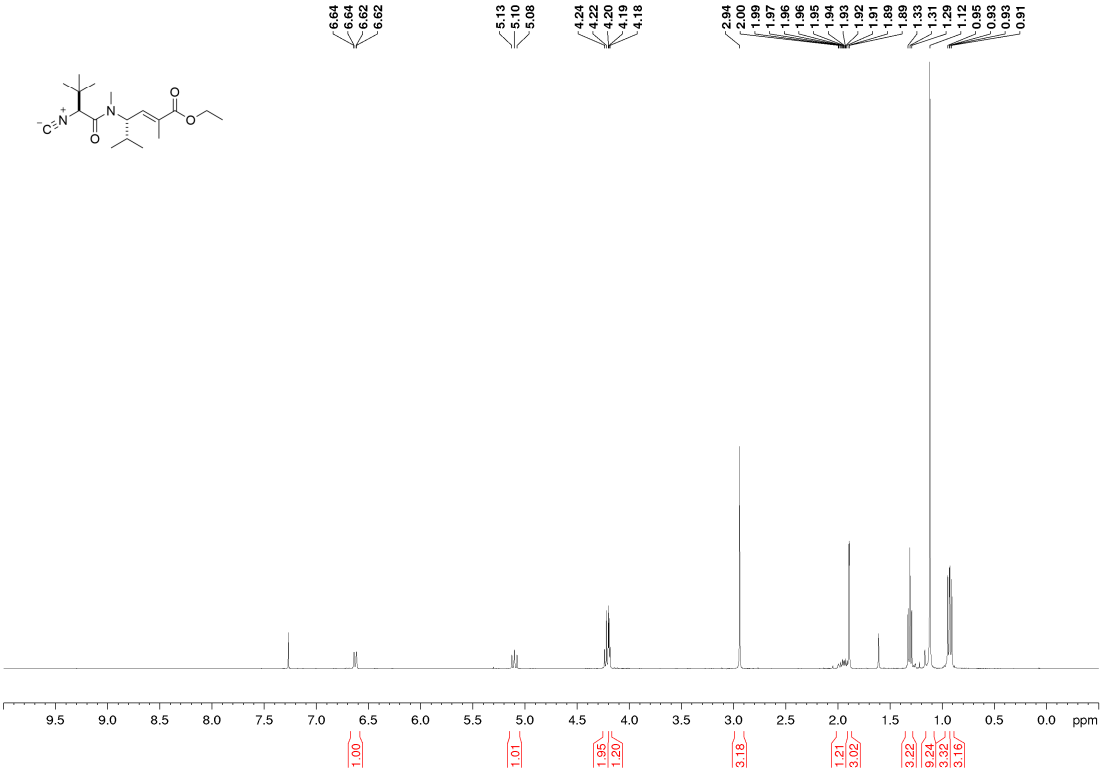

^{13}C-NMR

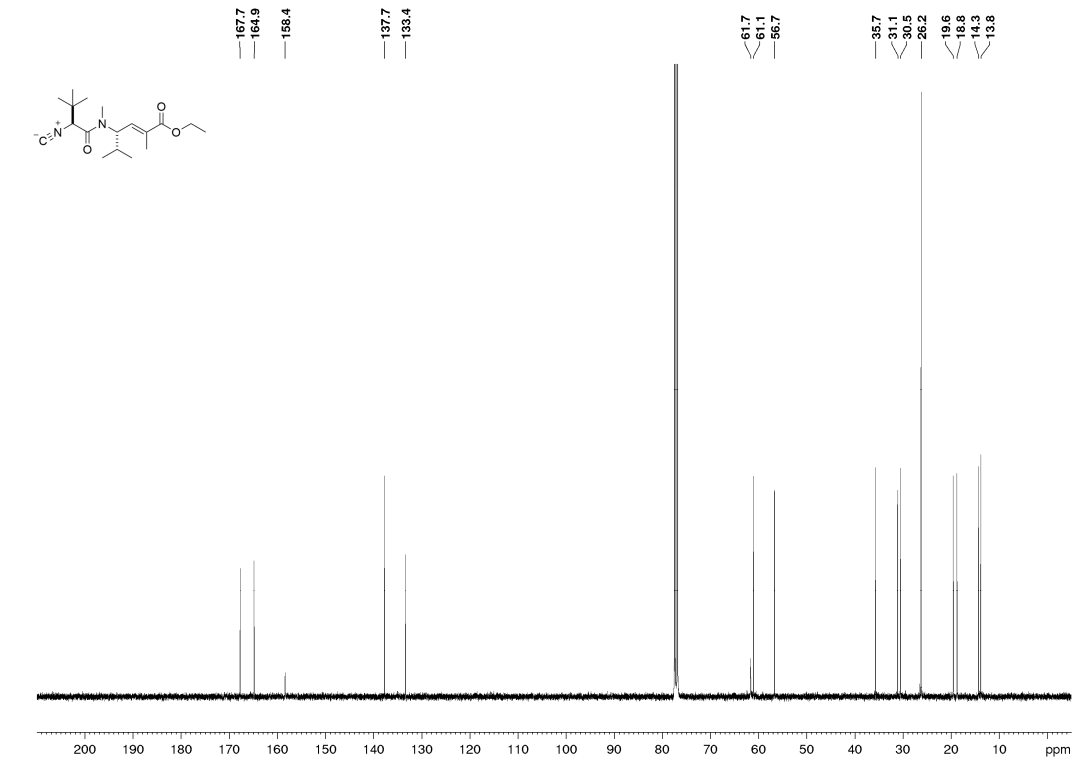

N-Trifluoroacetyl hemiasterlin ethyl ester (113a)

^{1}H-NMR

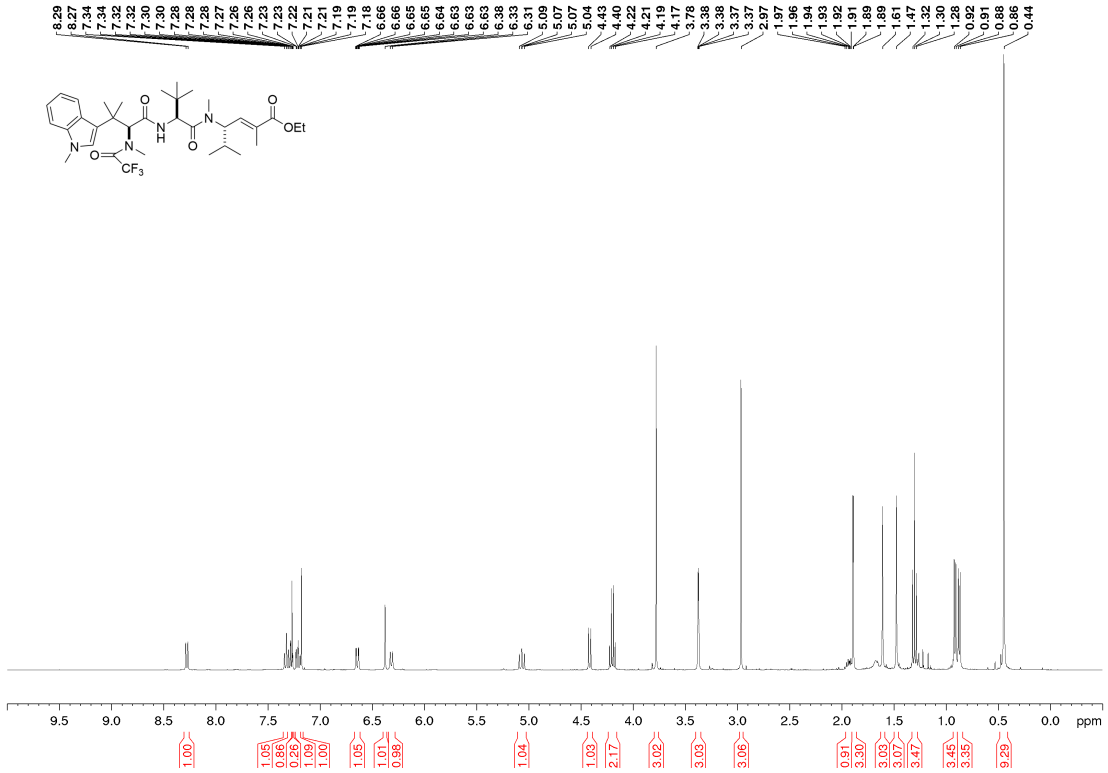

^{13}C-NMR

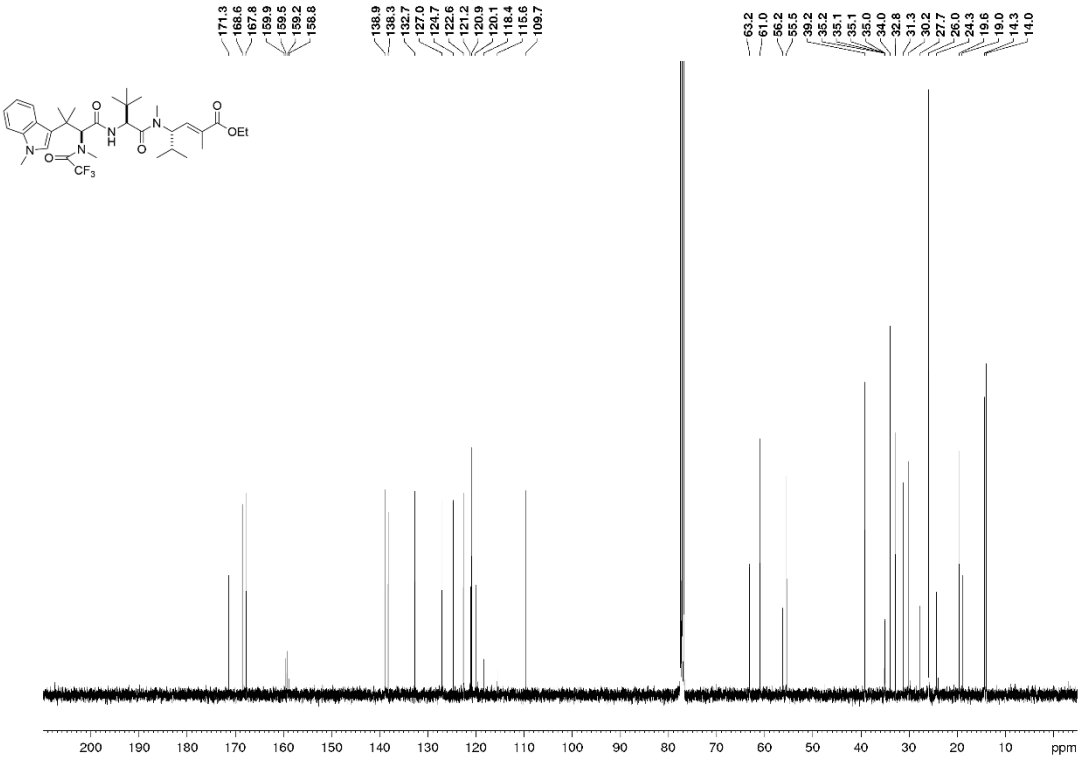

^{19}F-NMR

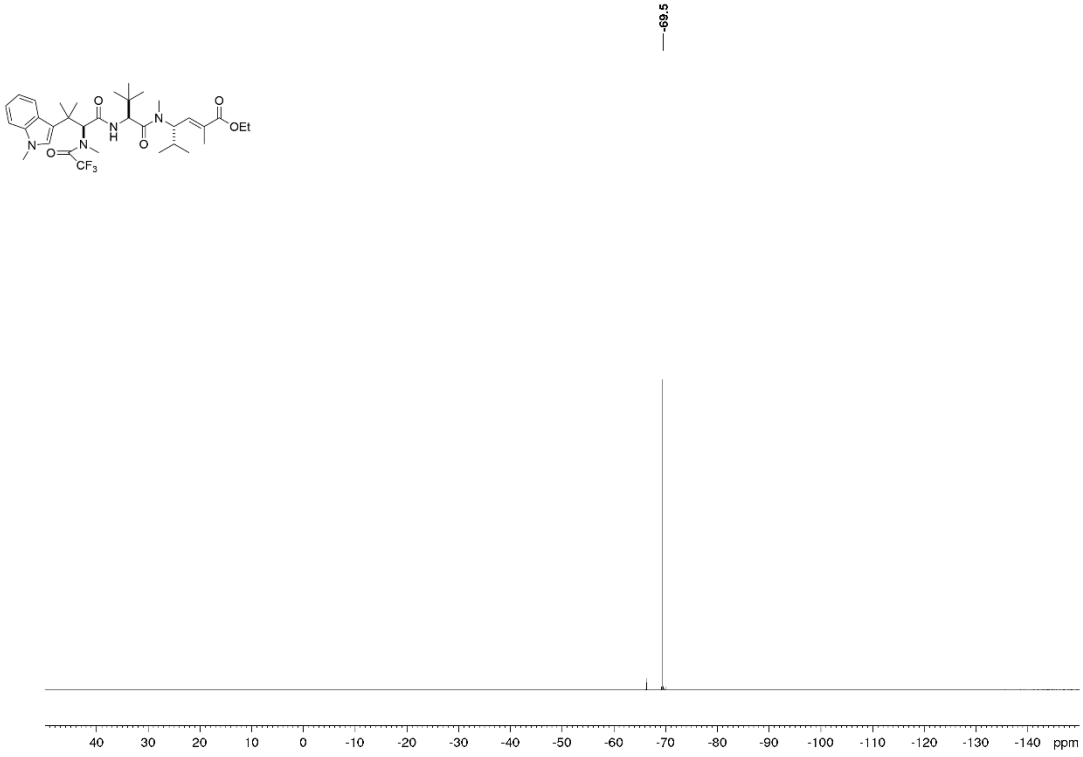

N-Trifluoroacetyl *epi*-hemiasterlin ethyl ester (113b)

^{1}H-NMR

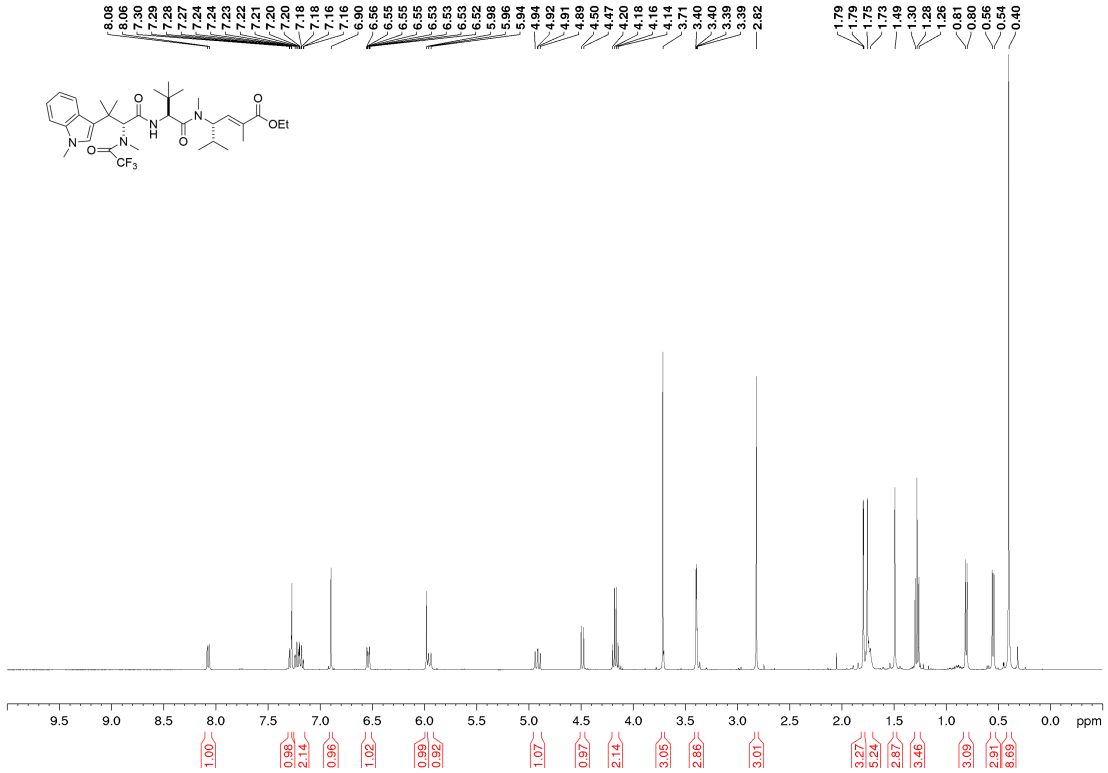

^{13}C-NMR

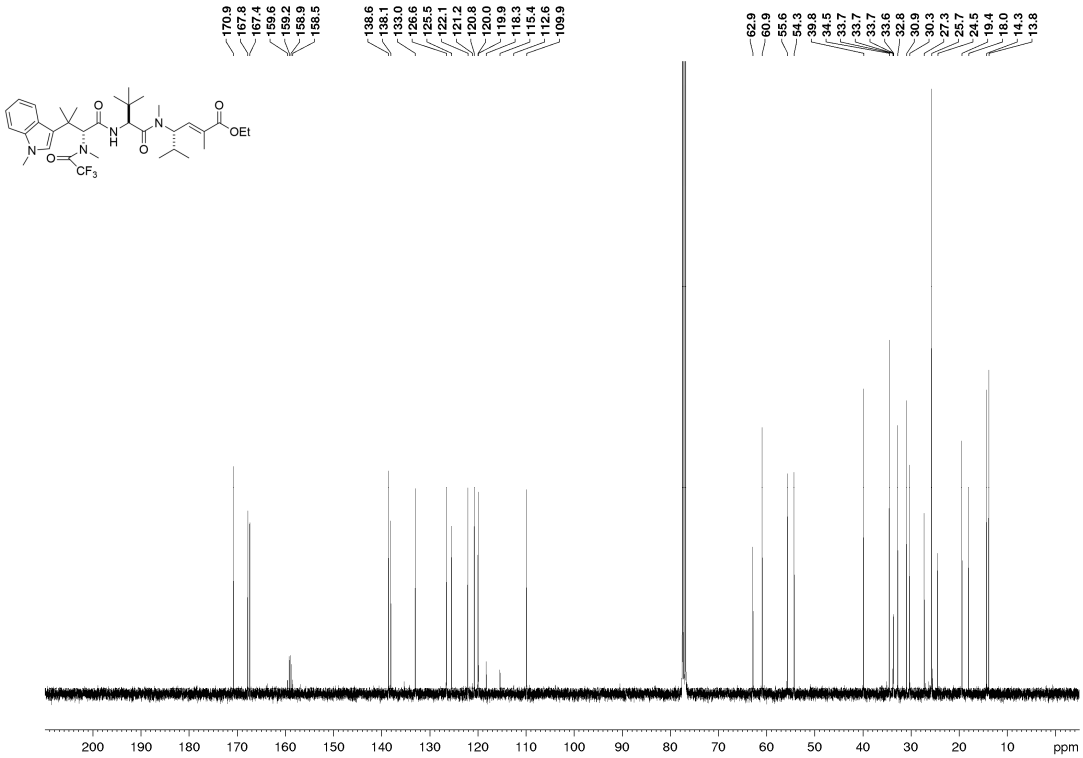

^{19}F-NMR

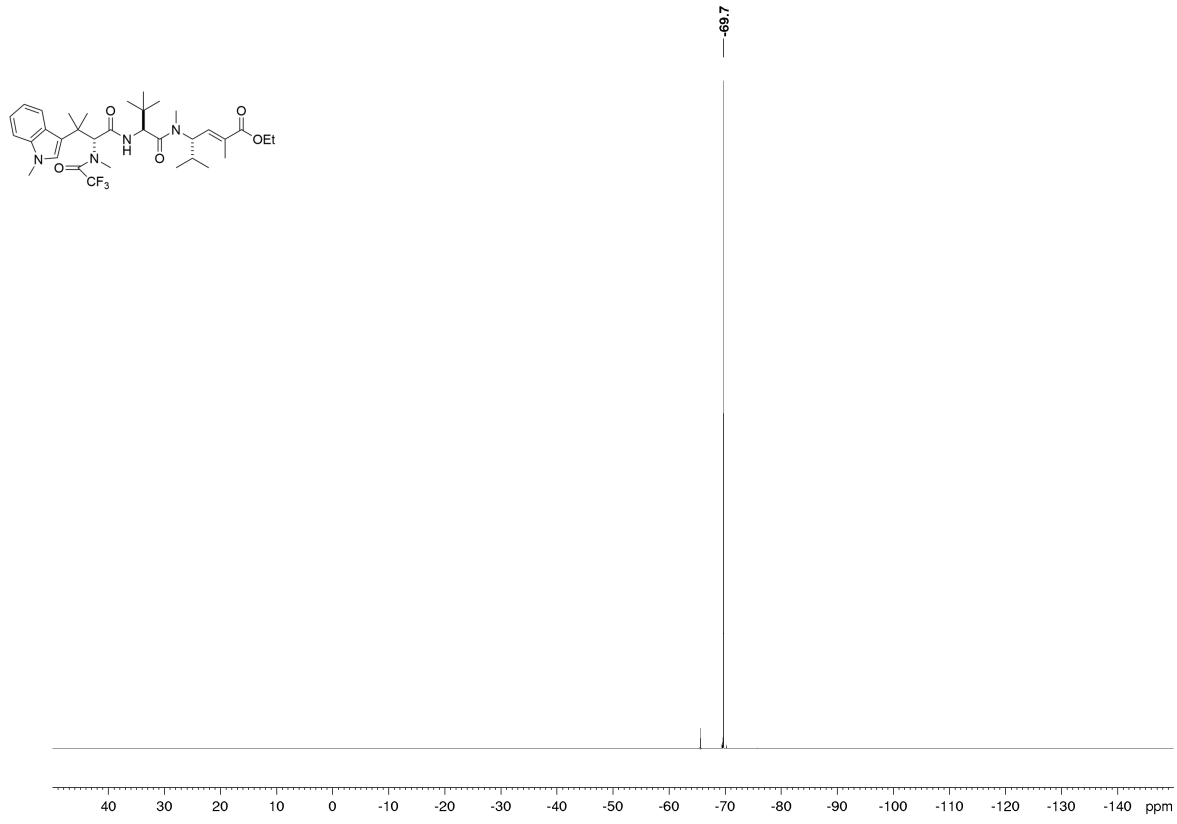

Hemiasterlin trifluoroacetate salt (56·TFA)

^{1}H-NMR

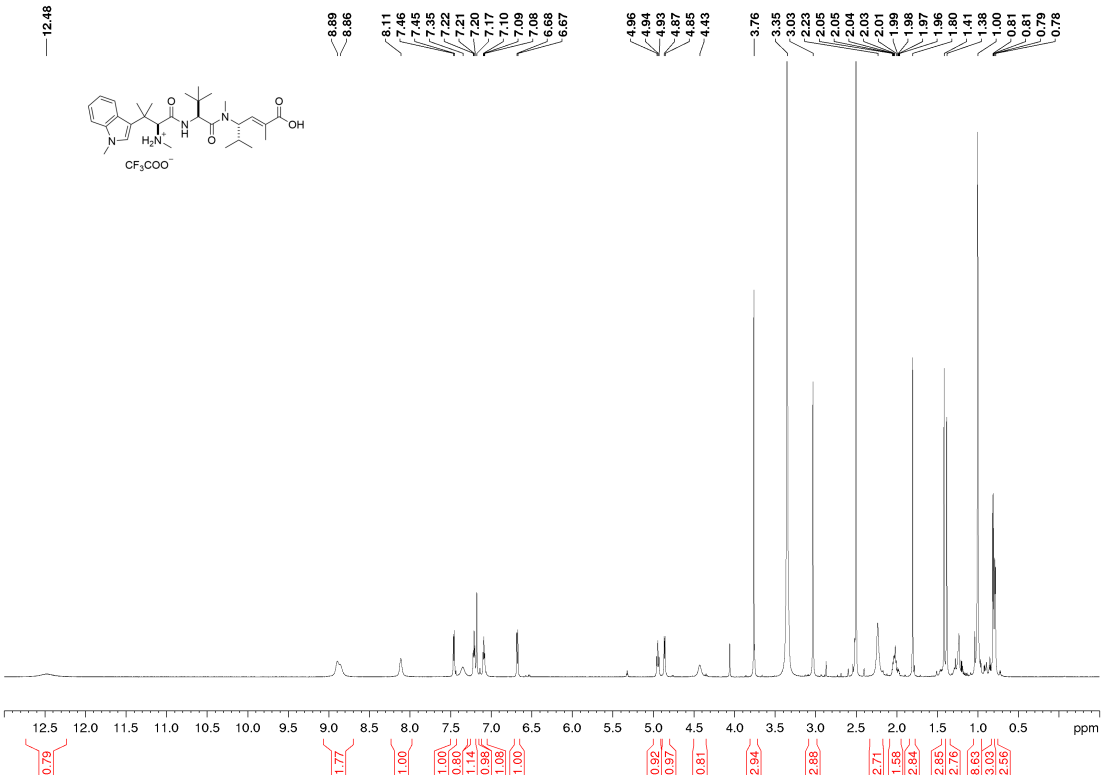

^{13}C-NMR

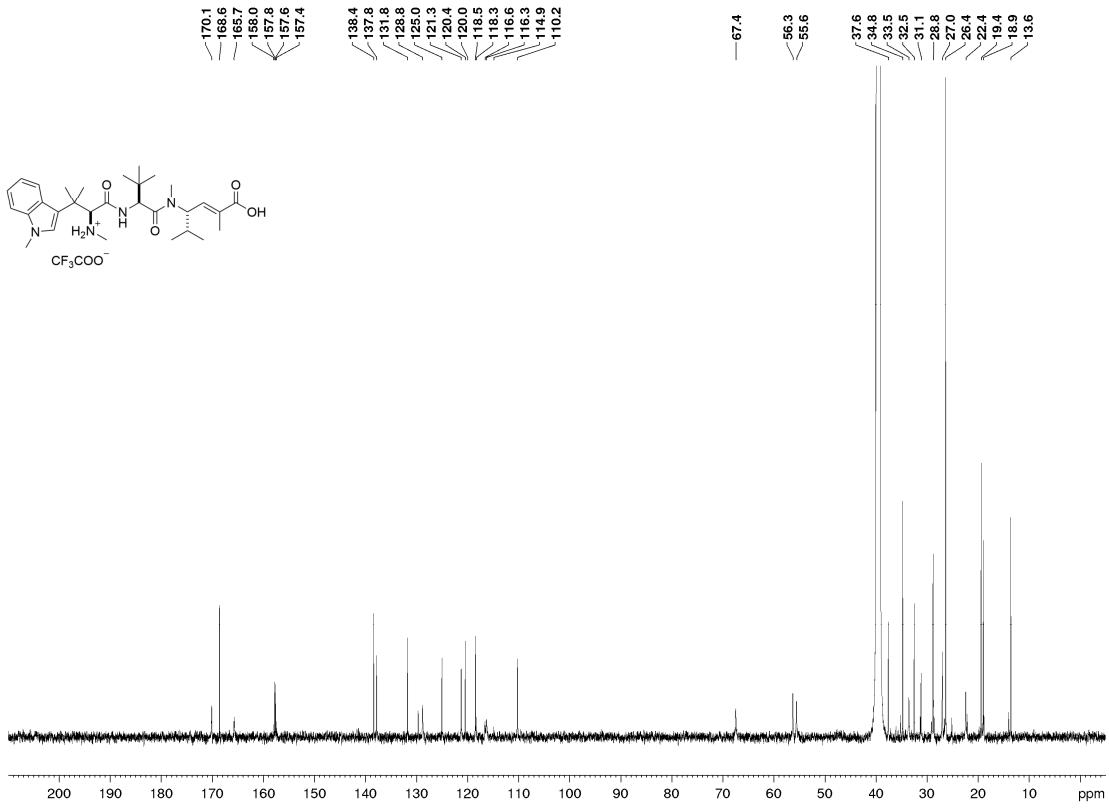

^{19}F-NMR

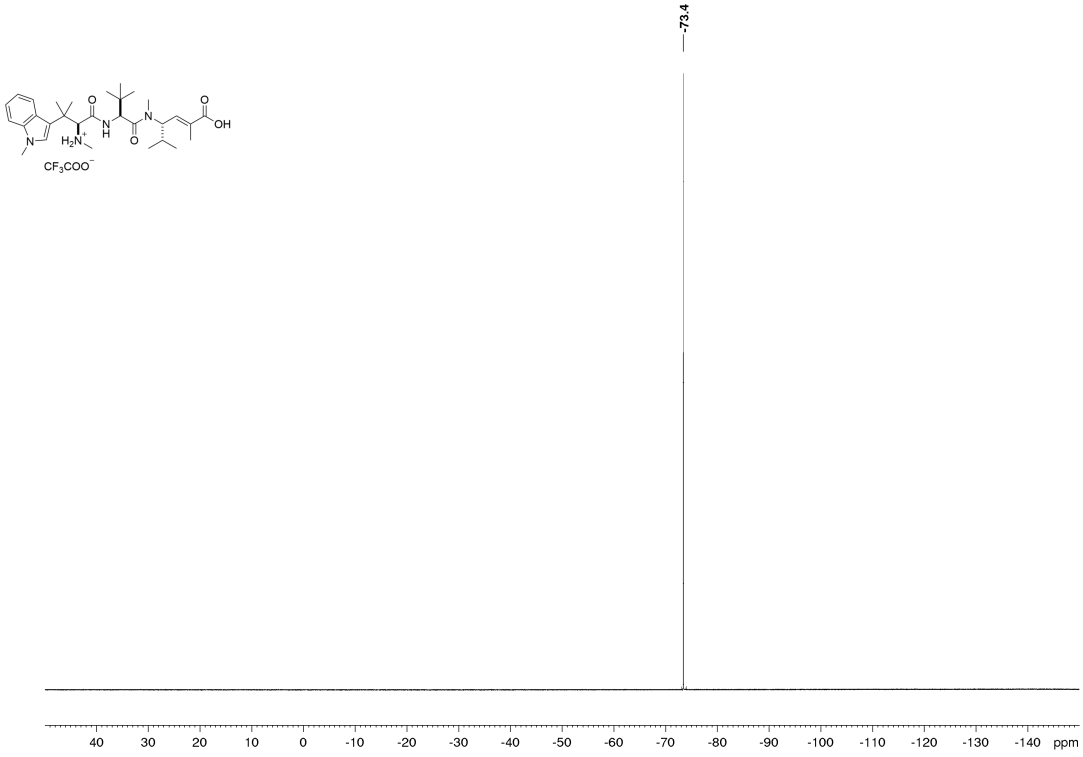

epi-Hemiasterlin trifluoroacetate salt (56b·TFA)

^{1}H-NMR

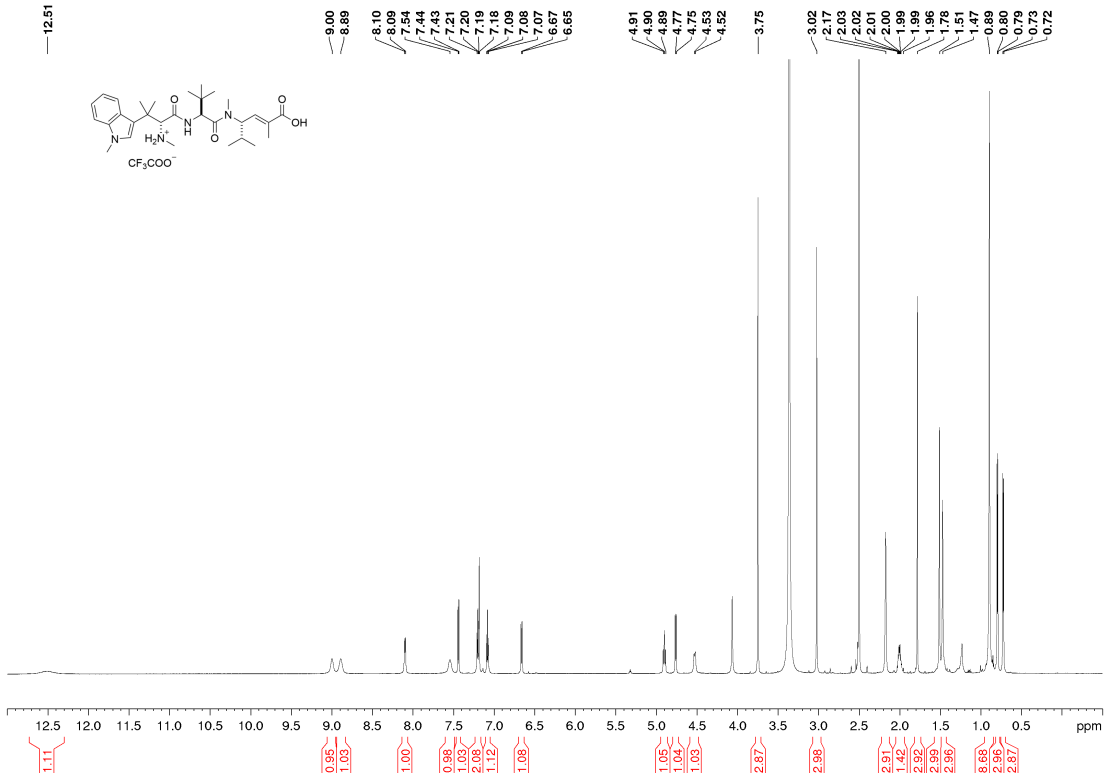

^{13}C-NMR

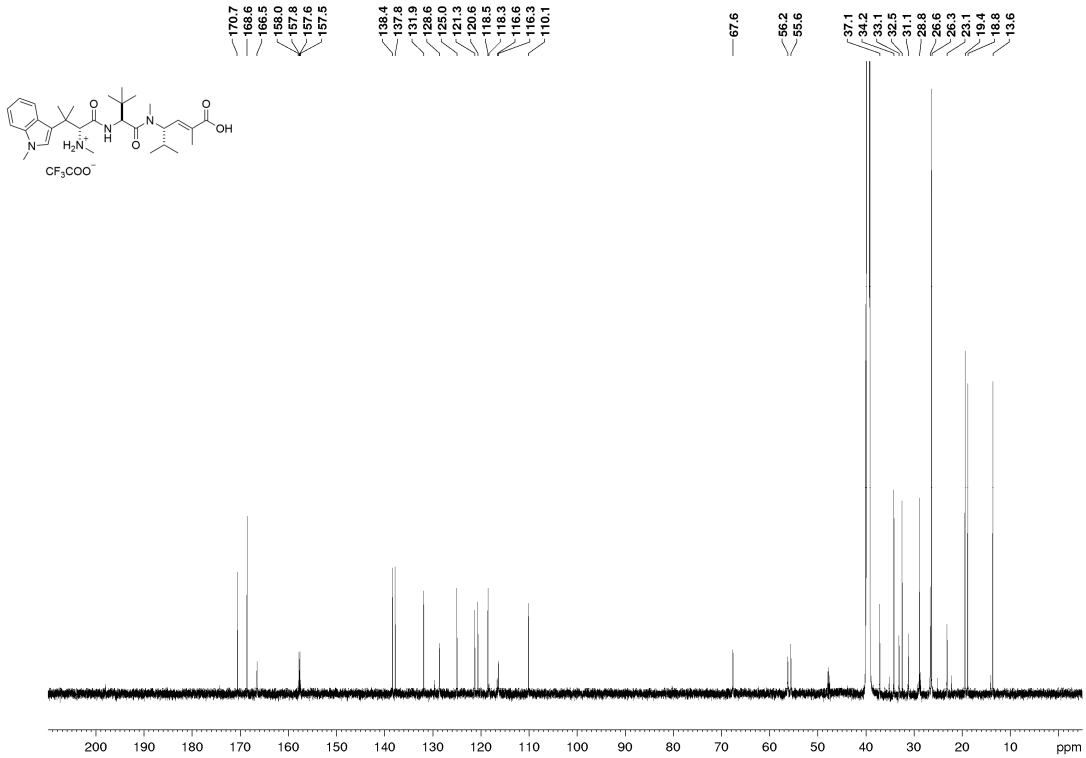

^{19}F-NMR

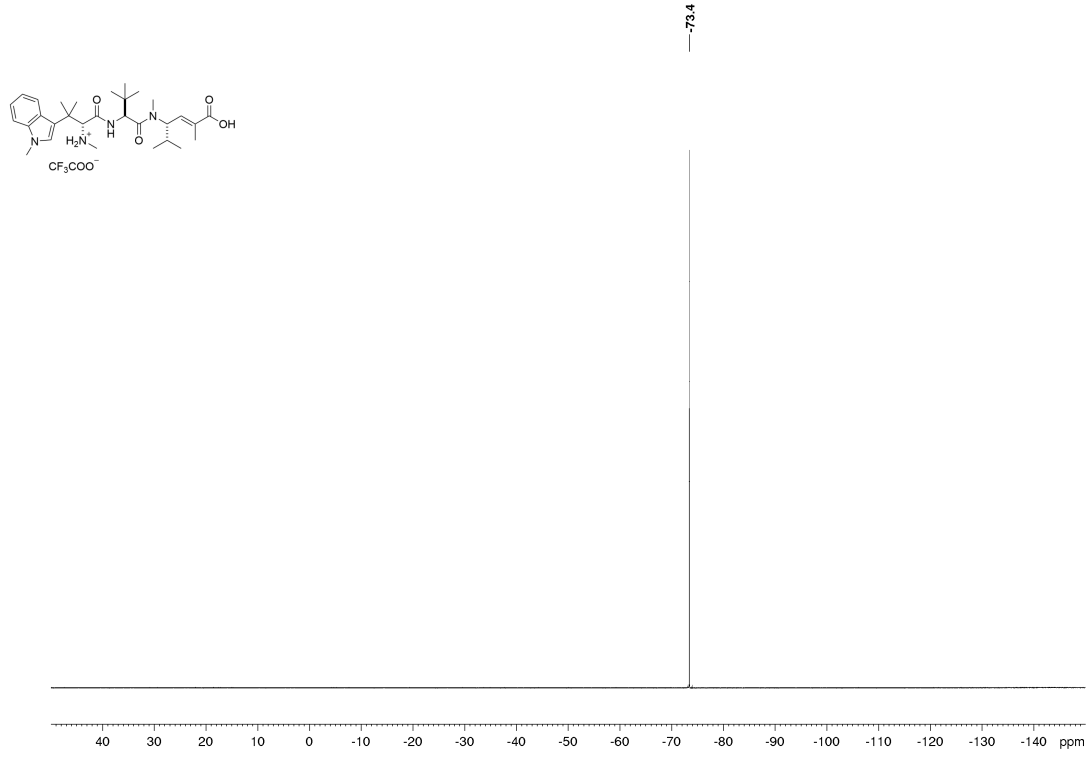

2-Methyl-2-phenylpropanal (120)

^{1}H-NMR

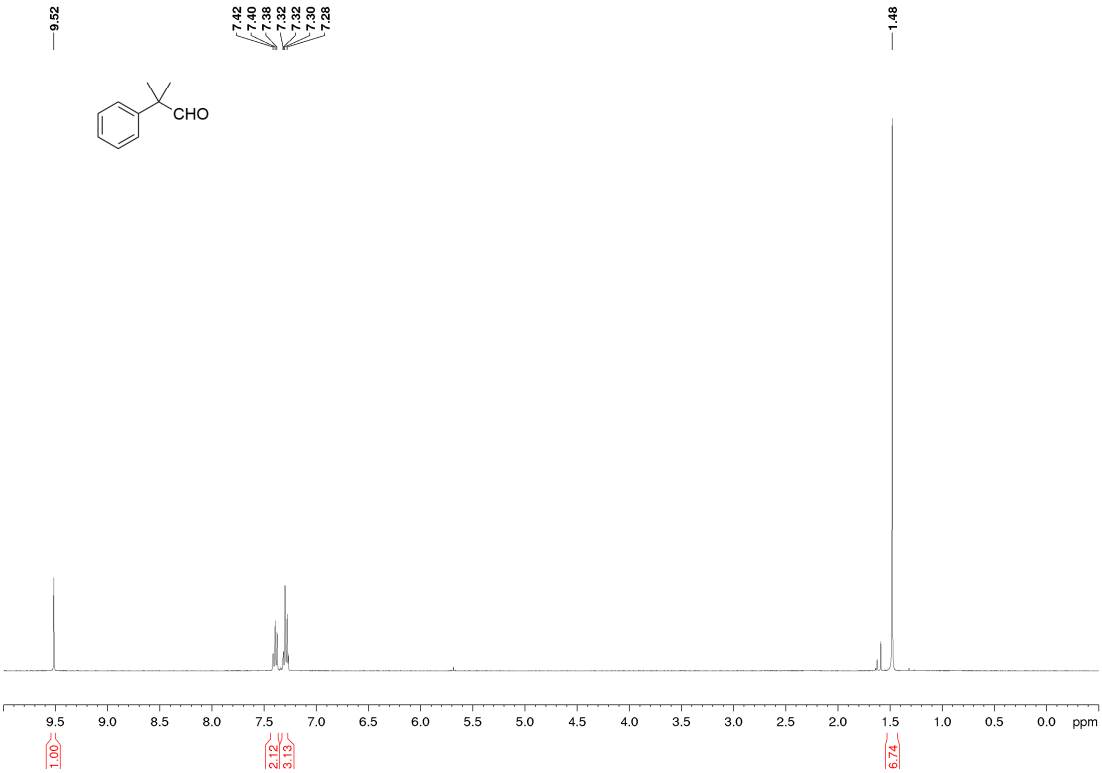

^{13}C-NMR

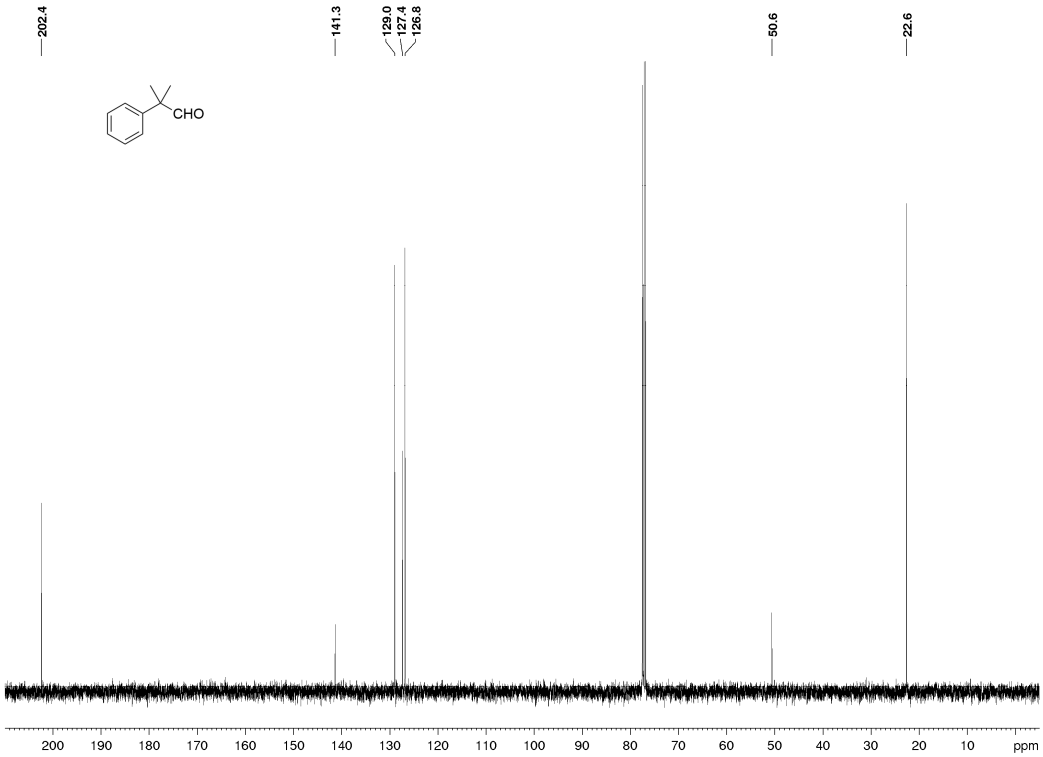

Taltobulin trifluoroacetate salt (57·TFA)

^{1}H-NMR

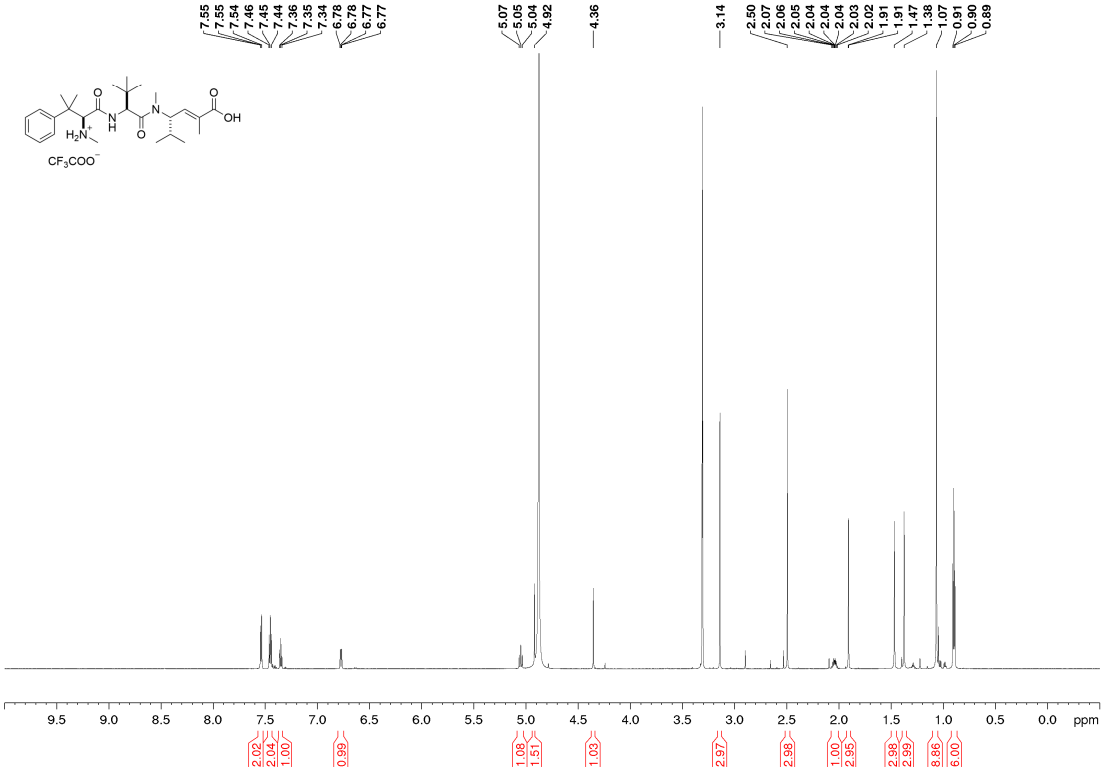

^{13}C-NMR

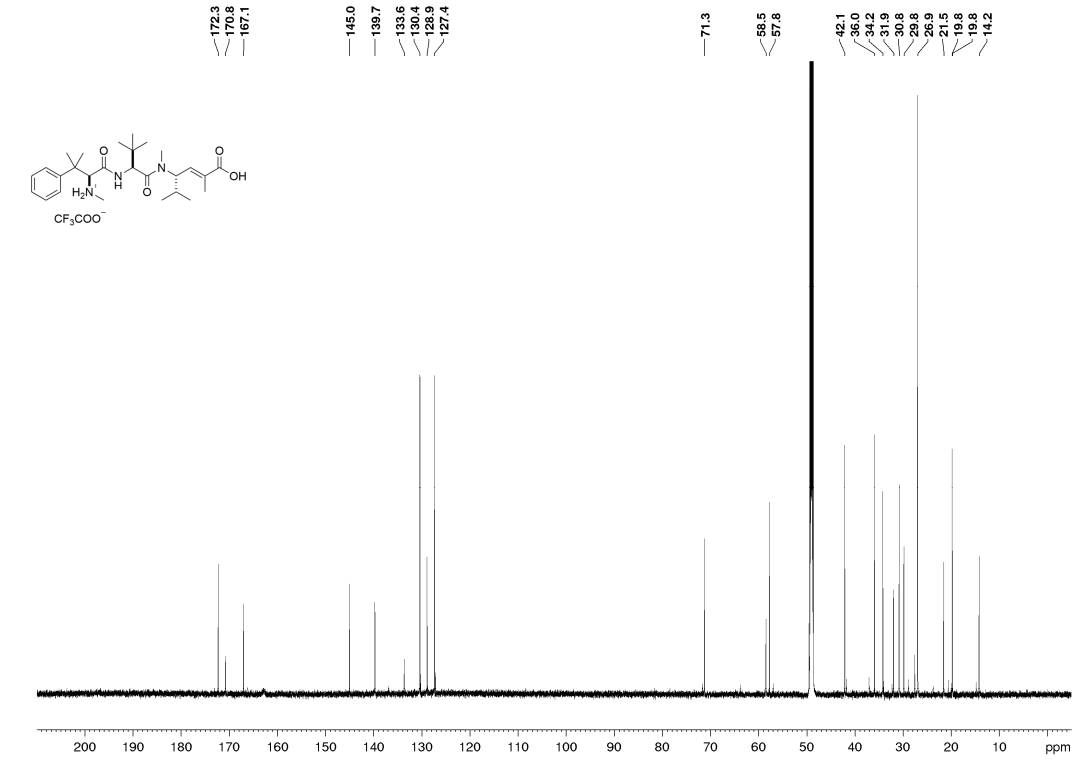

^{19}F-NMR

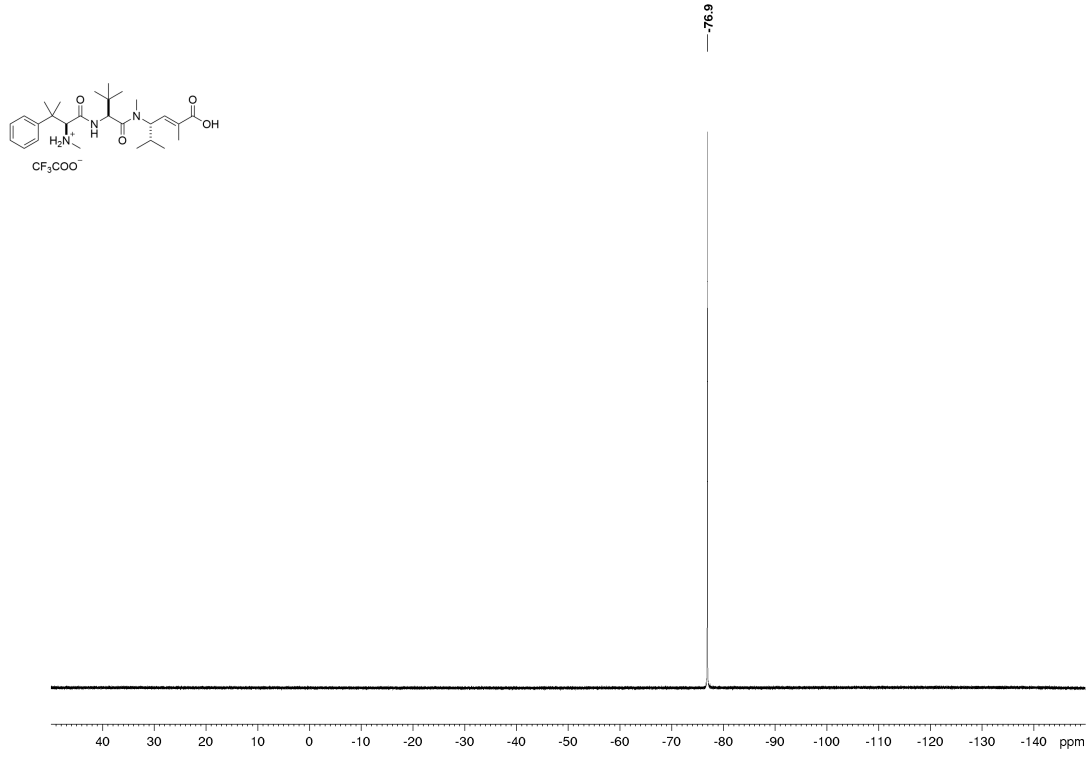

epi-Taltobulin trifluoroacetate salt (57b·TFA)

^{1}H-NMR

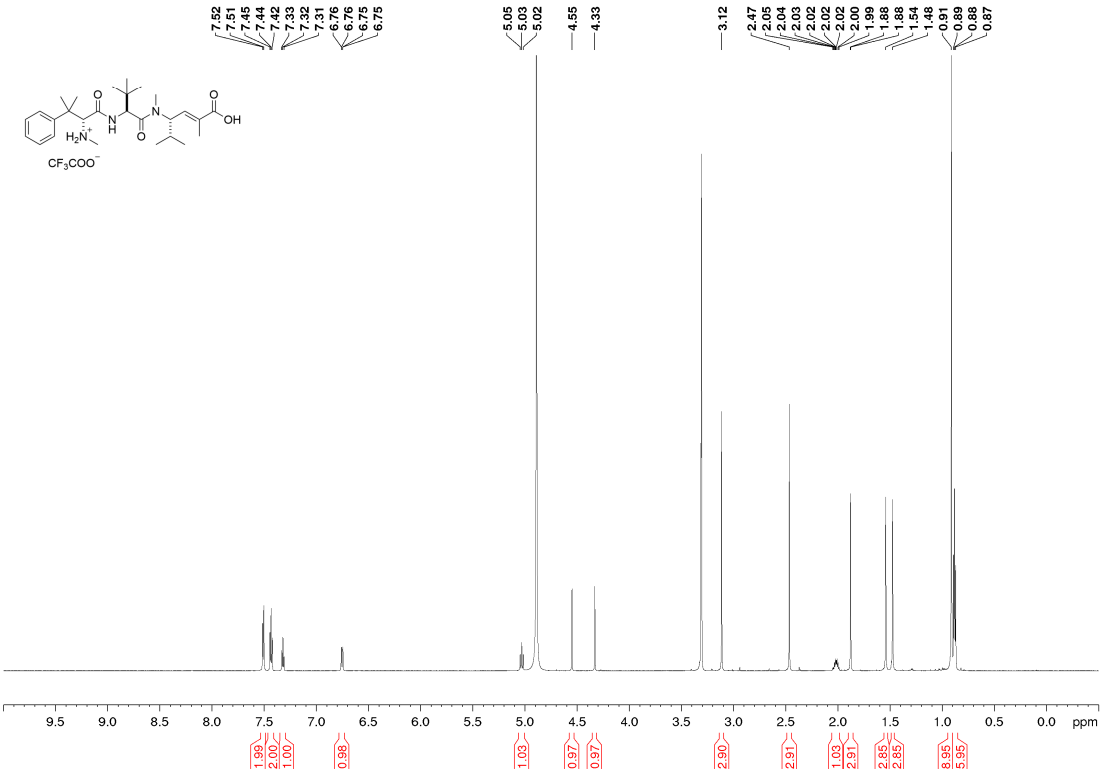

^{13}C-NMR

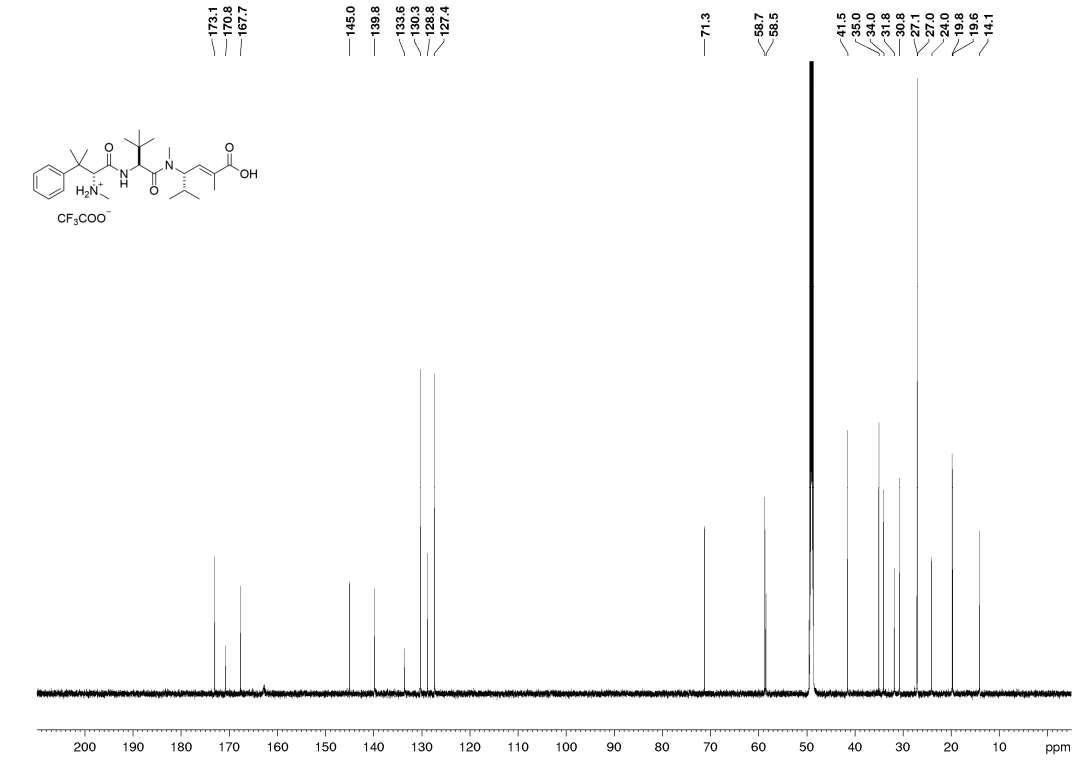

^{19}F-NMR

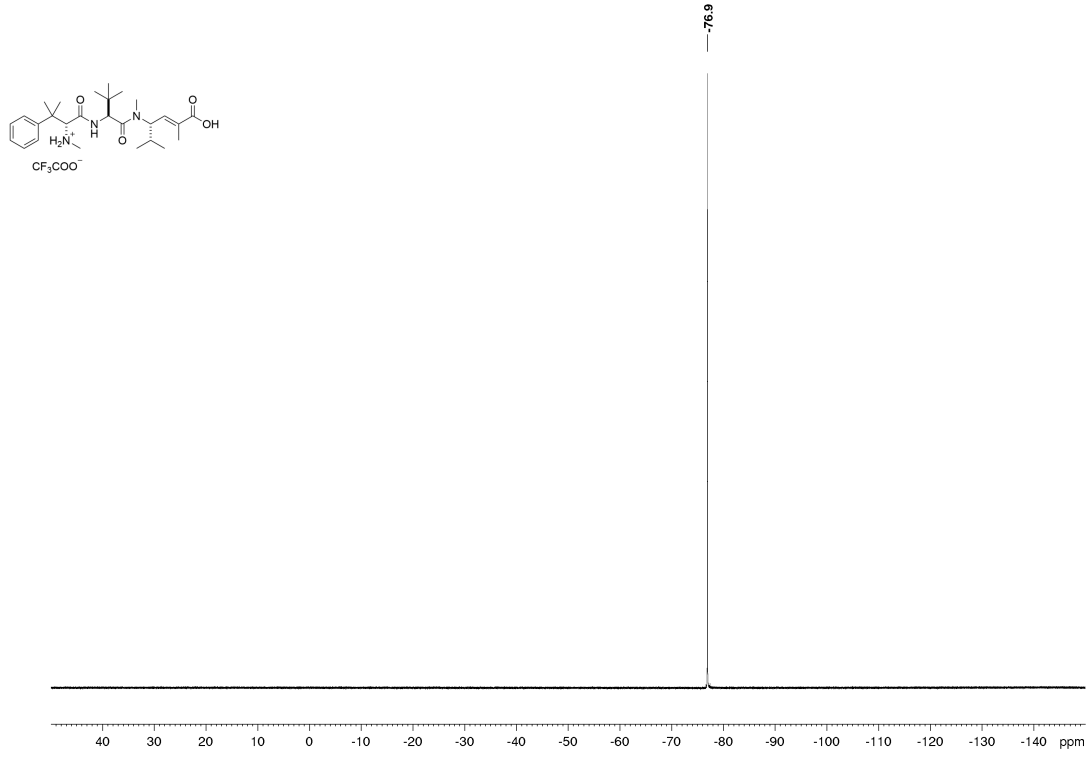

H-Val-Ala-PABA·TFA (134)

^{1}H-NMR

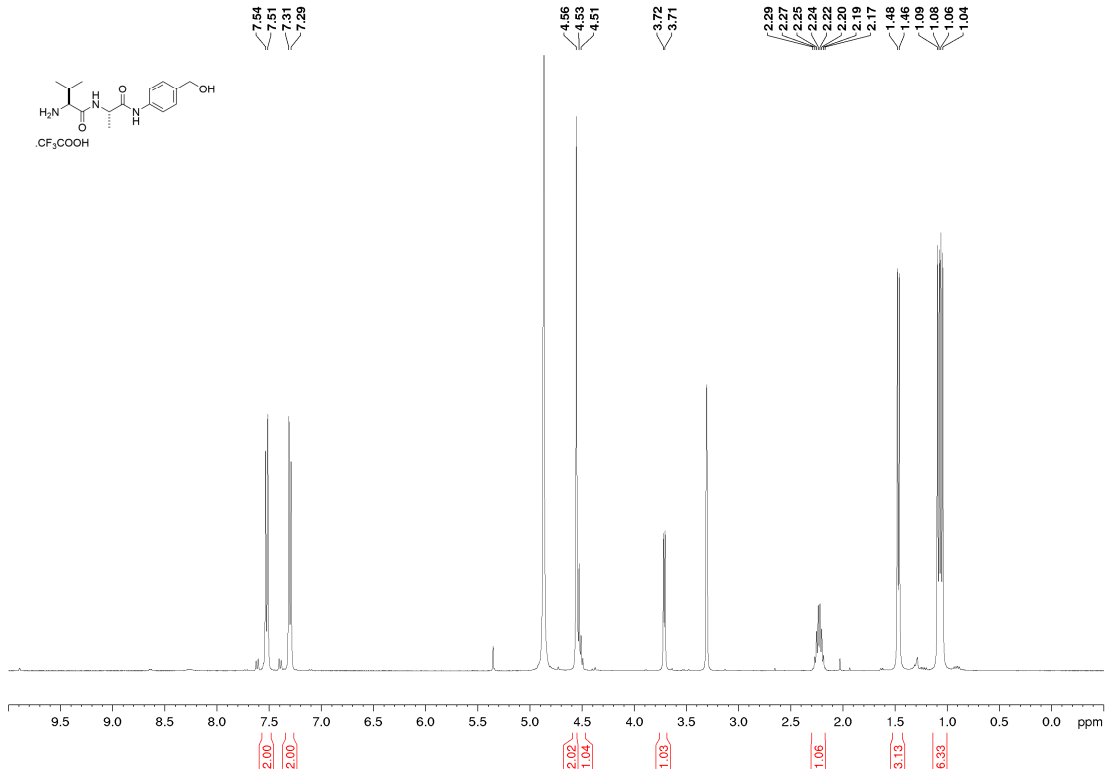

^{13}C-NMR

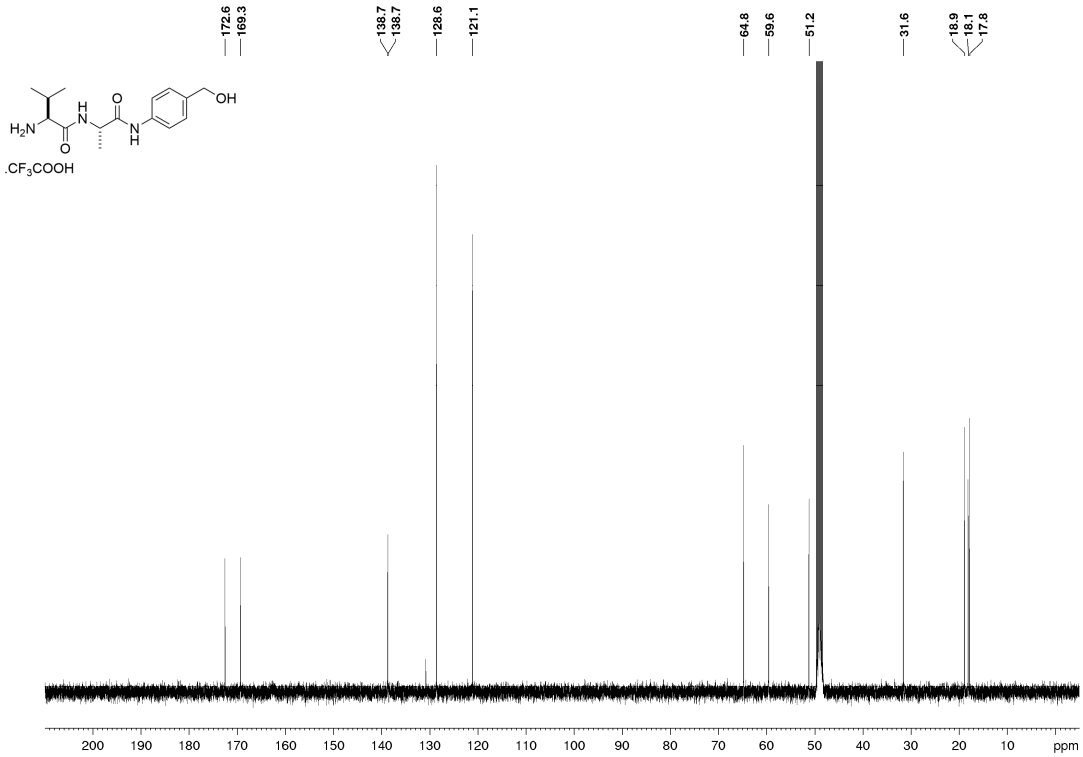

^{19}F-NMR

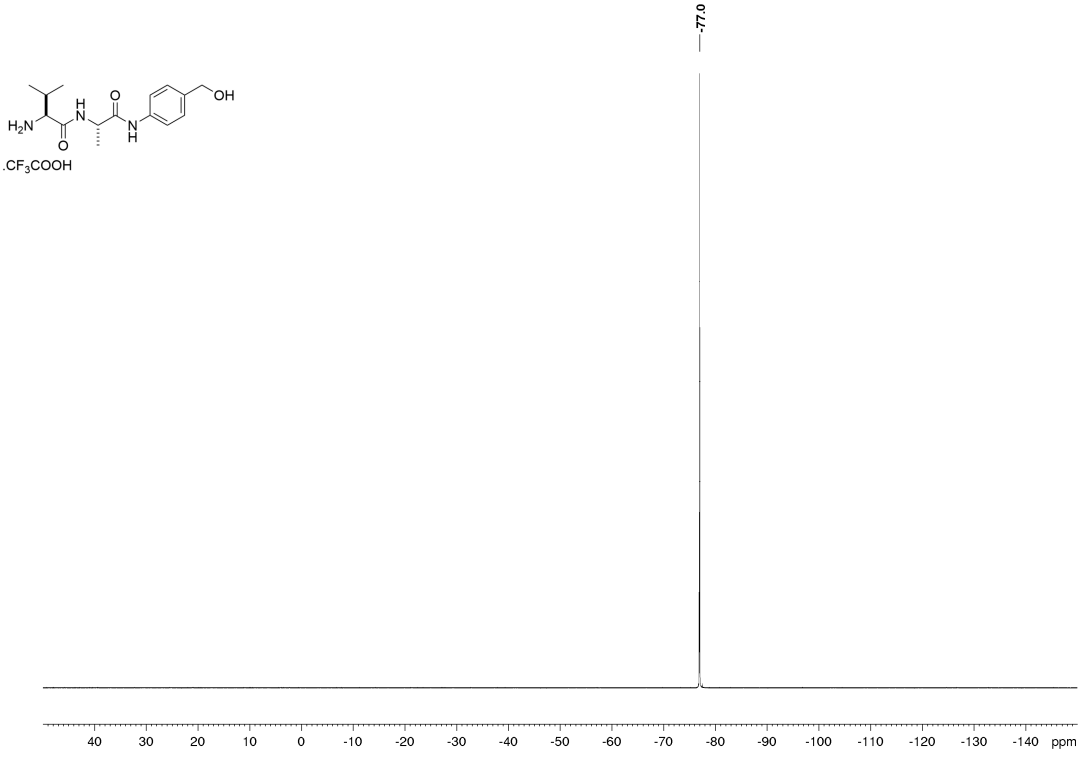
-77.0
H2N
O
H
N
O
N
H
OH
.CF3COOH
40 30 20 10 0 -10 -20 -30 -40 -50 -60 -70 -80 -90 -100 -110 -120 -130 -140 ppm

N_3-PEG_4-Val-Ala-PABA (135)

^{1}H-NMR

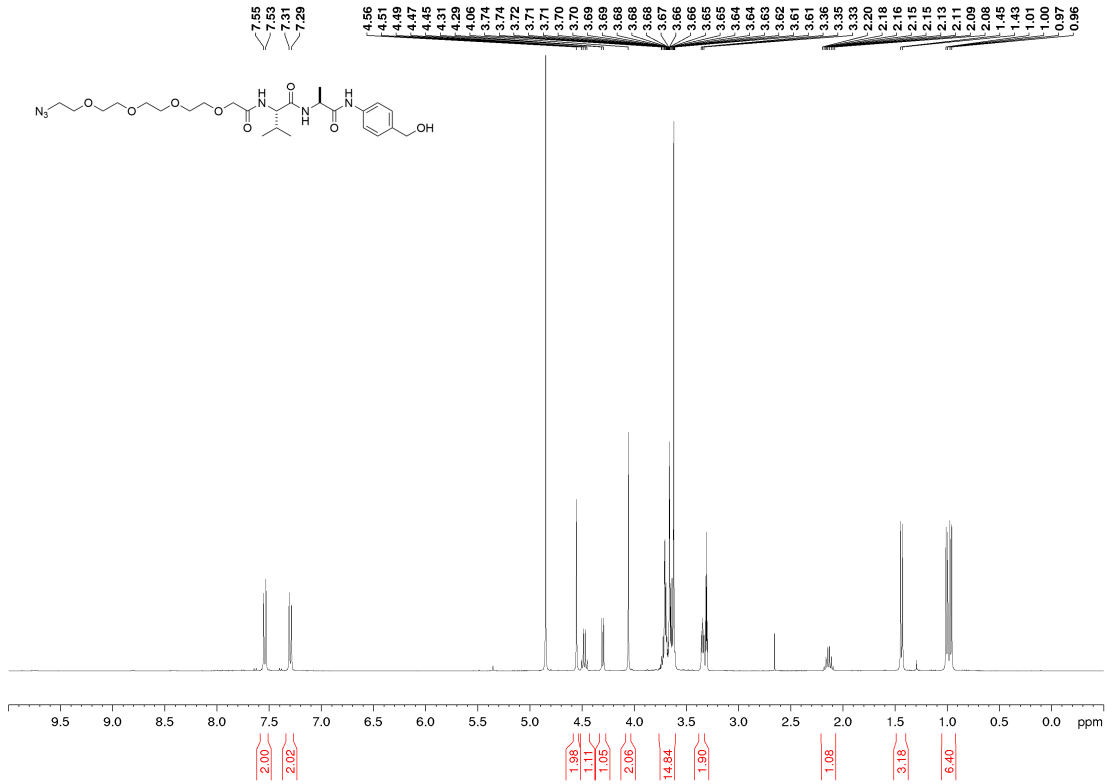

^{13}C-NMR

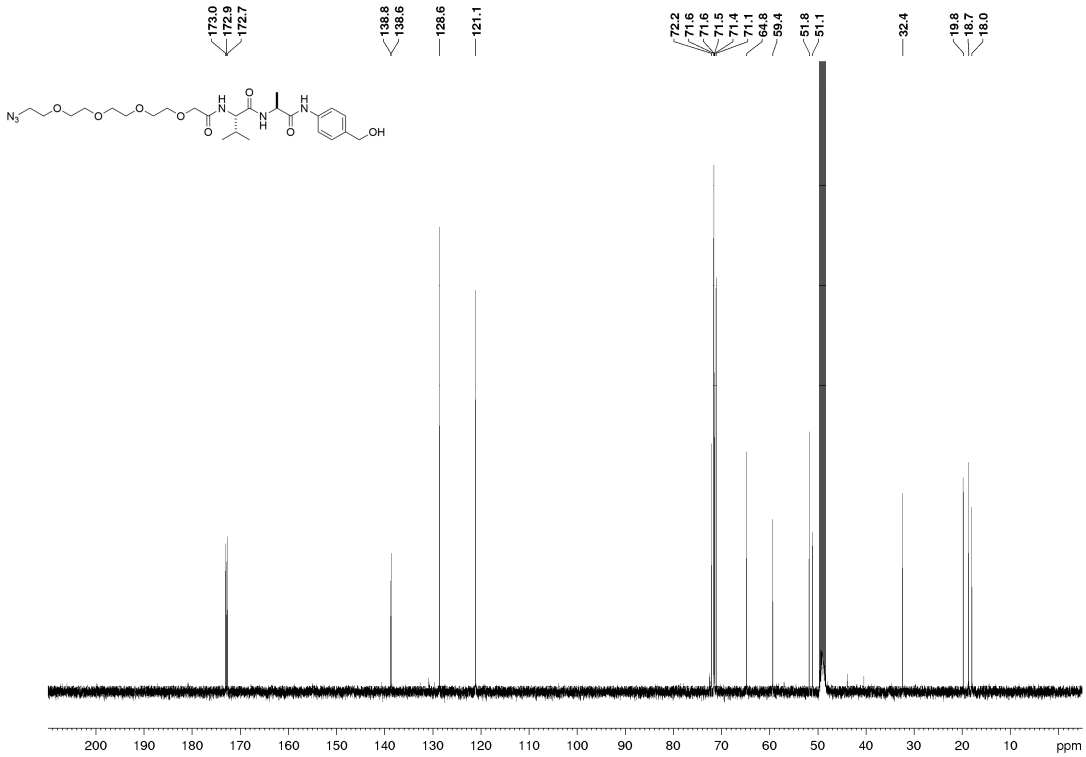

N_3-PEG_4-Val-Ala-PABC-OPNP (136)

^{1}H-NMR

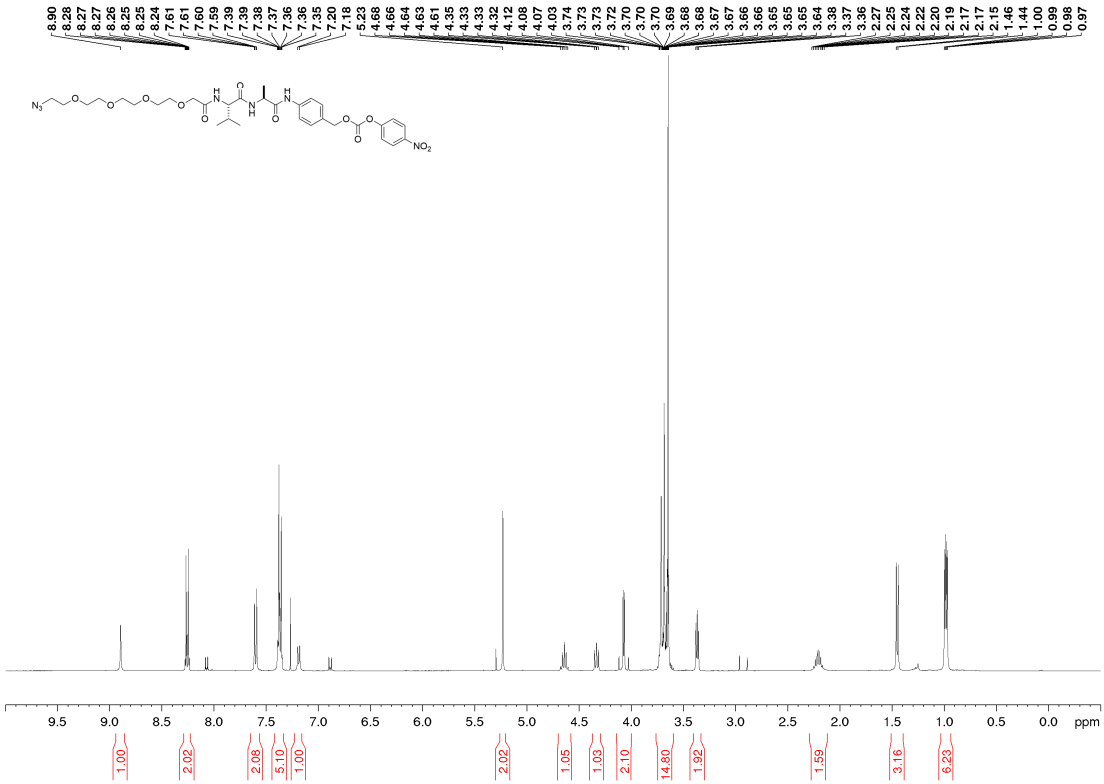

^{13}C-NMR

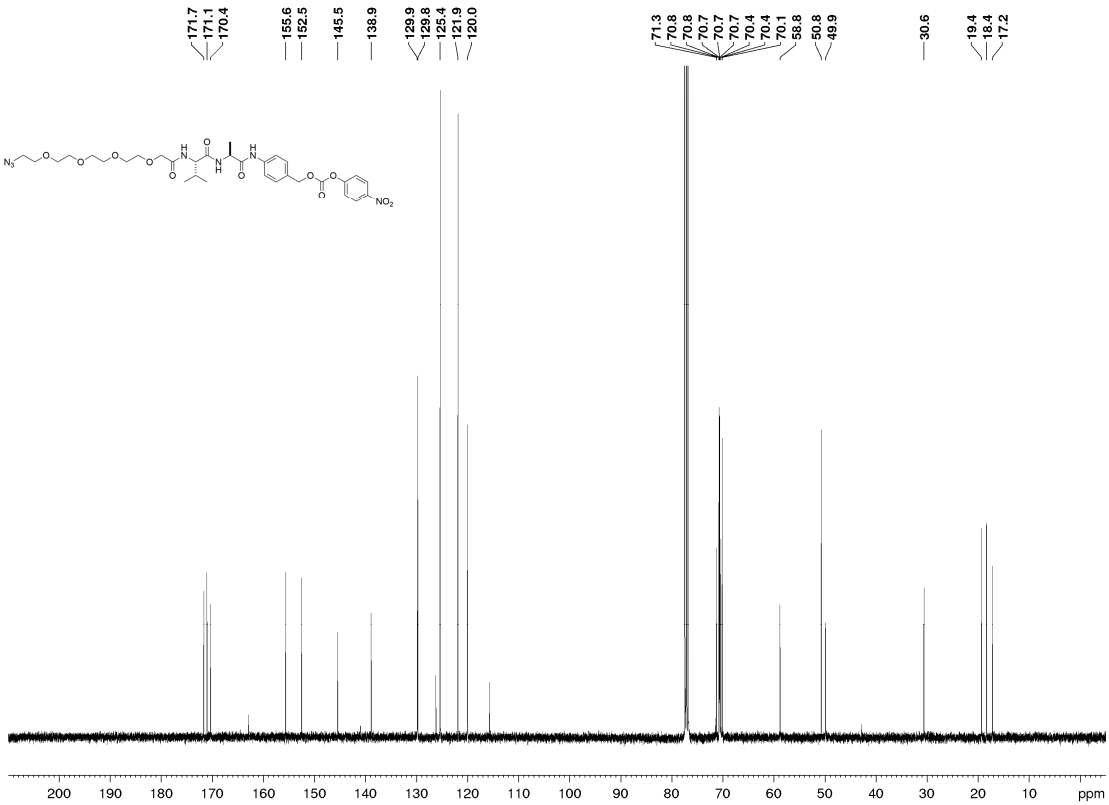

Hemiasterlin ethyl ester trifluoroacetate salt (137)

^{1}H-NMR

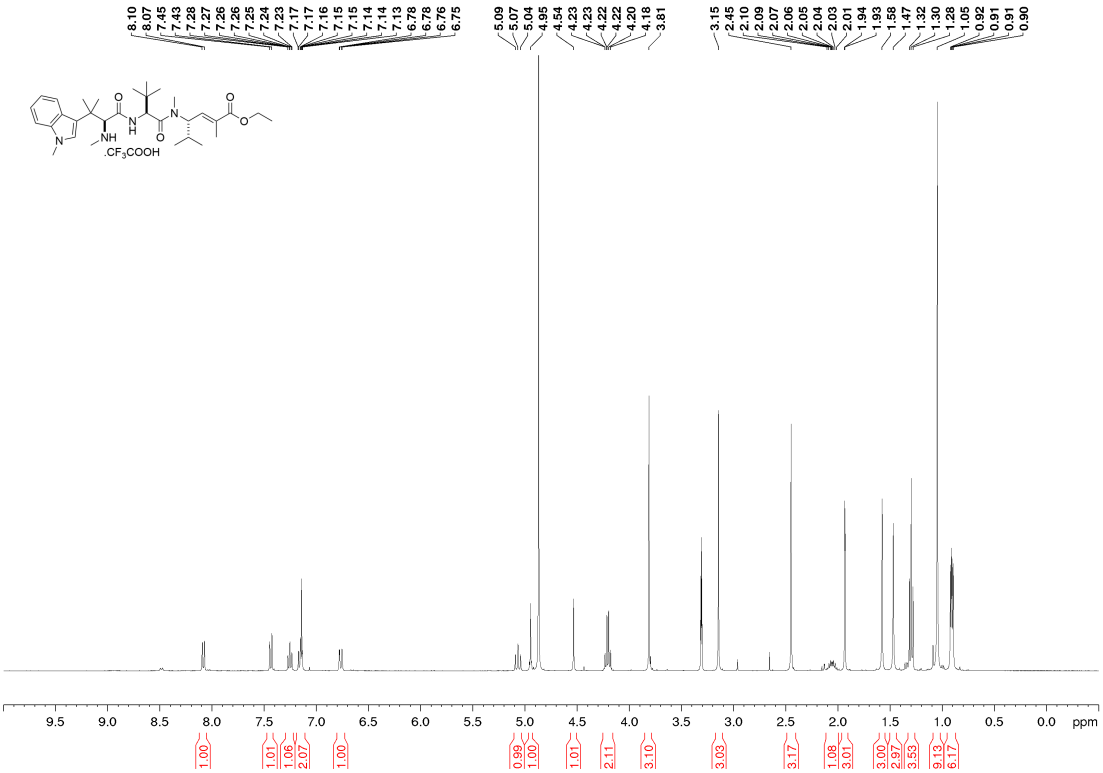

^{13}C-NMR

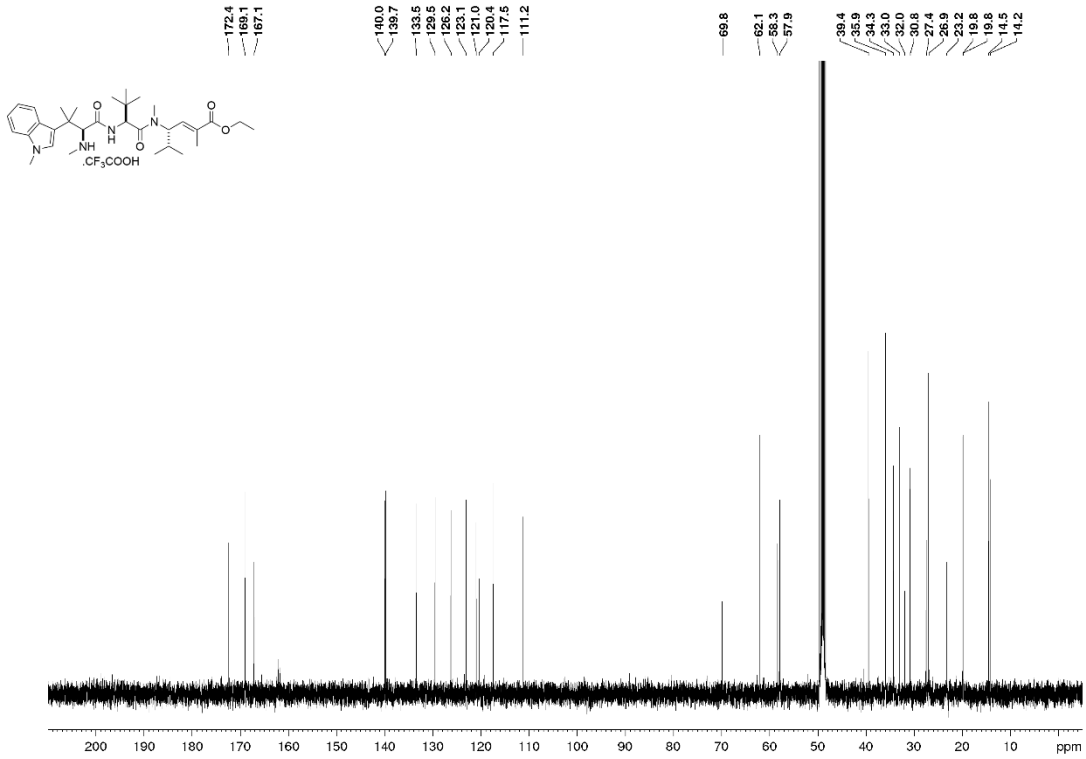

^{19}F-NMR

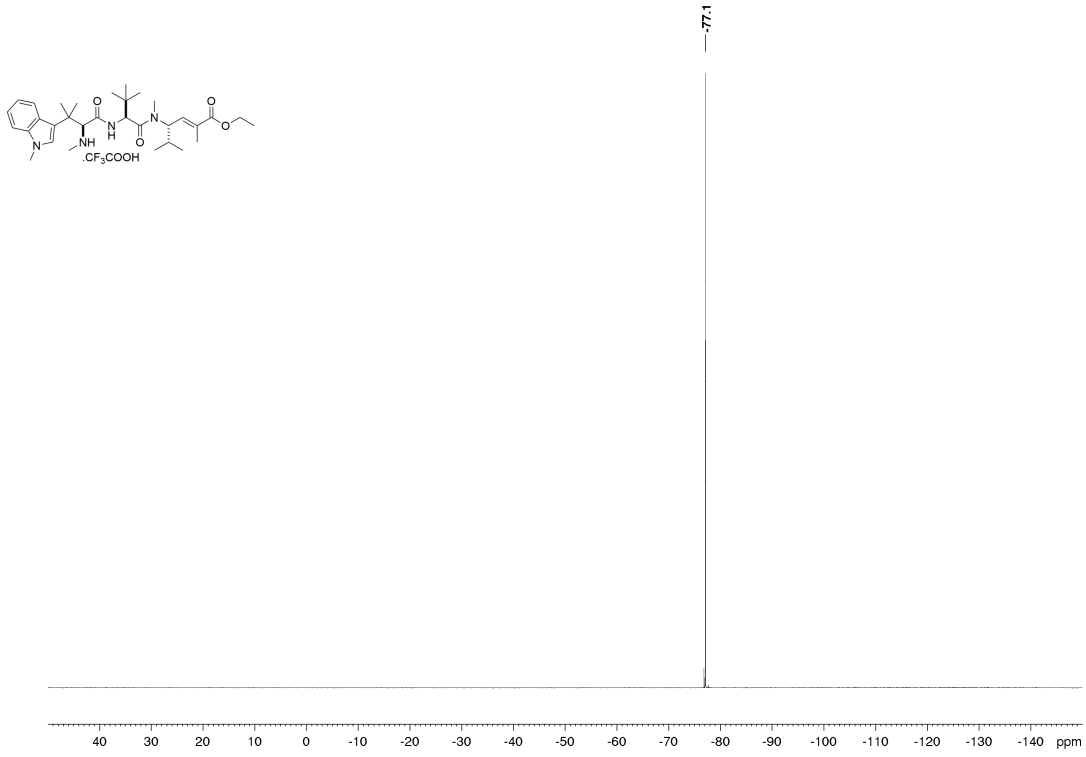

N_3-PEG_4-Val-Ala-PABC-hemiasterlin-OEt (139)

^{1}H-NMR

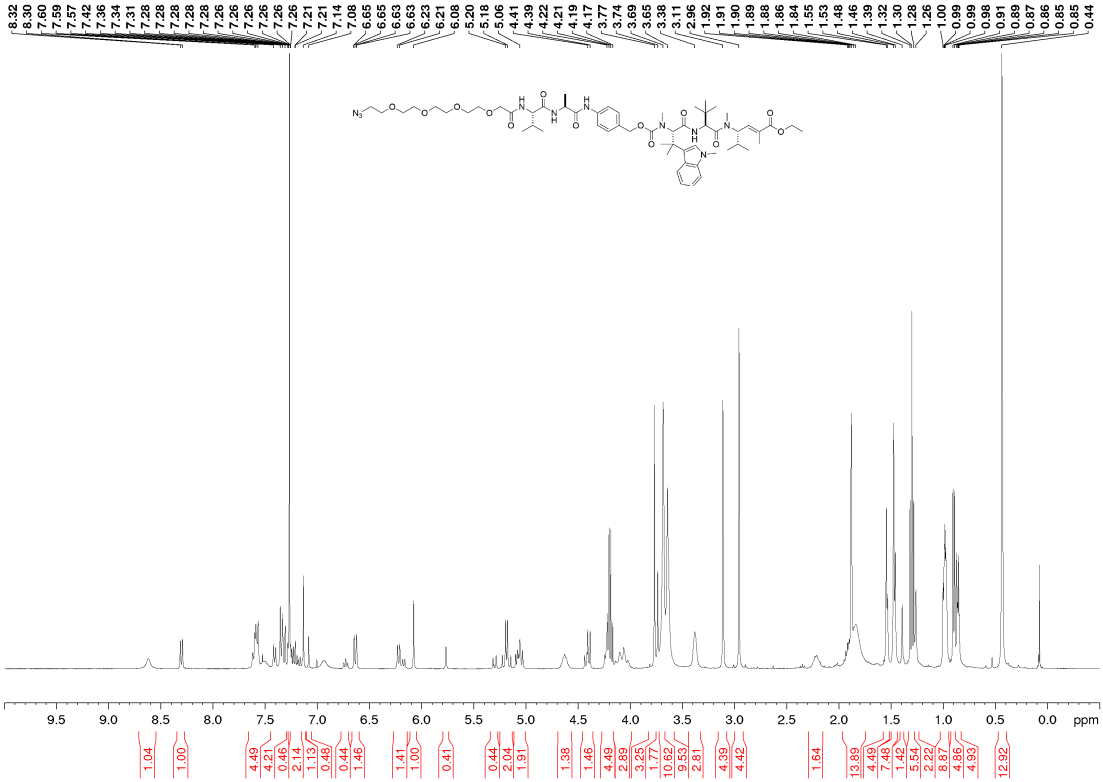

Taltobulin ethyl ester trifluoroacetate salt (138)

^{1}H-NMR

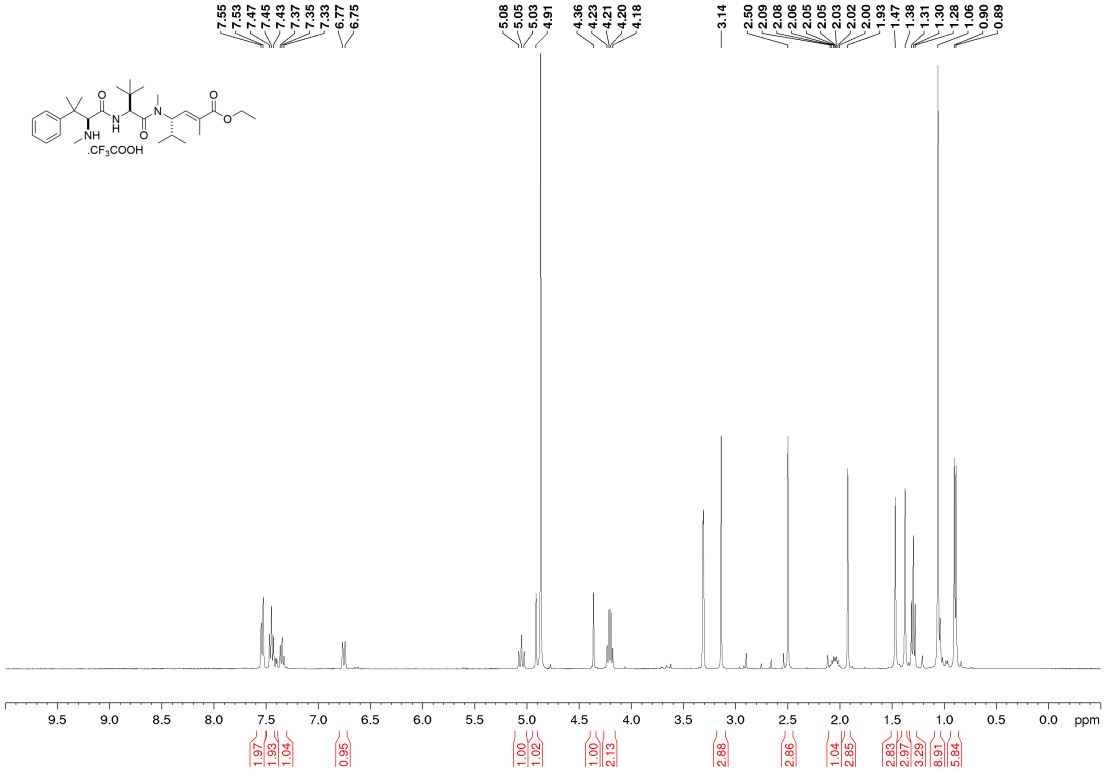

^{13}C-NMR

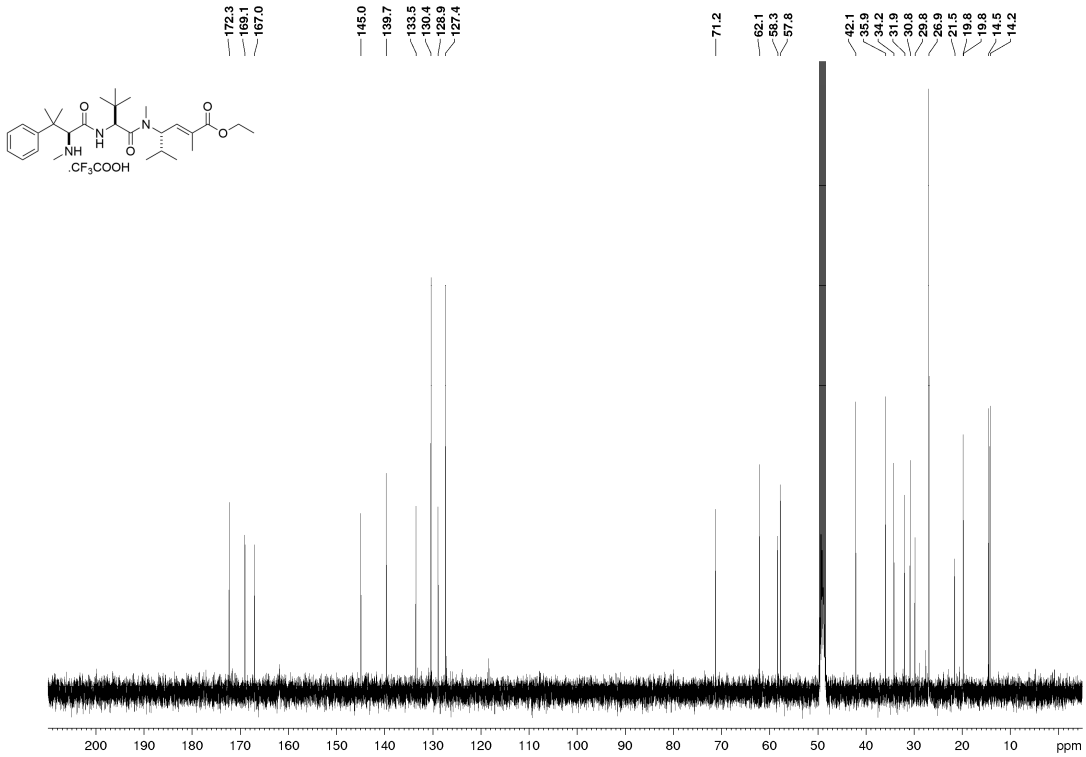

^{19}F-NMR

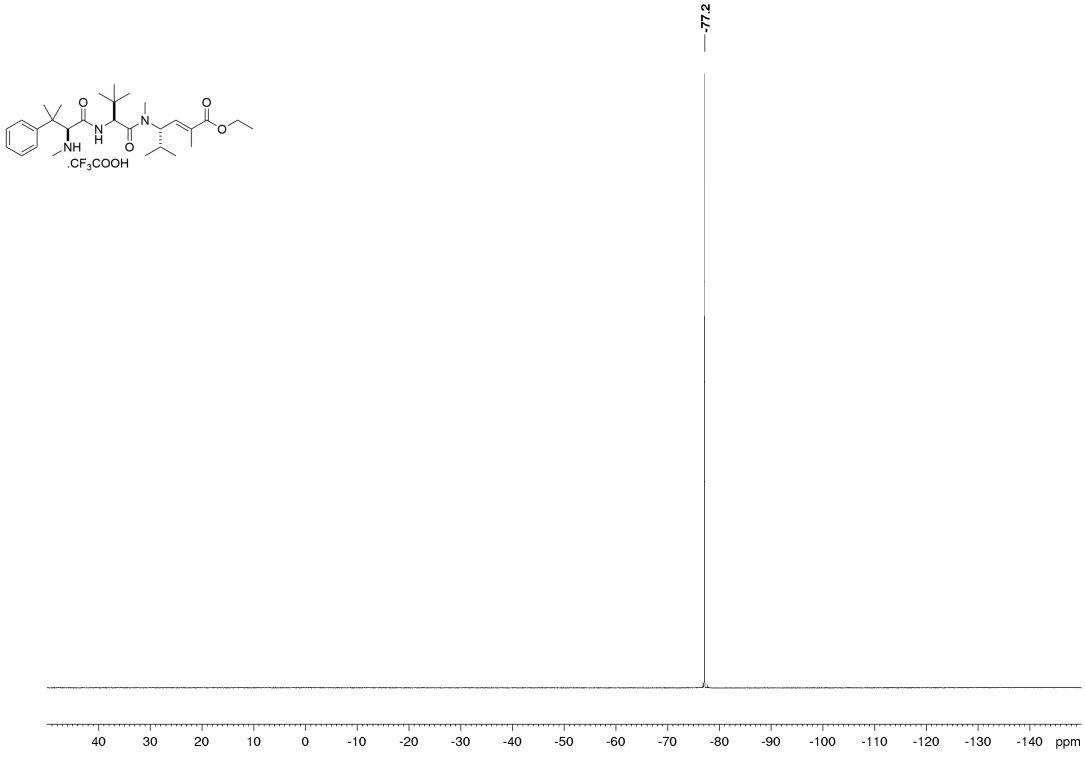
-77.2
NH
.CF3COOH
40 30 20 10 0 -10 -20 -30 -40 -50 -60 -70 -80 -90 -100 -110 -120 -130 -140 ppm

N_3-PEG_4-Val-Ala-PABC-taltobulin-OEt (140)

^{1}H-NMR

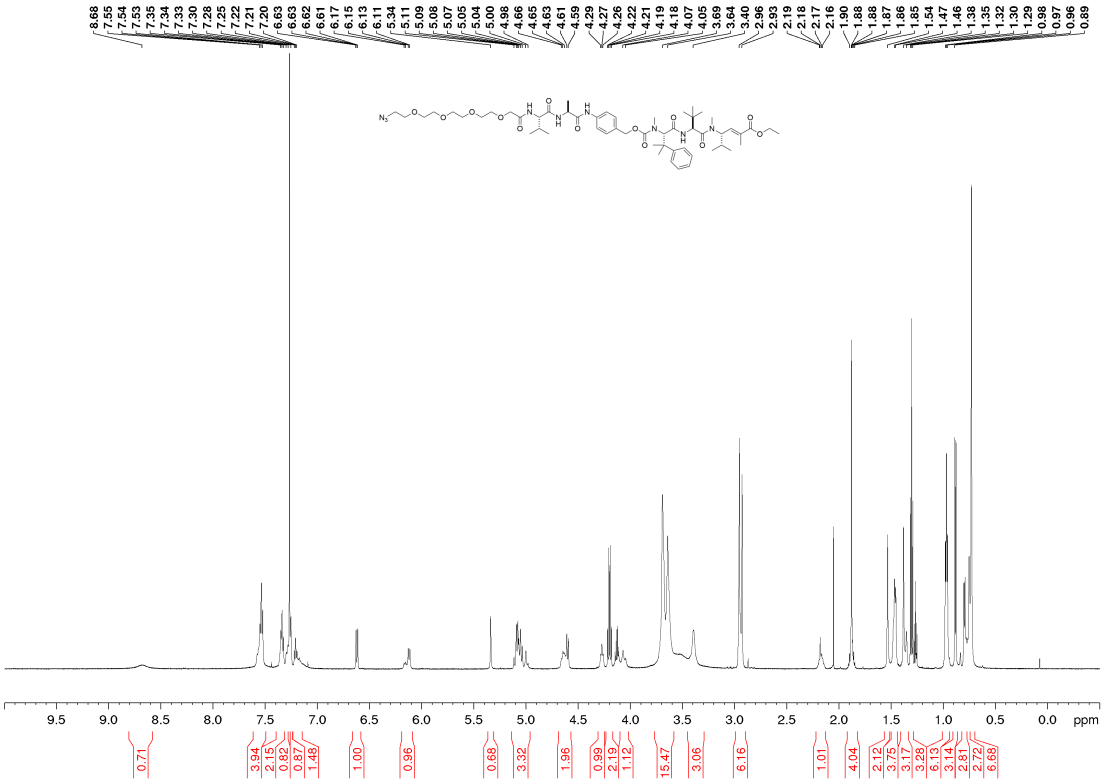

(*S*)-3,3-Dimethyl-2-((*S*)-3-methyl-3-(1-methyl-1*H*-indol-3-yl)-2-(2,2,2-trifluoro-*N*-methylacetamido)butanamido)butanoic acid (109a)

^{1}H-NMR

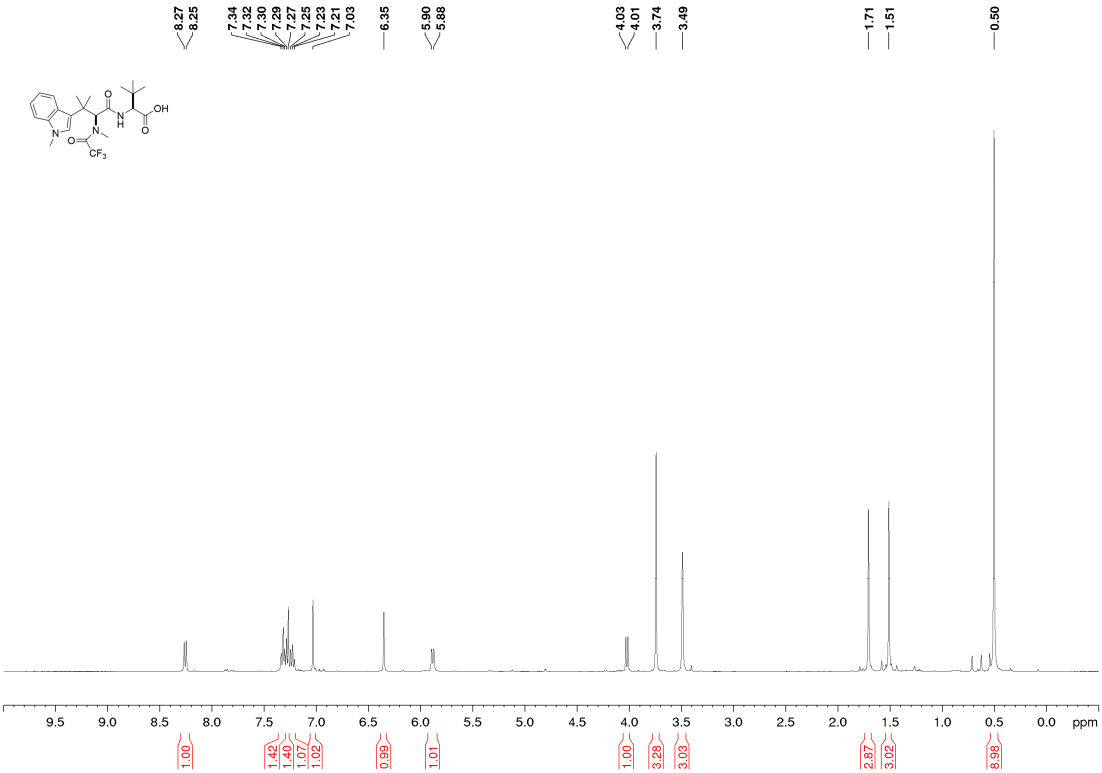

^{13}C-NMR

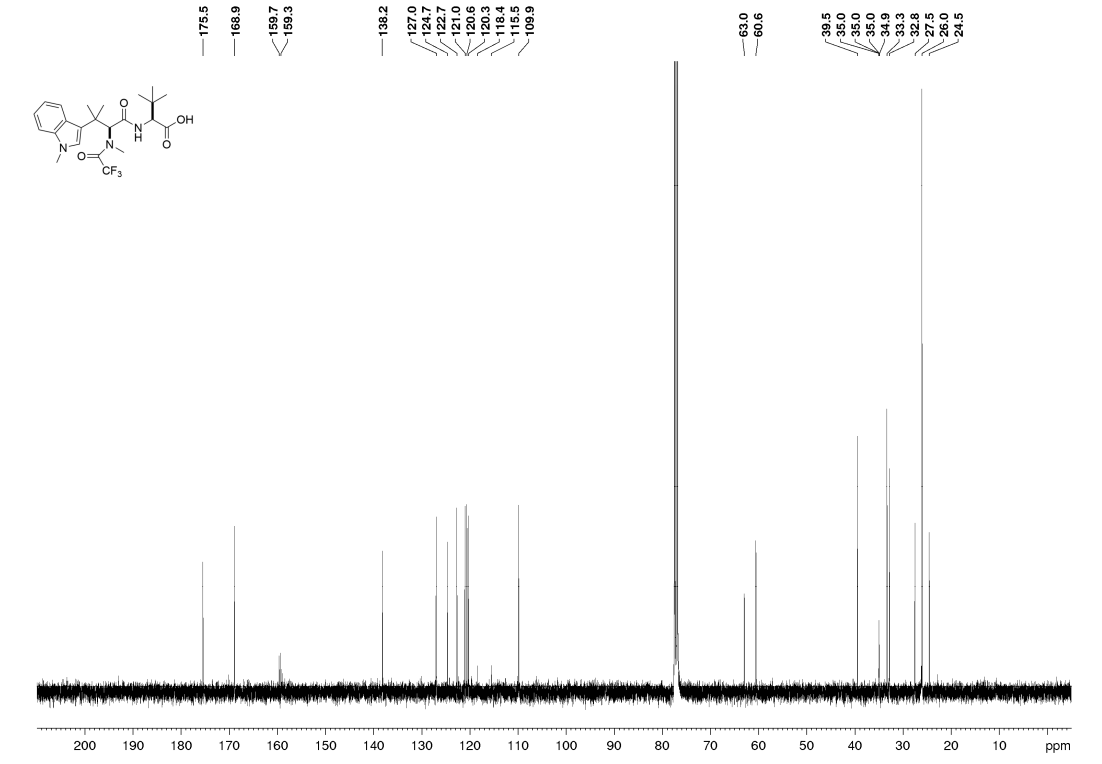

^{19}F-NMR

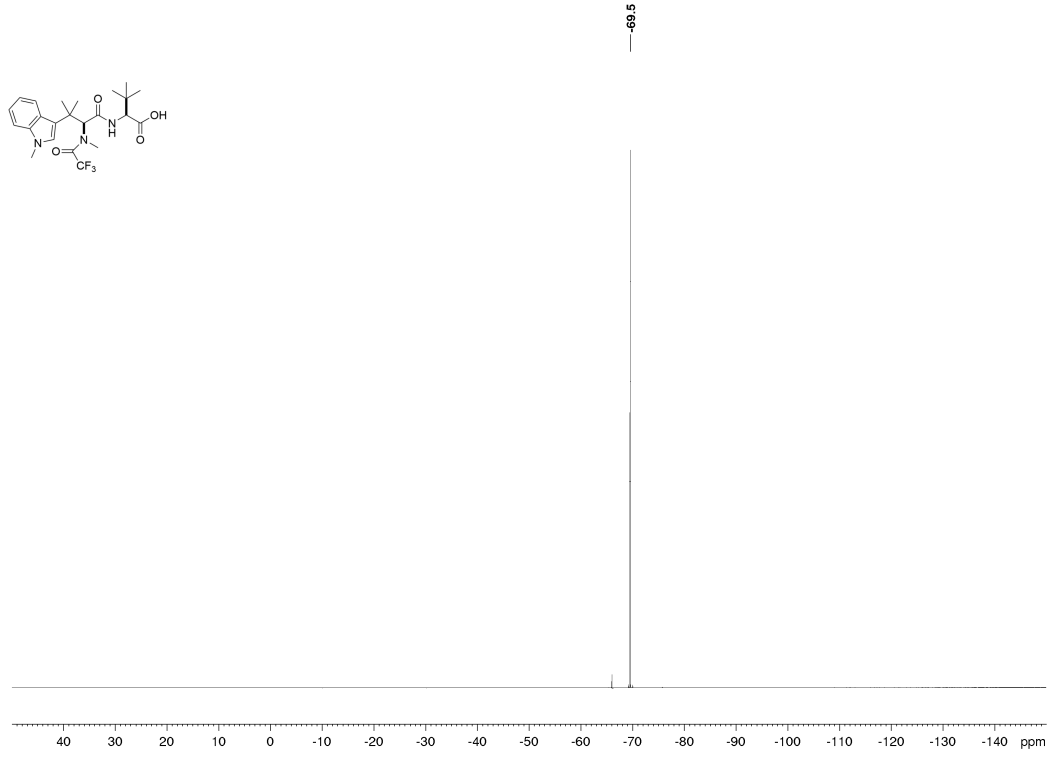

(*S*)-3,3-Dimethyl-2-((*R*)-3-methyl-3-(1-methyl-1*H*-indol-3-yl)-2-(2,2,2-trifluoro-*N*-methylacetamido)butanamido)butanoic acid (109b)

^{1}H-NMR

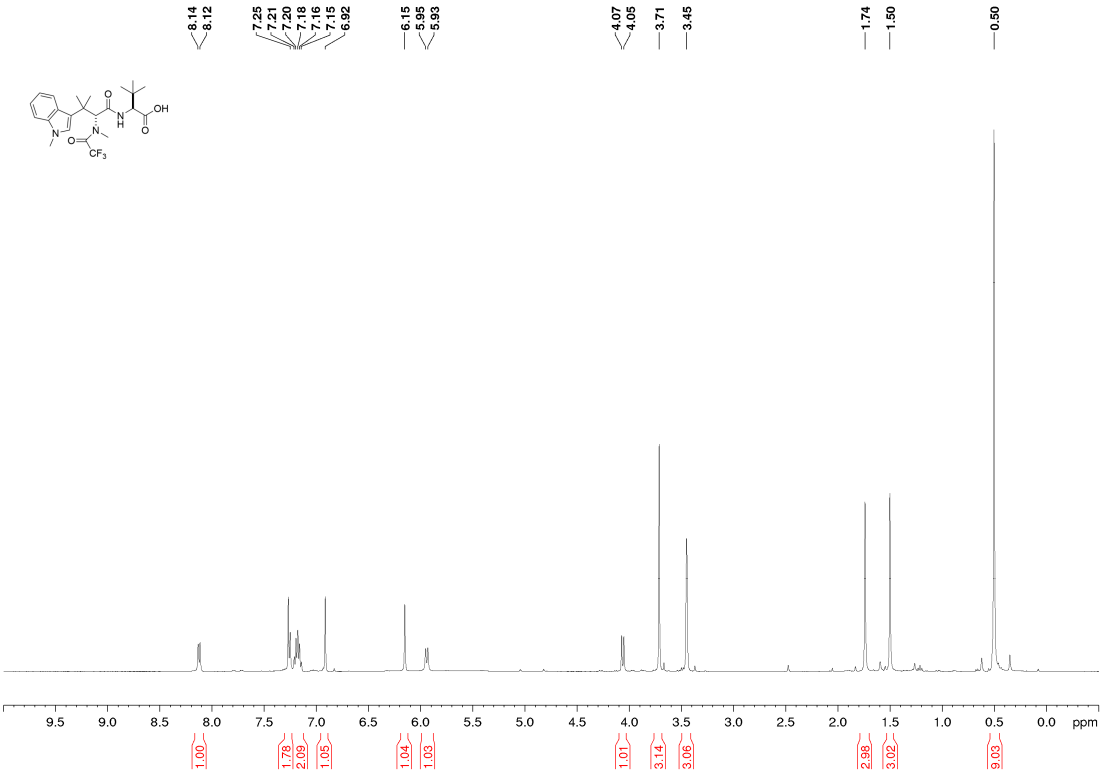

^{13}C-NMR

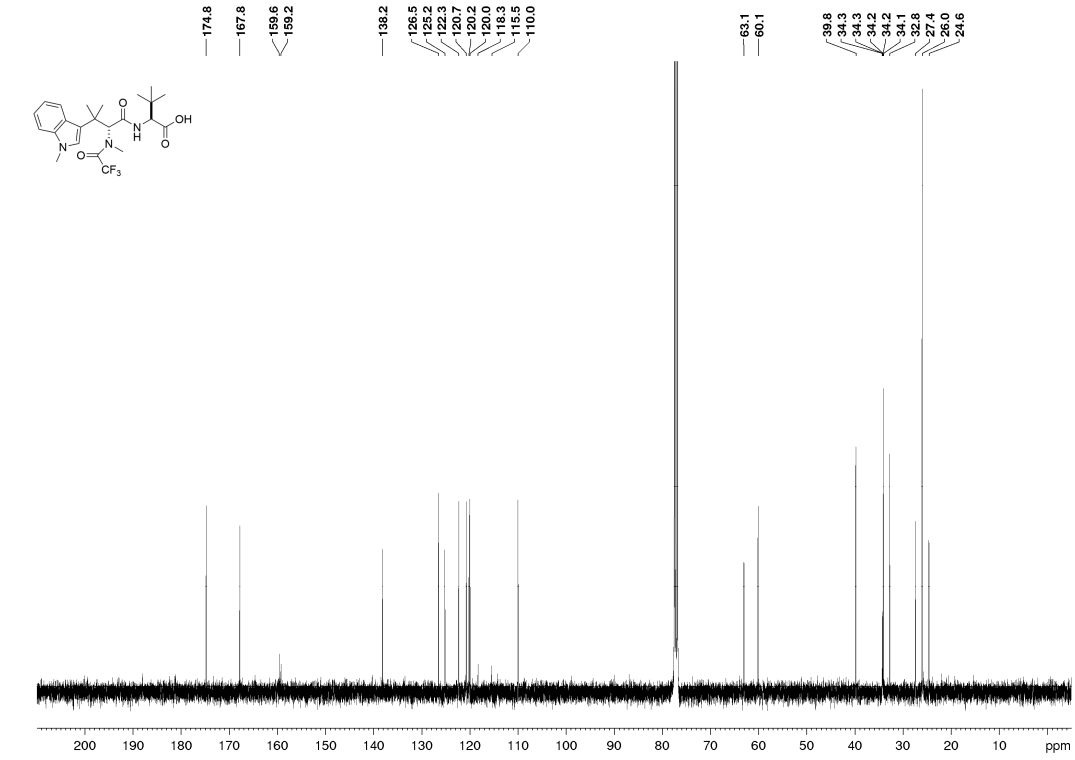

^{19}F-NMR

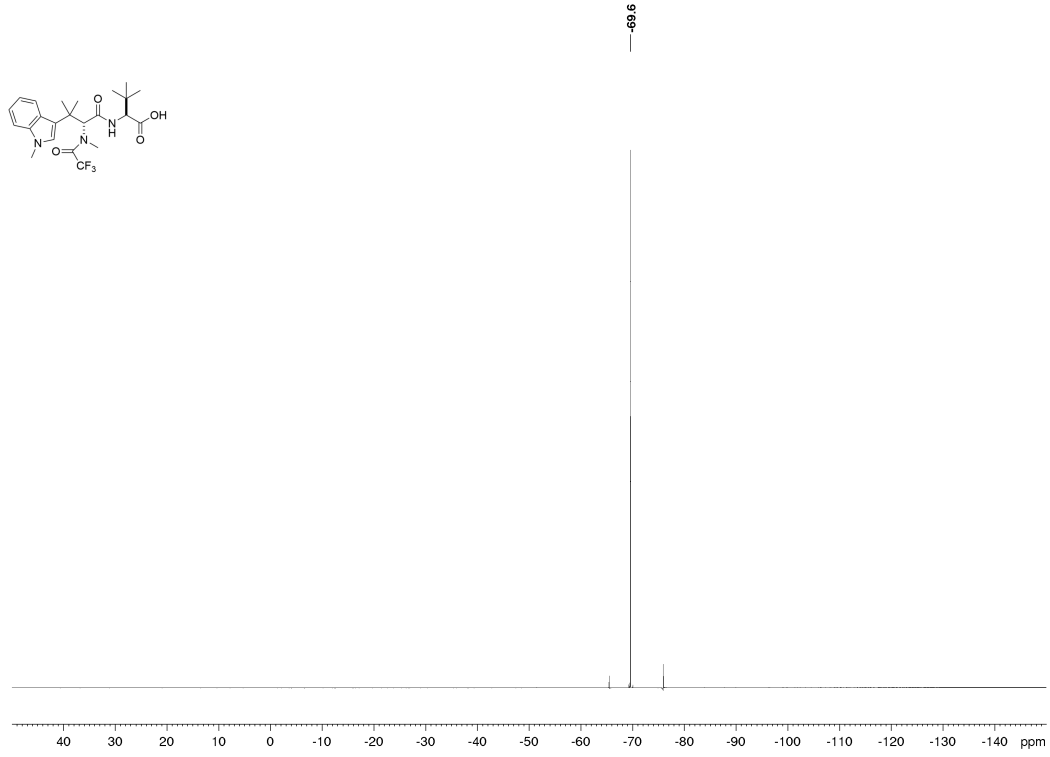

***N*-((1*S*)-1-(4-(*tert*-Butyl)-5-oxo-4,5-dihydrooxazol-2-yl)-2-methyl-2-(1-methyl-1*H*-indol-3-yl)propyl)-2,2,2-trifluoro-1*N*-methylacetamide (114, as an inseparable diastereomeric mixture of 1.7:1 *dr*)**

^{1}H-NMR

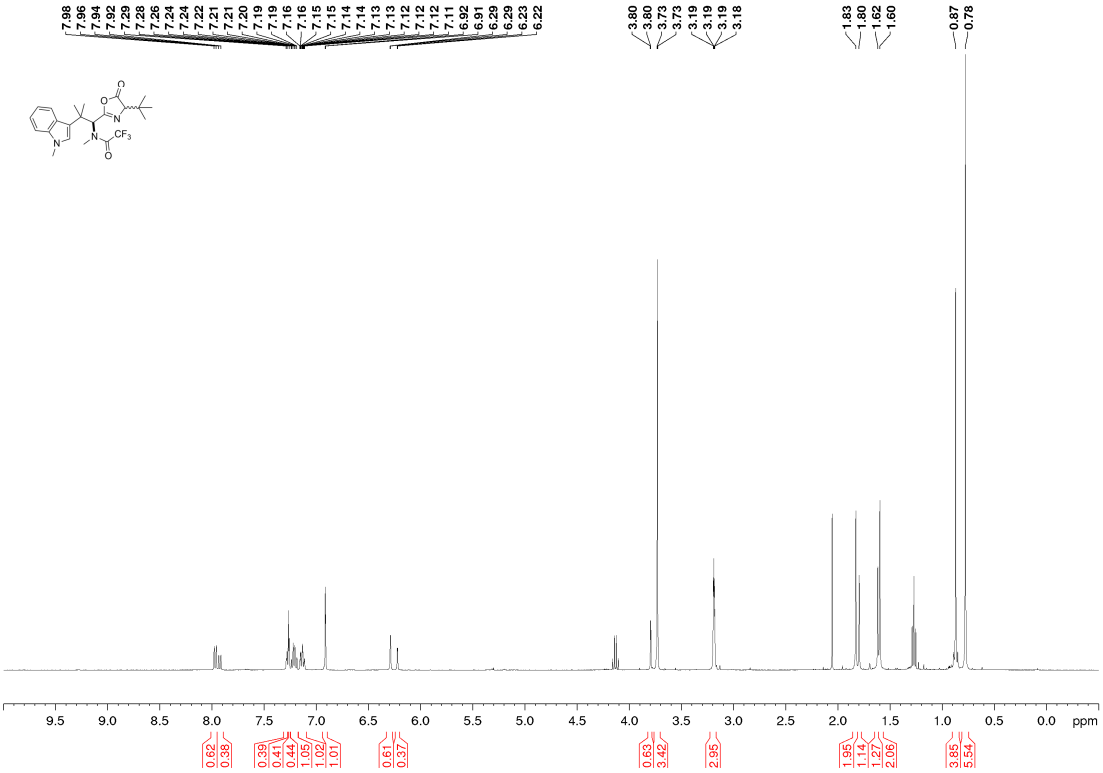

^{13}C-NMR

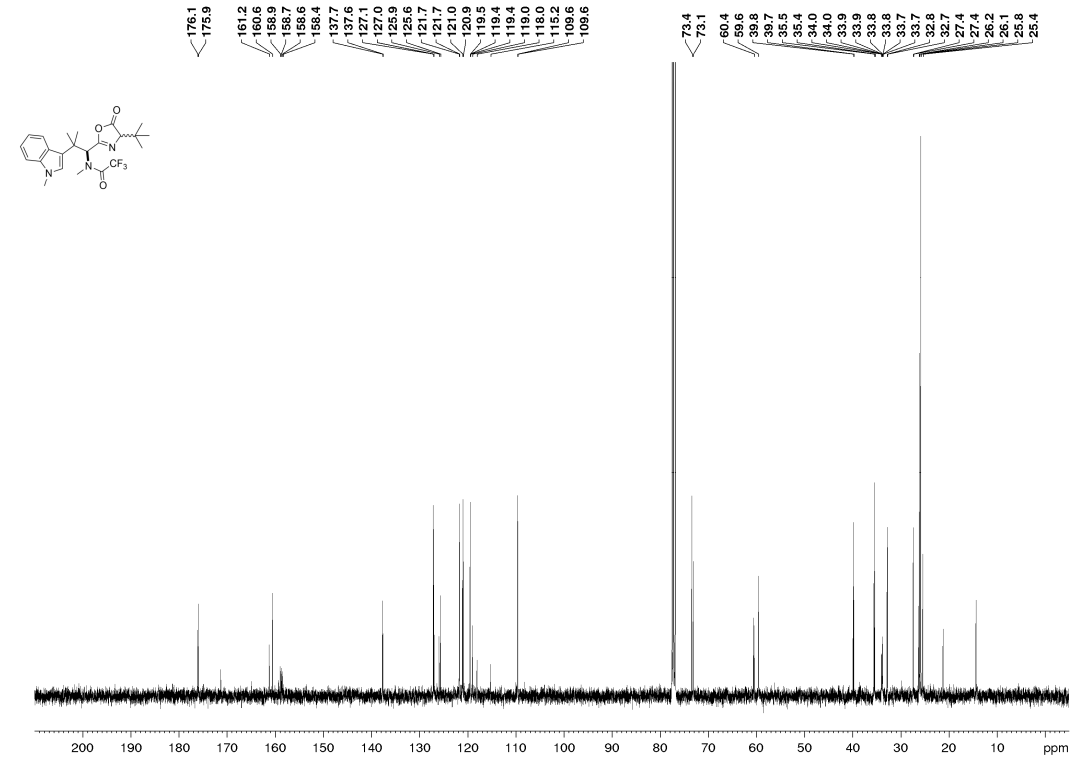

^{19}F-NMR

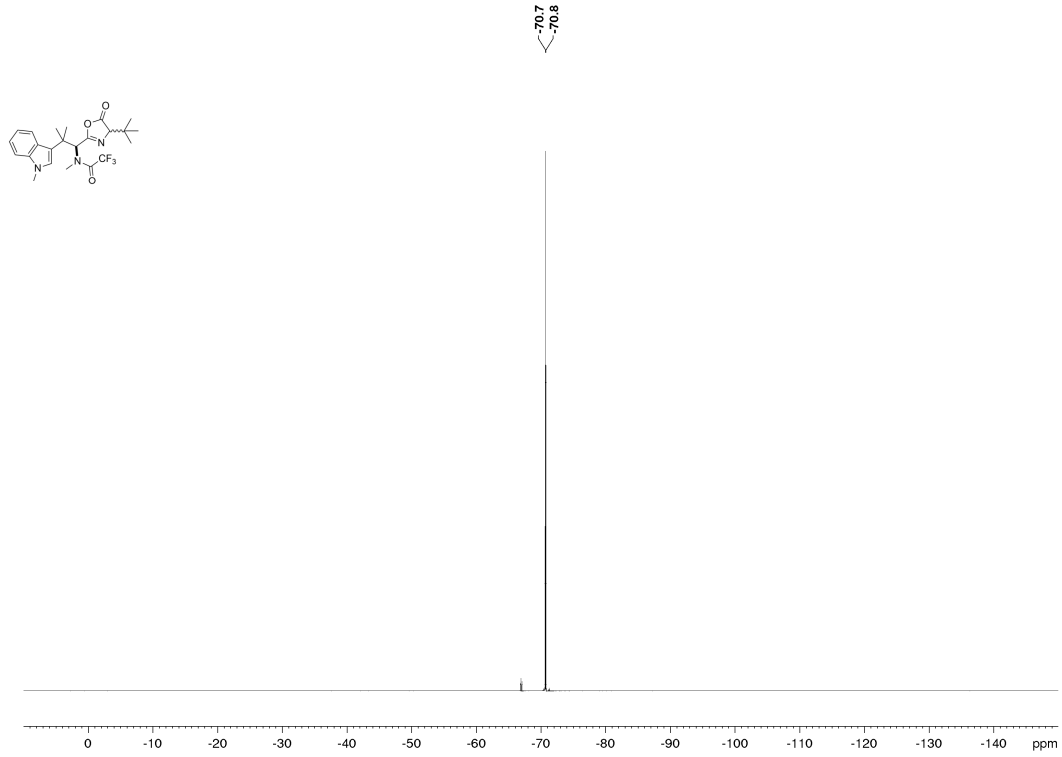

(*S*)-3,3-Dimethyl-2-((*S*)-3-methyl-3-(1-methyl-1*H*-indol-3-yl)-2-(methylamino)butanamido)butanoic acid trifluoroacetate salt (127a)

^{1}H-NMR

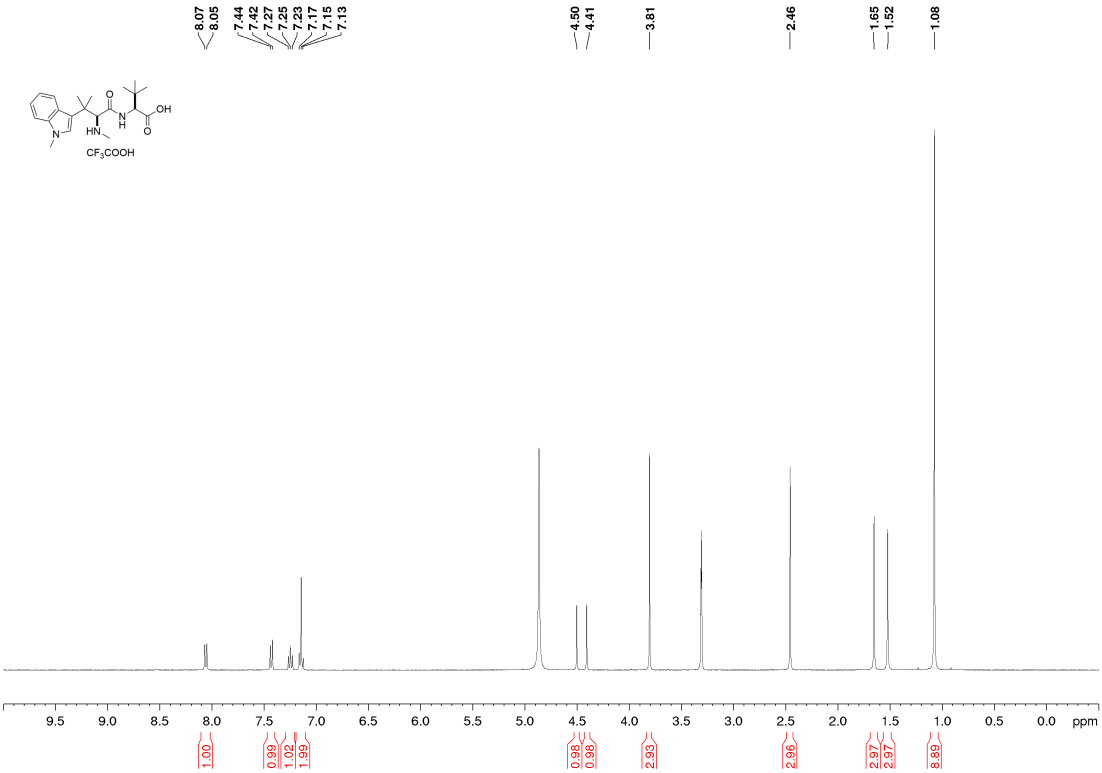

^{13}C-NMR

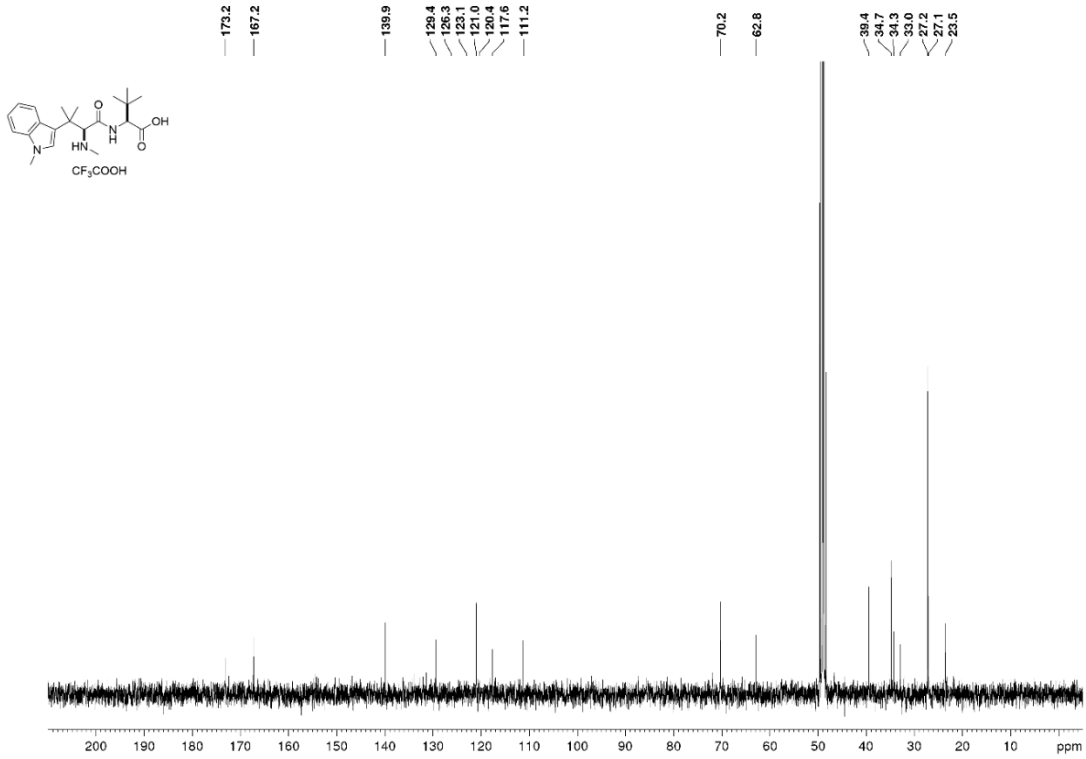

^{19}F-NMR

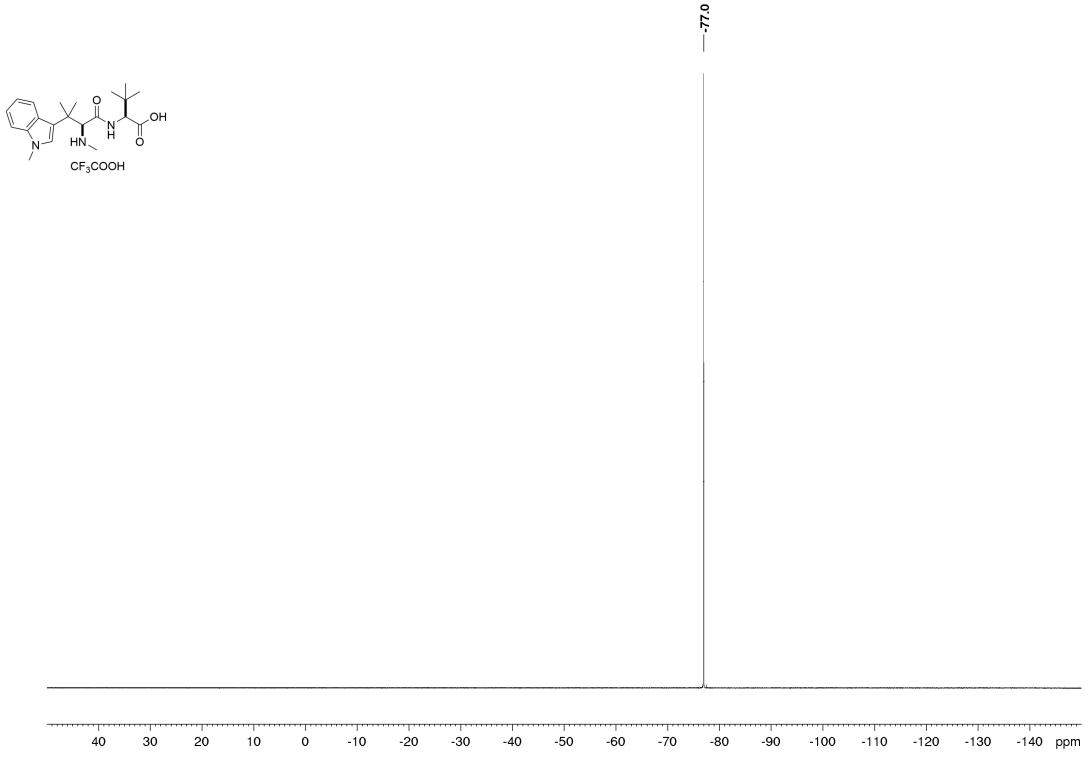
-77.0
OH
HN
CF3COOH
40 30 20 10 0 -10 -20 -30 -40 -50 -60 -70 -80 -90 -100 -110 -120 -130 -140 ppm

Methyl (*S*)-3,3-dimethyl-2-((*S*)-3-methyl-3-(1-methyl-1*H*-indol-3-yl)-2-(methylamino)butanamido)butanoate trifluoroacetate salt (129a)

^{1}H-NMR

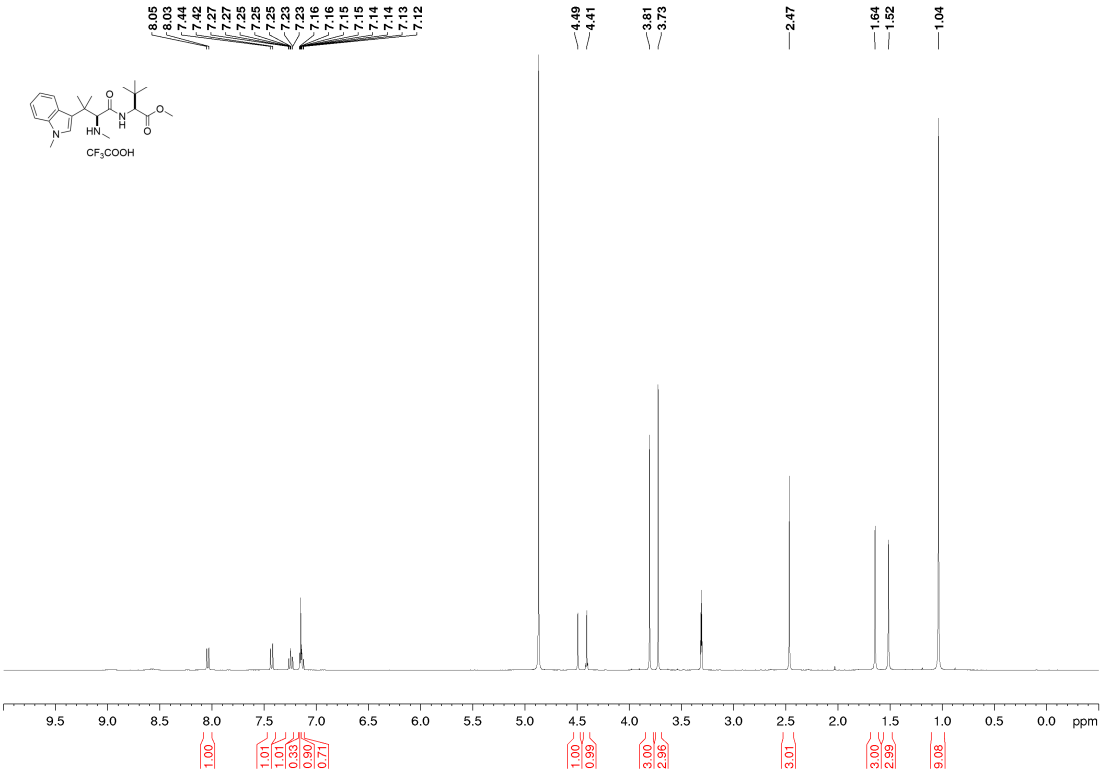

^{13}C-NMR

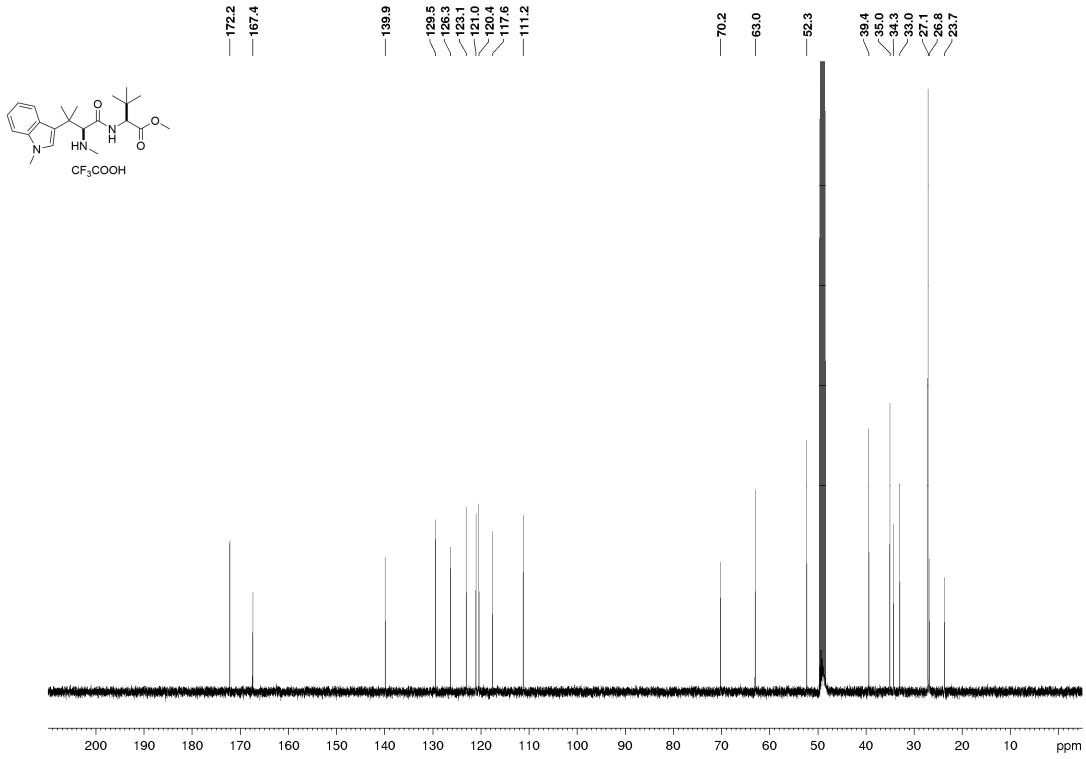

Methyl (*S*)-3,3-dimethyl-2-((*R*)-3-methyl-3-(1-methyl-1*H*-indol-3-yl)-2-(methylamino)butanamido)butanoate trifluoroacetate salt (129b)

^{1}H-NMR

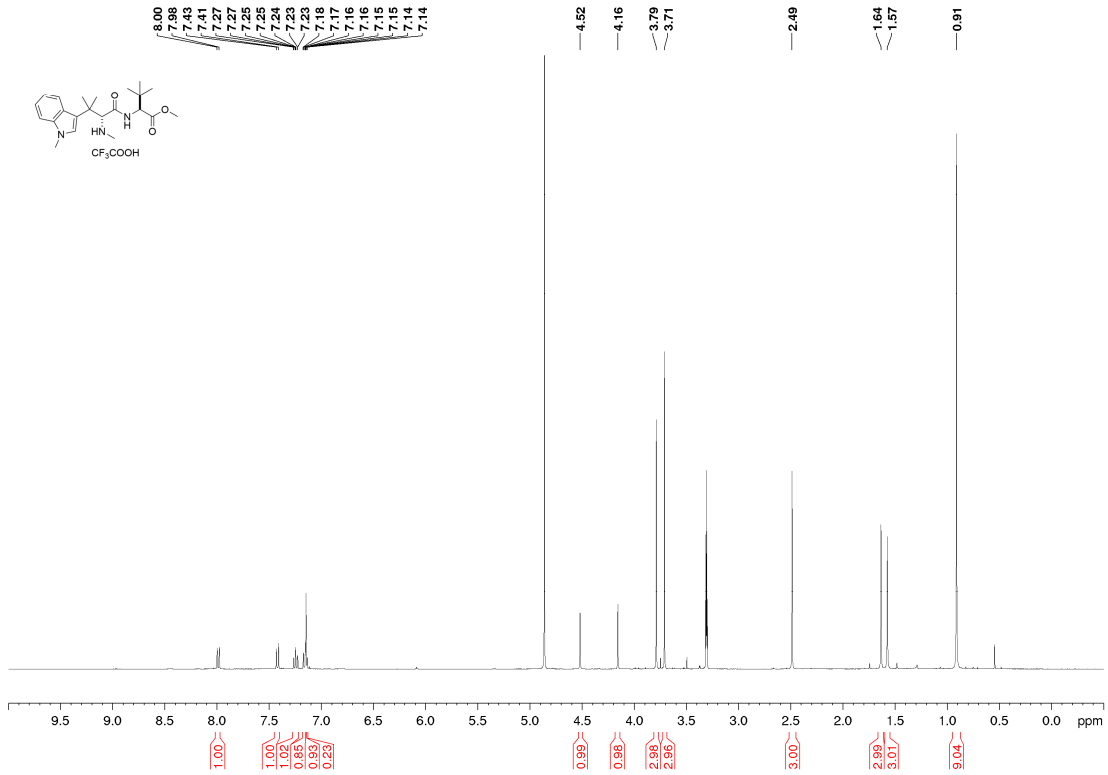

^{13}C-NMR

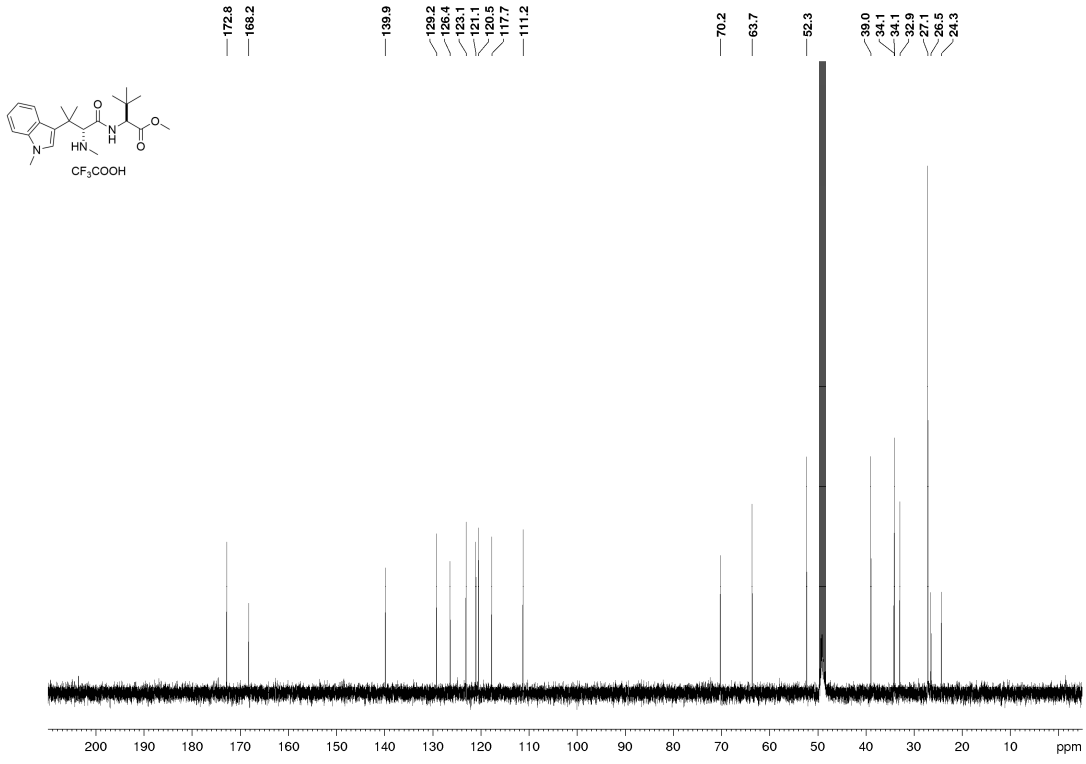

^{19}F-NMR

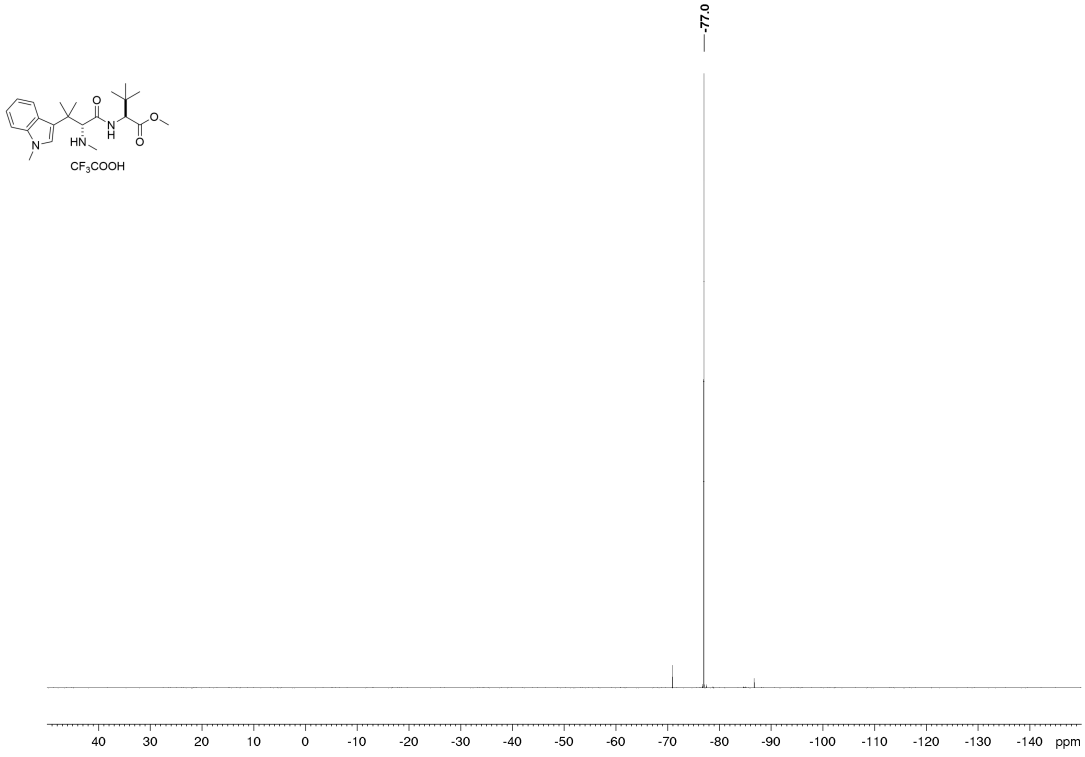
-77.0
CF3COOH
40 30 20 10 0 -10 -20 -30 -40 -50 -60 -70 -80 -90 -100 -110 -120 -130 -140 ppm

Alloc-Val-Ala-PABC-OPNP (123)

^{1}H-NMR

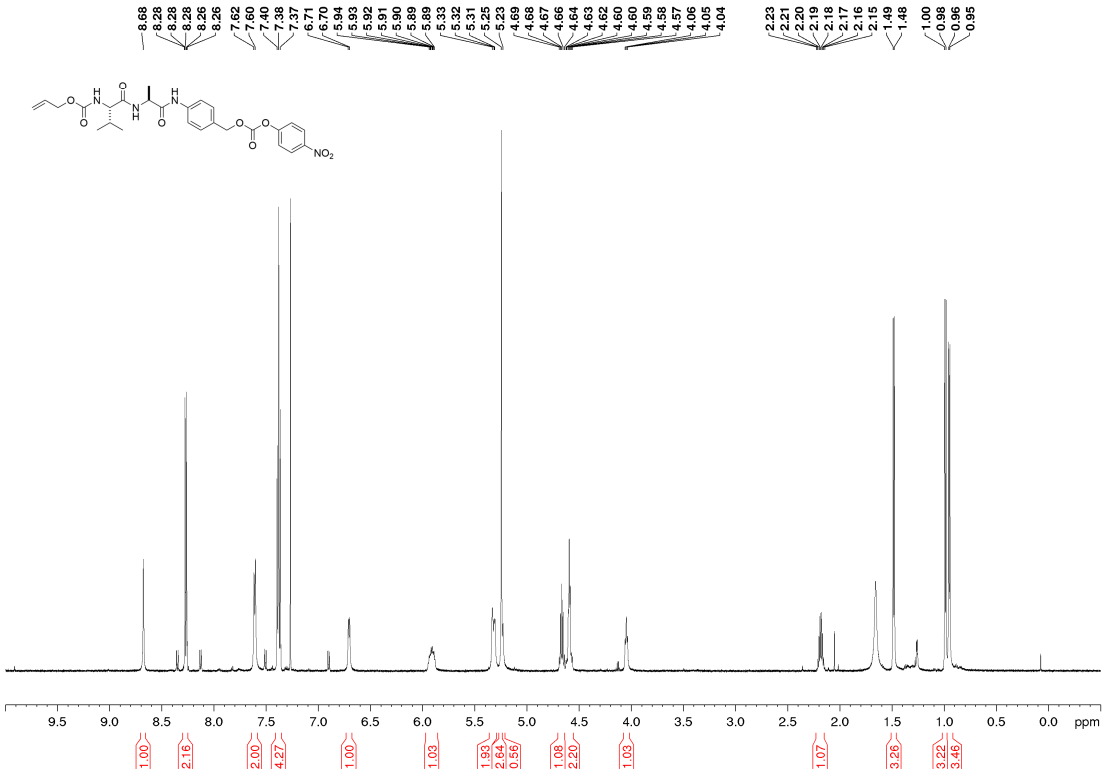

Carbamate 128b

^{1}H-NMR (rt, DMSO)

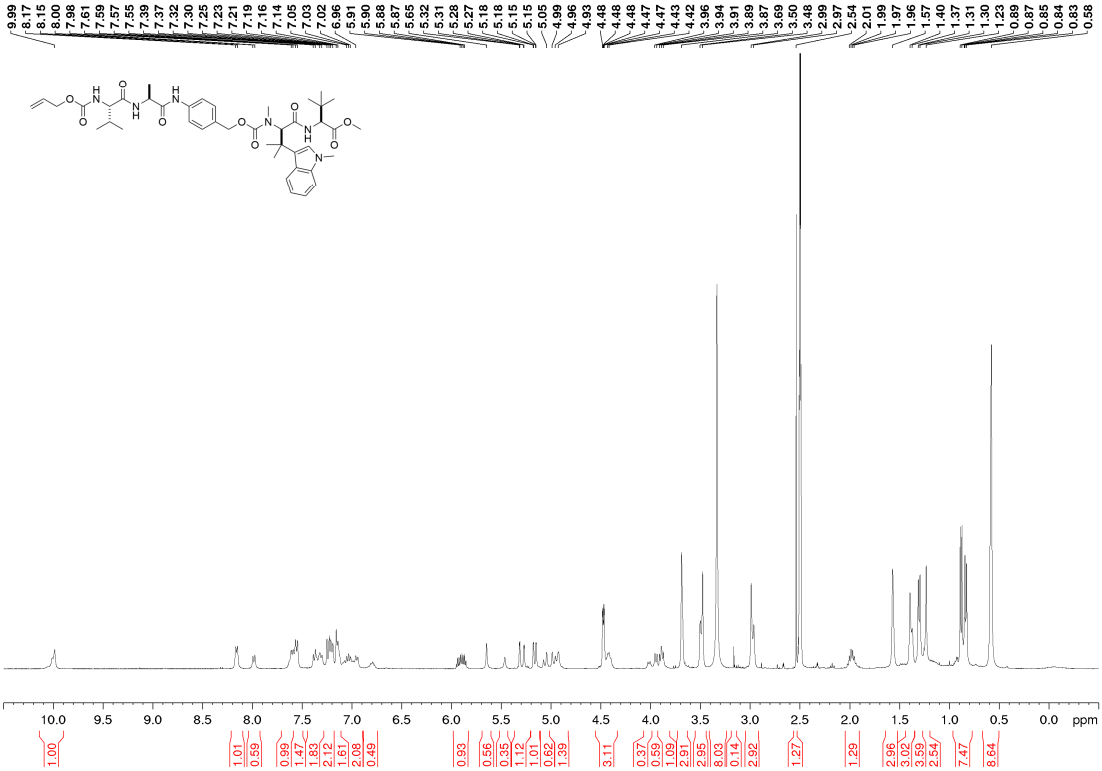

^{1}H-NMR (130 °C, DMSO)

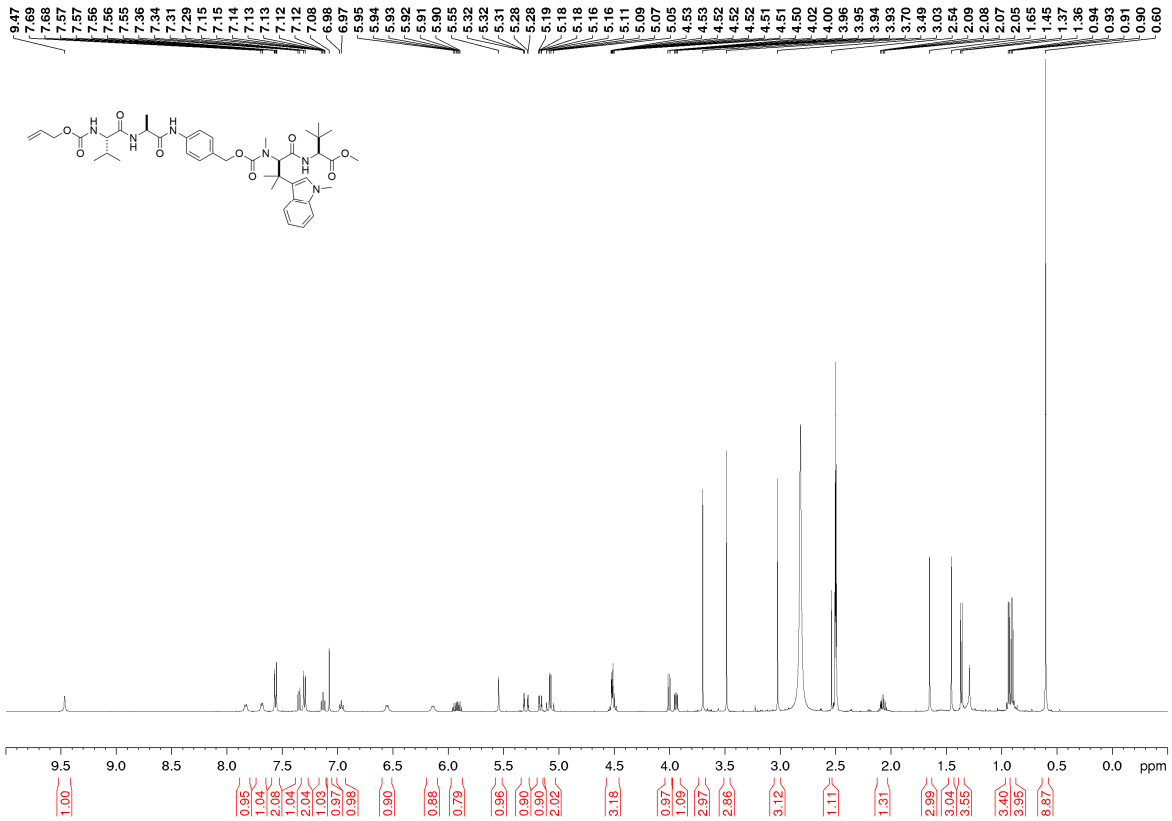

^{13}C-NMR (rt, $CDCl_3$)

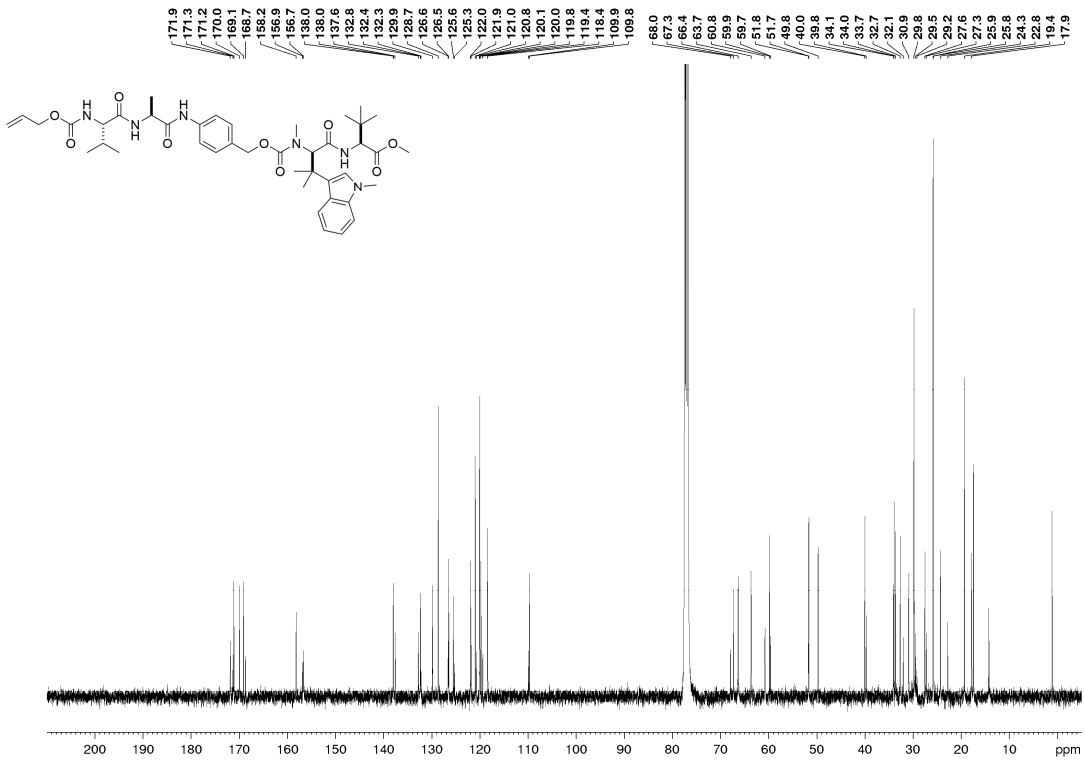

^{1}H-NMR comparison at different temperatures for carbamate 128b

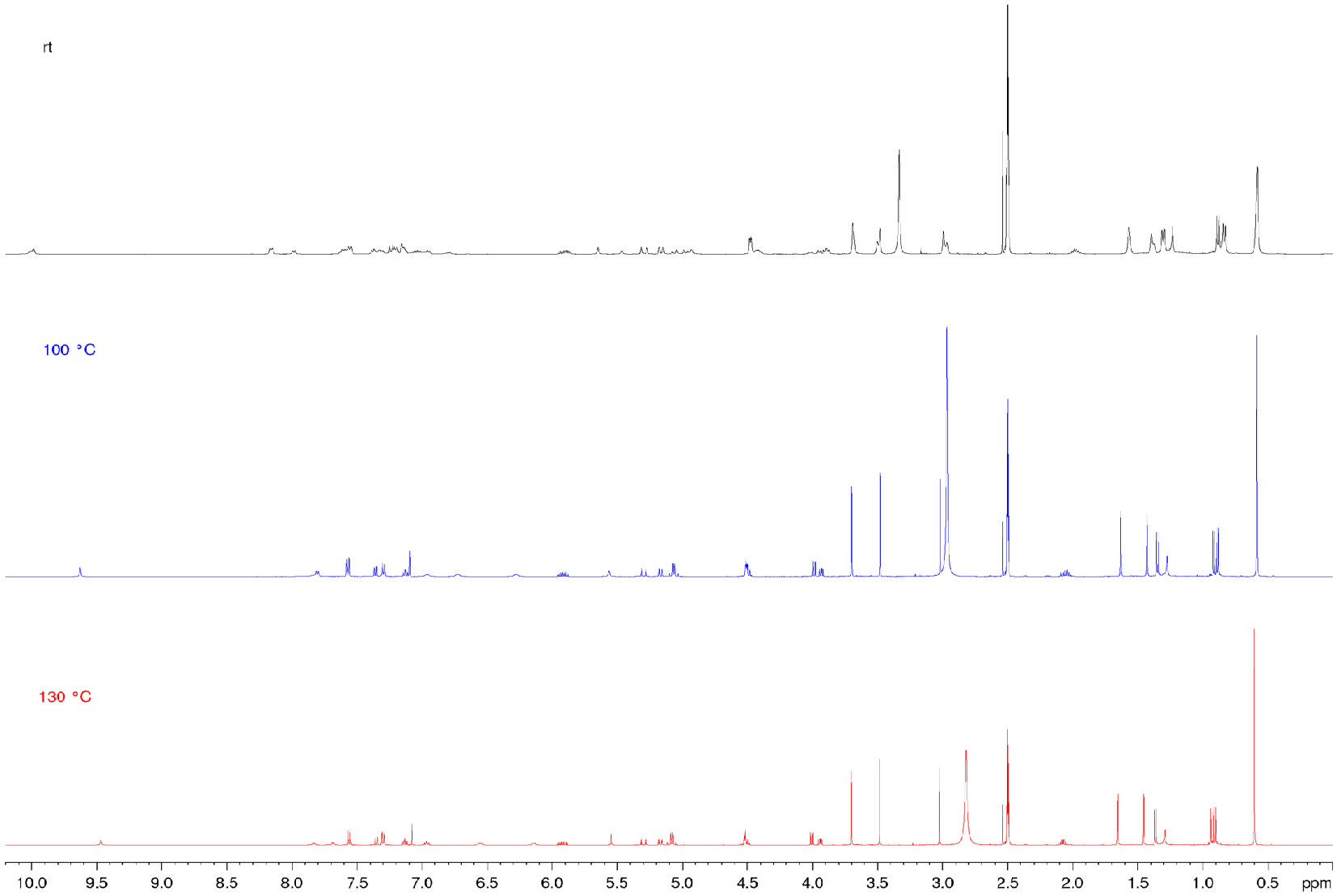

Appendix C — Selected analytical HPLC and LCMS traces

For HPLC analysis, unless stated otherwise, all compounds were analysed using 5-95%B over 15 min gradient and monitored at 220 nm. In some HPLC chromatographs, there exists a peak at $t_R \approx 2$ min, corresponding to DMSO.

C.1. Chapter 4

P1

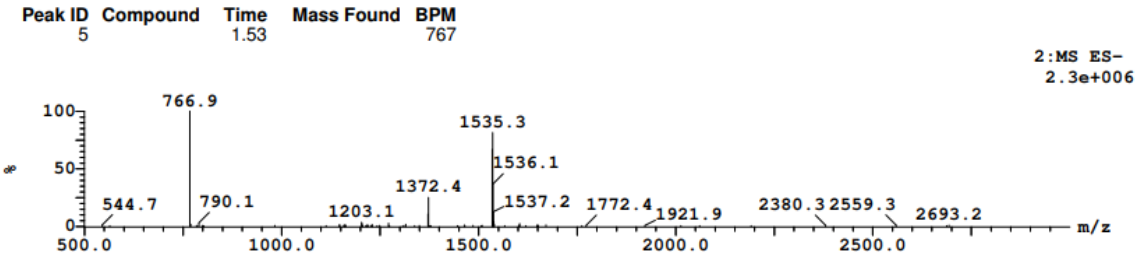

Gradient: 30-80%B over 15 min

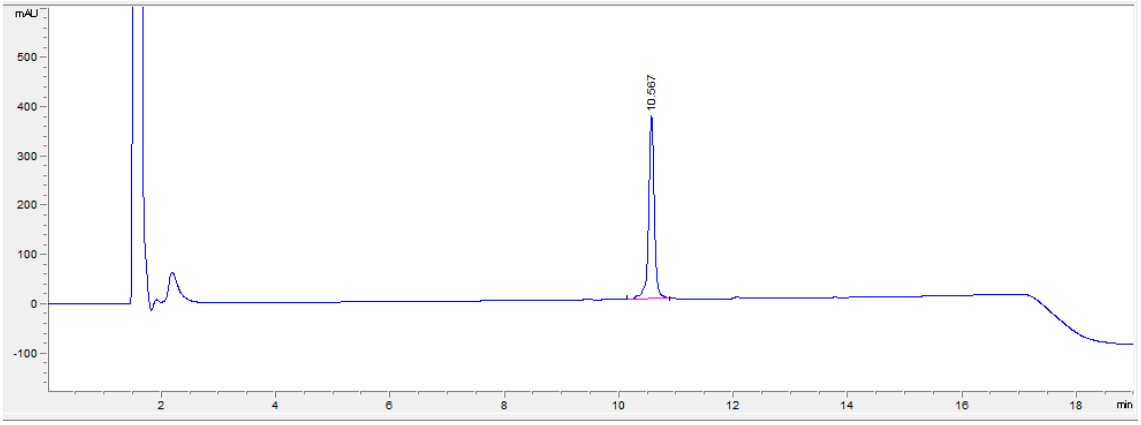

P3

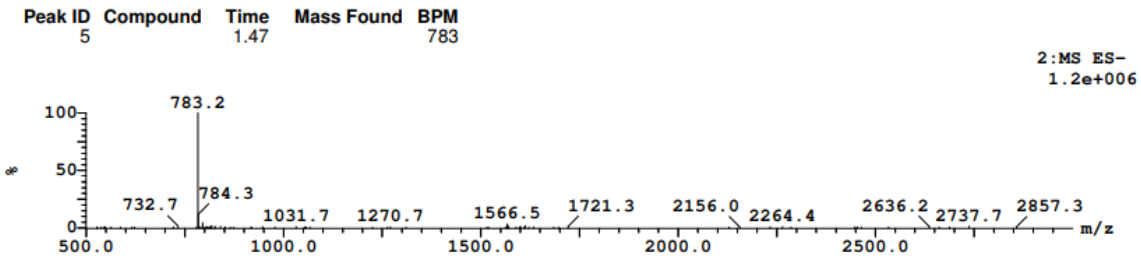

Gradient: 10-80%B over 15 min

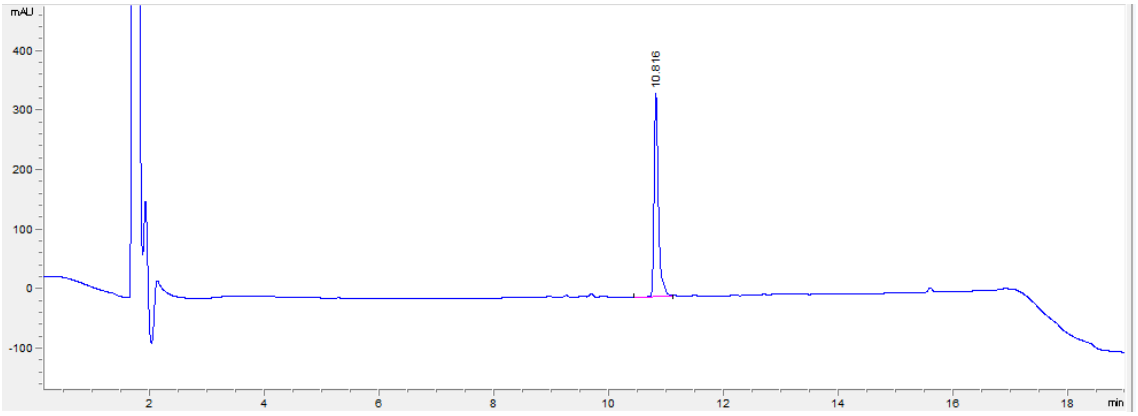

P4

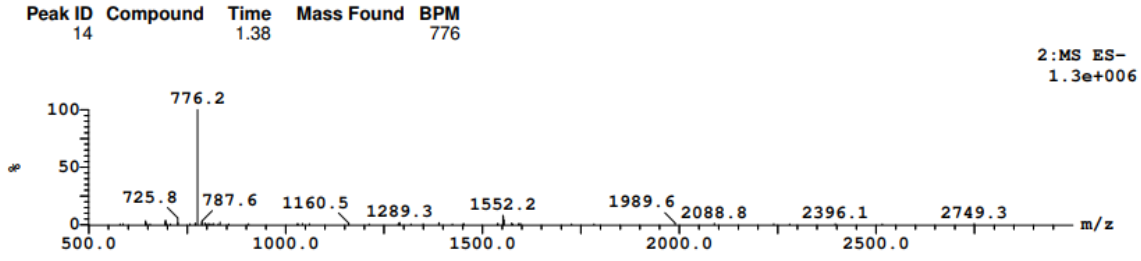

Gradient: 20-60%B over 15 min

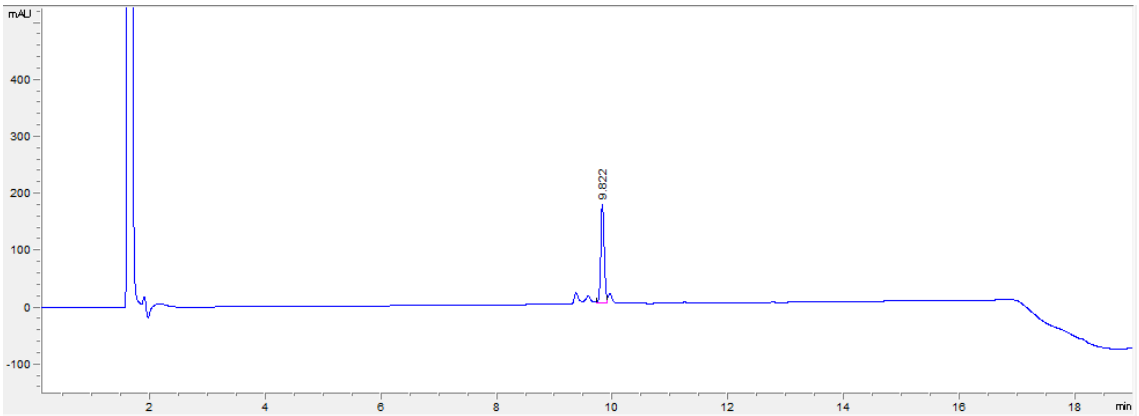

P5

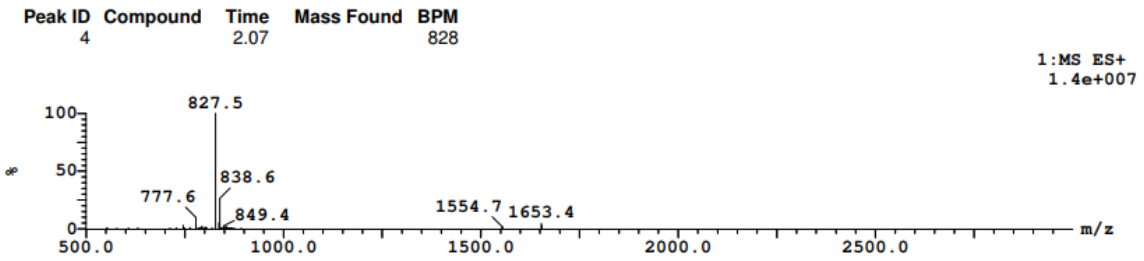

Gradient: 20-60%B over 15 min

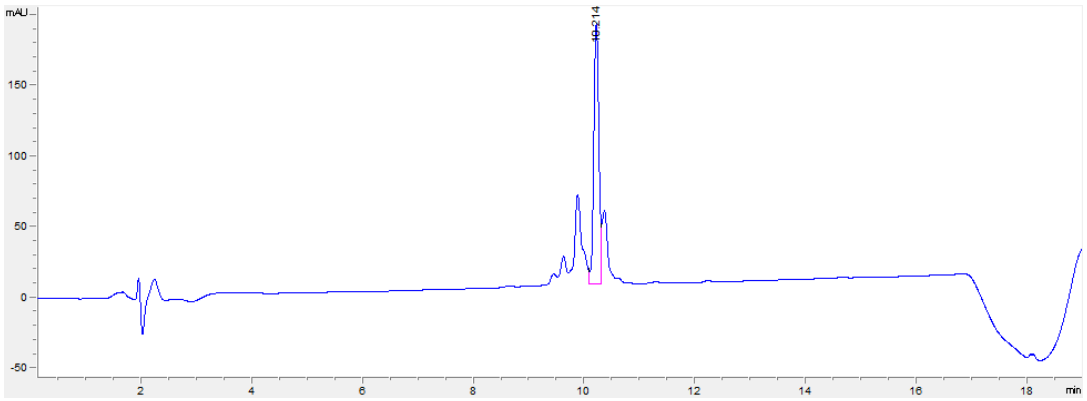

P6

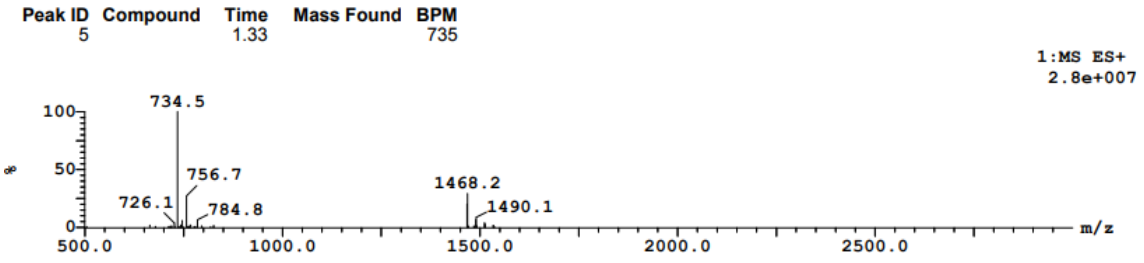

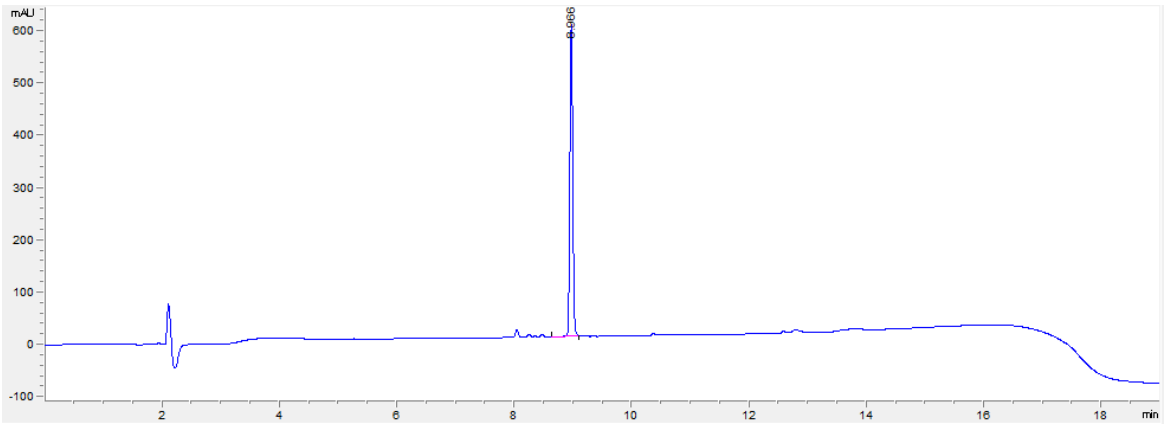

WT PMI

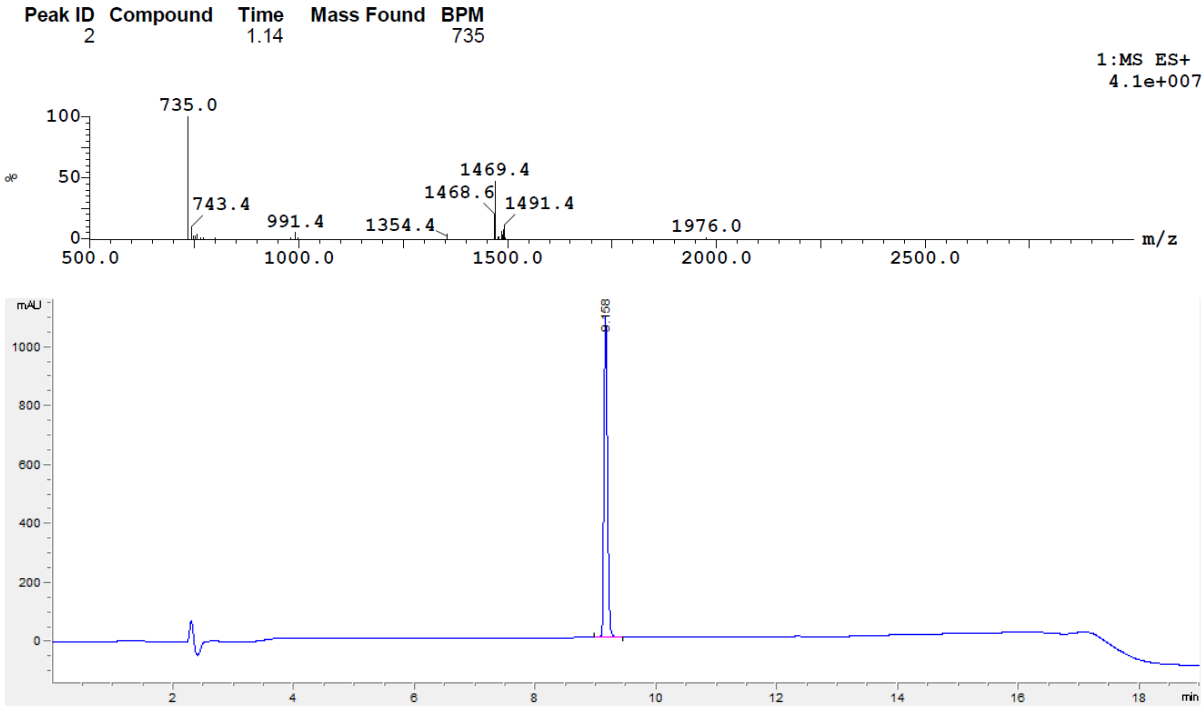

P5-81

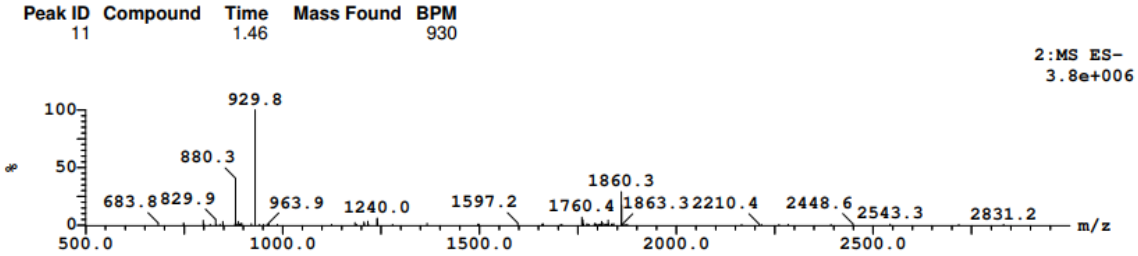

Gradient: 20-60%B over 15 min

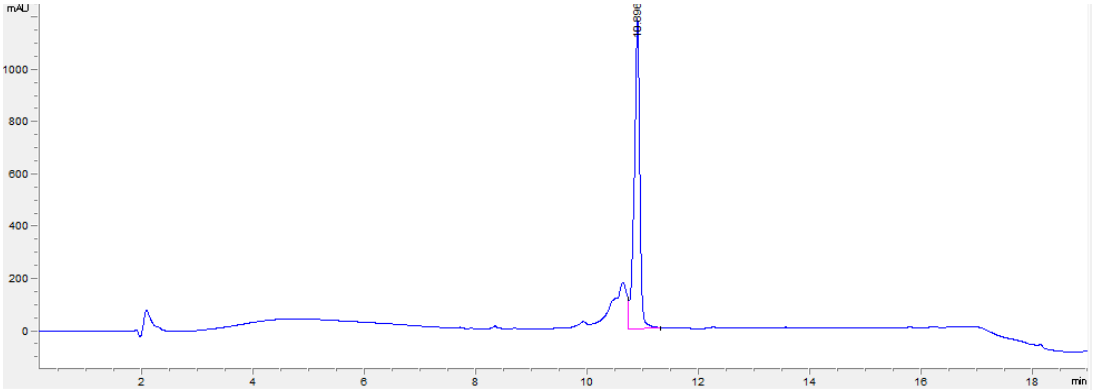

P6-81

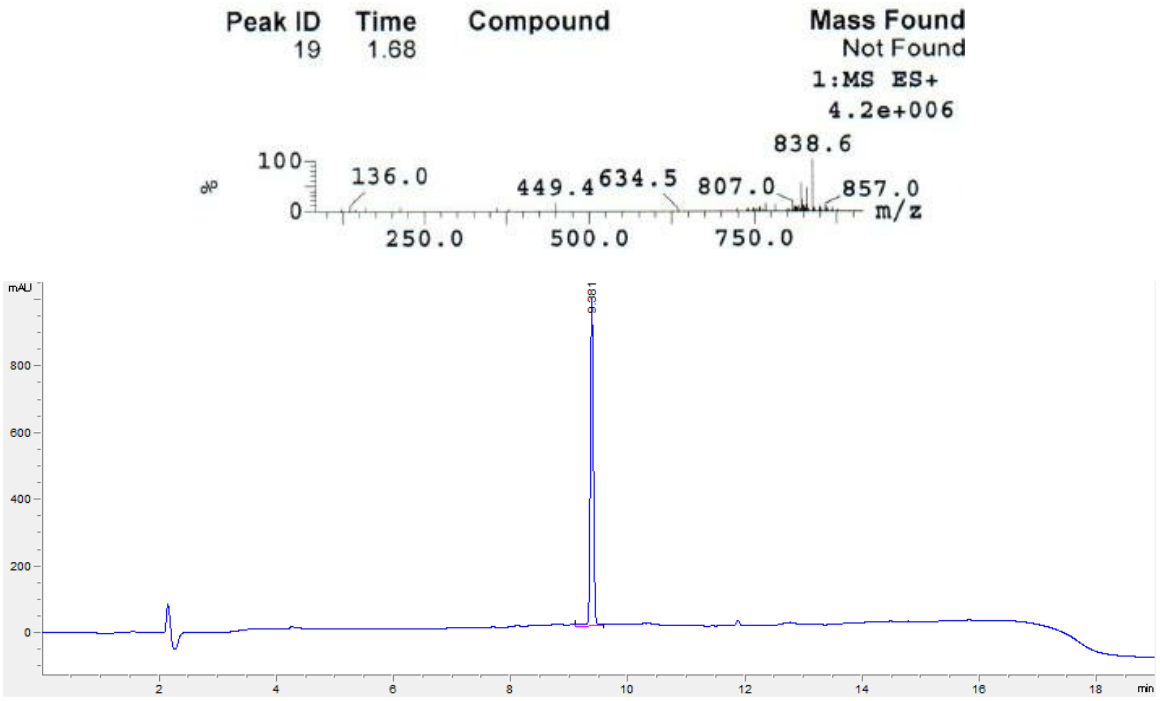
Peak ID
19
Time
1.68
Compound
Mass Found
Not Found
1:MS ES+
4.2e+006
838.6
100
0
136.0
449.4
634.5
807.0
857.0
m/z
250.0
500.0
750.0
mAU
9.981
800
600
400
200
0
2
4
6
8
10
12
14
16
18
min

P6-92

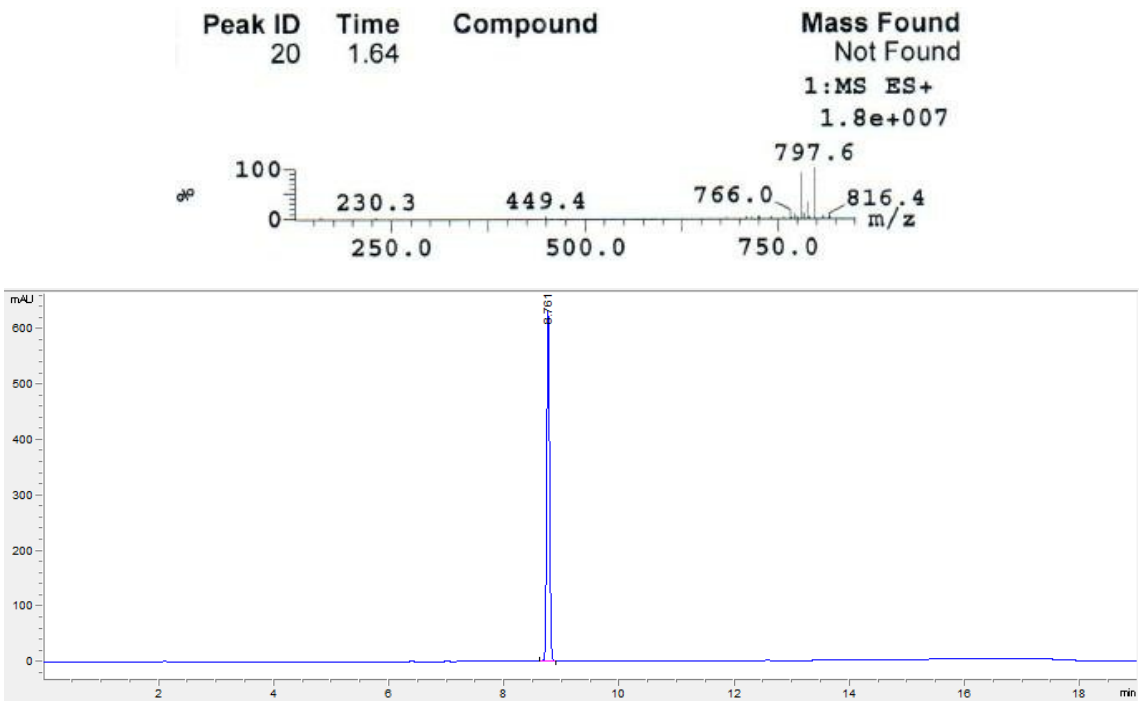
Peak ID
20
Time
1.64
Compound
Mass Found
Not Found
1:MS ES+
1.8e+007
797.6
100
0
230.3
449.4
766.0
816.4
m/z
250.0
500.0
750.0
mAU
9.761
600
500
400
300
200
100
0
2
4
6
8
10
12
14
16
18
min

P6-93

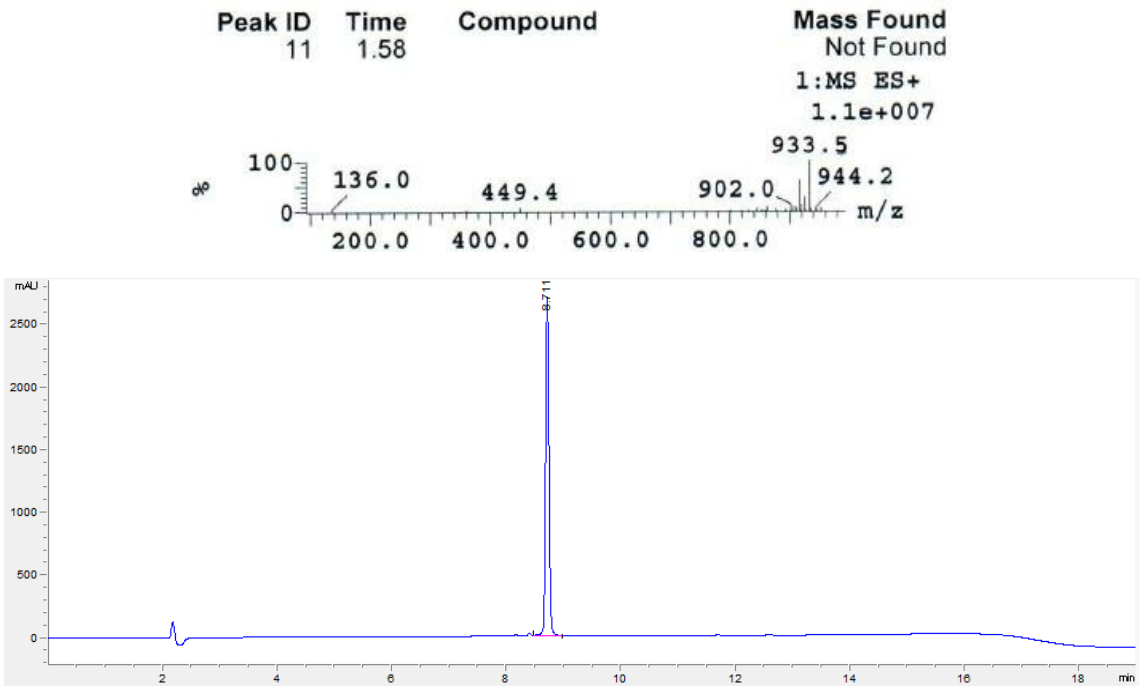
Peak ID
11
Time
1.58
Compound
Mass Found
Not Found
1:MS ES+
1.1e+007
933.5
944.2
902.0
136.0
449.4
100
0
%
m/z
200.0
400.0
600.0
800.0
mAU
2500
2000
1500
1000
500
0
8.711
2
4
6
8
10
12
14
16
18
min

C.2. Chapter 5

Hemiasterlin trifluoroacetate salt (56·TFA)

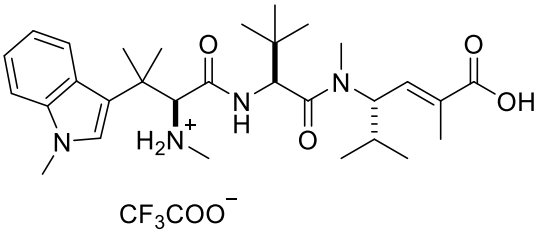

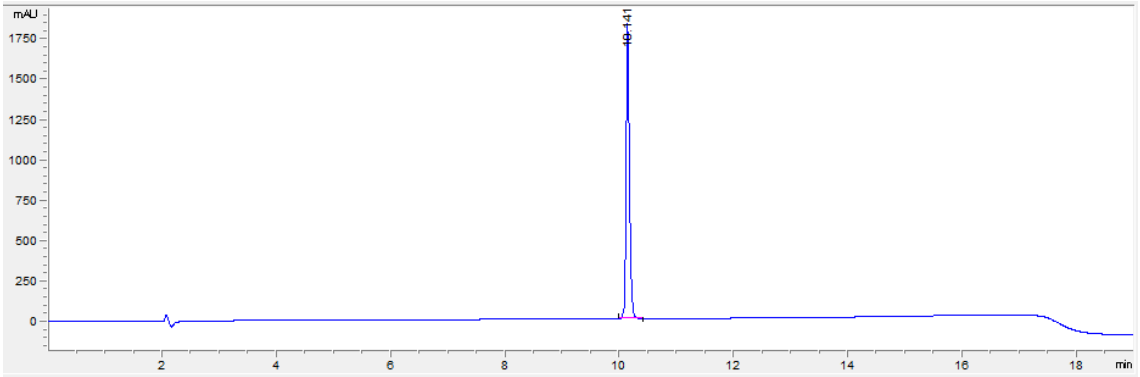

epi-Hemiasterlin trifluoroacetate salt (56b·TFA)

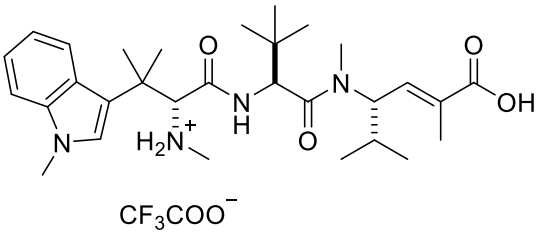

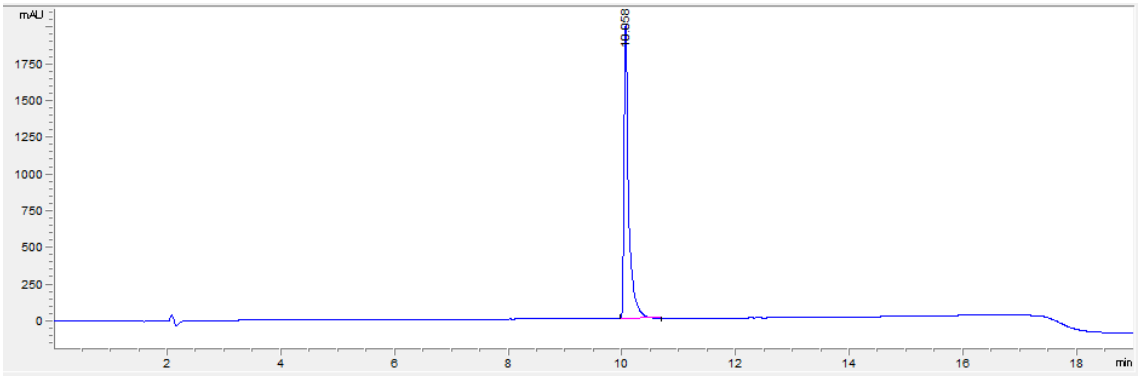

Taltobulin trifluoroacetate salt (57·TFA)

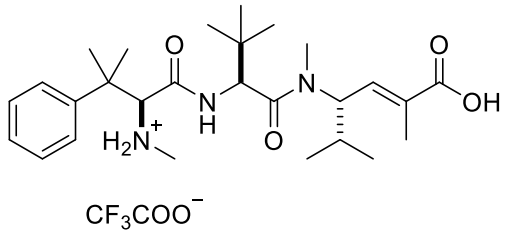

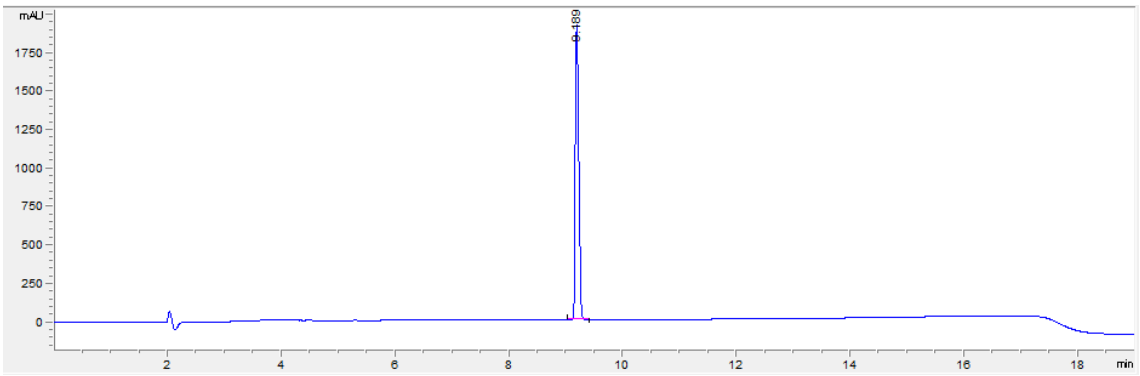

***epi*-Taltobulin trifluoroacetate salt (57b·TFA)**

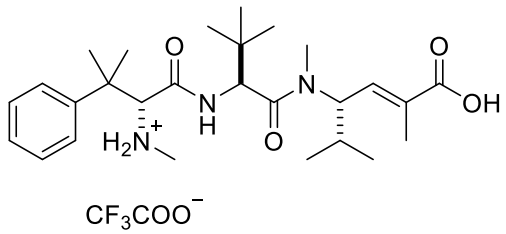

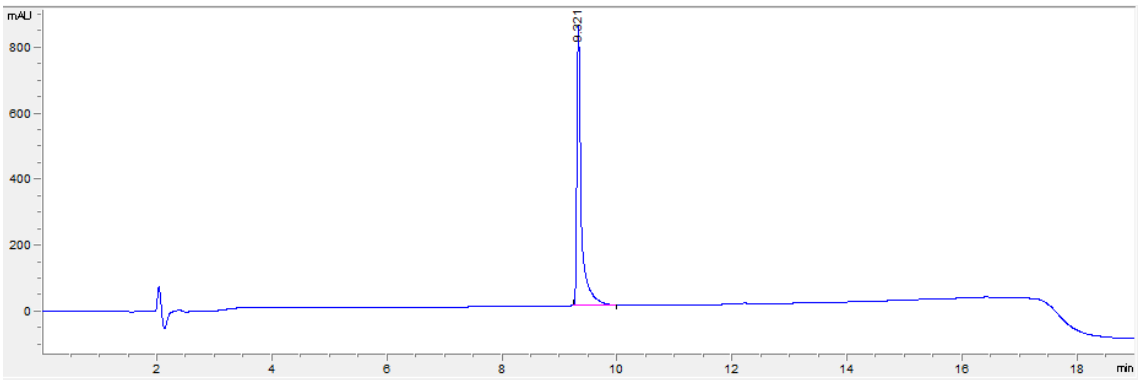

H-Val-Ala-PABA·TFA (134)

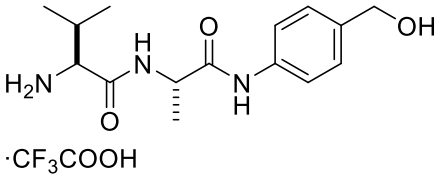

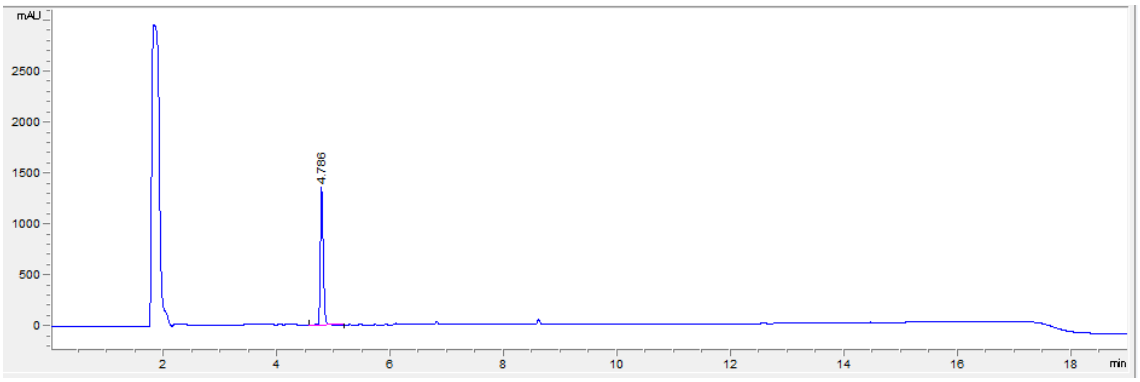

N_3-PEG_4-Val-Ala-PABA (135)

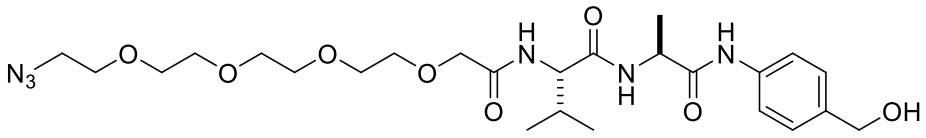

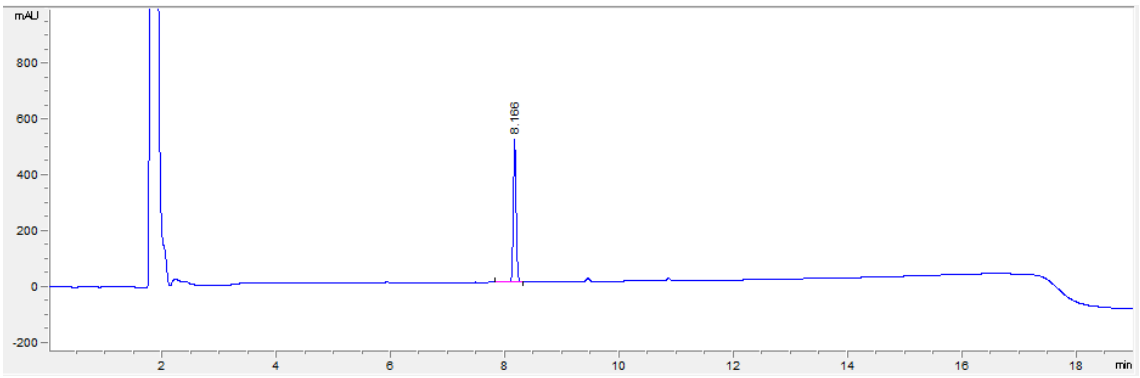

Hemiasterlin ethyl ester trifluoroacetate salt (137)

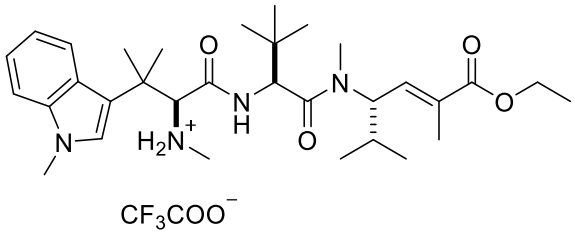

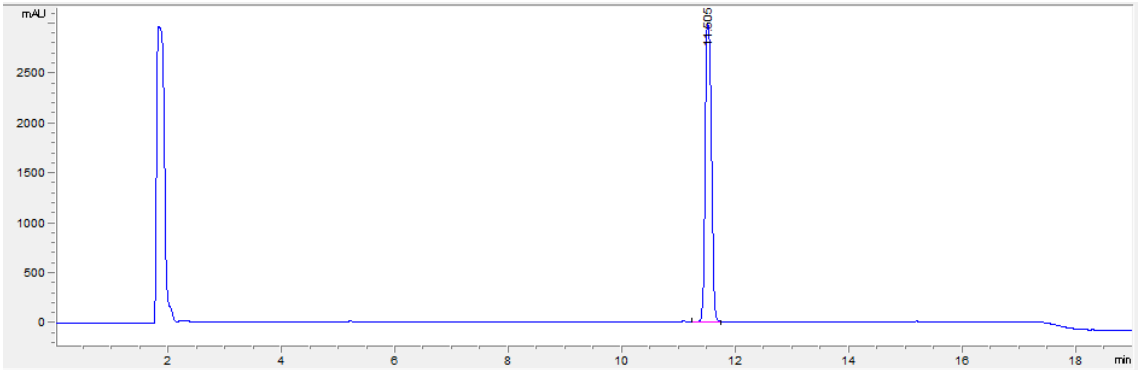

N_3-PEG_4-Val-Ala-PABC-hemiasterlin-OEt (139)

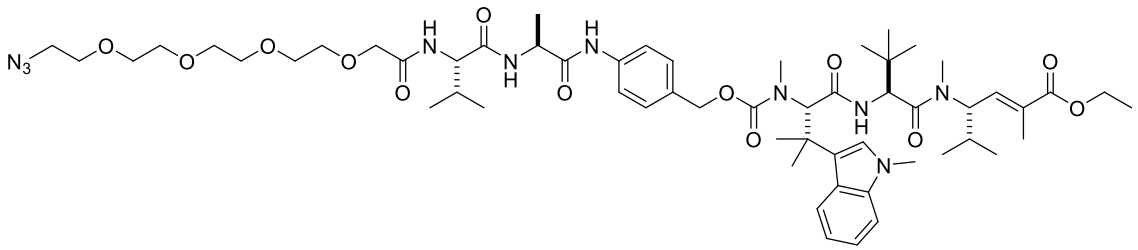

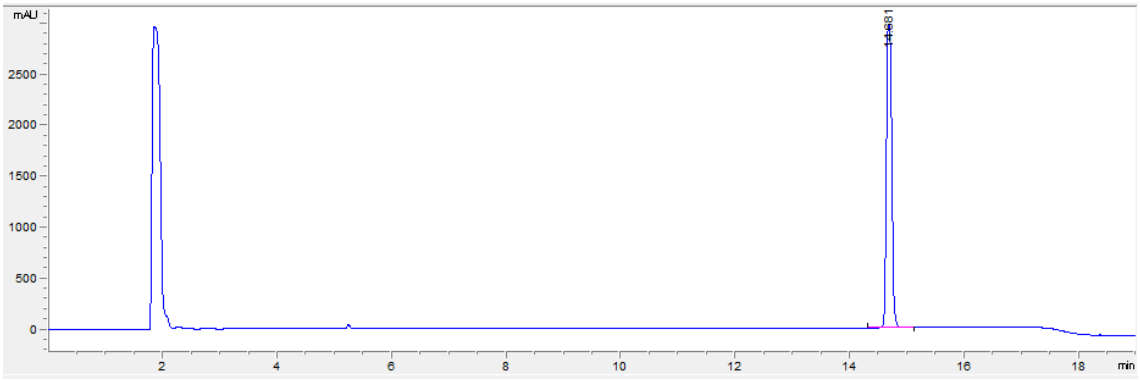

Taltobulin ethyl ester trifluoroacetate salt (138)

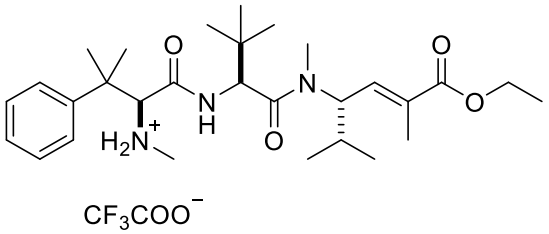

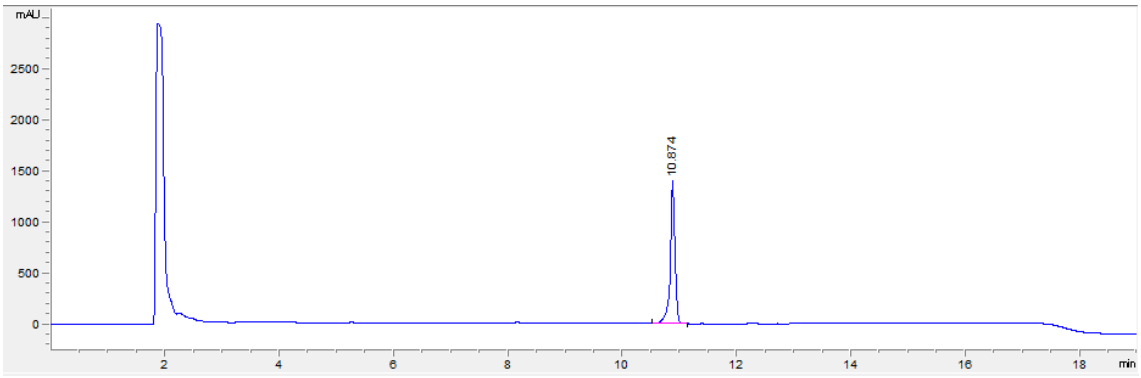

N_3-PEG_4-Val-Ala-PABC-taltobulin-OEt (140)

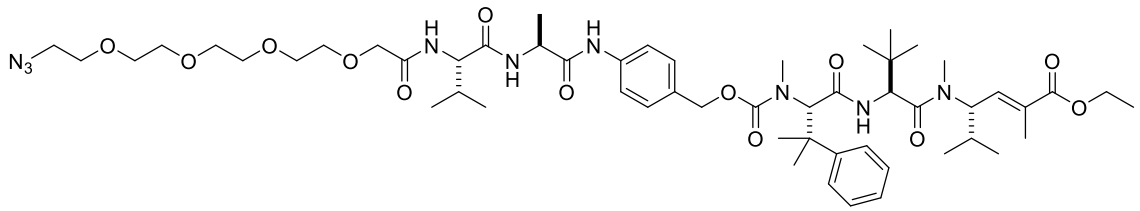

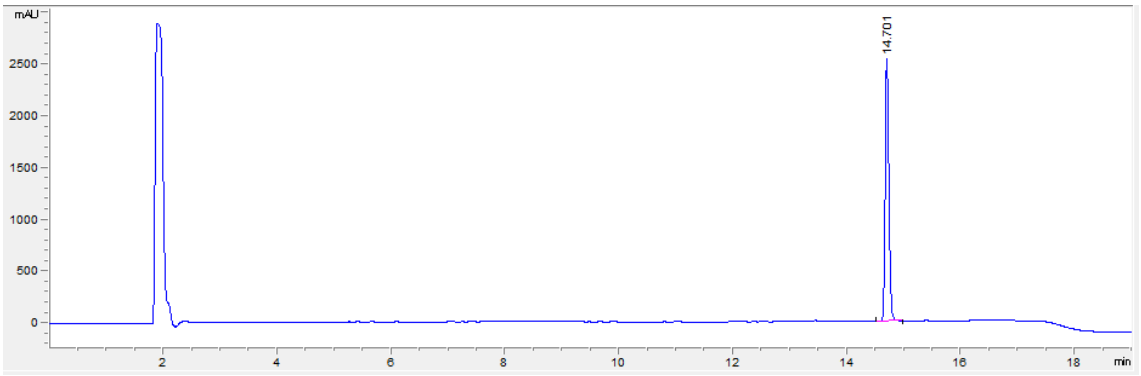

H-PEG$_2$-Glu$_3$-PEG$_2$-propargylGly-NH$_2$·TFA (141)

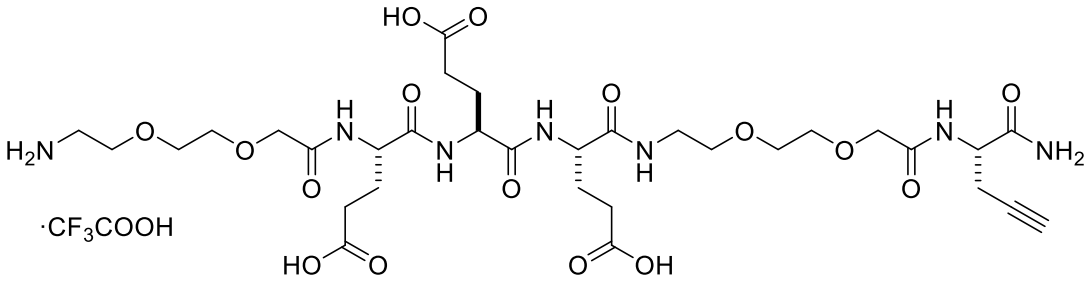

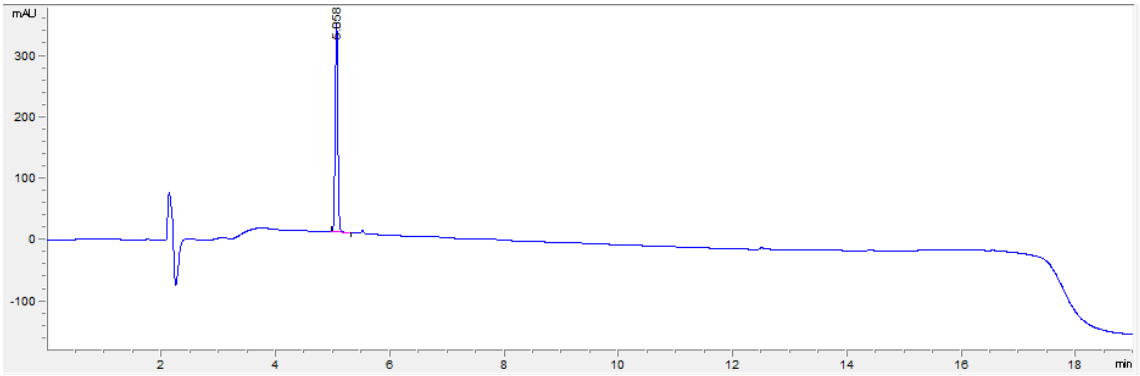

DVP-PEG$_2$-Glu$_3$-PEG$_2$-propargylGly-NH$_2$ (143)

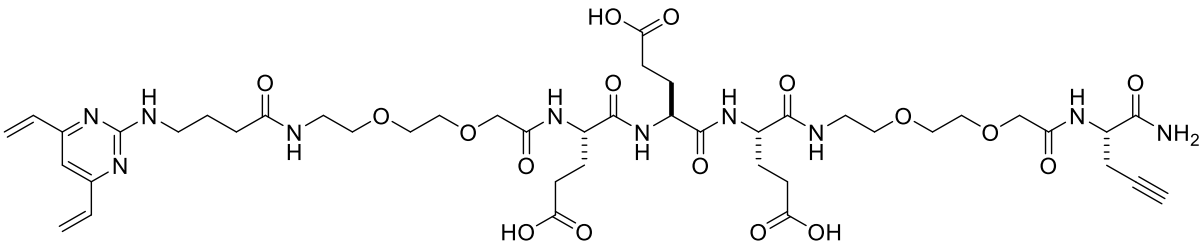

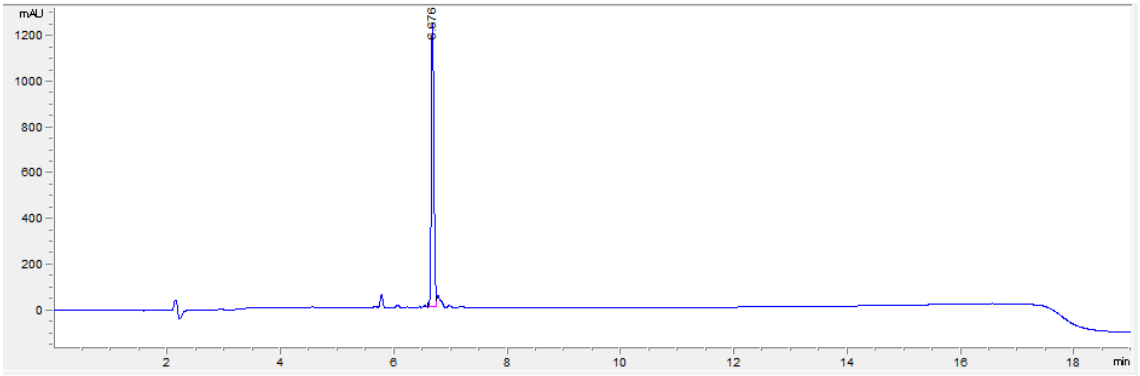

DVP-PEG$_2$-Glu$_3$-PEG$_2$-triazole-PEG$_4$-Val-Ala-PABC-hemiasterlin ammonium salt (144)

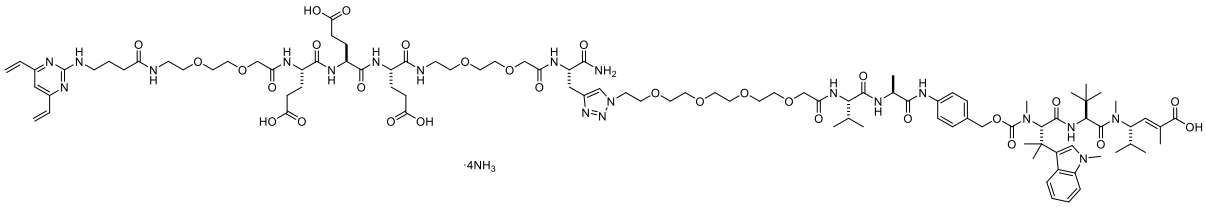

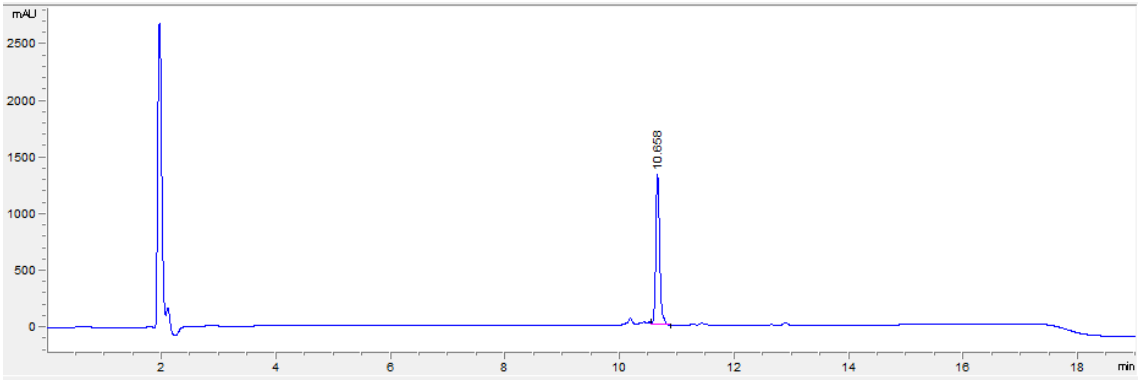

DVP-PEG$_2$-Glu$_3$-PEG$_2$-triazole-PEG$_4$-Val-Ala-PABC-taltobulin ammonium salt (145)

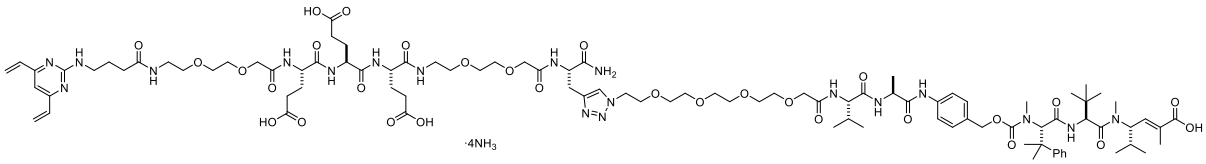

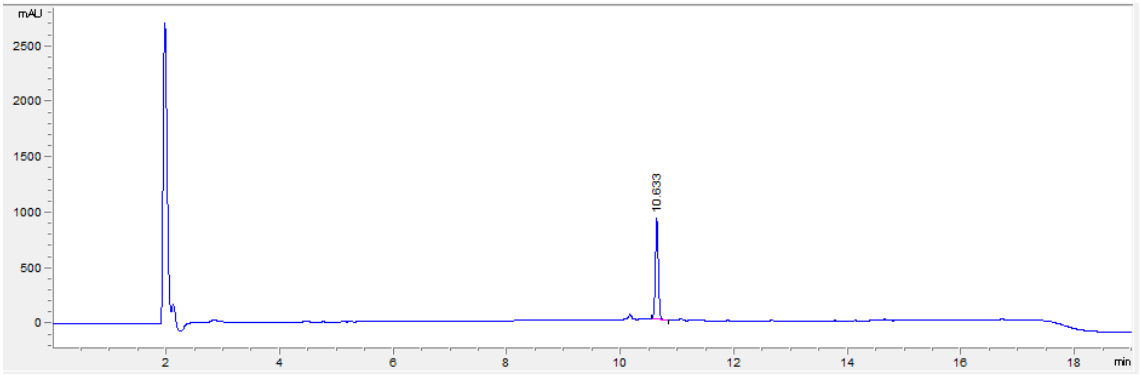

(*S*)-3,3-Dimethyl-2-((*S*)-3-methyl-3-(1-methyl-1*H*-indol-3-yl)-2-(methylamino)butanamido)butanoic acid trifluoroacetate salt (127a)

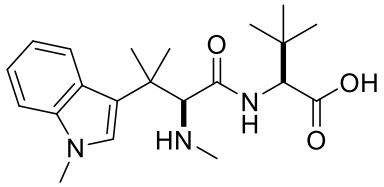

·CF_3COOH

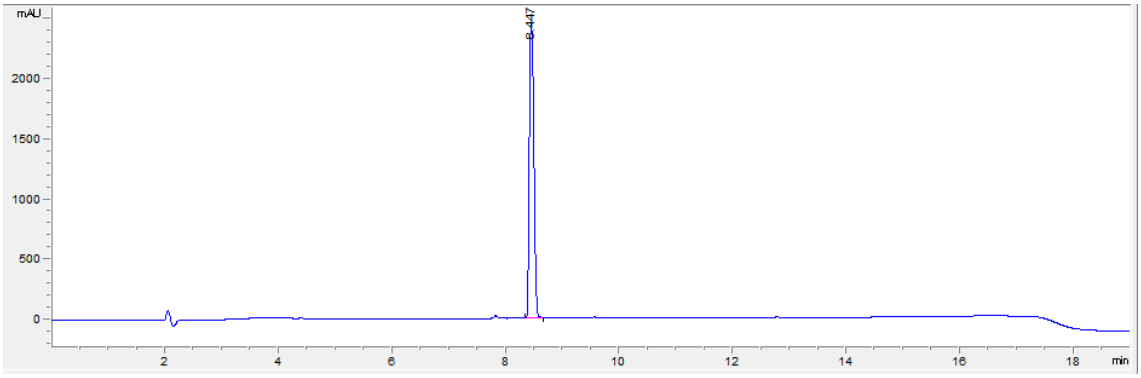

Methyl (*S*)-3,3-dimethyl-2-((*S*)-3-methyl-3-(1-methyl-1*H*-indol-3-yl)-2-(methylamino)butanamido)butanoate trifluoroacetate salt (129a)

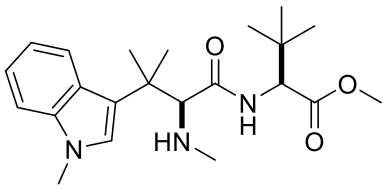

·CF_3COOH

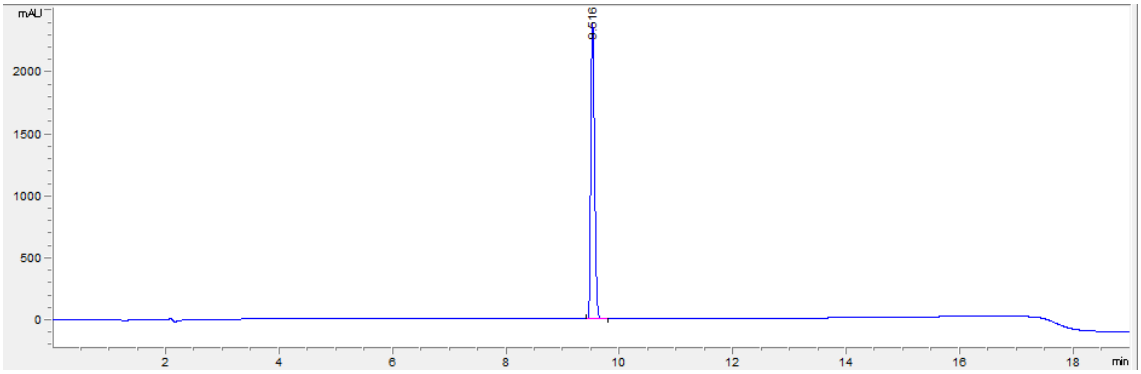

Methyl (*S*)-3,3-dimethyl-2-((*R*)-3-methyl-3-(1-methyl-1*H*-indol-3-yl)-2-(methylamino)butanamido)butanoate trifluoroacetate salt (129b)

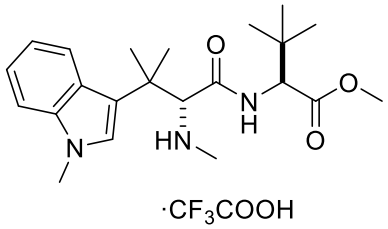

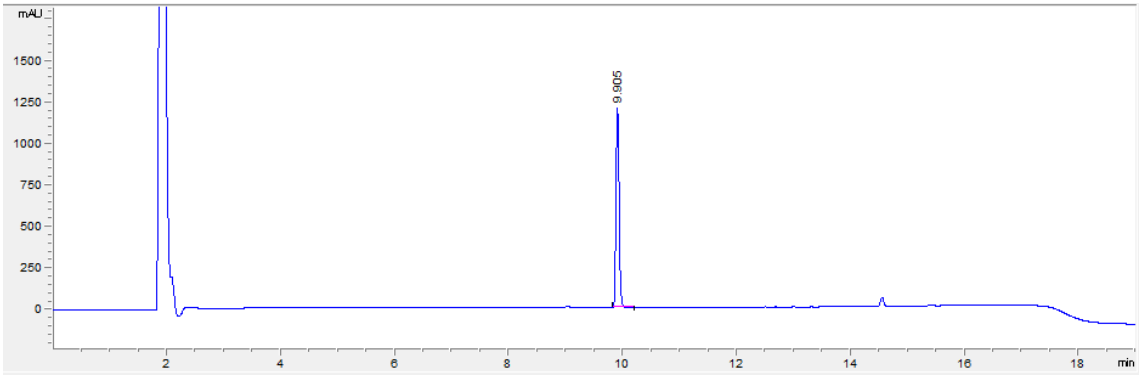

Carbamate 128b (35-95%B over 15 min)

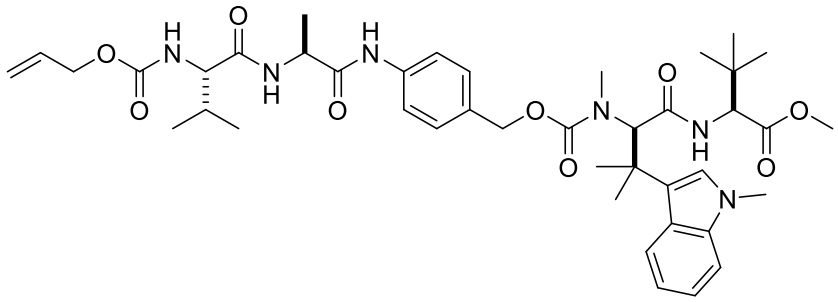

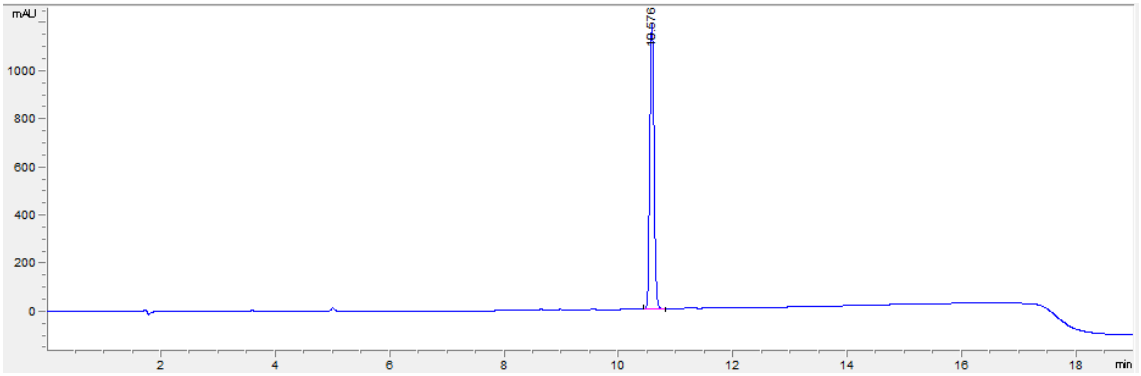

Appendix D — Selected HPLC traces from stability and reactivity traces

Stability tests in CuAAC peptide stapling condition

Compound **81**

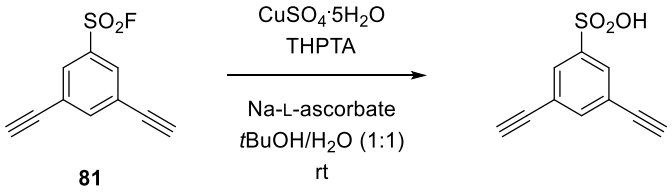

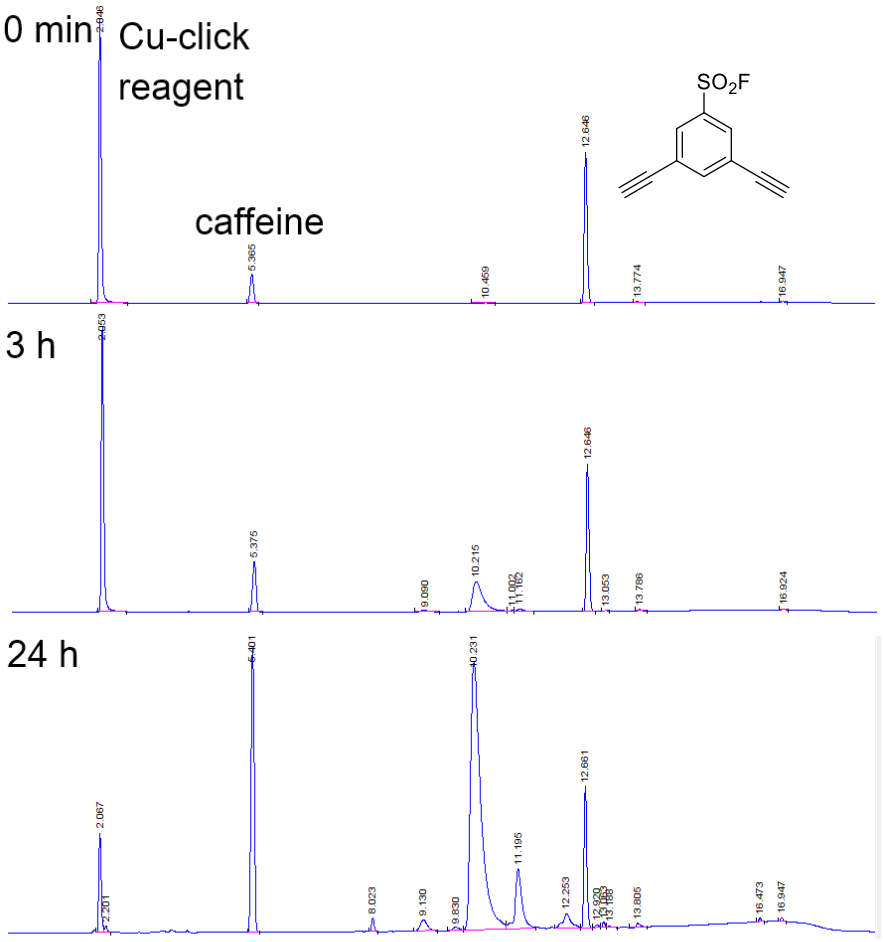

Compound **93**

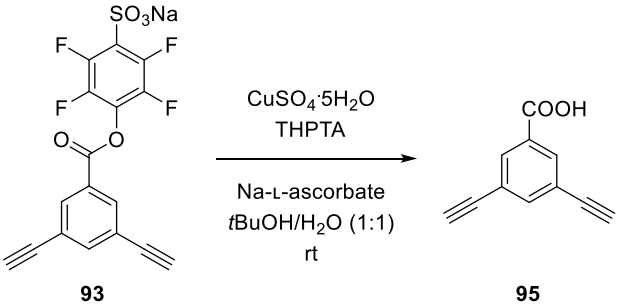

93 **95**

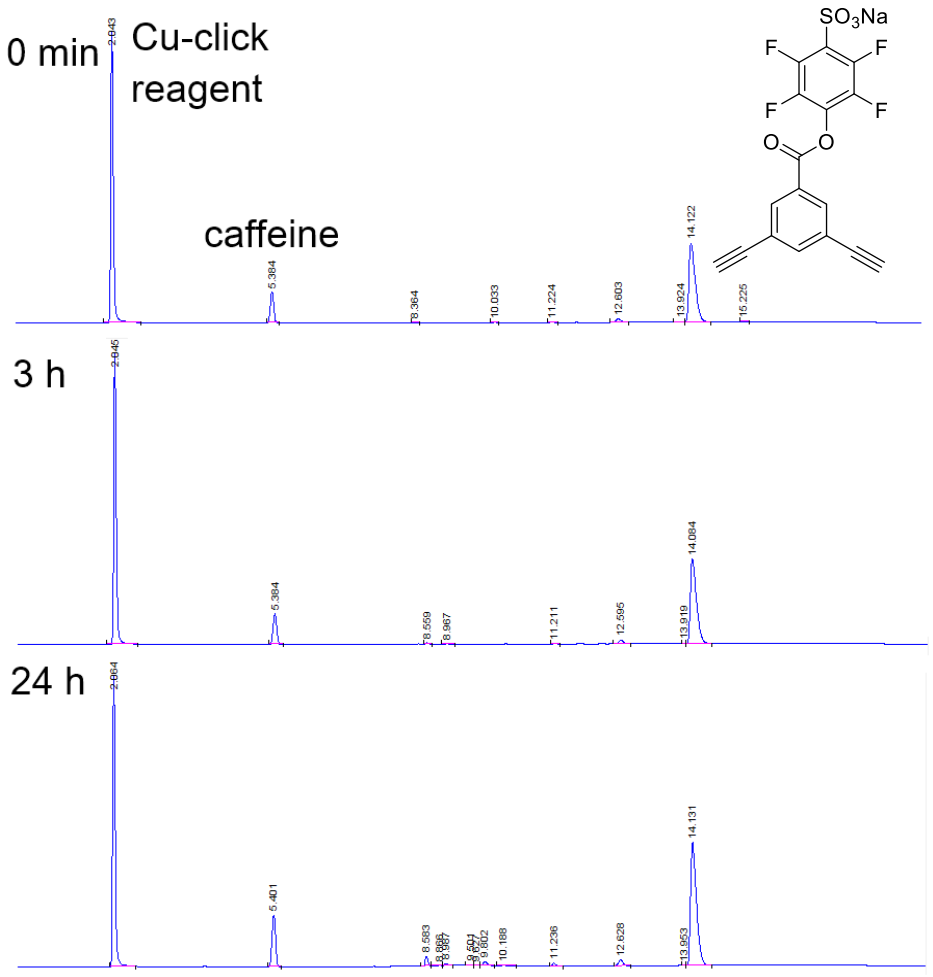

Stability tests in aqueous media

Compound **81**

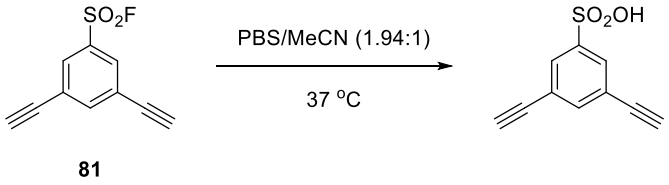

81

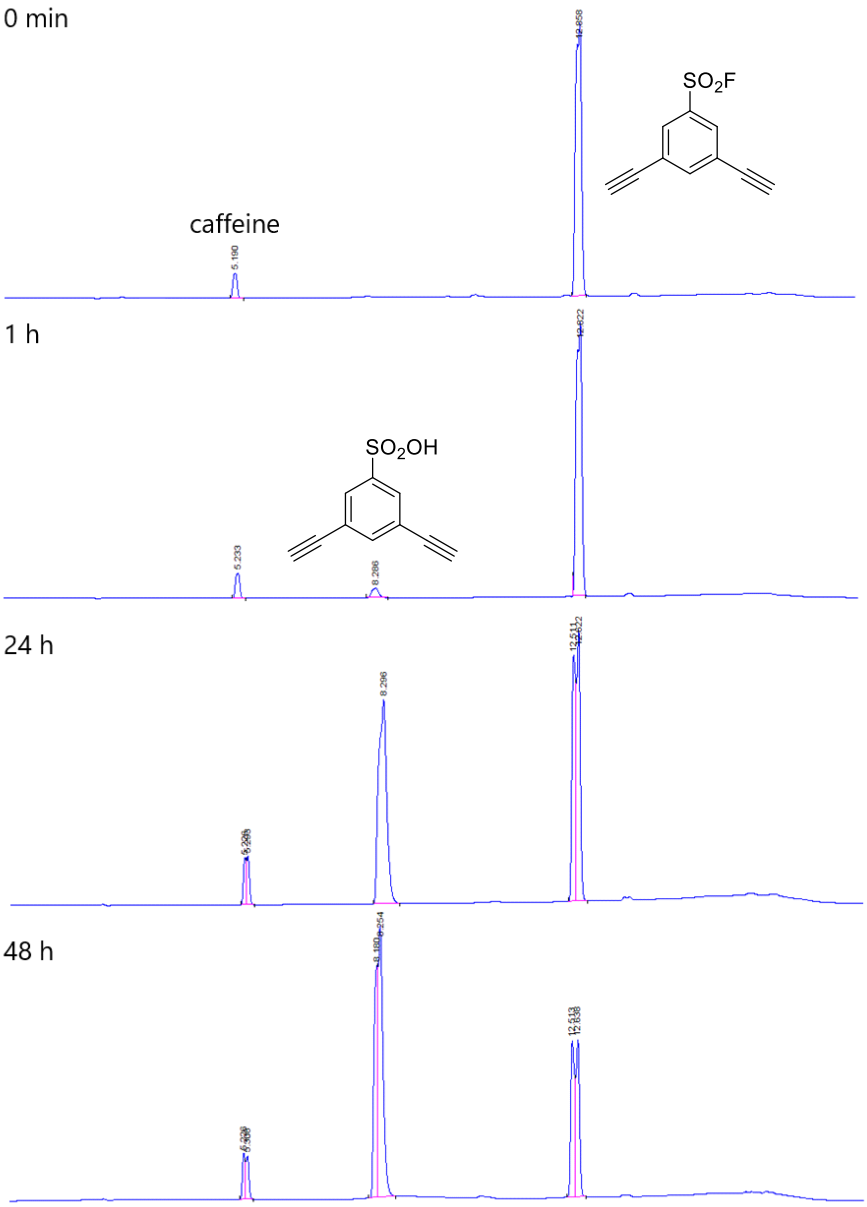

Compound **93**

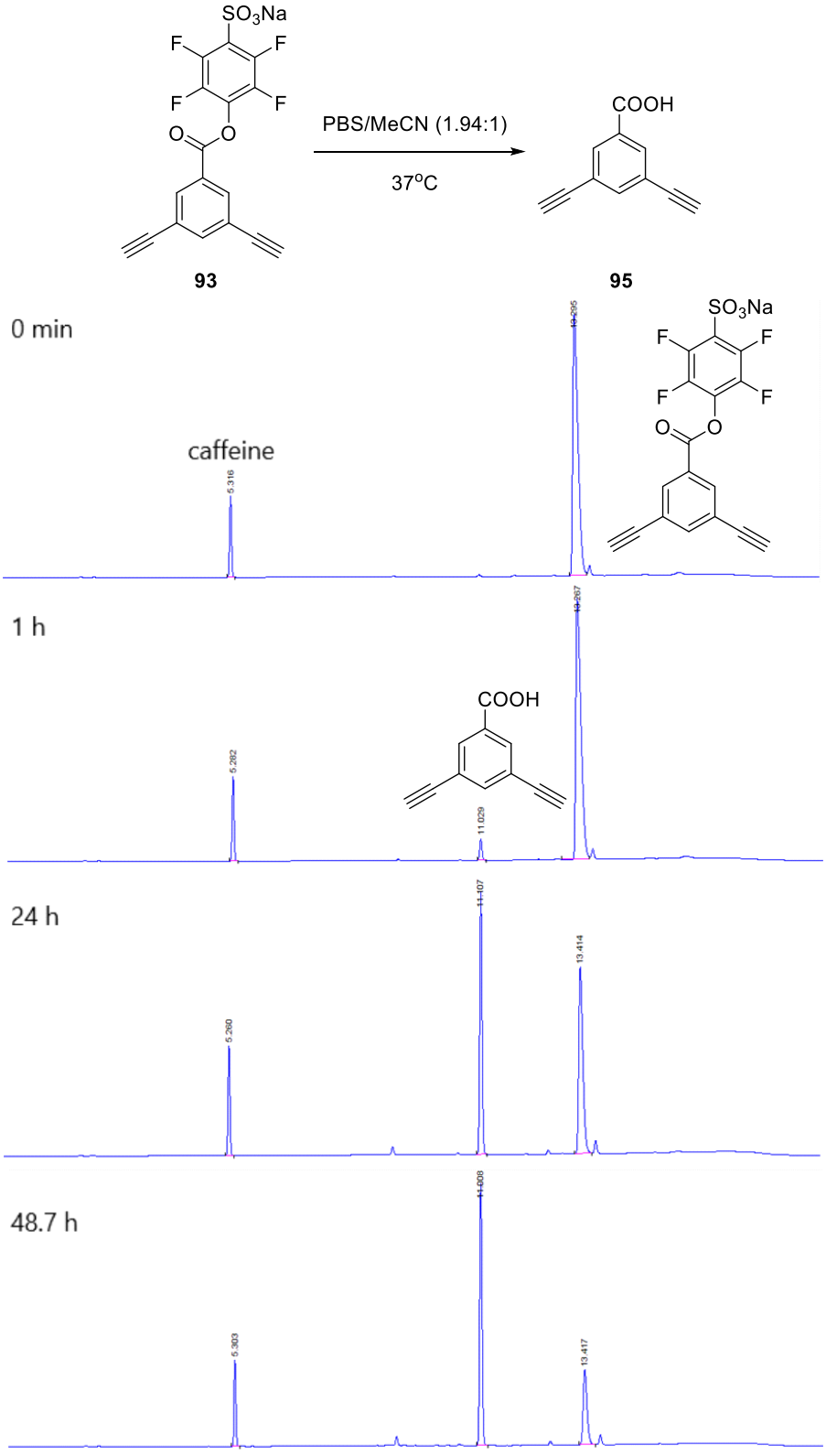
SO3Na
F
F
F
F
O
O
PBS/MeCN (1.94:1)
37°C
COOH
93
95
0 min
caffeine
5.316
13.295
SO3Na
1 h
COOH
5.282
11.029
13.287
24 h
5.280
11.107
13.414
48.7 h
5.303
11.009
13.417

Reactivity tests with Lys

Compound **81**

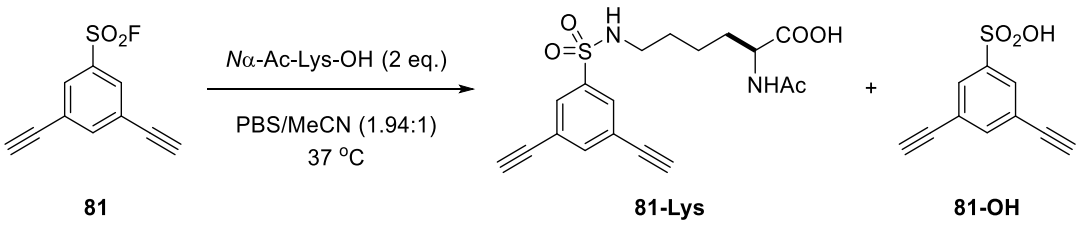

81 **81-Lys** **81-OH**

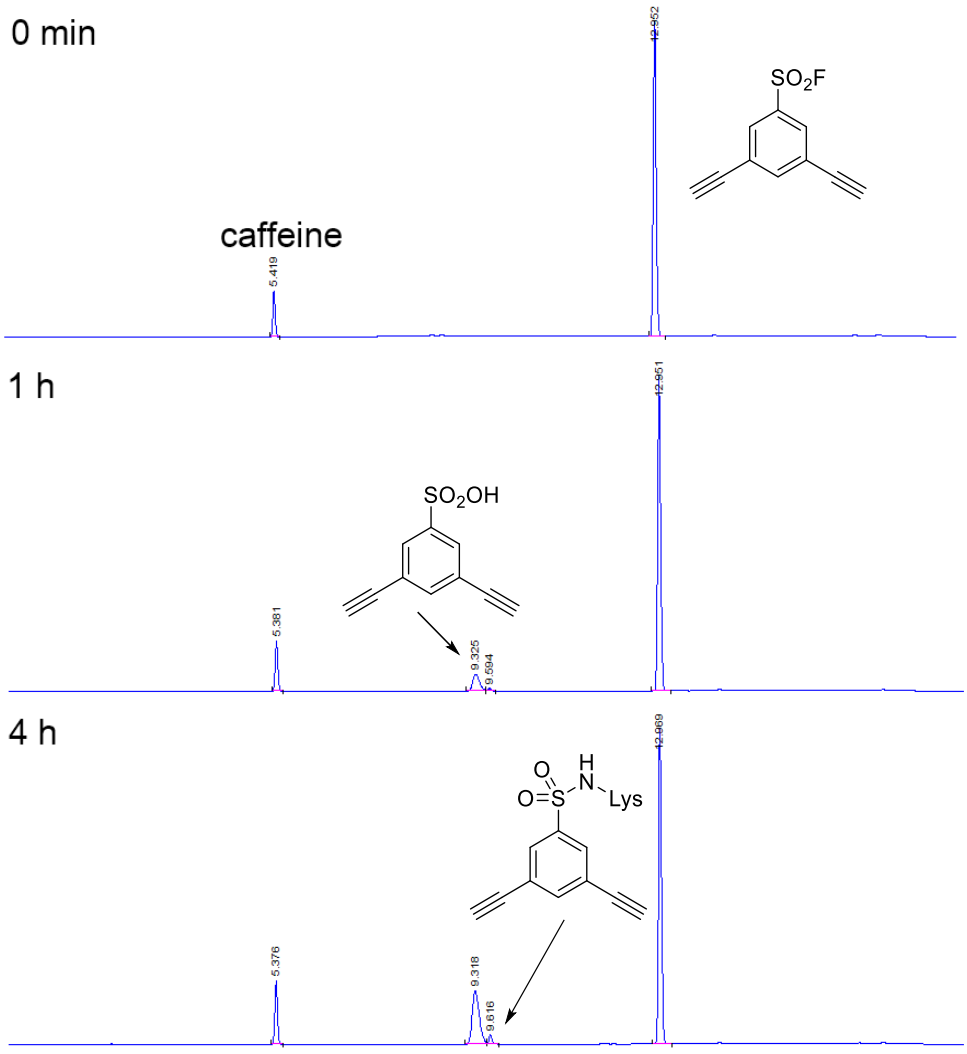

Compound **93**

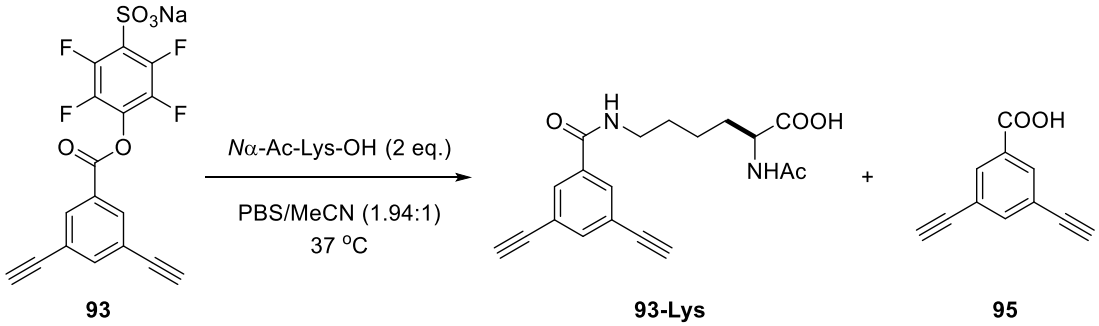

93 **93-Lys** **95**

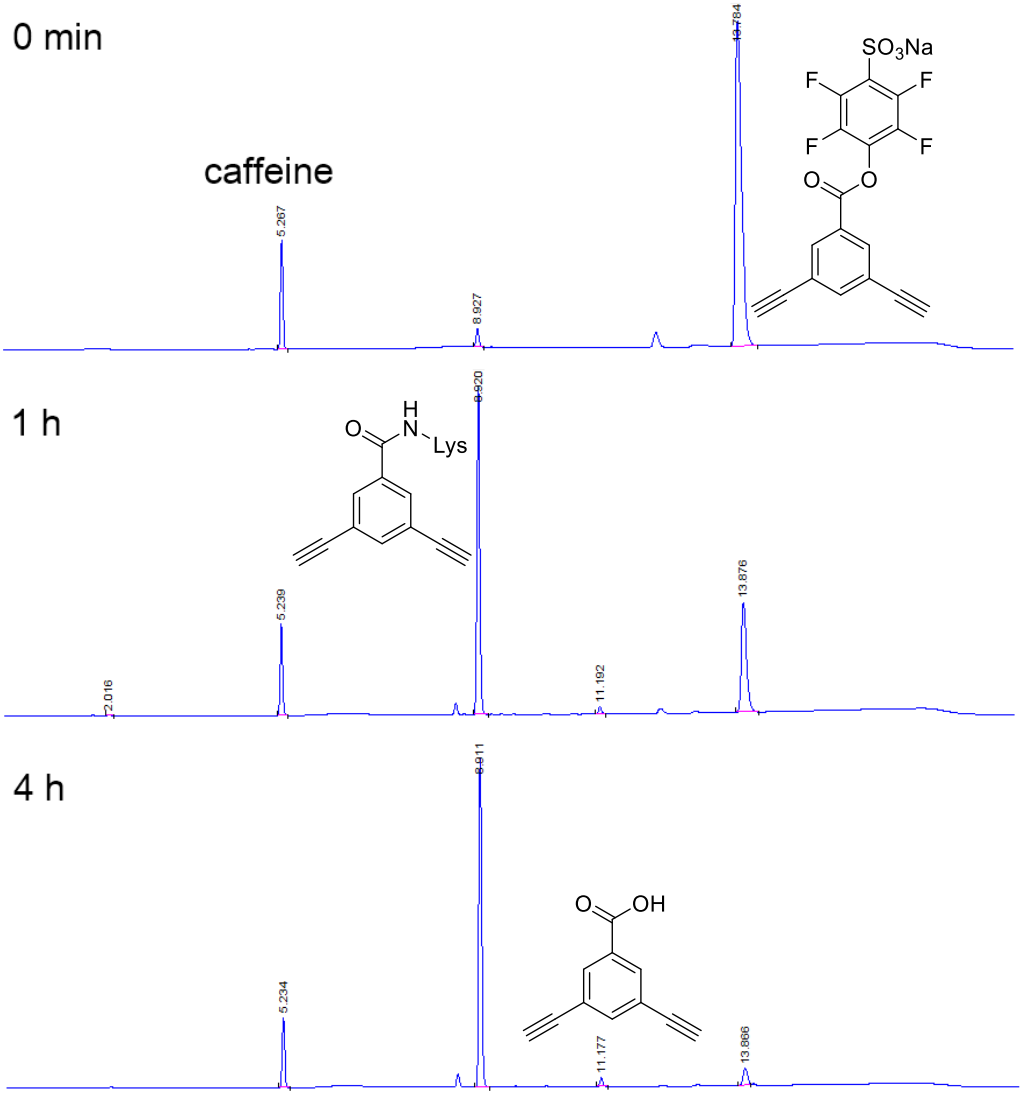

Reactivity tests with Cys

Compound **93**

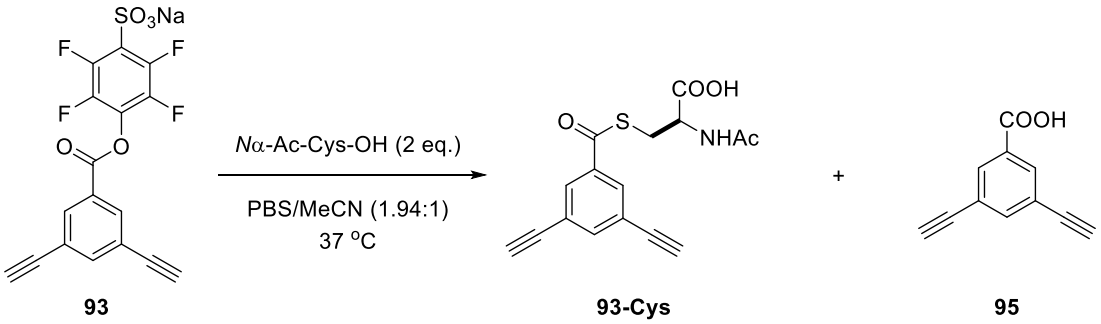

93 **93-Cys** **95**

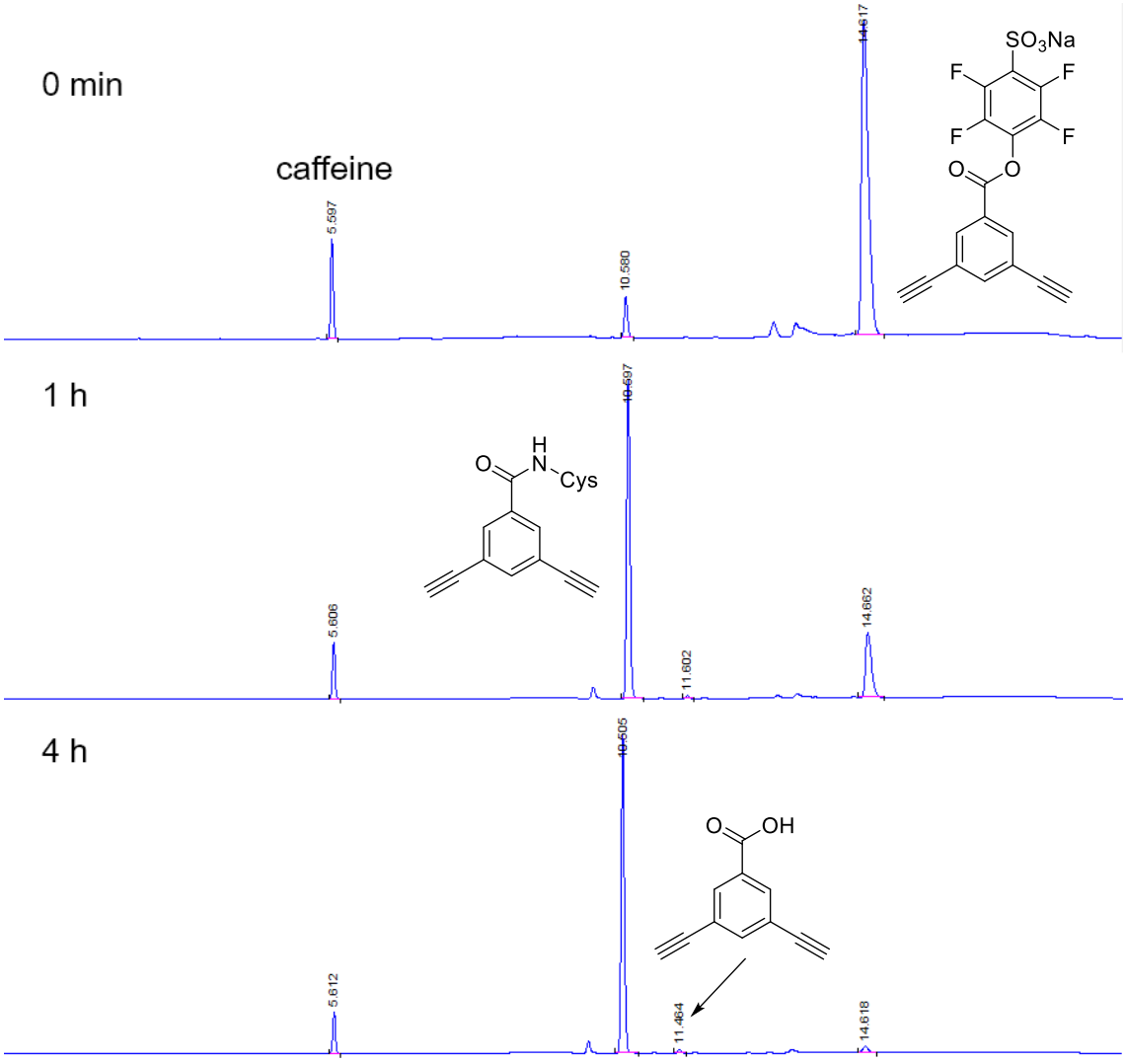

Appendix E — Publication list

J. Charoenpattarapreeda, Y. S. Tan, J. Iegre, S. J. Walsh, E. Fowler, R. S. Eapen, Y. Wu, H. F. Sore, C. S. Verma, L. Itzhaki and D. R. Spring, Targeted covalent inhibitors of MDM2 using electrophile-bearing stapled peptides, *Chem. Commun.*, 2019, **55**, 7914–7917.

J. Charoenpattarapreeda, S. J. Walsh, J. S. Carroll and D. R. Spring, Expeditious Total Synthesis of Hemiasterlin through a Convergent Multicomponent Strategy and Its Use in Targeted Cancer Therapeutics, *Angew. Chem. Int. Ed.*, 2020, DOI:10.1002/anie.202010090.